IMPACT AND MANAGEMENT OF IRON CORROSION BY-PRODUCTS ON DRINKING WATER QUALITY IN DISTRIBUTION SYSTEMS

by

Md. Safiur Rahman

Submitted in partial fulfilment of the requirements
for the degree of Doctor of Philosophy

at

Dalhousie University
Halifax, Nova Scotia
February 2014

Dedication

To

My beloved mother

Who passed away in 2010, April 09 (Friday)

And

Who was the main inspiration for my PhD Degree

TABLES OF CONTENTS

LIST OF TABLES

LIST OF FIGURES

ABSTRACT

Cast iron pipes were installed broadly in North American water utilities. Many of these cast iron pipes are corroded and are continuous sources of Fe(II) ions in drinking water distribution systems. Recent studies have reported that soluble or particulate iron decreases water quality in distribution systems.

In this study, an array of bench scale experiments were conducted to evaluate the impact of most common water parameters (e.g., pH, PO_4, Cl_2, and DOM) on the oxidation rate of Fe(II) ions, and on the formation of iron suspense in synthetic water samples. This was accomplished using a 2^4 full factorial design approach at a 95% confidence level. This study demonstrated that a lower content of iron suspension color, turbidity, and smaller particle size would appear to be obtained in presence of a phosphate based corrosion inhibitor at a pH value of 6.5 compared to a pH value of 8.5.

To investigate the impact of Fe(II) ions, phosphate, pH and reaction time, and their interaction on DBPs formation in water samples, this study was conducted following an experimental design approach. Considering all the significant ($\alpha = 0.05$, $p < 0.05$) factors, mathematical models for HAAs and THMs prediction were developed using 80 experiments. The models' adequacy was checked thorough the statistical and graphical diagnostics. Different sources of natural water samples collected from three main water treatment plants in Halifax, Canada, were used to validate the models. This study suggested that the models' performance were found to be excellent under a wide range of studied variables. Consequently, the most predominant iron oxides (goethite and magnetite) were used to investigate their impact on chlorine decay and DBPs formation study. Goethite and magnetite were also used for the adsorption of DBPs precursor (DOM). The DOM adsorption data illustrated to fit well with the Langmuir adsorption isotherm, indicating monolayer coverage. Molecular weight (MW) distributions of DBPs precursor (DOM) revealed that the higher molecular weight fractions adsorbed preferentially onto goethite followed by magnetite surface. The change of MW distribution of DOM was found to be in reasonable agreement with the change of DBPs formation in iron-water systems.

LIST OF ABBREVIATIONS AND SYMBOLS USED

°C	Degree Celsius
ANOVA	Analysis of variance
BCAA	Bromochloroacetic acid
BDCM	Bromodichloromethane
BDCAA	Bromodichloroacetic acid
BET	Burnauer Emmet and Teller
$CaCO_3$	Calcium carbonate
CDBAA	Chlorodibromoacetic acid
Cl^-	Chloride
cm	Centimeter
Da	Dalton
DBAA	Dibromoacetic acid
DBCM	Dibromochloromethane
DBPFP	Disinfection byproduct formation potential
DBPs	Disinfection byproducts
DCAA	Dichloroacetic acid
DO	Dissolved oxygen
DOC	Dissolved organic carbon
DOM	Dissolved organic matter
Fe(II)	Ferrous ions
FTIR	Fourier-transform infrared
h	Hour
HAA	Haloacetic acid
HCl	Hydrochloric acid
HPSEC	High performance size exclusion chromatography
ICP-MS	Inductively coupled plasma mass spectrometry
k	Constant value for Langmuir isotherm or rate constant
MBAA	Monobromoacetic acid

MCAA	Monochloroacetic acid
MDL	Method detection limit
mg/L	Milligrams per liter
min	Minute
mm	Millimeter
MN	Molecular number
MTBE	Methyl *tert*-butyl ether
mV	Millivolt
MW	Molecular weight
$NaHCO_3$	Sodium bicarbonate
NaOCl	Sodium hypochloride
NaOH	Sodium hydroxide
nm	Nanometer
NTU	Nephelometric turbidity units
OCl^-	Hypochlorite ion
Q	Adsorption density
QC	Quality control
Q_{max}	Maximum adsorption density
R^2	Coefficient of determination
RPM	Revolutions per minute
SEM	Scanning electron microscope
SO_4^{2-}	Sulfate
TBAA	Tribromoacetic acid
TCAA	Trichloroacetic acid
TEM	Transmission electron microscope
THM	Trihalomethane
UV_{254}	Ultra violet absorbance at 254 nm
XRD	X-day difractiometer
µg/L	Micrograms per liter
µL	Micro liter

ACKNOWLEDGEMENT

I wish to express my deepest sense of gratitude, profound appreciation and indebtedness to my reverend teacher and PhD supervisor Dr. Graham A. Gagnon. Your skilful supervision and keen interest throughout the coursework, proposal writing, papers' writing and in the preparation of this dissertation has shown me how to be a good academic. Your generous supports and continuous encouragement has been instrumental in getting me to this point.

It is my great pleasure and proud privileges to express my heartiest thanks and gratefulness to my committee members Dr. Lei Liu and Dr. Rob Jamieson. Thanks due to Dr. Marc Lamourex and Dr. Young J.C.O. (Chemistry Dept., St. Mary's University). Each of your inspiration, suggestions and guidance have helped to shape my project and given me new ideas to think about and to incorporate into my thesis. I am grateful to all of you, and I do appreciate you all.

I would like to express my thanks to Dr. Marc Whalen (Chemistry Dept., Dalhousie Univ.) for providing me technical supports during conducting FTIR experiments. The authors also would like to acknowledge Dr. Z. Farhat (Process Engg Dept.), Dr. Ping Li (Biology Dept.) Dr. Jeff Dahn (Physics and Atmospheric Science Dept), Patricia Scallion (Institute for Research in Materials) of Dalhousie University for providing enthusiastic assistances throughout the XRD, TEM, BET surface area and SEM-EDX experiments.

I would like to acknowledge the contributions of technical support from members of the water quality laboratory. In particular, I would like to thank our research chemist Heather Daurie for helping me to handle analytical instruments and to analysis my samples. Many thanks are due to Jessica Cambell, Amina Stoddart, Meghan Gibbons, Alisha Knowles, Eliman Camara, Elsadig Abdallah, Sarah J. Payne, Wendy Krkosek, Joelle D. Doubrough, Krysta R. Montreuil and many others.

The authors gratefully acknowledge the financial support of the Natural Sciences and Engineering Research Council of Canada (NSERC), Halifax Regional Water Commission (HRWC), Canadian Water Network (CWN), and Faculty of Graduate Studies (FGS), Dalhousie University, Canada.

Thank you to my parents and siblings, for encouraging me to fulfill my dreams, cheering for me through my success. Without your support and encouragement in my all academic life, it's not possible to come to this point. A special thanks as well to Lamisa S. Rahman and Meher N. Chowdhury.

CHAPTER 1. INTRODUCTION

1.1. Perspective

The drinking water, that is also well-known as "potable water" should be safely used for drinking, cooking, bathing and washing. The safe drinking water should not contain the minerals, the organic ingredients, or the disease causing organisms. It should be aesthetically suitable and free from the apparent turbidity, odor, color, objectionable taste, and any contamination/s (natural or anthropogenic). However, the water quality in distribution systems has been reported to be deteriorated (O'Connor and O'Connor, 2000). The water quality deterioration in distribution systems can adversely affect consumers' health as well the aesthetic properties of water (Sadiq et al., 2010). Sadiq et al. (2010) have identified several major deterioration mechanisms in drinking water distribution systems, which include: contaminant intrusion, interior corrosion, leaching, biofilm development, disinfectant loss and DBPs formation, and permeation that may contribute to water quality failure.

Cast iron pipes were installed broadly in North American water utilities, particularly in older cities such as Halifax, NS; and other cities in the Northeastern portions of Canada and the US. In US only, the majority of distribution system pipes are composed of iron material: cast iron (38%), ductile iron (22%), and steel (5%) (AWWA, 1996). Many of these cast iron pipes are corroded, and are continuous sources of iron in drinking water. Therefore, the problem of corrosion related water quality changes is significant. Metal corrosion is one of the most complicated and costly problems facing drinking water utilities. In drinking water transmission and distribution systems, the internal surfaces of the unlined cast iron pipes are normally exposed to an oxidizing atmosphere that causes corrosions. The reduction of pipe wall is directed as a zero-valent iron (Fe°); and correspondingly when Fe° ions come in contact with water,

ferrous iron (Fe^{2+}) start to appear in drinking water distribution systems (Hozalski et al. (2008)). As a result, Fe^{2+} ions are continuously coming into drinking water (Sarin et al., 2004a) and the concentrations of Fe^{2+} ions are site specific to water quality. The concentration of Fe^{2+} ions was found to be 7.2 mg/L, dry weight basis in a center sample, and 17.1 mg/L, dry weight basis in a side sample of 40-50 years-old iron pipe collected from the distribution systems in Melbourne, Australia (Lin et al., 2001). The discharge of iron from drinking water distribution systems materials and the nature of iron corrosion scales are organized by the redox reactions (Sarin et al., 2004a). Previously, several studies have been examined Fe^{2+} ions oxidation in natural water (Stumm and Lee, 1961; Theis and Singer, 1974; Millero et al., 1995; Azher et al., 2008; Gonz´alez et al., 2010). These studies have encouraged a number of additional measurements of the rate of Fe^{2+} ions oxidation in well-defined aqueous solutions.

The soluble Fe^{2+} ions are oxidized to comparatively insoluble Fe^{3+} ions by different types of oxidants present in water (e.g., dissolved oxygen and disinfectant residual), which is a vital reaction in both natural and engineering water systems. Conversely, it has been stated in literature that dissolved organic matter (DOM) can lead to accelerate, abate, or have no conclusion on the oxidation of ferrous iron (Stumm and Lee, 1961; Theis and Singer, 1974; Liang et al., 1993). The effects of DOM on Fe^{2+} ions oxidation has been shown to be dependent on a number of factors including pH (Stumm, 1990; Millero et al., 1995; Morgan and Lahav, 2007; Gonz´alez et al., 2010) and the concentration iron and oxygen in aqueous media (Rose and Waite, 2002). On the other hand, chlorine based disinfectants have been most broadly used as a secondary disinfectant for drinking water distribution systems since 1913 in North America (White, 1992). Generally, an increament in disinfectants (oxidants) concentrations would be expected to accelerate corrosion rate. This is experimentally substantiated by Eisnor and Gagnon (2004), who conducted cast-iron pipe loop experiments for the reaction periods of 6 and 12 h using three different types of disinfectants, and they observed that free chlorine and chloramine would increase iron release from background water quality

levels. To prevent corrosion, different types of corrosion inhibitors have also been using with phosphate based corrosion inhibitors having a popular treatment technique for low alkalinity water (Maddison et al., 2001).

However, the iron corrosion by-products through a drinking water distribution system cause several problems, i.e., unpleasant metallic taste, increase color, turbidity, odor, metal contents, and loss of the disinfectant residuals in water. Nearly all of the reports published on corrosion control deal only with the control of Fe(II) and Fe(III) ions release rather than the production or reduction of turbidity and color in drinking water distribution systems. On the other hand, it has been hypothesized that these corrosion by-products (e.g., Fe(II) ions, goethite, and magnetite) might be reacted with free chlorine, and they might have adsorbed DOM. Consequently these corrosion by-products might have impact on disinfectant byproducts (DBPs) formation in drinking water distribution systems. However, relatively few key studies have been published concerning corrosion by-products and corrosion inhibitors on the changes in drinking water quality (Valentine et al., 2000; Chun et al., 2005). Therefore, a simulated distribution system (SDS) test is important to evaluate the impact of individual iron corrosion by-products (e.g., Fe(II) ions, goethite, and magnetite) alone, and with corrosion inhibitor on chlorine decay, DBPs formation, and subsequently change of water quality in distribution systems.

To recognize the corrosion mechanisms, to reduce metal release from corroded pipe and to know their impacts on disinfectant residual decay and DBPs formation in distribution systems, a good number of researches have been conducted in recent years. In most studies, traditional one-factor-at-a-time experiments have been conducted, while the influences of the significant environmental factors simultaneously are very limited. To identify the most important factors, and their interactions that affect the change of rate constants in ferrous iron oxidation processes, iron suspension and DBPs formation in a simulated distribution system, will be an important element to improve water quality in

drinking water treatment and distribution systems. This might be accomplished using a 2^n full factorial design approach at a statistical significance level. The factorial design determines which factors have significant effects on the response as well as how the effect of one factor varies with the level of the other factors (Montgomery, 2009). Different types of software (e.g., Statistica, Minitab, SPSS, and SAS) use to analysis data for developing a mathematical model. The development of consistent models is progressively documented as an essential methodological basis for calculating the formation of DBPs, which may be an alternative for monitoring of DBPs in the fields. On the other hand, the models can also be very useful in validating key operational and water quality parameters, which may help to explain the DBPs formation potential in distribution systems (Rodriguez et al., 2003).

Dissolved organic matter (DOM) is reported to be one of the main precursors in DBPs formation, which is consisted of an extensive range of molecular weight varies from a few hundred to a few thousands Daltons (Da) (Leenheer and Croué, 2003). The higher molecular weight components of DOM in water are mainly hydrophobic fractions (Eikebrokk et al., 2004). The hydrophobic fractions are described to be the most reactive DOM components in DBPs formation study (Marhaba and Van, 2000; Chang et al., 2001). Therefore, it is an important filed of study to evaluate the impact of different variables on the changes in molecular weight (MW) distributions of DOM in water sample, and their correlation with the DBPs formation in drinking water distribution systems.

On the other hand, dissolved organic matter can potentially change the surface properties and reactivity of the hydrous mineral oxides, hydroxides due to adsorption onto iron particles. Consequently, DOM present in water can play a major role on conducts (e.g., transport and fate) of many environmental organic and inorganic contaminants by changing surface charge of the mineral particles. The behaviors (e.g.,

electrophoretic mobility, transport and interaction) of these mineral colloids might also be altered due to DOM adsorption onto mineral surfaces (Davis, 1982; Sposito, 1984; Stevenson, 1994; Wang et al., 1997; Guan et al., 2006). Therefore, it is important to investigate the mechanisms controlling DOM adsorption onto iron oxides surfaces.

1.2. Research hypotheses and objectives

The hypothesis of this thesis was that the different environmental variables had significant impact on the processes of iron corrosion and oxidation, and on the formation of iron suspension that might alter drinking water quality in distribution systems. It was also hypothesized that DOM and chlorine residual, and disinfectant byproducts (produce from the reactions of DOM and chlorine), might have altered by the iron corrosion by-products. The manner in which these mechanisms function in distribution systems are depicted in Figure 1.1. These hypotheses are tested through the completion of five main objectives. It has been expected that the findings of this study should be advance knowledge to understand the mechanistic roles of iron corrosion by-products on the changes in drinking water quality in distribution systems.

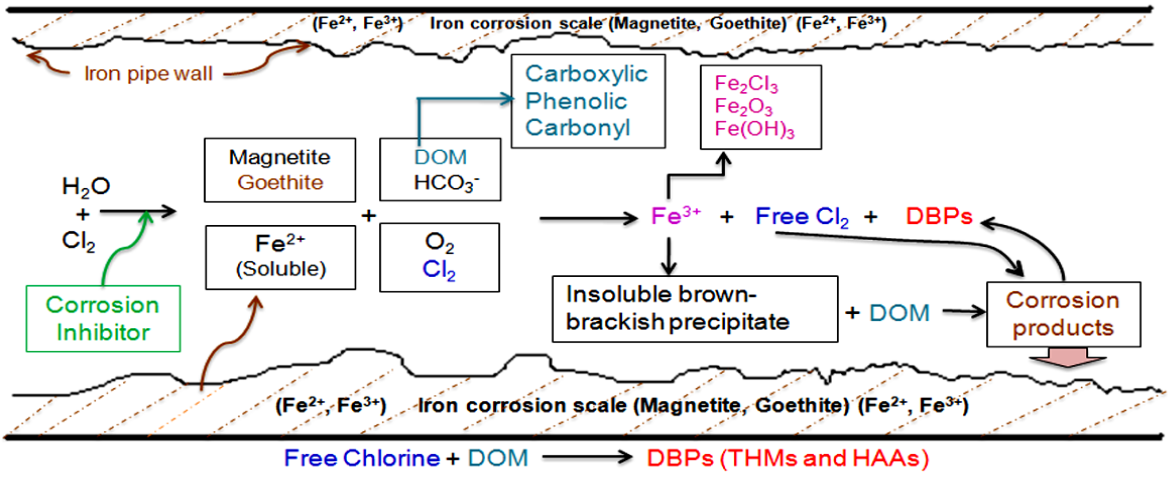

Figure 1.1. The role of iron corrosion by-products (e.g., soluble iron, goethite, and magnetite), and corrosion inhibitor on water quality changes in distribution systems.

Objectives:

Five research objectives were defined to complete this research project. The following schematic diagram (Figure 1.2) represents at a glance of the research objectives which were conducted in this study.

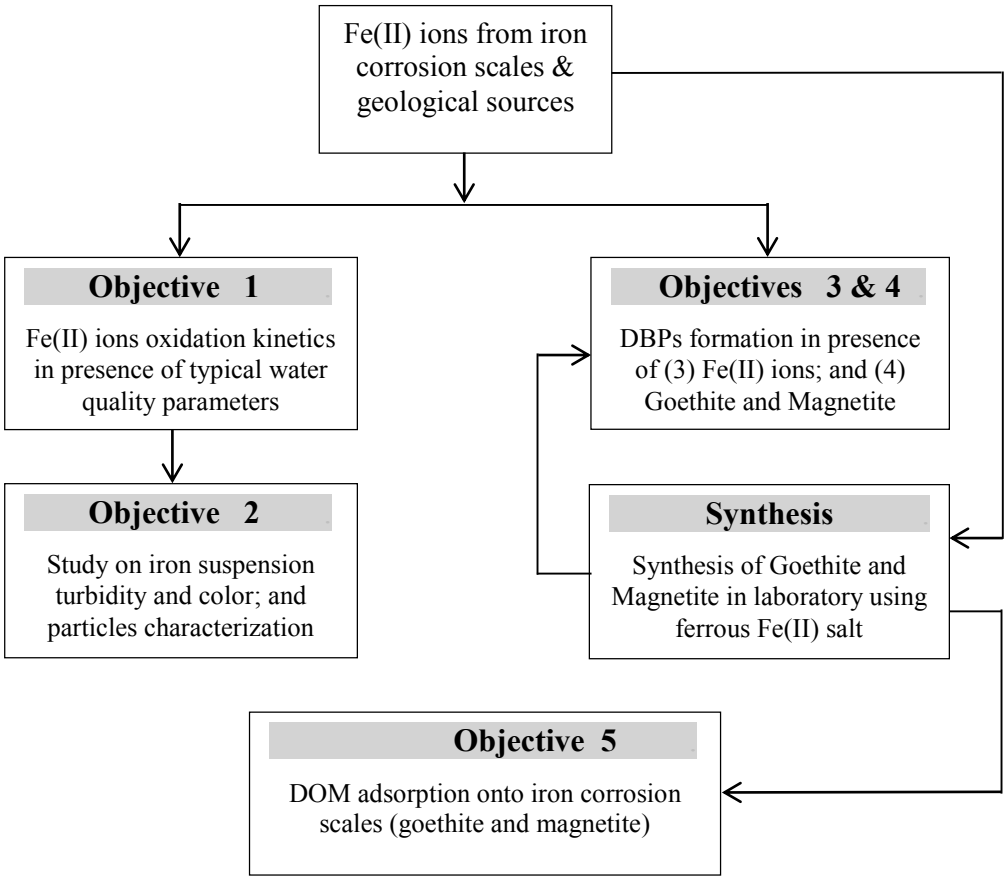

Figure 1.2. Organization of the study for the objectives 1 through 5.

Objective 1: The objectives of this research were to identify and quantify the most significant factors and their interaction influencing on change in rate constants of ferrous iron oxidation processes in a system containing four factors: (1) pH, (2) DOM, (3) disinfectant, and (4) phosphate based corrosion inhibitor in $NaHCO_3$ buffered synthetic water. A 2^4 full factorial design approach at a 95% confidence level was designed to follow for the bench scale experiments. The correlation between the rate constants of Fe(II) ions oxidation and the various factors (acting independently) was aimed to determine. In addition to the factorial design approach, an extensive study for different variables with their wide range of levels were also directed to investigate their impact on Fe(II) ions oxidation processes. Understanding both homogeneous and heterogeneous parameters that affects Fe(II) ions oxidation process will be an important element to improve water quality in drinking water treatment and distribution systems.

Objective 2: Nearly all of the reports published on corrosion control deal only with the control of Fe(II) and Fe(III) ions release rather than the production or reduction of turbidity and color in drinking water distribution systems. Therefore, the aims of this study were to evaluate the impacts of most significant environmental parameters on the formation of iron suspension color and turbidity following a 2^4 full factorial design approach. A comprehensive study was directed to investigate the mechanisms causing high color and turbidity in drinking water. The iron particles derive from the oxygenation of Fe(II) ions in presence of different variables were targeted to characterize using the different tools, i.e., zeta potential, particle size distribution, X-ray diffraction (XRD), and transmission electron microscopy (TEM).

Objective 3: The objectives of this study were to investigate comprehensively the effects of four potential water quality parameters, i.e., pH, Fe(II) ions, phosphate, and stagnation time with a wide range of levels for each variable on HAAs and THMs formation and distribution in $NaHCO_3$ buffered synthetic water under the laboratory conditions

simulated to distribution systems. The molecular weight (MW) distribution of DOM was aimed to conduct using a high performance size exclusion chromatography (HPSEC) to evaluate the effects of studied variables on the changes in MW distribution of DOM in water samples. In addition with the comprehensive study, a 2^4 full factorial design with center point levels approach was followed to conduct HAAs and THMs formation study with the typical drinking water quality parameters. Based on the statistical analysis of the experimental data, the mathematical models for HAAs and THMs prediction were intended to develop. To evaluate the models' adequacy, graphical and numerical diagnostic methods were directed to follow. An independent set of data for DBPs formation in natural water for the presence of different variables at different levels, was expected to assess the effectiveness of the fitted modeling equations.

Objective 4: To better understand the chlorine decay and the regulated DBPs formation mechanisms in presence of iron corrosion scales, it is an important study on the interection between individual iron oxide and drinking water disinfectant that my help to elucidate the reactive mechanisms in distribution systems. Therefore, the objectives of this study were to assess the role of most predominant iron oxides present in corrosion scales, i.e., goethite (α-FeOOH) and magnetite (Fe_3O_4) on the changes in residual chlorine concentrations; and ultimate impact on the changes in disinfection byproducts (DBPs) formation in post filtered water sample collected from JDK water treatment plant. Magnetite and goethite were synthesized in our laboratory, and were confirmed using XRD, SEM-EDX, BET surface area. Thereafter, goethite and magnetite were used in bench scale study to conduct chlorine decay and DBPs formation in the post filtered water samples.

Objective 5: It is important to understand the behaviors of DOM sorption onto iron oxides since the presence of DOM and DOM associated metal oxides greatly affect the fate and transport of many organic and inorganic pollutants and the formation of DBPs in

drinking water transmission and distribution systems. Therefore, the motivation of this study was to investigate the mechanisms controlling the DOM adsorption onto metal oxides. The particular objectives here were to (1) quantify the adsorption of DOM in synthetic water by two main iron oxides (goethite and magnetite), (2) evaluate the change of DOM molecular weight distribution due to adsorption onto goethite and magnetite, (3) examine the role of solution pH on adsorption mechanisms using goethite and magnetite, and (4) investigate the correlation between independent and dependent variables involving with the DOM adsorption processes.

1.3. Organization of thesis

In order to present the research outcomes according to the five research objectives outlined above, the thesis was organized in the following chapters. The main chapters (Chapters 4 through 8) of this thesis are prearranged and formatted with the purposes of being submitted for possible publication in the referred journals. For that reason, each chapter contains an abstract, introduction, materials and methods, results and discussion, and conclusions. In Appendices A through E, raw and supplemental data for the Chapters 4 through 8 are presented respectively. Appendice F contains the letters of copyright permission/acceptance from the respective journals.

Chapter 2 provides an appraisal of important background information on the factors influencing Fe(II) ions oxidation process, iron suspension formation, disinfection byproducts (DBPs) formation/reduction in iron pipe water distribution systems. This chapter also provides information on the main iron corrosion scales, i.e., goethite and magnetite formation; and their significant impacts on the changes in drinking water quality especially on the reduction of disinfectant's residual, and the formation in disinfection byproducts. In addition, dissolved organic matter adsorption onto iron pipe corrosion scales (e.g., goethite and magnetite) is also discussed. Most of the relevant

information related to this thesis has been cited from the peer reviewed journals and books.

Chapter 3 entitled "Materials and methods" describes all of the methods, materials that are common for most of the experimental works presented in Chapters 4, 5, 6, 7 and 8. An overview of all chemicals preparation, analytical equipments, experimental setup, and statistics is included in this chapter.

Chapter 4 is entitled "Bench-scale evaluation of ferrous iron oxidation kinetics in drinking water: Effect of corrosion control and dissolved organic matter". This chapter investigates the impact of most common water quality parameters on the kinetics of Fe(II) ions oxidation process in $NaHCO_3$ buffered synthetic water. Ranking of each variable is evaluated following a full factorial design approach. A comprehensive investigation is conducted at a wide range of pH values, different dosages of DOM, phosphate based corrosion inhibitor and disinfectant (chlorine solution). This study is carried out under the conditions simulating as closely as possible to potable water distribution systems; and its principle aim is to enhance understanding of Fe(II) ions oxidation processes in iron pipe distribution systems. Eventually, the results of this study coupled with the results of other have led to develop a conceptual model explaining visually the role of different variables on the changes in rate constants of Fe(II) ions oxidation processes. This work is aimed to publish in the *Journal of Environmental Science and Health, Part A* (*Toxic/Hazardous Substances and Environmental Engineering*), Tailor & Francis Group.

Chapter 5 is entitled "Bench-scale evaluation of drinking water treatment parameters on iron particles and water quality". This chapter investigates the mechanisms causing high color and turbidity in iron water systems. This study is designed to characterize the iron

particles using different techniques, i.e., X-ray diffraction (XRD), scanning electron microscope (SEM), transmission electron microscope (TEM), dynamic light scattering (DLS). This study is carried out at different environmental parameters (e.g., pH, DOM, PO_4, and Chlorine) to investigate the most significant factor/s, and to rank their significant impacts on the formation in iron suspension color and turbidity. This work is intended to publish in the *Water Research Journal* (a journal of the International Water Association, IWA), Elsevier Inc.

Chapter 6 is entitled "Evaluation of Fe(II) ions on DBPs formation in drinking water distribution systems: Experimental assessment and model development". In this chapter, the effect of four potential explanatory factors including Fe(II) ions, pH, phosphate based corrosion inhibitor and stagnation time on DBPs (HAAs and THMs) formation are investigated in synthetic water samples following a 2^4 full factorial design with center point approach. A windows version software Minitab® 16 (MINITAB Inc., State College, Pennsylvania, USA) is used to analysis the data. The statistical significance is determined based on the Student *t*-test and the values of probability *p*. The model equation for the prediction of response factor is determined by Fisher's test. Based on the statistical analysis using research data, the mathematical models for HAAs and THMs formation are developed. The post filtered water samples are collected from three major water treatment plants in Halifax, NS to conduct DBPs formation using different pH values, in presences of different dosages of Fe(II) ions and phosphate for different reaction times. The DBPs formation data for the natural water samples have been used to validate the developed mathematical models for HAAs and THMs prediction. This work is targeted to be published in the *Journal of Water Supply*: *Research and Technology –AQUA* (IWA Publishing).

Chapter 7 is entitled "The role of model iron corrosion scales (goethite and magnetite) on the changes in chlorine residual and disinfection byproducts in drinking water

distribution systems". In this chapter, two main iron corrosion scales, i.e., goethite (α-FeOOH) and magnetite (Fe_3O_4) are synthesized in our water chemistry laboratory; and they are confirmed by BET surface area, XRD and SEM-EDX. The post filtered water samples (before adding any chemicals) are collected from JDK water treatment plant, Halifax. These water samples are used to conduct bench scale study for chlorine decay kinetics and DBPs formation/reduction study. This work is expected to publish in the *Journal of Hazardous Materials* (Elsevier Inc.).

Chapter 8 is entitled "Adsorption of dissolved organic matter (DOM) onto the synthetic iron pipe corrosion scales (goethite and magnetite): Effect of pH". In this work, two main iron corrosion scales, i.e., goethite and magnetite are used for DOM adsorption study in $NaHCO_3$ buffered synthetic water samples at a wide range of pH values. Zeta potentials and FTIR are used before and after conducting DOM adsorption study. The adsorption isotherms study is conducted for different pH values to find out the impact of pH on DOM adsorption onto the surfaces of iron oxides. HPSEC test is also conducted to compare the changes in molecular weight (MW) distribution of DOM in solutions in the presence of different dosages of goethite and magnetite. This work is aimed to publish in the *Chemical Engineering Journal* (Elsevier Inc.).

Chapter 9 summarizes the findings as conclusions that discussed in the previous chapters (Chapters 4 to 8) in this dissertation. Several recommendations and opportunities for future research projects that were beyond the scope of this thesis, but merit additional research have been discussed in this chapter.

CHAPTER 2. CURRENT STATE OF KNOWLEDGE

This chapter discusses the detailed mechanisms on the roles of different water quality parameters in iron corrosion and oxidation processes; and the impact of the iron corrosion by-products on chlorine decay, disinfection byproducts (DBPs) formation, and DOM adsorption in drinking water distribution systems. More specifically, Section 2.1 discusses the mechanisms of corrosion depending on different environmental variables, while Section 2.2 discusses the role corrosion by-products: soluble Fe(II) ions, and corrosion scales (goethite and magnetite) on the formation or reduction of DBPs in drinking water distribution systems. Section 2.3 of this chapter discusses the DOM adsorption mechanisms onto the main iron corrosion products, i.e., goethite and magnetite. All the discussions have been cited from the previous published journal papers and books.

2.1. Corrosion

Corrosion is defined as the destruction or deterioration of a material (usually a metal) due to the physiochemical reactions between a metal, and its surroundings that consequences on changes in the properties of the metals (Schock, 1999). The basic reason of corrosion is the instability of metal in its refined form. The process of corrosion is the affinity of a metal to return to its natural state. Nevertheless, metal corrosion is one of the most problematical and costly problems facing drinking water utilities. Drinking water corrosiveness differs depending on water quality characteristics and treatment train procedures. Raw and finished water parameters such as alkalinity, pH and hardness can affect the corrosiveness, as well as the means of corrosion control, if any. Due to the presence of disinfectant residual, finished water always tends to be somewhat corrosive (Eisnor and Gagnon, 2004). Corrosion of metal pipes in a distribution system can cause different types of problems. The corrosion products interior the water mains deliver a key

reactive component that affects water quality. Iron releases from corrosion products causes “red water” problem (Sarin et al., 2001; Eisnor and Gagnon, 2004). Red water or rusty water is commonly endorsed to ferric hydroxide. Ferric hydroxide forms from the reaction of insoluble (ferric) iron with water after the oxidation of soluble (ferrous) iron to the insoluble ferric iron in water through iron pipe distribution systems.

Corrosion can happen in many different forms, which are classified based on the appearances of the corroded metals. Although the classifications of corrosion are unique, the same basic electrochemical principles apply to all processes. The types of corrosions range from uniform to localized attacks (Schock, 1999).

Uniform corrosion is the most general form of corrosion, and it happens when the corrosive environments must have the similar access to all parts of the metal surfaces, and the metal itself must be metallurgically and compositionally uniform (Jones, 1992). In a distribution system, uniform corrosion happens inside a pipe when anodic and cathodic areas are very minor and near to one another. Uniform corrosion outcomes from the heterogeneous nature of the metal pipes (Schock, 1999). However, uniform corrosion is relatively easily measured and predicted. It is also known as general corrosion. This type of corrosion is not the most severe form of corrosions. Uniform corrosion is also considered and stated as a mass loss per unit area and unit of time, i.e., mm/year.

On the other hand, localized corrosion happens in the presence of persistent local nonuniformalities in the pipe or the water quality adjacent to it in distribution systems (AWWA, 1999). They are usually rust colored and soft on the outside, and are both harder and darker towards the inside (Schock, 1999). Areas of localized corrosion are often quite small at the surfaces, and are easily hidden by apparently inoffensive corrosion products. The consequence of localized corrosion can be a great deal more

severe than uniform corrosion. Because, failure occurs generally without warning and after a surprisingly short period of use or exposure. Therefore, it has been suggested that localized corrosion is much less predictable than uniform corrosion.

The factors affecting corrosion are dissimilar, and as such will vary from site to site. Therefore, corrosion studies tend to be fairy site specific and results are not easily carried over to other distribution systems. However, the following three steps have been reported that govern the corrosion rates (Schock, 1999):

(1) Transport of dissolved reactants to the metal surfaces,
(2) Electron transfer at the surface, and
(3) Transport of dissolved products from the reaction site.

2.1.1. Corrosion in water distribution systems

Corrosion is an alarm for many engineering applications, principally in drinking water distribution systems. Corrosion can cause cost-effective and environmental damages. For instance, the replacement of iron pipe due to corrosion in drinking water distribution systems causes a great economical cost. In addition to the basic repair costs associated with corrosion, failure could cause additional costs in water loss, property damage and safety problems (Schock, 1999). A survey of the 100 largest utilities members of the American Water Works Association Research Foundation (AWWARF) found in 1997 that the most common distribution system problem was corrosion of cast-iron pipe (McNeil and Edwards, 2001). The majority of distribution systems pipes are composed of iron material: cast iron (38%), ductile iron (22%), and steel (5%) (AWWA, 1996). Now metal pipe is gradually replacing to improve the water quality. The American Water Works Association (AWWA) estimates that it will cost US water utilities $325 billion over the next 20 years to upgrade water distribution systems (AWWA, 1999).

Table 2.1. Water main material and percentage of Halifax Regional Municipality, HRM

Pipe material	Total pipe length (m)	%
Asbestos cement	1176.41	0.2
Brass	73.42	0.0
Cast iron	253143.91	33.7
Copper	945.56	0.1
Ductile iron	368265.15	49.0
Ductile iron hyprotec	5382.02	0.7
HDPE	1169.61	0.2
Hyprescon	38268.76	5.1
Hyprescon C-301	7366.37	1.0
Hyprescon C-303	4350.33	0.6
PVC	39866.51	5.3
Stainless steel	713.10	0.1
Unknown	30759.67	4.1

Like as America, the majority of the distribution systems in Canada are still comprised of old-cast iron pipes. The water distribution system in Halifax consists of a mixture of cast iron, ductile iron, PVC (plyvinyl chloride) and other pipe materials (Table 2.1). The majority of iron pipes in distribution systems are corroded as well they have been installed before 1960. These cast iron pipes are replacing with new ductile iron pipes as a part of the distribution replacement program in Halifax (Halifax Water, 2012). The majority of the distribution main replacement projects are undertaken in partnership with Halifax Regional Municipality (HRM) road or sewer renewal projects in order to reduce public disruption and to improve cost benefit. Currently, approximately 4.5

kilometers of cast iron pipes are replaced annually. The ductile iron mains used in Halifax are cement mortar lined with an asphaltic coating (Halifax Water, 2012).

2.1.2. Iron oxidation and corrosion chemistry

Metals are commonly unsteady in this planet. Because, they are trying to lower their energy by naturally reacting to form solutions or compound that have better thermodynamic stability (Bradford, 1993). Corrosion is happende by the transfer of electronic charge in aqueous media between anodic and cathodic sites in iron. Since metal is not homogeneous, sites along the metal surfaces act as anodes or cathodes with different electrical potential (Volk et al., 2000). The aqueous environment (water) acts an electrolyte solution to conduct reaction between the anodes and the cathodes. For iron, corrosion converts elemental iron ($Fe°$) to ferrous iron (Fe^{2+}), releasing 2 electrons, which can be expressed in a simple way:

$$Fe^{o} \leftrightarrow Fe^{2+}_{(aq)} + 2e^{-} \tag{2.1}$$

According any oxidation-reduction reaction, an electron acceptor must be present in solution to balance the reactions. In the case of corrosion of iron, the predominant electron acceptors are oxygen and chlorine in the distribution systems (Sung and Morgan, 1980; Scherer et al., 1999; Frateur et al., 1999; Lytle et al., 2004). In distribution systems, the cathodic reaction is typically reduction of oxygen (Eq. (2.2)), or aqueous chlorine in chlorinated systems (Eq. (2.3)):

$$\frac{1}{2}O_{2\,(aq)} + 2H^{+} + 2e^{-} \leftrightarrow H_2O \tag{2.2}$$

$$HOCl + H^{+} + 2e^{-} \leftrightarrow Cl^{-} + H_2O \tag{2.3}$$

Once the Fe^{2+} ions are released from iron pipe surface, it is available to react further with the chemicals present in water. A number of competing oxidation and precipitation reactions are occurred with Fe^{2+} ions. Moreover, the overall redox equations for the conversion of Fe^{2+} to Fe^{3+} in presence of oxygen and chlorine are given below (Eqs. (2.4) and (2.5)). It should be noted that the ferrous iron is highly reactive with chlorine compared to oxygen.

$$4Fe^{2+}_{(aq)} + O_{2\,(aq)} + 10H_2O \leftrightarrow 4Fe(OH)_{3\,(s)} + 8H^+ \qquad (2.4)$$

$$2Fe^{2+}_{(aq)} + HOCl + 5H_2O \leftrightarrow 2Fe(OH)_{3\,(s)} + Cl^{-+} + 5H^+ \qquad (2.5)$$

Several commonly inorganic anions, including phosphate (Lytle and Snoeyink, 2002; Aitken-Rogers, 2004; Gonz´alez et al., 2010), sulfate (Truong et al., 2004) and carbonate/bicarbonate (King et al., 1995) play a role in moderating Fe^{2+} ions oxidation processes. On the other hand, natural dissolved organic matter (DOM), which possesses the structural features of humic substances, can lead to accelerate, abate, or have no conclusion on the oxidation of ferrous iron (Stumm and Lee, 1961; Theis and Singer, 1974; Liang et al., 1993). The level of the effects has been revealed to be dependent on a number of factors including iron, oxygen and chlorine concentration (Rose and Waite, 2002), and pH values (Stumm, 1990; Millero et al., 1995; Morgan and Lahav, 2007; Gonz´alez et al., 2010).

However, the released iron as ferrous iron (Fe^{2+} ions) in the bulk water systems may eventually oxidize to ferric iron (Fe^{3+} ions), which form particles because of its low solubility. Subsequently, ferric iron contributes to color and turbidity in water (Sarin et al., 2004b). The composition and structure of iron scales in pipes of distribution system varies on the basis of several factors including water quality parameters, fluctuations of water temperature in different seasons, and water flow parameters (McNeill and

Edwards, 2001). However, scales from different systems can have similarities in compositions, compounds often found in iron corrosion scales. A list of typical composition in iron corrosion scales is shown in Table 2.2.

Table 2.2. Corrosion scales present in cast iron pipes (adapted from McNeill and Edwards, 2001).

Name of iron oxide	Chemical formula	Iron oxide state
Ferrous hydroxide	$Fe(OH)_2$	II
Ferric hydroxide	$Fe(OH)_3$	III
Wustite	FeO	II
Goethite	α- FeOOH	III
Akaganeite	β–FeOOH	III
Lepidocrocite	γ- FeOOH	III
Hematite	α– Fe_2O_3	III
Maghemite	γ– Fe_2O_3	III
Magnetite	$Fe_3O_4(FeO.Fe_2O_3)$	II and III
Ferric oxy-hydroxide	$FeOx(OH)_{3-2x}$	III
Siderite	$FeCO_3$	II
Iron hydroxyl-carbonate	$Fe_x(OH)_y(CO3)_z$	III
Green rust	$Fe(III)_{x1}Fe(II)_{x2}(OH)_3(CO_3.SO_4)_2$	II and III
Vivianite	$Fe_3(PO_4)_2.8H_2O$	II
Strengite	$FePO_4$	III
Schreibersite	Fe_3P	Not known

Corrosion products are a mixture of ferrous and ferric iron minerals, and other minor constituents including natural dissolved organic matter (DOM) and trace metals. It has been hypothesis that ferric iron generated from the oxidation of ferrous iron, are trapped with DOM and deposited on the surface of iron pipe in distribution systems. However, iron pipe corrosion scales in water distribution systems are found to be composed of ferrous (9.3% ~ 15.6%) and ferric (83.1% ~ 90.7%) oxides along with other oxy-hydroxides (Sarin et al., 2001). Magnetite represents both ferrous and ferric component of the pipe deposits, while goethite represents the ferric component of the pipe deposits (Schwertman and Cornell, 2000). A study has been conducted in Boston pipe deposits and it has been reported that iron pipe deposit contains 25% magnetite and 75% goethite (Sarin et al., 2001).

2.1.3. Factors affecting iron corrosion and oxidation

It is an essential element for water utilities to recognize how water quality parameters that may affect the corrosion processes in iron piping. There are a number of vital studies that explore the mechanisms of iron corrosion under stagnate conditions (Schwertman and Cornell, 2000). The most common factors including pH, alkalinity (carbonate), pipe age, time, oxygen concentrations, corrosion inhibitors and disinfectant residual may participate in iron corrosion processes. A brief description on the impacts of major water quality parameters in iron corrosion and oxidation processes has been discussed below:

2.1.3.1. Effect of pH

The pH value is a vital water quality parameter to occur corrosion by iron oxidation process in distribution system (Droste, 1997; Schock, 1999). Metal corrodes rapidly at a lower pH value ($pH < 5$), while higher pH values ($pH > 9$) may protect pipes and decrease corrosion rates (Eisnor, 2002; Lasheen et al., 2008; Tam and Elefsiniotis, 2009). However, one study found that both weight loss and iron concentration was

decreased as pH was raised from 8.5 to 9.2 (Kashinkunti et al., 1999). Wight loss is generally incorporated with the degree of tuberculation.

Fe^{2+} ions that come in drinking water through the corrosion processes, were reported to be more reductant at a higher pH value. On the other hand, the iron oxidation reactions in solution were appeared as a complex function of the solution pH with an apparent hydroxide ion dependency. Several authors (Stumm, 1990; King et al., 1995; Millero et al, 1995) have assumed this complex pH dependence to occur due to the parallel oxidation of Fe^{2+} ions and its hydroxo complexes i.e. ($Fe(OH)^{+}$, $Fe(OH)_2$ and $Fe(OH)_3^{-}$). The 'hydrolysed' ferrous iron species are more readily oxidized than non-hydrolyzed ferrous species in the following order $Fe(OH)^{0}_{2(aq)}$ >> $Fe(OH)^{+}$ >> Fe^{2+} (Morgan and Lahav, 2007), and the hydroxyl (OH^{-}) ligands donate electron density to the Fe^{2+} atoms through both the σ and π systems (Stumm, 1990); and that might be a reason to make Fe^{2+} ions more reductant at a higher pH value.

2.1.3.2. Effect of alkalinity

Alkalinity is a directory of the buffering capability of water. Thus pH fluctuations in solution are more at lower alkalinity. At lower pH, corrosion rate has been observed to increase (Droste, 1997). In most Canadian surface waters, alkalinity is thoroughly linked to hardness as their alkalinity is due to the presence of carbonates and biocarbonates (Health Canada, 1995). Many important reactions in corrosion chemistry, i.e., ability of water to form protective metallic carbonate scale or passivating film have been affected by the carbonate and bicarbonate species. On the other hand, alkalinity is stated in equivalent of calcium carbonate ($CaCO_3$) like as hardness. At a higher alkalinity, carbonate reacts with iron to procedure ferric carbonate ($FeCO_3$). Therefore, a reduction of alkalinity in solutions may elevate the dissolution of a carbonate-containing iron such as $FeCO_3$, which leads to rise in iron release.

2.1.3.3. Effect of dissolved oxygen (DO)

Dissolved oxygen (DO) is an important electron acceptor in the oxidation of ferrous iron (Fe^{2+}) or iron corrosion scales. DO reacts with ferrous iron, and oxidizes it to the more stable ferric forms. Ferric hydroxides later dehydrate or further oxidize to form oxide scales like goethite and lepidocrocite (AWWARF, 2002). The ferric iron gathers at the point of corrosion causing tubercles or settles out at dead-ends and interfering with flow (Schock, 1999). However, the effects of DO on iron release and iron oxidation depends on the characteristics of the iron scales present. For instance, DO may easily react with metal iron present in the porous iron scales,, and may cause the release of Fe^{2+} ions in solution. On the other hand, when the scales are more solid, oxygen is devoured by both in the corrosion reactions of the iron metal, and in the oxidation of the ferrous iron (Fe^{2+}) into ferric iron (Fe^{3+}) that may be participated, making the scales denser and less permeable to Fe^{2+} diffusion (Sarin et al., 2004b; Alshehri, 2008).

On the other hand, Shipley et al. (1925) have reported that in absence of dissolved oxygen, previously deposited ferric scales (e.g., lepidocrocite and γ-FeOOH) can act as electron acceptors to facilitate the iron corrosion process that is known as "Kuch Mechanism" (Kuch, 1984). This Kuch reaction produces ferrous iron (Fe^{2+}) following the equation (2.6), and allows the corrosion reaction to continue even after DO is depleted (McNeil and Edward, 2001).

$$Fe_{(metal)} + 2FeOOH_{(scale)} + 2H^{+} \leftrightarrow 3Fe^{2+} + 4OH^{-} \qquad (2.6)$$

2.1.3.4. Effect of chlorine

Free chlorine is the most widely applied disinfectant for treating drinking water in North America (AWWA, 2000). The WHO drinking water standards state that 2 to 3 mg/L

chlorine should be added to water in order to gain a satisfactory disinfection and residual concentration for protecting water from microbial contamination in water distribution systems (WHO, 2008). On the other hand, many disinfectants including chlorine are used as oxidant to control color, taste, and odor, biological growth inside various treatment units, and other organic and inorganic compounds. The process is commonly referred to as preoxidation or prechlorination when chlorine is used (Xie, 2003). Conversely, several studies have shown that disinfectant residuals (e.g., free chlorine and chloramine) also degrade water quality and pipe materials in distribution systems due to causing pipe corrosion (McNeill and Edwards, 2000; Eisnor and Gagnon, 2004). A previous study (Eisnor and Gagnon, 2004) in our research group conducted cast-iron pipe loop experiments for the reaction periods of 6 and 12 h using three different types of disinfectants, and observed that free chlorine and chloramine would increase iron release from background water quality levels. Consequently, a previous study in which deionized water (water extremely low alkalinity and hardness) having pH 7 in contact with iron pipe showed that a 4 mg/L free chlorine residual was much more corrosive than an equivalent amount of monochloramine residual as a disinfectant (LeChevallier et al., 1990). However, several researchers have reported that free chlorines participate predominantly in Fe(II) ions oxidation processes in iron pipe drinking water distribution systems, and also participate in iron corrosion processes (Maddison et al., 2001; Cantor et al., 2003; Gagnon et al., 2008). Three forms of chlorine including molecular chlorine (Cl_2), un-ionized hypochlorous acid (HOCl), and the hypochlorite ions (OCl^-) are involved in these reactions, and they are defined as free available chlorine. Their relative proportions depend on solution pH, temperature and dissolved solids. However, the corrosivity of water in contact with iron has been reported to increase in presence of free chlorine (Cantor et al., 2003).

2.1.3.5. Effect of PO_4

Last one century, different types of phosphate based corrosion inhibitors are widely used as chemical additives for mitigating iron corrosion in drinking water distribution systems.

In the US, around 67% of water utilities use polyphosphate or a blend of polyphosphate and orthophosphate and rest of the utilities (33%) add orthophosphate as a corrosion inhibitor to the finished water (Edwards and McNeill, 2002). The general formula of polyphosphates is defined as $M_{n+2}P_nO_{3n+1}^{-(n+2)}$, in which M is a monovalent ion, and the ratio of M_2O to P_2O_5 is defined as the average chain length (Lytle and Snoeyink, 2002). Plyphospghates react with water or hydrolyze, with time, breaking down into a mixture of shorter chain polyphosphate and orthophosphate, and ultimately to only orthophosphate. This process is related to pH, temperature and the presence of cations (Lytle and Snoeyink, 2002). In addition of corrosion inhibitor (phosphate), corrosion may be controlled by maintaining proper pH, alkalinity and hardness.

Nevertheless, several researchers have stated the benefits of using phosphate to control corrosion, and to decrease or to prevent iron, manganese, and calcium precipitation in distribution systems (Larson, 1957; McNeill and Edwards, 2000; Maddison et al., 2001). The effect of phosphate dosages on the Fe(II) ions oxidation have been reported in the literature often with higher PO_4 concentration ranging from 6.5 to 1665 mg-PO_4/L (0.07 to 17.5 mM PO_4) (Mitra and Matthews, 1985; Aitken-Rogers, 2004; Gonz´alez, et al., 2010). In general, it has been reported that higher dosages of phosphate increase Fe(II) ions oxidation rate (Mitra and Matthews, 1985; Aitken-Rogers, 2004; Gonz´alez, et al., 2010). However, using a lower phosphate dosage, which is more typical in drinking water distribution systems, only a key studies were reported to decrease or to retard the Fe(II) ions oxidation processes (Wolthoorn et al., 2004; Lytle, 2005). Lytle (2005) has conducted Fe(II) ions oxidation batch tests in $NaHCO_3$ buffered synthetic water systems, and has reported that the addition of orthophosphate (3 mg-PO_4/L) in iron water systems significantly decreased the rate of Fe(II) ions oxidation. On the other hand, the heterogeneous oxidation of Fe(II) ions in the synthetic ground water samples has been reported to be retarded when phosphate is present along with other ions (Wolthoorn et al., 2004). The effect of PO_4 on Fe(II) ions

oxidation process seems to be contradictory depending on pH, temperature and the presence of disinfection residual and cations.

2.1.3.6. Effect of DOM

Dissolved organic matter (DOM), which possesses the structural features of humic substances can lead to accelerate, abate, or have no conclusion on the oxidation of ferrous iron (Stumm and Lee, 1961; Theis and Singer, 1974; Liang et al., 1993). Theis and Singer (1974) have conducted polarographic analyses on the complexation of Fe(II) ions with organic acids, and have demonstrated that organic matter irrevocably bound to Fe(II) ions. Therefore, the reaction mechanisms limit Fe(II) ions oxidation processes, and its release into solutions. On the other hand, Morgan and Stumm (1964) have suggested that the inhibition of ferrous iron oxidation by organic species has involved the catalytic oxidation of Fe(II) ions followed by the reduction of Fe(III) ions by organic substances. Thereby, affecting the Fe(II) ions reactivity might be given in Eqs. (2.7) and (2.8) (Morgan and Stumm, 1964; Theis and Singer, 1974), if one considers the following interrelated reactions:

$$\mathrm{Fe(II)} + \mathrm{Org.} \rightleftarrows \mathrm{Fe(II)} - \mathrm{Org.} \xrightarrow{+\,O_2} \mathrm{Fe(III)} \qquad (2.7)$$

$$\mathrm{Fe(III)} + \mathrm{Organic} \rightarrow \mathrm{Fe(II)} + \mathrm{Oxidized\ Organic} \qquad (2.8)$$

The magnitude of the roles of dissolved organic matter has been shown to be dependent on several factors including iron and oxygen concentration (Rose and Waite, 2002), and pH (Stumm, 1990; Millero et al., 1995; Morgan and Lahav, 2007; Gonz´alez et al., 2010).

2.1.4. Iron suspension color and turbidity

When iron corrosion scales are released from the pipe wall due to sudden change of flow velocity of water, red water is appeared. In most cases, ferric hydroxide floc is found in red water rather than crystalline matters. In addition, high concentration of ferrous iron is also observed, especially when free residual chlorine is absent (AWWARF, 1996). However, discoloration of water resulting from suspended iron particles is one of the main customer complaints received by water suppliers. Iron can originate from the source water and from distribution system materials. The concentration of Fe(II) ions depend on the iron pipe age and corrosion condition. The concentration of Fe(II) ions in water distribution systems were reported up to 3 mg/L (0.054 mM) (Kirmeyer et al., 2000), and under anoxic conditions, aqueous Fe(II) ions concentrations of up to 1.11 mg-Fe(II)/L (0.02 mM) were observed in a pipe loop reactor that was constructed using a 70 years old galvanized iron pipe (Sarin et al., 2004a). The levels of Fe(II) ions has been reported to be site specific to the water quality. USEPA recommends the secondary drinking water guideline for dissolved iron as 0.3 mg/L, and when iron presents larger than 0.3 mg/L in drinking water, can reason of unpleasant metallic taste and rusty color (Cham et al., 2010). Several trace impurities (e.g., metals, organic compounds, and microorganisms) adsorb onto iron particles surfaces and may cause adverse health effects (Lytle and Snoeyink, 2002).

Deposited iron formed by oxidized Fe(II) ions in the distribution systems, leads to high turbidity (Sharma et al., 2001). The release of soluble or particulate iron corrosion by-products to the water declines its aesthetic quality (such as taste, color, staining, turbidity), and often leads to common problem of ‘red water’ at tap (Sharma et al., 2001; Lytle and Snoeyink, 2002; Cham et al., 2010). The formation of red water depends on different factors and a sequence of steps including oxidation, hydrolysis, polymerization, and precipitation (Lytle et al., 2004). Red water or rusty water is commonly recognized to ferric hydroxide. Upon contact to mainly oxygen or disinfectant during water treatment and distribution systems, soluble Fe(II) ions are oxidized to

insoluble Fe(III) ions form following the equations 2.4 and 2.5 (McNeill and Edwards, 2000; Lytle et al., 2004), which readily precipitate and accountable for colore in water. Effect of chlorine has been usually stated to accelerate Fe(II) ions oxidation rates. Conversely, water industries use chlorine as oxidant to control color, taste, and odor, biological growth inside several treatment units and in drinking water distribution systems. The procedure is usually mentioned to as preoxidation or prechlorination when chlorine is used (Xie, 2003). Subsequently, the role of chlorine on iron suspension color and turbidity has been reported to decrease in literature (Lytle et. al., 2004). Lytle et al. (2004) have conducted 5 mg-Fe/L iron suspension formation study in presence of 5 mg Cl_2/L for different pH values (7 to 10), and they have found that iron suspension color and turbidity are lower in presence of chlorine compared with the control systems for all studied pH values.

In the US, around 67% of water utilities use polyphosphate or a blend of polyphosphate and orthophosphate and rest of the utilities (33%) add orthophosphate as a corrosion inhibitor to the finished water (Edwards and McNeill, 2002). Phosphate (polyphosphate and, or orthophosphate) is mostly used to decrease the influence of both source water iron and iron released from the distribution systems materials (Vik et al., 1996; Lytle and Snoeyink, 2002). Vik et al. (1996) reported that orthophosphate decreased corrosion rate of steel, as well as iron release rate. They found that small amount of orthophosphate greatly decreased the iron release rates, and the increase in orthophosphate dosages from 0.5 to 1.0 mg/l PO_4 decreased iron released by two thirds. Phosphate has noteworthy effect to reduce both turbidity and color of iron suspension especially higher dosages of phosphate (Deng, 1996; Lytle and Snoeyink, 2002), which showed color and structural differences in iron colloids when formed in the presence of orthophosphate and polyphosphate.

Conversely, natural dissolved organic matter (DOM), which possess the structural features of humic substances can lead to accelerate, abate, or have no conclusion on the oxidation of Fe(II) ions (Stumm and Lee, 1961; Serikov et al., 2009) and iron suspension formation. However, the effect of DOM on iron suspension formation has been shown to be dependent on a number of factors including iron and oxygen concentrations (Rose and Waite, 2002), and pH (Morgan and Lahav, 2007). These factors have significant influence on the aggregation behavior of DOM with the iron colloids that might be one of the reasons to degrade water quality (Stumm and Lee, 1961; Serikov et al., 2009).

2.2. Disinfection byproducts

Disinfection byproducts are formed when certain disinfectants react with natural dissolved organic matter (DOM) (Wallace et al., 2002), and/or with organic contaminants present in water (Chang and Young, 2000). So far, chlorination byproducts are the most common types of byproducts known to scientists. Byproducts of the chlorination process, specifically four trihalomethanes in drinking water were first identified as disinfection byproduct in treated water in the Netherland and USA in 1974 (Bellar et al., 1974; Rook, 1974). Since that time, hundreds of additional chlorinated organic disinfection byproducts (DBPs) have been identified. Haloacetic acids (HAAs) were later identified as second class of disinfection byproducts (DBPs). Some other frequently identified halogenated DBPs found at low concentrations including haloacetonitriles, haloketons, chlopicrin, cynaogen chloride and chloral hydrate. Besides these identified DBPs, 51% of the total chloride that are produced when natural DOM is exposed to chlorine are unidentified (Zhang et al., 2000).

Trihalomethanes (THMs) are the most common groups of DBPs formed in water. These volatile compounds make up an estimated 20 percent (%) of total DBPs, and it has

been used as surrogates of total exposure to DBPs. There are four common THM species: trichloromethane (chloroform), bromodichloromethane, dibromochloromethane and tribromomethane (bromoform). Chloroform is the most commonly occurring THM and constitutes approximately 90% of the total THM concentration (Sadiq et al., 2002). The chemical names, common acronyms and properties of THM species are listed in Table 2.3. These four THM species are obtained by replacing three hydrogen atoms of methane with halogen atoms, including chlorine and bromine (Xie, 2005), which is shown in Figure 2.1. Xie (2005) has stated that chloroform and other THM species are not only formed for the reaction between chlorine and methane, rather it should be said that THM species are formed due a complex reaction between halogen (chlorine and/or bromide) and natural DOM (humic and or fulvic subatances) as shown in Equation 2.9.

Trichloromethane Bromodichloromethane Chlorodibromomethane Tribromomethane

Figure 2.1 Molecular structure of four trihalomethane (THMs) species

$$\text{Natural DOM} + \text{Chlorine} + \text{Bromide} \longrightarrow \text{THMs} \qquad (2.9)$$

Haloacetic acids (HAAs) are the second major class of chlorinated DBPs. There are nine species of haloacetic acids. However, of the nine, five HAAs including: monochloroacetic acid, dichloroacetic acid, trichloroacetic acid, monobromoacetic acid, and dibromoacetic acid are currently regulated. The chemical names, common acronyms and properties of nine haloacetic acids are listed in Table 2.3. Partially or completely, a total of nine HAAs are obtained by the replacing hydrogen atoms of acetic acid with halogen atoms (Figures 2.2 to 2.4). There are three groups of HAAs and their formation, and biological and chemical properties are significantly different (Xie, 2005).

Monohaloacetic acid (CH_2X-COOH) is formed by replacing one hydrogen atom by one halogen atom (Figure 2.2), while dihaloacetic acids (CHX_2-COOH) and trihaloacetic acids (CX_3-COOH) are formed by replacing two and three hydrogen atoms with halogen atoms respectively (Figures 2.3 and 2.4). Again, the formation of HAAs in chlorinated water is not due to the reaction between acetic acid and chlorine. HAAs are formed by the reaction between natural organic matter and chlorine (Xie, 2005), as shown in Equation 2.10.

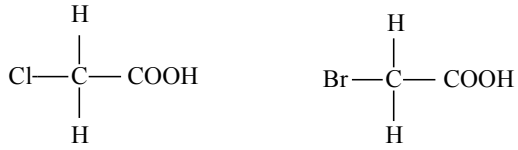

Monochloacetic acid Monobromoacetic acid

Figure 2.2 Molecular structure of two monohaloacetic acids

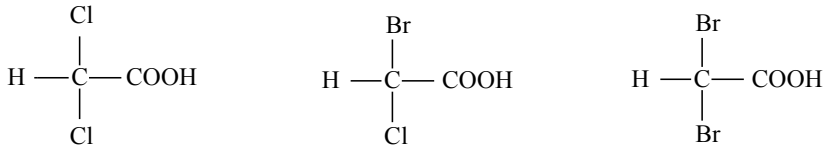

Dichloacetic acid Bromochloroacetic acid Dibromoacetic acid

Figure 2.3 Molecular structure of three dihaloacetic acids

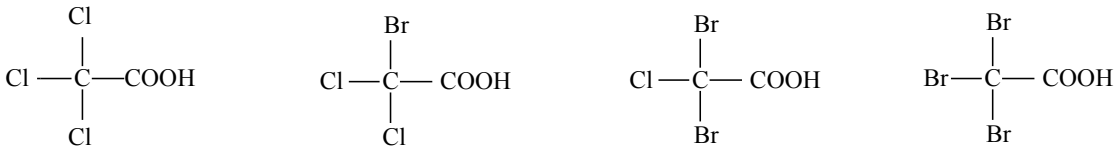

Trichloacetic acid Bromdiochloroacetic acid Chlorodibromoacetic acid Tribromoacetic acid

Figure 2.4 Molecular structure of four trihaloacetic acids

$$\text{Natural DOM} + \text{Chlorine} + \text{Bromide} \longrightarrow \text{HAAs} \qquad (2.10)$$

Table 2.3. Properties of THMs and HAAs (Adapted from Shorney, 1998)

	DBPs Species	Acronym	Molecular Weight (g/mol)	Boiling Point (°C)
THMs Species				
1	Trichloromethane (Chloroform)	TCM	119.5	61
2	Dichlorobromomethane	DCBM	163.9	87
3	Chlodibromoromethane	CDBM	208.3	116
4	Tribromomethane (Bromoform)	TBM	252.7	151
HAAs Species				
1	Monochloroacetic acid	MCAA	94.5	184
2	Monobromoacetic acid	MBAA	137.9	208
3	Dichloroacetic acid	DCAA	129.0	193
4	Trichloroacetic acid	TCAA	163.5	197
5	Bromochloroacetic acid	BCAA	173.4	215
6	Dibromoacetic acid	DBAA	217.8	233
7	Bromodichloroacetic acid	BDCAA	207.9	--
8	Chlorodibromoacetic acid	CDBAA	252.3	--
9	Tribromoacetic acid	TBAA	296.7	245

While HAAs and THMs have in common that they are formed in drinking water by water chlorination, however they are very different in their chemical structures and their properties (Table 2.3). HAAs formation has been found to form more quickly than THMs (Liang and Singer, 2003), while HAAs have found to be less stable than THMs (Baribeau et al., 2005). The concentration of HAAs to THMs in drinking water distribution systems was found to be dependent on different factors including the type of natural DOM present in water samples and treatment procedures. For instance in Canada,

the highest concentration trihalomethanes (THMs) were observed in Manitoba followed by Nova Scotia and Saskatchewan, while haloacetic acids were highest in Nova Scotia followed by Newfoundland and Labrador (Chowdhury et al., 2011). On the other hand, HAAs formation has been found to increase in the distribution systems or increase to some maximum value in the distribution systems and then decrease (Chen and Weisel, 1998; Speight and Singer, 2005). This decrease in HAAs concentration has been attributed to biodegradation and chemical decomposition.

After the discovery of DBPs (HAAs and THMs) in drinking water, the USEPA began assessing the extent of human exposure to DBPs, and the possible health effects associated with DBPs in drinking water. In Canada only, approximately 700 cancer cases may be caused by exposure to THMs in drinking water. Medical expenses associated with these cancer incidents are estimated at some $140 million/year (Chowdhury et al., 2011). Disinfection byproducts (DBPs) exposure occurs in our body through multiple routes. Primary exposure to chloroform resulting from ingestion of chlorinated drinking water poses significant health risk to humans. Inhalation and dermal contact are the two other exposure pathways besides ingestion (Dyck et al., 2011). Exposure pathways like inhalation and dermal absorption can cause more exposure to volatile organic compounds than pathways like ingestion. Humans are subjected to all these three kind of exposures through activities such as showering, bathing, cooking, toilet use, washing dishes, washing clothes and drinking (Legay et al., 2011). On the other hand, the impact of individual THM and HAA species are varies from each other. For instance, dichloroacetic acid (DCAA) is believed to be more carcinogenic than any of the trihalomethanes (Bull and Kopfler, 1991). Rodriguez et al. (2004) reported that DCAA and TCAA were generally present at the highest percentages out of HAA_5 studied. However, due to the toxicity and carcinogenicity of different THM and HAA species in various animal studies, USEPA has designated TCM, BDCM, TBM, DCAA as Class B2 carcinogen compounds (probable human carcinogens), while CDBM and TCAA are designated as Class C carcinogen compound (USEPA, 2006).

Since the identification of disinfection byproducts (THMs and HAAs) in halogenated water, various epidemiological investigations have been conducted to evaluate the possible health risks causes from chlorinated and chloraminated waters. Some reports suggest that these compounds may have a more profound impact on human health. By evaluating 12 epidemiological examinations, Morris et al. (1992) suggested that 9% of bladder cancer cases and 15% of the rectal cancer cases that is 10,000 additional cancer cases per year could be attributed to chlorinated water and its byproducts.

Considering the impact of DBPs produce in drinking, and their health risks, DBPs are regulated in drinking water distribution systems by the USEPA. THMs are currently regulated under the Stage 2 D/DBPs Rule produced by the Environmental Protection Agency. Based on widespread DBPs occurrences, potential health risks (disease and chemical toxicity) and cost-effective treatment technologies, the maximum contaminant level (MCL) for THMs set by the EPA is 0.08 mg/L (USEPA, 2006). Consequently, HAA_5 are currently regulated under the Stage 2 D/DBP Rule produced by the EPA, and have a MCL currently set at 0.06 mg/L (USEPA, 2006).

2.2.1. Factors affecting DBPs formation

2.2.1.1. Effect of iron

The internal surfaces of an unlined cast iron water distribution pipe are typically exposed to an oxidizing environment that causes corrosion. Hozalski et al. (2008) have reported that the reduction of pipe wall as a zero-valent iron (Fe°), and correspondingly when Fe° ions come in contact with water, Fe^{2+} ions start to appear in water through iron corrosion (Eq. (6.1)). Therefore, Fe^{2+} ions are being added continuously in drinking water distribution systems from the corrosion products (Sarin et al., 2004a). Several laboratory

studies have reported that Fe° is a robust reductant that reduces different types of halogenated solvents including chlorinated byproducts: carbon tetrachloride (Matheson and Tratnyek, 1994), trichloro(nitro)-methane (chloropicrin) (Pearson et al., 2005), haloacetic acids (Zhang et al., 2004; Hozalski et al., 2008), 1,1,1-trichloroethane (Fennelly and Roberts, 1998), and pentachlorophenol (Kim and Carraway, 2000). Several brominated compounds, for instance, 1,2-dibromoethane (Rajagopal and Burris, 1999), 1,2-dibromo-3-chloropropane were reported to reduce by zero-valent iron (Siantar et al., 1996). In addition to the study on impact of zero valent iron (Fe°) on reduction of halogenated compounds, Chun et al. (2005) investigated a study using synthetic iron corrosion scales, i.e., magnetite and goethite, which contain both Fe^{2+} and Fe^{3+} ions. Subsequently, the authors found that selected synthetic disinfection byproducts (e.g., trichlonitromethane, trichloacetonitrile, 1,1,1-trichloropropanone and trichloroacetaldehyde hydrate) significantly reduced in presence of magnetite and goethite in solution. The degradation rate for trichloronitromethane (TCNM), a non-regulated DBPs has been reported to be dependent on water-soluble iron in water systems (Lee et al., 2008). Conversely Hassan et al. (2006) reported that THMs and HAAs formation was increased in presence of synthetic goethite, while a reverse trend was observed to decrease THMs and HAAs formation in presence of synthetic magnetite in two different sources of natural water samples.

2.2.1.2. Effect of chlorine

The first use of chlorine as a disinfectant in drinking water was in the 1880's in England, believed to be in the form of hypochlorite or chloride of lime (White, 1992). First application of chlorine in North America was in 1896 in Louisville Kentucky, and then continuous use was introduced in Boonton, New Jersey in 1908 (White, 1992). Its popularity arises worldwide for its high oxidation potential, relative low cost, excellent disinfection effectiveness. To keep the water safe free from microbial contamination, a certain level of residual chlorine must be present in water (WHO, 2008). One weakness of using free chlorine is related to its high and nonselective reactivity leading to the

formation of unwanted byproducts. When waters are chlorinated, free chlorine will react rapidly, (i.e. within a few minutes) with dissolved organic matter (DOM) naturally present in water to form organic byproducts following the reaction (Eq. (2.11)). The formation of DBPs was reported to increase with the increase in chlorine dosages. In general, the impact of chlorine concentration is greater during primary disinfection than during secondary disinfection as well chlorine reacts rapidly with DBPs precursors (Rahman and Gagnon, 2013). However, during primary disinfection, a smaller amount of chlorine is added than the long term demand. Therefore, the concentration of chlorine is often insufficient to react with all DBPs precursors in water samples. On the other hand, DBPs formation is often limited during secondary disinfection even though excess disinfectant is added, because during water treatment process, excess DBPs precursors are removed from water (Reckhow et al., 1990). Nevertheless, Johnson and Jenson (1986) have stated that chlorine related DBPs are formed more specially either by oxidation of dissolved organic matter (by accepting electrons from organic substrate) or by substitution into the organic matrix.

$$\text{Free Chlorine } (HOCl + OCl^{-} + Cl_2) + \text{DOM}_{\text{(precursor)}} \rightarrow \text{DBPs} \qquad (2.11)$$

On the other hand, several researches have been demonstrated that there is an increased demand for chlorine by the most common pipe materials “cast iron” in distribution systems. It happens due to reaction of chlorine with cast iron, resulting in a high chlorine decay rate in pipe. The rate of chlorine decay is related to a variety of factors including: source water quality, velocity, pH, temperature, residence time (Rossman et al., 2001; DiGiano and Zhang, 2005). As a result of the high demand of chlorine from the cast iron pipes (Rossman et al., 2001), and from iron corrosion by-products (Rahman and Gagnon, 2014), a lesser portion of chlorine will be presented in drinking water systems. Therefore, it has been suggested that lesser amount of chlorine will be available to react with DBPs precursor to form DBPs.

2.2.1.3. Effect of pH

Typical pH values in drinking water treatment and distribution systems have been reported to be 6.5 to 9.0 (Chun et al., 2005). Small changes in pH can have impact on the speciation between hypochlorous acid and hypochlorite ions. Hypochlorite ions are the dominant species of free chlorine at pH above 7.5, and are less reactive with DOM than hypochlorous acid. The pH can also affect functional groups associated with organic precursors by changing the degree of protonation and structure of the organic precursor (Liang and Singer, 2003). Therefore, formation of DBPs is expected to be influenced by pH. Generally, an increase in pH values led to increase in THMs formation, and a decrease in HAAs formation (Summer et al., 1996). Summer et al. (1996) found that THMs formation was approximately 50% higher when the pH of influent water was 9.0 as compared to a pH value of 7.0. Many researchers (Rook, 1974; Morris and Baum, 1977; Miller and Uden, 1983) have suggested that the increases in THMs (mainly chloroform) formation at high pH are associated with the base-catalyzed halo form type reactions. The decrease of trichloroacetic acid (TCAA), one of main HAAs species with the increases in pH values is related to the corresponding increase in THMs formation if TCAA and THMs share common precursors (Boyce and Horning, 1983; Reckhow et al., 1990). At pH 5 and 7, TCAA formation was observed to be same, while it was observed to decrease at pH 9.4 (Pourmoghaddas et al., 1993). Miller and Uden (1983) showed that DCAA formation decreased slightly with the increase in pH values, and that TCAA decreased slightly when pH was above 7. In general, the overall HAAs formation decreases with the increase in pH values. At high pH values, hydrolysis of many halogenated DBPs occur (Krasner et al., 1989); and therefore, total organic halide (TOX) concentration is lower at pH > 8 (Reckhow et al., 1990). Another study conducted by Ye et al. (2009), acknowledged that increasing the pH values from 6.0 to 8.5, did not change significantly the content of HAAs. However, it has been suggested that pH dependence for the formation of individual DBPs species is complicated.

2.2.1.4. Effect of time

The concentration of DBPs in full-scale distribution systems has been reported to change with the change in residence time (Singer, 1995; Arora et al., 1997; Williams et al., 1997; Rodriguez and Serodes, 2001). In most cases, DBPs concentration was reported to increase with the increase in time. Zou et al. (1997) reported that about 55 to 75% of the one-day total halogen formation potential (TOXFP) was produced within 30 min. Rodriguez and Serodes (2001) conducted a field study of three distribution systems in the province of Quebec, and they reported that THMs concentration was increased from 20 µg/L to 40 µg/L at 6 h and 24 h respectively in the distribution systems. Similar observation was reported by Amy et al. (1987), who conducted THMs formation at reaction time ranging from 0.1 to 168 h, and they found that THMs formed rapidly in the initial 8 h, and slowly thereafter if precursor and free chlorine were still present. A bench-scale study for THMs formation conducted by Rossman et al. (2001) showed that THMs increased significantly within 24 h of reaction time, and this was also correlated with a decrease in free chlorine concentrations. On the other hand, HAAs concentration was reported to decrease with residence time along in distribution systems (Arora et al., 1997). However, another study conducted in a North Carolina drinking water distribution system showed that for a high residual chlorine level, HAAs formation increased along the systems (Singer, 1995). The effect of residence time might be dependent on the chemical and physical properties of individual DBPs, water quality conditions (pH, chlorine dosage, DOM). On the other hand, Xie (2005) has suggested that if DBPs are intermediate products, then the increase in reaction times may decrease the formation of DBPs. The author mentioned that some DBPs, including trihalopropanes, trihaloacetaldehydes, and trihalonitromethanes undergo hydrolysis reactions. Therefore, the increase in reaction times, especially when chlorine and DBPs precursors are exhausted, the hydrolysis reactions will be more noticeable to reduce the concentration of these DBPs.

It should be clarified that there is a difference between stagnation time and retention time. Stagnation time refers to the length of time the water has been under

stagnant conditions, while retention time refers to the hydraulic retention time or time that the water has traveled in the drinking water distribution system under flow conditions (McDonald, 2007). A uniform formation condition (UFC) for simulated distribution system (SDS) uses a stagnation time of 24 h. However, most of the DBPs formation occurred within the first day but formation continued to increase for remaining four days in the study under stagnation conditions (Summers et al., 1996).

2.2.1.5. Effect of PO_4

In recent years, different types of efforts have been made to understand the corrosion mechanisms and to control metal release from corroded pipe. Increasing pH and/or alkalinity are two cost effective and useful methods to reduce metal corrosion. Phosphate based corrosion inhibitors are alternative additive in drinking water for mitigating metal corrosion protection, red water control, and turbidity reduction (Maddison et al., 2001). Corrosion inhibitors such as polyphosphate (or poly/orthophosphate blends) have been historically added to water for sequestering Fe(II) ions to treat 'red water'. Phosphate based corrosion inhibitors are typically dosed into their treated water at a dosage of 0.5 to 3 mg-PO_4/L (Kirmeyer et al., 2000; Maddison et al., 2001). Unfortunately, published research concerning the reactivity of phosphate based corrosion inhibitors on the formation of disinfection byproducts (DBPs) in the presence and absence of soluble iron is not well established yet.

2.2.2. Simulated distribution system test

The simulated distribution system (SDS) test following the Standard Method 5710C (APHA-AWWA-WEF, 2005) allows to predict HAAs and THMs formation under the same conditions as in the distribution systems, with the exception of distribution system material exposure. It has become a common practice in water quality research. The test uses the water quality conditions including pH, temperature, stagnation time, corrosion

inhibitor, iron corrosion by-products simulating an actual distribution system. The SDS test can be done in two ways: (1) pilot treatment plant and (2) bench scale studies. Pilot treatment plant is used for the purpose of conducting a production process on a relatively small scale but same as actual full scale treatment plant. A pilot plant helps to understand each stage of operation, and ultimately help to optimize the current treatment practices using the same natural water sample that uses in the full scale treatment plant. On the other hand, in the bench scale studies, the synthetic and/or natural water samples are used, and the reaction conditions need to be adjusted to simulate as closely as possible to the actual distribution systems considering all major variables present in water. A pH buffer should be added to get stable pH in solution in synthetic samples. In bench scale study, a series of chlorine demand free amber color glass bottles with polypropylene screw caps and teflon-lined septa are generally used for incubation of the water samples under the same conditions (chlorine dosage, temperature, pH, DOC concentration, phosphate dosage etc.) as in the distribution systems. For conducting DBPs formation study at various temperatures considering different seasons (e.g., summer, winter, and spring), a water bath with lid can be used to adjust temperature. After different stagnation times, the incubated water samples are analyzed to determine DBPs concentration. By subtracting the initial DBPs concentration from the DBPs concentration for each incubation period can show the impact of each stagnation time on DBPs formation (Rahman and Gagnon, 2014a). The DBPs results for simulated distribution system can be compared with the DBPs results in an actual distribution system. The comparison should be included both DBPs concentration and speciation. The effect of corrosion inhibitor and iron corrosion by-products on the alternation in DBPs formation results obtained from the bench scale study can be evaluated by comparing with the results obtained from control study.

2.2.3. Modeling

The formation of DBPs and their species distribution is a complex phenomenon and depends on several factors including the characteristics of water, treatments procedures,

and water distribution pipe materials. Previous studies have mostly reported both the formation of DBPs and their reduction in full scale distribution systems (Singer et al., 1995; Arora et al., 1997; Williams et al., 1997; Pecher et al., 2002; Hozalski et al., 2008; Amold et al., 2010). In addition to the field/observation data, several important models considering the most significant factors (e.g., pH, temperature, chlorine dosage, TOC, Br concentration, and time) for predicting DBPs formation in real distribution systems have been proposed (Sung et al., 2000; Clark et al., 2001; Shimazu et al., 2005; Uyak et al., 2007; Zhang et al., 2011). In fact, after the discovery of chloroform in chlorinated drinking water (Bellar et al., 1974; Rook, 1974), some research efforts have been made to develop mathematical models for predicting DBPs formation. Previously excellent review of the various models for DBPs prediction has been reported in literature (Amy et al. 1987; Sadiq and Rodriguez 2004b). Most of these models provided some understanding of DBPs formation from synthetic humic substances or raw/untreated natural waters basing on various conditions.

Due to the complex nature of DBPs precursors (humic and fulvic substance) and their corresponding reactions with different variables, the empirical approaches involving major water quality parameters have been used to develop mathematical models for the prediction of DBPs formation in drinking water. Several steps including formulation, calibration and validation are required for the development of a predicted model (Amy et al., 1987). The development of a model design involves defining a conceptual framework of general functionalities, while a calibration is a process of the model with known input and output information that is used to adjust or estimate factors. Consequently, an independent data set with a number of water quality and operation parameters (e.g., concentration of Fe(II) ions, phosphate dosages, pH, and stagnation times) in real iron pipe water distribution systems, are needed to validate the model. It should be noted that the criterion of model fitness is met if a predicted value falls within $\pm$ 20 percent (%) of the measured values.

2.3. Adsorption

2.3.1. Adsorption theory

Adsorption is a mass transfer process by which a substance is transferred from the liquid phase to the surface of a solid, and becomes bound by physical and/or chemical interactions (Babel and Kurniawan, 2003). Sorption depends heavily on individual experimental conditions such as pH, adsorbent dosage, adsorbate concentration, temperature, contact time, competing ions (Chuah, 2005; Rahman and Islam, 2009a). The constituent that undergoes adsorption is referred to as the adsorbate, and the solid onto which the constituent is adsorbed is referred to as the adsorbent (Droste, 1997; Crittenden et al., 2012). Adsorption processes are used in drinking water treatment for the removal of organic and inorganic constituents and significant progress has been made in the past two decades.

2.3.2. Adsorption types

Based on the nature of the bonding between the molecule and the surface, adsorption phenomena can be classified as (i) Chemical reaction (chemisorption) and (ii) Physical attraction (physical adsorption).

Chemisorption**:** Chemical adsorption (chemisorption) is a type of adsorption whereby a molecule adheres to a surface through a covalent bond or ionic bond. Chemisorption is typically not reversible because the adsorbate is chemically attached to the surface. Due to the specificity of the bond between adsorbate and surface, adsorbates bound by chemisorption to a surface generally cannot accumulate at more than one molecule layer (Crittenden et al., 2012). The bond may also be precise to specific sites or functional groups on the surface of the adsorbent. The charged surface groups attract the opposite charges and repel like charges according to Coulomb's law (Crittenden et al.,

2012). For adsorption of ionic species to surfaces, the most important mechanism is electrostatic attraction, which is highly dependent on pH and ionic strength (Crittenden et al., 2012).

Physical adsorption**:** Physical adsorption (physisorption) is a type of adsorption in which the adsorbate adheres to the surface only through Van der Waals (weak intermolecular) interaction. In some cases, the difference between physical and chemical adsorption may not be that distinct. However, physical adsorption is reported to be less specific compared to chemical adsorption. In physical adsorption process, compounds absorb to surface sites have weaker forces and energies of bonding, and is more reversible (Crittenden et al., 2012). Physical adsorption happens quickly and operates over longer distances (multiple layers). In fact, they begins as a mono-molecular (unimolecular) layer or monolayer, and it can then become 2, 3 or more layers thick (multi-molecular). In the physical adsorption process, if the pores are close to the size of the molecules, more adsorption occurs until the pores are filled with adsorbate. Consequently, the maximum capability of a porous adsorbent can be more related to the pore volume than to the surface area (Crittenden et al., 2012).

2.3.3. Adsorption equilibrium/isotherms

Adsorption equilibrium is usually described through adsorption isotherms. An adsorption isotherm is a constant (*iso*-) temperature (*-therm*) equilibrium relationship between the amount or concentration of adsorbate that accumulates on the adsorbent and the equilibrium concentration of dissolved adsorbate (Droste, 1997). Adsorption isotherms are obtained by exposing a known quantity of adsorbate in a fixed volume of liquid to various dosages of adsorbent. The equilibrium concentrations for all batch adsorption experiments are used to the adsorption isotherm equations to determine coefficients and isotherm curves. These coefficients are useful for modeling adsorption in experiments. Both the coefficients and isotherm curves are an indicator of whether ideal (optimal)

adsorption behavior is observed between an adsorbent and adsorbate (Benjamin and Lawler, 2013). There are two widely used models for use an adsorption process: (i) The Langmuir and (ii) The Freundlich adsorption isotherm.

An American chemist, Irving Langmuir, developed a theoretical equilibrium isotherm relating the amount of solute sorbed on a surface to the concentration of solute (Langmuir, 1916). This equation is derived from simple mass action kinetics, assuming chemisorption (Jeon et al., 2001). The Langmuir adsorption isotherm has found wide range of applications, including water treatment. Its advantages include simplicity, having some physical basis, and its ability to fit a broad range of experimental data. The Langmuir model assumes that the uptakes of ions occur on a homogenous surface by monolayer adsorption without any interaction between adsorbed ions. The Langmuir model can be described as given below (Eq. (2.12)).

$$q_e = \frac{q_m K_L C_e}{1 + K_L C_e} \tag{2.12}$$

where, q_e is the adsorption density achieved in mg/g solid (adsorbent); C_e is the solution adsorbate equilibrium concentration (mg/L); K_L is the mono layer adsorption constant, and q_m is the maximum adsorption capacity mg/g solid. The linearized form of the Langmuir equation can be written as given below (Eq. (2.13)):

$$\frac{C_e}{q_e} = \frac{1}{K_L q_m} + \frac{1}{q_m} C_e \tag{2.13}$$

On the other hand, an empirical sorption isotherm was presented by a German physical chemist Herbert Max Finley Freundlich (Freundlich, 1926). This isotherm assumes that the metal ions uptakes occur on heterogeneous surfaces by multilayer adsorption and the amount of adsorbate adsorbed increases with an increase in concentration. The Freundlich isotherm is expressed as given below (Eq. (2.14)):

$$q_e = K_F C_e^{1/n} \tag{2.14}$$

where, q_e is the adsorption density achieved in mg-C/g solid, C_e is the solution adsorbate equilibrium concentration (mg/L), K_F is the Freundlich adsorption constant indicating adsorption capacity, and 1/n is adsorption equilibrium constant. The linearized form of the Freundlich equation can be written as given below (Eq. (2.15)):

$$logq_e = logK_F + \frac{1}{n} logC_e \tag{2.15}$$

2.3.4. DOM adsorption onto iron oxide surfaces

A wide variety of iron oxides and hydroxides (hematite, goethite, magnetite, maghemite, etc.) occurs in nature (Illés and Tombácz, 2004), and generates in corroded iron pipes in distribution systems (Sarin et al., 2001). On the other hand, the majority (80 to 90%) of natural organic matter (NOM) is often as dissolved form in water (Karanfil et al., 2005). However, significant amount of DOM adsorption onto a variety of natural and synthetic iron oxides and hydroxides have been reported in the literature (Davis, 1982; Benjamin et al., 1990; McKnight et al., 1992; Gu et al., 1995; Rahman et al., 2013). Due to adsorption affinity of DOM, it might have significant impacts on conducts (e.g.

transpoand fate) of many environmental organic and inorganic contaminants as well as the behaviors (e.g. electrophoretic mobility, transport, and interaction) of mineral colloids (Davis, 1982; Sposito, 1984; Stevenson, 1994; Wang et al., 1997; Guan et al., 2006).

Previously several studies have been stated that the variety of functional groups (e.g. carboxylates, phenolic hydroxyls) associated with DOM, and the heterogeneous nature of the solid surface, the adsorption process is expected to be very complex (Hayes et al., 1989; Illés and Tombácz, 2004). These acidic functional groups dissociate in aqueous media, leads to the formation of negatively charges bound chemically to the cross-linked carbon network of DOM macromolecules (Illés and Tombácz, 2004). To assess the role of organic acidity in DOM adsorption onto metal oxides, several research works have been published in the literature (Davis, 1982; Benjamin et al., 1990; McKnight et al., 1992; Edwards et al., 1996). Davis (1982) has conducted DOM adsorption study on aluminum oxide, and found that component of DOM selectively removed according to the steric arrangement of functional groups present in DOM. The same type of study has been conducted by Edwards et al. (1996); and they have predicted that very strongly acidic groups (acid groups ionized at $pH < 3.0$) are the key to the formation of strong surface complexes between organic molecules and metal oxide surfaces. McKnight et al. (1992) observed that dissolved organic matter enriched with aromatic moieties, carboxylic acid groups, and amino residues were preferentially removed along a hydrologic flow path in a stream system. The NMR (nuclear magnetic resonance) analysis of untreated and treated DOM showed that DOM sorbing to metal oxide surfaces had a higher carboxylic content than the nonadsorbing fractions (Benjamin et al., 1990).

Dissolved organic matter (DOM) is a complex and heterogeneous mixture of organic components having a wide range of molecular weights (MWs) fractions, and different chemical moieties. DOM may also have a broad distribution of sorption

affinities onto the mineral surfaces within a particular bulk material (Hur and Schlautman, 2003). In recent times, the adsorption of humic substances (HS) onto metal oxide and hydroxide based on MW distribution using high performance size exclusion chromatography (HP-SEC) has been investigated (Davis and Gloor, 1981; Tipping, 1981; Thurman and Malcolm, 1983; Rahman et al., 2013). Tipping (1981) has shown that humic substances are bound to lab-synthesized goethite, hematite, and amorphous Fe gels, with larger molecular-weight humics exhibiting a greater adsorption relative to smaller humic molecules. Consequently, Davis and Gloor (1981) have indicated that NOM adsorption density by Al_2O_3 has been increased by the higher molecular weight fractions. Based upon binding experiments using nonpolar organic probe molecules, Chin et al. (1994) have reported that the hydrophobicity of humic materials increases with the increase in molecular weight of DOM. Gu et al. (1995) demonstrated that on a carbon weight basis, larger size hydrophobic fractions were preferentially adsorbed over smaller size hydrophilic fractions. Therefore, it has been suggested that higher molecular weight compounds in DOM tend to be more aromatic in nature (Thurman and Malcolm, 1983); therefore, they might have larger number of reaction sites than smaller MW compounds in DOM.

Several studies have shown that the molecular weight, aromatic content, and acidic functional groups of the DOM may play an important role on DOM adsorption onto mineral oxides (Davis, 1982; Benjamin et al., 1990; McKnight et al., 1992; Edwards et al., 1996). However, the mechanisms of DOM adsorption onto mineral oxide surfaces are still not fully identified. Several major mechanisms governing DOM adsorption onto metal oxides, hydroxides may be accounted: (i) ligand exchange surface complexing, (ii) anion exchange (electrostatic interaction), (iii) hydrophobic interaction, (iv) cation bridging (v) entropic effects, and (vi) hydrogen bonding. A comprehensive description of these mechanisms has been presented by Sposito (Sposito, 1984).

CHAPTER 3. MATERIALS AND METHODS

The purpose of this chapter is to elaborate the analytical methods, chemicals and equipment that are used to conduct various types of experiments during the course of the experiments in chapters 4 through 8. Unless otherwise specified, all experiments to complete the research tasks have been conducted in Water Chemistry Laboratory, Centre for Water Resources Studies, Dalhousie University, NS, Canada.

3.1. Glassware

Throughout the experiments, all glassware and sampling bottles were detergent dish-washed, soaked in a 10% nitric acid (HNO_3) solution for 24 h, rinsed several times in Milli-Q water, dried, covered with parafilm plastic (Pechiney Plastic Packing, Chicago, IL), and stored in a dry and dust-free place prior to use for conducting experiments. All dish washed glassware especially amber color bottles (reactor) used for DBPs formation study were chlorine demand free by soaking with concentrated sodium hypochlorite solution (~ 300 mg/L as Cl_2) for at least 24 h. Thereafter, the bottles were rinsed thoroughly three times with deionized water and finally with Milli-Q water, and were heated at 110 °C temperature in an oven (Fisher Scientific, USA) overnight following the Standard Methods (APHA-AWWA-WEF, 2005).

3.2. Reagents and solutions

A brief description about the chemicals use in this study is presented in Table 3.1. Milli-Q water is used for any chemical preparation.

Table 3.1. Information of the main chemicals those are used for this project.

No	Name of the chemical	Chemical formula	Purity	Manufacturer
1	Ammonium chloride	NH_4Cl	99.6%	Fisher Scientific, USA
2	Blended phosphate (25% zinc orthophosphate, 75% Polyphosphate)	$Zn_3(PO_4)_2$ $(.5ZnPO_3)_3.ZnO$	25%, 75%	Carus Chemical Corporation, USA
3	Diethylene glycol monoethyl ether	$C_6H_{14}O_3$	99%	Sigma-Aldrich, USA
4	Ethyl ether anhydrous (Diethyl ether)	$(CH_3\ CH_2)_2O$	99%	Sigma-Aldrich, USA
5	Ferrous sulfate	$FeSO_4.7H_2O$	100%	Fisher Scientific, USA
6	Ferric nitrate	$Fe(NO_3)_3$	98 -101%	Fisher Scientific, USA
7	Humic acid		Tech. grade	Sigma Aldrich, USA
8	Haloacetic acids calibration mix	HAAs		EPA, USA
9	Methyl *tert*-butyl ether (MTBE)	$(CH_3)_3COCH_3$	99.8%	Sigma-Aldrich, Germany
10	Methanol	CH_3OH	99.9%	Fisher Scientific, USA
11	Nitric acid	HNO_3	68-70%	Fisher Scientific, USA
12	N,N-diethyl-p-phenylenediamine (DPD)	$C_8H_{12}N_2$	Powder pillow	HACH Co., USA
13	N-methyl-N-nitroso-p-toluene sulfonamide	$C_8H_{10}N_2O_3S$	99%	Spectrum Chemical MFG Corp., USA
14	Potassium nitrate	KNO_3	99%	Fisher Scientific, USA
15	Potassium hydroxide	KOH	87.3%	Fisher Scientific, USA
16	Pentane	C_5H_{12}	99.6	Fisher Scientific, USA
17	Sodium hydroxide	NaOH	100%	Fisher Scientific, USA
18	Sulfuric acid	H_2SO_4	98%	Fisher Scientific, USA
19	Sodium bi-carbonate	$NaHCO_3$	99%	Fisher Scientific, USA
20	Sodium sulfite (anhydrous)	Na_2SO_3	100%	Fisher Scientific, USA
21	Sodium sulfate (anhydrous)	Na_2SO_4	99.4%	Fisher Scientific, USA
22	Phosphoric acid	H_3PO_4	85%	Fisher Scientific, USA
23	Sodium hypochlorite soln	NaOCl	5.65-6%	Fisher Scientific, USA
24	Trihalomethanes calibration mix	THMs	2000 µg/L	Supelco, USA
25	1-2 dibromopropane	$C_3H_6Br_2$	99%	Acros Organics, USA
26	1,10 –Phenanthrdine (Fe(II) ions reagent)	$C_{12}H_8N_2$	Powder pillow	HACH Co., USA
27	pH buffer solution	NA		Fisher Scientific, USA

3.2.1. DOM solution

Humic acid (Technical grade, Sigma Aldrich, USA) was used as a source of DOM in synthetic water samples (Yang and Shang, 2004; Li and Zhao, 2006). Humic acid was chosen, because it contains 48.95% carbon (by weight), while natural freshwater contains 48 to 54% carbon. A stock solution for the humic acid (HA) was prepared by dissolving an aliquot of HA in 1 L Milli-Q water at $pH > 10$. The solution was stirred for 24 h at laboratory (lab) temperature (21 ± 1 °C). The solution was then filtered through 0.45 µm filter paper (Micron-PSE, Polysulfone), which produced a DOM solution of 280 to 300 mg/L as DOC (dissolved organic carbon). The purified HA stock solution was kept at 4 °C for subsequent use.

3.2.2. Chlorine stock soluteion

A chlorine stock solution of 500 mg-Cl_2/L was prepared using a 5% aqueous sodium hypochlorite (NaOCl) solution (Fisher Scientific, USA) following the Standard Method 5710B (APHA-AWWA-WEF, 2005). Ultrapure water obtained from a Milli-Q® integral water purification system (EMD Millipore Corporation, Billerica, MA, USA) was used to prepare all solutions. All the solutions were kept in freezer at 4 °C for subsequent use. The concentration of chlorine in solution decays at minimum level even if it stores in an amber color bottle. Therefore, it has been suggested to measure chlorine concentration each time prior to use it for conducting the experiments.

3.2.3. Sulfonamide (Diazald) solution

15 mL of diethylene glycol ($(HOCH_2CH_2)_2O$), 15 mL of ether and 3 g of N-methyl-N-nitroso-p-toluene sulfonamide (Diazald) was added to a 40 mL amber vial. The 40 mL vial was shaken until 3 g of Diazald were completely dissolved in solutrion. This solution was used to make diazomethane and can be stored at 4 °C for up to 30 days.

3.2.4. Diazomethane (CH_2N_2) generation

Diazomethane (CH_2N_2) is a gas at room temperature, liquefies at -23 °C and freezes at -145 °C. It is the most common methylating reagent for carboxylic and haloacetic acids. It is reported as highly toxic and a carcinogen. It has been known to explode both as a gas and in solution.

A diazomethane generation apparatus was set up following the Standard Methods (APHA-AWWA-WEF, 2005). The schematic diagram of diazomethane generation apparatus is shown in Figure 3.1. Both N_2 tubes were placed into the rubber tube supplied with the diazomethane apparatus, and parafilm was used to seal the attachments at both ends of the rubber tube. The first tube was filled with ether to a depth of 3 cm. Potassium hydroxide solution (370 g/L KOH in Milli-Q® water) was added into the second tube, so that it is just touching the base of the impinger. Sulfonamide solution was added above the KOH using a long Pasteur pipette with a special care by gently depositing along the side of the tube to ensure no mixing was occurred. In the last tube 4 mL of methyl *tert*-butyl ether (MTBE) was added, and put in a beaker of ice such that the MTBE was submerged.

After getting all the chemicals in the respective places of the diazomethane generation apparatus, the nitrogen gas feed was connected to the in-port of the diazomethane generator, and the gas flow was turned slowly. Therefore, nitrogen gas was bubbled through the apparatus slowly until the MTBE solution became yellow (approximately as yellow as the Diazald solution). This solution would be enough for the extraction of 40 HAAs samples. The diazomethane would be stored at 4 °C in an amber vial for up to 24 h for subsequent use.

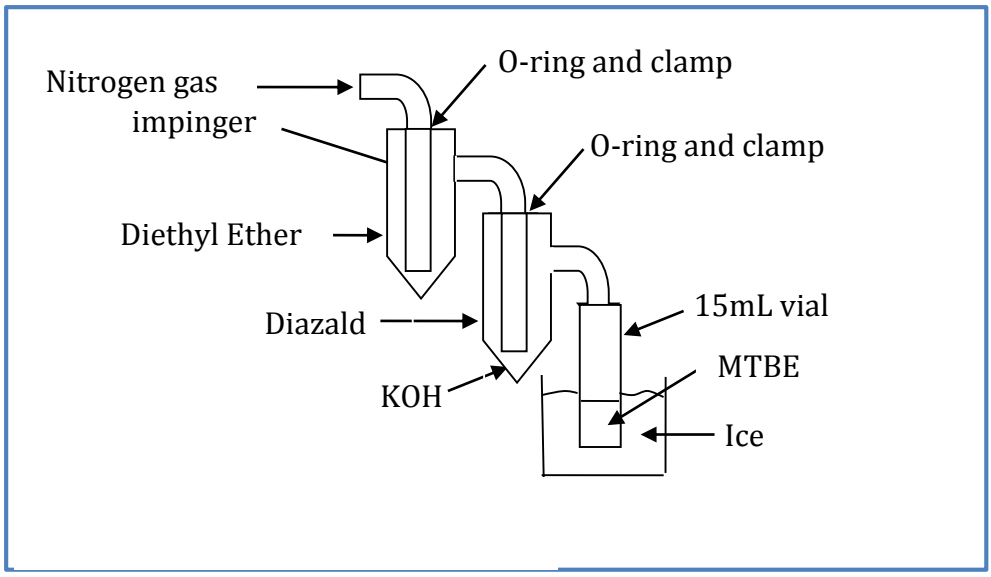

Figure 3.1. Schematic diagram of diazomethane generator.

3.2.5. Synthesis and characterize of goethite and magnetite

Goethite: The iron oxide, goethite (α-FeOOH) was prepared from an alkaline system in accordance with the methods outlined by Schwertmann and Cornwell (2000) with some modifications. The method consisted of the preparation of a 1M $Fe(NO_3)_3$ and a 5M KOH solution. A 100 mL of the 1M $Fe(NO_3)_3$ solution was added to a 2000 mL polyethylene flask followed by the rapid addition of 180 mL of the 5M KOH solution. A red-brown ferrihydrite precipitate was quickly formed. Thereafter, the solution was diluted to 2 liters with Milli-Q water. The flask was sealed and placed in an oven (Fisher Scientific, USA) at 70 °C for 60 h (Figure 3.2). During this drying period, the voluminous red-brown suspension of ferrihydrite was converted to a compact, yellow brown precipitate of goethite. The goethite solution was then centrifuged at a minimum of 2500 rpm for 1 h using centrifuge machine (IEC Centra GP8R, Thermo Electronic Corporation). The liquid was decanted and the process was repeated with Milli-Q water at least 4 times to remove OH^-, NO_3^- and other ions. The sample was then dried in an oven over night at 40 °C. The goethite sample was appeared to be red-brown (Figure 3.3), which was consistent with the typical goethite color (Schwertmann and Cornwell, 2000). The synthetic goethite

sample was confirmed by X-ray diffraction (XRD D8 Advance, Bruker, Germany) technique (Figure 3.4); and scanning electron microscope (SEM, Hitachi S-4700, Japan) coupled with energy dispersive X-ray (EDX, INCA, UK) analysis (Figures 3.5 and 3.6) technique in the Department of Material Engineering at Dalhousie University, Canada.

Figure 3.2. Preparation of goethite (α-FeOOH) in an oven placed at 70 °C for 60 h.

Figure 3.3. Synthesized goethite sample (α-FeOOH) after air dried.

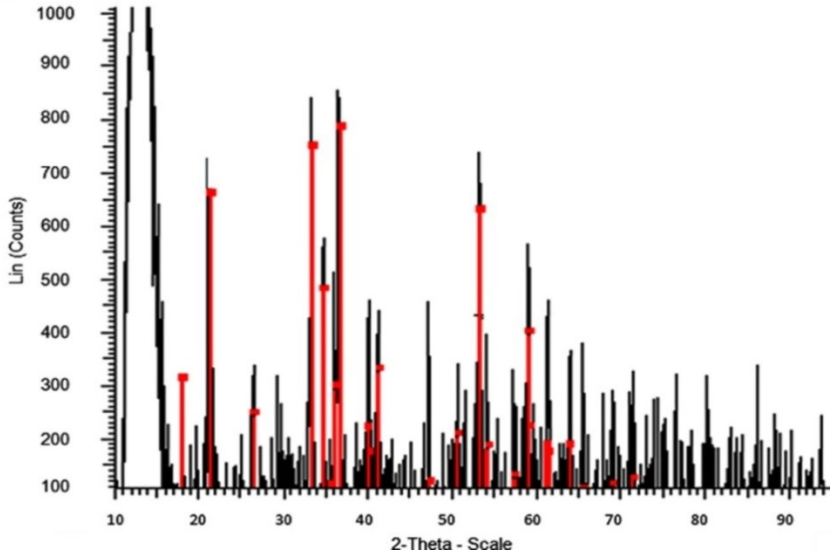

Figure 3.4. XRD patterns of the synthesized goethite (α-FeOOH) using a high-speed XRD system (XRD D8 Advance, Bruker, Germany). Black colored spectrums represent the peaks for model raw goethite and red colored spectrums represent synthesized goethite (Type: 2Th/Th locked – Start: 20.000° -End: 95.197° -Step: 0.050° - Temp.: 25 °C (Room) –T Operation: Strip kAlpha2 0.500.

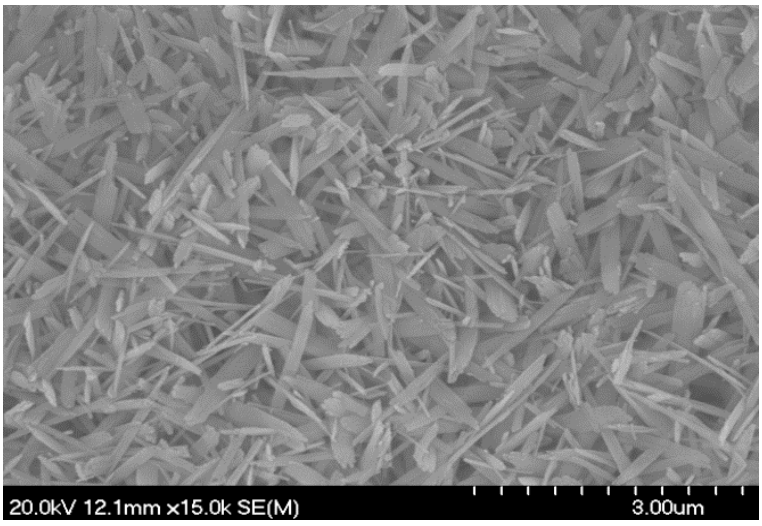

Figure 3.5. Typical SEM micrographs (magnification: 15,000x) for goethite.

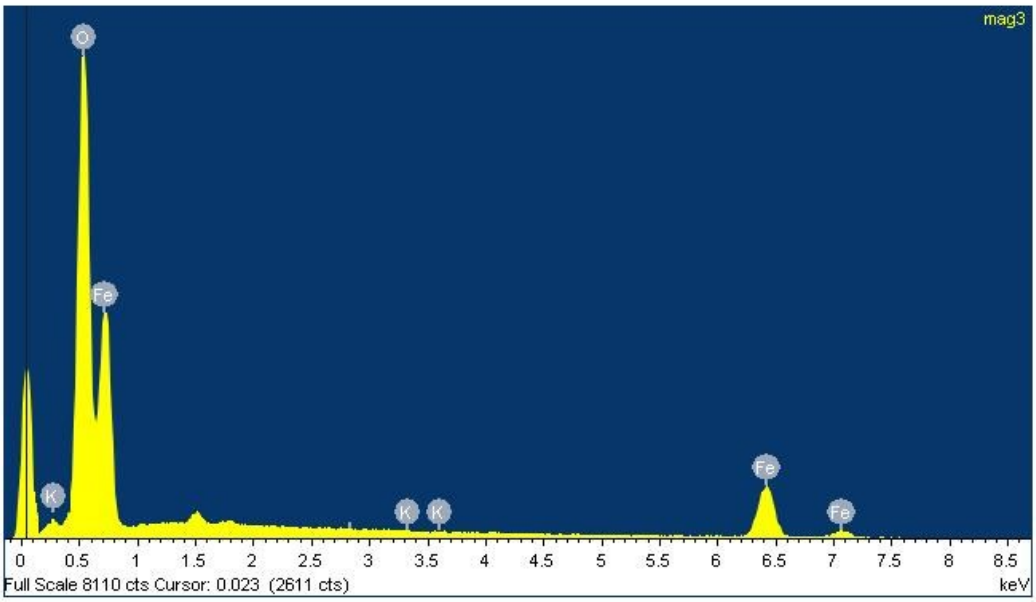

Figure 3.6. Energy dispersive X-ray analysis of synthesized goethite.

Magnetite: The magnetite (Fe_3O_4) was prepared from oxidation of a ferrous solution following the method outlined by Schwertmann and Cornwell (2000) with some modifications. A 80 g ferrous sulfate ($FeSO_4.7H_2O$) was added in 560 mL of Milli-Q water, which had been purged previously using nitrogen gas. The reaction vessel was composed of a 1 liter Erlenmeyer flask, which was sealed with a rubber stopper. The stopper had four holes drilling into it: one for insertion of a thermometer, one for insertion of a separatory funnel, one for nitrogen gas and one for releasing gas (Figure 3.7). The reaction vessel was placed in a water bath which had a temperature of 90 °C. To eliminate the presence of any oxygen in the system, the reaction vessel was continuously purged by bubbling nitrogen gas through the solution. Once the reaction temperature was reached, 240 mL of an oxygen free solution which contained 6.46 g KNO_3 and 44.9 g KOH was added drop wise over approximately 5 min. After adding of this solution, the reaction flask was heated for another 20-60 min, and allowed to cool overnight (Figure 3.8).

The magnetite solution is then centrifuged using a centrifuge machine (IEC Centra GP8R, Thermo Electronic Corporation) at a minimum of 2500 rpm for 1 h. The liquid was decanted and the process had been repeated with Milli-Q water at least 4 times to remove OH^-, NO_3^- and other ions. The sample was then dried at 40 °C in an oven (Fisher Scientific, USA) over night. The magnetite sample was appeared to blackish (Figure 3.8), which was consistent with the typical magnetite color (Schwertmann and Cornwell, 2000). The synthetic magnetite sample was confirmed by X-ray diffraction (XRD D8 Advance, Bruker, Germany) technique (Figure 3.9); and scanning electron microscope (SEM, Hitachi S-4700, Japan) coupled with energy dispersive X-ray (EDX, INCA, UK) analysis (Figures 3.10 and 3.11) technique in the Department of Material Engineering at Dalhousie University.

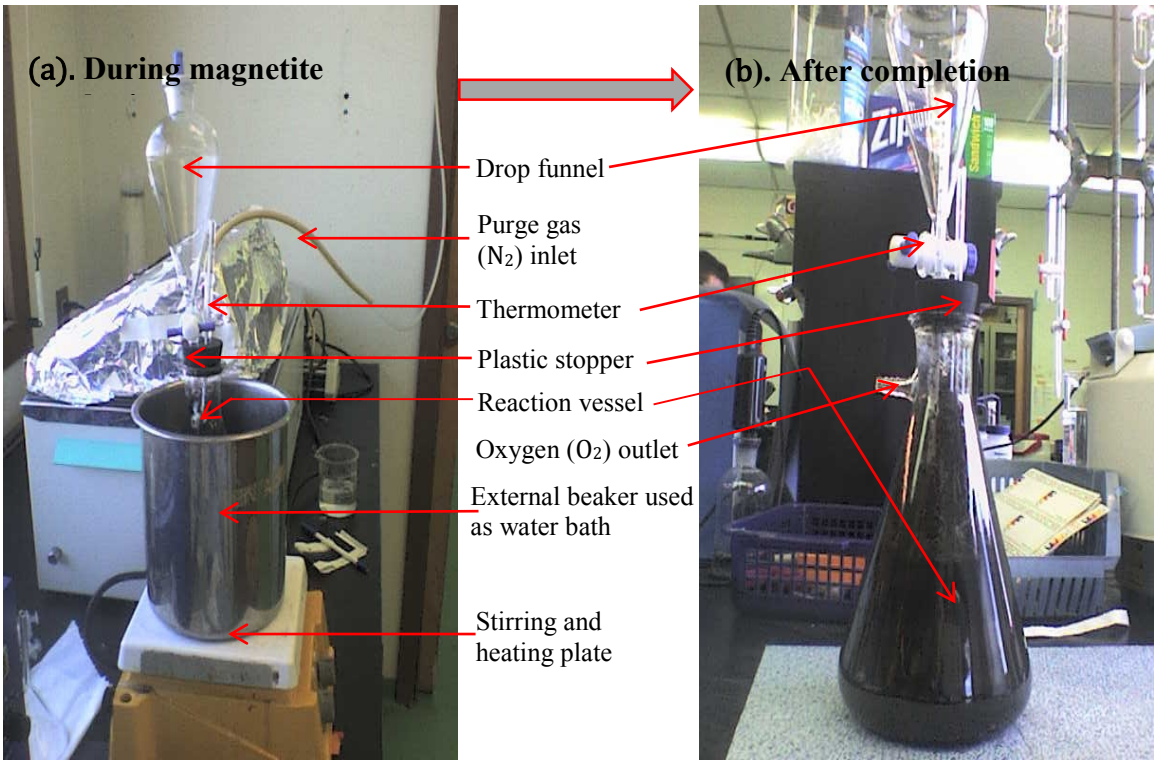

Figure 3.7. A typical equipment for magnetite (F_3O_4) synthesis (a) during magnetite synthesis and (b) after completion synthesis.

Figure 3.8. Synthesized magnetite sample (Fe_2O_3).

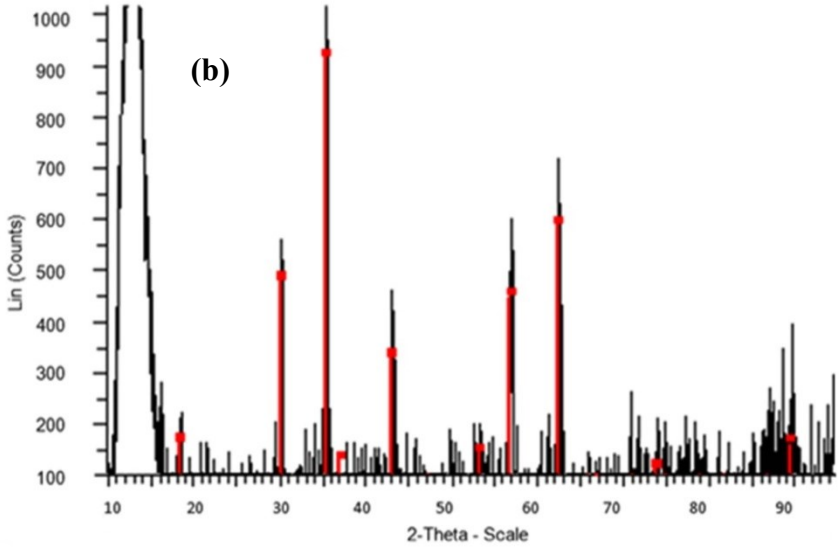

Figure 3.9. XRD patterns of the synthesized magnetite (Fe_3O_4), using a high-speed XRD system (XRD D8 Advance, Bruker, Germany). Black colored spectrums represent the peaks for model raw magnetite, and red colored spectrums represent synthesized magnetite (Type: 2Th/Th locked – Start: 20.000° -End: 95.197° -Step: 0.050° - Temp.: 25 °C (Room) –T Operation: Strip kAlpha2 0.500.

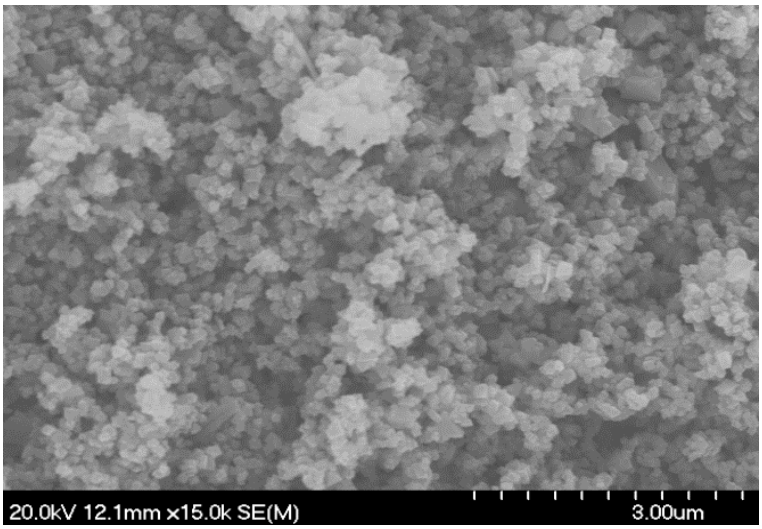

Figure 3.10. Typical SEM micrographs (magnification: 15,000x) for magnetite.

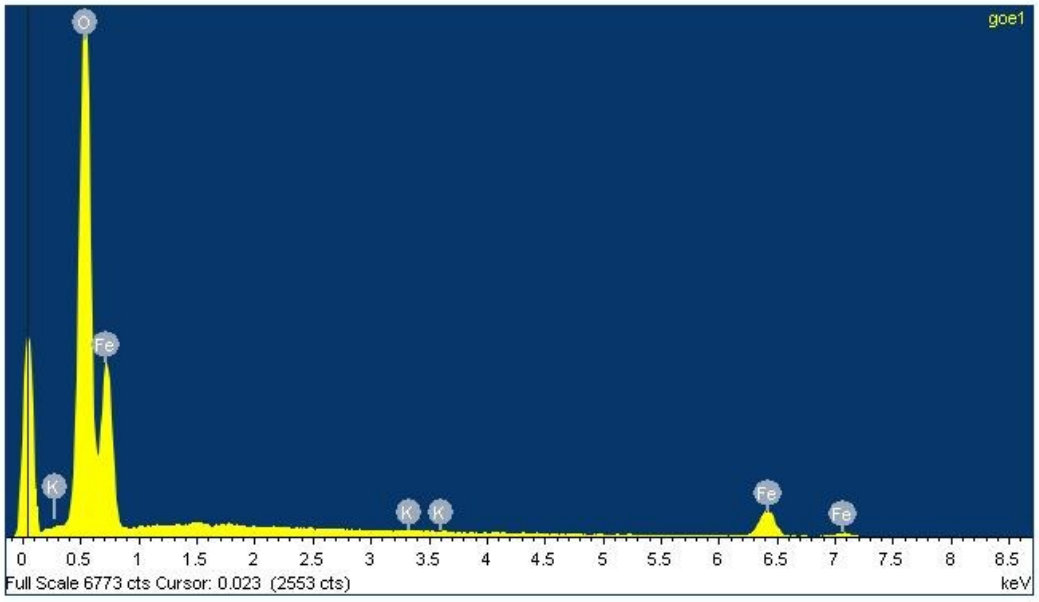

Figure 3.11. Energy dispersive X-ray analysis of synthesized magnetite.

3.3. Water samples

3.3.1. Synthetic water

Ultrapure synthetic (Milli-Q) water was prepared by passing distilled water through a Milli-Q Plus© cartridge deionized water system (Millipore: Milli-Ro 5 plus and Milli-Q plus 185), which produced water with a resistivity $\geq$ 18.2 MΩ. Cm. All clean glassware was ringed several times with the Milli-Q water before using for this study. This water was also used to prepare all chemicals. For adjusting water quality, 35 g of $NaHCO_3$ was added to obtain 5 mg-C/L as dissolved inorganic carbon (DIC) in the synthetic water samples (Lytle and Snoeyink, 2002). The synthetic $NaHCO_3$ buffered water samples were used mostly to conduct all batch tests for Fe(II) ions oxidation kinetics, iron suspension, BDPs formation, and DOM adsorption isotherms study.

3.3.2. JDKWTP water

J. Douglas Kline Water Supply Plant (JDKTSP) uses Pockwock Lake water as a raw water to treat it in the plant through coagulation, hydraulic flocculation followed by direct filtration. In the post filtered water sample, phosphate is added as a corrosion inhibitor, chlorine as a disinfectant and fluoride as dental care. The finished water then flows by gravity in the distribution system to satisfy the needs of Halifax residents. Currently JDKWTP operates 90 ML/day (20 Million igpd) water (Halifax Water, 2012). The post filtered water samples were collected from the JDK water treatment plant to perform DBPs formation study in different reaction conditions.

3.3.3. LMWSP water

Lake Major is the source water for the Lake Major Water Supply Plant (LMWSP), Dartmouth, Nova Scotia, which has a low pH and low alkalinity. The key treatment

processes in this plant include alum coagulation, flocculation and sedimentation followed by filtration and disinfection. LMWSP uses lime for pH control, and alum as a coagulant, and a major treatment consideration is the removal of iron and manganese. Currently JDKTSP operates 43 ML/day (9.5 Million igpd) water (Halifax Water, 2012). The post filtered water samples were collected from the LM Water Supply Plant to perform DBPs formation study in different reaction conditions.

3.3.4. BLWSP water

Bennery Lake Water Supply Plant (BLWSP) uses Bennery Lake water as a raw water to treat it in the plant through coagulation, flocculation followed by direct filtration. In the post filtered water sample, phosphate is added as a corrosion inhibitor, chlorine as a disinfectant. Currently BLWSP operates 12 ML/day (0.257 Million igpd) water (Halifax Water, 2012). The post filtered water samples were collected from the BLWSP to perform DBPs formation study in different reaction conditions.

3.4. Analytical techniques

3.4.1. Water quality parameter

pH and temperature measurements in all studied water samples were made using an Accumet electrode and Accumet Excel, XL50 (Dual channel pH/ion/conductivity) meter (Fisher Scientific, Singapore). The pH meter was standardized daily using a three-point calibration with pH 4 (SB101-500), pH 7 (SB107-500), and pH 10 (SB115-500) buffer solutions respectively (Fisher Scientific, USA). The temperature probe was also calibrated daily using a mercury thermometer (Fisher Scientific, USA). DO was measured with a DO meter (VWR, SP5OD, SympHony, Thermo Orion, USA) with a DO probe (VWR, SympHony, Thermo Orion, UK). The probe was calibrated against water saturated air at the experimental temperature. Color in water sample was measured using a DR/5000 UV

Visible Spectrophotometer (HACH Co., Loveland, USA) at a wavelength of 455 nm. HACH 2100 AN Turbidimeter was used to measure the turbidity in water sample.

Phosphate concentration was measured by an ion chromatograph (761 Compact IC, Metrohm). Free chlorine concentration was determined using the colorimetric version of the N,N-diethyl-p-phenylenediamine (DPD) following the HACH 8021 method (HACH, 2005) at a wavelength of 530 nm using a DR/5000 UV Visible Spectrophotometer (HACH Co., USA). Fe(II) ions concentration was measured colometrically by the 1,10-phenanthroline method at a wavelength of 510 nm using a DR/5000 UV Visible Spectrophotometer (HACH, 2005). The total iron concentration was measured using inductive couple plasma mass spectrometry (Thermo Scientific X-Series2 ICP-MS).

Total and dissolved organic carbon (TOC and DOC) were analyzed using a TOC-V_{CHP} Total Organic Carbon Analyzer (Shimadzu, Japan) with a Shimadzu ASI-V auto sampler (Shimadzu, Japan), and catalytically aided combustion oxidation non dispersive infrared detector (NDIR) having a method detection limit of 0.08-mg/L (Shimadzu, Japan). For TOC and DOC analysis, the TOC analyzer operating conditions were as follows: TOC standard platinum catalyst, injector volume 50 µL, oven temperature 680 °C, carrier gas flow 150 mL/min, potassium hydrogen phthalate standards 0 to 10 mg/L, and correlation > 0.99. For measuring TOC, water samples are first transformed to 40 mL vials, headspace free, and phosphoric acid is added into the water samples to reduce the pH to approximately 2 to 3. At this low pH, any inorganic carbon that is present is liberated as CO_2 into a nitrogen carrier gas. Any remaining carbon in the sample is assumed to be TOC. DOC was measured following the same method as TOC, but after filtering the sample through 0.45 µm polysulfone membrane filter (Cole-Parmer® Nylon Membranes) that had been pre-ringed with 500 mL of milli-Q water following the Standard Method 5310C (APHA-AWWA-WEF, 2005).

3.4.2. X-ray diffraction (XRD)

X-ray diffraction analyzer (XRD D8 Advance, Bruker, Germany) was used to identify the crystalline phase of iron particles. The iron particles samples were centrifuged at 40,000 rpm for 30 min using a centrifuge machine (IEC Centra GP8R, Thermo Electronic Corporation). The precipitates were washed once in Milli-Q water before being centrifuged again. Finally, the particles were dried at 30 °C for 24 h, and thereafter kept at lab temperature (21 ± 1 °C) until characterization (usually within 2 to 3 weeks) following the method described elsewhere (Gunnars et al., 2002). The iron particles products were identified by X-ray diffraction (XRD) method employing a high-speed Bruker D8 Advance XRD system using Cu-Ka radiation having a wave length of 1.54 A°, tube voltage of 40 kV, and tube current of 40 mA. The experiment for XRD was conducted in the Department of Process Engineering at Dalhousie University.

3.4.3. BET surface area

Specific surface area of synthesized goethite (α-FeOOH) and magnetite (Fe_3O_4) were determined with BET method (the Brunauer-Emmett-Teller isotherm) in the Department of Physics and Atmosphoric Science at Dalhousie University, Canada. The BET isotherm is the basis for determining the extent of nitrogen (N_2) adsorption on a given surface. To conduct this experiment, 1 to 2 g of goethite and magnetite were transferred into small bottles, and heated them at 150 °C for 2 h to remove any gases that might be adsorbed by the samples. After the degasification process, the sample bottles were immersed in a liquid nitrogen bath. Then the bottles were exposed to a high purity gas mixture containing nitrogen and helium gas under ambient pressure. The number of moles of nitrogen adsorbed at monolayer coverage was determined from a BET plot, and from this surface area of the sorbent (each N_2 molecule occupies an area of 16.2×10^{-20} m^2). Replicate analysis of adsorption/desorption were performed at each mole fraction of nitrogen with an overall error of approximately 4%.

3.4.4. Scanning electron microscope (SEM)

The goethite and magnetite samples before and after DOM adsorption study were first coated with a thin layer of conductive materials, namely, gold and palladium. Coating was performed with a small device called a sputter coater (Hitachi E-1030, Japan). A detailed method for SEM sample preparation is described elsewhere (Rahman, 2007). Briefly, the sputter coater used argon gas and a small electric field. The samples were first fixed on double sided adhesive carbon tapes attached to one end of SEM stubs, and then the samples were attached with carbon tapes. The samples were placed in a small chamber which was at vacuum. Argon (Ar) gas was then introduced, and an electric field was used to add a positive charge to the atoms. The Argon ions were then attracted to a negatively charged piece of gold and palladium foil. Gold and palladium atoms now settled onto the surface of the sample, producing a gold-palladium coating. The thickness of the coating was approximately 30 nm, and the density was 19.32 g/cm^3. The morphology of the coated goethite and magnetite samples were investigated using a SEM (Hitachi S-4700, Japan). The elemental analysis in goethite and magnetite samples were conducted by an energy-dispersive X-ray spectrometry (EDX) system (INCA, UK) equipped with SEM in institute of research materials (IRM), Dalhousie University. Five fields per sample were analyzed and the most representative images are presented.

3.4.5. Transmission electron microscope (TEM)

TEM (transmission electron microscope) is a microscopy technique, where a beam of electrons is transmitted through a specimen, and passes through a series of lenses (Sellers, 2009). It determines the image resolution and obtains a magnified image using an image processing system such as a computer. To obtain TEM images of the iron nanoparticles, a 10 mL supernatant was first sonicated for about a min, and then a droplet of it was placed on a 200-mesh gold grid of carbon film (Electron Microscopy Sciences, Hatfield, PA, USA). The 200-mesh grid was set on tissue paper and allowed to dry before being placed in a special holder. Consequently, the samples were loaded under a vacuum

in the FEI Tecnai-12 for image capturing. The TEM images of the iron nanoparticle samples were recorded by the FEI Tecnai-12 with a MegaView II camera and AnalySIS software in the Department of Biology at Dalhousie University.

3.4.6. Zeta (ζ) potential (ZP)

The electrophoretic mobility (EMF) of iron particles was measured over a wide range of pH from 3 to 11 at 25 ± 0.1 °C using Zetasizer Nano (Malvern Instruments Ltd., UK). The ζ-potential was calculated from the EMF using the default instrument software following Henry's equation with the Smoluchowski relationship. During the ζ-potential measurement at different pH values in solution, pH was adjusted by addition of 0.01 M NaOH and 0.01 M HCl using multiple purpose auto-titrator (MPT-2, Malvern Instruments Ltd., UK). The experimental temperature (25 ± 0.1 °C) was set by Zetasizer Nano (Malvern Instruments Ltd., UK). At least three measurements in each sample were performed as x-potential at certain pH value, and the average values were used to represent the data. Prior to the measurement of each new sample, approximately 20 mL of milli-Q water was ringed through the cell followed by a rinse with 10 mL of the sample to be measured. Each sample was measured over a time period of 15-20 min with a 20 sec time interval between each measurement at 25 °C.

3.4.7. Dynamic light scattering (DLS)

The average particle size and size distribution of iron nanoparticles were measured at a fixed pH value of 6.5 and at 25 °C temperature following the dynamic light scattering (DLS) technique using a Zetasizer Nano Series (Zetasizer Nano-ZS, Malvern, UK). The temperature in solution was adjusted (25 °C) automatically by the Zetasizer. The Zetasizer was equipped with a 633 nm wavelength of green laser and was operated at a non-invasive back scattering angle of 173°. This instrument is suitable to determine the particle sizes ranging from 0.6 nm to 6 μm. To determine the particle size distribution in

solution, 1.3 mL portion of each sample was filled in a cuvette, which was then capped, cleaned from the outside by Kimwipes, and loaded in the Zetasizer cell. The average particle size produced by DLS could be presented as an intensity, volume, or number distribution. However, the reported average particle size is always an intensity mean size (also called a cumulant mean).

3.4.8. High performance size exclusion chromatography (HPSEC)

High performance size exclusion chromatography (HPSEC) (Perkin Elmer, Series 200) with a UV/VIS detector was used to determine the molecular weight (MW) distribution of DOM present in water samples. The samples were analyzed using a TSK G3000SW column (7.5 mm × 300 mm) with a TSKgel SW guard column (7.5 mm × 70 mm). The media in the TSK column is consisted of silica with a pore size of 10 µm. These columns are connected to the Perkin Elmer Series 200 Auto sampler and the Perkin UV/VIS detector, which is set at UV 254 nm. However, the column was calibrated with sodium polystyrene sulphonate (PSS) standards with different molecular weight (14900, 7540, 5180, 1530 Da). All PSS standards and samples were detected at a wavelength of 254 nm. The water samples were first passed through a 0.45 µm membrane filter (Micron-PSE, Polysulfone), and transferred into 2 mL SEC vial. The SEC vials were kept in freezer at 4 °C for a maximum of one week prior to analysis. For the SEC analysis, the samples were put into the auto sampler tray and a 20 µL of each sample was injected and passed through the columns at a flow rate of 0.7 mL/min. A sample run time of 30 min was established, whereby all of the compounds in the sample had passed through the column. Molecular weight, which is related to the size of solute molecules, was plotted against retention time. The reproducibility of the measurements was assured by running duplicates.

3.4.9. Gas Chromatography (GC)

HAAs and THMs samples obtained by the liquid-liquid extraction (LLE) procedure with methyl *tert*-butyl ether (MTBE) and pentane respectively, and were analyzed by gas chromatography (CP-3800 GC, Varian Inc.), coupled with an electron capture detector (GC-ECD) according to the USEPA Methods 551.1 and 552.2 (USEPA, 1995a and b). The Varian CP-3800 gas chromatography was equipped with a VF-5 column and a Varian CP-8400 auto-sampler (Varian Inc.).

The GC operating conditions for HAAs analysis were as follows: injector temperature 200 °C, detector temperature 300 °C, injection volume 1µL, flow rate 1 mL/min, sample injected at 35 °C and held for 10 min, temperature increased to 65 °C at a rate of 2.5 °C/min with no hold, temperature increased to 85 °C at a rate of 10 °C/min with no hold, temperature is increased to 205 °C at a rate of 20 °C/min, and held for 7 min. A coefficient of determination $R^2 > 0.95$ was consistently achieved for the calibration curves for all nine HAAs analytes. Samples were analyzed for the following nine haloacetic acids: monochloroacetic acid, dichloroacetic acid, trichloroacetic acid, bromochloroacetic acid, bromodichloroacetic acid, monobromoacetic acid, dibromoacetic acid, chlorodibromoacetic acid and tribromoacetic acid. A typical GC chromatograph for the calibration curve of individual HAA standard is shown in Figure 3.12.

The GC operating conditions for THMs was little bit different from that of HAAs follows as: injector temperature 220 °C, detector temperature 320 °C, injection volume 1 µL, flow rate 1 mL/min, sample injected at 50 °C and held for 7 min, temperature increased to 115 °C at a rate of 5 °C/min with no hold, temperature increased to 295 °C at a rate of 50 °C/min and held for 0.5 min. A coefficient of determination $R^2 > 0.95$ was consistently achieved for the calibration curves for all four THMs compounds. Samples were analyzed for four THM compounds: chloroform, bromodichloromethane, dibromochloromethane and bromoform. A typical GC chromatograph for the calibration curve of individual HAAs standard is shown in Figure 3.13.

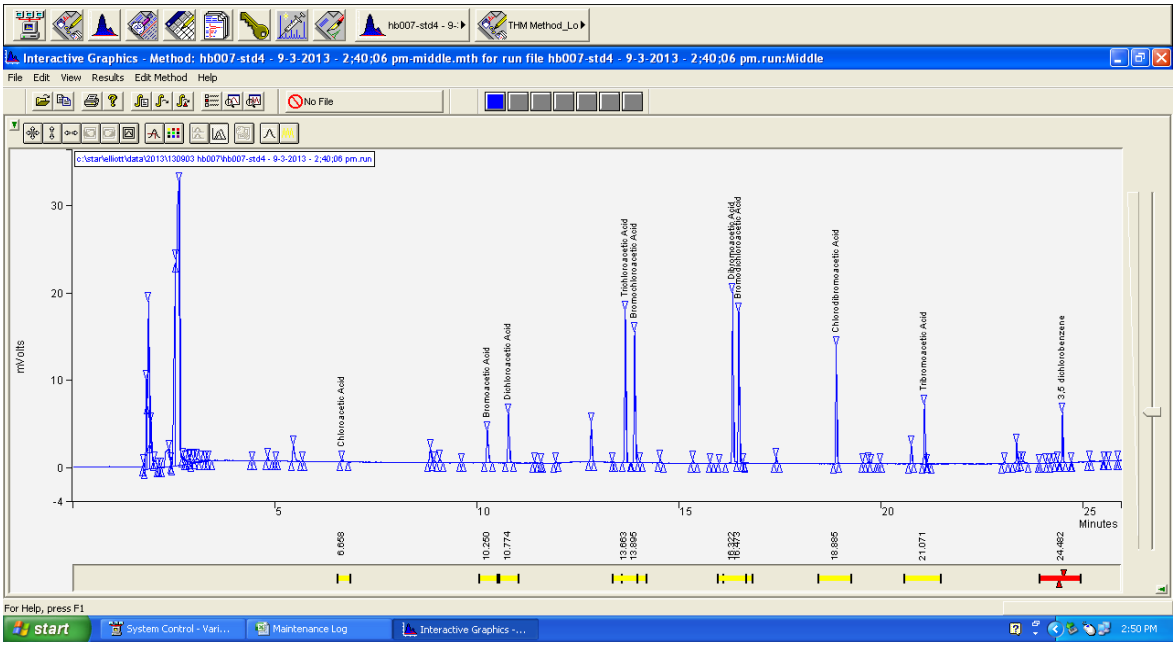

Figure 3.12. A typical GC chromatograph for the calibration curve of HAA species.

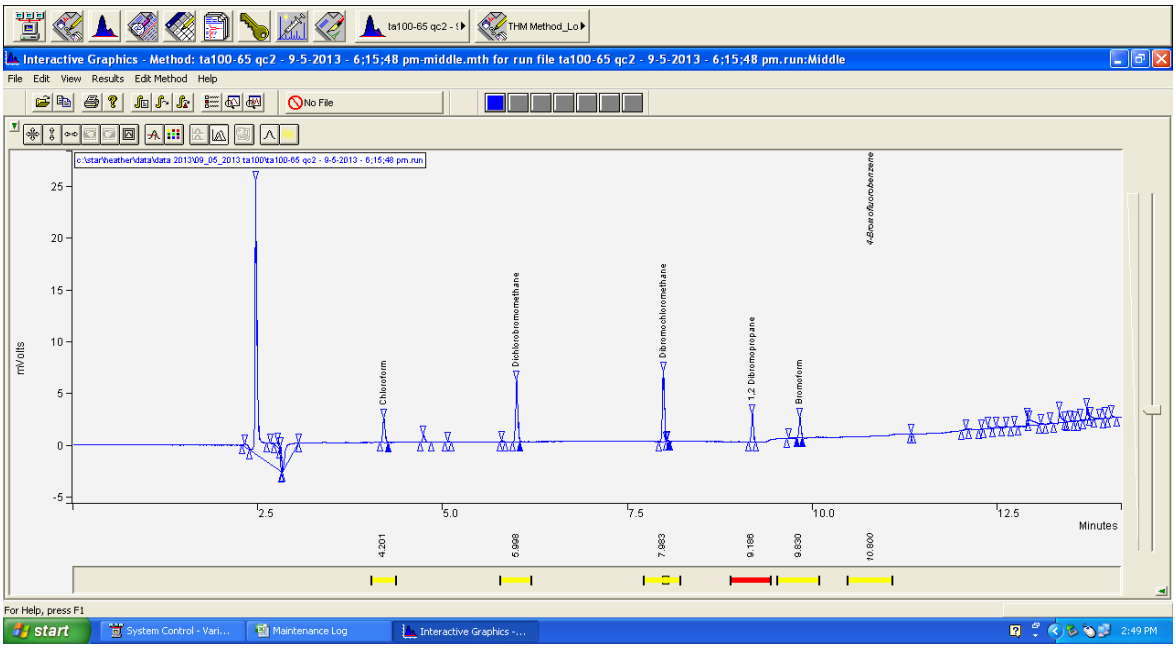

Figure 3.13. A typical GC chromatograph for the calibration curve of THM species.

3.4.10. Fourier transform infrared (FTIR) spectroscopy

The samples for FTIR (Fourier transform infrared) analysis were prepared following the method reported elsewhere (Fu and Quan, 2006; Giasuddin et al., 2007). Briefly, after completion of the DOM adsorption study, the DOM solutions treated with goethite and magnetite were centrifuged and the precipitate was dried over night at an ambient temperature, and ground to yield powder. All dried powder samples were stored in a desiccator until the FTIR analysis. FTIR spectra was measured on KBr pellets prepared by pressing mixtures of 1 mg dry powder sample and 100 mg spectrometry grade KBr powder (Sigma-Aldrich, USA) under vacuum, with precaution taken to avoid moisture uptake. Solid-state FTIR spectra were recorded for a wavenumber range of 3600 to 400 using a FTIR spectrometer (Spectrum 100, Perkin Elmer, USA) in the Department of Chemistry at Dalhousie University.

3.5. Bench scale experiments

3.5.1. Fe(II) ions oxidation and iron suspension

Experiments were conducted in a 1000 mL glass reaction cell. The pH electrode, thermometer, and DO (dissolved oxygen) electrode were clamped firmly from the top of the reaction cell. The reaction cell was set on a magnetic stirrer plate (VWR Advanced Hot Plate Stirrer, USA) to mix the solution gently and homogeneously (Figure 3.14). All experiments were conducted at lab temperature (21 ± 1 °C).

To start an experiment, 1 L of ultrapure synthetic water was added to a reaction cell. For adjusting water quality, 35 g of $NaHCO_3$ (assay: 100%, Fisher Scientific, USA) was added to obtain 5 mg-C/L as dissolved inorganic carbon (DIC) in water samples (Lytle and Snoeyink, 2002). The DO concentration in the reaction solutions was kept saturated and constant during each run corresponding to an oxygen partial pressure of

0.21 atm (DO ≈ 8.5 mg/L) using oxygen (Ultra Pure, Praxair, Canada). At the required pH for the particular Fe(II) ions oxidation experiment, pH adjustment was performed using high-purity 0.6 M HCl (assay: 37.4%, Fisher Scientific, Canada) and 0.6 M NaOH (assay: 100%, Fisher Scientific, Canada). The pre-settled pH levels were maintained constant at least 30 min before starting each experiment. After the stabilization of the desired pH levels in water solution, $FeSO_4.7H_2O$ (assay: 100%, Fisher Scientific, NJ, USA) was added into the water samples to obtain an initial soluble Fe(II) ions concentration of approximately 3 mg/L (5.37×10^{-5} M). After each desired reaction period, a 20 mL of sample was withdrawn from the reaction cell and Fe(II) ions concentration was measured immediately following the HACH 8146 method (HACH, 2005). Temperature, DO and pH were also monitored over the time of the experiments. According to the 2^4 full factorial design experimental protocols, the same experiments were conducted for different pH values (6.5 and 8.5) in the presence and absence of DOM, corrosion inhibitor (blended phosphate) and disinfectant (chlorine solution) in $NaHCO_3$ buffered synthetic water systems. A purified Humic acid (HA) (Technical grade, Sigma Aldrich, USA) stock solution was used as a source of DOM for this study. A chlorine stock solution of 500 mg-Cl_2/L was prepared using a 5% aqueous sodium hypochlorite (NaOCl) solution (Fisher Scientific, USA) following the Standard Method 5710B (APHA-AWWA-WEF, 2005). To prevent precipitation of source water iron, phosphate was added prior to chlorination (Klueh, 1988). Blended phosphate (Virchem 937, Carus Chemical Corporation, USA) composed of 25% zinc phosphate and 75% polyphosphate were used as a source of phosphate for this study. During the experiments, the solutions were stirred gently with a Teflon-coated magnetic stirrer bar and magnetic stirrer plate (VWR Advanced Hot Plate Stirrer, USA). After 30 min of completion of ferrous ions oxidation processes, samples were drawn out of the cell with a clean syringe for iron suspension study. In addition to the 2^4 factorial design experimental protocols, extended studies were conducted for different pH values of 5.5 to 8.5, different initial Fe(II) ions concentration of 0.4 to 3 mg/L (0.72×10^{-5} to 5.37×10^{-5} M), different chlorine dosages of 2.2 to 5.7 mg/L (6.19×10^{-5} to 16.06×10^{-5} M), and different phosphate dosages of 0.5 to 20 mg-PO_4/L (0.53×10^{-5} to 21.06×10^{-5} M PO_4) respectively in the same water conditions.

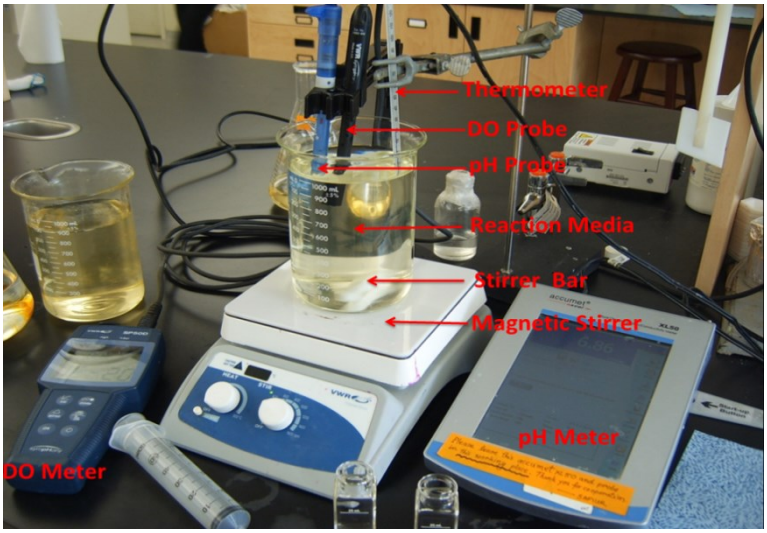

Figure 3.14. Bench scale study for ferrous iron oxidation kinetics and iron suspension formation for different reaction media in $NaHCO_3$ buffered synthetic water.

3.5.2. Disinfection byproducts (DBPs) formation

Bench scale experiments were conducted for DBPs (HAAs and THMs) formation analysis using synthetic water samples consisting of differing characteristics. Humic acid (Sigma-Aldrich, USA) stock solution was used as a source of dissolved organic matter in synthetic water samples (Vikesland et al., 1998; Chang et al., 2001; Yang and Shang, 2004; Li and Zhao, 2006). A required amount of purified humic acid stock solution was employed as the surrogate for DOM (2.85 mg/L as DOC) in $NaHCO_3$ buffered synthetic water systems (5 mg-C/L as dissolved inorganic carbon). Humic acid was chosen, because it contains 48.95% carbon (by weight), while natural freshwater contains 48 to 54% carbon. The required pH values of the buffered water samples were adjusted using 0.5N HCl acid and 0.5N NaOH solution. The water samples were chlorinated (chlorine to carbon mole ratio of 0.79). The solutions were mixed properly, and transferred

immediately into 250 mL chlorine demand free serum bottles (reactor) with PTFE (Polytetrafluoroethylene) faced screw caps. The serum bottles were filled with the samples head-space-free. Finally the serum bottles (reactors) were wrapped with aluminum foil to prevent photochemical reaction and kept in dark place for the designated reaction times. The same experiments were conducted in the presence of different dosages of Fe(II) ions and phosphate for different pH values and different reaction times.

After each designated reaction period (e.g., 3.5, 24, 48, 84, and 130 h) for different water characteristics, the chlorinated water samples were collected into headspace-free 25 mL glass vials with polypropylene screw caps and teflon-lined septa. The vials were cautiously filled with the water samples, so that tapping of air bubbles inside was prevented. Chlorinated samples for HAAs samples were quenched with ammonium chloride (Fisher Scientific, NJ, USA), while THMs samples were quenched by sodium sulfite (Fisher Scientific, NJ, USA) to prevent further formation of HAAs and THMs respectively. All samples were refrigerated at 4 °C not more than 2 weeks prior to extraction. Total experiments were conducted at lab temperature (21 ± 1 °C). All of the experiments were conducted in duplicate to test the reproducibility of the results. For each batch test control samples were used following the procedure as the test sample but without the designed variables (e.g., ferrous ions and phosphate) at different pH values and reaction times.

In addition to conduct DBPs formation study in synthetic water samples, the post filtered water samples collected from 3 major water treatment plants in Halifax, Nova Scotia: (1) JDK water treatment plant, (2) Lake Major water treatment plant and (3) Bennery Lake water treatment plant were used in HAAs and THMs formation study. This study was conducted for the different pH values (5.5 to 8.5), different dosages of Fe(II)

ions (0.5 to 3 mg/L) and phosphate (0 to 1.5 mg/L); and different reaction times (3.5 to 24 h) to validate HAAs and THMs formation model equations.

3.5.2.1. DBPs samples preparation and analysis

The HAAs analysis in water samples was prepared following the EPA 552.2 method (USEPA, 1995a) employing liquid-liquid extraction with the MTBE. Briefly, the chlorinated water sample was transferred to 40 mL glass vial. A 6 g of anhydrous sodium sulfate (assay: 99.4%, Fisher Scientific, NJ, USA), 2 drops (100 g/L) of $NaHCO_3$ solution (assay: 100%, Fisher Scientific, NJ, USA), 1 mL of analytical grade concentrated H_2SO_4 (assay: 98%, Fisher Scientific, Canada), and 4 mL of MTBE (assay: 99.8%, Sigma-Aldrich, Germany) were added into the 40 mL vial of each HAAs water sample. The vials were sealed, manually shaken for 2 min, and allowed to stand for 10 min for separating the organic phase. Then, the organic layer containing HAAs was extracted by Pasteur pipette, and transferred to a 2 mL GC vial. A 20 µL (1 mg/L) of internal standard (1,2-dibromopropane) and a 100 µL of freshly prepared diazomethane were added into the GC vials.

The THMs analysis in water samples was performed following the EPA 551.1 method (USEPA, 1995b) employing liquid-liquid extraction with the pentane. Briefly, the incubated water samples were transferred into 40 mL amber colored vials. A 6 g of anhydrous sodium sulfate (assay 99.4%, Fisher Scientific, NJ, USA) and 4 mL of pentane (assay 99.6%, Fisher Scientific, NJ, USA) were added into each water sample; and the bottles were gently shaken for 2 min. The upper portion of the organic phase was separated by Pasteur pipette into a 2 mL vial. 20 µL (1 mg/L) of internal standard (1,2-dibromopropane) was added into the 2 mL GC vial of each THMs extracted sample.

The GC vials containing HAAs and THMs samples were shaken lightly and kept in a freezer for a maximum of 14 days for GC analysis. The calibration curves for HAAs and THMs were prepared using the standard solutions for HAAs and THMs before starting analysis in the DBPs samples. HAAs and THMs analyses in samples were quantified by gas chromatography (Varian, CP 3800 Gas Chromatography) with electron capture detector (GC/ECD). At the beginning of each analytical run, solvent blanks and solvent samples containing the internal standard were injected to condition the GC, and to verify that interferences were absent. Other quality assurance/quality control (QA/QC) procedures, such as QC check standards and matrix spikes were taken through the analysis.

3.5.3. DOM adsorption study

Batch experiments for DOM adsorption were conducted in a series of 250 mL Pyrex conical flasks with stopper. Initially, a 150 mL of DOM stock solution with desired concentration (mg/L as DOC) was taken in each 250 mL conical flask. The final solutions were adjusted to an ionic strength of 0.01 M using NaCl and the desired pH values were adjusted using 0.01 M NaOH or 0.01M HCl acid. The pH values of each solution were stabilized for at least 30 min before adding adsorbent (goethite or magnetite). An appropriate amount of adsorbents (goethite or magnetite) were added into DOM solutions. The suspensions were then shaken at 175 rpm using a shaker table (Barnstead/Lab-Line MaxQ™ 2000) at lab temperature (21 ± 1 °C) for 5 days, which provided sufficient time for our systems to equilibrate, based upon preliminary kinetic studies. After 5 days, the samples (suspensions) were centrifuged at 25000 rpm for 30 min using a centrifuge machine (IEC Centra GP8R, Thermo Electronic Corporation), which was found to be sufficient for separation of the adsorbent from the adsorbate. The supernatants were then filtered instantly through 0.45 μm membrane filter (Micron-PSE, Polysulfone), and filtered were immediately pipetted into glass vial for the measurement of dissolved organic carbon (DOC) and molecular weight distribution of DOM in solution.

DOC in each sample was measured in triplicate using TOC-V_{CHP} analyzer. The amount of DOM adsorbed was determined from the difference between the initial and final (after adsorption) DOC concentration in solution after equilibration. The adsorption experiments were conducted for the different dosages of DOM and different pH values in the same experimental setup. Control flasks containing no sorbent were prepared and treated similarly to monitor other possible losses of organic carbon. The equilibrium adsorption capacity was calculated using the following expression (Rahman and Islam, 2009b).

$$q_e\,(mg/g) = \frac{(C_o - C_e)V}{m} \qquad (3.1)$$

where, q_e is equilibrium adsorption capacity (mg C/g), C_o and C_e are initial and equilibrium concentration (mg C/L) of DOM in solution respectively; V is volume of aqueous solution (mL); and m is dry weight of the adsorbent (g).

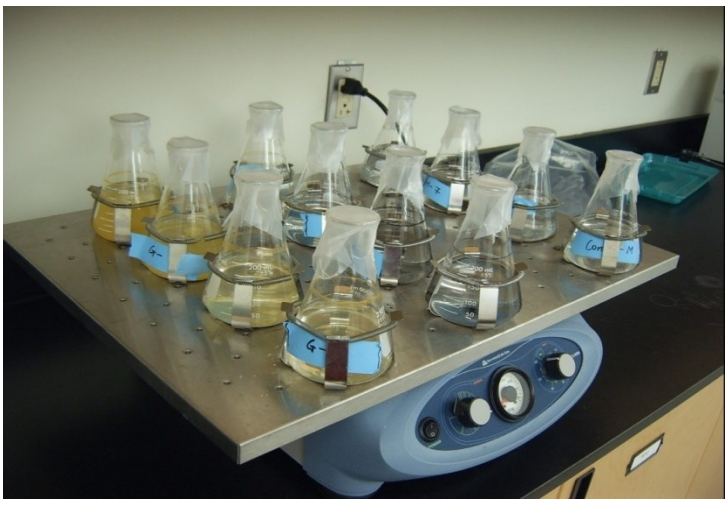

Figure 3.15. DOM adsorption study using goethite and magnetite in synthetic water samples at lab temperature and 150 rpm.

CHAPTER 4. BENCH SCALE EVALUATION OF FERROUS IRON OXIDATION KINETICS IN DRINKING WATER: EFFECT OF CORROSION CONTROL AND DISSOLVED ORGANIC MATTER[1]

4.1. Abstract

This paper reports on experiments that were conducted in bicarbonate buffered synthetic water in order to determine the effects of corrosion control (pH and phosphate) and dissolved organic matter (DOM) on the rate constants in Fe(II) ions oxidation processes. A factorial design approach elucidated that pH ($p = 0.007$, contribution $= 42.5\%$) and phosphate ($p = 0.025$, contribution $= 22.7\%$) were the statistically significant factors in Fe(II) ions oxidation processes at a 95% confidence level. The comprehensive study elucidated a significant dependency relationship between the Fe(II) ions oxidation rate constants (k) and PO_4 –to– Fe(II) mole ratio. At pH 6.5, the optimum mole ratio was found to be 0.3 to reduce the k values. Conversely, the k values were observed to increase for the PO_4 –to– Fe(II) mole ratio > 1. This study showed that a typical chlorine dosage (2.2 mg/L) and DOM concentration (2.85 mg-C/L) present in drinking water were not statistically significant ($\alpha = 0.05$, $p > 0.05$) for a change in rate constants of a 3 mg/L initial Fe(II) ions in solution. However, an increment of the chlorine to ferrous iron mole ratio by a factor of ~ 2.5 resulted in an increase k values by a factor of ~ 10. The study conclusively suggested that the lowest Fe(II) ions oxidation rate constant would be obtained under low pH conditions (pH ≤ 6.5); chlorine dosage less than 2.2-mg/L and PO_4 –to– Fe(II) mole ratio ≈ 0.03 in the iron water systems. The findings for this study might have practical consequence for some water treatment processes and iron pipe distribution system issues.

[1] Rahman, M.S., Gagnon, G.A. 2014. Bench-scale evaluation of ferrous iron oxidation kinetics in drinking water: Effect of corrosion control and dissolved organic matter. *J Environ. Sci. Health A* **49** (1), 1-9.

4.2. Introduction

Cast iron pipes have been used to transport potable water for over 500 years, and corroded iron pipes are a constant source of Fe(II) ions in drinking water distribution systems (Sarin et al., 2004a). While the levels of Fe(II) ions are site specific to the water quality. The concentration of Fe(II) ions was found to be 7.2 mg/L, dry weight basis in a center sample; and 17.1 mg/L, dry weight basis in a side sample of 40–50 years-old iron pipe collected from the distribution systems in Melbourne, Australia (Lin et al., 2001). The release of iron from drinking water distribution system materials, and the nature of iron corrosion scales are controlled by the oxidation of Fe(II) ions (Sarin et al., 2004a).

Fe(II) ions are transient species in a redox system that continuously cycles iron between the two oxidation states. Thus, the rate at which Fe(II) ions are oxidized to Fe(III) is a critical determinant of how much iron is in the reduced state at any time. Over the last 35 years, a large number of studies have been made investigating Fe(II) ions oxidation in natural water (Stumm and Lee, 1961; Theis and Singer, 1974; Millero et al., 1995; Azher et al., 2008; Gonz´alez et al., 2010). These studies encouraged a number of additional investigations of the rate of Fe(II) ions oxidation process in well-defined aqueous solutions. Oxidation of aqueous Fe(II) ions by dissolved oxygen (DO) generates several secondary oxidants, i.e., superoxide ($O_2^{\cdot-}$), hydrogen peroxide (H_2O_2), hydroxyl radical ($OH^{\cdot}$), that may also contribute in Fe(II) ions oxidation processes (Tamura et al., 1976; King et al., 1995; Millero et al., 1995). The enormousness of their impacts on the overall rate constants of Fe(II) ions oxidation is a complex function of their association constants with Fe(II) ions (King et al., 1995; Millero et al., 1995), their ability to rummage $OH^{\cdot}$ and superoxide and their reactivity to their corresponding radicals (Rose and Waite, 2002). The most conventional mechanisms and sequences to describe the Fe(II) ions oxidation with O_2 in natural waters is the following Harber-Weiss mechanism (Weiss, 1935):

$$Fe(II) + O_2 \longrightarrow Fe(III) + O_2^{\cdot -} \quad (4.1)$$

$$Fe(II) + O_2^{\cdot -} + 2H^+ \longrightarrow Fe(III) + H_2O_2 \quad (4.2)$$

$$Fe(II) + H_2O_2 \longrightarrow Fe(III) + OH^{\cdot} + OH^- \quad (4.3)$$

$$Fe(II) + OH^{\cdot} \longrightarrow Fe(III) + OH^- \quad (4.4)$$

The overall rate constants for the reactions (1) to (4) are a function of the composition and physical-chemical properties of the solutions. The complete oxidation of Fe(II) ions by DO occurs over seconds to hours (h) depending on water chemistry during iron removal treatment or during water transport in iron pipe distribution systems.

Several commonly inorganic anions, including phosphate (Mitra and Matthews, 1985; Lytle and Snoeyink, 2002; Aitken-Rogers, 2004; Gonz´alez et al., 2010), chlorine (Folkes et al., 1995; Maddison et al., 2001; Gagnon et al., 2004; Lytle et al., 2004), and carbonate/bicarbonate (King et al., 1995) play a role in moderating Fe(II) ions oxidation processes. Dissolved organic material (DOM), which possesses the structural features of humic substances can lead to accelerate, abate, or have no effect on ferrous iron oxidation processes (Stumm and Lee, 1961; Theis and Singer, 1974; Liang et al., 1993). The magnitude of the effects has been shown to be dependent on a number of factors including iron and oxygen concentration (Rose and Waite, 2002), pH (Stumm, 1990; Millero et al., 1995; Morgan and Lahav, 2007; Gonz´alez et al., 2010), and free chlorine concentration (McNeill and Edwards, 2000). Free chlorine is the most widely applied disinfectant for treating drinking water in North America (AWWA, 2000; Health Canada, 2009). Studies have shown that disinfectant residuals (e.g., free chlorine and chloramine) also degrade water quality and pipe materials in distribution systems due to causing pipe corrosion (McNeill and Edwards, 2000; Eisnor and Gagnon, 2004). A previous study (Eisnor and Gagnon, 2004) in our research group conducted cast-iron pipe loop

experiments for the reaction period of 6 and 12 h using three different types of disinfectants; and observed that free chlorine and chloramine would increase iron release from background water quality levels. Therefore, it has been hypothesized that increase in the concentrations of disinfectants would be expected to increase Fe(II) ions oxidation. Last one century, different types of phosphate based corrosion inhibitors are widely used as chemical additives for mitigating iron corrosion in drinking water distribution systems. Several researchers have reported the benefits of using phosphate to control corrosion, and to reduce or to prevent iron, manganese, and calcium precipitation in distribution systems (Larson, 1957; McNeill and Edwards, 2000; Maddison et al., 2001).

In most previous studies, traditional one-factor-at-a-time experiments were tested to control the corrosion, while the influence of environmental factors simultaneously on the rate constants in Fe(II) ions oxidation is very limited. The objectives of this research were to identify and quantify the most important factors and their interaction on the changes in rate constants in ferrous iron oxidation processes in the systems containing four factors: (A) pH, (B) DOM, (C) phosphate and (D) disinfectant. This was accomplished using a 2^4 full factorial design approach at a 95% confidence level. The correlation between the rate constants of Fe(II) ions oxidation and the various factors (acting independently) was aimed to determine. To carry out this study in laboratory under the conditions simulating as closely as possible to potable water distribution systems, its principle aim is to enhance understanding of the Fe(II) ions oxidation processes in distribution systems. Understanding both homogeneous and heterogeneous parameters that affect the Fe(II) ions oxidation processes will be an important element to improve water quality in drinking water treatment and distribution systems.

4.3. Materials and methods

4.3.1. Kinetics of Fe(II) ions oxidation experiment

Fe(II) ions oxidation experiments were conducted in 1000 mL glass reaction cells using 1 L of ultrapure synthetic water. To start an experiment, 1 L of ultrapure synthetic water was added to a reaction cell. For adjusting water quality, 35 g of $NaHCO_3$ (assay: 100%, Fisher Scientific, USA) was added to obtain 5 mg-C/L as dissolved inorganic carbon (DIC) in water samples (Lytle and Snoeyink, 2002). The DO concentration in the reaction solutions was kept saturated and constant during each run corresponding to an oxygen partial pressure of 0.21 atm (DO $\approx$ 8.5 mg/L) using oxygen (Ultra Pure, Praxair, Canada). The Fe(II) ions oxidation kinetics experiments were conducted following a 2^4 full factorial design approach (Table A1 and A2 of Appendix A). The detailed method for Fe(II) ions oxidation kinetics experiments was described in Section 3.5.1 of Chapter 3. In addition to the 2^4 factorial design experimental protocols, extended kinetic studies were conducted for different pH values: 5.5 to 8.5, different concentrations of initial Fe(II) ions: 0.35 to 3 mg/L (0.72 x 10^{-5} to 5.37 x 10^{-5} M), different dosages of chlorine: 2.2 to 5.7 mg/L (6.19 x 10^{-5} to 16.06 x 10^{-5} M), and different dosages of phosphate: 0.5 to 12.5 mg-PO_4/L (0.53 x10^{-5} to 13.16 x 10^{-5} M PO_4) respectively in the same reaction systems.

4.3.2. Analytical methods

All pH measurements were made using an Accumet electrode and Accumet Excel, XL50 (Dual channel pH/ion/conductivity) meter (Fisher Scientific, Singapore). The pH meter was standardized daily using a three-point calibration with pH 4 (SB101-500), pH 7 (SB107-500), and pH 10 (SB115-500) buffer solutions (Fisher Scientific, USA) before taking reading in samples. DO was measured with a DO meter (VWR, SP5OD, SympHony, Thermo Orion, USA) with a DO probe (VWR, SympHony, Thermo Orion, UK). Phosphate concentration was measured by an ion chromatograph (761 Compact IC, Metrohm). Free chlorine concentration was determined using the colorimetric version of the N,N-diethyl-p-phenylenediamine (DPD) following the HACH 8021 method (HACH, 2005) at a wavelength of 530 nm using a DR/5000 UV Visible Spectrophotometer (HACH Co., Loveland, USA). Fe(II) ions concentration was measured colometrically by

the 1,10-phenanthroline method at a wavelength of 510 nm using a DR/5000 UV Spectrometer (HACH, 2005). The detailed description of analytical procedures for the measurement of water quality parameters such as pH, DO, DOC, free chlorine, Fe(II) ions and phosphate concentration are described in Section 3.4.1 of Chapter 3.

4.3.3. Kinetics

The kinetics of Fe(II) ions oxidation by oxygen (O_2) in laboratory systems have been first established by Stumm and Lee (1961), and the general rate law was found to be:

$$\frac{-d[\mathrm{Fe(II)}]}{dt} = k[\mathrm{Fe\ (II)}]\mathrm{P}o_2(\mathrm{OH}^-)^2 \qquad (4.5)$$

At constant pH and Po_2, equation (4.5) reduces to a first order reaction (Sung and Morgan, 1980):

$$\frac{-d[\mathrm{Fe(II)}]}{dt} = k_1[\mathrm{Fe(II)}] \qquad (4.6)$$

After integrating eq. (4.6) with time '*0*' to *'t'*, we can write

$$-ln\frac{[\mathrm{Fe\ (II)}]_t}{[\mathrm{Fe\ (II)}]_0} = k_1 t \qquad (4.7)$$

$$[Fe(II)]_t = [\mathrm{Fe(II)}]_o exp^{-k_1 t} \qquad (4.8)$$

The Pseudo-first-order rate constant, k_1 can be determined using the experimental data for the designed reaction periods (the slope of a linear plot of $(\ln[\mathrm{Fe(II)}/\mathrm{Fe(II)}_o]$ vs time). The Pseudo-first order kinetics with respect to Fe(II) ions also exhibit in the presence of inorganic/organic anions and DOM (Tamura et al., 1976; Davidson and Seed, 1983).

4.4. Results

In this study, a statistical approach based on a two-level (low and high) with four factors full factorial design experiments was chosen (Table A1 of Appendix A) to investigate the various parameters, and their possible interactions affecting the kinetics of Fe(II) ions oxidation processes. The range and levels of the studied variables corresponding to the response factor (rate constants, *k*) for this study is presented in Table 4.1. These variables and their levels were chosen based on the typical values in many drinking water distribution systems.

The significant factors affecting the iron oxidation rate constants were determined following the model marix of 2^4 full factorial design approach (Table A2 of Appendix A) by using windows version program, Minitab® 16 (MINITAB Inc., State College, Pennsylvania, USA) at a 95% confidence level; and the results are presented in Table 4.2. This study demonstrated that two main factors, i.e., pH and phosphate were statistically significant ($\alpha = 0.05,\ p < 0.05$) for changing the Fe(II) ions oxidation rate constants. However, DOM and chlorine, and their interactions did not have statistically significant effect ($\alpha = 0.05$) on the rate constants of Fe(II) ions oxidation process. The effects of input parameters on the kinetics of ferrous iron oxidation are graphically shown in Figure 4.1 to access visually their impact on Fe(II) ions oxidation process. Figure 4.1 depicts that the change in solution pH values from a lower (pH 6.5) to a higher level (pH 8.5) have a sharp effect in increase of Fe(II) ions oxidation rate constants having a positive

slope of 0.013. However, when the phosphate concentration was increased from a lower level (0 mg/L) to a higher level (1.5 mg-PO_4/L), a reverse trend was observed to decrease the rate constants (k) with a negative slope of -0.0094. A slight increment of Fe(II) ions oxidation rate constants was observed when chlorine concentration was increased from 0 to 2.2 mg/L with a positive slope of 0.0045 (Figure A3, Appendix A). However, DOM ($\approx$ 2.85 mg/L as DOC) did not show statistically ($\alpha = 0.05$) any significant impact on the rate constants in Fe(II) ions oxidation processes.

Table 4.1. Design matrix and experimental results for the iron oxidation rate constants, k (min^{-1}).

Exp. No.	Composition of synthetic water	Factors: pH unit (A)	DOM conc. (B)[I]	PO_4^{3-} conc. (C)[II]	Chlorine conc. (D)[III]	Reaction rate (k) constants (min^{-1})	r^2
1	$Fe(II) + O_2$	6.5	0.00	0.0	0.0	0.0085	0.99
2	$Fe(II) + O_2$	8.5	0.00	0 .0	0.0	0.0337	0.99
3	$Fe(II) + O_2 + DOM$	6.5	2.85	0.0	0.0	0.0097	0.99
4	$Fe(II) + O_2 + DOM$	8.5	2.85	0.0	0.0	0.016	0.98
5	$Fe(II) + O_2 + PO_4^{3-}$	6.5	0.00	1.5	0.0	0.0046	0.98
6	$Fe(II) + O_2 + PO_4^{3-}$	8.5	0.00	1.5	0.0	0.0018	0.97
7	$Fe(II) + O_2 + DOM + PO_4^{3-}$	6.5	2.85	1.5	0.0	0.0056	0.98
8	$Fe(II) + O_2 + DOM + PO_4^{3-}$	8.5	2.85	1.5	0.0	0.014	0.97
9	$Fe(II) + O_2 + Cl_2$	6.5	0.00	0.0	2.2	0.0087	0.98
10	$Fe(II) + O_2 + Cl_2$	8.5	0.00	0.0	2.2	0.0329	0.94
11	$Fe(II) + O_2 + DOM + Cl_2$	6.5	2.85	0.0	2.2	0.0102	0.98
12	$Fe(II) + O_2 + DOM + Cl_2$	8.5	2.85	0.0	2.2	0.0298	0.97
13	$Fe(II) + O_2 + PO_4^{3-} + Cl_2$	6.5	0.00	1.5	2.2	0.0048	0.94
14	$Fe(II) + O_2 + PO_4^{3-} + Cl_2$	8.5	0.00	1.5	2.2	0.0203	0.99
15	$Fe(II) + O_2 + DOM + PO_4^{3-} + Cl_2$	6.5	2.85	1.5	2.2	0.0085	0.97
16	$Fe(II) + O_2 + DOM + PO_4^{3-} + Cl_2$	8.5	2.85	1.5	2.2	0.0148	0.95

[I, II and III] Unit: mg/L

Table 4.2. Estimated effects, statistical significance for Fe(II) ions oxidation rate constants (min^{-1})

Code	Term	Effect Estimate	SE Coef	*t*-value	*p*-value	Remark	Impact
Main effects							
A	pH	0.0128	0.0015	4.340	0.007	*Significant*	42.5%
B	DOM	-0.0008	0.0015	-0.280	0.788	*Insignificant*	0.2%
C	PO_4^{3-}	-0.0094	0.0015	-3.170	0.025	*Significant*	22.7%
D	Chlorine	0.0045	0.0015	1.530	0.188	*Insignificant*	5.2%
Interaction effects							
AB	pH and DOM	-0.0027	0.0015	-0.910	0.405	*Insignificant*	1.9%
AC	pH and PO_4^{3-}	-0.0060	0.0015	-2.020	0.099	*Insignificant*	9.2%
AD	pH and Chlorine	0.0036	0.0015	1.200	0.282	*Insignificant*	3.3%
BC	DOM and PO_4^{3-}	0.0037	0.0015	1.250	0.268	*Insignificant*	3.5%
BD	DOM and Chlorine	0.0000	0.0015	0.000	0.997	*Insignificant*	0.0%
CD	PO_4^{3-} and Chlorine	0.0011	0.0015	0.370	0.728	*Insignificant*	0.3%

Table 4.3. Pearson's correlation matrices between the rate constants (*k*), solution pH, DOM, phosphate and chlorine concentration in iron water systems.

Variable	*k*	pH	DOM	PO_4^{3-}	Chlorine
Fe(II) ions oxidation rate constants, *k*	1				
Solution pH	0.69[b]	1			
Dissolved organic matter (DOM)	0.09	0.24	1		
Phosphate dosage (PO_4^{3-})	-0.41[a]	0.02	0.02	1	
Chlorine concentration	0.27	0.175	0.18	-0.06	1

[a] Correlation is significant at the 0.05 level (2-tailed)

[b] Correlation is significant at the 0.01 level (2-tailed)

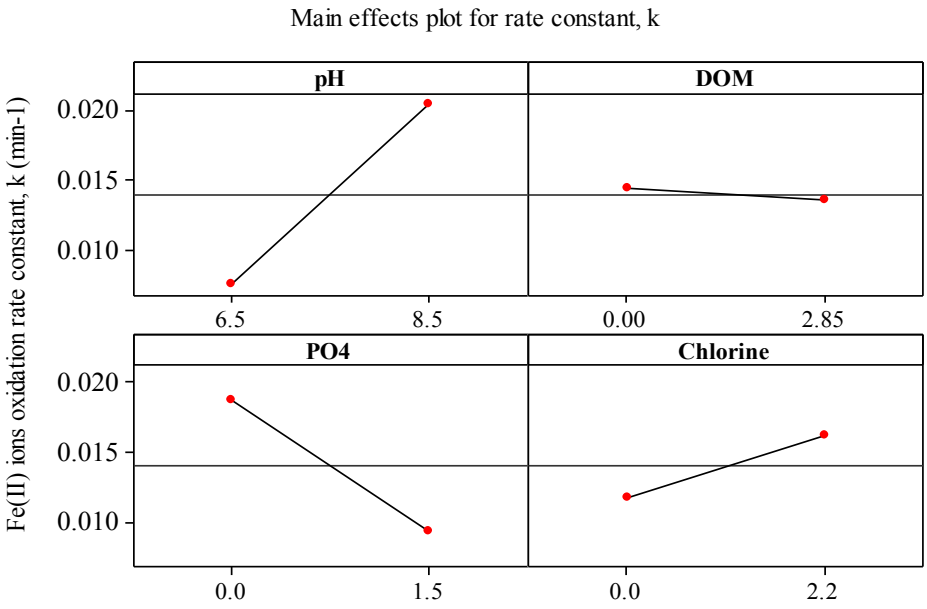

Figure 4.1. Plots of Fe(II) ions oxidation rate constants for the main effects of solution pH, DOM, phosphate and chlorine dosages following 2^4 full factorial design approach ($\alpha = 0.05$, $p < 0.05$).

The Pearson's correlation matrix analysis between all the independent (e.g., pH, DOC, PO_4, and chlorine); and the dependent (rate constant, k) variables in synthetic water samples (No of observation 48) was performed using the software, 'IBM SPSS Statistic 20' for windows (IBM, USA), and the results are presented in Table 4.3. This analysis revealed a positive and strong correlation between the solution pH values and the rate constants ($r = 0.69$, $p < 0.0001$); and a negative and moderate correlation between the phosphate dosages and the rate constants ($r = 0.41$, $p < 0.05$). The correlation among the other factors can also be found in Table 4.3. Further details of the correlation can be found elsewhere (Montgomery, 2009). The results of Pearson's correlation matrix were observed to be consistent with the factorial design analysis data (Table 4.2).

However, in addition to the factorial design approach for typical water quality parameters, consequently a comprehensive study was conducted herein with a wide range of the variables to find out the impact of different levels of each individual variable on Fe(II) ions oxidation processes (rate constants) in $NaHCO_3$ buffered synthetic water systems.

4.4.1. Effect of pH

From the factorial design approach, it was observed that pH was the most significant factor ($\alpha = 0.05$, $p = 0.007$) on the kinetics of Fe(II) ions oxidation processes among all factors studied here (Table 4.2). This study elucidated that the change in pH values from a lower (pH 6.5) to a higher level (pH 8.5) accounted to decrease the Fe^{2+} ions oxidation rate constants of 42.5% for total variability. Consequently, in addition to the factorial design approach, an extended study for the pH values of 5.5 and 7.5 were carried out in the control water systems (in absence of DOM, chlorine and phosphate), and the results are shown in Figure 4.2. The study examining Fe(II) ions oxidation kinetics by oxygen revealed that the rate constants (k) were increased with the increase in pH values from 5.5 to 8.5.

The kinetics study revealed that after 60 min of the reaction period, the percentages of Fe(II) ions oxidation were 28.34, 41.33, 67.27, and 72.27 for the pH values of 5.5, 6.5, 7.5, and 8.5 respectively for an initial Fe(II) ions concentration of 3 mg/L (5.37×10^{-5} M) in solutions. However, the results of this study revealed that over the reaction period of 150 min, 55.67%, 72.66%, 97.69%, and 99 % of the 3 mg/L Fe(II) ions were oxidized for the pH values of 5.5, 6.5, 7.5 and 8.5, respectively (Table A5 of Appendix A). This study demonstrated that over the reaction period of 150 min, almost the total Fe(II) ions in solution were converted to Fe(III) ions for the pH values of 7.5 and above. Therefore, it could be concluded that apparently, Fe(II) ions oxidation

rates were increasingly faster above the pH value of 6.5. The same trend was observed by other researchers who conducted the Fe(II) ions oxidation processes for different pH values in synthetic water (Davidson and Seed, 1983), fresh water (Tamura et al., 1976; Millero et al., 1995; Azher et al., 2008) and seawater (Gonz´alez et al., 2010). Figure 4.2 shows that the evaluation of Fe(II) ions with reaction time for the studied pH values follow an exponential decrease. This study revealed that the change in pH values from 5.5 to 8.5, the apparent half-life ($t_{1/2}$) of the ferrous iron oxidation is decreased 6 times (Table A5 of Appendix A).

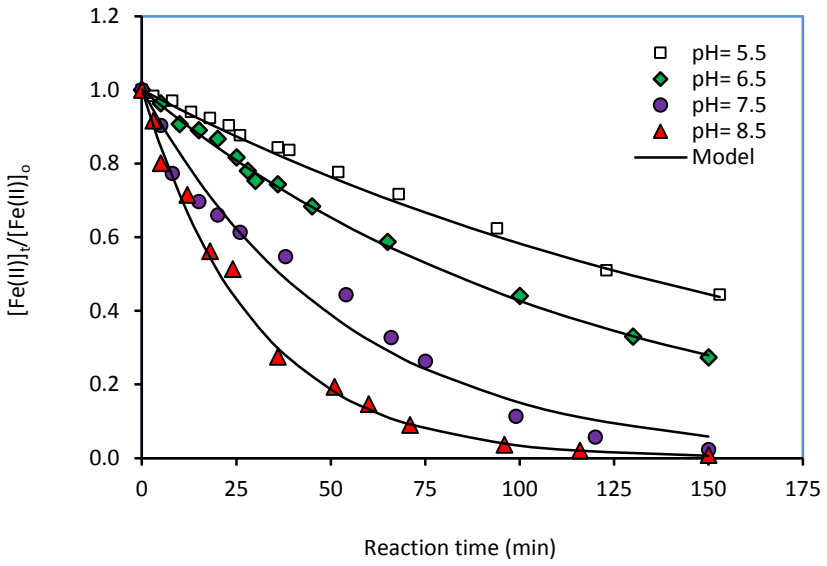

Figure 4.2. Effect of pH on the oxygenation kinetics of ferrous iron in synthetic water samples ($[Fe(II)]_o \approx 3$ mg/L, 21 ± 1 °C).

4.4.2. Effect of phosphate

The factorial design approach elucidated that PO_4 was the second significant factor ($\alpha = 0.05$, $p = 0.025$); and the change in phosphate dosages from 0 to 1.5 mg/L accounted to decrease the overall rate constants 22.7% of total variability in Fe(II) ions oxidation process (Table 4.2).

The effect of phosphate dosages in the Fe(II) ions oxidation have been reported in the literature often with the higher dosages of PO_4 ranging from 6.5 to 1665 mg-PO_4/L (0.07 to 17.5 mM PO_4) (Mitra and Matthews, 1985; Aitken-Rogers, 2004; Gonz´alez et al., 2010). However, only a few key studies have been shown to use a lower content of phosphate in Fe(II) ions oxidation processes. In general, it has been reported that higher dosages of phosphate increase Fe(II) ions oxidation rate (Mitra and Matthews, 1985; Aitken-Rogers, 2004; Gonz´alez et al., 2010). Using a lower phosphate dosage of 1.5 mg-PO_4/L (1.6×10^{-5} M PO_4), which is more typical in drinking water distribution systems, this study showed that iron oxidation rate constants were decreased compared with the control water systems (in absence of phosphate) (Figure 4.3). Our results corroborate similar observation by other investigators (Wolthoorn et al., 2004; Lytle, 2005). Lytle (2005) has conducted Fe(II) ions oxidation batch tests in $NaHCO_3$ buffered synthetic water systems, and has reported that the addition of orthophosphate (3 mg-PO_4/L) in iron water systems significantly decreased the rate of Fe(II) ions oxidation. On the other hand, the heterogeneous oxidation of Fe(II) ions in the synthetic ground water systems has been reported to be retarded when phosphate is present along with other ions (Wolthoorn et al., 2004).

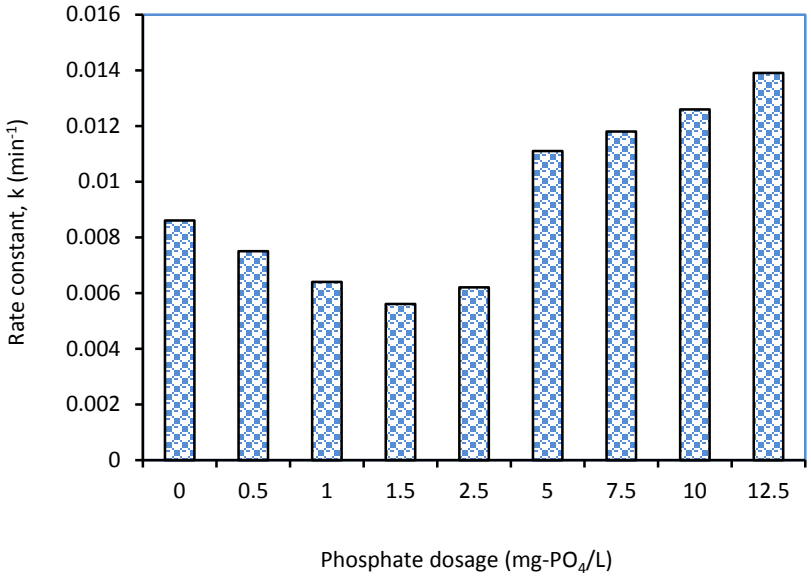

Figure 4.3. Effect of phosphate dosage on the rate constants in Fe(II) ions oxidation processes in synthetic water samples ($[Fe(II)]_o \approx 3$ mg/L, pH= 6.5, 21 ± 1 °C).

The effect of phosphate on Fe(II) ions oxidation processes seems contradictory; therefore along with the factorial design approach, a more extensive investigation was subsequently carried out to explore the effect of different dosages of phosphate ranging from 0.5 to 12.5 mg (0.53×10^{-5} to 13.16×10^{-5} M PO_4) in the same reaction systems. Consequently, it was observed that in the presence of different dosages of phosphate in solution for the initial Fe(II) ions concentration of 3 mg/L, and at a constant pH value of 6.5, the rate constants decreased gradually with the increase in phosphate dosages, and reached an optimum level that was maintained at 1.5 mg-PO_4/L (PO_4 –to– Fe(II) mole ratio ≈ 0.3) in solution (Figure 4.3). Figure 4.3 shows that when the initial phosphate ions concentration is increased to 5 mg-PO_4/L (PO_4 –to– Fe(II) mole ratio ≈ 1), the iron oxidation rate constants are observed to increase compared with the systems having no phosphate in solution.

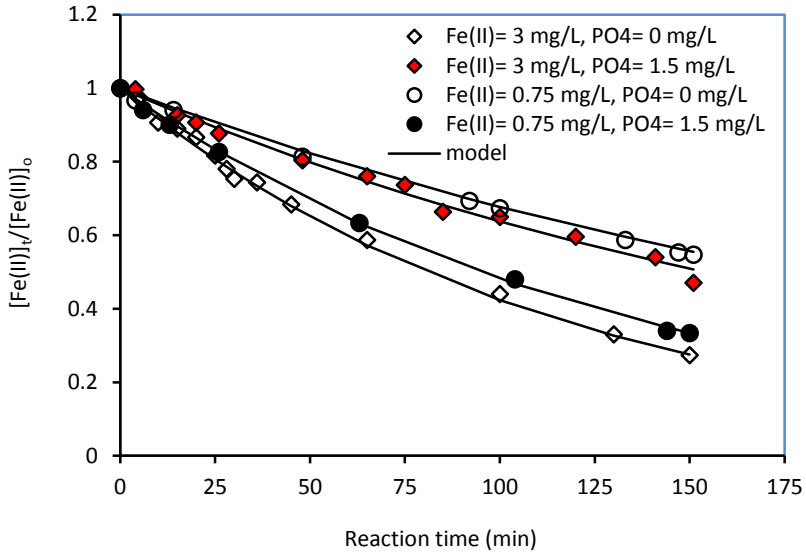

Figure 4.4. Effect of phosphate and initial Fe(II) ions concentrations on oxidation rate constants in synthetic water samples (pH= 6.5, 21 ± 1 °C).

The effect of different concentrations of Fe(II) ions in solution for a fixed initial phosphate ions concentration of 1.5 mg-PO_4/L (1.6 x 10^{-5} M PO_4), was also investigated. This study revealed that the addition of phosphate (1.5 mg-PO_4/L) for the initial Fe(II) ions concentration of 3 mg-PO_4/L (PO_4 –to– Fe(II) mole ratio ≈ 0.29) at pH 6.5, reduced the *k* values from 0.0086 to 0.0046 min^{-1} compared with the systems, where phosphate was not present. In contrast, when a lower concentration of Fe(II) ions (0.75 mg/L) was used for the same phosphate dosage of 1.5 mg-PO_4/L (PO_4 –to– Fe(II) mole ratio ≈ 1.15) in the solution, an opposite trend was observed to increase *k* from 0.0039 to 0.0073 min^{-1} (Figure 4.4). This finding corroborates similar observation for the effect of different phosphate dosages on changing rate constants. Therefore, it has been suggested that with the increase in PO_4 –to– Fe(II) mole ratios ≥ 1, the oxidation rate constants of Fe(II) ions are increased. However, it is assumed that Fe(II) ions oxidation rate constants are correlated with the phosphate dosages and the initial Fe(II) ions

concentration in aqueous systems. This hypothesis is statistically substantiated by the Pearson's correlation matrix presents in Table 4.3 that shows a moderate correlation between the phosphate dosages and the rate constants.

4.4.3. Effect of chlorine

The WHO drinking water standards state that 2 to 3 mg/L chlorine should be added to water in order to gain a satisfactory disinfection and residual concentration for protecting water from microbial contamination in water distribution systems (WHO, 2008). Therefore, 2.2 mg/L chlorine dosage was selected for the factorial design study. This study revealed that 2.2 mg/L of free chlorine (HOCl and OCl^-) was mostly occupied by the 3 mg/L of Fe(II) ions within a short reaction time (Figure 4.5). In contrast, when the concentrations of Fe(II) ions were reduced for the same chlorine dosage of 2.2 mg/L in solutions, the measurable chlorine concentrations were found at the end of the designated reaction periods of 150 min, even though after 3 days (4320 min) of the reaction period (Figure 4.5). The result from this study demonstrates that the oxidation of Fe(II) ions is one of the main reaction mechanisms to reduce the disinfectant residuals in iron water systems. These findings are in general agreement to the reported results published in literature (Maddison et al., 2001; Cantor et al., 2003; Gagnon et al., 2008), which acknowledge that chlorine could be chemically reduced by the corrosion products, i.e., Fe(II) ions in iron pipe drinking water distribution systems, and also participating in iron oxidation processes. However, this study exhibited that Fe(II) ions were oxidized much faster at the initial stage within a few minutes, when the designated chlorine dosage (2.2 mg/L) was introduced into the systems. Thereafter, the oxidation rate for chlorine along with oxygen was very close to the oxidation rate for oxygen alone. Previous studies have demonstrated the same trend that Fe(II) ions react with HOCl much faster than other oxidant/s (Folkes et al., 1995).

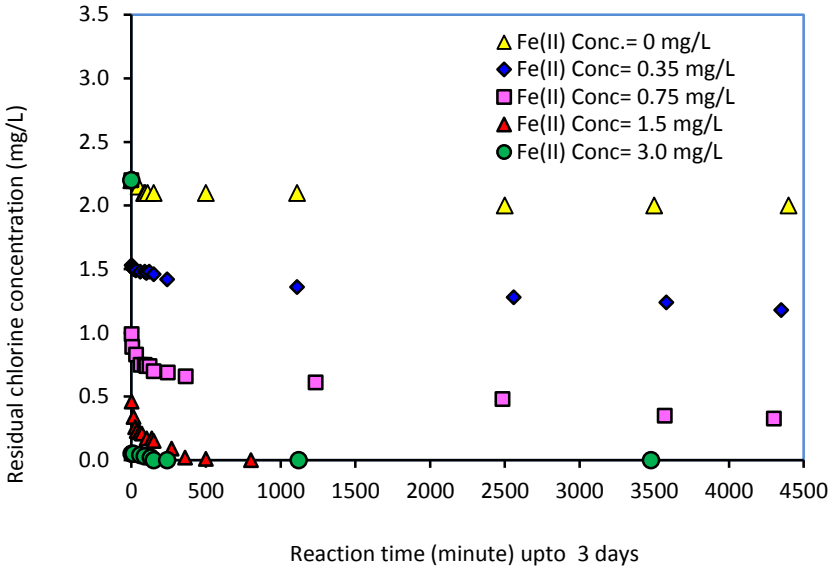

Figure 4.5. Effect of the initial concentrations of Fe(II) ions on the residual chlorine concentrations in synthetic water samples (pH= 6.5, 21 ± 1 °C).

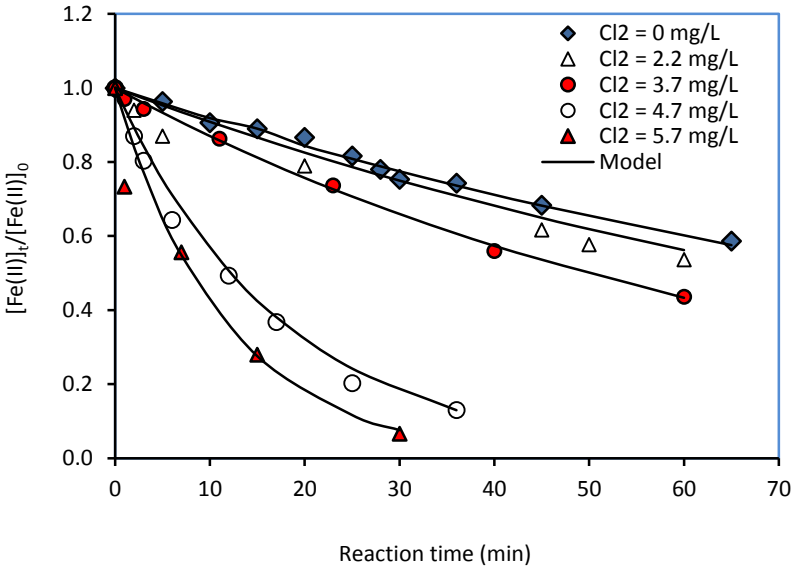

Figure 4.6. Effect of initial chlorine concentration on the rate of ferrous iron oxidation process ($[Fe(II)]_o \approx 3$ mg/L, pH= 6.5, 21 ± 1 °C).

The factorial design approach illustrated that a dosage of 2.2 mg/L free chlorine was not statistically significant ($\alpha = 0.05, p > 0.05$) on the kinetics for 3 mg/L of Fe(II) ions oxidation processes. However, the statistical analysis revealed that chlorine at designated dosage (2.2 mg/L) had overall contribution of 5.2% to increase k (Table 4.2). Therefore, an extended study for the various chlorine dosages ranging from 2.2 to 5.7 mg/L (6.19 x 10^{-5} to 16.06 x 10^{-5} M) were used to conduct experiments. The results of this study revealed that the oxidation rates of Fe(II) ions for the chlorine concentrations of 2.2 to 2.7 mg/L plus oxygen was very close to the oxidation rate for oxygen alone (Table 4.4). However, when the chlorine concentration was increased to 4.7 mg/L (chlorine : Fe(II) ≈ 2.5), a big difference was observed to increase the Fe(II) ions oxidation rates (Figure 4.6). It was also observed that after the reaction period of 35 min, the Fe(II) ions concentrations in the solutions were almost zero for using the chlorine dosages of 4.7 and 5.7 mg/L in the same reaction systems. This study revealed an important finding that an increment of the chlorine to Fe(II) mole ratio by a factor of ≈ 2.5 resulted an increase in oxidation rate constants by a factor of ≈ 10 (Table 4.4).

Table 4.4. Effect of initial chlorine dosage on the oxidation rate constants, k of Fe(II) ions in $NaHCO_3$ buffered synthetic water ($[Fe(II)]_o \approx 3$ mg/L, pH= 6.5, 21 ± 1 °C).

Exp. No.	pH value in solutions	Initial chlorine concentration (mg/L)	Mole ratio of chlorine –to-Fe(II) ions	Rate constants k (min^{-1})
1	6.5	0.0 mg/L	-	0.0085
2	6.5	2.2 mg/L	1.153	0.0087
3	6.5	2.7 mg/L	1.154	0.0096
4	6.5	3.7 mg/L	1.941	0.0139
5	6.5	4.7 mg/L	2.465	0.0578
6	6.5	5.7 mg/L	2.99	0.0877

4.4.4. Effect of dissolved organic matter

The factorial design approach for this study revealed that 2.85 mg-C/L of DOM in synthetic water systems was not statistically significant ($\alpha = 0.05$, $p = 0.788$) on the changes of rate constants in Fe(II) ions oxidation processes. The statistical analysis illustrated that the designated DOM concentration accounted for only 0.19% contribution of total variability on the changes of overall rate constants values in the Fe(II) ions oxidation processes (Table 4.2, Figure 4.1). Therefore, it has been suggested that there is little influence of DOM on the changes of rate constants in the same reaction systems for the reaction period of 2.5 h. The findings of this study are within a reasonable agreement with the published work by Liang et al. (1993), who have demonstrated that the DOM containing mainly carboxylic (COOH) functional groups are bound to soluble Fe(II) ions center forming a bidentate complex or forming a ring structure, and these Fe(II)−organic complexation is hypothesized to be the mechanism for retarding the Fe(II) ions oxidation as follows (Eqs. (4.7) and (4.8)):

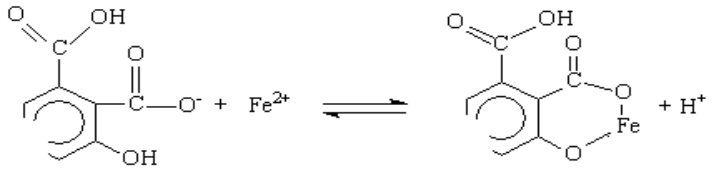

(4.7)

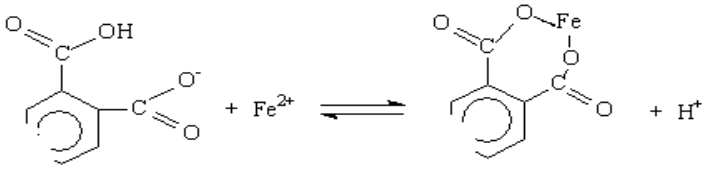

(4.8)

4.5. Discussion

This study examining Fe(II) ions oxidation kinetics by oxygen revealed that the rate constants (k) were increased with the increase in pH values from 5.5 to 8.5, which indicates that Fe^{2+} ions were more reductant at a higher pH value. The reactions were looked as a complicated function of the solution pH with an evident hydroxide ion dependency. Several authors (Stumm, 1990; King et al., 1995; Millero et al., 1995) have presumed this complex pH necessity to happen due to the consistent oxidation of Fe(II) ions and its hydroxo complexes ($Fe(OH)^{+}$, $Fe(OH)_2$, $Fe(OH)_3^{-}$). The "non-hydrolyzed ferrous species" are less willingly oxidized than "hydrolysed ferrous iron species" in the following order $Fe^{2+} << Fe(OH)^{+} << Fe(OH)^{o}_{2(aq)}$ (Morgan and Lahav, 2007). On the other hand, the hydroxyl (OH^{-}) ligands provide electron density to the Fe^{2+} atoms through both the σ and π systems (Stumm, 1990); and that might be a reason to make Fe^{2+} ions more reductant at a higher pH value.

A dependency relationship of the iron oxidation rate constants with the PO_4 –to– Fe(II) mole ratios were elucidated in this investigation. It was observed that the Fe(II) ions oxidation rate constants were shown to be decreased gradually with the increase in phosphate dosages, and reached an optimum level that was maintained at 1.5 mg-PO_4/L (PO_4 –to– Fe(II) mole ratio ≈ 0.3). However, for the increases in phosphate to iron mole ratios above 1, the rate constants were observed to increase compared with the systems having no phosphate in solutions. This can be attributed to two main reasons. First: when PO_4 –to– Fe(II) mole ratios are ≤ 0.5, Fe(II) ions possibly dominate the reactions; and vivianite, $Fe_3(PO_4)_2$ (Wang and Waite, 2010; Walpersdorf et al., 2012); and Fe(II)-phosphate species: $FeH_2PO_4^{+}$, $FeHPO_4$ and $FePO_4^{-}$ (Mao et al., 2011) are formed. It has been reported that vivianite ($Fe_3(PO_4)_2$) forms at high Fe(II) ions concentration in solution (Walpersdorf et al., 2012); and it is an important sink for dissolved Fe(II) ions (Miot et al., 2009). On the other hand, $FeH_2PO_4^{+}$ and $FeHPO_4$ were less reactive with oxygen (Mao et al., 2011). Therefore, this might be a possible reason to decrease/retard

Fe(II) ions oxidation. Second: when the PO_4 –to– Fe(II) mole ratio > 1, PO_4^{3-} possibly dominate the reactions; and the excess phosphate species (e.g., $H_2PO_4^-$, HPO_4^{2-}, and PO_4^{3-}) increase the binding of phosphate with Fe(II) ions, thereby shifting its redox potential to more negative and thus facilitating its oxidation (Cheng and Chasteen, 1991).

Consequently, this study demonstrated that a typical chlorine dosage of 2.2 mg/L was not statistically significant on the change in oxidation rates for an initial 3 mg/L Fe(II) ions in solutions. However, the comprehensive study revealed that a higher dosage of chlorine, especially chlorine to Fe(II) mole ratio > 2, a significant change on the rate constant in Fe(II) ions oxidation process was observed, and it was more pronounced with the increase in chlorine dosages in solutions. This could have happened due to the reasons that with the increase of initial chlorine concentrations in iron water systems, it oxidizes Fe(II) ions more shows in Eqs. 4.9 and 4.10, and afterword, it generates chloride ions (Wang et al., 2012). Consequently, these chloride ions are increased in parallel, and excess chloride ions produce some intermediate oxidants (chlorine radical i.e., Cl_3^-, Cl_2^-), which might have participated in the iron oxidation processes shows in Eqs. (4.11) to (4.13) (Hochhauser and Taube, 1947; Crabtree and Schaeper, 1966).

$$6Fe^{2+} + 3OCl^- + 3H_2O \rightleftharpoons 2Fe(OH)_3 + 4Fe^{3+} + 3Cl^- \quad (4.9)$$

$$2Fe^{2+} + HOCl + H^+ \rightleftharpoons 2Fe^{3+} + Cl^- + H_2O \quad (4.10)$$

$$Fe^{2+} + Cl_3^- \rightarrow Fe^{3+} + Cl_2^- + Cl^- \quad (4.11)$$

$$Fe^{2+} + Cl_2^- \rightarrow Fe^{3+} + 2Cl^- \quad (4.12)$$

$$Fe^{2+} + 2Cl^- \rightarrow Fe^{3+} + Cl_2 \quad (4.13)$$

The results of this investigation also revealed that at pH value of 6.5, a typical concentration of dissolved organic matter (2.85 mg-C/L) present in solution increased slightly the Fe(II) ions oxidation rates. The experimental design approach demonstrated only 0.18% contribution of DOM on the changes of overall rate constants. Several possible reasons behind the role of DOM on Fe(II) ions oxidation process have been reported in the literature (Theis and Singer, 1974; Liang et al., 1993). Theis and Singer (1974) have conducted polarographic analyses on the complexation of Fe(II) ions with organic acids, and have demonstrated that organic matter irrevocably bound to Fe(II) ions. Therefore, the reaction mechanisms limit Fe(II) ions oxidation processes, and its release into solutions. Conversely, the inhibition of Fe(II) ions oxidation by organic species has involved the catalytic oxidation of Fe(II) ions followed by the reduction of Fe(III) ions by organic substances Theis and Singer, 1974; Liang et al., 1993.

Eventually, the total results of this study coupled with the results of other have led to develop a conceptual model to explain visually the role of phosphate based corrosion inhibitor, DOM, and disinfectant residuals on the changes in rate constants of Fe(II) ions oxidation processes. A schematic of this model is illustrated in Figure 4.7. Figure 4.7 shows that in absence of corrosion inhibitor and DOM, Fe(II) ions are oxidized slowly by oxygen (Reaction 4.1a of Figure 4.7), and when chlorine is introduced in the system, the oxidation is quite rapid especially with the increase in pH values (Reaction 4.1b of Figure 4.7). In the presence of lower dosage of PO_4 (PO_4 –to– Fe(II) mole ratios ≤ 0.5), several soluble iron-phospate complexation species are formed (Reaction 4.2a of Figure 4.7). However, Fe(II) ions are oxidized to Fe(III) when a higher dosage of phosphate (PO_4 –to– Fe(II) mole ratios > 1) is introduced into the systems (Reaction 4.2b of Figure 4.7). On the other hand, when a significant concentration of DOM is present, a complex reaction with Fe(II) ions is occurred (Reaction 4.3 of Figure 4.7). The oxidation of Fe(II)−DOM complexed proceeds via a slow step (experimental design approach shows in Table 4.2 that for a reaction period of 2.5 h, DOM has only 0.19% contribution of Fe(II) ions rate constant) to form the corresponding Fe(III−DOM) complex. The

fractions of ferrous iron complexed or oxidezed depend on the pH value and quantity of DOM present in the systems (Theis and Singer, 1974).

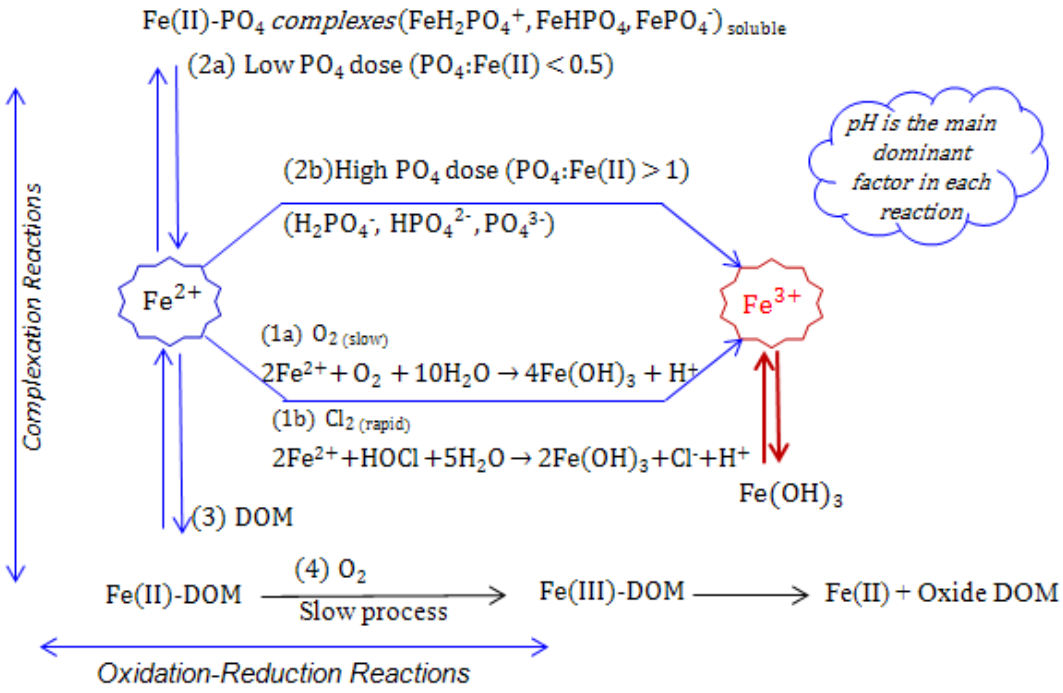

Figure 4.7. Schematic diagram for a conceptual model which describes the role of phosphate based corrosion inhibitor, dissolved organic matter and disinfectant on the behaviors of iron in drinking water distribution systems. Oxidation-reduction reactions are indicated horizontally, while the complexation reactions are indicated vertically.

4.6. Conclusions

The kinetics study for all reaction systems in bicarbonate buffered water exhibits the first order behavior with respect to the concentration of Fe(II) ions having a good agreement with r^2 values. The study revealed that pH was the most ($\alpha = 0.05$, $p < 0.05$) significant factor on the change of rate constants in the ferrous iron oxidation processes followed by phosphate. The Pearson's correlation matrices revealed a strong correlation ($r = 0.69$, $p < 0.001$) between the rate constants and the pH values; and a moderate correlation ($r = 0.41$, $p < 0.05$) between the rate constants and the phosphate dosages. A dependency relationship of the iron oxidation rate constants with pH and the PO_4 –to– Fe(II) mole ratios were elucidated in this investigation. This study revealed that a typical DOM (2.85 mg-C/L) and chlorine (2.2 mg/L) concentrations present in drinking water did not significantly ($\alpha = 0.69$, $p > 0.05$) affect the rate constants for an initial Fe(II) ions concentration of 3 mg/L in solution. However, an increment of the chlorine to the Fe(II) mole ratio of ~ 2.5 fold showed an increment of the iron oxidation rate constants of 10 fold. The investigation involved four factors with different levels shows that the lowest Fe(II) ions oxidation rate constants would appear to be obtained when pH value was 6.5, chlorine dosage was < 2.2 and PO_4 –to– Fe(II) mole ratio was ≈ 0.3 in the iron water systems. The research findings have practical implications related to both iron pipe drinking water distribution systems and water treatment issues.

CHAPTER 5. BENCH-SCALE EVALUATION OF DRINKING WATER TREATMENT PARAMETERS ON IRON PARTICLES AND WATER QUALITY[2]

5.1. Abstract

Discoloration of water resulting from suspended iron particles is one of the main customer complaints received by water suppliers. However, understanding the mechanisms of discoloration as well as role of materials involved in the processes is limited. In this study, an array of bench scale experiments were conducted to evaluate the impact of the most common variables (e.g., pH, PO_4, Cl_2, and DOM) on the properties of iron particles and suspensions, which derived from the oxygenation of Fe(II) ions in $NaHCO_3$ buffered synthetic water systems. The most important factors as well as their rank influencing iron suspension color and turbidity formation were identified for a range of typical water quality parameters. This was accomplished using a 2^4 full factorial design approach at a 95% confidence level. The statistical analysis revealed that phosphate was found to be the most significant factor to alter color (contribution: 37.9%) and turbidity (contribution: 45.5%) in iron-water system. A comprehensive study revealed that phosphate and chlorine produced iron suspension with reduced color and turbidity, made ζ-potential more negative, reduced average particle sizes, and increased iron suspension stability. In the presence of DOM, color was observed to increase but a reverse trend was observed to decrease the turbidity and to alter particle size distribution. HPSEC results suggest that higher molecular weight fractions of DOM tend to adsorb onto the surfaces of iron particles at early stage, resulting in alteration of the surface charge of iron particles. This in turn limits particles aggregation and makes iron colloids highly stable. This study conclusively demonstrated that a lower content of iron suspension color and turbidity would appear to be obtained in presence of a phosphate based corrosion inhibitor at a pH value of 6.5 compared to a pH value of 8.5. The same trend was observed in presence of DOM. This study also suggested that iron colloid suspension color and turbidity in chlorinated drinking water systems could be lower than non-chlorinated systems.

[2] Rahman, M.S., Gagnon, G.A. 2014. Bench-scale evaluation of drinking water treatment parameters on iron particles and water quality, *Water Res.* 48, 137-147.

5.2. Introduction

In water distribution systems, most of the iron pipes have been in place for more than a century and are corroded, leading to continuous release of Fe(II) ions into drinking water distribution systems. These Fe(II) ions are oxidized to Fe(III) ions (Sarin et al., 2004a) that cause coloration in water. The concentrations of Fe(II) ions in water distribution systems were reported up to 3 mg/L (Kirmeyer et al., 2000), and under anoxic conditions, aqueous Fe(II) ions concentrations of up to 1.11 mg-Fe(II)/L (0.02 mM) were observed in a pipe loop reactor that was constructed using a 70 years old galvanized iron pipe (Sarin et al., 2004a). USEPA recommends the secondary drinking water regulation for dissolved iron as 0.3 mg/L, and when iron is present greater than 0.3 mg/L in drinking water, can cause unpleasant metallic taste and rusty color (Cham et al., 2010). Iron alone in water does not pose an identified human health hazard; however, some trace impurities (e.g., metals, organic compounds, and microorganisms) adsorb onto iron particles and may reason adverse health effects (Lytle and Snoeyink, 2002).

Deposited iron formed by oxidized Fe(II) ions lead to high turbidity in the distribution systems (Sharma et al., 2001). The releases of soluble or particulate iron corrosion by-products into water reduces its aesthetic quality (i.e., color, staining, turbidity), and frequently leads to common problem of 'red water' at the tap (Sharma et al., 2001; McNeill and Edwards, 2001, Sarin et al., 2004a). The formation of red water depends on several factors and a sequence of steps including oxidation, hydrolysis, polymerization, and precipitation (Lytle et al., 2004). Red water, or rusty water, is generally attributed to ferric hydroxide. Upon contact to mainly oxygen or disinfectant during water treatment and distribution systems, soluble Fe(II) ions are oxidized to insoluble Fe(III) form following the equations 5.1 and 5.2 (McNeill and Edwards, 2000; Lytle et al., 2004), which readily precipitate and responsible for colored water.

$$4Fe^{2+} + O_2(aq) + 10H_2O \rightarrow 4Fe(OH)_3(s) + 8H^+ \quad (5.1)$$

$$Fe^{2+} + HOCl + 5H_2O \rightarrow 2Fe(OH)_3(s) + Cl^- + 5H^+ \quad (5.2)$$

Previously it has been reported in literature that oxygen is not a strong oxidant, and the rate of Fe(II) ions oxidation is strongly dependent on pH that is also influenced by other water chemistry factors, i.e., residual chlorine, phosphate based corrosion inhibitor and DOM (Stumm and Lee, 1961; Tamura et al., 1976; Mitra and Matthews, 1985; Millero et al., 1995; Maddison et al., 2001; Gagnon et al., 2004; Lytle et al., 2004). Free chlorine is the most extensively applied disinfectant for treating drinking water in North America (AWWA, 2000). Studies have shown that residual chlorine reacts rapidly with soluble Fe(II) ions at pH values found in drinking water distribution systems (Clement et al., 2002; Eisnor and Gagnon, 2004; Rahman and Gagnon, 2014b). Conversely, phosphate based corrosion inhibitors are alternative additive for drinking water for mitigating metal corrosion (Maddison et al., 2001; Edwards and McNeill, 2002) and red colored water problems. Dissolved organic matter (DOM), which possess the structural features of humic substances can lead to accelerate, abate, or have no effect on oxidation of Fe(II) ions (Stumm and Lee, 1961; Serikov et al., 2009). In addition, the magnitude of the effects for DOM has been shown to be dependent on several factors including iron and oxygen concentrations (Rose and Waite, 2002), and pH (Morgan and Lahav, 2007). These factors have significant influence on the aggregation behavior of DOM with the iron colloids that might be one of the reasons to degrade water quality (Stumm and Lee, 1961; Serikov et al., 2009). The manner in which these mechanisms function to change the color and particle size in drinking water through the iron pipe distribution systems is depicted by the following schematic diagram (Figure 5.1).

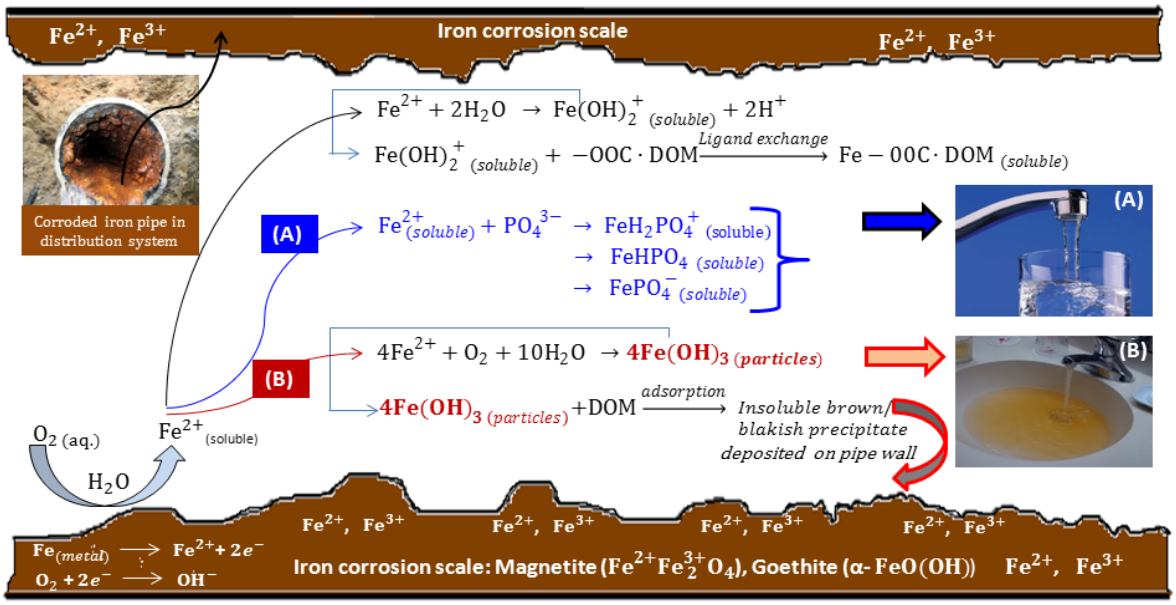

Figure 5.1. Schematic diagram for the reaction mechanisms that possibly occur to change the water color and particle size in distribution system.

Nearly all of the reports published on corrosion control deal only with the control of Fe(II) and Fe(III) ions release rather than the production or reduction of turbidity and color in drinking water distribution systems. Turbidity and color in drinking water caused by the oxidation of soluble Fe(II) ions to insoluble Fe(III) ions are most noticeable and probably the most important to consumers, which are not documented well as a part of corrosion study. Understanding the impact of different factors on the properties of the resulting iron particles is very important to improve the water quality in drinking water treatment and distribution systems. Unfortunately, the mechanisms and materials causing discolor in water are limited in current literature. Therefore, the aims of this study are (1) to evaluate the most important environmental parameters on the formation of iron suspension color and turbidity following a 2^4 full factorial design approach, (2) to investigate the mechanisms causing high color and turbidity in water, (3) to characterize

the iron particles derived from the oxygenation of Fe(II) ions, and (4) to investigate the complexions of the iron ions with DOM. The research findings might have useful repercussion related to both water treatment (iron removal) and drinking water distribution system issues (reduce color, odor and turbidity).

5.3. Materials and methods

5.3.1. Reagents and glassware

Sodium bi-carbonate ($NaHCO_3$, assay: 100%), sodium hydroxide (NaOH, assay: 100%), hydrochloric acid (HCl, assay: 36.5-38%) were obtained from Fisher Scientific, USA. Blended phosphate (Virchem 937, Carus Chemical Corporation, USA) composed of 25% zinc phosphate and 75% polyphosphate were used as a source of phosphate for this study. Ferrous sulfate ($FeSO_4.7H_2O$, assay: 100%, Fisher Scientific, USA) was used as a source of initial Fe(II) ions in solution. Humic acid (HA) (Technical grade, Sigma Aldrich, USA) was used as a source of DOM. The detailed method for preparation of purified HA stock solution is described in Section 3.2.1 of Chapter 3. A chlorine stock solution of 500 mg-Cl_2/L was prepared using a 5% aqueous sodium hypochlorite (NaOCl) solution (Fisher Scientific, USA) following the Standard Method 5710B (APHA-AWWA-WEF, 2005). Ultrapure water obtained from a Milli-Q® integral water purification system (EMD Millipore Corporation, Billerica, MA, U.S.A.) was used to prepare all solutions.

All laboratory experiments were conducted according to the procedure described in the Standard Methods (APHA-AWWA-WEF, 2005). To avoid contamination, all laboratory glassware used for sample collection and preservation were detergent dish-washed, soaked in a 10% nitric acid (HNO_3) solution for 24 h, rinsed several times in Milli-Q water, dried, covered with parafilm plastic (Pechiney Plastic Packing, Chicago, IL), and stored in a dry and dust-free place prior to use. To conduct the experiments in

presence of chlorine, all laboratory glassware were soaked using a concentrated sodium hypochlorite solution (~ 300 mg/L as Cl_2) for at least 24 h. Thereafter, the bottles were rinsed thoroughly three times with deionized water and finally with Milli-Q water, and were dried at 110 °C overnight (APHA-AWWA-WEF, 2005).

5.3.2. Batch test

To start an experiment, 1 L of ultrapure water was added into a reaction cell. A detailed description on iron suspension color and turbidity formation is described in Section 3.5.1 of Chapter 3. Briefly, 35 g of $NaHCO_3$ was added to buffer the water samples (Lytle and Snoeyink, 2002) and dissolved oxygen (DO) concentration in the reaction solutions was kept saturated and constant during each run corresponding to an oxygen partial pressure of 0.21 atm (DO ≈ 8.5 mg/L). At the required pH for the iron colloids formation study, pH adjustment was performed using high-purity 0.6 M HCl (assay: 38%, Fisher Scientific, USA) and 0.6 M NaOH (assay: 100%, Fisher Scientific, USA). The pre-settled pH levels were maintained constant at least 30 min before starting each experiment. After stabilization of the desired pH levels in water solution, $FeSO_4.7H_2O$ was added into the water samples to get initial Fe(II) ions concentration of approximately 3 and 6 mg/L (5.37×10^{-5} M and 10.74×10^{-5} M) depending on the goal of the experiments. Temperature, DO, pH and iron concentration were monitored over the time of the experiments. Using syringe, the samples were drawn out from the reaction cell approximately after 3.5 h of the reaction period. The same experiments were conducted for different pH values (5.5 to 8.5) in absence and presence of different dosages of DOM, phosphate based corrosion inhibitor and chlorine based disinfectant in the $NaHCO_3$ buffered synthetic water systems. Samples were analyzed in duplicate, and the average values are reported.

5.3.3. Analytical methods

All pH measurements were made using an Accumet electrode and Accumet Excel, XL50 (Dual channel pH/ion/conductivity) meter (Fisher Scientific, Singapore) calibrated with NBS buffer solutions (Fisher Scientific, USA). DO was measured using a DO meter (VWR, SP5OD, SympHony, Thermo Orion, USA) with a DO probe (VWR, SympHony, Thermo Orion, UK). Phosphate concentration was measured by an ion chromatograph (761 Compact IC, Metrohm). Free chlorine concentration was determined using the colorimetric version of the N,N-diethyl-p-phenylenediamine (DPD following the HACH 8021 method (HACH, 2005) at a wavelength of 530 nm using a DR/5000 UV Visible Spectrophotometer (HACH Co., Loveland, Colorado, USA). Concentration of Fe(II) ions was measured colometrically by the 1,10-phenanthroline following HACH 8146 method (HACH, 2005) using a DR/5000 UV Visible Spectrophotometer at wavelength of 510 nm, and total iron concentration was measured by ICP-MS (Thermo Scientific X-Series2 ICP-MS). Color in water sample was measured using a DR/5000 UV Visible Spectrophotometer (HACH Co., Loveland, USA) at a wavelength of 455 nm. HACH 2100AN Turbidimeter was used to measure the turbidity in water samples. DOM was measured as DOC with a TOC-V_{CPH} analyzer equipped with an auto-sampler ASI-V (Shimadzu Corp., Kyoto, Japan) according to the Standard Method 5310B (APHA-AWWA-WEF, 2005). The detailed description of the analytical procedures for the measurement of water quality parameters such as pH, DO, DOC, free chlorine, Fe(II) ions and phosphate concentration are described in Section 3.4.1 of Chapter 3.

5.3.3.1. Zeta (ζ) potential and particle size distribution

The electrophoretic mobility (EMF) of iron particles was measured over a wide range of pH values from 3 to 11 at 25 $\pm$ 0.1 °C temperature, using Zetasizer Nano (Malvern Instruments Ltd., UK). The ζ-potential was calculated from the EMF using the default instrument software following Henry's equation with the Smoluchowski relationship. During the ζ-potential measurement at different pH values, pH was adjusted by multiple purpose titrator (MPT-2, Malvern Instruments Ltd., UK). The experimental temperature (25 $\pm$ 0.1 °C) was set by Zetasizer Nano (Malvern Instruments Ltd., UK). The average

particle size and particle size distribution of iron particles was measured at a fixed pH value of 6.5 and at 25 °C temperature using a dynamic light scattering instrument (Zetasizer Nano-ZS, Malvern, UK), which is suitable for particle sizes ranging from 0.6 nm to 6 μm.

5.3.3.2. High performance size exclusion chromatography (HPSEC)

High performance size exclusion chromatography (HPSEC) (Perkin Elmer, Series 200) with a UV/VIS detector was used to determine the molecular weight (MW) distribution of DOM present in water samples. The samples were passed through a 0.45 μm membrane filter (Micron-PSE, Polysulfone) and analyzed using a TSK G3000SW column (7.5 mm × 300 mm). The column was calibrated with sodium polystyrene sulphonate (PSS) standards with different MW (14900, 7540, 5180, 1530 Da). All PSS standards and samples were detected at a wavelength of 254 nm. The reproducibility of the measurements was assured by running duplicate. A description about the method can be found in Section 3.4.8 of Chapter 3.

5.3.3.3. X-ray difraction (XRD)

XRD was used to identify the crystalline phase of iron particles. The iron particles samples were centrifuged at 40,000 rpm for 30 min using a centrifuge (IEC Centra GP8R, Thermo Electronic Corporation). The precipitates were washed once in Milli-Q water before being centrifuged again. Finally, the particles were dried at 30 °C for 24 h, and thereafter, kept at room temperature until characterization (usually within 2 to 3 weeks) following the method described elsewhere (Gunnars et al., 2002). The iron particles products were identified by X-ray diffraction (XRD) method employing a high-speed Bruker D8 Advance XRD system using Cu-Ka radiation having a wave length of 1.54 A°, tube voltage of 40 kV, and tube current of 40 mA.

5.3.3.4. Transmission electron microscope (TEM)

The TEM images of the iron nanoparticles were recorded by the FEI Tecnai-12 with a MegaView II camera and AnalySIS software. A 10 mL supernatant was first sonicated for about a minute, and then a droplet of it was placed on a 200-mesh gold grid of carbon film (Electron Microscopy Sciences, Hatfield, PA, USA). The 200-mesh grid was set on tissue paper and allowed to dry before being placed in a special holder, and loaded under a vacuum in the FEI Tecnai-12 for image capturing.

5.3.3.5. Statistical analysis

Data that were obtained from the experiments was entered into a computer system and the statistical analysis of a 2^4 full factorial design approach was performed by using a windows version program Minitab® 16 (MINITAB Inc., State College, Pennsylvania, USA). The analysis provided relevant statistical parameters including the *F*-test associated with probability $p(F)$. Unless otherwise mentioned, all statistical analyses were conducted at a 95% confidence level. The Pearson's correlation coefficients analysis between all the variables (e.g., pH, chlorine, DOM, phosphate, turbidity, and color) in synthetic water samples was performed using windows version software, 'IBM SPSS Statistics 20' (IBM, USA).

5.4. Results

In drinking water treatment and distribution systems, soluble Fe(II) ions are oxidized to insoluble Fe(III) ions by the different variables and different reaction mechanisms that defines the chemistry of a typical drinking water distribution system. In this study, the addition of phosphate based corrosion inhibitor represents the particle sequestering approach in which visible Fe precipitation is prevented in real distribution systems. Humic acid solution was employed as the surrogate for DOM (2.85 mg/L as DOC), and

chlorine was used as disinfectant in solutions. The levels of each factor for the particles formation studied here were selected simulating as closely as possible characteristics encountered in drinking water. In this article, the terms "colloid" was defined as a subset of particles having diameter less than 1 μm (Lytle and Snoeyink, 2002).

5.4.1. Evaluating treatment factors affecting color and turbidity

To evaluate the significant factor/s on the formation of iron suspension color and turbidity, a full factorial (2^4) design approach (Tables B1 and B4 of Appendixes B) was followed to conduct the bench scale experiments considering the existing water treatment facilities. Four main experimental factors and their levels were: (A) pH (6.5 to 8.5), (B) DOM (0 to 2.85 mg/L as DOC), (C) PO_4 (0 to 1.5 mg/L), and (D) Cl_2 (0 to 2.2 mg/L) respectively. The experimental data was analyzed with a windows version program Minitab® 16, and the results are summarized in Table 5.1. The statistical significance was determined based on Student's *t*-test and the value of probability *p*. The statistical analysis revealed that PO_4 was the most significant factor to reduce the solution color (37.9% contribution) and turbidity (45.5% contribution) at a 95% confidence level (Table 5.1). pH and DOM were also statistically significant factors ($\alpha = 95\%$) to increase the color but the interaction factor for pH and DOM were observed to decrease the color. On the other hand, PO_4 and Cl_2 were significant ($\alpha = 95\%$) factors to reduce the turbidity, and the reverse trend was observed for the interaction effects of PO_4 and Cl_2. The rank of each main and interaction factor and their statistical significance can also be found in Table 5.1. The contour plots for the interaction effects on color and turbidity, generated by the software 'Minitab® 16' using the factorial design approach data, is graphically shown in Figure 5.2. It should be noted here that the level of curvature in contour plots is an indication of the interaction between two variables on the responses (Montgomery, 2009).

Table 5.1. Effects estimates and statistical significance for iron suspension color (Co-Pt) and turbidity (NTU).

Code	Term	Color (Pt-Co)				Turbidity (NTU)			
		Effect estimate	*t* value	*P* value	Impact (%)	Effect estimate	*t* value	*p* value	Impact (%)
Main Factor									
A	pH	55.24	4.49	0.006[a]	14.9	0.94	3.2	0.024[a]	14.4
B	DOM	70.50	5.73	0.002[a]	24.2	-0.79	-2.69	0.043[a]	10.2
C	PO_4	-88.25	-7.17	0.001[a]	37.9	-1.67	-5.7	0.002[a]	45.5
D	Chlorine	-44.51	-3.62	0.015[a]	9.6	-0.42	-1.43	0.213	2.9
2 -way interactions									
AB	pH·DOM	-32.0	-2.60	0.048[a]	4.9	-0.34	-1.15	0.301	1.9
AC	pH·PO_4	4.25	0.35	0.744	0.1	-0.17	-0.57	0.592	0.5
AD	pH·Cl_2	12.0	0.98	0.374	0.7	-0.13	-0.44	0.681	0.3
BC	DOM·PO_4	26.1	2.11	0.088	3.3	0.79	2.73	0.042[a]	10.4
BD	DOM·Cl_2	8.75	0.71	0.509	0.4	0.01	0.03	0.981	0.0
CD	PO_4·Cl_2	8.00	0.65	0.544	0.3	0.66	2.25	0.075	7.1

[a] Significant at 95% confidence level and critical value of t for this test is 2.571.

The Pearson's correlation coefficients between all the variables are determined using the windows version software, 'IBM SPSS Statistics 20' (IBM, USA), and the results are presented in Table 5.2. This statistical analysis revealed a strong positive correlation between color and turbidity ($r = 0.72$, $p < 0.0001$) that was consistent with the color and turbidity observation experiments. The most significant negative correlation was observed between PO_4 dosage; and color ($r = -0.61$, $p < 0.0001$), and turbidity ($r = -0.75$, $p < 0.0001$), which stated that with the increase in PO_4 dosage, iron suspension color and turbidity decreased accordingly. This study also revealed that pH had positive and moderate correlation with color and turbidity formation in solutions. The correlation

among other factors can also be found in Table 5.2. Further details of the correlations can be found elsewhere (Montgomery, 2009).

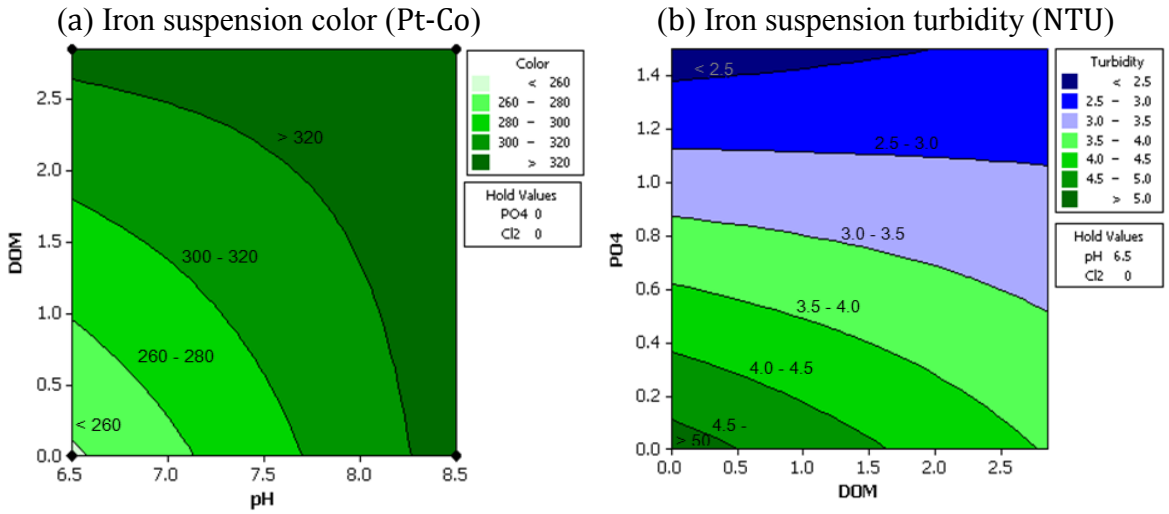

Figure 5.2. Contour plots of (a) effect of DOM and pHon color, holding constants PO_4 and chlorine; and (b) effect of PO_4 and DOM on turbidity, holding constants pH and chlorine.

However, in addition to the factorial design experiments conducted with the existing water quality parameters, an extensive study for different levels of each individual variable was conducted consequently herein to find out the impact of different variables on iron suspension color and turbidity formation in $NaHCO_3$ buffered synthetic water systems.

Table 5.2. Pearson's correlation coefficients between the dependent variables (iron suspension color and turbidity) and the independent variables (pH, DOM, PO_4 and chlorine in solution).

Variable	Color	Turbidity	pH	DOC	PO_4	Chlorine
Color	1					
Turbidity	0.717[b]	1				
pH	0.534[b]	0.374[a]	1			
DOC	0.602[b]	-0.440[a]	0.269	1		
PO_4	-0.610[b]	-0.752[b]	-0.025	-0.116	1	
Chlorine	-0.116	-0.045	-0.077	0.012	-0.298	1

[a] Correlation is significant at the 0.05 level (2-tailed).

[b] Correlation is significant at the 0.01 level (2-tailed).

5.4.1.1. Effect of pH

The effect of different pH values ranging from 5.5 to 10.5 on the iron suspension property (e.g., turbidity and color) was evaluated in $NaHCO_3$ buffered synthetic water containing DO $\approx$ 8.5 mg/L (saturated oxygen). This study revealed that the apparent color and turbidity in water samples were increased with the increase in pH values (Figure 5.3(a)). A major increment for iron suspension color (41.3%) and turbidity (81.9%) was observed for changing pH value from 5.5 to 7.5; and after that color and turbidity appeared relatively stable. The same trend was observed by Lytle and Snoeyink (2002), who reported that the apparent color was increased with the increase in pH values in the control water systems.

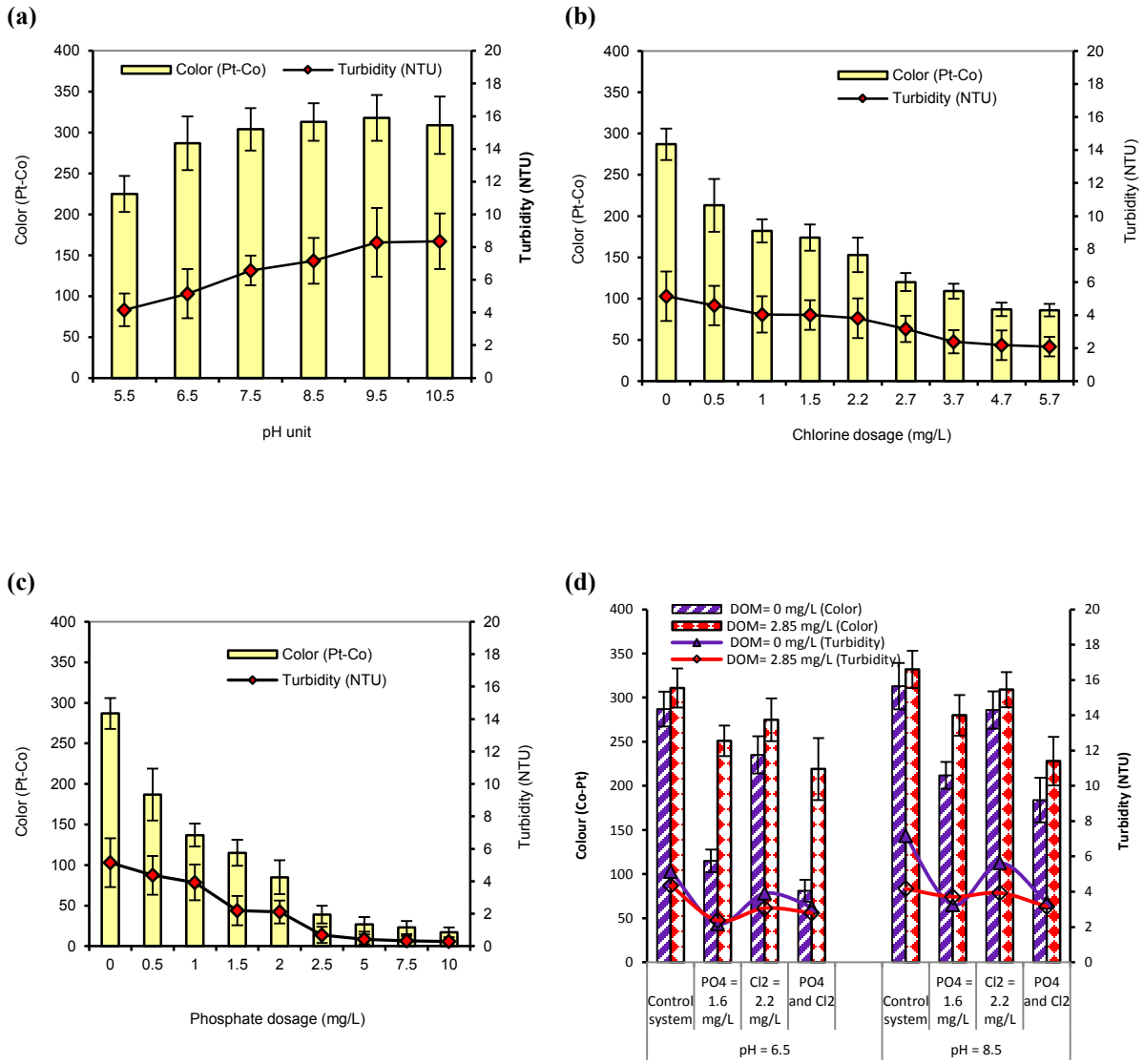

Figure 5.3. Effect of (a) pH, (b) chlorine dosage, (c) phosphate dosage and (d) dissolved organic matter (DOM) on the formation of iron particles suspension color (Pt-Co) and turbidity (NTU) in $NaHCO_3$ buffered synthetic water at lab

5.4.1.2. Effect of chlorine

The effect of different dosages of free chlorine ranging from 0.5 to 5.7 mg/L on iron suspension color and turbidity at pH 6.5 is shown in Figure 5.3(b). NaOCl solution was added in water samples before adding iron in solution. This study revealed that in the presence of 0.5 mg/L free chlorine in the iron water systems (chlorine –to– iron mole ratio ≈ 0.26), 25.8% color and 11.1% turbidity were reduced. This finding is consistent with the reported result by Lytle et. al. (2004), who have conducted 5 mg-Fe/L iron suspension formation study in presence of 5 mg Cl_2/L for different pH values (7 to 10) in synthetic water samples. Lytle et. al. (2004) have found that iron suspension color and turbidity are lower in presence of chlorine compared with the control water systems for all pH values. In addition, this study revealed that the reduction (%) of iron suspension was gradually increased with the increase in free chlorine dosages in solutions. Consequently, no significant decreases in color and turbidity were observed above a chlorine dosage of 4.7 mg-Cl_2/L (chlorine –to– iron mole ratio ≈ 2.47). Further, settled particles were not observed for the chlorine dosages greater than or equal to 4.7 mg/L; and the iron colloid suspensions remained stable for days (Figure B9 of Appendix B).

5.4.1.3. Effect of phosphate

The measured apparent iron suspension color and turbidity at a constant pH value of 6.5 in control water system (in absence of phosphate) were 287 platinum-cobalt (Pt-Co) units and 5.15 NTU respectively (Figure 5.3(c)). On the other hand, an addition of 0.5 mg/L of phosphate (PO_4 -to- iron mole ratio ≈ 0.098), the iron suspension color and turbidity were reduced 34.8% and 15.2% respectively. The reduction (%) was increased with the increase in PO_4 dosages (0.5 to 10 mg/L) studied here. Greater than 90% reduction of color and turbidity was observed in presence of 5 mg/L phosphate (PO_4 -to- iron mole ratio ≥ 1) in solution (Figure 5.3(c)). This finding is similar to the published work in literature, which acknowledges that color and structural difference have been observed due to the presence of phosphate in iron water systems (Deng, 1996; Lytle and Snoeyink,

2002). These results demonstrate that with the increase in phosphate dosages in iron water systems, iron suspension color subsequently decreases (Figure B10 of Appendix B). For the phosphate dosage at 5 mg/L and above, iron suspension was appeared clear and almost colorless; and iron colloid suspensions remained stable for months. An increase in suspension stability with the increase in phosphate dosages is predicted to decrease particle-particle interactions.

5.4.1.4. Effect of organic matter

The effect of DOM on the properties of iron particles and suspensions was examined in $NaHCO_3$ buffered synthetic water using an initial DOM concentration of 2.85 mg/L in the different reaction systems. This study revealed that in presence of DOM, iron suspension color was observed to increase in the different reaction systems (Figure 5.3(d)). Conversely, a reverse trend was observed to decrease turbidity in presence of DOM for the same reaction systems. A possible explanation for this fact is that DOM itself contains color that contributes to increase the color in solution. Nevertheless, DOM adsorbs onto the surface of iron particle at early stage and limits the aggregation of particles. Therefore, it has been suggested that the reduction of particle sizes, reduce the turbidity in solutions. This study also revealed that iron suspension color and turbidity formation in presence of DOM was lower at pH value of 6.5 compared to pH value of 8.5.

5.4.2. Role of treatment factors through materials characterization

5.4.2.1. Zeta (ζ) potential

The ζ-potential of the iron particles alone; and along with chlorine, phosphate and DOM was measured as a function of pH ranging from 3 to 11 in bicarbonate buffered (5 mg-C/L as DIC) synthetic water systems. The pH for point zero charge (pH_{PHC}) of the iron particles in the control systems was shown to be at pH 6.1. This observation is consistent

with that found in other study (Lytle et. al., 2004). This study also demonstrated that the ζ-potential values were decreased gradually with the increase in pH values from approximately 13.3 mV at pH 3 to - 42.2 mV at pH 10.8 (Figure 5.4), which was in good accordance with the reported results by Lytle and Snoeyink (2002). In presence of 4.7 mg/L of chlorine (chlorine -to- iron mole ratio = 2.47), the ζ-potential values of the iron particles were close to the values for the particles in control water system (Figure 5.4). This study elucidated that an addition of 5 mg-PO_4/L (PO_4 -to- Fe(II) mole ratio ≥ 1), in the iron water systems caused a more negative ζ-potential of the iron particles; and it decreased gradually with the increase in pH values. Therefore, interaction between the colloids was reduced by strong electrostatistic charge repulsion; and inhibited the extent of aggregation and colloid size. On the other hand, this study revealed that DOM (2.85 mg/L as DOC) made the ζ-potential of iron particles more negative. Therefore, the interactions between the particles decreased significantly, which limited particles aggregation. This study illustrates a significant impact of DOM on the change of ζ-potential values of the iron particles in solutions (Figure 5.4).

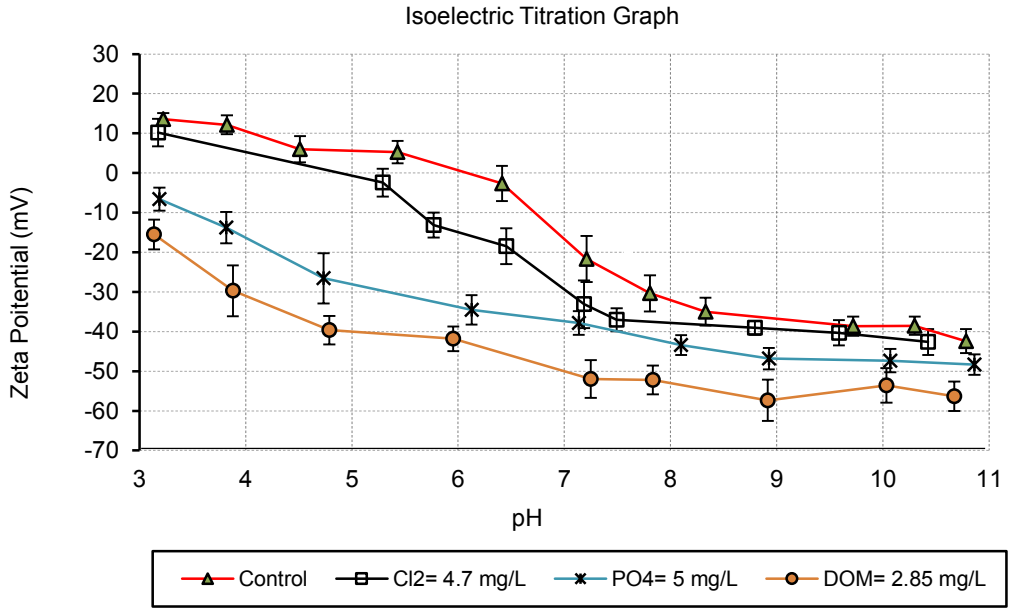

Figure 5.4. Effect of pH, chlorine (4.7 mg/L), phosphate (5 mg/L), and DOM (2.85 mg-C/L) on change of ζ-potential of the iron particles in $NaHCO_3$ buffered synthetic water.

5.4.2.2. Particle size distribution

Dynamic light-scattering (DLS) was used to analyze the particle size distributions by intensity of iron in solutions in control water systems; and in presence of chlorine, phosphate and DOM in $NaHCO_3$ buffered synthetic water at pH value of 6.5 (close to pH_{PHC}). Figure 5.5 shows a typical log-normal particle size distribution (x axis) of the iron nano particles based on the percentage of intensity (y axis). The median diameter of the iron particles is located at about 287.5 ± 17.6 nm, and the average (mean) diameter of the iron particles was found to be 422.8 ± 61.9 nm that formed in the control water systems (Figure 5.5(a)). Conversely, in presence of 4.7 mg/L chlorine (particle size: 176.2 ± 3.3 nm), 10 mg/L phosphate (particle size: 31.16 ± 0.59 nm) and 2.85 mg/L organic matter (particle size: 97.5 ± 0.8 nm), the average iron particle sizes were observed to be altered show in Figures 5.5(a), (c), and (d) respectively. The findings for the change of particle size distributions were coincided with the change in zeta potential values of iron particles mentioned above for different reaction systems (Figure 5.5). In addition, the statistical analysis for F test ($F_{obs} = 320.9 > F_{0.01,3,8} = 7.59$) illustrated that the average iron particles size distributions was significantly ($p < 0.05$) changed in presence of chlorine, phosphate and DOM compared with the control water systems (Table B7 and B8 of Appendix B). An extended study using different dosages of phosphate (0.5 to 10 mg/L) revealed that the average particle sizes of iron particles were gradually decreased with the increase in phosphate dosages (Table B9 to B23 of Appendix B), and the particle sizes were relatively comparable for a phosphate dosage greater than or equal to 5 mg/L (PO_4 -to- iron mole ratio ≥ 1) (Table 5.3). The particles size distributions data for different phosphate dosages was used to develop the following linear regression model ($F_{obs} = 19.25 > F_{0.01,1,6} = 13.75$), which indicating a significant ($\alpha = 0.05$, $p = 0.004$) relationship between the increase in phosphate dosages, and the decrease in iron particle size distributions in solutions.

$$\hat{y} = 313.98 - 35.52x \qquad (5.3)$$

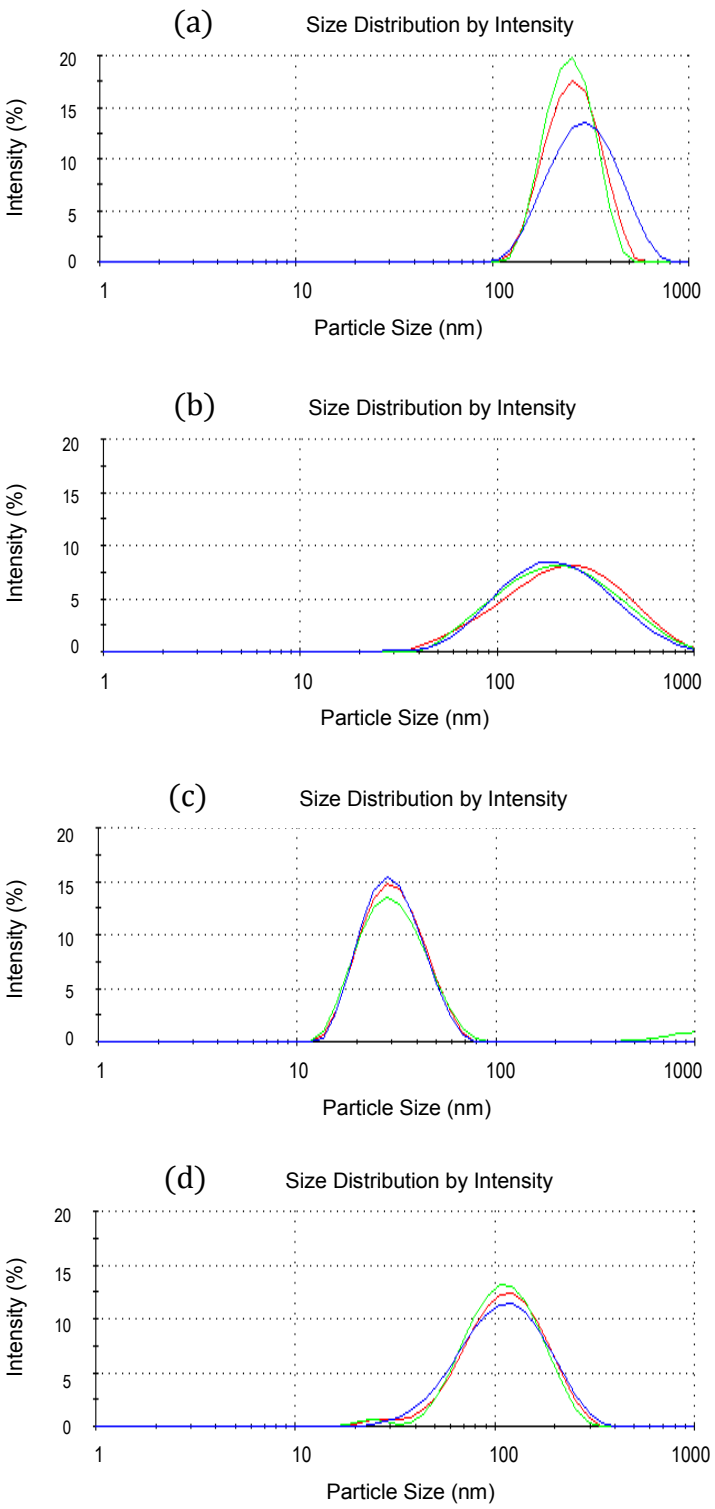

Figure 5.5. Iron particles size distribution by intensity (a) control system; and (b) in presence of 4.7 mg/L chlorine, (c) 10 mg/L of PO_4, and (d) 2.85 mg/L of DOM.

Table 5.3. Effect of phosphate dosage on iron particles size distribution (nm).

Sl No	pH	No. of observation	Phosphate mg/L as PO_4	PO_4 to iron mole ratio	Particle size (nm)
1	6.54	5	0.0	-	422.8 ± 61.9
2	6.49	5	0.5	0.098	350.2 ± 28.1
3	6.61	6	1.0	0.196	246.1 ± 11.6
4	6.52	6	1.5	0.294	192.3 ± 10.2
5	6.45	6	2.5	0.481	169.9 ± 6.4
6	6.51	6	5.0	0.981	43.5 ± 0.6
7	6.48	6	7.5	1.469	43.3 ± 2.3
8	6.53	5	10	1.961	31.2 ± 0.6

5.4.2.3. Molecular weight distribution

High performance size exclusion chromatography (HPSEC) was used to investigate the formation of complexes between different molecular weight (MW) fractions of DOM; and chlorine, phosphate and iron colloids. This study revealed that in control water system (in absence of chlorine, phosphate and iron), the molecular weight distribution of DOM in water ranged from 58000 to 150 dalton (Da). A detailed molecular weight distribution of this studied DOM can be found elsewhere (Rahman and Gagnon, 2013). Nevertheless, similar molecular weight distribution of DOM was observed in presence of chlorine and phosphate (Figure 5.6). Conversely this study revealed that in presence of iron colloids, the MW distribution of DOM in water have been heavily modified comparing to that of control water systems. The change of chromatograms was observed pronouncedly for the higher MW fractions having MW of 57987.2 ± 645.5 Da (Figure 5.6). Consequently, this study suggests that higher MW of organic fractions of DOM tend to adsorb onto the surfaces of iron particles that alter the surface charge of iron particles, limit the particles

aggregation and make iron particles highly stable in solution. This finding is consistent with the iron particles size distribution study in the presence of DOM (Figure 5.5(d)).

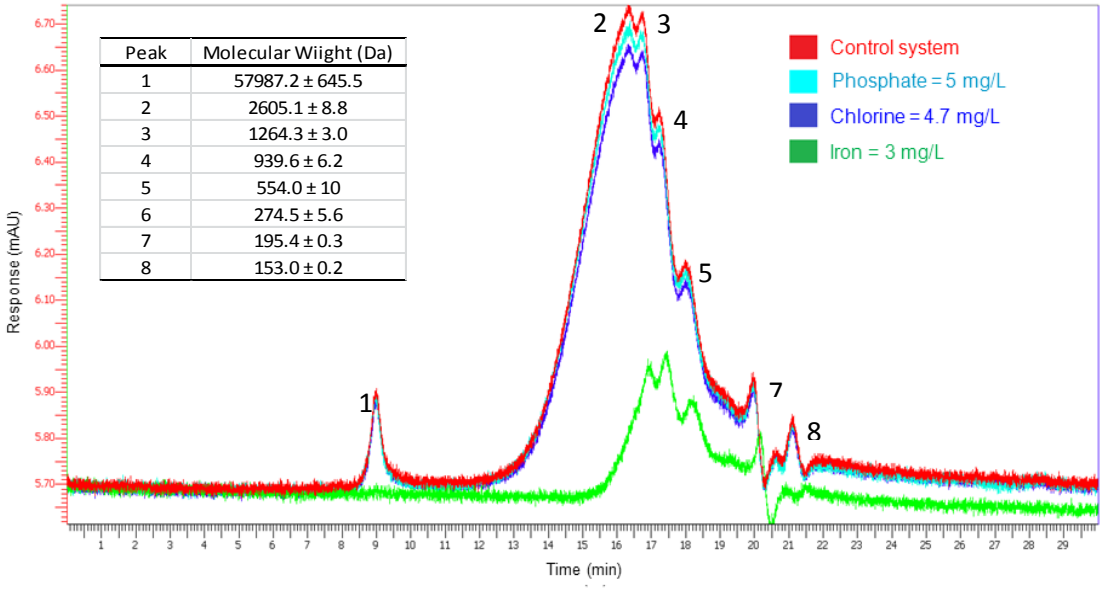

Figure 5.6. High performance size exclusion (HPSEC) chromatograms for the control system containing 2.85 mg/L DOM; and in presence of phosphate (5 mg/L), chlorine (4.7 mg/L) and iron (3 mg/L) in the same reaction systems.

5.4.2.4. Structural properties of iron particles

XRD (X-ray diffraction) was conducted on iron particles formed in the control water systems (in presence of oxygen only). This study revealed that goethite (α-FeOOH) was the dominant specie in iron particles followed by hematite (Fe_3O_4) and lepidocrocite (γ-

FeOOH) (Figure 5.7). This result was in agreement with the previous study conducted on iron pipe's corrosion scales analysis (Cornell and Giovanoli, 1985; Lin et al., 2001; Hove et al., 2008; Pédrot et al., 2011), who reported that goethite was found predominantly (α-FeOOH, 75.6%) with magnetite (Fe_3O_4, 21.5%) and lepidocrocite (γ-FeOOH, 2.9%) in iron corrosion scales. It should be noted here that ferrihydrite ($Fe_2O_3 \cdot 0.5H_2O$) forms initially and then turns into goethite by dissolution and precipitation within 24 h (Cornell and Giovanoli, 1985).

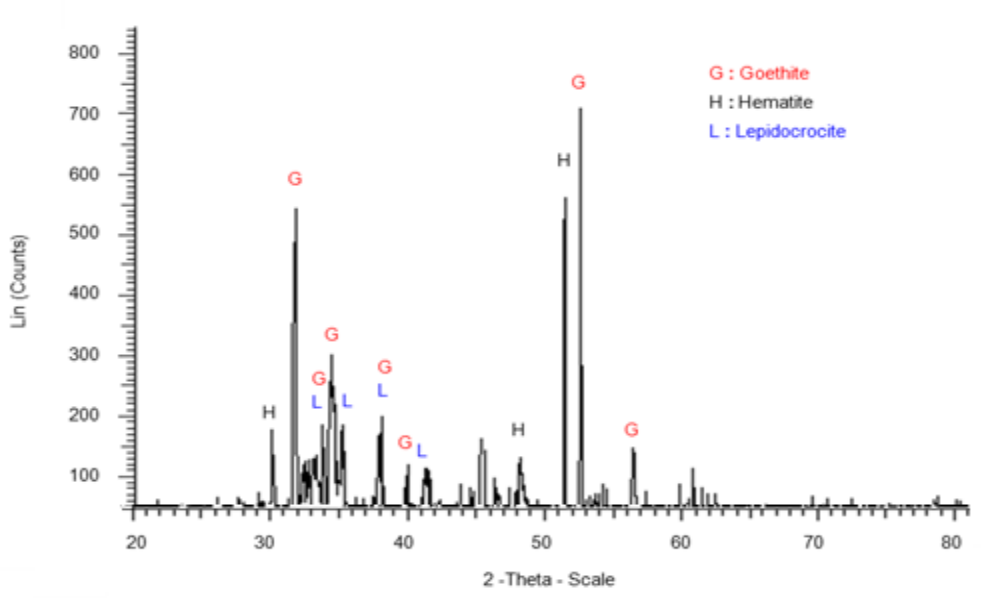

Figure 5.7. X-ray diffractogram of iron particles in control system.

A comparison study on the structural properties of iron colloids/particles in control water systems (in absence of phosphate, chlorine and DOM); and in presence of phosphate, chlorine, and DOM at pH 6.5 was conducted using transmission electron

microscope (TEM). This study showed that the iron particles formed in control water systems were appeared as singular, dense masses with needle like morphology of goethite (α-FeOOH) particles (Cornell and Giovanoli, 1985), and poorly crystalline morphology of lepidocrocite (γ-FeOOH) particles (Pédrot et al., 2011) shows in Figure 5.8(a). This finding is consistent with our XRD study (Figure 5.7) indicating that goethite is the predominant iron species in iron(III) oxide-hydroxide (FeOOH) particles. However, in the presence of phosphate, chlorine and DOM, the TEM micrographs show clearly a pronounced change of the iron colloids/particles shape and size. Phosphate and chlorine changed the iron particles shape from needle like crystalline shape to a rice grain type shape (Figure 5.8(b) and (c)). In the presence of chlorine, the iron particles that formed by the oxidation reactions of Fe(II) ions into Fe(III) ions, were composed of aggregates of small subunits and less transparent to the electron beam (Figure 5.8(b)). Conversely, in the presence of phosphate, the iron particles appeared to be relatively sponge like porous (Figure 5.8(c)), giving the impression that they had lower density than ones formed in the control system (Figure 5.8(a)). TEM observation of the Fe-DOM system revealed the presence of dense and opaque nanoparticles diffusely distributed (Figure 5.8(d)). This finding is in reasonable agreement with the published work by Pédrot et al. (2011), who have observed the same type of morphology for Fe-HA colloids, and have smaller sizes of 30 ± 15 nm for Fe-HA colloids. Nevertheless, the TEM micrographs results for the iron particles that formed in different reaction systems (Figure 5.8) are comparable with the iron particles size distribution results by DLS, which has been mentioned above (Figure 5.5).

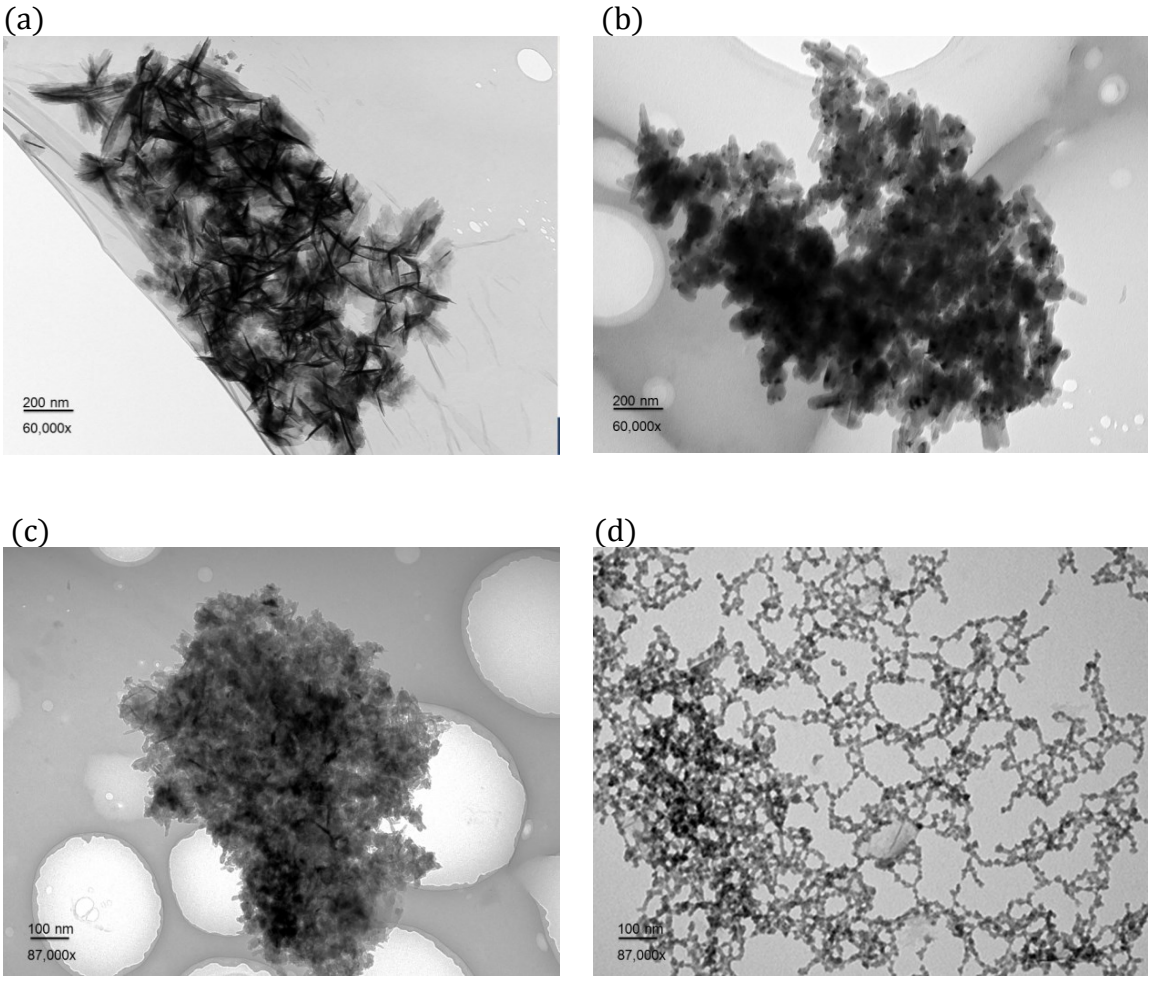

Figure 5.8. Transmission electron microscopes of iron particles formed at pH 6.5 in $NaHCO_3$ buffered synthetic water at 21 ± 1 °C; for (a) control systems; and (b) in presence of 4.7 mg/L chlorine, (c) 5 mg/L of PO_4, and (d) 2.85 mg/L of DOM.

5.5. Discussion

This study revealed that iron suspension color and turbidity were greatest when only a weak oxidant (oxygen) was present. With the increase in pH values, turbidity and color were observed to increase, which indicated that the reactions were a complex function of the solution pH. Several authors (King et al., 1995; Millero et al., 1995) have assumed this complex pH dependence to occur due to the parallel oxidation of Fe(II) ions and its hydroxo complexes ($Fe(OH)^{+}$, $Fe(OH)_2$, $Fe(OH)_3^{-}$). In contrast, iron suspension color and turbidity were observed to decrease in the presence of chlorine, and this was more pronounced with the increase in chlorine dosages in solutions. On the other hand, phosphate greatly reduced both turbidity and color of iron suspensions especially for a higher dosage of phosphate. These results are in agreement with the reported results in literature (Deng, 1996; Lytle and Snoeyink, 2002), which showed color and structural differences in iron colloids when formed in the presence of orthophosphate and polyphosphate. In addition, this study showed that phosphate made the zeta potential of the iron particles more negative, inhibited the extent of aggregation and colloid size, and increased suspension stability. The decrease of ζ-potential values in the presence of phosphate may be due to the fact that when phosphate adsorbs onto the surfaces of iron particles at early stage of particles aggregation, probably involves the interaction of PO_4^{3-} with two Fe(III) ions to form relatively stable Fe $-PO_4-$ Fe linkages or binuclear inner-sphare complexes (Hsu, 1982; Stumm and Sulzberger, 1992). Fourier transform infrared (FTIR) adsorption studies also support this type of Fe-phosphate bond (Atkinson et al., 1974; Parfitt et al., 1975). However, the observation suggests that adsorption of phosphate causes a more negative zeta potential of the iron particles compared with the control water systems (Figure 5.4). Conversely, a noteworthy effect on the aggregation behavior of the iron colloids was observed due to the presence of DOM. This study revealed that DOM effectively reduced the iron particle sizes, thus confirming the break of the aggregates into individual particles. In presence of DOM, ζ-potential decreased significantly in the pH values ranging between 3 and 11 compared to the control water systems (in absence of DOM). Therefore, particle-particle interactions were decreased that made the iron colloids highly stable in the studied pH values. A possible explanation

for this fact is that DOM containing carboxyl groups have a strong affinity for metal oxide-surfaces, which change particle surface charges, and make iron colloids very stable in solutions (Balistrieri and Murray, 1987; Tombacz et al., 2004; Serikov et al., 2009).

The particle size measurements (measured by DLS) confirmed the presence of small colloids in solutions due to the presence of dissolved organic matter, phosphate and chlorine compared to the control water systems. The average size differences between iron particles formed in presence of chlorine, different dosages of phosphate and DOM in solutions agreed well with the observation data for the turbidity and color difference. The findings of this study advocate that particle size is directly correlated most of the cases with color and turbidity change. The DLS data corroborate similar observation by TEM that shows clearly a pronounced change of iron colloids/particles shape and size in the presence of chlorine, phosphate and DOM compared with the control water systems. Such a phase, however, has not been previously identified in drinking water distribution systems.

In addition with the above finding, HPSEC study suggests that higher molecular weight (MW) fractions of DOM tend to adsorb onto iron particle surfaces that alter the surface charge of the iron colloids, limit the particles aggregation and make the iron colloids highly stable. The possible reason for the change of MW distribution due to the presence of iron colloids is that the higher MW compounds tend to be more aromatic in nature (Thurman and Malcolm, 1983). Therefore, they might have larger number of reaction sites than the smaller MW compounds, which might be adsorbed onto the surface of iron particles. Our HPSEC results were consistent with the ^{13}C-NMR results conducted by McKnight et al. (1992), who reported the privileged sorption of aromatic moieties on iron oxides.

5.6. Conclusions

The investigation reported in this article shows that the existing water quality parameters, i.e., pH, residual chlorine, phosphate based corrosion inhibitor and DOM have significant impact on the properties of iron particles (shape and size) and suspension (color and turbidity) in a drinking water distribution system. PO_4 based corrosion inhibitor was observed to be the most significant factor ($p \leq 0.05$, $\alpha = 0.05$) reducing the color and turbidity. In addition, PO_4 decreased the iron particle sizes, created more negative zeta potential, and increased iron suspension stability in iron water systems. Consequently, DOM made the ζ-potential of iron particles more negative. Therefore, the interactions between the particles decreased significantly, which limited particles aggregation. These results were observed to be more pronounced at a pH value of 6.5 compared to a pH value of 8.5 in solutions. This study also suggests that iron colloid suspension color and turbidity in chlorinated drinking water systems could be lower than non-chlorinated systems. The practical implication of this research finding for drinking water distribution system issues should be considered in future research.

CHAPTER 6. EVALUATION OF Fe(II) IONS ON DBPs FORMATION IN DRINKING WATER DISTRIBUTION SYSTEMS: EXPERIMENTAL ASSESSMENT AND MODEL DEVELOPMENT[3,4]

6.1. Abstract

Cast iron pipes were installed br oadly in North American water utilities, particularly in older cities such as Halifax, NS and other cities in the Northeastern portions of Canada and the US. Many of these cast iron pipes are corroded and are continuous source of Fe(II) ions in drinking water distribution systems. Recent studies have reported on the formation and reduction of disinfection byproducts (DBPs), i.e., haloacetic acids (HAAs) and trihalomethanes (THMs) in full scale iron pipe water distribution systems. In this chapter, a comprehensive study was conducted to evaluate the impacts of Fe(II) ions, phosphate, pH and reaction time with their different levels on DBPs formation in synthetic waters. In addition with the comprehensive study, a 2^4 full factorial design study was conducted with the typical water quality parameters. This study elucidated that the main effect of Fe(II) ions really dominated the reduction of DBPs formation processes, accounting for over 50.85% and 60.41% of total variability for HAAs and THMs formation respectively. Two way ANOVA test revealed that the studied reaction times were not statistically significant ($\alpha = 0.05$, $p > 0.05$) on the changes in HAAs formation in presence of different concentrations of Fe(II) ions in solutions. However, the reaction times were statistically significant ($\alpha = 0.05$, $p < 0.005$) on the changes in THMs formation in the same reaction systems. In this study, the solution pH values had an obvious impact on the formation of HAAs and THMs in presence of Fe(II) ions and a phosphate based corrosion inhibitor. Significant factors (main and interaction) influencing DBPs formation/reduction were identified using a 2^4 full factorial design approach. Considering the effects of all significant factors, mathematical models for HAAs and THMs formation were developed using 80 experiments. The models' adequacy was checked thorough the statistical and graphical diagnostics. The models were validated by an independent data set, obtained from using the natural water samples collected from three major water treatment plants in Nova Scotia, Canada. The models were found to be a reasonable predictor for HAAs and THMs formation in drinking water distribution systems. These research findings have practical implications related to both water treatment and distribution system issues.

[3] Rahman, M.S., Gagnon, G.A. 2013. Bench scale evaluation of Fe(II) ions on haloacetic acids (HAAs) formation in synthetic water. *J. Water Supply Res. Technol. –AQUA*, **63** (3), 155-168.

[4] Rahman, M.S., Gagnon, G.A. 2014. Iron corrosion as a factor contributing to haloacetic acids formation in the distribution system: experimental assessment and model development. *J. Water Supply Res. Technol. –AQUA* (in press, doi:10.2166/aqua.2014.071).

6.2. Introduction

According to AWWA survey, the majority of distribution system pipes in USA are composed of iron materials: cast iron (38%), ductile iron (22%), and steel (5%) (AWWA, 1996). The internal surface of an unlined cast iron water distribution pipe is usually exposed to an oxidizing environment that reasons corrosion. Hozalski et al. (2008) have reported that the reduction of pipe wall as a zero-valent iron Fe^{o}; and correspondingly when Fe^{o} ions come in contact with water, Fe^{2+} ions start to appear in water through iron corrosion releasing electrons (Eq.(6.1)). Oxidants such as oxygen and free chlorine (HOCl and OCl^{-}) or monochloramine (NH_2Cl) may be efficient to accept these released electrons (Eq. (6.2) to (6.4)) (Sarin et al., 2004a). Consequently, the concentration of Fe^{2+} ions in drinking water distribution systems increases under these corrosion conditions (Kirmeyer et al., 2000). In addition, Kuch (1984) and Kirmeyer et al. (2000) have hypothesized that ferric (Fe^{3+}) oxides present in the iron corrosion scales, act as an another oxidant for letting the iron corrosion (and Fe^{2+} release) to occur during water stagnation/oxygen depletion conditions. However, ferric oxides in iron corrosion are reduced and Fe^{2+} ions are formed according to the following reaction (Eq. (6.5)) "Kuch Mechanism" (Kuch, 1984):

$$Fe^{o} \rightarrow Fe^{2+} + 2e^{-} \quad (6.1)$$

$$O_2 + 4H^{+} + 2e^{-} \rightarrow 2H_2O \quad (6.2)$$

$$HOCl + H^{+} + 2e^{-} \rightarrow Cl^{-} + H_2O \quad (6.3)$$

$$NH_2Cl + 2H^{+} + 2e^{-} \rightarrow Cl^{-} + NH_4^{+} \quad (6.4)$$

$$Fe_{(s)} + 2FeOOH_{(s)} + 6H^{+} \longrightarrow 3Fe^{2+} + 4H_2O \quad (6.5)$$

Therefore, it has been stated that Fe^{2+} ions are being added continuously in drinking water distribution systems from the iron pipe corrosion products (Sarin et al., 2004a). A laboratory study revealed that the release rate of Fe^{2+} ions ranges from 0.003 mg $m^{-1}h^{-1}$ in iron pipe loops with flowing oxygenated water to 0.01 mg $m^{-1}h^{-1}$ under stagnant anoxic conditions (Sarin et al., 2004b). However, corroded iron pipes are assumed to be the main source of aqueous Fe^{2+} ions in drinking water distribution systems. The concentration of Fe^{2+} ions was found to be 7.2 mg/L, dry weight basis in a center sample and 17.1 mg/L, dry weight basis in a side sample of 40–50 years-old iron pipe collected from the distribution system in Melbourne, Australia (Lin et al., 2001).

Reduction of pipe walls could be said by zero-valent iron (Fe^{o}) or by the ferrous iron contained in or sorbed to iron oxide corrosion products (Hozalski et al., 2008). Numerous laboratory studies have stated that Fe^{o} is a robust reductant that reduces different types of halogenated solvents including chlorinated byproducts: carbon tetrachloride (Matheson and Tratnyek, 1994), haloacetic acids (Zhang et al., 2004; Hozalski et al., 2008), pentachlorophenol (Kim and Carraway, 2000), trichloro(nitro)-methane (chloropicrin) (Pearson et al., 2005), and 1,1,1-trichloroethane (Fennelly and Roberts, 1998) . Several brominated compounds, for instance, 1,2-dibromoethane (Rajagopal and Burris, 1999), 1,2-dibromo-3-chloropropane (Siantar et al., 1996) have also been reported to reduce by zero-valent iron (Fe^{o}). Consequently, Chun et al. (2005) have discovered the susceptible reduction of some halogenated DBPs compounds (e.g., trichloro-nitromethane, trichloroacetonitrile, 1,1,1-trichloropropanone, and trichloroacetaldedyde hydrate) by Fe^{2+} ions associated with the synthetic main iron corrosion scales (e.g., magnetite and goethite). Ferrous iron (Fe^{2+}) can also a cause of unpleasant metallic taste and rusty color in water, when dissolved iron is found to be greater than USEPA recommended level 0.3 mg/L (Cham et al., 2010).

Chlorine has been used most extensively and efficiently as a secondary disinfectant since 1913 (White, 1992; AWWA, 2000); and has played an important role to eliminate maximum waterborne diseases (e.g., typhoid and cholera) in developing countries. Approximately 90% of the water supply systems in Canada use chlorine for disinfection purposes (Health Canada, 2009). However, increased concentrations of chlorine would be expected to increase disinfection byproducts formation (Sadiq and Rodriguez, 2004a), and to increase corrosion rate. Increasing corrosion rate was experimentally substantiated by Eisnor and Gagnon (2004), who conducted cast-iron pipe loop experiments for the reaction period of 6 and 12 h using three different types of disinfectants. They observed that free chlorine and chloramine would increase iron release from background water quality levels. Therefore, it has been hypothesized that these corrosion scales and Fe^{2+} ions react with free chlorine, and might have impact on DBPs formation in drinking water distribution systems.

In recent years, different types of efforts have been executed to understand the corrosion mechanisms, and to control metal release from corroded pipe. Increasing pH and/or alkalinity are two cost effective and useful methods to reduce the metal corrosion. Phosphate based corrosion inhibitors are alternative additive in drinking water for mitigating metal corrosion protection, red water control, and turbidity reduction (Maddison et al., 2001; Rahman and Gagnon, 20014c). In the US, around 67% of water utilities use polyphosphate or a blend of polyphosphate and orthophosphate; and rest of the utilities (33%) add orthophosphate as a corrosion inhibitor into the finished water (Edwards and McNeill, 2002). Corrosion inhibitors such as polyphosphate (or poly/orthophosphate blends) have been historically added to water for sequestering Fe^{2+} ions to treat 'red water' (Maddison et al., 2001; Edwards and McNeill, 2002). Unfortunately, published research concerning the reactivity of phosphate based corrosion inhibitors on the formation or reduction of disinfection byproducts (DBPs) in presence and absence of soluble iron is not well established yet. However, it has been hypothesized that corrosion by-products react with phosphate, free chlorine and organic matter; and

they might have impact on reduction or formation of total DBPs in drinking water distribution systems. The manner in which these mechanisms function in iron pipe distribution systems are depicted the schematic diagram (Figure 6.1).

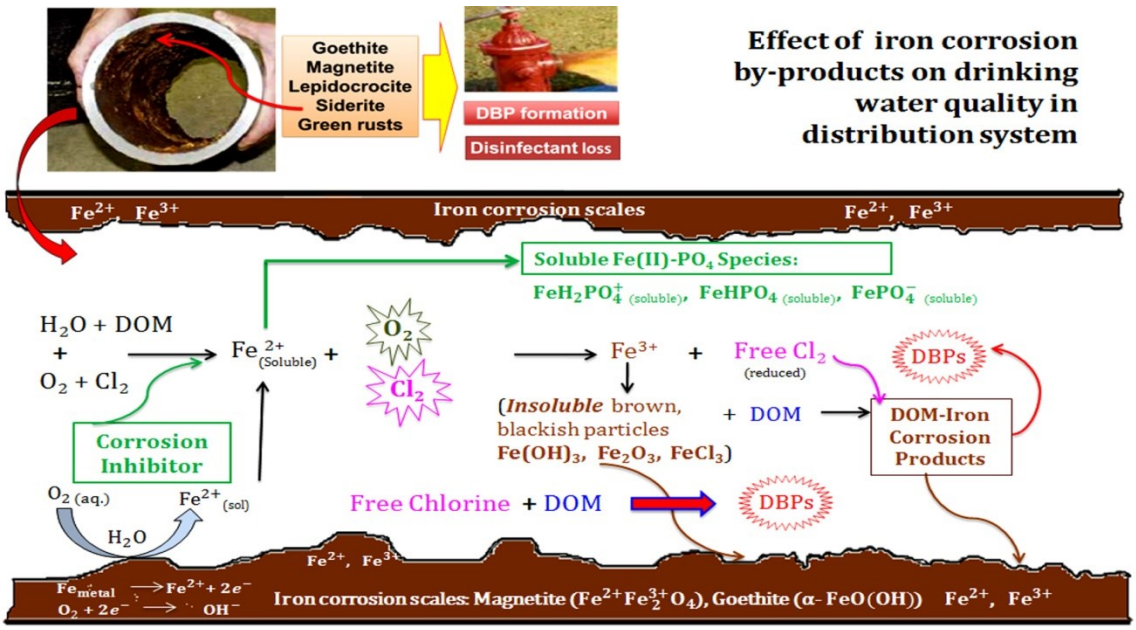

Figure 6.1. Schematic diagram for the reaction mechanisms that possibly occur in iron pipe distribution systems.

The formation of disinfection byproducts (DBPs) and their species distribution is a common and complex occurrence, and depends on several factors including the characteristics of water, treatment procedures, and water distribution pipe materials (Rahman and Gagnon, 2013). Previous studies have mostly reported on both the formation of DBPs and their reduction in full scale distribution systems (Singer et al.,

1995; Arora et al., 1997; Williams et al., 1997; Pecher et al., 2002; Hozalski et al., 2008; Amold et al., 2010). In addition to the reported data for DBPs formation study, some models considering the most significant factors (e.g., pH, reaction time, temperature, different concentration of chlorine, bromine and DOM) for predicting DBPs formation in real distribution systems have been proposed (Sung et al., 2000; Clark et al., 2001; Shimazu et al., 2005; Uyak et al., 2007; Zhang et al., 2011). Previously excellent reviews on the various models for DBPs prediction were reported in literature (Amy et al., 1987; Sadiq and Rodriguez, 2004b). Nevertheless, the development of HAAs and THMs formation models in the presence of soluble Fe^{2+} ions in water, and their relationship with phosphate based corrosion inhibitors for the different pH values and different stagnation times are very limited in existing literature.

In this present study, the effect of four potential explanatory factors including pH, Fe(II) ions, phosphate based corrosion inhibitor and reaction time for HAAs and THMs formation were investigated in $NaHCO_3$ buffered synthetic water under the laboratory conditions. In addition with the DBPs formation studies, the molecular weight (MW) distribution of DOM study was conducted using a high performance size exclusion chromatography (HPSEC) to evaluate the effect of the studied variables on the changes in MW distribution of DOM, and it's correlation with DBPs formation in the studied water samples. The synthetic water samples with the different water characteristics were prepared simulating as closely as possible characteristics encountered in drinking water. The goal of this study was to investigate the most significant factors, and their interactions influencing HAAs and THMs formation using a 2^4 full factorial design with center point approach, which was used to seed the development of the mathematical models. Graphical and numerical diagnostic methods were used to evaluate the models' adequacy. To validate the developed models, an independent set of data was used to assess the effectiveness of the fitted models equations.

6.3. Experimental section

6.3.1. Reagents and glassware

Ferrous sulfate ($FeSO_4.7H_2O$, assay: 100%, Fisher Scientific, USA) was used as a source of initial Fe(II) ions in solution. Ammonium chloride (NH_4Cl, assay: 99.6%), sodium sulfite (Na_2SO_3, assay: 100%) and sodium bi-carbonate ($NaHCO_3$, assay: 100%), sodium sulfate (Na_2SO_4, assay: 99.4%), sodium hydroxide (NaOH, assay: 100%), sulfuric acid (H_2SO_4, assay: 98%), hydrochloric acid (HCl, assay: 36.5-38%) were obtained from Fisher Scientific, USA. Blended phosphate composed of 25% zinc phosphate and 75% polyphosphate (Virchem 937, Carus Chemical Corporation, USA) was used as a source of phosphate for this study.

A purified humic acid (HA) stock solution was prepared by dissolving an aliquot of HA in 1 L Milli-Q water. A detailed method for HA stock solution preparation and purification is described in Section 3.2.1 of Chapter 3. A chlorine stock solution of 5 mg-Cl_2/L was prepared using a 5% aqueous sodium hypochlorite (NaOCl) solution (Fisher Scientific, USA) following the Standard Method 5710B (APHA-AWWA-WEF, 2005). All solutions were prepared in ultrapure water obtained from a Milli-Q® integral water purification system.

HAAs standard stock solution was prepared in a 5 mL volumetric flask containing methyl-tertiary-butyl-ether, MTBE ($(CH_3)_3COCH_3$, assay 99.8%, Sigma-Aldrich, Germany) by addition of 50 µL HAA_9 mix solution (EPA 552.2 Acids Calibration Mix, Supelco, PA, USA). The stock solution was used to prepare different concentrations (10 to 100 µg/L) of HAAs standard solutions to calibrate the gas chromatography (GC). The diluted stock solution will be good up to 24 h. Diazomethane (CH_2N_2) solution for HAAs samples extraction was prepared freshly each day in our water chemistry laboratory. A procedure for diazomethane preparation is described briefly in Section 3.2.4 of Chapter

3. Nine HAAs were measured in this study including: monochloroacetic acid (MCAA), monobromoacetic acid (MBAA), dibromoacetic acid (DBAA), dichloroacetic acid (DCAA), bromochloroacetic acid (BCAA), bromodichloroacetic acid (BDCAA), dibromochloroacetic acid (DBCAA), trichloroacetic acid (TCAA) and tribromoacetic acid (TBAA). To calibrate GC for THMs analysis, a certified commercial mix standard solution (Supelco, USA; purity $> 99\%$) for different known concentrations (10 to 150 $\mu g/L$) was used. Each standard solution contained four THM species including: trichloromethane (TCM), bromodichloromethane (BDCM), dibromochloromethane (DBCM), and tribromomethane (TBM). A details information on nine HAA and four THM species has been provide in Section 2.2 of Chapter 2.

All dish-washed glassware especially amber color bottles (reactor) used for this study were soaked using a concentrated sodium hypochlorite solution (~ 300 mg/L as Cl_2) for at least 24 h. Thereafter, the bottles were rinsed thoroughly three times with deionized water and finally with Milli-Q water; and the bottles were heated at 110 °C in an oven (Fisher Scientific, USA) overnight (APHA-AWWA-WEF, 2005).

6.3.2. Analytical methods

DOC measurements were performed with a TOC-V_{CPH} analyzer equipped with an auto-sampler ASI-V (Shimadzu Corp., Kyoto, Japan) according to the Standard Method 5310B (APHA-AWWA-WEF, 2005). Free chlorine concentration was determined using the colorimetric version of the N,N-diethyl-p-phenylenediamine (DPD) following the HACH 8021 method (HACH, 2005) at a wavelength of 530 nm using a DR/5000 UV Visible Spectrophotometer (HACH Co., Loveland, USA). Concentration of Fe(II) ions was measured colometrically with the 1,10-phenanthroline following the HACH 8146 method (HACH, 2005) at a wavelength of 510 nm using a DR/5000 UV Visible Spectrophotometer. An ion chromatograph (761 Compact IC, Metrohm) was used to

measure the phosphate concentration in solution. All pH measurements were made using an Accumet electrode and Accumet Excel, XL50 (Dual channel pH/ion/conductivity) meter (Fisher Scientific, Singapore). The pH meter was standardized daily using a three-point calibration with pH 4 (SB101-500), pH 7 (SB107-500), and pH 10 (SB115-500) buffer solutions (Fisher Scientific, USA) before taking reading in samples.

6.3.3. Batch experiments

Bench scale experiments were conducted for DBPs (HAAs and THMs) formation analysis using synthetic water samples consisting of differing characteristics. Humic acid was used as a source of dissolved organic matter (Vikesland et al., 1998; Chang et al., 2001; Yang and Shang, 2004; Li and Zhao, 2006). A required amount of purified humic acid stock solution was employed as the surrogate for DOM (2.85 mg/L as DOC) in $NaHCO_3$ buffered synthetic water systems (5 mg-C/L as dissolved inorganic carbon). Humic acid was chosen, because it contains 48.95% carbon (by weight), while natural freshwater contains 48 to 54% carbon. The required pH values in the water samples were adjusted using 0.5N HCl acid and 0.5N NaOH solution. The water samples were chlorinated (chlorine to carbon mole ratio of 0.79), and $FeSO_4.7H_2O$ (assay: 100%, Fisher Scientific, USA) was added to get the required amount of Fe(II) ions in solution. A comprehensive study for HAAs and THMs formation was conducted in presence of different dosages of Fe(II) ions (0.35 to 3.0 mg/L), phosphate ions (0 to 1.5 mg/L), different pH values (6.5 to 8.5), and at different reaction time (3.5 to 130 h) following the same procedures However, the solutions were mixed gently and homogeneously using a Teflon-coated magnetic stirrer bar and magnetic stirrer plate (VWR Advanced Hot Plate Stirrer, USA). Thereafter, the chlorinated solutions were transferred into headspace-free 250 mL chlorine demand free serum bottles (reactor). The bottles were capped immediately using PTFE (Polytetrafluoroethylene) screw cap with teflon-lined septa. Finally the serum bottles (reactors) were wrapped with aluminum foil to prevent photochemical reaction, and kept in dark for the designated reaction periods. After each designated reaction period (e.g., 3.5, 24, 48, 84, and 130 h), the chlorinated water samples were collected

into headspace-free 25 mL glass vials with polypropylene screw caps and teflon-lined septa. The vials were cautiously filled with the water samples, so that tapping of air bubbles inside was prevented. The chlorinated samples for HAAs analysis were quenched with ammonium chloride (Fisher Scientific, NJ, USA), while the sample for THMs analysis were quenched by sodium sulfite (Fisher Scientific, NJ, USA) to prevent further formation of HAAs and THMs respectively. All samples were refrigerated at 4 °C not more than two weeks prior to extraction for HAAs and THMs. Total experiments were conducted at lab temperature (21 ± 1 °C).

Table 6.1. Experimental range and level of different variables in DBPs formation study

Code	Variable	Unit	Level		
			Low level (-)	Center (+)	High level (+)
A	Fe(II) ions conc.	mg-Fe(II)/L	0.0	1.5	3.0
B	pH	Unit	6.5	7.5	8.5
C	Corrosion inhibitor	mg-PO_4/L	0.0	0.75	1.5
D	Reaction Time	hour (h)	3.5	13.5	24

In addition with the comprehensive study, a 2^4 full factorial design approach with center point level was followed to conduct the HAAs and THMs formation study with the typical drinking water quality parameters (Table 6.1). All of the experiments were conducted in duplicate to test the reproducibility of the results. For each batch test, control samples were used following the same procedure as the test samples but without the designed variables (e.g., ferrous ions and phosphate).

However, all haloaccetic acids (HAAs) and trihalomethanes (THMs) samples were extracted following the liquid-liquid extraction procedure, and the extracted organic phase was transferred into 2 mL of GC vial. A detailed method for HAAs and THMs extraction was described in Section 3.5.2.1 of Chapter 3. The GC vials containing HAAs and THMs samples were kept in a refrigerator for a maximum of 14 days prior to analysis. The calibration curves for HAAs and THMs were prepared using the standard solutions for HAAs and THMs before analysis the samples. The concentration of HAAs and THMs was quantified by gas chromatography (Varian, CP 3800 Gas Chromatography) with an electron capture detector (GC/ECD). Further details on the operating conditions of GC-ECD for HAAs and THMs analysis are provided in Tables C1 and C2 of Appendix C. At the beginning of each analytical run, solvent blanks and solvent samples containing the internal standard were injected to condition the GC and to verify that interferences were absent. Other quality assurance/quality control (QA/QC) procedures, such as QC check standards and matrix spikes were taken through the analysis.

Consequently, the post filtered water samples collected from three major water treatment plants in Halifax, Nova Scotia including: (1) JD Kline water treatment plant (JDKWTP), (2) Lake Major water treatment plant (LMWTP), and (3) Bennery Lake water treatment plant (BLWTP) were used for HAAs and THMs formation study. This study was conducted in presence of different dosages of Fe(II) ions and phosphate, at different pH values and different reaction times. The results of this study were followed to validate the developed HAAs and THMs prediction model equations. The water quality parameters for three water supply plants are presented in Table 6.2.

Table 6.2. Raw and treated water quality for J. Douglas Kline (JDK), Lake Major (LM) and Bennery Lake (BL) water treatment plant (WTP).

Parameter	JDK-WTP[a] (Pockwock)		LM-WTP[a] (Lake Major)		BL-WTP[a] (Bennery Lake)	
	Raw water	Treated water	Raw water	Treated water	Raw water	Treated water
pH (unit)	5.6	7.4	5.4	7.3	6.1	7.3
Alkalinity ($CaCO_3$)	<1.0	19.0	<1.0	14.5	<5.0	45.0
TOC	2.7	1.9	4.0	1.5	4.2	2.0
Iron (Total)	<0.063	<0.05	0.16	<0.02	0.23	<0.05
Chloride	6.5	9.0	6.0	8.0	8.0	11.5
Chlorate	<0.1	<0.1	<0.1	<0.1	<0.1	0.70
Chlorite	<0.1	<0.1	<0.1	<0.1	<0.1	<0.1
HAA_5 (avg.)	<0.005	0.062	<0.005	0.061	–	0.072
THMs (avg.)	–	0.073	–	0.089	<0.001	0.080

Unit: milligrams per liter unless shown otherwise

[a] Source: Annual Report of Halifax Regional Water Commission, 2012

6.3.4. Experimental design and data analysis

A 2^4 full factorial design approach was followed to evaluate the importance and interaction of the Fe(II) ions, pH values, phosphate ions and reaction times on the formation of HAAs and THMs. Four experiments were carried out at the center point level for estimation of experimental error. The range and levels of the studied variables for this study is presented in Table 6.1. Data that were obtained from each DBPs (HAAs and THMs) formation experiments was entered into a computer system. Thereafter, the statistical analysis of the experimental data was performed by the windows version programs: (1) Minitab® 16 (MINITAB Inc., State College, Pennsylvania, USA) and (2) Microsoft Excel® 2010 (Redmond, WA, USA). The analysis provided relevant statistical

parameters including the *F*-test associated with probability p (F); determination of the coefficient, r^2. The statistical significance of the regression coefficient was determined by the Student's *t*-test associated with probability p (t). The Fisher's test was followed for determining the model equations. The models adequacy was checked statistically following numerical and graphical diagnosis. The models were validated against an independence data set. The predicted values of HAAs and THMs were compared with the measured values in accordance with the following equation (Eq. (6.6)). It should be noted that the criterion of model fitness is met if a predicted value falls within $\pm$ 20 percent (%) of the measured values.

$$\text{Absolute model deviation} = \left[\frac{\text{Predicted value} - \text{Observed value}}{\text{Observed value}}\right] * 100 \qquad (6.6)$$

6.4. Results and discussion

To determine the effects of Fe(II) ions and other factors on HAAs and THMs formation, and their speciation in different reaction systems; a methodical comprehensive investigation was conducted in water samples. Bromine was not present significantly in the studied water samples and method detection limit (MDL) for bromine for this study was found to be 0.105 mg/L. As a consequence, the formation of major brominated species was found to be below the detection limit in most of the cases throughout the study. Therefore, major brominated species were not included in the results and discussion part. MDL for nine HAA and four THM species are provided in Tables C3 and C4 of Appendix C. Nevertheless, the effects of different factors studied are presented below.

6.4.1. Factors affecting DBPs formation

6.4.1.1. Effect of Fe(II) ions and reaction time

To understand the effect of Fe(II) ions on HAAs and THMs formation, different dosages of ferrous iron was added into the buffered synthetic water samples having pH 6.5 and DOC 2.85 mg/L, and chlorine to carbon mole ratio of 0.79. This bench scale comprehensive study was conducted for the different reaction periods ranging from 3.5 to 130 h. As mentioned previously, cast iron pipes are a constant source of Fe(II) ions in drinking water distribution systems (Sarin et al., 2004a). The concentration of Fe(II) ions in drinking water distribution systems were reported up to 3 mg/L (Kirmeyer et al., 2000); and under anoxic condition, aqueous Fe(II) ions concentrations up to 1.11 mg-Fe(II)/L (0.02 mM) were observed in a pipe loop reactor constructed using a 70 years old galvanized iron pipe (Sarin et al., 2004a). Therefore, different dosages of Fe(II) ions ranging from 0.3 to 3 mg/L were chosen for this study.

This study revealed that in presence of 0.35 mg/L Fe(II) ions, HAAs and THMs formation was significantly reduced from 41.5 to 51.9%, and from 23.5 to 34.8% compared with the control water systems (in absence of Fe(II) ions) for the studied reaction periods ranging from 3.5 to 130 h respectively (Figures 6.2(a) and (b)). This study also revealed that HAAs and THMs formation was reduced gradually from 41.5 to 71.1%, and 23.5 to 45.1% with the increase in Fe(II) ions concentration from 0.35 to 3 mg/L correspondingly (Table 6.3) for the reaction period of 3.5 h. This finding is consistent with the reported results by numerous studies (Amonette et al., 2000; Pecher et al., 2002; Elsner et al., 2004; Chun et al., 2005; Lee et al., 2008), which have mentioned that iron oxides surface (e.g., magnetite and goethite) accelerated the reduction rates of various organic compounds and halogenated byproducts. Lee et al. (2008) have stated that the degradation rate for a non-regulated DBP, (trichloronitromethane), depends on water-soluble iron in water systems. It has been reported that Fe(II) is a strong reductant (Amold et al., 2010); and when the

concentration of Fe(II) ions increases, it increases the reactive surface area, via oxidation of Fe(II) to Fe(III) by residual disinfectants along with other oxidants, and consequent precipitation. As several studies have stated that free chlorine is used up preliminarily by iron oxides (Rossman et al., 2001), therefore it is presumed that smaller amount of free chlorine is available to react with DBPs precursors to form DBPs. However, the current bench scale experiments showed that the formation of HAAs and THMs were lower in presence of Fe(II) ions compared with the control water systems (in absence of Fe(II) ions). Consequently, HAAs and THMs formation was decreased gradually with the increase in Fe(II) ions concentration in water samples (Figures 6.2(a) and (b)). In addition to chlorine reactivity with Fe(II) ions, it is also thought that DBPs those are formed at initial stage in interaction of chlorine with DOM, are adsorbed on the iron oxides surfaces.

Table 6.3. Effect of Fe(II) ions concentrations (mg/L) and different reaction times (h) for HAAs and THMs formation study in synthetic water samples.

Concentration of Fe(II) ions	Reaction time (h)				
	3.5 h	24 h	48 h	84 h	130 h
HAAs reduction percentage (%)					
0.35 mg/L	41.50 %	51.89 %	48.26 %	45.99 %	43.45 %
0.7 mg/L	61.26 %	62.85 %	56.48 %	58.46 %	60.68 %
1.5 mg/L	60.42 %	68.43 %	68.24 %	68.81 %	69.45 %
2.0 mg/L	70.63 %	72.34 %	65.35 %	68.73 %	72.50 %
3.0 mg/L	71.02 %	68.22 %	68.77 %	70.79 %	73.05 %
THMs reduction percentage (%)					
0.35 mg/L	23.53 %	25.06 %	34.32 %	34.52 %	34.76 %
0.7 mg/L	36.27 %	41.13 %	54.46 %	54.24 %	53.97 %
1.5 mg/L	38.92 %	41.52 %	49.79 %	45.63 %	40.64 %
2.0 mg/L	36.45 %	42.80 %	52.58 %	47.00 %	40.31 %
3.0 mg/L	45.07 %	49.13 %	59.79 %	60.01 %	60.26 %

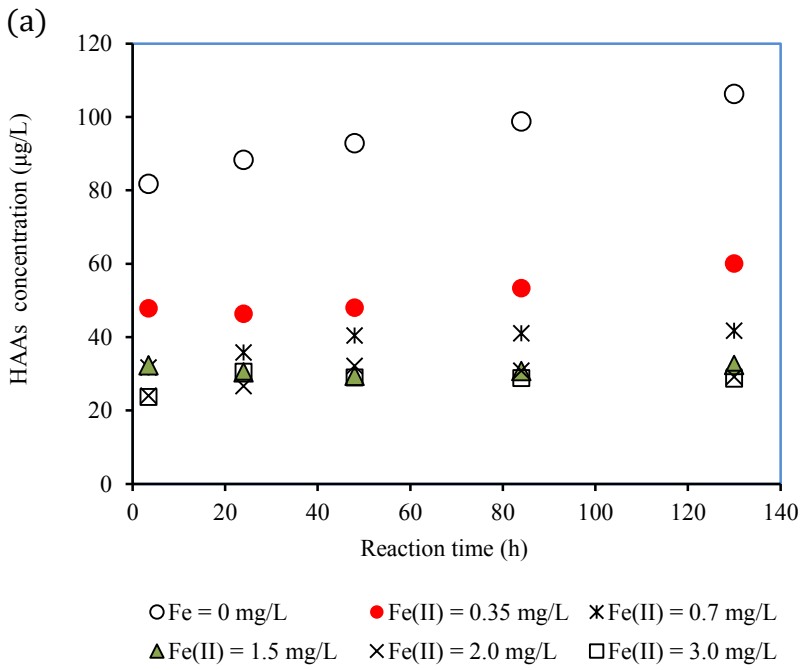

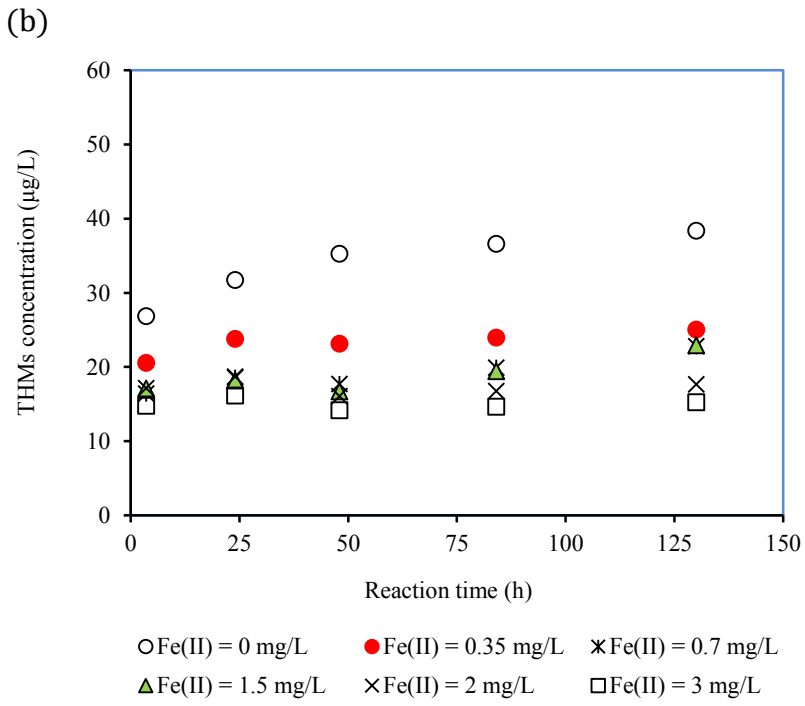

Figure 6.2. Effect of Fe(II) ions concentrations (mg/L) and reaction times (h) on (a) HAAs and (b) THMs formation in synthetic water samples (chlorine to carbon mole ration 0.79, pH 6.5, lab temperature 21 ± 1 °C).

Table 6.4. Two way ANOVA test on effect for different concentrations of Fe(II) ions (mg/L) and different reaction times (h) for HAAs and THMs formation study (chlorine to carbon mole ratio of 0.79, pH 6.5, lab temperature 21 ± 1 °C).

Source of variation	*SS*	*df*	*MS*	*F*	*P-value*	*F crit*
Haloacetic acids (*HAAs*)						
Fe(II) conc. (mg/L)	2022.16	4	505.54	36.01	< 0.001	3.007
Reaction time (h)	164.35	4	41.09	2.92	> 0.05	3.007
Error	224.68	16	14.04			
Total	2411.19	24				
Trihalomethanes (*THMs*)						
Fe(II) conc. (mg/L)	185.39	4	46.36	27.93	< 0.001	3.007
Reaction time (h)	39.45	4	9.86	5.94	< 0.004	3.007
Error	26.55	16	1.66			
Total	251.39	24				

The major portion of HAAs and THMs formation in all samples were observed at the initial 3.5 h of the reaction period (Figures 6.2(a) and (b)). However, HAAs and THMs formation was monitored up to 130 h (5.5 days) of the reaction periods. It was found that the HAAs and THMs concentrations in the control water systems were gradually and slightly increased with the increase in reaction times. Conversely, in the presence of different of dosages of Fe(II) ions in solution, HAAs and THMs formation were appeared relatively constant after 48 h of the reaction period. Statistical analysis (two-way ANOVA) for the HAAs formation data revealed that Fe(II) ions significantly reduced the formation of HAAs ($p < 0.001$) and THMs ($p < 0.001$) at a 95% confidence level (Table 6.4). The results of this study suggested that the presence of ferrous iron in solutions changed the reactivity between chlorine and DOM, which led to a net decrease in the formation of HAAs and THMs. ANOVA test revealed that the studied reaction times were not statistically significant ($\alpha = 0.05$, $p > 0.05$) for the change in HAAs formation.

Conversely, the reaction times were statistically significant for the changes in THMs formation for the different dosages of Fe(II) ions in the iron water systems (Table 6.4).

6.4.1.2. Effect of pH

Typical pH values in drinking water treatment and distribution systems have been reported to be 6.5 to 9.0 (Chun et al., 2005). Therefore, this comprehensive study was conducted at pH value of 6.5 and 8.5 for chlorine to carbon mole ratio of 0.79 in four different reaction systems. This study revealed that in the control water systems (in absence of Fe(II) ions and PO_4), the change in pH values from 6.5 to 8.5, the average HAAs formation was not significantly changed (Figure 6.3(a)), while THMs formation was observed to increase in the same reaction systems (Figure 6.3(b)).

Consequently, this study revealed that in presence of Fe(II) ions and phosphate based corrosion inhibitor, solution pH had an obvious impact on the formation and distribution of HAAs and THMs. In presence of 3 mg/L Fe(II) ions in solutions, the change in pH values from 6.5 to 8.5, led to a 2.5 fold increment of HAAs formation (Figure 6.3(a)); and a 9 fold increment on THMs formation (Figure 6.3(b)) following the same reaction conditions. The results of this study was in agreement with the research by Liu et al. (2011), who indicated that in the presence of ferric iron during chlorination, solution pH had a noticeable impact on the formation and distribution of HAAs and THMs. This study also demonstrated that a lower pH value of 6.5 contributed a lower content of HAAs and THMs compared with a higher pH value of 8.5 in the iron water systems. The influence of pH in the formation and distribution of HAAs and THMs in iron water systems could be affected by the following possible reasons: (1) at a higher pH level, the dissolved metal ions could directly enhance chloride ions ($OCl^- \rightarrow O_2 + Cl^-$, Gray et al., 1977), (2) increase in pH values from 6.5 to 8.5, Fe(II) ions oxidation increases significantly to generate Fe(III) oxides (Davidson and Seed, 1983), (3) Fe(III)

oxides profoundly adsorb DOM compare to Fe(II) oxides (Rahman et al., 2013), and (4) Fe(III) oxides interaction with DOM increases the number of DOM reactive sites for chlorine attack as well as modify the DOM characteristics (Hassan et al., 2006). Therefore, the results of this study might have implications for understanding the facts that pH change in drinking water distribution systems not only affects the Fe(II) ions oxidation processes, but has also impact on the formation of HAAs and THMs as well as to affect the reactivity between DOM and chlorine (Liu et al., 2011).

Nevertheless, this study revealed that HAAs formation was lower at a pH value of 6.5, compared with the pH value of 8.5 in presence of phosphate (1.5 mg-PO_4/L) associated with Fe(II) ions (3 mg/L) in solutions (Figure 6.3(a)), while an adverse trend was observed for THMs formation study in the same reaction systems (Figure 6.3(b)). However, when pH values were changed from 6.5 to 8.5 in the presence of phosphate ions alone, HAAs and THMs formation were observed to decrease. The same trends were found for both the reaction periods of 3.5 and 24 h respectively.

This study revealed that in the control water systems, DCAA formation was favored at a high pH value of 8.5 but an adverse trend was observed for TCAA formation (Figure 6.4). Figure 6.4 demonstrates that TCAA formation is exceeded DCAA formation at pH 6.5 in control water systems. These findings are consistent with the reported results in the literature (Liang and Singer, 2003; Uyak et al., 2007). Conversely, in the presence of Fe(II) ions alone, and along with phosphate; an increment for DCAA, TCAA and BCAA was observed for the change in pH values from 6.5 to 8.5. This can be attributed to the facts that the changes in pH values can change iron oxidation rate even though in presence of phosphate. However, this study has been suggested that the impact of pH on the formation of HAAs is complicated; because the rate of HAAs formation and hydrolysis varies for each individual species in different reaction systems.

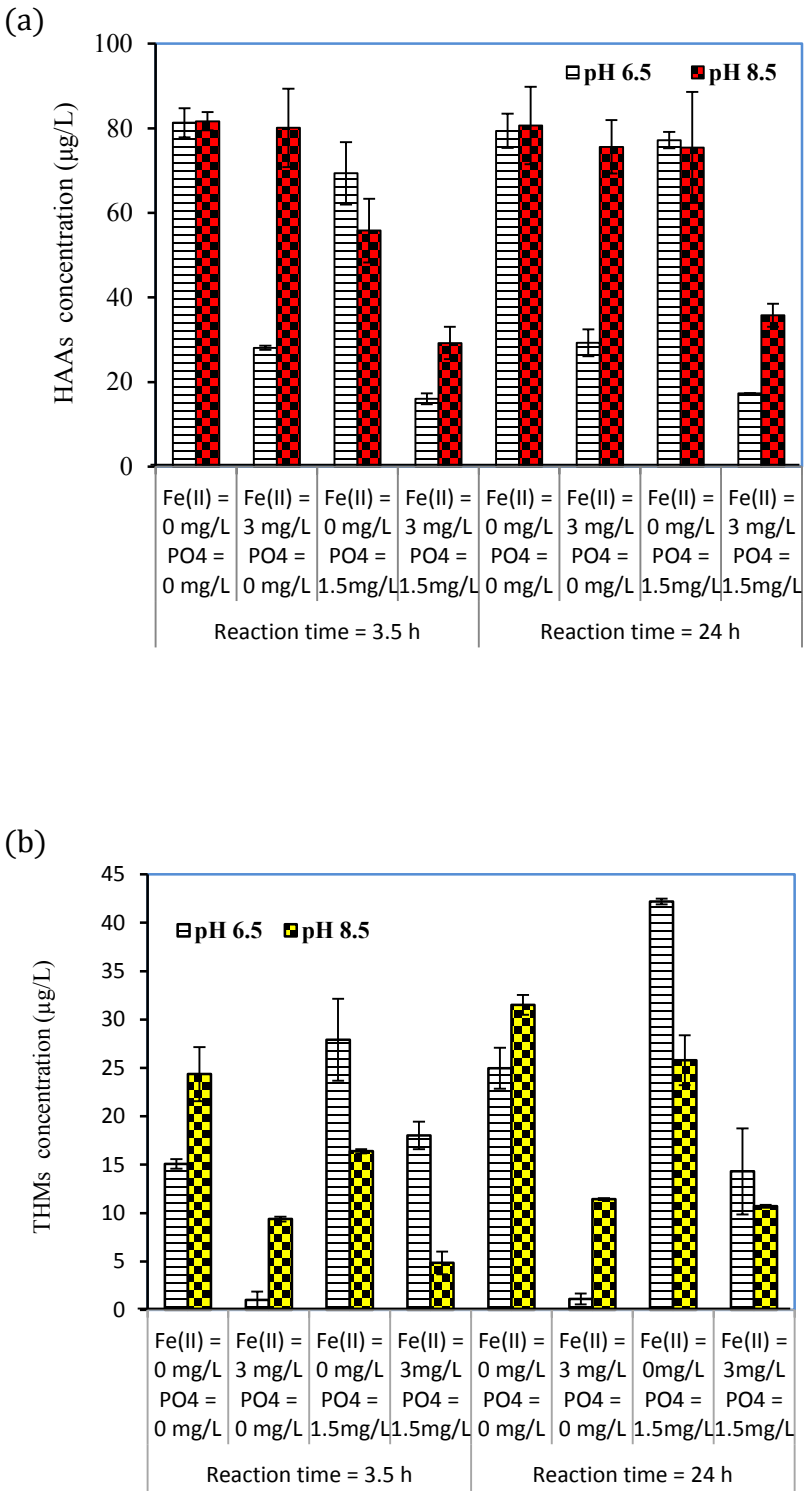

Figure 6.3. Effect of pH on (a) HAAs and (b) THMs formation in synthetic water for different reaction systems (chlorine to carbon mole ration 0.79, temperature 21 ± 1 °C).

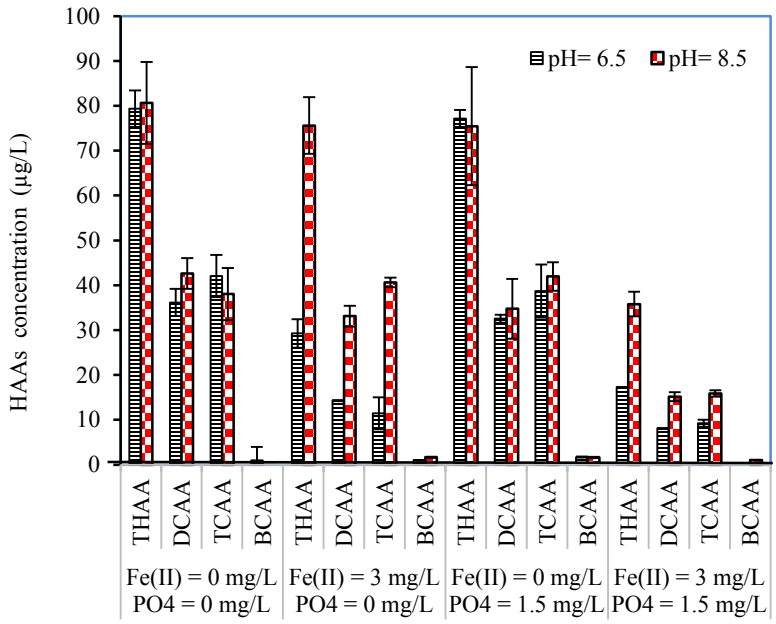

Figure 6.4. Effect of pH on HAAs formation and speciation in different reaction systems (chlorine to carbon mole ratio of 0.79, reaction period of 24 h at 21 ± 1 °C temp).

Chloroform was mainly found in all THM speciation studies, and other species were not present significantly in the studied reaction systems. This finding is within reasonable agreement with the published literature of Sadiq et al. (2002), who have been reported that chloroform is the most usually THM species, and constitutes nearly 90% of total THMs concentration. However, total THMs concentration was discussed in this study. THM speciation and distribution was not discussed here.

6.4.1.3. Effect of PO_4 dosage and reaction time

Phosphate based corrosion inhibitors are typically dosed into their treated water at a dosage of 0.5 to 3 mg-PO_4/L (Kirmeyer et al., 2000; Maddison et al., 2001). Therefore,

a 1.5 mg/L, phosphate dosage was selected for this bench scale comprehensive study. This study was conducted in presence of different dosages of Fe(II) ions in synthetic water samples at different reaction times and different pH values. This comprehensive study revealed the interaction effects of a phosphate based corrosion inhibitor with the different dosages of Fe(II) ions on the formation of HAAs and THMs (Figures 6.5 and 6.6).

The paired Student *t*-test illustrated that HAAs formation was significantly lower for the presence of phosphate (1.5 mg-PO_4/L) in iron water systems compared with the iron water systems only (no phosphate) for the reaction periods of 24 h ($p = 0.008$), 48 h ($p = 0.042$), 84 h ($p = 0.036$) and 130 h ($p = 0.005$) respectively (Figures. 6.5(b), (c), (d), and (e)) at a confidence level of 95% (Table 6.5). This finding was in agreement with the research by Zhang and Andrews (2012), who indicated that HAAs formation was decreased significantly in the presence of phosphate associated with iron coupon compared with the presence of iron coupon only. However, for the reaction period of 3.5 h, this study showed that the phosphate based corrosion inhibitor (1.5 mg-PO_4/L) was not statistically ($\alpha = 0.05$, $p = 0.878$) significant to reduce HAAs formation in the same reaction systems (Figure 6.5(a)). The finding of this study was in agreement with the research by Zhang and Andrews (2012), who conducted batch tests using three metals (Fe, Cu and Pb) coupons in presence of 1 mg/L phosphate, and in absence of phosphate. They reported that during a short reaction period (< 12 h), phosphate did not considerably affect HAAs formation. The analysis of the results illustrated that in presence of a phosphate based corrosion inhibitor (1.5 mg-PO_4/L) in the iron water systems, the statistical variation ($\alpha = 0.05$, $p \leq 0.005$) of HAAs formation was higher (Table 6.5) for the reaction period of 130 h (Figure 6.5(e)), compared with the reaction periods of 84, 48, 24 and 3.5 h respectively (Figures 6.5(a) – (d)).

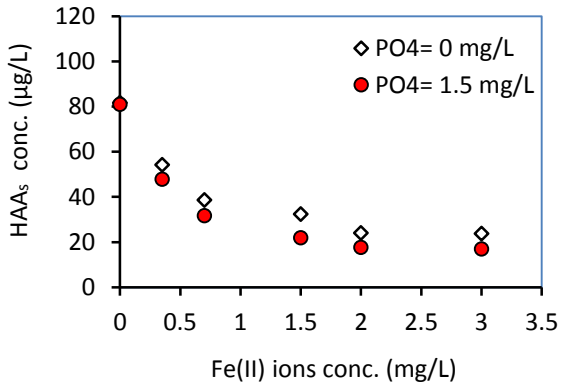

(a). Reaction time: 3.5 h

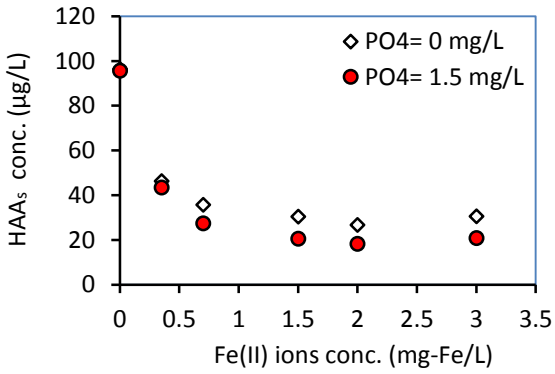

(b). Reaction time: 24 h

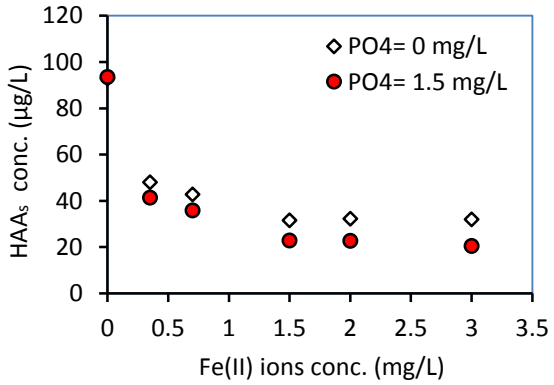

(c). Reaction time: 48 h

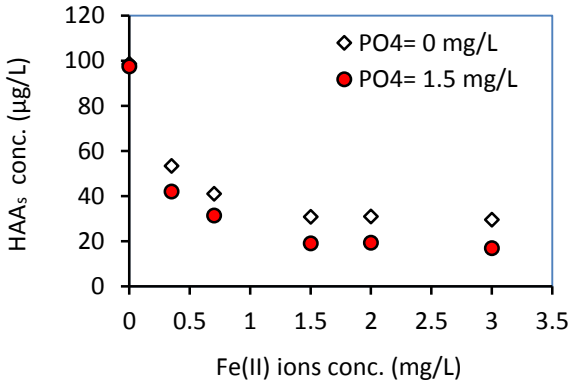

(d). Reaction time: 84 h

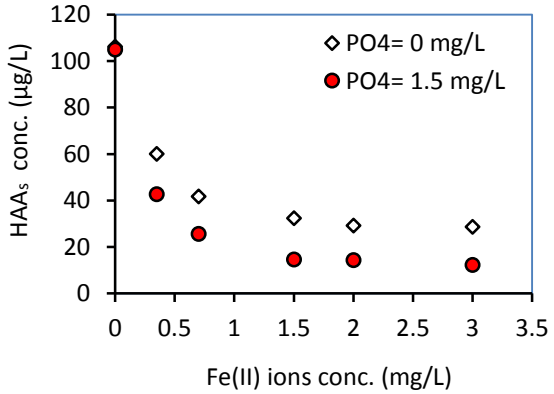

(e). Reaction time: 130 h

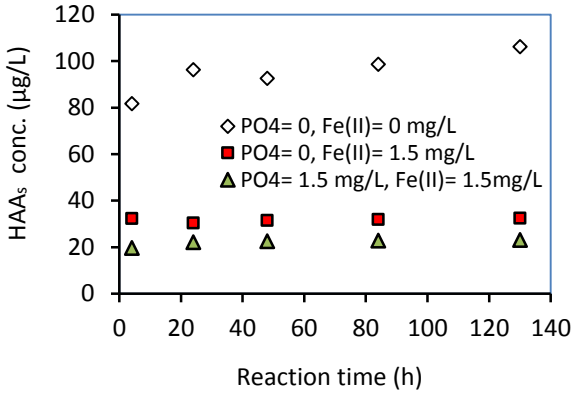

(f). Effect of PO_4 for all reaction periods

Figure 6.5. Effect of phosphate (1.5 mg-PO_4/L) on HAAs formation in synthetic water for (a) 4 h, (b) 24 h, (c) 48 h, (d) 84 h, (e) 130 h, and (f) all reaction periods together (chlorine to carbon mole ration 0.79, pH 6.5, lab temperature 21 $\pm$ 1 °C).

For the THMs formation study, it was observed that an addition of phosphate (1.5 mg-PO_4/L) in the control water system for a pH value of 6.5, THMs formation was significantly increased. Nevertheless, in iron water systems, a same trend was observed to increase THMs formation in presence of phosphate for a pH value of 6.5. The increment of THMs formation was observed for both the reaction periods of 3.5 and 24 h respectively in the same reaction systems (Figure 6.6). However, when the reactions were conducted at a pH value of 8.5, the adverse trend was observed to decrease THMs formation for both the reaction periods of 3.5 and 24 h in both reaction systems. Therefore, it has been suggested that the impact of phosphate on the formation of THMs is dependent on solution pH values.

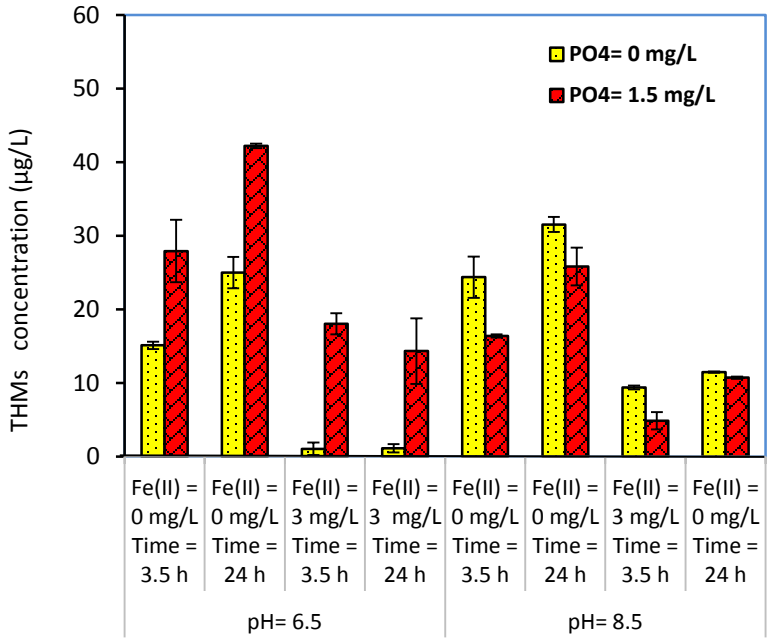

Figure 6.6. Effect of phosphate (1.5 mg-PO_4/L) on THMs formation in synthetic water samples (chlorine to carbon mole ration 0.79, pH 6.5, lab temperature 21 ± 1 °C).

Table 6.5. The paired Student's *t*-test for the effect of phosphate dosage on HAAs formation in synthetic water samples at different reaction times (chlorine to carbon mole ratio of 0.79, pH 6.5, lab temperature 21 ± 1 °C).

Statistical factors	Reaction time (h)				
	4 h	24 h	48 h	84 h	130 h
Pooled variance	48.97	14.92	39.51	36.04	36.92
t Stat	1.54	3.324	2.07	2.69	3.79
t Critical	1.94	1.943	1.943	1.94	1.94
P(T<=t)	0.087	0.008	0.042	0.036	0.005
Remark	*Insignificant*	*Significant*	*Significant*	*Significant*	*Significant*

6.4.1.4. Overall correlation

Several previous studies have provided results that DCAA, TCAA and MCAA are the main HAAs species in the chlorinated drinking water supplies (Rodriguez et al., 2004; Zhang and Andrews, 2012). In the current study, MCAA was not found in most of the samples. However, the results of our study revealed that DCAA and TCAA were found to be the most common HAA species with a content of over 90% of total HAAs. This study revealed that TCAA was the most abundant HAA species ($51.93 \pm 11.4\%$), followed by DCAA ($45.34 \pm 7.5\%$), and BAA ($1.14 \pm 1.6\%$) respectively in the control water systems. This study also illustrated that less formation of DCAA, TCAA and BCAA was occurred, when 1.5 mg/L phosphate was added in iron water systems compared with the absence of phosphate (Figure 6.4). Bromine was not present in the synthetic water systems. Consequently, no major brominated HAAs and THMs species were significantly observed in this study. However, small amount of BCAA was found due to the presence of trace amount of bromide in NaOCl solution. Conversely, chloroform was mainly observed for THMs formation study in the different reaction systems.

Table 6.6. The Pearson's correlations between THMs, HAAs, DCAA, TCAA, BCAA, pH, PO_4 dosage, Fe(II) ions and reaction time.

Variable	THMs	HAAs	DCAA	TCAA	BCAA	pH	PO_4	Fe(II)	Time
THMs	1								
HAAs	0.56[b]	1							
DCAA	0.52[b]	0.96[b]	1						
TCAA	0.60[b]	0.98[b]	0.88[b]	1					
BCAA	0.08[b]	0.69[b]	0.62[b]	0.68[b]	1				
pH	0.16	0.45[b]	0.42[b]	0.40[b]	0.74[b]	1			
PO_4 dose	0.25[a]	-0.48[b]	-0.51[b]	-0.46[b]	-0.12	-0.04	1		
Fe(II) ions	-0.79[b]	-0.47[b]	-0.43[b]	-0.48[b]	-0.07	0.26[a]	0.17	1	
Time	0.26[a]	-0.09	-0.22	0.01	-0.19	-0.36[b]	-0.04	-0.16	1

[a] Correlation is significant at the 0.05 level (2-tailed).

[b] Correlation is significant at the 0.01 level (2-tailed).

The Pearson's correlation matrix between all the variables (e.g., Fe(II) ions, pH, phosphate dosage, reaction time, total THMs, total HAAs, and HAA species) in synthetic water samples (number of observations 79) was performed using a windows version software 'IBM SPSS Statistics 20' (IBM, USA); and the results are presented in Table 6.6. This study revealed a significant positive correlation between the pH values and the formation of total HAAs ($r = 0.45$, $p < 0.0001$) and individual HAA species: DCAA ($r = 0.42$, $p < 0.0001$), TCAA ($r = 0.49$, $p < 0.0001$) and BCAA ($r = 0.74$, $p < 0.0001$). Conversely, a negative and moderate correlation was observed between the phosphate based corrosion inhibitor and the formation of total HAAs ($r = 0.48$, $p < 0.0001$), DCAA ($r = 0.51$, $p < 0.0001$), and TCAA ($r = 0.46$, $p < 0.0001$) in the same reaction systems. The Pearson's correlation analysis showed a moderate and negative relationship between

Fe(II) ions and the formation of total HAAs ($r = 0.47$, $p < 0.0001$), DCAA ($r = 0.43$, $p < 0.0001$), and TCAA ($r = 0.48$, $p < 0.0001$) respectively. The correlation coefficients values between total HAAs and individual HAA species were higher ranging from 0.62 to 0.98 ($p < 0.0001$), showing that each HAA species was strongly related to the other HAA species.

On the other hand, an attempt was made to determine the correlation between total THMs (mainly chloroform), total HAAs, and also different variables studied here. This study showed that Fe(II) ions had a strong negative correlation with the THMs formation ($r = -0.79$, $p < 0.0001$) compared with the HAAs formation ($r = -0.48$, $p < 0.0001$). This is indicating that Fe(II) ions has more impact to reduce THMs formation study. The Pearson's correlation matrix showed a strong positive correlation between THMs and HAAs, DCAA, TCAA, indicating that the formation of total THMs and HAA species increases in parallel. A medium correlation between Fe(II) ions and pH ($\alpha = 0.05$, $p = 0.023$) was observed, indicating that an interaction may exist between the two independent variables. Therefore, the affiliation between one of the independent variables (pH or Fe(II) ions), and the dependent variable (HAAs and THMs) was dependent upon the values of the other independent variables. The Pearson's correlation matrix showed a correlation between reaction time and pH values ($\alpha = 0.05$, $p = 0.001$). This finding from the statistical analysis ($\alpha = 0.05$, $p = 0.023$) is similar with the pH monitoring data (not presented in here), acknowledges that the increase in reaction times, decrease the pH values in different reaction systems. The correlation among the other factors can also be found in Table 6.6.

6.4.2. Molecular weight (MW) distribution and DBPs formation

The HPSEC chromatograms were used to determine the molecular weight (MW) distribution of DOM in the studied water samples for control water systems; and in

presence of chlorine and iron. This study revealed that in presence of chlorine, no significant change in MW distribution of DOM in water samples was observed. Conversely, in presence of iron a pronounced change was observed (Figure 6.7). The same trend was reported in the literature (Świetlik et al., 2002), who conducted an experiment with ClO_2, and showed that there was no significant change on molecular weight distribution of DOM in presence of ClO_2 compared with the control water system (in absence of ClO_2).

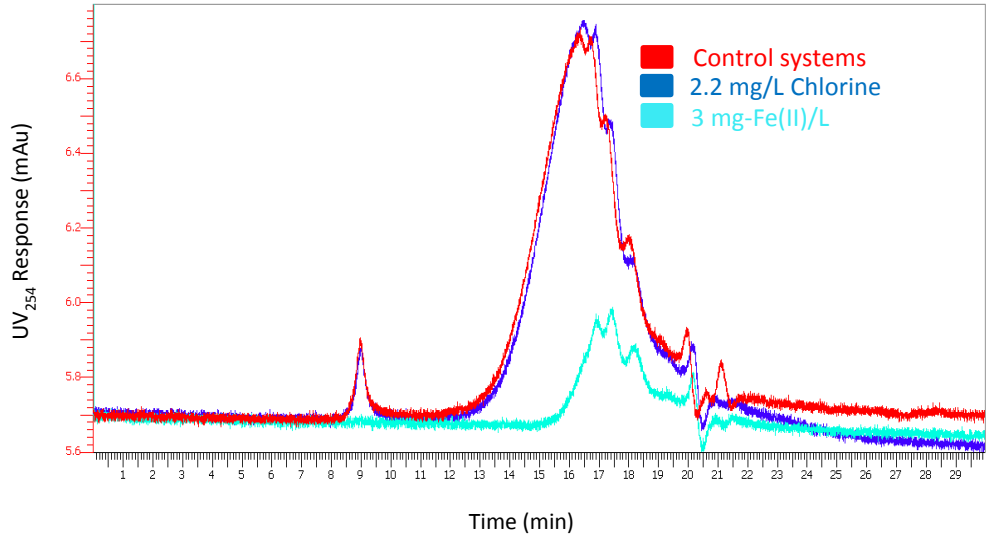

Figure 6.7. High performance size exclusion chromatograph for DOM in studied water samples for the control system, for the presence of chlorine and iron.

It should be noted here that the higher MW organic fractions are eluted from the column first and lower MW organic fractions are eluted later. The entire MW distribution

of DOM in the samples was obtained by integrating the total area of the sample using Totalchrom software (Perkin Elmer, Ontarion, Canada) (Figure 6.7). The data for elution times and MW distribution associated with different peaks for three different reaction systems are provided in Tables C30 to C32 of Appendix C. HPSEC analysis revealed that the higher molecular weight fractions (> 2000 Da) were consisted more than 50% of the chromatograph areas in the control water systems. However, the higher MW fractions of DOM were observed to modify significantly in presence of iron in solutions than that of lower MW fractions of DOM in solution (Figures 6.7 and 6.8). It could be happed due to the reason that the higher MW compounds tend to be more aromatic in nature, so they might have a larger number of reaction sites than smaller MW compounds. The change in MW distribution of DOM is coincident with that of the DBPs formation study in presence and absence of iron in solutions. Consequently, this study suggested that iron significantly reduced the DBPs formation by altering the MW distribution in solutions. This hypothesis was in agreement with the previous researches (Eikebrokk et al., 2004), which stated that the hydrophobic fractions of DOM in water generally contained higher molecular weight components of DOM. On the other hand, hydrophobic fractions were reported to be the most reactive DOM components in DBPs formation study (Marhaba and Van, 2000; Chang et al., 2001).

Therefore, this study has been suggested that the determination of MW distribution of DOM in water samples can provide important information on the impact of most available metals (e.g., Cu, Pb, and Zn) in water with the specific fractions of DOM that may play a vital role in the formation of DBPs in distribution systems.

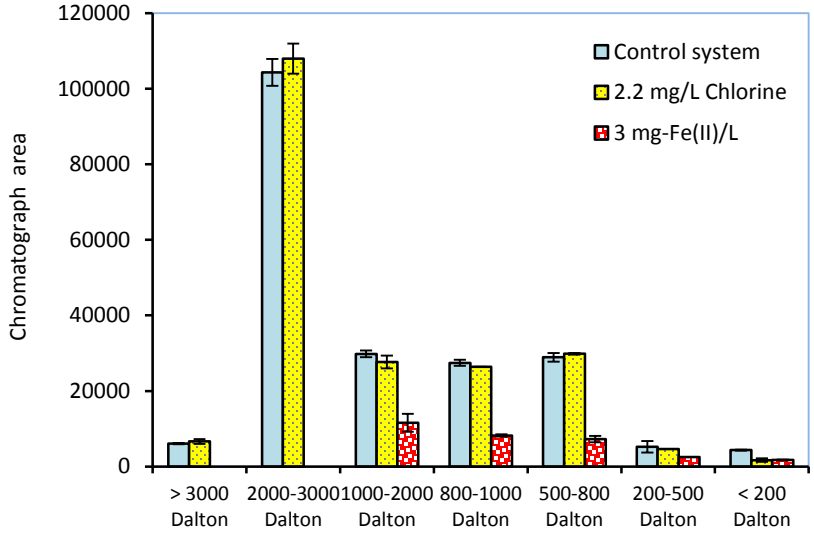

Figure 6.8. Chromatogram area counts for different molecular weight fractions of DOM in studied water samples for the control system, for the presence of chlorine and iron.

6.4.3. Model development

The mathematical models for HAAs and THMs formation were developed based on a 2^4 full factorial design with center points approach including four potential explanatory variables, i.e., (A) Fe(II) ions, (B) pH, (C) phosphate based corrosion inhibitor, and (D) reaction time. All experiments for the factorial design approach for HAAs and THMs formation were conducted in duplicate and the repeatability was checked by paired Student's *t*-test at a 95% confidence level (Tables C53 and C57, Appendix C). The average values for HAAs and THMs concentrations were used for the statistical analyses. The experimental conditions associated with the two data sets were used in the development of HAAs and THMs prediction models which are shown in Table 6.7. These values were chosen because they are typical values in many drinking water distribution

systems. Statistical analysis of the experimental data (number of observation 80) was conducted using Minitab® 16 statistical package (MINITAB Inc., State College, Pennsylvania, USA). The results of the analysis are presented in Tables 6.8(a) and (b), which show the estimated parameter values, their standard errors, and summarization of the hypothesis results for the significance of each parameter. The statistical significance was determined based on the Student's *t*-test associated with the values of probability (p). The statistical significance is represented in terms of Prob > | t | in Tables 6.8(a) and (b). It should be noted that if the value of Prob > | t | for a factor is less than 0.05, the factor is considered to be statistically significant (Montgomery, 2009).

In this study, the negative value of coefficient indicated that a high level setting of the factor provided lower content for DBPs formation than the low level setting, and vice versa for the positive value of the coefficients. Statistical analysis for HAAs formation results are presented in Table 6.8(a). This study revealed that the concentration of Fe(II) ions (factor *A*) was the most significant factor ($p < 0.0001$, contribution 50.85%) on the formation of HAAs followed by the phosphate based corrosion inhibitor ($p < 0.0001$, contribution 14.96%) and pH ($p \leq 0.01$, contribution 7.92%) respectively at a 95% confidence level (Table C54 in Appendix C). Several interaction factors including *AB* (Fe(II) ions and pH, contribution 13.94%), *AC* (Fe(II) ions and phosphate dosage, contribution 3.65%) and *BC* (pH and phosphate dosage, contribution 3.97%) were also shown to be statistically ($\alpha = 0.05$, $p < 0.05$) significant on the formation of HAAs (Table 6.8(a)). However, for the THMs formation study, the statistical analysis ($\alpha = 0.05$) indicated that the most significant main factors were Fe(II) ions ($p < 0.0001$, contribution 60.41%) followed by reaction time ($p = 0.009$, contribution 6.49%) and phosphate based corrosion inhibitor ($p = 0.013$, contribution 5.46%) respectively (Table C58 in Appendix C). The most significant interaction factors on the formation of THMs were *BC* (pH and phosphate, $p = 0.001$, contribution 20.07%) followed by *AD* (Fe(II) ions and reaction time, $p = 0.021$, contribution 4.25%) respectively (Table 6.8(b)).

Table 6.7. Matrix of the experimental study for a 2^4 full factorial design with center points approach for HAAs and THMs formation in synthetic water samples.

Exp No	Factors				DBPs Species (µg/L)			
	Fe(II) mg/L (A)	pH unit (B)	PO_4 mg/L (C)	Time min (D)	HAAs formation		THMs formation	
					Response 1	Response 2	Response 1	Response 2
1	0 mg/L	6.5	0 mg/L	3.5 h	78.87	83.75	14.74	15.43
2	3 mg/L	6.5	0 mg/L	3.5 h	27.76	28.43	0.44	1.65
3	0 mg/L	8.5	0 mg/L	3.5 h	75.56	74.95	22.38	26.34
4	3 mg/L	8.5	0 mg/L	3.5 h	86.67	73.51	9.2	9.55
5	0 mg/L	6.5	1.5 mg/L	3.5 h	64.12	74.74	30.91	24.92
6	3 mg/L	6.5	1.5 mg/L	3.5 h	15.13	16.93	17.02	19.03
7	0 mg/L	8.5	1.5 mg/L	3.5 h	61.12	50.48	16.24	16.54
8	3 mg/L	8.5	1.5 mg/L	3.5 h	26.51	31.91	4.03	5.68
9	0 mg/L	6.5	0 mg/L	24 h	75.51	81.49	23.47	26.47
10	3 mg/L	6.5	0 mg/L	24 h	29.13	29.39	0.72	1.53
11	0 mg/L	8.5	0 mg/L	24 h	80.16	83.18	32.23	30.79
12	3 mg/L	8.5	0 mg/L	24 h	80.07	71.16	11.51	11.38
13	0 mg/L	6.5	1.5 mg/L	24 h	75.83	78.55	41.99	42.4
14	3 mg/L	6.5	1.5 mg/L	24 h	17.31	17.30	11.17	17.46
15	0 mg/L	8.5	1.5 mg/L	24 h	84.74	66.15	27.62	23.98
16	3 mg/L	8.5	1.5 mg/L	24 h	33.85	37.72	10.60	10.81
I	1.5 mg/L	7.5	0.7 mg/L	13.5 h	67.57	64.23	16.54	18.38
II	1.5 mg/L	7.5	0.7 mg/L	13.5 h	61.12	52.12	15.54	13.94
III	1.5 mg/L	7.5	0.7 mg/L	13.5 h	37.72	40.30	21.01	17.05
IV	1.5 mg/L	7.5	0.7 mg/L	13.5 h	50.48	45.78	15.44	17.04

Table 6.8(a). Estimated parameters and their significance for HAAs formation study in synthetic water samples.

Code	Term	Effect	Coef	SE Coef	t	p	Comments
	Constant		56.62	1.73	32.82	0.000	
A	Fe(II) ions conc. (mg/L)	-35.4	-17.7	1.73	-10.26	0.000	Significant
B	pH Unit	13.97	6.98	1.73	4.05	0.010	Significant
C	Phosphate (mg-PO_4/L)	-19.2	-9.6	1.73	-5.56	0.003	Significant
D	Reaction time (h)	4.44	2.22	1.73	1.29	0.254	
AB	Fe(II) · pH	18.53	9.27	1.73	5.37	0.003	Significant
AC	Fe(II) · Phosphate	-9.48	-4.74	1.73	-2.75	0.040	Significant
AD	Fe(II) · Time	-3.31	-1.65	1.73	-0.96	0.382	
BC	pH · Phosphate	-9.9	-4.95	1.73	-2.87	0.035	Significant
BD	pH · Time	2.6	1.3	1.73	0.75	0.486	
CD	Phosphate · Time	4.37	2.18	1.73	1.27	0.261	

$t_{0.025,\ 1,\ 5} = 2.571;\ t_{observed} > t_{critical}$ *is significant at* 95% *confidence level*

Table 6.8(b). Estimated parameters and their significance for THMs formation study

Code	Term	Effect	Coef	SE Coef	t	p	Comments
	Constant		17.45	0.69	25.39	0.000	
A	Fe(II) ions conc. (mg/L)	-17.17	-8.58	0.69	-12.49	0.000	Significant
B	pH Unit	-1.28	-0.64	0.69	-0.93	0.394	
C	Phosphate (mg-PO_4/L)	5.16	2.58	0.69	3.76	0.013	Significant
D	Reaction time (h)	5.63	2.81	0.69	4.10	0.009	Significant
AB	Fe(II) · pH	1.75	0.87	0.69	1.27	0.259	
AC	Fe(II) · Phosphate	1.07	0.53	0.69	0.78	0.473	
AD	Fe(II) · Time	-4.55	-2.28	0.69	-3.31	0.021	Significant
BC	pH · Phosphate	-9.89	-4.95	0.69	-7.20	0.001	Significant
BD	pH · Time	0.49	0.25	0.69	0.36	0.734	
CD	Phosphate · Time	0.83	0.42	0.69	0.60	0.572	

$t_{0.025,\ 1,\ 5} = 2.571;\ t_{observed} > t_{critical}$ *is significant at* 95% *confidence level*

A half-normal probability plot is used to evaluate graphically the statistical significance of the parameters on the formation of disinfection byproducts (DBPs), shows in Figures 6.9(a) and (b). The statistically significant effects on HAAs and THMs formation are indicated by the solid square signs showing a large deviation from the normal distribution line. However, the insignificant effects tend to follow a normal distribution (Montgomery, 2009). The data for HAAs and THMs present in graphs are completely consistent with the analysis performed for significant results present in Tables 6.8(a) and (b).

The effect of the simultaneous variability for the concentrations of Fe(II) ions, pH values, phosphate dosages and different reaction times on the formation of HAAs and THMs are shown in the contour plots (Figures 6.10 and 6.11). Curvature in the contour plots indicates the presence of two factors interactions (Montgomery, 2009; Chowdhury et al., 2010). In this study, the contour plots for the significant interactions on HAAs formation depict that the interaction effect of *BA* (Fe(II) ions and pH) play a major role to reduce HAAs formation showing curvature (Figure 6.10(a)). Figure 6.10(a) shows that two factors: *A* (Fe(II)) ions) and *B* (pH) are also interacted strongly with the factor *C* (phosphate dosage) showing curvature for *CA* and *CB* (Figures 6.10(b) and (d)). However, the contour plots show that there are no significant interactions effect for *DA* (time and Fe(II) ions), *DB* (time and pH) and *DC* (time and phosphate) for HAAs formation study (Figures 6.10(c), (e) and (f)), which are consistent with the results present in Table 6.8(a).

(a)

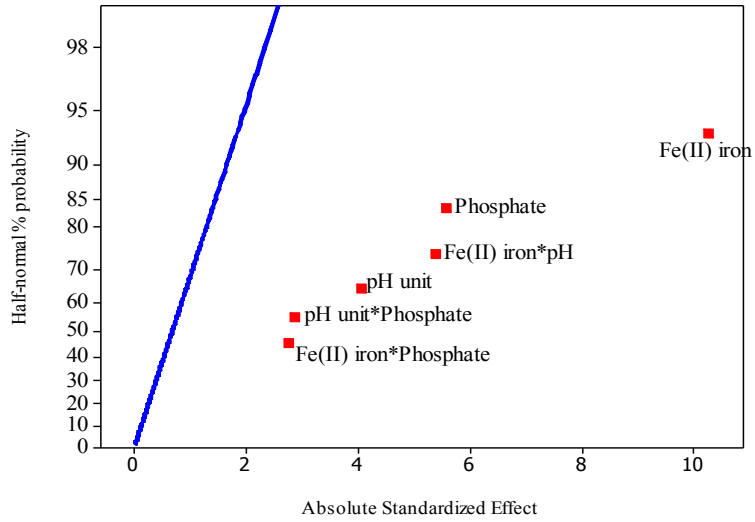

(b)

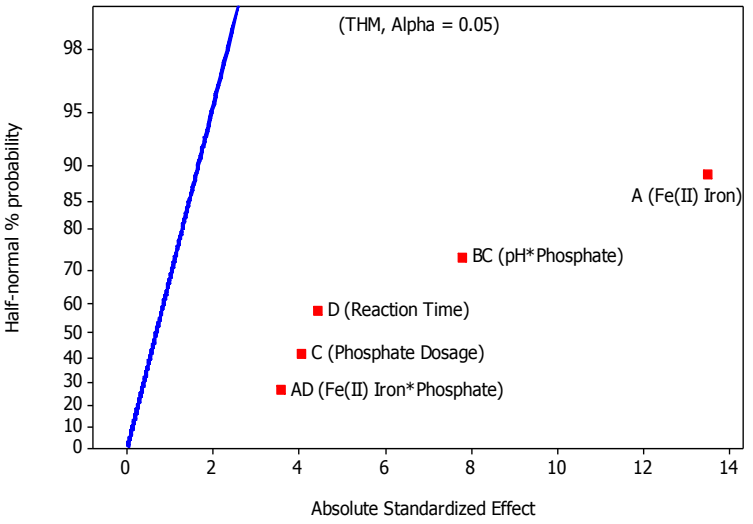

Figure 6.9. Half-normal plot showing the effect of studied factors and their interaction on (a) HAAs, and (b) THMs formation study.

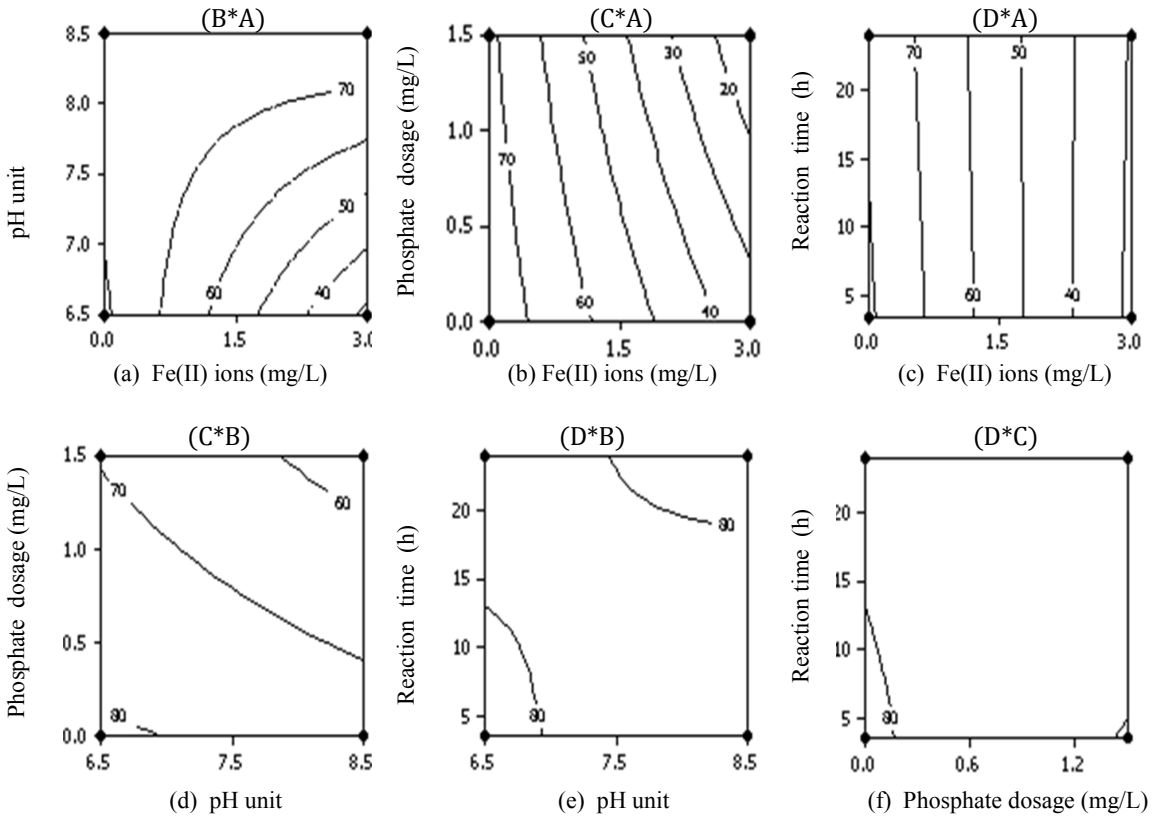

Figure 6.10. Contour plots for the interaction effects on HAAs formation in synthetic water samples following a 2^4 full factorial design approach.

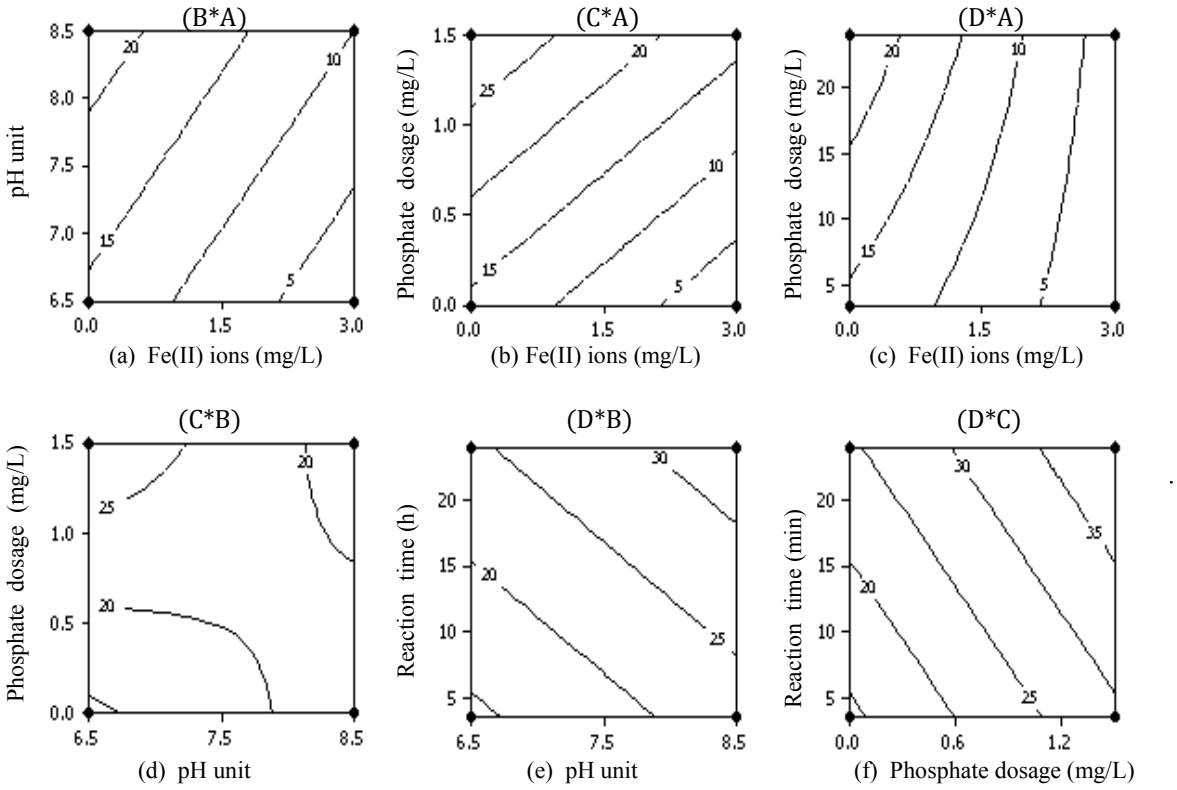

Figure 6.11. Contour plots for interaction effects on THMs formation in synthetic water samples following a 2^4 full factorial design approach.

The main and interaction effects of the significant variables in this study are plotted in Figures 6.12 and 6.13 to assess visually their impact on HAAs and THMs formation. The signs of the effects indicate the direction of the effects. It has been observed in Figure 6.12(a), that the main factors of Fe(II) ions concentration (factor *A*)

and phosphate dosage (factor *C*) are negative having slopes -35.4 and -19.2 respectively. Therefore, it has been indicated that when Fe(II) ions concentration and phosphate dosage are changed from a lower to a higher level, it reduces HAAs formation. However, a reverse trend is observed for the main effect of pH value (factor *B*) having slope +13.9 (Figure 6.12(a)). One of the major benefits of factorial design approach is that it gives more insight about the interaction between the input parameters on the responses (Hines et al., 2003; Montgomery, 2009). The interaction effects of the studied factors (e.g., *AB, AC, BC, AD, BD*, and *CD*) on HAAs formation are plotted in Figure 6.12(b). The non-parallel lines in these figures are indication of interaction between the two factors (Hines et al., 2003). The interaction plots for the factors of Fe(II) ions and pH demonstrate that the effect of Fe(II) ions concentration is very large to reduce HAAs formation when the pH value is at a low level (pH 6.5); but small when the pH value is at a high level (pH 8.5). However, the Fe(II) ions and PO_4 ions interaction plots show opposite trend, which indicate that Fe(II) ions has more impact to reduce HAAs formation at a high level of phosphate (1.5 mg/L) compared with a low level of phosphate dosage (0 mg/L) (Figure 6.12(b)). On the other hand, the interaction plots for pH and phosphate dosages indicate that higher level of phosphate (1.5 mg/L) has lower interaction effect but a reverse trend is observed for the lower phosphate dosage in solution. Conversely, the interaction plots between Fe(II) ions and reaction time (*AD*); pH and reaction time (*BD*); phosphate and reaction time (*CD*) show the parallel lines indicating that there is no interaction effects (Montgomery, 2009) on HAAs formation (Figure 6.12(b)). Therefore, this study illustrated that the lowest content of HAAs formation would appear to be obtained when the pH value was at a low level (6.5) and the phosphate dosage was at the high level (1.65 mg/L) in iron water systems.

The main effects of input parameters on THMs formation are graphically shown in Figure 6.13(a). It is observed that initial Fe(II) ions has a sharp effect (slope = -17.17) to reduce THMs formation (Figure 6.13(b) and Table 6.8(b)). However, when phosphate concentration and reaction time are increased, THMs formation is observed to

increase, that is consistent with the statistical analysis data. The effect of the solution pH shows a slight decrease (slope = -1.28) on THMs formation, as stated in the previous discussion that pH had not significant impact at a 95% confidence level for THMs formation study (Table 6.8(b)). The interaction plots for THMs formation are shown in Figure 6.13(b), which plots the mean response of two factors at all possible combination of their settings. The interaction plots for *AB* (Fe(II) ions and pH); *AC* (Fe(II) ions and PO_4 dosage), *BD* (pH and reaction time) and *CD* (PO_4 dosage and reaction time) show parallel lines indicating no interaction between the two factors (Montgomery, 2009) on THMs formation. However, the interaction plots for *BC* (pH and PO_4 dosage), and *AD* (Fe(II) ions and reaction time) show non-parallel lines revealing the interaction effect for THMs formation (Figure 6.13(b)). The interaction effects for *AD* (Fe(II) ions and reaction time) depict that at lower iron dosage, THMs formation is increased with the increase in reaction times; and that is consistent with the reported results in literature (Liang and Singer, 2003). However, in the presence of higher dosages of Fe(II) ions, the reaction time is shown to be insignificant. The interaction plots for *BC* (pH and PO_4 dosage), provide an interesting findings showing that at a lower PO_4 dosage (0 mg/L) increasing solution pH from 6.5 to 8.5, increases THMs formation but a reverse trend is observed when the solution pH is increased in the presence of higher dosage of PO_4 (1.5 mg/L) in the control water systems. Therefore, this study illustrated that the lowest content of THMs formation would appear to be obtained when PO_4 was present at 1.5 mg/L having a lower level of solution pH 6.5 in water systems.

According to the student's *t*-test, *F*-test and graphical analysis of the data for HAAs and THMs formation study, the effect of the reaction times (factor *D*) for HAAs formation; and the effect of pH (factor *B*) for THMs formation and several interaction effects, which were statistically insignificant compared with the other effects were discarded. Therefore, the parameters estimated for the final HAAs and THMs model are summarized in Tables 6.9(a) and (b). Subsequently, the regression models for prediction of HAAs and THMs can be presented as the following equations (Eqs. (6.8) and (6.10)):

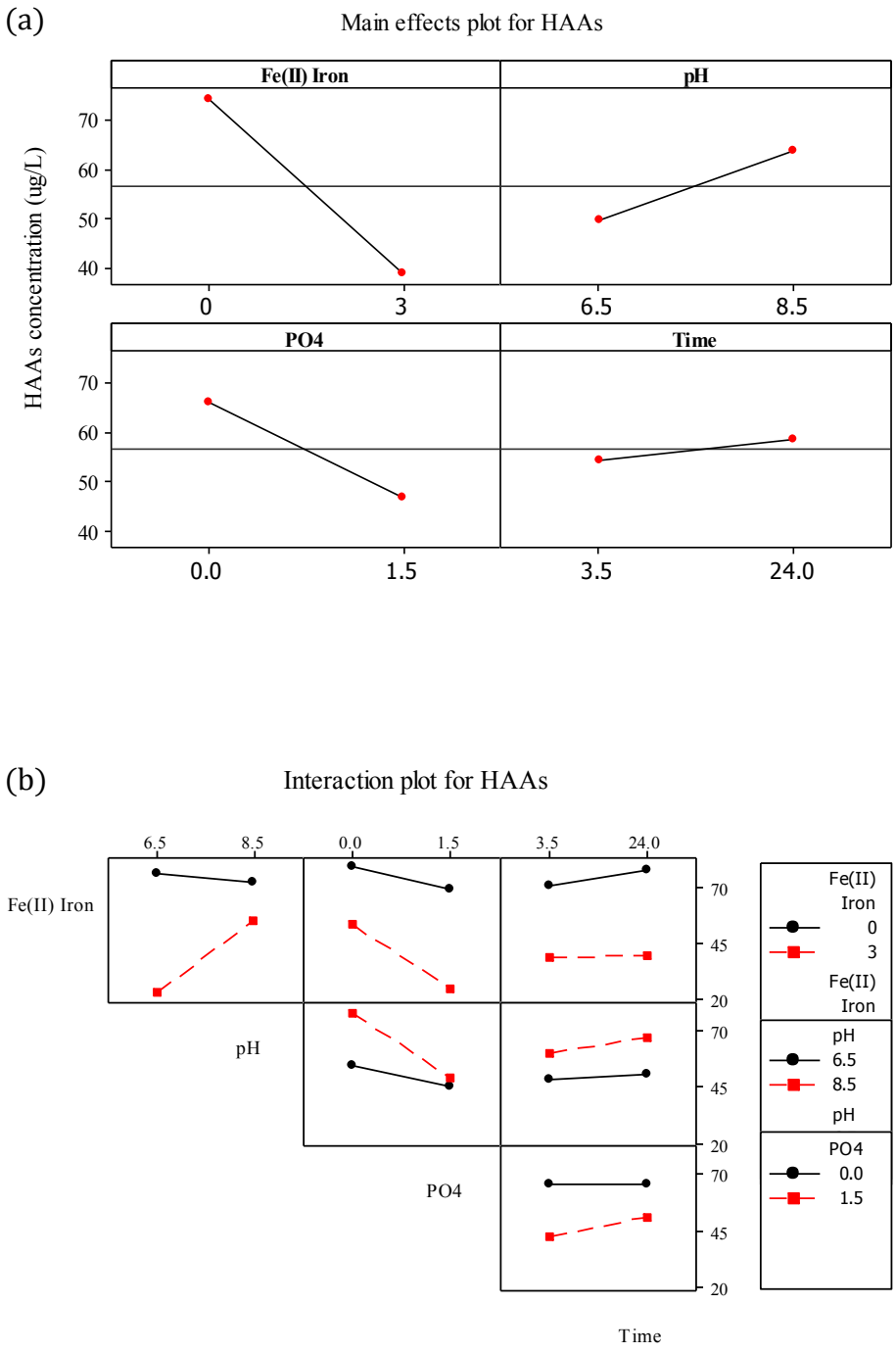

Figure 6.12. Plots of HAAs formation in synthetic water samples for (a) main effects, and (b) interaction effects following a 2^4 full factorial design approach.

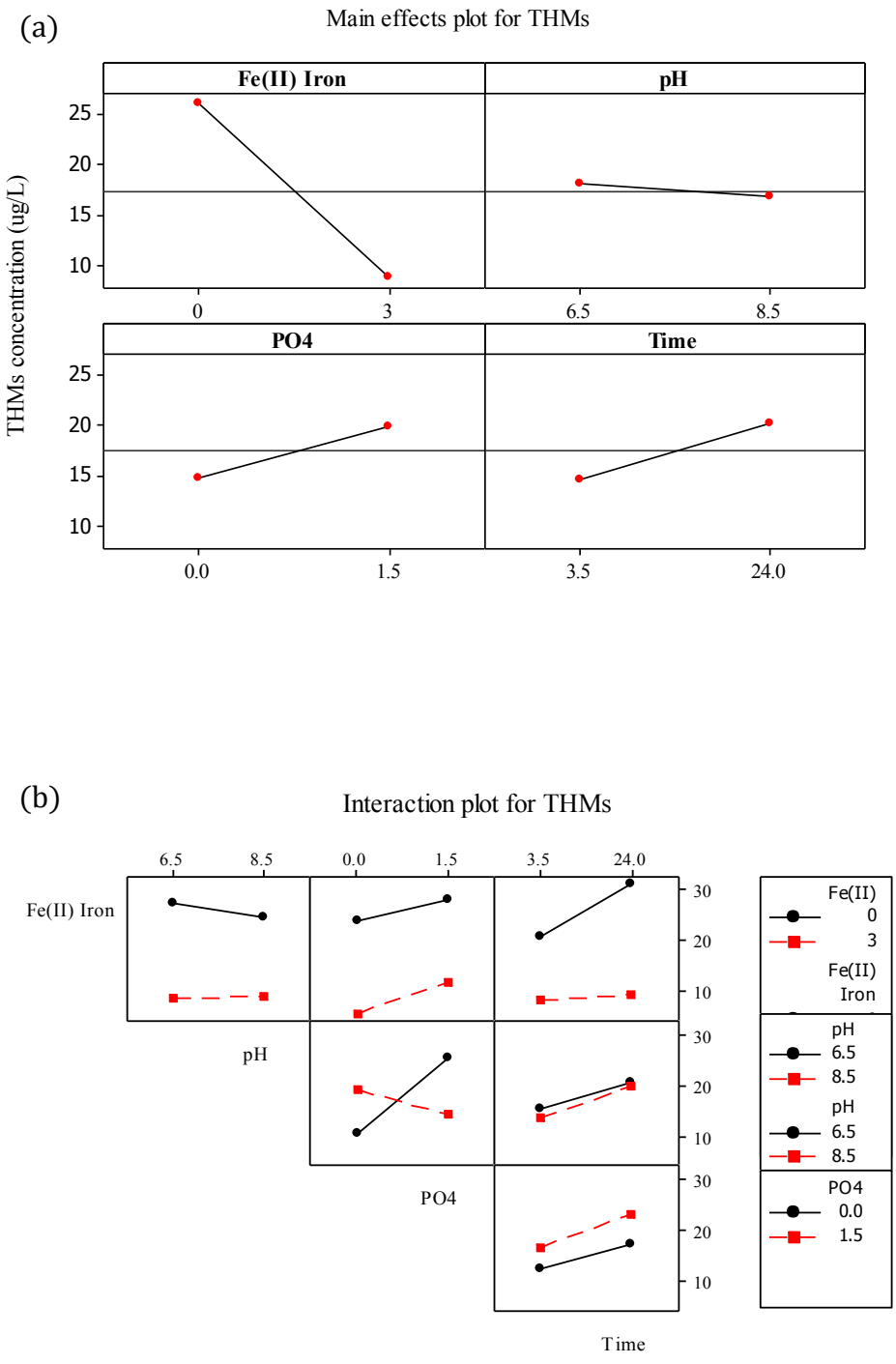

Figure 6.13. Plots of THMs formation in synthetic water samples for (a) main effects, and (b) interaction effects following a 2^4 full factorial design approach.

Table 6.9(a). Parameter estimates for HAAs formation model

Term	Parameter	Effect	Coef	SE Coef	*t*- value	*p*-value	Remark
Constant	β_o		56.62	1.80	31.54	0.000	
Fe(II) ions (mg/L)	β_1	-35.40	-17.70	1.80	-9.86	0.000	Decrease
pH unit	β_2	13.97	6.98	1.80	3.89	0.004	Increase
Phosphate (mg/L)	β_3	-19.20	-9.60	1.80	-5.35	0.000	Decrease
Fe(II) · pH	β_{12}	18.53	9.27	1.80	5.16	0.001	Increase
Fe(II) · Phosphate	B_{13}	-9.48	-4.74	1.80	-2.64	0.027	Decrease
pH · Phosphate	β_{23}	-9.90	-4.95	1.80	-2.76	0.022	Decrease

Table 6.9(b). Parameter estimates for THMs formation model

Term	Parameter	Effect	Coef	SE Coef	*t*- value	*P*-value	Remark
Constant	β_o		17.45	0.64	27.43	0.000	
Fe(II) ions (mg/L)	β_1	-17.17	-8.58	0.64	-13.50	0.000	Decrease
Phosphate (mg/L)	β_2	5.16	2.58	0.64	4.06	0.003	Increase
Reaction time (h)	β_4	5.63	2.81	0.64	4.42	0.002	Increase
Fe(II) · time	β_{14}	-4.55	-2.28	0.64	-3.58	0.006	Decrease
pH · Phosphate	β_{23}	-9.89	-4.95	0.64	-7.78	0.000	Decrease

***HAAs prediction model*:**

$$\hat{y}_{HAAs} = \hat{\beta}_0 + \hat{\beta}_1 A + \hat{\beta}_2 B + \hat{\beta}_3 C + \hat{\beta}_{12} AB + \hat{\beta}_{13} AC + \hat{\beta}_{23} BC \qquad (6.7)$$

where, $\hat{\beta}_0$ represents the global mean and $\hat{\beta}_i$ represents the regression coefficients. Substituting $\hat{\beta}_0$ and $\hat{\beta}_i$ in Eq. (6.7) by their values from the Table 6.9(a), the equation can be written as follows:

$$\hat{y}_{\mathrm{HAAs}} = 56.62 - 17.7(\mathrm{Fe}^{2+}) + 6.98(\mathrm{pH}) - 9.6(\mathrm{PO}_4) + 9.27(\mathrm{Fe}^{2+}.\mathrm{pH}) - 4.74(\mathrm{Fe}^{2+}.\mathrm{PO}_4) - 4.95(\mathrm{pH}.\mathrm{PO}_4) \quad (6.8)$$

***THMs prediction model*:**

$$\hat{y}_{THMs} = \hat{\beta}_0 + \hat{\beta}_1 A + \hat{\beta}_2 C + \hat{\beta}_3 D + \hat{\beta}_{14} AD + \hat{\beta}_{23} BC \quad (6.9)$$

where, $\hat{\beta}_0$ represents the global mean and $\hat{\beta}_i$ represents the regression coefficients. Substituting $\hat{\beta}_0$ and $\hat{\beta}_i$ in Eq. (6.9) by their values from the Table 6.9(b), the equation can be written as follows:

$$\hat{y}_{\mathrm{THMs}} = 17.45 - 8.58(Fe^{2+}) + 2.58(PO_4) + 2.81(Time) - 2.28(Fe^{2+}.Time) - 4.95(pH.PO_4) \quad (6.10)$$

Here, $\hat{y}_{\mathrm{HAAs}}$ and $\hat{y}_{\mathrm{THMs}}$ are the predicted formation (μg/L) of total haloacatic acids and total trihalometanes respectively in the studied water samples, pH is solution pH value, PO_4 is phosphate based corrosion inhibitor dosage (mg-PO_4/L), and time is reaction period (h).

The analysis of variance (ANOVA) tests for the fitting linear models and the lack of fit (LOF) tests for the HAAs and THMs formation models are presented in Tables 6.10 (a) and (b). In this study, the F_{model} value for HAAs (21.8) and THMs (66.43) were greater than their critical values ($F_{0.05,6.11} = 3.09$ and $F_{0.05,5,3} = 9.01$). The p-values for the models were very low ($p < 0.005$) demonstrating a high significance for the

regression models (Montgomery, 2009). The goodness of fit for the models was checked by the determination coefficient (r^2). In this case, the coefficients of the determination for the models were found to be 91.64% and 96.58% respectively, which indicated that only 8.367% and 3.42% of the total variations were not explained by the proposed models for HAAs and THMs formation. The values of the adjusted determination coefficients ($adj\ r^2$) were also high to advocate for a high significance of the models. The *F*-values for the lack of fit (LOF) test associated with the elimination of a few factors were 2.89 and 2.22 for the linear models of HAAs and THMs respectively. The *F*-values for the LOF test can be compared with the tabulated value at a 95% confidence level for the appropriate number of degrees of freedom. Since the mean sum square ratios (*F*-values) for these lack of fit tests were smaller than the tabulated values ($F_{0.05,1.11} = 4.84$ and $F_{0.05,9.3} = 8.81$), and the p values for the lack of fit tests were larger (Tables 10(a) and (b)). Therefore it could be concluded that these eliminated factors did not have statistical significance on the linear models for HAAs and THMs formation. However, the LOF tests show in Tables 6.10(a) and (b) provide additional evidence that the models adequately fit the data for HAAs and THMs formation study.

In this study, the residuals also had to be examined for normal distribution as well as the residual of multiple regression models play an important role in judging model adequacy (Montgomery, 2009). The values of the calculated residuals for the response factors are plotted in a normal probability plot; and the results are shown in Figures 14(a) and (b) respectively. It is observed that all data points for the response factors lay close to a straight line, and within the 95% confidence intervals line with mean value near to zero. Since the residuals lay approximately along a straight line, we did not suspect any severe non-normality in the data (Hines et al., 2003). The models predictions were compared with the experimental data; and it was observed that there was a strong linear correlation having a strong coefficient ($r^2 = 0.93$ for HAAs and $r^2 = 0.95$ for THMs) between experimental and predicted data (Figures C8 and C12, Appendix C).

Table 6.10(a). Quantitative diagnosis for final model for HAAs formation

Source	*DF*	*Seq SS*	*SS (Adj)*	*MS*	*F*	*P*
Model	6	9361.60	9361.69	1560.28	21.80	< 0.05
Residual Error	12	858.90	858.86	71.57		
Lack of Fit (LOF)	1	179.20	179.16	179.16	2.89	0.117
Pure Error	11	679.70	679.71	61.79		
Total	19	10278.50				

Table 6.10(b). Quantitative diagnosis for final model for THMs formation

Source	*DF*	*Seq SS*	*Adj SS*	*Adj MS*	*F*	*P*
Model	5	1886.65	1886.65	377.33	67.59	< 0.005
Residual Error	12	66.99	66.99	5.58		
Lack of Fit (LOF)	9	58.24	58.24	6.47	2.22	0.316
Pure Error	3	8.75	8.75	2.92		
Total	19	1961.73				

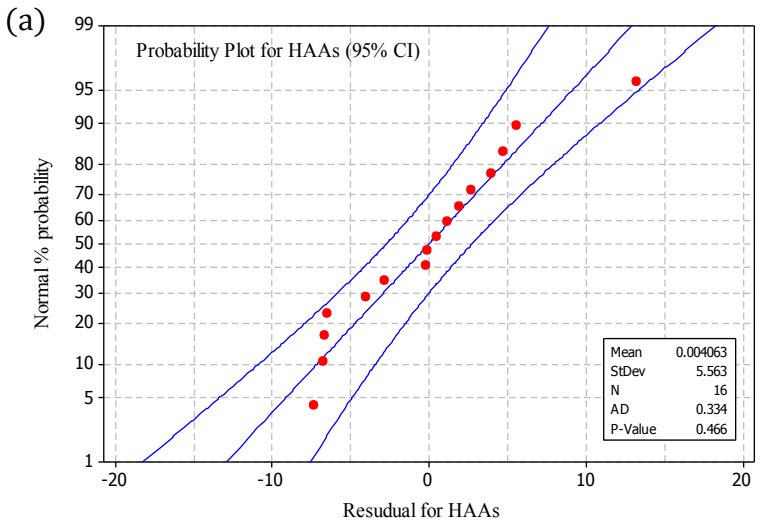

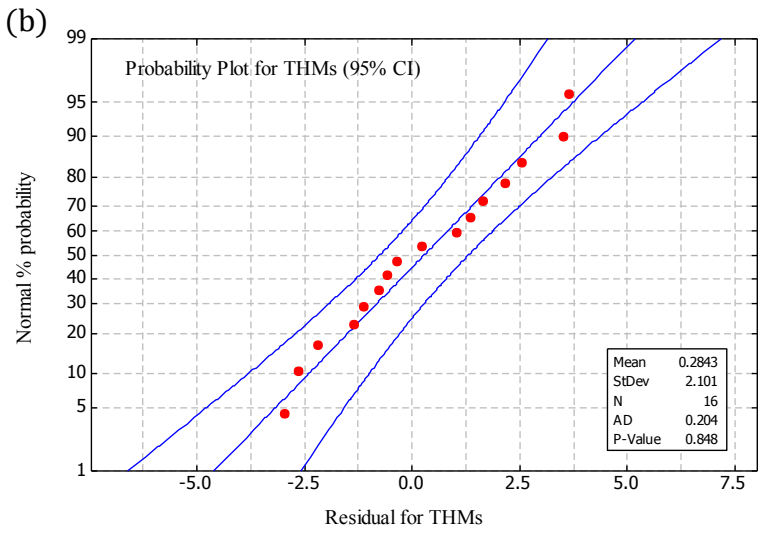

Figure 6.14. Normal probability plot of the residuals at 95% confidence interval for the response factor (a) HAAs formation and (b) THMs formation.

6.4.4. Model validation

An independent data set including a number of water quality and setup parameters (e.g., concentration of Fe(II) ions, phosphate dosages, pH, and stagnation times) in real iron pipe water distribution systems are wanted to validate the models. pH and phosphate based corrosion inhibitor dosage and stagnation time in the water treatment plants and in distribution systems can be obtained easily. Whereas it is a challenge to obtain the actual Fe(II) ions concentration in distribution systems especially for the different stagnation times (Benjamin and Miller, 1990). The variability of Fe(II) ions can be attributed to the inorganic compounds, bio-geochemical processes, leaching due to the iron pipe corrosion and environmental conditions. However, there are no reported data for the concentrations of Fe(II) ions, PO_4 ions, pH, THMs and HAAs in drinking water distribution systems, Nova Scotia, Canada. Therefore, the post filtered natural water samples collected from three major water treatment plants in Halifax, Nova Scotia (Table 6.2), were spiked with the different dosages of Fe(II) ions (0.5 to 3 mg/L) for the different pH values (5.5 to 8.5) and different reaction times (3.5 to 24 h) in the absence and presence of a phosphate based corrosion inhibitor (1.5 mg-PO_4/L) for HAAs and THMs formation study. The data for HAAs and THMs concentration in natural water obtained from this current study were used to validate the developed models (Eqs. (6.8) and (6.10)).

Figures 6.15(a) and (b) illustrate the results of the validation analysis for HAAs and THMs formation models. This study shows that the correlation coefficients (r^2) for the predicted and measured values of HAAs and THMs formation in the natural water samples were found to be 0.87 and 0.92 respectively, which indicated the goodness of fit for the models. The results for the percentage of absolute model deviation (Eq. (6.6)) revealed that 83.33% of the total observed HAAs formation data lay within $\pm$ 20% of the predicted values. However, 91.67% THMs formation data of the total observed data lay within $\pm$ 20% of the predicted values. The validation results seem to be at a satisfactory level for the explanation of the observed variability under these experimental conditions, which indicate the variation of Fe(II) ions, pH, phosphate dosages and reaction times.

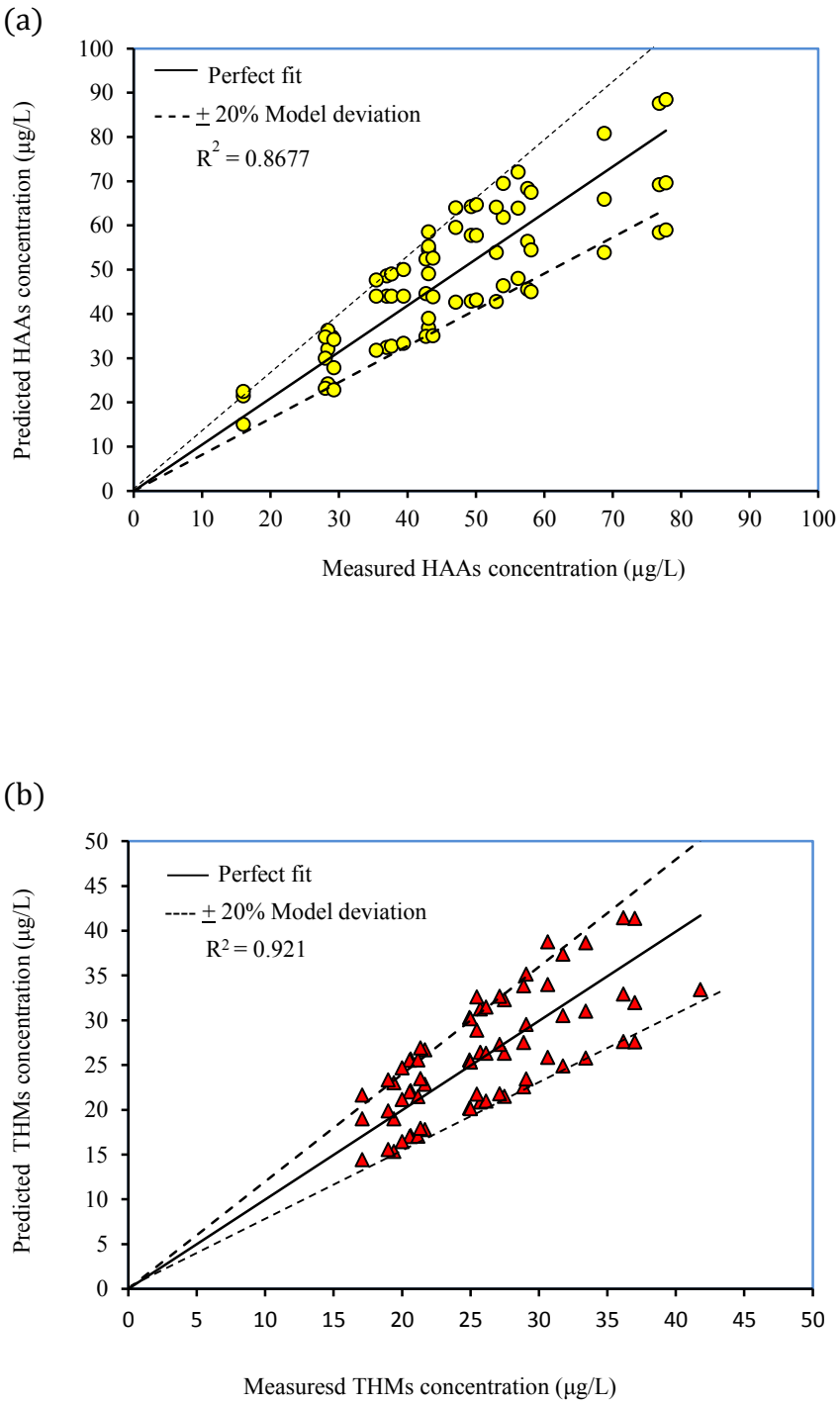

Figure 6.15. Model predictions and measured concentrations of (a) HAAs, and (b) THMs concentrations in natural water sample collected from three water supply plants in Nova Scotia, Canada.

6.5. Summary and conclusions

The goal of this comprehensive study was to evaluate the effect of Fe(II) ions concentrations along with a phosphate based corrosion inhibitor for the different pH values and different reaction times on the formation of HAAs and THMs. In addition with the comprehensive study, a 2^4 full factorial design with center points approach was followed using the most common water parameters to develop mathematical models for the prediction of HAAs and THMs in drinking water distribution systems.

The comprehensive study revealed that the formation of HAAs and THMs in iron water systems was lower compared with the control water systems for the different reaction periods (3.5 to 130 h). This study substantially showed that the solution pH had an obvious impact on the formation and distribution of HAAs and THMs in presence of Fe(II) ions and a phosphate based corrosion inhibitor. A 2.5 fold increment for HAAs formation, and a 9 fold increment for THMs formation were observed, when the solution pH was changed from 6.5 to 8.5 in the iron water systems following the same reaction conditions. These results conclusively demonstrated that a lower pH value of of 6.5 might have contributed a lower content of HAAs and THMs compared with the higher pH value of 8.5 in iron water systems. Therefore, the results of this study might have implications for understanding the facts that pH change in drinking water not only affects Fe(II) oxidation process, but has also an impact on the DBPs precursors as well as to affect reactivity between DOM and chlorine. This study illustrated that in the presence of a phosphate based corrosion inhibitor (1.5 mg-PO_4/L) along with the different dosages of Fe(II) ions, HAAs formation significantly (at a confidence level of 95%) reduced compared with the presence of Fe(II) ions only for the different reaction periods. However, an adverse trend was observed to increase THMs formation in the presence of phosphate (1.5 mg-PO_4/L) in iron water systems at a pH value of 6.5.

The full factorial design approach revealed that Fe(II) ions, pH and phosphate based corrosion inhibitor were the main significant factors for HAAs formation study. However, this study showed that Fe(II) ions concentration really dominated this process, accounting for over 50.9% of total variability for HAAs formation, whereas phosphate dosage and pH accounting for about 14.9% and 7.9 respectively. Several interaction factors were also showed to have significant effects at a 95% confidence level on the changes in HAAs formation. On the other hand, pH was not statistically significant for THMs formation in the studied reaction systems. Conversely, Fe(II) ions, phosphate and reaction time were statistically significant ($\alpha = 0.05,\ p < 0.05$) accounting for over 60.4%, 5.5% and 6.5% respectively of total variability for THMs formation.

In this study, considering the effect of several significant main and interaction factors in iron water systems, the mathematical models for HAAs and THMs formation were developed. The adequacy of the developed models was tested statistically using the numerical and graphical diagnostics. The models were found to be statistically significant, and the lack of fit tests was found to be insignificant. No visible trends were observed in the residuals plots. The normal probability plots for the residual values for HAAs and THMs revealed that all data points for the response factors lay close to a straight line; and within the 95% confidence intervals line with mean value near to zero. The graph for predicted and experimental concentrations for HAAs and THMs showed that there were no systematic deviations with the correlation coefficients (r^2) of 0.93 and 0.97 respectively, indicating that the models functioned well during the course of the entire range of experimental conditions.

The validation of the model using three different sources of natural waters collected from the main water treatment plants in Halifax, Canada, illustrated that 83.3% of the total observed HAAs formation data, and 91.7% of the total observed THMs formation data lay within $\pm$ 20% of the predicted values. The models performance were

found to be excellent under a wide range of Fe(II) ions and, DBPs (HAAs and THMs) concentrations. No systematic under or over prediction was noticed throughout the whole range of DBPs concentrations. This study showed that there was a good agreement between the experimental and model values. However, modeling results demonstrated that it could be possible to estimate HAAs and THMs level in iron pipe water distribution systems following the developed models. Conversely, the models can also be very useful in verifying key operational and water quality parameters, which may help to explain the HAAs and THMs formation potential. Therefore, model may be used as decision making tools by the drinking water industries. However, it should be said that it is difficult to develop the universal applicable HAAs and THMs formation models due to the complexity of HAAs and THMs formation reaction depending on different factors.

CHAPTER 7. THE ROLE OF MODEL IRON CORROSION SCALES (GOETHITE AND MAGNETITE) ON CHANGES OF CHLORINE RESIDUAL AND DISINFECTION BYPRODUCTS IN DRINKING WATER DISTRIBUTION SYSTEMS

7.1. Abstract

The objective of this study was to assess the role of most predominant iron oxides in corrosion scales, i.e., goethite (α-FeOOH) and magnetite (Fe_3O_4) on residual chlorine concentrations, and ultimate impact on disinfection byproducts (DBPs) formation in the post filtered water samples collected from JDK water treatment plant, NS, Canada. Magnetite and goethite were synthesized in our laboratory, and were confirmed using XRD, SEM-EDX, BET surface area. The energy dispersive X-ray analysis of the treated goethite and magnetite in chlorine solutions revealed that both iron oxides consumed chlorine. However, magnetite surfaces consumed a greater mass of chlorine than that of goethite surfaces. ANOVA test revealed that chlorine consumption rate was significantly ($\alpha = 0$, $p < 0.05$) increased with the increase in magnetite and goethite dosages in water samples. Chlorine consumption was observed to be more profound in aqueous-magnetite systems compared to aqueous-goethite systems. The bench scale study revealed that in presence of synthetic goethite, HAAs and THMs formation was observed to increase compared with that of aqueous systems, and this was more reflective with the increases in reaction times. Conversely, a reverse trend was observed to decrease HAAs and THMs formation in presence of magnetite in the same reaction systems. Chlorine stock solution was found to be the main source of bromide ions that might have contributed to generate brominated DBP species in drinking water distribution systems.

7.2. Introduction

Due to worthy mechanical properties and economically cheap, iron pipe is mostly used in drinking water distribution systems for over 500 years. According to a survey in 1996, the majority of distribution system pipes in USA are composed of iron material: cast iron (38%), ductile iron (22%), and steel (5%) (AWWA, 1996). When drinking water is transported through water mains, it interacts with the resources present at the pipe-water interfaces. Iron pipe is often exposed to numerous harsh environments. For instance, chlorine media representing one of the most common as well chlorine is as a strong electron acceptor, can be consumed on metal oxide surfaces either strong or weak chemisorption bonds (Peljhan and Kokalj, 2009) or participate in oxidation processes (Rossman et al., 2001; Sarin et al., 2001). Therefore, chlorine consumption by iron corrosion by-products (iron oxides surfaces) represents a key issue for understanding the mechanisms and kinetics of chlorine decay and DBPs formation/reduction in iron pipe distribution systems. The manners in which these mechanisms function in a distribution system are depicted by a schematic diagram (Figure 7.1).

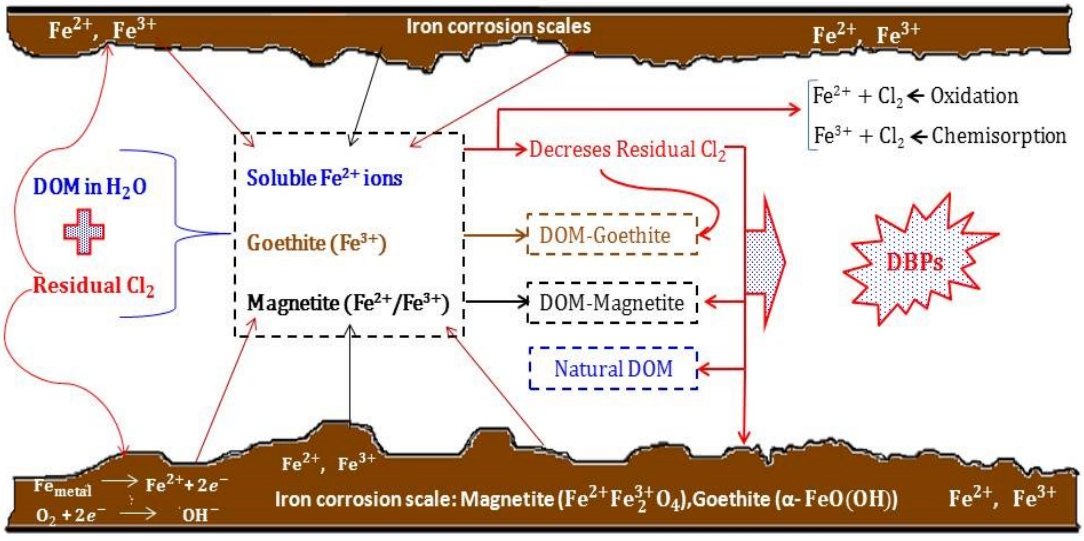

Figure 7.1. Schematic diagram for chlorine decay and DBPs formation in presence of iron corrosion products (magnetite and goethite) in drinking water distribution system.

Corrosion products are a combination of ferrous and ferric iron minerals. Goethite (α-FeOOH) is reported to be the most predominant iron minerals in corrosion deposits, followed by magnetite (Fe_3O_4), lepidocrocite (γ-FeOOH), and green rusts ($Fe_4^{II}Fe_2^{III}(OH)_{12}(CO_3)$). In addition with the iron oxides, other mionor constituents including dissolved organic matter and trace metals are found in corrosion deposits in drinking water distribution systems (Tuovinen et al., 1984; Lin et al., 2001; Sarin et al., 2001; Crittenden et al., 2012). The composition of pipe deposit in water distribution system of Boston, MA reported to contain 75% of a misture of goethite and lepidocrocite, and 25% of magnetite (Sarin et al., 2001). Sarin et al. (2001) have also reported that magnetite is composed of ferrous (Fe^{2+}) and ferric (Fe^{3+}) ions (> 50% Fe^{2+}), whereas goethite is composed of mainly ferric (Fe^{3+}) ions. Nevertheless, different types of problems including protecting/defending microorganisms from disinfection (Tuovinen et al., 1984; LeChevallier et al., 1993), decreased disinfection competence (LeChevallier et al., 1993; Vikesland et al., 1998), increased disinfectant byproducts formation (Tuovinen et a., 1984; Valentine et al., 2000; Hassan et al., 2006), and increased color, metallic taste and odor (Sharma et al., 2001; McNeill and Edwards, 2001; Sarin et al., 2004a; Rahman and Gagnon, 2014c) might be caused due to corrosion of metal pipes in a drinking water distribution system. Therefore, metal pipe is now gradually replacing to improve the water quality. In USA only, it will cost US water utilities $325 billion over the next 20 years to upgrade the water distribution systems (AWWA, 1999).

Recent studies have shown that there is an increased demand for chlorine by the unlined cast iron pipe wall, such as corrosion products and biofilm slime, and it can cause a substantial chlorine decay rate in a distribution system (Frateur et al., 1999; Rossman et al., 2001). To keep the water free from any microbial contamination, it has been recommended that a drinking water distribution system should be kept residual chlorine concentration more than 0.2 mg/L at consumers (WHO, 2008). On the other hand, two regulated DBPs (e.g., THMs and HAAs) concentration must be maintained below the maximum contaminant level (MCL) 80 µg/L for THM_4 (chloroform,

bromodichloromethane, dibromochloromethane, and bromoform) and 60 μg/L for HAA_5 (monochloroacetic, dichloroacetic, trichloroacetic, bromoacetic, and dibromoacetic acid) as set by EPA (USEPA, 2006). DBPs have confirmed positive for carcinogenetic and adverse pregnancy consequences, and reflected to execute risk to human health. Therefore, chlorine decay and DBPs formation in treatment plants and distribution systems has drawn an important attention due to the microbial contamination for chlorine decay, and suspected health effects of DBPs formation (Bove et al., 2002; Chun et al., 2005). However, drinking water utilities have been required to assess their disinfection, treatment practices and distribution systems to meet increasingly stringent regulatory limits (USEPA, 2006).

There are four major issues including water quality conditions, chlorine dosage, nature of DOM and pipe deposits that could cause the chlorine decay and the formation or reduction rate of DBPs in drinking water distribution systems (Tuovinen et al., 1984; Frateur et al., 1999; Valentine et al., 2000; Rossman et al., 2001; Brereton and Mavinic, 2002; Hassan et al., 2006). Tuovinen et al. (1984) conducted THMs as well as HAAs formation study using actual iron pipe deposit collected from distribution systems and they found that DBPs formation was much greater in presence of actual iron pipe deposit than without pipe deposit. A same trend has been reported by Hassan et al. (2006), who acknowledge that THMs formation increases substantially with time in the presence of synthetic iron corrosion scale, i.e., goethite. Conversely, Brereton and Mavinic (2002) have showed lower levels of THMs formation in the presence of pipe materials conducting field and materails-specific simulated distribution systems. A recent study on degradation of selected synthetic disinfection byproducts by synthetic goethite and magnetite associated with Fe(II) ions addition has been reported by (Chun et al., 2005). Chun et al. (2005) added several synthetic DBPs in 123 mL serum bottles contaning synthetic water at pH 7.5, and they found that trichloronitromethane was degraded via reduction, while trichloroacetonitrile, 1,1,1-richloropropanone, and trichloroacetaldyde hydrate were transformed via both hydrolysis and reduction; and chloroform and

trichloroacetic acid were unreactive in the presence of 0.8 g/L goethite and magnetite suspension in addition of 1 mM (55.85 mg/L) of Fe(II) ion in the same solutions. Consequently, the importance of disinfectant decay and EPA regulated DBPs formation in drinking water distribution systems has been attracted great experimental interest over the past years. However, there is a limited works using individual iron oxides (e.g., goethite and magnetite) on chlorine decay and regulated DBPs formation/reduction in drinking water have been reported.

Till today the mechanisms and controlling factors for DBPs formation in iron pipe distribution systems are remain unclear (Hassan et al., 2006). To better understand the chlorine decay and the regulated DBPs formation mechanisms in presence of iron corrosion scales, it is an important to evaluate the interections between individual iron oxide and drinking water disinfectant that my help to elucidate their reactive mechanisms in distribution systems. Synthetic goethite and magnetite were selected for this study due to their common presence and occurrence as iron pipe corrosion products (Benjamin et al., 1996; Sarin et al., 2001). The main objective of this paper is to explain the impact of individual model iron corrosion products (magnetite and goethite) on chlorine decay, DBPs formation in post filtered water sample collected from J. Douglas Kline Water Treatment Plant (JDKWTP), Halifax, Canada.

7.3. Materials and methods

7.3.1. Water source

The post filtered water samples were collected from JDK water treatment plant (JDKWTP). The source water for JDKWTP is Pockwock Lake, and this plant supplies water most of Halifax with a daily flow rate of 100 ML/d (Halifax Water, 2012). This water was collected before adding any disinfectant or any chemicals in the treatment plant (before discharging into distribution systems). The plant follows the treatment

processes adding $KMNO_4$ for pre-oxidation, alum for coagulation, NaOH for pH adjustment, and chlorine as disinfectant. JDK water treatment plant serves their finished water through different sections of the systems, and is not blended during distribution. However, the water is characterized as low pH and low alkalinity (Table 7.1).

Table 7.1. Typical water quality parameters in raw and treated water in JDK water treatment plant (Halifax Water, 2012).

Parameter	Unit	Raw water	Treated water
Alkalinity	mg/L, As $CaCO_3$	<1.0	18.0
Ammonia	mg/L (N)	<0.05	<0.05
Iron (Total)	mg/L	0.061	<0.05
pH	pH Unit	5.6	7.4
Potassium	mg/L	0.32	0.41
Total Dissolved Solid	mg/L	22.0	49.3
Sulfate	mg/L	4.0	9.1
Total Organic Carbon	mg/L	2.7	1.8

7.3.2. Reagents and glassware

Ultra-pure water obtained from a Milli-Q® integral water purification system (EMD Millipore Corporation, Billerica, MA, U.S.A) was used to prepare all reagents and stock solutions. A detailed method to prepare the required chemicals for this study has been mentioned earlier in Section 3.2 of Chapter 3. Chlorine demand free glassware are essential for DBPs formation study (Summers et al., 1996). To make the chlorine demand free, amber colored incubation bottles (with PTFE-faced caps) were soaked in detergent at least overnight, rinse four times with hot tap water, two times with Milli-Q®

water. After washing, a 10-20 mg/L chlorine solution (made with DI water) was taken into headspace-free glass bottles with polypropylene screw caps and teflon-lined septa, and kept the bottles in dark place for at least 24 h. The bottles were rinsed four times with DI water, and then one to two times with Milli-Q® water. Subsequently, the chlorine demand free glassware were dried at 140 °C in an oven (Fisher Scientific, USA) at least overnight.

7.3.3. Synthesis of iron corrosion scales

Synthesis of magnetite (Fe_3O_4) and goethite (α-FeOOH) was performed in water quality laboratory, Dalhousie University following the method outlined by Schwertmann and Cornwell (2000) with some modification. A detailed method for the preparation of magnetite and goethite has been described earlier in Section 3.2.5 of Chapter 3. The synthetic magnetite and goethite samples were confirmed by SEM microphotograph (Scanning Electron Microscope, Hitachi, Japan) and X-ray Diffraction technique (XRD D8 Advance, Bruker, Germany) in the Department of Material Engineering at Dalhousie University. The data for SEM and XRD has been shown earlier in Figures 3.4-3.6 and 3.9-3.11 of Section 3.2.5 in Chapter 3.

7.3.4. Bench scale experiments

This study was carried out in 250 mL serum bottles containing 4 g/L of the most predominant iron oxides in corrosion scales (e.g., magnetite and goethite). To simulate the bench scale study with existing water treatments plant facilities, the experiments were conducted at pH value of 7.4 and chlorine dosage of 2.4 mg/L. To find out the effect of different chlorine dosages and different reaction times in different reaction systems (e.g., aqueous, aqueous-magnetite, and aqueous-goethite), a comprehensive bench scale experiments were conducted in JDKWTP's post filtered water samples. After each reaction period for different reaction systems, water samples were collected for the test of

pH, TOC, DOC, selective anions, concentration of residual chlorine; and sampling for THMs and HAAs analyses.

7.3.5. Analytical procedures

All water samples were analyzed based on the procedures described in the Standard Methods (APHA-AWWA-WEF, 2005). DOC analysis was conducted using a TOC-V_{CPH} analyzer (Shimadzu Corp., Japan) equipped with an auto-sampler ASI-V (Shimadzu Corp., Japan) according to the Standard Method 5310B (APHA-AWWA-WEF, 2005). Residual (free) chlorine concentrations were measured using the colorimetric version of the N, N-diethyl-p-phenylenediamine (DPD) following the HACH 8021 method (HACH, 2005) at a wavelength of 530 nm using a DR/5000 UV Visible Spectrophotometer (HACH Co., USA). Bromide and sulfate concentration were measured by an ion chromatograph (761 Compact IC, Metrohm). High pressure size exclusion chromatography (HPSEC, Series 200, Perkin Elmer, USA) was used to determine molecular weight (MW) distribution of DOM in solutions. The detailed analytical procedures to determine water quality parameters have been described earlier in materials and methods section (Chapter 3).

7.4. Results and discussion

7.4.1. Changes of water parameters

The post filtered water samples (before adding any chemical) were collected from JDK water treatment plant (JDKWTP), Halifax to conduct bench scale study. To evaluate water quality change in presence of goethite and magnetite, this study was conducted for a chlorine dosage of 2.4 mg/L, pH value of 7.4, and a reaction period for 48 h at lab temperature (21 ± 1 °C). The change of average water quality parameters is summarized in Table 7.2. This study revealed that bromide was not found in the control water system

(post filtered water without adding any chemicals). However, in addition of chlorine stock solution (sodium hypochlorous acid solution) in all reaction systems, a significant amount of bromide was found (Table 7.2). It was also interesting to observe that bromide concentration was remained almost same in the presence of synthetic magnetite and goethite for their different dosages ranging from 1 to 5 g/L. Therefore, it has been suggested that the chlorine stock solution is the main source of bromide ions that might be contributed to generate brominated DBP species in drinking water distribution systems. This study also revealed that sulfate concentration was observed to increase as double to triple after addition of chlorine in solutions. The same trend was observed in annual report of Halifax Regional Water Commission (HRWC), which acknowledges increasing sulfate concentration twice/thrice in treated water compared with the raw water in JDK water treatment plant (Halifax Water, 2012) (Table 2.1). However, different dosages of magnetite and goethite do not have significant impact on the changes of sulfate ions in solutions. It has been assumed that chlorine solution (HOCl and OCl^-) is occupied to oxidize the sulfite ions present in water to sulfate ions following the equations (Eqs. (7.1) to (7.3)). During these reaction processes, hypochlorous acid and hypochlorite ions are reduced to chloride ions (Fogelman et al., 1989). In presence of different dosages of goethite and magnetite, DOC concentrations were observed to decrease and this was more prominent in presence of goethite (Table 2.2). This is consistent with the reported result in literature (Rahman et al., 2013), which acknowledges that at pH 7.4 goethite adsorbed more DOM than magnetite as well the isoelectric point of goethite and magnetite are 8.09 and 6.65 respectively.

$$OCl^- + SO_3^{2-} \rightarrow Cl^- + SO_4^{2-} \qquad (7.1)$$

$$HOCl + SO_3^{2-} \rightarrow ClSO_3^- + 2H^+ + OH^- \qquad (7.2)$$

$$ClSO_3^- + H_2O \rightarrow SO_4^{2-} + Cl^- + 2H^+ \qquad (7.3)$$

Table 7.2. Physico-chemical properties (average value) of water samples during each stage of experiment using different amount of magnetite and goethite.

Water parameter	JDK post filtered water	Magnetite dosage (g/L) in water					Goethite dosage (g/L) in water				
		1 g/L	2 g/L	3 g/L	4 g/L	5 g/L	1 g/L	2 g/L	3 g/L	4 g/L	5 g/L
Bromide	0.00	0.46	0.34	0.33	0.37	0.34	0.31	0.36	0.34	0.33	0.36
Sulfate	8.11	20.1	19.3	18.9	18.7	19.3	14.77	14.7	19.6	18.6	18.8
DOC	1.80	1.42	1.38	1.26	1.29	1.66	1.27	1.22	1.19	1.17	1.06

7.4.2. Changes of MW distribution

The HPSEC chromatograms were used to determine the molecular weight (MW) distribution of DOM in the studied water samples in control water systems; and in presence of goethite, magnetite and different dosages of chlorine. It should be noted that the higher MW organics are eluted from the column first and lower MW organics are eluted later. The entire MW distribution of DOM in the samples was obtained by integrating the total area of the sample using Totalchrom software (Perkin Elmer, Ontarion, Canada) (Figures 7.2 and 7.4). The elution times and MW distribution associated with different peaks for three reaction systems are provided in Figures D1 to D6 of Appendix D.

HPSEC analysis revealed that the higher molecular weight fractions (> 800 Da) were consisted more than 50 % of the chromatograph areas in the control water systems (without adding magnetite and goethite). In presence of goethite, the higher MW fractions of DOM were observed to modify significantly than that of the lower MW of DOM in JDK post filtered water samples (Figures 7.2 and 7.3). Figure 7.3 shows that in aqueous-

goethite system, the molecular weight fraction of DOM for > 1000 Da and 800-1000 Da are completely removed; and a significant change was observed for 400-800 Da molecular weight fraction of DOM. Conversely, this study showed that higher molecular weight fraction of DOM did not change significantly in aqueous-magnetite systems as it was observed in aqueous-goethite systems (Figure 7.3). This study has suggested that goethite has more impact to alter the properties of DOM in JDK post filtered water samples. It might be happed due to the reason that goethite is composed of mainly ferric oxide, and the higher MW compounds tend to be more aromatic in nature (Thurman and Malcolm, 1983), so they might have a larger number of reaction sites than smaller MW compounds to adsorb onto ferric oxide surfaces. However, our results were in reasonable agreement with the published works in literature (Davis and Gloor, 1981; Chin et al., 1994). Davis and Gloor (1981) indicated that the higher molecular weight fractions of natural DOM profoundly adsorbed by Al_2O_3. Based upon binding experiments using nonpolar organic probe molecules, Chin et al. (1994) and Eikebrokk et al. (2004) have reported that the hydrophobicity of humic materials increases with the increase in molecular weight fraction of DOM. Therefore, the DOM molecular weight distribution study has been suggested that the interaction of hydrophobic aromatic fractions with goethite surfaces (mainly ferric oxides) resulting larger molecular weight fractions preferentially adsorbed from the solutions compared with the magnetite surface (> 50% ferrous oxide).

HPSEC study also conducted in presence of different dosages of chlorine solutions ranging from 0.55 to 8.5 mg/L using the same JDKWSP post filtered water samples with the same reaction conditions (pH 7.4, temp 21 ± 1 °C, reaction time 48 h). This study revealed that in presence of different dosages of chlorine, no significant change in molecular weight distribution of natural DOM was observed (Figure 7.4). The finding is consistent with the reported results by Świetlik et al. (2002), who have conducted an experiment with ClO_2, and showed that there is no change on molecular weight distribution in presence of ClO_2.

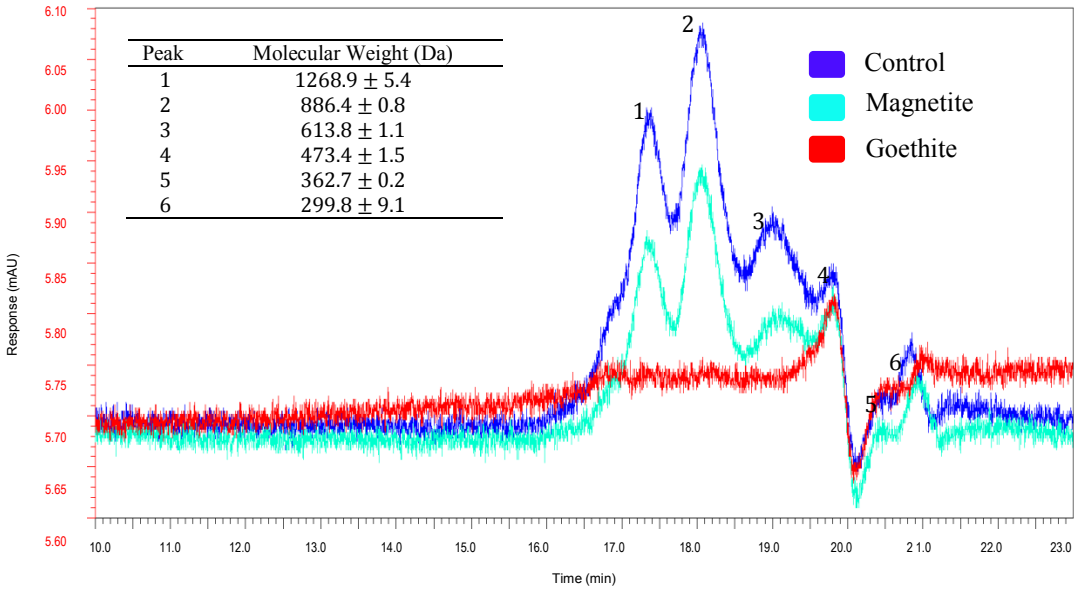

Figure 7.2. High performance size exclusion chromatograph for DOM in studied water samples for the control water system, and for the presence of magnetite and goethite.

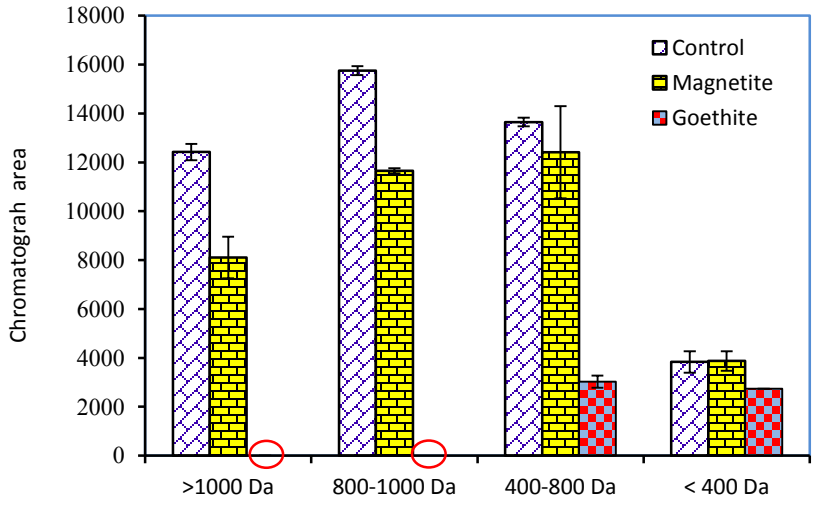

Figure 7.3. Chromatogram area counts for different molecular weight fractions of DOM in water samples for the control water system, and for the presence of magnetite and goethite.

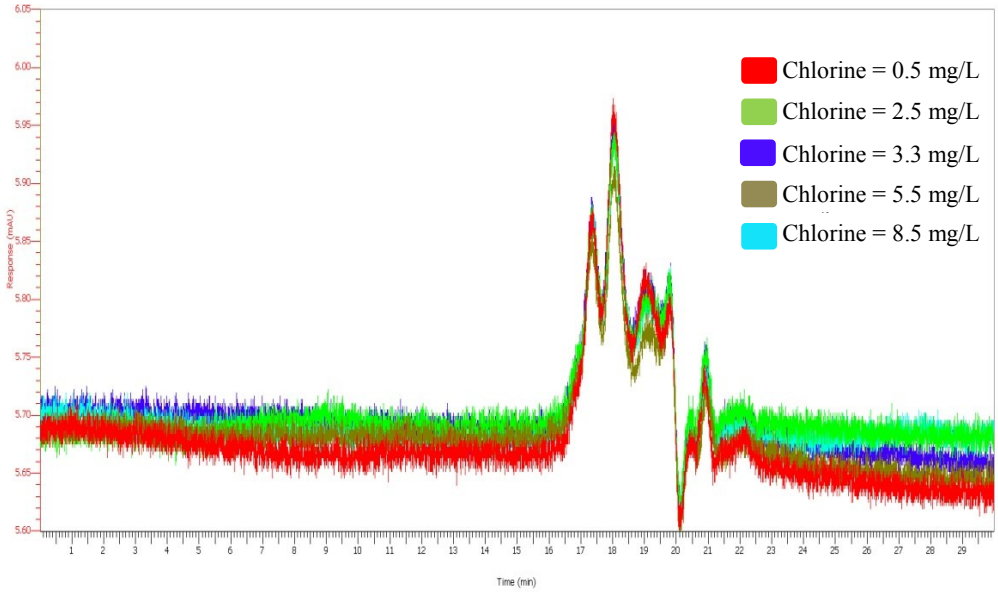

Figure 7.4. Effect of different dosages of chlorine on the changes of molecular weight distribution of DOM in post filtered water sample collected from JDKWTP.

7.4.3. Changes of elemental analysis

EDX-SEM (Energy dispersive X-ray couple of scanning electron microscopy) analysis provided the X-ray diffractograms of the elemental composition for untreated and treated magnetite and goethite with chlorine in solutions (Figures 7.5 to 7.8). Energy dispersive X-ray spectrum (data shows in Chapter 3) and elemental composition revealed that untreated magnetite contained 71.13% of iron as well it contains both ferrous and ferric iron, whereas goethite contains 44.64 % of iron as well it is composed of ferrous-iron only. X-ray analysis demonstrated that both model iron oxides (magnetite and goethite) consumed chlorine. The elemental composition of magnetite and goethite before and after chlorine consumption is presented in Table 7.3. This study showed that magnetite exhibited a preference for chlorine consumption (0.91 weight %) than goethite (0.05 weight %).

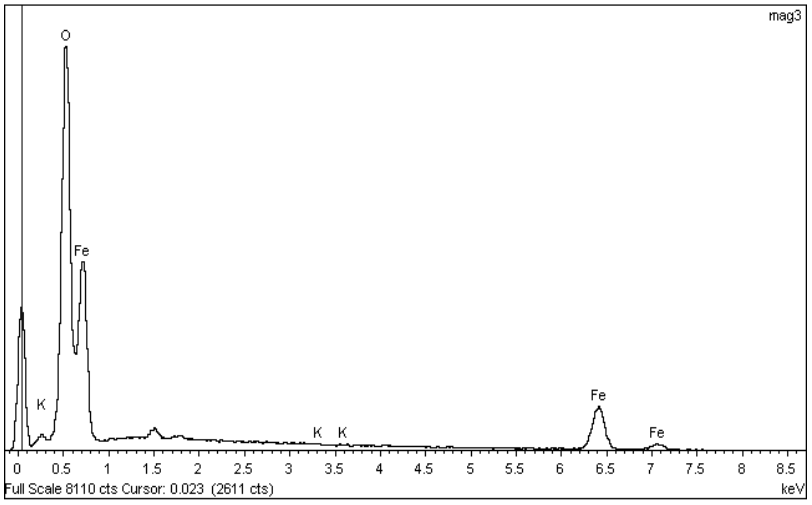

Figure 7.5. EDX diffractograms of magnetite elemental composition before chlorine consumption.

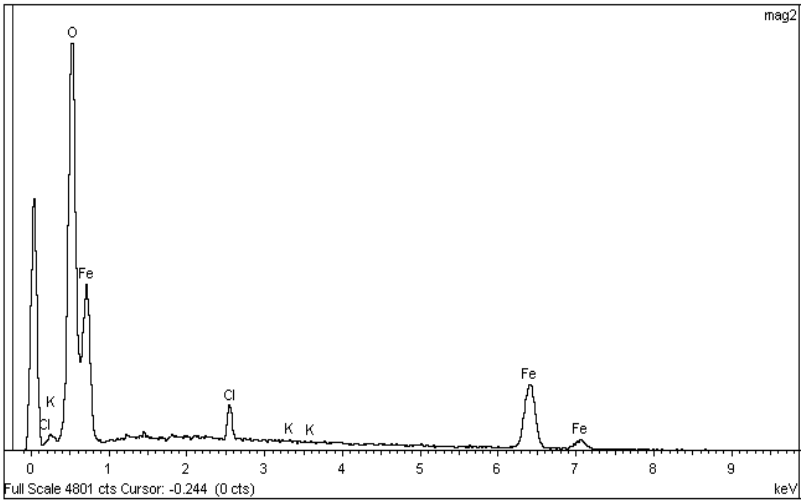

Figure 7.6. EDX diffractograms of magnetite elemental composition after chlorine consumption.

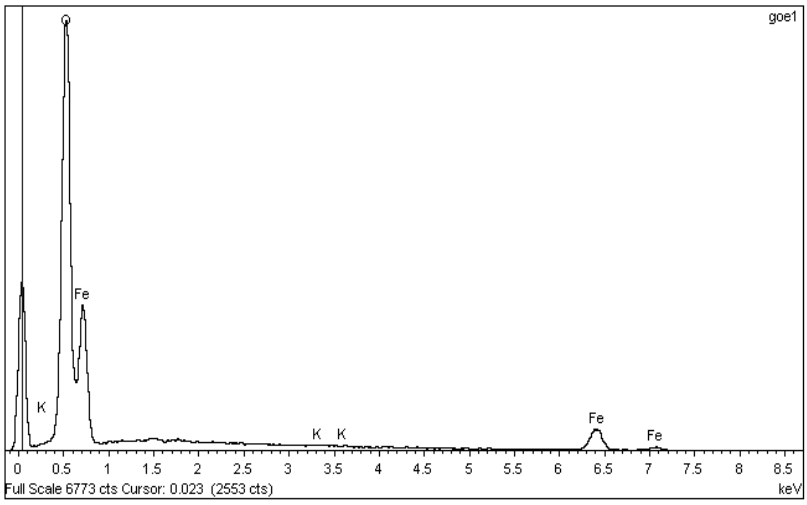

Figure 7.7. EDX diffractograms of goethite elemental composition before chlorine consumption.

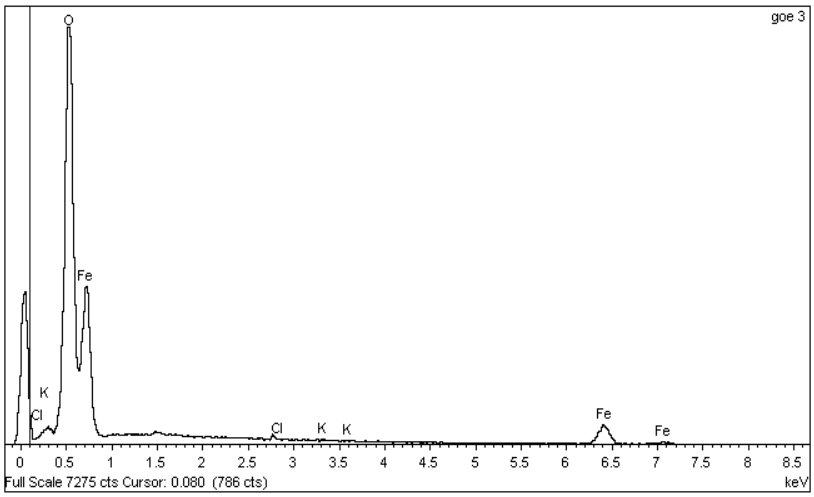

Figure 7.8. EDX diffractograms of goethite elemental composition after chlorine consumption.

Table 7.3. Elemental composition of magnetite and goethite before and after chlorine consumption.

Name of Elements	Elemental composition in magnetite				Elemental composition in goethite			
	Before		After		Before		After	
	Weight %	Atomic %	Weight %	Weight %	Atomic %	Weight %	Weight %	Atomic %
O	28.73	58.43	30.69	61.08	54.21	80.35	54.52	80.36
K	0.14	0.12	0.14	0.11	1.15	0.70	1.24	0.73
Fe	71.13	41.45	68.26	38.21	44.64	18.95	44.19	18.86
Cl	--	--	0.91	0.60	--	--	0.05	0.05
Total	100.00	100.00	100.00	100.00	100.00	100.00	100.00	100.00

7.4.4. Changes of chlorine concentration

7.4.4.1. Effect of magnetite and goethite dosage

For this study, the initial chlorine concentration was 2.4 mg/L (chlorine to carbon mole ratio $= 1.2$), and the chlorine decay tests were performed following the UFC protocol at lab temperature (21 ± 1 °C) for a single pH value of 7.4. This study illustrated that the percentage of chlorine consumption was increased rapidly with the increase in magnetite and goethite dosages (Figure 7.9). It was also observed that magnetite consumed more chlorine than that of goethite. Statistical analysis revealed that in the presence of 1 g/L magnetite, 75% chlorine was consumed, while in the presence of 1 g/L goethite, 57% chlorine was observed to consume. Figure 7.9 shows that with the increase in goethite and magnetite dosages from 1 to 5 g/L, the percentage (%) of chlorine consumption is appeared relatively constant. However, the analysis of variance (two-way ANOVA) test for the chlorine consumption data revealed that chlorine consumption rate is significantly increased with the increase in magnetite and goethite dosages at a 95% confidence level

($p < 0.05$; $F_{stat} = 6.55 > F_{critic} = 6.39$). Statistically a great difference of chlorine consumption between in aqueous-magnetite and aqueous-goethite systems was observed at 95% confidence level ($p = 0.001$; $F_{stat} = 222.07 > F_{critic} = 7.71$) (Table D7 of Appendix D). It could be happened due to the reason that magnetite is composed of 50% ferrous iron, whereas goethite is composed of mainly ferric iron (Schwertmann and Cornwell, 2000; Sarin et al., 2001). Therefore, it has been hypothesized that magnetite consumes more chlorine for the Fe(II) ions oxidation into Fe(III) ions that decrease residual chlorine concentration more in aqueous-magnetite systems. Similar observation has been reported by Frateur et al. (1999) for iron pipe distribution systems. Therefore, it has been suggested that magnetite has more impact on the reduction of residual chlorine concentration in drinking water distribution systems compared with aqueous-goethite systems.

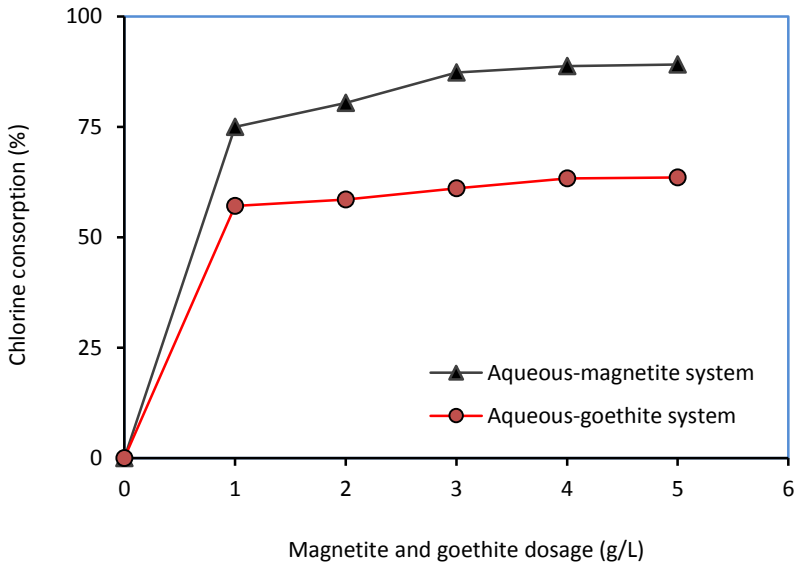

Figure 7.9. Effect of magnetite and goethite dosage on residual chlorine concentration (%) in JDK post filtered water sample (Chlorine dosage 2.4, pH 7.4, temp 21 $\pm$ 1 °C, reaction time 24 h).

7.4.4.2. Effect of reaction time

In Milli-Q water system (in absence of DOM), chlorine concentration was observed to remain stable for the different reaction periods studied here. However, this study revealed that the residual chlorine concentrations were gradually decreased with the increase in reaction times from 1 to 120 h in JDK post filter water samples (Figure 7.10). Several researchers have reported the same type of findings. Speight and Singer (2005) found that water chlorine dosages of 3 mg/L almost decayed by 7 d in natural water samples. However, this study revealed an identical trend in aqueous-goethite and aqueous-magnetite systems. On the other hand, it has been advised that a drinking water distribution system should be maintained residual chlorine concentration greater than 0.2 mg/L at consumers to protect the water from any microbial contamination (WHO, 2008). This study illustrated that in presence of both magnetite and goethite JDK water samples can keep that residual chlorine concentration (0.2 mg/L) upto 48 h of the reaction period. However, in aqueous media alone, the residual chlorine concentration is close to 0.2 mg/L upto 5 d of reaction period (Figure 7.10). The comparison on chlorine decay among three reaction media showed that chlorine was consumed more by the magnetite for the studied all reaction periods studied here. Because some part of chlorine was occupied to react with ferrous ions oxidation process in aqueous-magnetite systems along with the chemisorption process onto the iron oxide surfaces (Peljhan and Kokalj, 2009). Therefore, it has been suggested that the residence time (water age) is also one of the factors on the change in residual chlorine concentrations as shows in Figure 7.10 in different reaction systems.

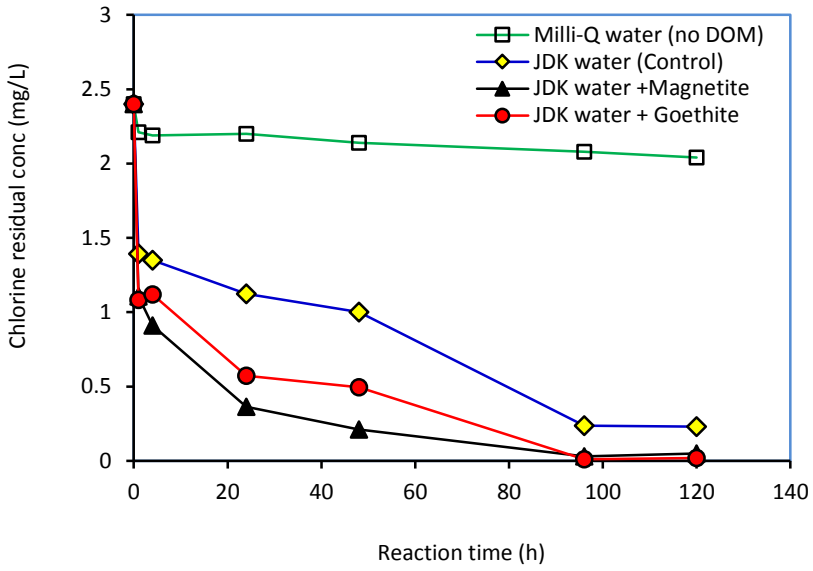

Figure 7.10. Kinetic study on chlorine decay in JDK post filtered water samples (Chlorine dosage 2.4 mg/L, magnetite dosage 4 mg/L, goethite 4 mg/L, pH 7.4, temp 21 ± 1 °C).

7.4.5. Changes of BDPs formation

Nine HAAs (e.g., monochloroacetic acid, dichloroacetic acid, trichloroacetic acid, bromochloroacetic acid, bromodichloroacetic acid, monobromoacetic acid, dibromoacetic acid, chlorodibromoacetic acid, and tribromoacetic acid), and four THMs (e.g., chloroform, dibromochloromethane, bromodichloromethane, and bromoform) were determined in each sample for this bench scale study in JDK post filtered water samples. The average results for total THMs and HAAs were used to represent the data.

The effect of model iron oxides (e.g., magnetite and goethite) on DBPs formation was studied at lab temperature (21 ± 1 °C) for a pH value of 7.4, and a constant chlorine dosage of 2.4 mg/L for the different reaction periods ranging from 2 to 120 h respectively. From this experimental study, it was observed that the major portion of total THMs and HAAs formation were happened at the reaction period of 24 h in the different reaction systems (e.g., aqueous, aqueous-magnetite, and aqueous-goethite systems) (Figures 7.11 and 7.12). This finding is consistent with the reported results in literature (Amy et al., 1987; Zou et al., 1997). Using a wide range of reaction time, (0.1 to 168 h) Amy et al. (1987) conducted THMs formation study, and they found that in the initial 8 h of reaction time THMs formed quickly, and afterword slowly if precursor and free chlorine were still present. Zou et al., (1997) reported that about 55 to 75% of the one-day total halogen formation potential (TOXFP) was produced within 30 min.

This study revealed that in presence of magnetite, DBPs formation was observed to be lower compared to the aqueous system only (without magnetite) (Figures 7.11 and 7.12). Our findings are in agreement with the reported result in literature by other authors (Rossman et al., 2001; Chun at al., 2005). Chun at al. (2005) have conducted synthetic DBPs degradation study in presence of iron oxide surfaces associated with Fe(II) ions. They have suggested that Fe(II), is a potent reductant when associated with iron oxide surfaces, and can mediate the reduction of halogenated organic compound. On the other hand, Rossman et al. (2001) have also reported that free chlorine is used up preliminary by Fe(II) ions enriched iron oxide surfaces (magnetite). Therefore, it has been presumed that in aqueous-magnetite systems, DBPs formation might be lower dur to less amount of free chlorine is available to react with DBPs precursor. However, after the reaction period of 24 h, the THMs and HAAs formation was observed to be parallel in aqueous and aqueous-magnetite systems. Based on the experimental results and literature finding, it has been assumed that the reduction of DBPs formation in presence of magnetite could be occurred due to the following reasons:

(1) Chlorine is consumed by non-DBP producing materials (for instance ferrous ions enriched corrosion products); and therefore, less amount of chlorine residual is present to react with DOM to produce DBPs (Rossman et al., 2001).

(2) The DBPs themselves may be oxidized by ferrous iron, which result in a decrease in the observed DBPs concentration in solution (Chun et al., 2005).

(3) The stoichiometric ratio of Fe(II)/Fe(III) in magnetite is 0.5 (Schwertmann and Cornwell, 2000). Therefore, ferrous iron that presents predominantly in magnetite might play an important role in reduction reactions of chlorinated aliphatic compounds at the metal-water interfaces (Scherer et al., 1998), reduced iron can react with oxygen to produce superoxide (Stumm, 1992), which can result in oxidation of organic compounds.

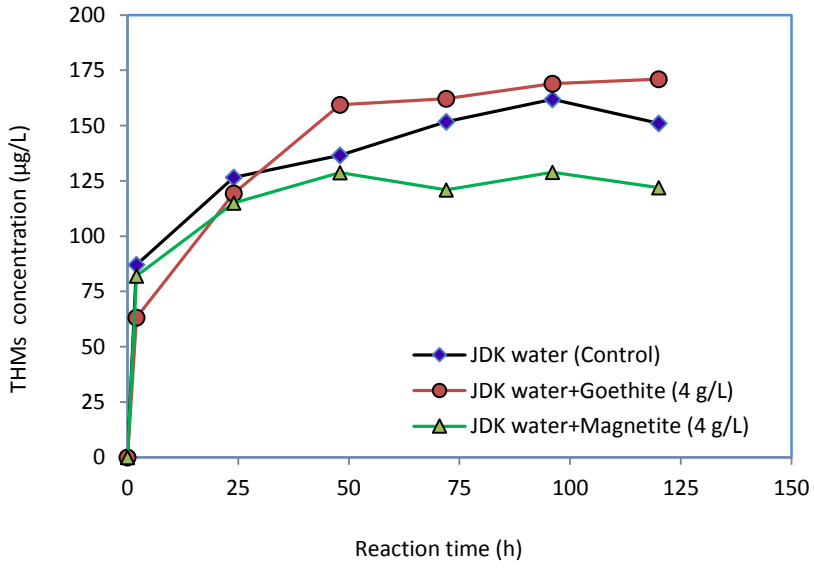

Figure 7.11. Effect of magnetite and goethite on changes in THMs formation for the reaction periods ranging from 2 to 120 h (pH 7.4, chlorine dosage 2.4 mg/L, 21 ± 1 °C).

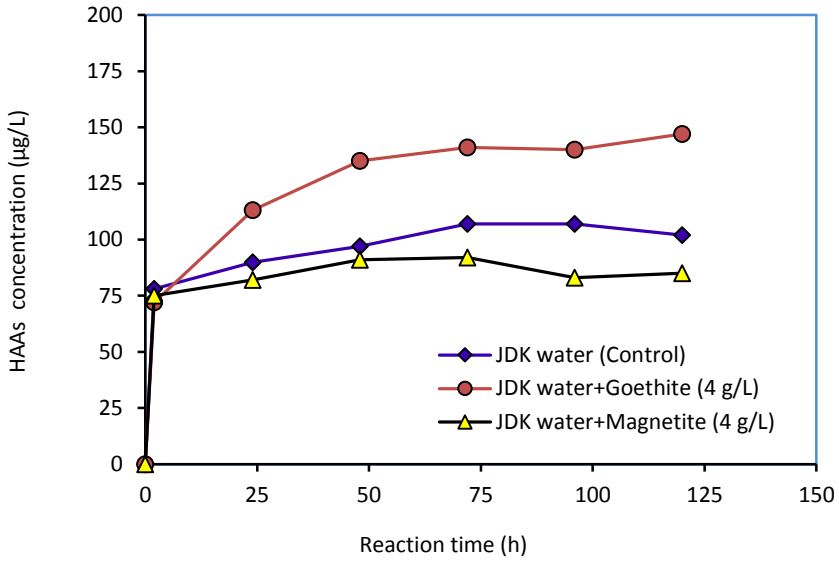

Figure 7.12. Effect of magnetite and goethite on changes in THMs formation for the reaction periods ranging from 2 to 120 h (pH 7.4, Chlorine dosage 2.4 mg/L).

On the other hand, it is interesting to observe that THMs and HAAs formation was higher in aqueous-goethite systems compared to the aqueous and aqueous-magnetite systems, especially after the reaction period of 24 h. The similar findings for THMs formation study have been reported by Valentine et al. (2000), who have found an increament of 185% increased THMs formation with the addition of 1 g/L goethite concentration over water only. As reported in literature, goethite contains mainly ferric iron (Sarin et al., 2001); and at pH 7.4, goethite ($pH_{PZC} \approx 8.09$) significantly adsorbed DOM compared to magnetite ($pH_{PZC} \approx 6.65$) in the same reaction condition. DOM adsorption isotherms using magnetite and goethite for different pH values have been determined as a part of separate study, which is presented in Chapter 8. However, it has been assumed that adsorbed DOM onto goethite surfaces generated some intermediate

factors those were more reactive to contribute more DBPs formation (Hassan et al., 2006). Consequently, this study revealed that THMs and HAAs formation was observed to increase with the increase of reaction time in aqueous-goethite systems (Figures 7.11 and 7.12). It might be happened due to the reasons that with the increase in reaction time, goethite interaction with natural DOM has increased the number of reactive sites those might be reacted with chlorine to generate DBPs formation. Our assumption is in good agreement with the reported results in literature (McBride et al., 1991; Pracht et al., 2001). The authors have reported that phenolic substances are commonly present in dissolved organic matter in water, which are oxidized in the presence of ferric iron surfaces. However, it has been assumed that the formation of these intermediates are more reactive to chlorine to produce DBPs in water.

7.4.6. Conclusions

The overall objective of this chapter was to assess the role of the predominant model iron oxides (e.g., magnetite and goethite) found in the corrosion scales, on the change of water quality. Both model iron pipe deposits have impact on chlorine decay and DBPs formation. However, the conclusions can be addressed by the following points:

- NaOCl was found to be the main source of bromide ions in the studied water samples that might be reacted with organic matter to produce brominated byproducts.

- The chlorine decay in control water systems (absence of DOM, goethite and magnetite) showed that chlorine concentrations were not change significantly in solutions. However, in presence of goethite and magnetite in natural water sample, residual chlorine concentrations were decayed significantly. Therefore, it has been suggested that chlorine is consumed by the corrosion by-products and DOM in drinking water distribution systems.

- Both magnetite and goethite surfaces were observed to consume chlorine compared to water alone. Chlorine consumption rate was higher in aqueous-magnetite systems than that of aqueous-goethite systems for all reaction times.

- The DBPs (both THMs and HAAs) formation in aqueous-magnetite systems was lower compared to control water systems (in absence of magnetite and goethite). The decrease in DBPs formation accompanished by increased chlorine consumption. However, a reverse trend was observed to increase DBPs formation in aqueous-goethite systems.

CHAPTER 8. ADSORPTION OF DISSOLVED ORGANIC MATTER (DOM) ONTO THE SYNTHETIC IRON PIPE CORROSION SCALES (GOETHITE AND MAGNETITE): EFFECT OF pH[5].

8.1. Abstract

This study was performed to investigate dissolved organic matter (DOM) adsorption equilibrium using synthetic iron pipe corrosion scales i.e. goethite and magnetite for different pH values ranging from 2.5 to 10.5. The synthesized goethite and magnetite were characterized by XRD, SEM and BET surface area. SEM micrographs for before and after DOM adsorption study revealed a significant change on the morphology of goethite and magnetite surfaces. Molecular weight distributions of DOM measured by HPSEC revealed that the higher molecular weight fractions adsorbed preferentially onto goethite and magnetite surfaces, and it was pronouncedly observed at lower pH. The DOM adsorption data illustrated to be fit well by the Langmuir adsorption isotherm indicating monolayer coverage. The standard Gibb's free energy ($\Delta G^{\circ}_{\mathrm{ads}}$) changes of adsorption process stating the DOM adsorption onto goethite and magnetite surface was spontaneous under the experimental conditions. However, the maximal adsorption capacity for goethite and magnetite were revealed to be 4.75 mg-C/g and 3.79 mg-C/g respectively at pH value of 2.5. The DOM adsorption study was observed to be highly pH dependent. Consequently, zeta (ζ) potential measurements revealed that surface charge of goethite and magnetite was modified due to DOM adsorption onto their surfaces, and their pH for point zero charge ($\mathrm{pH_{PZC}}$) was shifted to lower pH compared to that of in absence of DOM. Nevertheless, it has been suggested that ligand exchange between carboxyl/hydroxyl functional groups of DOM and, goethite and magnetite surfaces was the leading interaction mechanism for DOM adsorption process. FTIR spectroscopy study was in agreement with the conclusion cited above.

[5]Rahman, M.S. Whalen, M. and Gagnon, G.A. 2013. Adsorption of dissolved organic matter (DOM) onto the synthetic iron pipe corrosion scales (goethite and magnetite): Effect of pH. *Chem. Eng. J.* **234**, 149-157.

8.2. Introduction

Natural or dissolved organic matter (NOM or DOM) is pervasive in aquatic systems and it is present in all groundwater on earth, with concentrations ranging from 0.5 up to 10 mg/L as organic carbon (Genz et al., 2008). The natural organic matter (NOM) is often mainly (80 to 90%) as dissolved form (Karanfil et al., 2005). On the other hand, a wide variety of iron oxides and hydroxides (hematite, goethite, magnetite, maghemite, etc.) happens in nature (Illés and Tombácz, 2004), and generates in corroded iron pipes in distribution systems (Sarin et al., 2001). Subsequently, the surface properties and reactivity of the hydrous mineral oxides, hydroxides might be significantly changed due to adsorption of dissolved organic matter (DOM) onto these iron oxide particles. Consequently, DOM present in water can play a significant role on conducts (e.g., transport and fate) of many environmental organic and inorganic contaminants. The behaviors (e.g., electrophoretic mobility, transport and interaction) of these mineral colloids might be also atered due to DOM adsorption onto mineral surfaces (Davis, 1982; Sposito, 1984; Stevenson, 1994; Wang et al., 1997; Guan et al., 2006). Previous studies state that DOM contains a large number of mainly acidic (e.g., carboxylates, phenolic, and hydroxyls) functional groups (Hayes et al., 1989; Gagnon et al., 1997), and the chemical behaviors of these organic acids are very complex (Illés and Tombácz, 2004). In in aqueous media, the acidic functional groups of DOM dissociate and lead to the formation of negatively charges bound chemically to the cross-linked carbon network of DOM macromolecules (Illés and Tombácz, 2004). On the other hand, when the particles are dispersed in aqueous media, the surface of metal oxides, hydroxides, such as hydrous iron oxides becomes charged, (Fokkink et al., 1987; Sun et al., 1998; Schwertmann and Cornell, 2000; Rietra et al., 2000; Illés and Tombácz, 2004), and this charge development is controlled by the pH and ionic strength in aqueous solution (Lyklema, 1991). For instance, the reactions of surface $Fe-OH$ sites with H^+ and OH^- ions lead to the formation of positive ($Fe-OH+H^+ \rightarrow FeOH_2^+$) and negative ($Fe-OH+OH^- \rightarrow Fe-O^- + H_2O$) surface charges. However, the negatively charged DOM macromolecules are being able to bind with these positively charged metal oxides, hydroxides particles especially with large surface area. Zeta potential is frequently used to obtain surface

potential information, and has recently been used to investigate the effect of dissolved organic matter adsorption onto the surface charge of metal oxides (Zhang et al., 2012).

A wide variety of iron oxides and hydroxides (hematite, goethite, magnetite, maghemite, etc.) occurs in nature (Illés and Tombácz, 2004), and generates in corroded iron pipes in distribution systems (Sarin et al., 2001), which often adsorb DOM. Several researchers (Davis and Gloor, 1981; McKnight et al., 1992; Gu et al., 1994) have observed that the DOM adsorbed onto aluminum oxide and iron oxide mineral were enriched in carboxylic groups, a fractionation pattern consistent with surface complexation processes (e.g., ligand exchange). However, the mechanisms of DOM adsorption onto mineral oxide surfaces are still not fully identified. Several major mechanisms governing DOM adsorption onto metal oxides, hydroxides may be accounted: (i) ligand exchange surface complexing, (ii) anion exchange (electrostatic interaction),(iii) hydrophobic interaction, (iv) cation bridging (v) entropic effects, and (vi) hydrogen bonding. A comprehensive description of these mechanisms has been presented by Sposito (1984).

Dissolved organic matter (DOM) is a complex and heterogeneous mixture of organic components having a wide range of molecular weights (MWs) fractions, and different chemical moieties. DOM may also have a broad distribution of sorption affinities onto the mineral surfaces within a particular bulk material (Hur and Schlautman, 2003). In recent times, the adsorption of humic substances (HS) onto metal oxides and hydroxides based on MW distribution using high performance size exclusion chromatography (HPSEC) has been investigated. A number of equilibrium HS adsorption studies have been reported that the different molecular weight fractions of DOM have different adsorption affinity onto minerals (Davis, 1982; Wang et al., 1997; Namjesnik-Dejanovic et al., 2000; Zhou et al., 2001). However, to date, there is little information available regarding the change of DOM molecular weight distribution in aqueous media

due to adsorption process onto iron corrosion scales i.e. goethite and magnetite, especially depending on different pH values.

Understanding the behavior of DOM sorption onto iron oxides is important since the presence of DOM and DOM associated metal oxides greatly affect the fate and transport of many organic and inorganic pollutants in drinking water transmission and distribution systems; and also in aquatic environment. Therefore, the motivation of this study was to investigate the mechanisms controlling the DOM adsorption onto metal oxides that is shown in Figure 8.1. Our objectives here were to (1) quantify the adsorption of DOM in synthetic water by two main iron oxides (goethite and magnetite), (2) evaluate the change of DOM molecular weight distribution due to adsorption onto goethite and magnetite, (3) investigate the role of solution pH on adsorption mechanisms using goethite and magnetite, and (4) adsorption isotherms modeling.

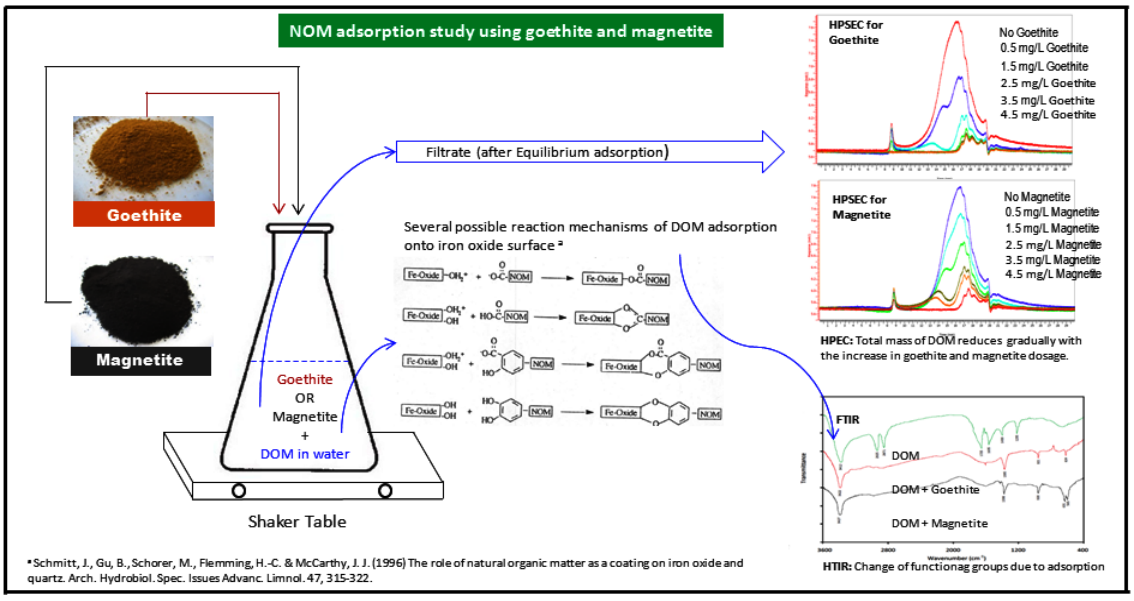

Figure 8.1. Schematic diagram for the mechanisms controlling DOM adsorption onto goethite and magnetite in synthetic water samples.

8.3. Materials and methods

8.3.1. Sorbents

A single batch of goethite and magnetite were prepared according to the procedure described by Shwertmann and Cornell (2000) with some modification. A brief description for the synthesis of goethite and magnetite used for this research is provided in the Section 3.2.5 of Chapter 3. X-ray diffraction (XRD) method employing a high-speed XRD system (XRD D8 Advance, Bruker, Germany) with Cu-Ka radiation having a wave length of 1.54 A°, tube voltage of 40 kV, and tube current of 40 mA was used to verify the synthesized goethite and magnetite. The BET surface area for goethite and magnetite were determined by N_2 gas adsorption. The morphology of goethite and magnetite, before and after DOM adsorption was analyzed by scanning electron microscopy (SEM, S-4700, Hitachi, Japan).

8.3.2. Sorbate

The purified humic acid (HA) (Technical grade, Sigma Aldrich, USA) stock solution was used as a source of DOM in water. The detailed method for preparation of purified HA stock solution is described elsewhere (Vikesland et al., 1998; Chang, et al., 2001; Yang and Shang, 2004; Li and Zhao, 2006; Rahman and Gagnon, 2013). Briefly, an aliquot of HA was dissolved in 1 L of buffered Milli-Q water at pH >10. The solution was stirred for 24 h at lab temperature (21 ± 1 °C). The solution was then filtered through 0.45 µm filter paper (Micron-PSE, Polysulfone), which produce a DOM solution. The stock solution was stored at 4 °C for subsequent uses.

8.3.3. Analytical methods

8.3.3.1. Dissolved organic carbon

The organic matter content of the stock solution was measured as dissolved inorganic carbon (DOC) using a TOC-V_{CPH} analyzer (Shimadzu Corp., Japan) equipped with an auto-sampler ASI-V (Shimadzu Corp., Japan) according to the Standard Method 5310B (APHA-AWWA-WEF, 2005).

8.3.3.2. Zeta (ζ) potential

Electrophoretic mobility (EMF) of suspended iron particles in solution was measured over a wide range of pH from 3 to11 at 25 ± 0.1 °C using Zetasizer (Zetasizer, Nano-ZS, Malvern Instruments, UK). During the measurements, pH was adjusted by 0.01 M NaOH and 0.01M HCl acid using a multiple purpose auto titrator (MPT-2, Malvern Instruments Ltd., UK). Zeta (ζ) potential was calculated from the electrophoretic mobility using the default instrument software following Henry's equation with the Smoluchowski relationship. At least three measurements were performed as x-potential at certain pH value and the average values were used to represent the data. Prior to the measurement of each new sample, approximately 20 mL of milli-Q water was ringed through the cell followed by a rinse with 10 mL of the sample to be measured. Each sample was measured over a time period of 15-20 min with a 20 sec time interval between each measurement at 25 °C settled by the instrument.

8.3.3.3. Size exclusion chromatography

High pressure size exclusion chromatography (HPSEC, Series 200, Perkin Elmer, USA) was used to determine molecular weight (MW) distribution of dissolved organic matter (DOM) in solution. The samples were passed through a 0.45 µm membrane filter (GE Water & Process Technologies, USA) and analyzed using UV detection at 254 nm with TSK G3000SW column (7.5 mm × 300 mm) and a TSK gel SW guard column (7.5 mm X 70 mm).

8.3.3.4. Fourier transform infrared (FTIR) spectroscopy

The samples for FTIR analysis were prepared following the method reported elsewhere (Fu and Quan, 2006; Giasuddin et al., 2007). Briefly, after completion of the DOM adsorption study, the DOM solutions treated with goethite and magnetite were centrifuged and the supernatants were discarded. The precipitate was dried over night at an ambient temperature, and ground to yield powder. All dried powder samples were stored in a desiccator until the FTIR analysis. FTIR spectra was measured on KBr pellets prepared by pressing mixtures of 1 mg dry powder sample and 100 mg spectrometry grade KBr powder (Sigma-Aldrich, USA) under vacuum, with precaution taken to avoid moisture uptake. Solid-state FTIR spectra were recorded for a wavenumber range of 3600 to 400 using a FTIR spectrometer (Spectrum 100, Perkin Elmer, USA).

8.3.4. Adsorption experiment

Adsorption batch experiments were conducted in 250 mL Pyrex conical flask with stopper. Initially, a 150 mL of DOM stock solution with desired concentration (mg/L as DOC) was taken in a 250 mL conical flask. The final solution was adjusted to an ionic strength of 0.01 M using NaCl, and the desired pH values were adjusted using 0.01 M NaOH or 0.01M HCl acid. The pH value of each solution was stabilized for at least 30 min before adding adsorbent (goethite, magnetite). An appropriate amount of adsorbents (goethite or magnetite) were added into DOM solutions. The suspensions were then shaken at 175 rpm using a shaker table (Barnstead/Lab-Line MaxQ™ 2000) at lab temperature (21 ± 1 °C) for 5 days, which provided sufficient time for our systems to equilibrate, based upon preliminary kinetic studies. After 5 days, the samples (suspensions) were centrifuged at 25000 rpm for 30 min using a centrifuge machine (IEC Centra GP8R, Thermo Electronic Corporation), which was found to be sufficient for separation of the adsorbent from the adsorbate. The supernatants were then filtered instantly through 0.45 μm membrane filter (Micron-PSE, Polysulfone), and filtered were immediately pipetted into glass vial for the measurement of dissolved organic carbon

(DOC) and molecular weight distribution of DOM. DOC in each sample was measured in triplicate using TOC analyzer. The detailed method for measuring is water sample has been described earlier in Section 3.4.1 of Chapter 3. The amount of DOM adsorbed was determined from the difference between the initial and final (after adsorption) DOM concentration in solution after equilibration. The adsorption experiments were conducted for the different dosages of DOM and different pH values in the same experimental setup. Control flasks containing no sorbent were prepared and treated similarly to monitor other possible losses of organic carbon. The equilibrium adsorption capacity was calculated using the following expression (Rahman and Islam, 2009).

$$q_e\,(mg/g) = \frac{(C_o - C_e)V}{m} \qquad (8.1)$$

where, q_e is equilibrium adsorption capacity (mg-C/g), C_o and C_e are initial and equilibrium concentration (mg-C/L) of DOM in solution respectively; V is volume of aqueous solution (mL); and m is dry weight of the adsorbent (g).

8.3.4.1. Adsorption isotherm

The Langmuir isotherm was selected for this analysis in order to estimate DOM adsorption capacity (mg-C/g) onto synthetic iron corrosion scales (e.g., goethite and magnetite), which has been previously applied to describe the adsorption of humic substances on mineral surfaces (Schlautman and Morgan, 1994; Tipping, 1981). The Langmuir adsorption isotherm equation is expressed as Eq. (2.12) in Chapter 2. The Langmuir adsorption isotherm was determined at different pH values ranging from 2.5 to 10.5.

Furthermore, the standard Gibb's free energy ($\Delta G^{\circ}_{\text{ads}}$) changes of adsorption (at atmosphere and 25 °C temp) process for different pH values were calculated using the adsorption constant (K_L) according to the equation (Eq. (8.2)) mention below:

$$\Delta G^{\circ}_{\text{ads}} = -RT\ ln\ (K_L) \tag{8.2}$$

8.3.5. Statistical analysis

All batch adsorption experiments were performed in duplicate. The paired student's t-test ($\alpha = 0.05,\ p < 0.05$) was used to check the similarity of the duplicate tests; and to evaluate the experimental isotherms data with the Langmuir isotherm models. Analysis of variance (ANOVA) tests at a significance level of 95% were used to compare the impact of the various combinations of pH value, and adsorbent type on the maximum DOM adsorption capacity. The Pearson's correlation matrix between all the variables was performed using the software, IBM SPSS Statistics 20 for Windows (IBM, USA).

8.4. Results and discussion

8.4.1. Properties of sorbents

Goethite (α-FeOOH) and magnetite (Fe_3O_4) were chosen for this study, because they are predominately (goethite 75% and magnetite 25%) present in iron corrosion scales of corroded iron pipe in water distribution systems (Sarin et al., 2001). XDR analysis revealed that the synthesized materials were matched exactly with that goethite and magnetite respectively having no detectable crystalline impurities. The X-ray diffraction patterns of synthesized goethite and magnetite are provided in Figures E1 and E2 of appendix E. The BET surface area for goethite and magnetite were determined by N_2 gas adsorption and the values were found to be 19.88 m^2/g and 12.12 m^2/g respectively.

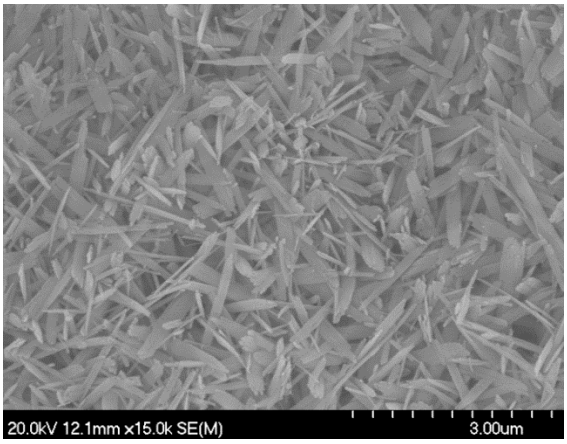

(a). Goethite (before DOM adsorption)

(b). Goethite (after DOM adsorption)

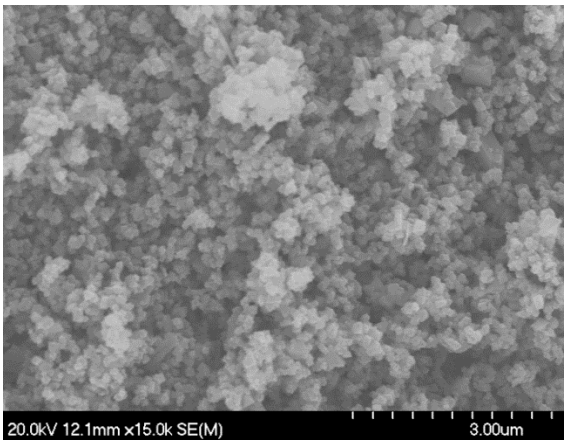

(c). Magnetite (before DOM adsorption)

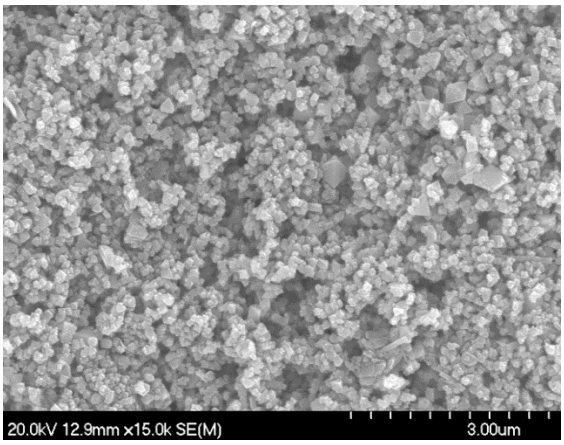

(d). Magnetite (after DOM adsorption)

Figure 8.2. Typical SEM micrographs (magnification: 15,000x) for goethite (a) before and (b) after DOM adsorption; and for magnetite (c) before

The surface structure of goethite and magnetite, before and after DOM adsorption was analyzed by scanning electron microscopy (SEM, Hitachi S-4700, Japan) with 15,000 magnifications. The SEM micrographs for goethite show needle like particles (Figures 8.2(a) and (b)), and magnetite show crystal structure (Figures 8.2(c) and (d)),

those have been resembled with the typical morphology of goethite and magnetite (Shwertmann and Cornell, 2000). The SEM micrographs for goethite and magnetite clearly revealed a change of surface structures and morphology, before and after DOM adsorption experiments. After adsorption both goethite (Figure 8.2(b)) and magnetite (Figure 8.2(d)) particles seem coated by DOM.

8.4.2.2. Effect of sorption on MW distribution of DOM

Previously several researchers (Gloor et al., 1981; Chin et al., 1994; Kilduff et al., 1996; Velten et al., 2011; Valencia et al., 2012; Gibert et al., 2013) have reported that HPSEC technique is perfectly suitable for measuring changes the MW distribution of macromolecules after adsorption onto mineral oxides and activated carbon. Therefore, HPSEC was used for this study to determine the change in MW distribution of DOM due to preferential adsorption of certain DOM fractions. The chromatograms of the initial DOM in solutions, and after adsorption onto different dosages of goethite and magnetite at pH 6.5 are shown in Figures 8.3(a) and (b). Figures 8.3(a) and (b) clearly reveal that with an increase in goethite and magnetite dosage, the total mass of DOM in solution is greatly reduced, and the overall molecular weight distribution chromatographs are shifted to smaller sizes. This can be attributed to the fact that when adsorbents dosage was low, less adsorption sites were available. Therefore, only the highest affinity components of DOM were adsorbed from the solutions. On the other hand, when the higher dosages of adsorbents were used, more adsorption sites were available, and a greater amount of less adsorbable fractions were removed from the solution (Figures 8.3(a) and (b)). Our data corroborate similar observation by other investigators (Kilduff et al., 1996; Wang et al., 1997; Summers and Robert, 1988), who have shown that molecular weight distribution chromatographs of polyelectrolytes shift to smaller sizes with the increase in dosages of granular activated carbon and metal oxides.

In addition, the response corresponding to short elution time, DOM with large molecular weight fractions (Chin et al., 1994) were removed preferentially from the solution by goethite and magnetite, while the response corresponding to longer elution times, DOM with low MW fractions were remained in solution (Figures 8.3(a) and (b)). It might be happened due to the reason that higher MW compounds tend to be more aromatic in nature (Thurman and Malcolm, 1983); therefore, they might have larger number of reaction sites than smaller MW compounds. However, our results were in reasonable agreement with the published works in literature (Davis and Gloor, 1981); Chin et al., 1994). Davis and Gloor (1981) has indicated that NOM adsorption density by Al_2O_3 has been increased by the higher molecular weight fractions. Based upon binding experiments using nonpolar organic probe molecules, Chin et al. (1994) have reported that the hydrophobicity of humic materials increases with increasing molecular weight. Therefore, the DOM molecular weight distribution study has been suggested that the interaction of hydrophobic aromatic fractions with goethite and magnetite surface resulting larger molecular weight fractions preferentially adsorbed from the solutions.

HPSEC study was also conducted in the equilibrium solutions for different pH values ranging from 10.5 to 2.5. In presence of both synthetic iron corrosion scales (goethite and magnetite), the weight-average DOM molecular weights fraction (Da) remaining in solution was gradually decreased with the decrease in pH values (Figure 8.4), that is consistent with the reported results in literature (Valencia et al., 2012). This study also revealed that the decrease of the weight-average DOM molecular weights fraction (Da) are more pronounced above the pH value of 6.5 (Table E22, Appendix E). A possible explanation for this fact is that in acidic media ($pH < 6.5$), the surface hydroxyls of iron are protonated that might render the surface hydroxyl groups more exchangeable (Gu et al., 1995), thus contribute to the pH dependent adsorption of higher molecular weight fractions of organic ligands. This study also revealed that when pH was increased in the presence of goethite and magnetite, the equilibrium concentration of

DOC in solution was higher compared to lower pH values in solution, which will be discussed in section 8.5 with adsorption isotherms data.

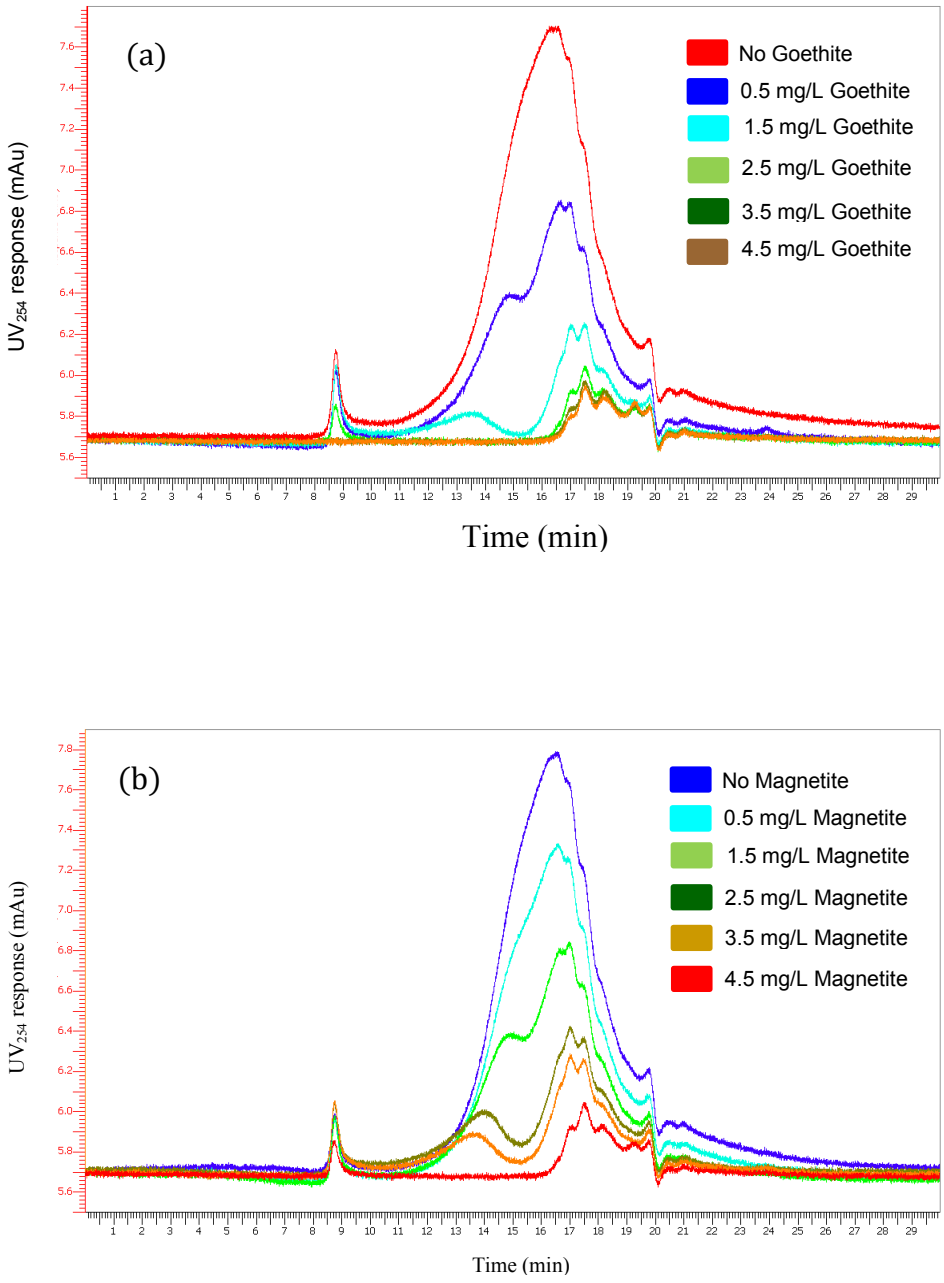

Figure 8.3. Molecular weight distribution of DOM in solution for the adsorption experiments using different dosages of (a) goethite and (b) magnetite at pH 6.5, temperature $21 \pm 1°C$.

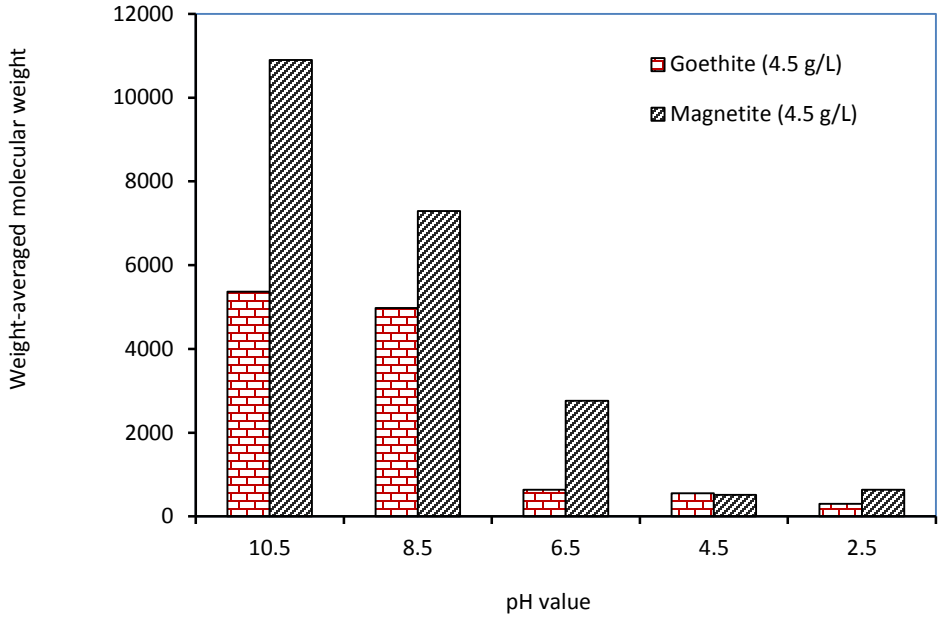

Figure 8.4. Effect of pH on weight average molecular weight fraction remain in solution after adsorption experiment using goethite and magnetite (initial DOM concentration 6.67 mg C/L, time 5 days, temperature 21 ± 1 °C).

8.4.3. Zeta Potential

The electrophoretic mobility in goethite and magnetite solutions alone, and in presence of DOM (6.67 mg-C/L) was measured to determine the pH for point zero charge (pH_{PZC}) at which net surface charge is zero. The pH_{PZC} for goethite and magnetite were found to be around 8.09 and 6.65 respectively, whereas pH_{PZC} was not observed for the DOM solution. Conversely, DOM showed negatively surface charged in the range of -28 mV to -63 mV (Figure 8.5). The findings of pH_{PZC} for goethite and magnetite in this study was in consistent with the literature values (pH_{PZC} of goethite is 8–10, and pH_{PZC} of magnetite is around 6; Schwertmann and Cornell, 2000). The ζ-potential measurements indicated clearly that in presence of DOM, the surface charges of goethite and magnetite particles changed considerably, and the position of pH for their point zero charges (pH_{PZC}) were shifted downward, resulting lower pH (pH 6.11 for goethite and pH 5.14

for magnetite) (Figure 8.5). A possible explanation for this fact might be a reason that DOM contains several functional groups, including major species such as carboxylic ($-COOH$) and phenolic ($-OH$) (Hayes et al., 1989; Gagnon et al., 1997), and specific adsorption of these highly reactive polar functional groups makes the surface of metal oxides negatively charged, which results in a shift of the pH_{PZC} of adsorbent (goethite and magnetite) to a lower pH value. It should be noted here that pH below the point zero charge, the surface of goethite ($pH_{PZC} < 8.09$) and magnetite ($pH_{PZC} < 6.65$) are positively charged due to the accumulation of H^+ ions on the surfaces of both iron oxides. Therefore, the positively charged of goethite and magnetite surfaces attack negatively charged organic ligands. However, when solution pH is above pH_{PZC}, the iron oxide surfaces become negatively charged and can form surface complexes with cations.

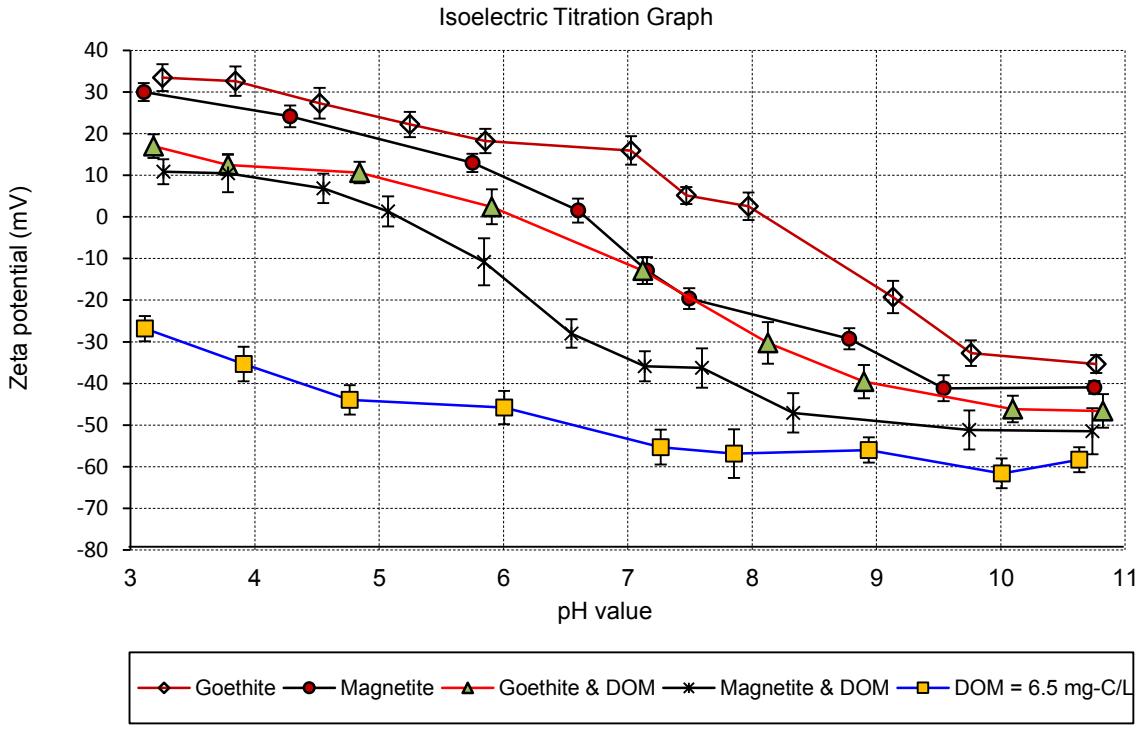

Figure 8.5. Zeta potential of goethite and magnetite as function of pH in the absence and presence of DOM (6.67 mg-C/L) in solution at 25 ± 0.1 °C.

8.4.4. FTIR Spectroscopy

Transmission FTIR spectra of DOM, DOM-goethite and DOM-magnetite are shown in Figure 8.6. DOM before adsorption appears with typical bands for humic substances in aquatic systems. Major adsorption bands for DOM (Figure 8.6, spectra (a)) were found at 3400/3425 cm^{-1} for phenolic O-H stretching, at 2940/2905 cm^{-1} for aliphatic C-H stretching of $-CH_3$ and $-CH_2$ groups, at 2865/2875 cm^{-1} for carboxylate ion, at 1730/1715 cm^{-1} for C-O stretching of –COOH and ketone; at 1635/1615 cm^{-1} associate to structural vibrations of aromatic C=C, and anti-symmetrical stretching of $-COO^-$ groups, and at 1240/1250 cm^{-1} for C–O stretching of ester, ethers and phenols (Stevenson, 1994; Giasuddin et al., 2007; Brigante et al., 2010).

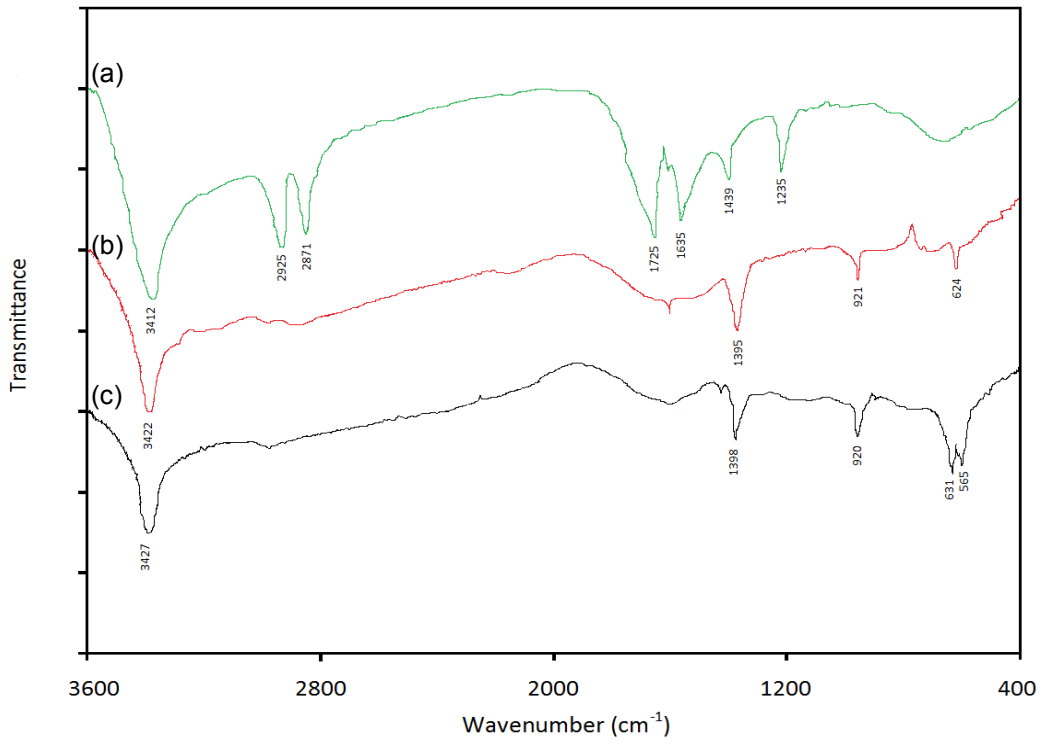

Figure 8.6. FTIR spectra of DOM (a) before, and after reaction with (b) goethite and (c) magnetite at pH 4.5, temperature 21 ± 1 °C.

When DOM adsorbed onto goethite and magnetite surfaces, some difference in FTIR spectra (Figure 8.6, spectra (b) and (c)) were observed compared with DOM spectra before adsorption (Figure 8.6, spectra (a)). Bands at 2925, 2871, 1725, 1439 cm^{-1} were observed to be partially or completely vanished as shown by spectra (b) and (c) in Figure 8.6, which indicated that several functional groups (mainly carboxyl and hydroxyl) of organic ligands participated in adsorption process onto iron oxide surface species ($Fe-OH_2^+$ or $Fe-OH$) by subsequently replacing H_2O and OH^- (Gu, et al., 1995). On the other hand, new strong bands at around 1395 and1098 cm^{-1} were appeared for DOM-goethite and DOM-magnetite spectra respectively that might be because of symmetric stretching of carboxyl functional groups complexed with iron or on iron oxide surfaces. This hypothesis has been supported by the fact that fulvic acid (FA) contains mainly carboxyl functional groups (Hayes et al., 1989; Gagnon et al., 1997), and the interaction of FA with iron to form iron fulvate and complexes with iron oxide appears a strong absorption band at about 1400 cm^{-1} (Sposito, 1984). Conversely, several small bands at 920, 631 and 565 cm^{-1} were observed in FTIR spectra for DOM-goethite (Spectra (b) in Figure 8.6) and DOM-magnetite (Spectra (c) in Figure 8.6) that might be Fe-O vibrations due to different stretching patterns in the different crystal phases (Fu and Quan, 2006; Giasuddin et al., 2007). However, considering the change of FTIR spectra for this study and the literature findings (Gu et al., 1995; Fu and Quan, 2006; Giasuddin et al., 2007), it has been suggested that carboxylate ion ($-COO^-$), phenolic group ($-OH$) and carboxyl group ($-COOH$) react with iron oxides/hydroxides (goethite and magnetite) by making an inner-sphere complexation with ligand exchange mechanism in adsorption processes.

8.4.5. Adsorption isotherm

The adsorption isotherms of DOM onto synthetic iron corrosion scales (e.g., goethite and magnetite) were investigated to determine the affinity of DOM for the iron oxides surfaces as a function of pH ranging from 2.5 to 10.5. Figures 8.7(a) and (b) show the plots of DOM uptake by goethite and magnetite against the equilibrium DOM

concentration in the solutions. The adsorption isotherms for the studied pH values for both goethite and magnetite showed an initial steep slope, and reached a plateau at an elevated equilibrium DOM concentration (Figures 8.7(a) and (b)), indicating a high affinity type interaction (Sposito, 1984) of the DOM with iron oxides/hydroxides surfaces. However, ANOVA test (Table E23 of Appendix E) revealed that the pH values were statistically significant (α = 0.05, $p < 0.005$ and $F_{stat} = 52.54 > F_{crit} = 6.39$) on the change in adsorption capacity onto the adsorbents. Several studies have shown a similar effect of pH on adsorption processes (Shi et al., 2012; Valencia et al., 2012). On the other hand, in ANOVA test, there was significant difference ($\alpha = 0.05$, $p < 0.005$ and $F_{stat} = 70.57 > F_{crit} = 7.71$) on adsorption capacity for goethite and magnetite in various solutions pH indicating that goethite and magnetite adsorbents performed differently at adsorbing DOM from the aqueous solutions.

However, results of this study have been suggested that DOM adsorption onto goethite and magnetite surfaces increase significantly with the decrease in pH values as has been reported previously for humic substances adsorption onto Al_2O_3 surfaces (Davis and Gloor, 1981). The increase in adsorption with the decrease in pH values might be continued until the organic anions in solution become protonated and the charge of the anions diminish (Filius et al., 1997). As a consequence of protonation, the adsorption envelope was observed to be less steep at higher pH; and therefore, the maximum adsorption density (q_m) of DOM on goethite and magnetite was observed at a lower pH 2.5 (Table 8.1; Figures 8.7(a) and (b)). This type of adsorption seems consistent with the ligand exchange (or electrostatic interaction) mechanism. In fact, the adsorption curves in Figure 8.7(a) and (b) are very similar to the adsorption curve of an organic acid with a pK value in the range of 3 to 5 on hydrous oxide as described by the ligand exchange of surface hydroxyls (Shen, 1999). It is thus reasonable to suppose that the primary sorption mechanism of DOM onto goethite and magnetite surface is ligand exchange. Other mechanisms might have influence on DOM adsorption by metal oxides/hydroxides. This study also revealed that higher adsorption densities were

observed between pH 2.5 and 6.5, especially evident for goethite (Figure 8.7(a)) compared to magnetite (Figure 8.7(b)). A possible reason may be explained by the fact that pH value between 2.5 to 6.5, the electrostatic attraction between the positive surfaces of goethite and magnetite, and negative functional groups of DOM is higher. However, a large decrease in sorption density was observed close to and above the pH for point zero charge of the goethite surface (pH_{PZC} = 8.09) and the magnetite surface (pH_{PZC} = 6.65) (Figures 8.7(a) and (b)). The zeta potential data discussed above (Figure 8.5) are consistent with the adsorption isotherms measured in this study (Figures 8.7(a) and (b)).

This study illustrated that the isotherm data on conversion to the Langmuir model yield straight lines for all the adsorption studies (Figures E3 to E12, Appendix E,), with the regression coefficient (r^2) more than 0.9 (Table 8.1). The values of r^2 are regarded as a measure of the goodness-of-fit of the experimental data on the isotherms models (Crittenden et al., 2012). Considering r^2 values for all the adsorption studies for different pH values, it might be concluded that the adsorption data perfectly fit the Langmuir isotherms model (Table 8.1), indicating monolayer cover of DOM over the goethite and magnetite surfaces. The paired student's *t*-tests revealed that there was no statistically significant difference ($\alpha = 0.05$, $p < 0.05$) between the Langmuir adsorption isotherm model and the experimental adsorption data (Tables E2, E4, E6, E8, E10, E12, E14, E16, E18 and E20, Appendix E). On the other hand, the standard Gibb's free energy (ΔG°_{ads}) changes of adsorption process (Eq. (8.2)) for goethite and magnetite were calculated using the Langmuir adsorption constants (K_L) for the different pH values showing negative (Table 8.1). The negative value of ΔG°_{ads} indicates the feasibility of adsorbents, and adsorption of DOM on the goethite and magnetite was spontaneous under the experimental conditions. Our data is consistent with the observations made by other investigators, where the adsorption of (poly)maleic and aquatic fulvic acid by metal oxide (Wang et al., 1997), adsorption of copper and cadmium ions by activated carbon (Teker and İmamoğlu, 1999) are described by the Langmuir equation; and show negative ΔG°_{ads} confirming the feasibility of the process and the spontaneous nature of the adsorption.

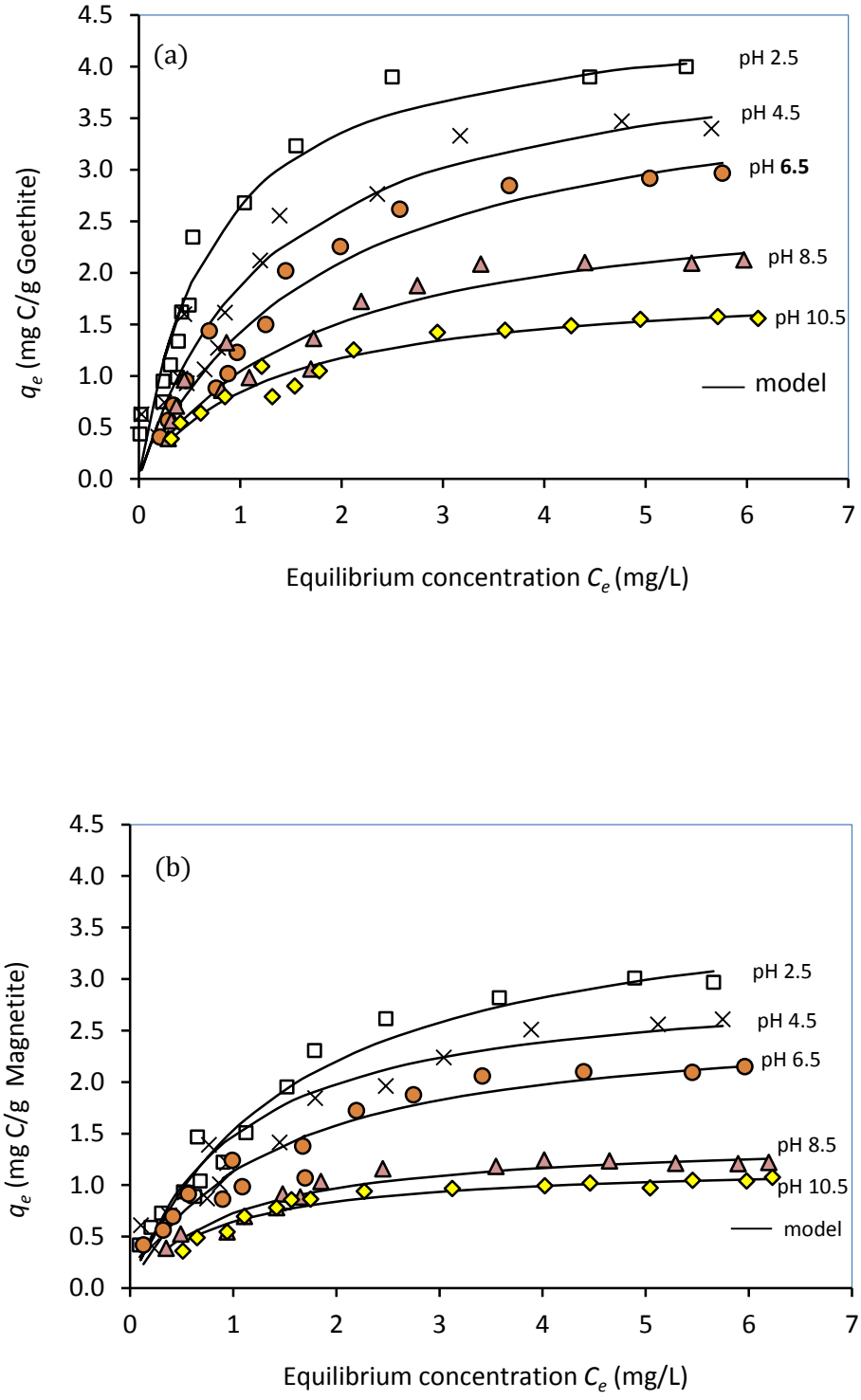

Figure 8.7. Effect of pH on the Langmuir adsorption isotherms using (a) goethite and (b) magnetite in synthetic water samples.

On the other hand, the DOM adsorption data was applied in the Freundlich adsorption isotherm equation. This study revealed that the r^2 values for the Freundlich isotherm in different adsorption studies were ranged between 0.4 to 8. However, the paired student's t-test revealed that there was statistically significant difference ($\alpha = 0.05, p < 0.05$) between the Freundlich adsorption isotherm model and the experimental adsorption data. Therefore, the Freundlich adsorption isotherm study was not included in this chapter.

Table 8.1. The Langmuir isotherm fitting parameters for DOM adsorption onto goethite and magnetite surface.

	Goethite					Magnetite				
	pH 2.5	pH 4.5	pH 6.5	pH 8.5	pH 10.5	pH 2.5	pH 4.5	pH 6.5	pH 8.5	pH 10.5
q_m	4.75	4.32	4.05	2.81	1.9	3.79	2.99	2.6	1.46	1.18
K_L	1.37	0.77	0.54	0.59	0.78	0.71	0.97	0.75	0.98	1.24
r^2	0.96	0.93	0.94	0.93	0.98	0.95	0.91	0.95	0.98	0.99
$q_m K_L$	6.27	3.32	2.18	1.65	1.51	2.70	2.91	1.95	1.43	1.46
$\Delta G^{\circ}_{\text{ads}}$	-34.9	-33.5	-32.7	-32.9	-33.6	-33.3	-34.1	-33.5	-34.1	-34.7

r^2 is the coefficient of determination, used in curve fitting to indicate the goodness-of-fit. $\Delta G^{\circ}_{\text{ads}}$ Gibbs free energy of adsorption (kJ/mol) according to equation, where, K_L is in units of L/kg (Baham and Sposito, 1994).

Based upon the Langmuir isotherm fitting results, the maximum adsorption capacity (q_m) of goethite was uniformly higher than that of magnetite over the entire pH range studied here (Table 8.1). A possible explanation for this fact is that BET surface area for goethite (19.88 m^2/g) was higher than that of magnetite (12.12 m^2/g).

Therefore, it has been assumed that the specific surface area of the synthetic iron corrosion scales has been influenced significantly DOM adsorption process. In addition of the surface area, another possible reason is that the pH for point zero charge of goethite (pH_{PZC} = 8.09) is greater than magnetite (pH_{PZC} = 6.65) (Figure 8.5). Therefore, at pH 6.5 and below, goethite has more positively charged surfaces, potentially leading to stronger interaction with negative charges in DOM molecules resulting higher adsorption affinity compared to magnetite surfaces.

8.4.6. Correlation

The Pearson's correlation matrix analysis between all the independent (e.g., pH, DOM, goethite, and magnetite dosage) and the dependent variables (e.g., C_e, q_e, MW, and MN) involving with the adsorption processes was performed using the software, 'IBM SPSS Statistic 20' for windows (IBM, USA), and the results are presented in Tables 8.2 and 8.3 respectively.

This analysis revealed a statistically significant negative correlation between goethite dosages; and MW ($r = 0.72$, $p < 0.05$) and; goethite dosages and MN ($r = 0.83$, $p < 0.01$) (Table 8.2). The findings of this study indicate that with an increase in goethite dosage, weight average molecular weight (MW) and average molecular number (MN) were decreased significantly ($p < 0.05$) that is consistent with the HPSEC chromatographs (Figures 8.3(a) and (b)). A same trend was observed in presence of magnetite that is presented in Table 8.3. This study also revealed a strong correlation between goethite dosage and q_e ($r = 0.96$, $p < 0.01$); and between magnetite dosage and q_e ($r = 0.81$, $p < 0.01$), that supports the Langmuir adsorption isotherm indicating monolayer coverage. Conversely, a positive significant ($\alpha = 0.05$) correlation was observed between pH and MW and MN in presence of goethite (Table 8.2) and magnetite (Table 8.3), which stated that pH has obvious role on the change of molecular weight

distribution and DOM adsorption mechanisms. The correlation among the other factors is presented in Tables 8.2 and 8.3. Further details of the correlation can be found elsewhere (Montgomery, 2009).

Table 8.2. The Pearson's correlation matrix analysis between all the independent (e.g., pH, DOM, and goethite dosage) and the dependent variables (e.g., C_e, q_e, MW, and MN).

	pH	DOM	Goethite	C_e	q_e	MW	MN
pH	1						
DOM (mg-C/L)	0.052	1					
Goethite (g/L)	0.108	-0.209	1				
C_e	0.260	0.340	-0.826 [b]	1			
q_e	-0.204	0.436	-0.960 [b]	0.792 [b]	1		
MW	0.485	0.326	-0.715 [a]	0.838 [b]	0.675 [a]	1	
MN	0.341	0.333	-0.832 [b]	0.944 [b]	0.769 [b]	0.815 [b]	1

[a] Correlation is significant at the 0.05 level (2-tailed).

[b] Correlation is significant at the 0.01 level (2-tailed).

C_e: Equilibrium concentration of DOM,

q_e: adsorption capacity

MW: molecular weight

MN: molecular number.

Table 8.3. The Pearson's correlation matrix analysis between all the independent (e.g., pH, DOM, and magnetite dosage) and the dependent variables (e.g., C_e, q_e, MW, and MN).

	pH	DOM	Magnetite	C_e	q_e	MW	MN
pH	1						
DOM (mg-C/L)	0.000	1					
Magnetite (g/L)	0.000	-0.236	1				
C_e	0.262	.0420	-0.884 [b]	1			
q_e	-0.155	0.573	-0.907 [b]	0.808 [b]	1		
MW	0.800 [b]	-0.199	-0.248	0.424	0.002	1	
MN	0.735 [a]	-0.257	-0.423	0.407	0.152	0.680 [a]	1

[a] Correlation is significant at the 0.05 level (2-tailed).

[b] Correlation is significant at the 0.01 level (2-tailed).

C_e: Equilibrium concentration of DOM,

q_e: adsorption capacity,

MW: molecular weight,

MN: molecular number.

8.5. Conclusions

The goal of this study was to explore the mechanisms of DOM adsorption onto synthetic iron pipe corrosion scales i.e. goethite and magnetite surfaces in order to understand the major appliances that control the DOM adsorption process, and change surface properties of goethite and magnetite particles. This study demonstrated that the adsorption data were fit well by the Langmuir adsorption isotherm indicating monolayer coverage. The standard Gibb's free energy ($\Delta G^{\circ}_{\text{ads}}$) changes of adsorption process obtained using the Langmuir equilibrium constant (K_L) indicating that the adsorption of DOM onto the

goethite and magnetite surface was spontaneous under the experimental conditions. However, the maximal adsorption capacity for goethite and magnetite were revealed to be 4.75 mg-C/g and 3.79 mg-C/g respectively at pH 2.5; and it was decreased with the increase in pH values. HPSEC chromatographs of DOM after adsorption demonstrated that total mass of DOM fractions from solution greatly adsorbed onto goethite and magnetite surfaces. More specifically, the higher molecular weight hydrophobic fractions are adsorbed onto goethite and magnetite surfaces and lower molecular weight fractions remained in solution. It's happened more pronouncedly at lower pH value ($pH < pH_{PZC}$). It has also been suggested that molecular weight distribution and organic acidity possibly control DOM adsorption onto goethite and magnetite surfaces. FTIR study revealed that DOM enriched in carboxylic functional groups are preferentially adsorbed by goethite and magnetite surfaces.

Although the DOM sample used in our study may not be representative of all aquatic DOM substances, however a general conclusion can be drawn for the results achieved from this study specify that DOM adsorption onto iron corrosion scales i.e. goethite and magnetite surface is largely due to the ligand exchange mechanisms. This study also demonstrated that the surface charges of goethite and magnetite were modified due to DOM adsorption onto their surfaces, and their pH for point zero charge (pH_{PZC}) was shifted markedly to lower pH compared to that of in absence of DOM. Therefore, it has been suggested that at normal pH of natural water samples, DOM adsorbed goethite and magnetite have a net negative charge, which would have possible impact on interact with inorganic cations/pollutants and to transport in iron pipe water distribution systems.

CHAPTER 9. CONCLUSIONS AND RECOMMENDATIONS

Conclusions

Overall, the results of this research allowed several key conclusions to be drawn about the impacts of different water quality parameters influencing the Fe(II) ions oxidation kinetics, iron suspension formation; and subsequently the impacts of iron corrosion by-products (e.g., Fe(II) ions, goethite, and magnetite) on the changes in disinfection residual concentrations and disinfection byproducts formation in drinking water distribution systems. The significant conclusions of the findings from this study are presented below by five sections in order to represent the conclusions of each experimental chapter:

- This research showed that certain water chemistry parameters had significant impact on the rate constants in Fe(II) ions oxidation processes for an initial 3 mg/L of Fe(II) ions in synthetic water samples. pH and phosphate were observed to be the most significant ($\alpha = 0.05$) factors contributing 42% and 23% of total variability in Fe(II) ions oxidation processes. Conversely, this study revealed that the typical concentrations for DOM (2.85 mg-C/L) and chlorine (2.2 mg/L) had not significant ($\alpha = 0.05$, $p > 0.05$) impact on the rate constants in Fe(II) ions oxidation processes. Conversely, a dependency relationship for the iron oxidation rate constants with pH and the PO_4 -to- Fe(II) mole ratios were revealed in this investigation. The investigation involved four factors with different levels showed that the lowest Fe(II) ions oxidation rate constants would appear to be obtained when pH value was 6.5, chlorine dosage was < 2.2, and PO_4 -to- Fe(II) mole ratio was ≈ 0.3 in the iron water systems. The research findings have practical implications related to both iron pipe drinking water distribution systems, and water treatment issues.

- This study revealed that the existing water quality parameters, i.e., pH, residual chlorine, phosphate based corrosion inhibitor and DOM had significant impacts on the properties of iron particles (shape and size) and suspension (color and turbidity) in a drinking water distribution system. The statistical analysis ($\alpha = 0.05$, $p > 0.05$) revealed that phosphate was observed to be the most significant factor reducing the color and turbidity in iron water systems. In addition, phosphate decreased the sizes of the iron particles, created more negative zeta (ζ) potential, and increased iron suspension stability in iron water systems. Consequently, DOM made the ζ-potential of iron particles more negative. Therefore, interactions between the particles were decreased significantly, which limited particles aggregation. These results were observed to be more pronounced at a pH value of 6.5 compared to a pH value of 8.5 in water samples. This study also suggests that iron colloid suspension color and turbidity in chlorinated drinking water distribution systems could be lower than non-chlorinated water systems. This study has suggested that water quality parameters have direct impact on the properties of iron suspension and the formation of iron particles in distribution systems.

- The formation of HAAs and THMs was observed to be lower in iron water systems compared with control water in different reactions systems. The results of this study demonstrated that in iron water systems, a lower pH value of 6.5 might have contributed a lower content of HAAs and THMs compared with the higher pH value of 8.5. Therefore, the results of this study might have implications for understanding the facts that pH change in drinking water not only affect Fe(II) ions oxidation processes, but has also an impact on DBPs formation as well as to affect reactivity between DOM and chlorine. Conversely, HAAs formation was observed to decrease significantly ($\alpha = 0.05$, $p < 0.05$) in presence of phosphate in iron water systems. This study revealed that Fe(II) ions was the most significant factor ($\alpha = 0.05$, $p < 0.05$) on HAAs and THMs formation study,

accounting over 50% of total variability. Mathematical models for HAAs and THMs prediction were successfully developed considering all the significant factors ($\alpha = 0.05$, $p < 0.05$), and the models were found to be noteworthy by the numerical and graphical diagnostics. The validation of the models using different sources of natural water samples collected from three main water treatment plants in Halifax, Canada, illustrated that $> 83\%$ of the total observed HAAs and THMs formation data lay within $\pm$ 20% of the predicted values, which suggested that the models performance was found to be excellent under a wide range of studied variables and DBPs (HAAs and THMs) concentrations. No systematic under or over prediction was noticed throughout the whole range of DBPs concentrations.

- This study revealed that the predominant iron oxides, i.e., magnetite and goethite which mainly present in iron pipe corrosion scales, consumed chlorine in drinking water distribution systems. Chlorine consumption rate was observed to increase significantly ($\alpha = 0.05$, $p < 0.05$) with the increase in magnetite and goethite dosages in water samples. This finding was more profound in aqueous-magnetite systems compared to aqueous-goethite systems. The bench scale study revealed that in presence of synthetic goethite, HAAs and THMs formation was observed to increase compared with that of aqueous systems, and this was more reflective with the increase in reaction times. Conversely, a reverse trend was observed to decrease HAAs and THMs formation in presence of magnetite in the same reaction systems. It was noticed in this study that chlorine stock solution was the main source of bromide ions, which might have contributed to generate brominated DBP species in drinking water distribution systems.

- This study demonstrated that the DOM adsorption onto the synthetic predominant iron pipe corrosion scales, i.e., goethite and magnetite data were fit well by the Langmuir adsorption isotherm indicating monolayer coverage. The standard

Gibb's free energy ($\Delta G^{\circ}_{\mathrm{ads}}$) changes of the adsorption processes obtained using the Langmuir equilibrium constant (K_L) indicating that the DOM adsorption onto the goethite and magnetite surfaces was spontaneous under the experimental conditions. The maximal adsorption capacity for goethite and magnetite was revealed to be $4.75\ \mathrm{mg\text{-}C/g}$ and $3.79\ \mathrm{mg\text{-}C/g}$ respectively at pH value of 2.5; and it was decreased gradually with the increase in pH values. HPSEC chromatographs of DOM before and after adsorption experiments demonstrated that total mass of DOM fractions from the solutions greatly adsorbed onto goethite surfaces followed by magnetite surfaces. More specifically, the higher molecular weight hydrophobic fractions of DOM are adsorbed onto goethite and magnetite surfaces, and lower molecular weight fractions remain in solutions. It's happened more pronouncedly at lower pH value ($\mathrm{pH} < \mathrm{pH_{PZC}}$). It has also been suggested that molecular weight distribution and organic acidity possibly control DOM adsorption onto goethite and magnetite surfaces. FTIR study revealed that DOM enriched in carboxylic functional groups was preferentially adsorbed by goethite surfaces followed by magnetite surfaces.

Recommendations

The research presented in this thesis has introduced a number of novel and interesting results. However, some of these results have raised supplementary questions or wants that are beyond the scopes of the original objectives, and can only be suitably addressed by directing further researches. The important recommendations for the future research works are presented below by five sections in order to represent limitation of each experimental chapter:

- Though the Fe(II) ions oxidation kinetics study showed some interesting finding in $NaHCO_3$ buffered synthetic water samples specially for using different dosages of phosphate for an initial Fe(II) ions concentration of 3 mg/L. Nevertheless, the findings of this study encourage further investigation in natural water samples with a wide range of Fe(II) ions concentrations. Because, the composition of natural water is complex having different inorganic and organic materials, and a wide range of Fe(II) ions concentrations has been reported to present in water samples. However, future research works should be considered a more detailed investigation including different mole ratios of phosphate to iron, and a detailed thermodynamic investigation in presence of other important variables those are present in natural water samples.

- The blended phosphate addition should be continued to minimize iron corrosion and oxidation processes, to reduce iron suspension color and turbidity, and to decrease the iron particles size in drinking water distribution systems. This study was conducted in the synthetic water samples at a fixed temperature (21 ± 1 °C), in presence of initial Fe(II) ions concentration of 3 mg/L for a fixed DOM concentration (2.85 mg/L) and for different pH values. Though the work on the influence of phosphate on iron particles stability provided admirable insights and

recommendation, a water utility must consider more water quality parameters specially a wide range of iron concentration and different pH values, when deciding the dosage of phosphate to control iron suspension problems. Because, the rate of iron corrosion, oxidation; and the formation of particles' shape and size are strongly affected by different water quality parameters.

- Although the model development results and its application in post filtered water samples, collected from three major water treatment plants of Halifax, Canada show that it is possible to estimate HAAs and THMs level in drinking water distribution systems. However, these models should be tested by real drinking water distribution or storage systems data. Conversely, it has been suggested that the models can also be very useful in verifying key operational and water quality parameters, which may help to explain the HAAs and THMs formation potential in distribution systems. Therefore, the models may be used as decision making tools by the drinking water industries. Nevertheless, it should be said that it is difficult to develop universal applicable HAAs and THMs formation models due to the complexity of HAAs and THMs formation reactions depending on different factors.

- Research concerning surface mediated reactions between iron pipe corrosion by-products (e.g., goethite and magnetite) and disinfectant that occurring in drinking water distribution systems should be continued to understand their impact on the change in water quality especially on the formation/reduction of carcinogenic disinfection byproducts (DBPs). Future researches should be designed to evaluate the impact of various pH values, and the different dosages of phosphate based corrosion inhibitor on DBPs formation study in presence of main iron pipe corrosion by-products, i.e., goethite and magnetite. Various chlorine dosages should be used to determine the balance between required chlorine dosage, and the lowest formation of DBPs in iron water systems.

This study showed that the predominant iron oxides present in corrosion scales, i.e. goethite and magnetite significantly adsorbed DOM from the synthetic water samples, which raises the possibility of iron oxides to use in water treatment plants. The DOM adsorption processes were observed to be more significant for a lower pH values ($pH < 6$). The pH values in raw (source) water uses in the Halifax water treatment and supply (HWTS) plant are lower than 6. On the other hand, both goethite and magnetite are abundant in nature, and both are nontoxic. Therefore, it has been suggested that both goethite and magnetite might be used as natural additives in water treatment plant to remove one of the main DBPs formation precursors, DOM from raw water during treatment processes in a plant.

REFERENCES

Aitken-Rogers, H., Singleton, C., Lewin, A., Taylor-Gee, A., Moore, G.R., Brun, N.E.L. 2004. Effect of phosphate on bacterioferritin-catalysed iron(II) oxidation. *J. Biol. Inorg. Chem*. **9** (2), 161-170.

Alshehri, A.R.A. 2008. *Impact of Corrosion Inhibitor Blended Orthophosphate on Water Quality in Water Distribution Systems*. Ph.D. Dissertation, University of Central Florida, Florida.

Amold, W.A., Hozalski, R.M., Pearson, C.R., Moore, K. 2010. TBAA reduction in reactors in simulated distribution systems pipes. *J. Am. Water Works Assoc*. **102** (3), 99-106.

Amonette, J.E., Workman, D.J., Kennedy, D.W., Fruchter, J.S., Gorby, Y.A. 2000. Dechlorination of carbon tetrachloride by Fe(II) associated with goethite. *Environ. Sci. Technol*. **34** (21), 4606-4613.

Amy, G.L., Chadik, P.A., Chowdhury, Z.K. 1987. Developing models for predicting trihalomethane formation potential kinetics. *J. Am. Water Works Assoc.* **79** (7), 89-96.

APHA-AWWA-WEF. 2005. *Standard Methods for the Examination of Water and Wastewater.* 20th Ed., APHA, AWWA and WEF, Washington DC, USA.

Arora, H., LeChevallier, M.W., Dixon, K.L. 1997. DBP occurrence survey. *J. Am. Water Works Assoc*. **89** (6), 60-68.

Atkinson, R.J., Parfitt, R.L., Smart, R. St.C. 1974. Infra-red study of phosphate adsorption on goethite. *J. Chem. Soc. Faraday Trans.* **1** (70), 1472-1479.

AWWA. 1996. *Water:/Stats, the Water Utility Database*: *1996 Survey* (CD), American Water Works Association: Denver, CO, USA.

AWWA. 1999. *AWWA Report: $325 billion for Pipes*. AWWA Mainstream.

AWWA. 2000. Water quality division disinfection systems committee report: Disinfection at large and medium size systems. *J. Am. Water Works Assoc*. **92** (5), 32-43.

AWWARF. 1996. *Internal Corrosion Control in Water Distribution Systems*. 2nd Ed. AWWA Research Foundation, DVGW-Technologiezentrum Wasser, Denver, USA.

AWWARF. 2002. *Development of Red Water Control Strategies* (90883). AWWARF and AWWA, USA.

Azher, N.E., Gourich, B., Vialb, C., Soulami, M.B., Ziyad, M. 2008. Study of ferrous iron oxidation in Morocco drinking water in an airlift reactor. *Chem. Eng. Process*. **47** (9), 1877-1886.

Babel, S., Kurniawan, T.A. 2003. Low-cost adsorbents for heavy metals uptake from contaminated water: A review. *J. Hazard. Mater*. **97** (1-3), 219-243.

Baham, J., Sposito, G. 1994. Adsorption of dissolved organic carbon extracted from sewage sludge on montmorillonite and kaolinite in the presence of metal ions. *J. Environ. Qual.* **23** (1), 147-153.

Balistrieri, L.S., Murray, J.W. 1987. The influence of the major ions of seawater on the adsorption of simple organic acids by goethite. *Geochim. Cosmochim. Acta* **51** (5), 1151-1160.

Baribeau, H., Pozos, N., Boulos, L., Crozes, G., Gagnon, G.A., Rutledge, S., Skinner, D., Hu, Z., Hofmann, R., Andrews, R.C., Alam, M.Z.B., Andrews, S.A., Dumancic, R., Chauret, C., Warn, E. 2005. *Impact of Changes in Distribution System Water Quality on Disinfection Efficacy*. AWWARF, Denver, CO, USA.

Bellar, T., Lichtenberg, J., Kroner, R. 1974. The occurrence of organohalides in chlorinated drinking water. *J. Am. Water Works Assoc.* **66** (12), 703-706.

Benjamin, M., Lawler, D. 2013. Chapter 7: Adsorption Processes-Part 1 Adsorption Equilibrium. *Water Quality Engineering*: *Chemical and Physical Processes.* Willy, USA.

Benjamin, M.M., Miller, M.W. 1990. *Chemistry of Corrosion Inhibitor in Portable Water.* AWWA Research Foundation, Denver, USA.

Benjamin, M.M., Sontheimer, H., Leroy, P. 1996. Chapter 2 In: *Internal Corrosion of Water Distribution Systems*. 2nd Ed. AWWARF, Denver, CO, USA.

Bove, F., Shim, Y., Zeitz, P. 2002. Drinking water contaminants and adverse pregnancy outcomes: A review. *Environ. Health Perspect*. **110** (Supplement 1), 61-74.

Boyce, S.D., Horning, J.F. 1983. Reaction pathways of trihalomethane formation from the halogenation of dihydroxyaromatic modelcompoun ds for humic acid. *Environ. Sci. Technol.* **17** (4), 202-210.

Bradford, S.A. 1993. *Corrosion Control*. Van Nostrand Reinhold, NY, USA.

Brereton, J.A., Mavinic, D.S. 2002. Field and material-specific simulated distribution system testing as aids to understanding trihalomethane formation in distribution systems. *Can. J. Civ. Eng.* **29** (1), 17-26.

Brigante, M., Zanini, G., Avena, M. 2010. Effect of humic acids on the adsorption of paraquat by goethite. *J. Hazard. Mater*. **184** (1-3), 241-247.

Bull, R.J., Kopfler, F.C. 1991. *Health Effects of Disinfectants and Disinfections By-products. Research Report*. American Water Works Research Foundation, Denver, CO, USA.

Cantor, A.F., Park, J.K., Vaiyavatjamai, P. 2003. Effect of chlorine on corrosion in drinking water systems. *J. Am. Water Works Assoc*. **95** (5), 112-123.

Cham, C.H., Gullick, R.W., Long, S.C., Kenel, P.P. 2010. *Operational Guide to AWWA Standard G300*: *Source Water Protection*. American Water Works Association, Denver, CO, USA.

Chang, E.E., Chiang, P.C., Ko, Y.W., Lan, W.H. 2001. Characteristics of organic precursors and their relationship with disinfection by-products. *Chemosphere* **44** (5), 1231–1236.

Chang, P.B.L., Young, T.M. 2000. Kinetics of methyl *tert*-butyl ether degradation and by-product formation during UV/H_2O_2 water treatment. *Water Res.* **34** (8), 2233-2240.

Chen, W.J., Weisel, C. 1998. Halogenated DBP concentrations in a distribution system. *J. Am. Water Works Assoc.* **90** (4), 151-163.

Cheng, Y.G., Chasteen, N.D. 1991. Role of phosphate in initial iron deposition in apoferritin. *Biochemistry* **30** (11), 2947-2953.

Chin, Y.-P., Aiken, G., O'Loughlin, E. 1994. Molecular weight, polydispersity, and spectroscopic properties of aquatic humic substances. *Environ. Sci. Technol*. **28** (11), 1853-1858.

Chowdhury, S., Champagne, P., McLellan, P.J. 2010. Investigating effects of bromide ions on trihalomethanes and developing model for predicting bromodichloromethane in drinking water. *Water Res.* **44** (10), 2349-2359.

Chowdhury, S., Rodriguez, M.J., Sadiq, R. 2011. Disinfection byproducts in Canadian provinces: associated cancer risks and medical expenses. *J. Hazard. Mater*. **187** (1-3), 574-584.

Chuah, T.G., Jumasiah, A., Azni, I., Katayon, S., Choong, S.Y.T. 2005. Rice husk as a potentially low-cost biosorbent for heavy metal and dye removal: An overview. *Desalination* **175** (3), 305-316.

Chun, C.L., Hozalski, R.M., Arnold, W.A. 2005. Degradation of drinking water disinfection byproducts by synthetic goethite and magnetite. *Environ. Sci. Technol*. **39** (21), 8525-8532.

Clark, R.M., Thurnau, R.C., Sivaganesan, M., Ringhand, P. 2001. Predicting the formation of chlorinated and brominated by-products. *J. Environ. Eng.-ASCE* **127** (6), 493-501.

Clement, J., Hayes, M., Sarin, P., Kriven, W., Bebee, J., Jim, K., Beckett, M., Snoeyink, V., Kirmeyer, G., Pierson, G. 2002. *Development of Red Water Control Strategies*. AWWARF, Denver, CO, USA.

Cornell, R.M., Giovanoli, R. 1985. Effect of solution conditions on the proportion and morphology of goethite formed from ferrihydrite. *Clays Clay Miner.* **33** (5), 424-432.

Crabtree, J.H., Schaeper, W.P. 1966. The oxidation of iron(II) by chlorine. *Inorg. Chem.* **5** (8), 1348-1351.

Crittenden, J.C., Trussell, R.R., Hand, D.W., Howe, K.J., Tchobanoglous, G. 2012. *MWH's Water Treatment*: *Principles and Design*. 3rd Ed., John Wiley & Sons, Inc., NJ, USA.

Davidson, W., Seed, G. 1983. The kinetics of the oxidation of ferrous iron in synthetic and natural waters. *Geochim. Cosmochim.-Acta* **47** (1), 67-69.

Davis, J.A. 1982. Adsorption of natural dissolved organic matter at the oxide/water interface. *Geochim.Cosmochim. Acta.* **46** (11), 2381-2393.

Davis, J.A., Gloor, R. 1981. Adsorption of dissolved organics in lake water by aluminum oxide. Effect of molecular weight. *Environ. Sci. Technol*. **15** (10), 1223-1229.

Deng, Y. 1996. Formation of iron(III) hydroxides from homogeneous solutions. *Water Res*. **31** (6), 1347-1354.

DiGiano, F.A., Zhang, W.D. 2005. Pipe section reactor to evaluate chlorine-wall reaction. *J. Am. Water Works Assoc.* **97** (1), 74-85.

Droste, R.L. 1997. *Physical-Chemical Treatment Processes. In*: *Theory and Practice of Water and Wastewater Treatment*. John Wiley & Sons, Inc., NY, USA.

Dyck, R., Sadiq, R., Rodriguez, M.J., Simard, S., Tardif, R. 2011. Trihalomethane exposures in indoor swimming pools: A level III fugacity model. *Water Res.* **45** (16), 5084-5098.

Edwards, M., Benjamin, M.M., Ryan, J.N. 1996. Role of organic matter acidity in sorption of natural organic matter (NOM) to oxide surfaces. *Colloid Surf. A* **107**. 297-307.

Edwards, M., McNeill, L.S. 2002. Effect of phosphate inhibitors on lead release from pipes. *J. Am. Water Works Assoc*. **94** (1), 79-90.

Eikebrokk, B., Vogt, R.D., Liltved, H. 2004. NOM increase in Northern European source waters: Discussion of possible causes and impacts on coagulation/contact filtration process. *Water Sci. Technol.*: *Water Supply* **4** (4), 47-54.

Eisnor, J.D., 2002. *Corrosion of Cast-Iron Water Distribution System Pipes*: *Impact of Secondary Disinfection*. MASc Dissertation, Dalhousie University, Canada.

Eisnor, J.D., Gagnon, G.A. 2004. Impact of secondary disinfectant on corrosion in a model water distribution system. *J. Water Supply Res. Technol.-AQUA* **53** (7), 441-452.

Elsner, M., Schwarzenbach, R.P., Haderlein, S.B. 2004. Reactivity of Fe(II)-bearing minerals toward reductive transformation of organic contaminants. *Environ. Sci. Technol*. **38** (3), 799- 807.

Fennelly, J.P., Roberts, A.L. 1998. Reaction of 1,1,1-trichloroethane with zero-valent metals and bimetallic reductants. *Environ. Sci. Technol*. **32**(13), 1980-1988.

Filius, J.D., Hiemstra, T., Van Riemsdijk, W.H. 1997. Adsorption of small weak organic acids on goethite: Modeling of mechanisms. *J. Colloid Interface Sci.* **195** (2), 368-380.

Fogelman, K.D., Walker, D.M., Margerum, D.W. 1989. Non-metal redox kinetics: Hypochlorite and hypochlorous acid reactions with sulfite. *Inorg. Chem.* **28** (6), 986-993.

Fokkink, L.G.J., de Keizer, A., Lyklema, J. 1987. Specific ion adsorption on oxides: Surface charge adjustment and proton stoichiometry. *J. Colloid Interface Sci.* **118** (2), 454-462.

Folkes, L.K., Candeias, L.P., Wardman, P. 1995. Kinetics and mechanisms of hypochlorous acid reactions. *Arch. Biochem. Biophys.* **323** (1), 120-126.

Frateur, I., Deslouis, C., Kiene, L., Levi, Y. Tribolle, B. 1999. Free chlorine consumption induced by cast iron corrosion in drinking water distribution systems. *Water Res.* **33** (8), 1781-1790.

Freundlich, H. 1926. *Colloid and Capillary Chemistry*. Methuen and Co., London, UK.

Fu, H., Quan, X. 2006. Complexes of fulvic acid on the surface of hematite, goethite, and akaganeite: FTIR observation. *Chemosphere* **63** (3), 403-410.

Gagnon, G.A., Baribeau, H., Rutledge, S.O., Dumancic, R., Oehmen, A., Chauret, C., Andrew, S. 2008. Disinfectant efficacy in distribution systems: A pilot-scale assessment. *J. Water Supply Res. Technol.-AQUA* **57** (7), 507-518.

Gagnon, G.A., Booth, S.D., Peldszus, S., Mutti, D., Smith, F., Huck, P.M. 1997. Carboxylic acids: Formation and removal in full-scale plants. *J. Amer. Water Work Assn*. **89** (8), 88-97.

Gagnon, G.A., O'Leary, K.C., Volk, C.J., Chauret, C., Stover, L., Andrews, R.C. 2004. Comparative analysis of chlorine dioxide, free chlorine and chloramines on bacterial water quality in model distribution systems. *J. Environ. Eng.* **130** (11), 1269-1279.

Genz, A., Baumgarten, B., Goernitz, M., Jekel, M. 2008. NOM removal by adsorption onto granular ferric hydroxide: Equilibrium, kinetics, filter and regeneration studies. *Water Res*. **42** (1-2), 238-248.

Giasuddin, A.B.M., Kanel, S.R., Choi, H. 2007. Adsorption of humic acid onto nanoscale zerovalent iron and its effect on arsenic removal. *Environ. Sci. Technol*. **41** (6), 2022-2027.

Gibert, O., Lefe`vre, B., Ferna´ndez, M., Bernat, X., Paraira, M., Pons, M. 2013. Fractionation and removal of dissolved organic carbon in a full-scale granular activated carbon filter used for drinking water production. *Water Res*. **47** (8), 2821-2829.

Gloor, R., Leidner, K., Wuhrmann, K., Fleishmann, T. 1981. Exclusion chromatography with carbon detection: A tool for further characterization of dissolved organic carbon. *Water Res*. **15** (4), 457-462.

Gonz´alez, A.G., Santana-Casiano, J.M., P´erez, N., Gonz´alez-D´avila, M. 2010. Oxidation of Fe(II) in natural waters at high nutrient concentrations. *Environ. Sci. Technol.* **44** (21), 8095-8101.

Gray, E.T., Taylor, R.W., Margerum, D.W. 1977. Kinetics and mechanisms of copper-catalyzed decomposition of hypochlorite and hypobromite -properties of a dimeric copper(III) hydroxide intermediate. *Inorg. Chem.* **16** (12), 3047-3055.

Gu, B., Schmitt, J. Chen, Z., Liang, L., McCarthy, J.F. 1994. Adsorption and desorption of natural organic matter on iron Oxide: Mechanisms and Models. *Environ. Sci. Technol*. **28** (1), 38-48.

Gu, B., Schmitt, J., Chen, Z., Liang, L., Mccarthy, J.F. 1995. Adsorption and desorption of different organic matter fractions on iron oxide. *Geochimica et Cosmochimica Acta* **59** (2), 219-229.

Guan, X.H., Li, D.L., Shang, C., Chen, G.H. 2006. Role of carboxylic and phenolic groups in NOM adsorption on minerals: A review. *Water Science & Technology*: *Water Supply* **6** (6), 155-164.

Gunnars, A., Blomqvist, S., Johansson, P., Andersson, C. 2002. Formation of Fe(III) oxyhydroxide colloids in freshwater and brackish seawater, with incorporation of phosphate and calcium. *Geochimica et Cosmochimica Acta* **66** (5), 745-758.

HACH. 2005. *DR 5000 Spectrophotometer Procedures Manual*. 2nd Ed., Loveland, CO, USA.

Halifax Water 2012. Water Quality [Online]. Available <http://www.halifax.ca/hrwc/WaterQuality.html>. (Accessed 04.07.02).

Hassan, K., Bower, K., Miller, C. 2006. Iron oxide enhanced chlorine decay and disinfection by-product formation. *J. Environ. Eng.* **132** (12), 1609-1616.

Hayes, M.H.B., MacCarthy, P., Malcolm, R.L., Swift, R.S., Ed. 1989. *Humic Substances II*: *In Search of Structure*. Wiley-Interscience, NY, USA.

Health Canada. 1995. *Guidelines for Canadian Drinking Water Quality -Hardness*. H48-10/1-49-1995-IN.

Health Canada. 2009. *Guidelines for Canadian Drinking Water Quality*: *Chlorine Guideline Technical Document*. Available at www.hc-sc.gc.ca/ewh-semt/pubs/water-eau/chlorine-chlore/index-eng.php (accessed 02.01.10).

Hines, W.W., Montgomery, D.C., Goldsman, D.M., Borror, C.M. 2003. *Probability and Statistics in Engineering*. 4th Ed., John Willey & Sons Inc., USA

Hochhauser, I.L. Taube, H. 1947. The direct and sensitized photochemically induced reaction of chlorine and oxalic acid. Comparison with the chemically induced reaction. *J. Am. Chem. Soc.* **69** (7), 1582-1589.

Hove, M., van Hille, R.P., Lewis, A.E. 2008. Mechanisms of formation of iron precipitates from ferrous solutions at high and low pH. *Chem. Eng. Sci*. **63** (6), 1626-1635.

Hozalski, R.M., Arnold, W.A., Chun, C., LaPara, T.M., Lee, J.Y., Pearson, C.R., Zhang, P. 2008. Degradation of halogenated disinfection byproducts in water distribution systems. *ACS Symposium Series*. **995**, 334-348.

Hsu, P.H. 1982. Crystallization of iron(III) phosphate at room emperature. *Soil Sci. Soc. Amer. J.* **46** (5), 928-932.

Hur, J., Schlautman, M.A. 2003. Molecular weight fractionation of humic substances by adsorption onto minerals. *J. Colloid Interface Sci.* **264** (2), 313-321.

Illés, E., Tombácz, E. 2004. The role of variable surface charge and surface complexation in the adsorption of humic acid on magnetite. *Colloids Surfaces A*: *Physicochem. Eng. Aspects* **230** (1-3), 99-109.

Jeon, C., Park, J.Y., Yoo, Y.J. 2001. Biosorption model for binary adsorption sites, *J. Microbiol. Biotechnol.* **11** (5), 781-787.

Johnson, J.D., Jensen, J.N. 1986. THM and TOX formation: Routes, rates, and precursors. *J. Am. Water Works Assoc.* **78** (4), 156-162.

Jones. D.A. 1992. *Principles and Prevention of Corrosion.* Macmillan Publishing Company, NY, USA.

Karanfil, T., Erdogan, I, Schlautman, M. 2005. The impact of filtrate turbidity on UV_{254} and $SUVA_{254}$ determinations. *J. Am. Water Works Assoc.* **97** (5), 125-136.

Kashinkunti, R.D., Metz, D.H., Hartman, D.J., DeMarco, J. 1999. How to reduce lead corrosion without increasing iron release in the distribution system. *Proc. AWWA Water Quality Technology Conference*. Tampa, FL, USA.

Kilduff, J.E., Karanfil, T., Chin, Y.P., Weber, W.J. 1996. Adsorption of natural organic plyelectrolytes by activated carbon: A size-exclusion chromatography study. *Environ. Sci. Technol*. **30** (4), 1336-1343.

Kim, Y.H., Carraway, E.R. 2000. Dechlorination of pentachlorophenol by zero valent iron and modified zero valent irons. *Environ. Sci. Technol*. **34** (10), 2014-2017.

King, D.W., Lounsbury, H.A., Millero, F.J. 1995. Rates and mechanism of Fe(II) oxidation at nanomolar total iron concentrations. *Environ. Sci. Techno*. **29** (3), 818-824.

Kirmeyer, G.J., Pierson, G., Clement, J., Sandvig, A., Snoeyink, V., Kriven, W., Camper, A. 2000. *Distribution System Water Quality Changes Following Implementation of Corrosion Control Strategies.* AWWA Research Foundation, Denver, CO, USA.

Klueh, K.G. 1988. Sequestration of iron in groundwater by polyphosphates. *J. Environ. Eng.-ASCE* **114** (5), 1192-1199.

Krasner, S.W., McGuire, M.J., Jacangelo, J.G., Patania, N.L., Reagan, K.M., Aieta, E.M. 1989. The occurrence of disinfection by-products in US drinking water. *J. Am. Water Works Assoc*. **81** (8), 41-53.

Kuch, A. 1984. Korrosion und Schutzchichtbildung Durch Leitungswasser. *Gwf-Das Gas-und Wasserfach* **81**, 611–615, 628–633.

Langmuir, I. 1916. The adsorption of gases on plane surface of glass, mica and platinum, *J. Am. Chem. Soc.* **40** (9), 1361-1368.

Larson, T.E. 1957. Evaluation of the use of polyphosphates in the water industry. *J. Am. Water Works Assoc*. **49** (12), 1581-1586.

Lasheen, M.R., Sharaby, C.M, El-Kholy,N.G., Elsherif, I.Y., El-Wakeel, S.T. 2008. Factors influencing lead and iron release from some Egyptian drinking water pipes. *J. Hazard. Mater.* **160** (2-3), 675-680.

LeChevallier, M.W., Lowry, C.D., Lee, R.G., Gibbon, D.L., 1993. Examining the relationship between iron corrosion and the disinfection of biofilm bacteria. *J. Am. Water Works Assoc.* **85** (7), 111-123.

LeChevallier, M.W., Lowry, C.D., Lee., R.G. 1990. Disinfecting biofilms in a model distribution system. *J. Am. Water Works Assoc*. **82** (7), 87-99.

Lee, J.Y., Pearson, C.R., Hozalski, R.M., Arnold, W.A. 2008. Degradation of trichloronitromethane by iron water main corrosion products. *Water Res*. **42**(8-9), 2043-2050.

Leenheer, J.A., Croue, J.-P. 2003. Characterizing dissolved aquatic organic matter. *Environ. Sci. Technol.* **37** (1), 18A-26A.

Legay, C., Rodriguez, M.J., Sadiq, R., Sérodes, J.B., Levallois, P., Proulx, F. 2011. Spatial variations of human health risk associated with exposure to chlorination by-products occurring in drinking water. *J. Environ. Manage*. **92** (3), 892-901.

Li, X., Zhao, H. 2006. Development of a model for predicting trihalomethanes propagation in water distribution systems. *Chemosphere* **62**(6), 1028-1032.

Liang, L., McNabb, J.A., Paulk, J.M., Guy, B., McCarthy, J.F. 1993. Kinetics of Fe(II) oxygenation at low partial pressure of oxygen in the presence of natural organic matter. *Environ. Sci. Technol*. **27** (9), 1864-1870.

Liang, L., Singer, P.C. 2003. Factors influencing the formation and relative distribution of haloacetic acids and trihalomethanes in drinking water. *Environ. Sci. Technol.* **37** (13), 2920-2928.

Lin, J., Ellaway, M., Adrien, R. 2001. Study of corrosion material accumulated on the inner wall of steel water pipe. *Corros. Sci*. **43** (11), 2065-2081.

Liu, S., Zhu, Z., Qiu, Y., Zhao, J. 2011. Effect of ferric and bromide ions on the formation and speciation of disinfection byproducts during chlorination. *J. Environ. Sci.* **23** (5), 765-772.

Lyklema, J. 1991. Electrified interfaces in aqueous dispersions of solids. *Pure Appl. Chem*. **63** (3), 895-906.

Lytle, D.A. 2005. *The Effect of Water Chemistry on the Propertied of Iron Particles.* PhD Dissertation, University of Illinois, USA.

Lytle, D.A., Magnuson, M.L., Snoeyink, V.L. 2004. Effect of oxidants on the properties of Fe(III) particles and suspensions formed from the oxidation of Fe(II). *J. Am. Water Works Assoc*. **96** (8), 112-124.

Lytle, D.A., Snoeyink, V.L. 2002. Effect of ortho-and polyphosphate on the properties of iron particles and suspensions. *J. Am. Water Works Assoc*. **94** (10), 87-99.

Maddison, L.A., Gagnon, G.A., Eisnor, J.D. 2001. Corrosion control strategies for the Halifax regional distribution system. *Can. J. Civ. Eng*. **28** (2), 305-313.

Mao, Y., Pham, A.N., Rose, A.L., Waite, T.D. 2011. Influence of phosphate on the oxidation kinetics of nanomolar Fe(II) in aqueous solution at circumneutral pH. *Geochimica et Cosmochimica Acta* **75** (16), 4601-4610.

Marhaba, T.F., Van, D. 2000. The variation of mass and disinfection by-product formation potential of dissolved organic matter fractions along a conventional surface water treatment plant. *J. Hazard. Mater*. **74**(3), 133-147.

Matheson, L.J., Tratnyek, P.G. 1994. Reductive dehalogenation of chlorinated methanes by iron metal. *Environ. Sci. Technol*. **28** (12), 2045-2053.

McBride, M.B., Kung, K.-H. 1991. Adsorption of phenol and substituted phenols by iron oxides. *Environ. Toxicol. Chem*. **10** (4), 441-448.

McDonald, B.C. 2007. *Factors Influencing Copper Corrosion and THM Formation in Low Alkalinity Drinking Water*. M.A.Sc. Dissertation, Dalhousie University, Canada.

McKnight, D.M., Bencala, K.E., Zellweger, G.W., Aiken, G.R., Feder, G.L., Thorn, K.A. 1992. Sorption of dissolved organic carbon by hydrous aluminum and iron oxides

occurring at the confluence of Deer Creek with the Snake River, Summit County, Colorado. *Environ. Sci. Technol.* **26** (7), 1388-1396.

McNeill, L.S., Edwards, M. 2000. Phosphate inhibitors and red water in stagnant iron pipes. *J. Environ. Eng*. **126** (12), 1096-1102.

McNeill, L.S., Edwards, M. 2001. Iron pipe corrosion in distribution systems. *J. Am. Water Works Assoc*. **93** (7), 88-100.

Miller, J.W., Uden, P.C. 1983. Characterization of nonvolatile aqueous chlorination products of humic substances. *Environ Sci Technol.* **17** (3), 150-157.

Millero, F.J., Yao, W.S., Aicher, J. 1995. The speciation of Fe(II) and Fe(III) in natural waters. *Mar. Chem.* **50** (1-4), 21-39.

Miot, J., Benzerara, K., Morin, G., Bernard, S., Beyssac, O., Larquet, E., Kappler, A., Guyot, F. 2009. Transformation of vivianite by anaerobic nitrate-reducing iron-oxidizing bacteria. *Geobiology* **7** (3), 373-384.

Mitra, A.K., Matthews, M.L., 1985. Effects of pH and phosphate on the oxidation of iron in aqueous solution. *Int. J. Pharm*. **23** (2), 185-193.

Montgomery, D.C. 2009. *Design and Analysis of Experiments*. 7th Ed., John Wiley & Sons Inc., NY, USA.

Morgan, B., Lahav, O. 2007. The effect of pH on the kinetics of spontaneous Fe(II) oxidation by O_2 in aqueous solution -basic principles and a simple heuristic description. *Chemosphere* **68** (11), 2080-2084.

Morgan, J.J., Stumm, W. 1964. The role of multivalent metal oxides in limnological transformations as exemplied by iron and manganese. *Proc. Second Intern. Water Pollution Research Conf.*, pp 103-131, Pergamon Press, Tokyo.

Morris, J.C., Baum, B. 1977. Precursors and mechanisms of haloform formation in the chlorination of water supplies. In: Jolley RL, editor. *Water Chlorination: Environmental Impact and Health Effects*. vol. 2. Ann Arbor, MI: Ann.

Morris, R.D., Audet, A., Angelillo, I.O., Chalmers, T.C., Mosteller, F. 1992. Chlorination, chlorination by-products, and cancer: A meta-analysis. *Am. J. Public Health* **82** (7), 955-963.

Namjesnik-Dejanovic, K., Maurice, P.A., Aiken, G.R. Cabaniss, S., Chin, Y-P., Pullin, M.J. 2000. Adsorption and fractionation of a muck fulvic acid on kaolinite and goethite at pH 3.7, 6, and 8. *Soil Sci.* **165** (7), 545-559.

O'Connor, T.L., O'Connor, J.T. 2000. Water quality deterioration in distribution systems. *Water Eng. Manage.* **147** (10), 34-38.

Parfitt, R.L., Atkinson, R.J., Smart, R.St.C. 1975. The mechanisms of phosphate fixation by iron oxides. *Soil Sci. Soc. Amer. Proc*. **39** (5), 837-841.

Pearson, C.R., Hozalski, R.M., Arnold, W.A. 2005. Degradation of chloropicrin in the presence of Fe(0*). Environ. Toxicol. Chem.* **24** (12), 48-53.

Pecher, K., Haderlein, S.B., Chwarzenbach, R.P. 2002. Reduction of polyhalogenated methanes by surface-bound Fe(II) in aqueous suspensions of iron oxides. *Environ. Sci. Technol*. **36** (8), 1734-1741.

Pédrot, M., Le Boudec, A., Davranche, M., Dia, A., Henin, O. 2011. How does organic matter constrain the nature, size and availability of Fe nanoparticles for biological reduction. *J. Colloid Interface Sci.* **359** (1), 75-85.

Peljhan, S., Kokalj, A. 2009. Adsorption of chlorine on Cu(111): A density-functional theory study. *J. Phys. Chem. C*. **113** (32), 14363-14376.

Pourmoghaddas, H., Stevens, A.A., Kinman, R.N., Dressman, R.C., Moore, L.A., Ireland, J.C. 1993. Effect of bromide ion on formation of HAAs during chlorination *J. Am. Water Works Assoc*. **85** (1), 82-87.

Pracht, J., Boenigk, J., Isenbeck-Schroter, M., Keppeler, F., Scholer, H.F. 2001. Abiotic Fe(III) induced mineralization of phenolic substances. *Chemosphere* **44** (4), 613-619.

Rahman, M.S. 2007. The Prospect of Natural Additives in Enhanced Oil Recovery and Water Purification Operation. MASc Dissertation, Dalhousie University, Canada.

Rahman, M.S., Islam, M.R. 2009a. Adsorption of Cd(II) ions from synthetic wastewater using Maple sawdust. Energy Sources Part A-recovery Utilization and Environmental Effects. 32 (3), 222-231.

Rahman, M.S., Islam, M.R. 2009b. Effects of pH on isotherms modeling for Cu(II) ions adsorption using maple wood sawdust. *Chem. Eng.* **149** (1-3), 273-280.

Rahman, M.S. Whalen, M., Gagnon, G.A. 2013. Adsorption of dissolved organic matter (DOM) onto the synthetic iron pipe corrosion scales (goethite and magnetite): Effect of pH. *Chem. Eng. J.* **234**, 149-157.

Rahman, M.S., Gagnon, G.A. 2013. Bench scale evaluation of Fe(II) ions on haloacetic acids (HAAs) formation in synthetic water. *J. Water Supply Res. Technol.-AQUA* **62** (3), 155-168.

Rahman, M.S., Gagnon, G.A. 2014a. Iron corrosion as a factor contributing to haloacetic acids formation in the distribution system: Experimental assessment and model development. *J. Water Supply Res. Technol. –AQUA* (in press, doi:10.2166/aqua.2014.071).

Rahman, M.S., Gagnon, G.A. 2014b. Bench-scale evaluation of ferrous iron oxidation kinetics in drinking water: Effect of corrosion control and dissolved organic matter. *J Environ. Sci. Health A* **49** (1), 1-9.

Rahman, M.S., Gagnon, G.A. 2014c. Bench-scale evaluation of drinking water treatment parameters on iron particles and water quality. *Water Res.* **48**, 137-147.

Rajagopal, V.K., Burris, D.R. 1999. Reduction of 1,2-dibromoethane in the presence of zero-valent iron. *Environ. Toxicol. Chem.* **18** (8), 1779-1782.

Reckhow, D.A., Singer, P.C., Malcolm, R.L. 1990. Chlorination of humic materials: Byproduct formation and chemical interpretations. *Environ. Sci. Technol*. **24** (11), 1655-1664.

Rietra, R.P.J.J., Hiemstra, T., van Riemsdijk, W.H. 2000. Electrolyte anion affinity and its effect on oxyanion adsorption on goethite. *J. Colloid Interface Sci.* **229** (1), 199-206.

Rodriguez, M.J., Se´rodes, J.B. 2001. Spatial and temporal evolution of trihalomethane in three distribution systems. *Water Res*. **35** (6), 1572-1586.

Rodriguez, M.J., Se´rodes, J.B., Levallois, P. 2004. Behavior of trihalomethanes and haloacetic acids in a drinking water distribution system. *Water Res*. **38** (20), 4367-4382.

Rodriguez, M.J., Vinette, Y., Serodes, J.B., Bouchard, C. 2003. Trihalomethanes in drinking water of Greater Quebec Region (Canada): Occurrence, variations and modelling. *Environ. Monit. Assess*. **89** (1), 69-93.

Rook J. 1974. Formation of haloforms during chlorination of natural waters. *J. Soc. Water Treat. Exam.* **23** (2), 234-243.

Rose, A.L., Waite, T.D. 2002. Kinetic model for Fe(II) oxidation in seawater in the absence and presence of natural organic matter. *Environ. Sci. Technol*. **36** (3), 433-444.

Rossman, L.A., Brown, R.A., Singer, P.C. Nuckols, J.R. 2001. DBP formation kinetics in a simulated distribution system. *Water Res*. **35** (14), 3483-3489.

Sadiq, R. Rodriguez, M.J. 2004b. Disinfection by-products (DBPs) in drinking water and predictive models for their occurrence: A review. *Sci. Total Envir.* **321** (1-3) 21-46.

Sadiq, R., Husain, T., Kar, S. 2002. Chloroform associated health risk assessment using bootstrapping: A case study for limited drinking water samples. *Water Air Soil Pollut*. **138** (1), 123-140.

Sadiq, R., Kleiner, Y., Rajani, B. 2010. Modelling the potential for water quality failures in distribution networks: framework (I). *J. Water Supply Res. Technol.-AQUA* **59** (4), 255-276.

Sadiq, R., Rodriguez, M.J. 2004a. Fuzzy synthetic evaluation of disinfection by-products -a risk-based indexing system. *J. Environ. Manage.* **73** (1), 1-13.

Sarin, P., Snoeyink, V.L., Bebee, J., Jim, K.K., Beckett, M.A., Kriven, W.M., Clement, J.A. 2004a. Iron release from corroded iron pipes in drinking water distribution systems: Effect of dissolved oxygen. *Water Res.* **38**(5), 1259-1269.

Sarin, P., Snoeyink, V.L., Bebee, M.A., Kriven, W.M., Clement, J.A. 2001. Physicochemical characteristics of corrosion scales in old iron pipes. *Water Res.* **35** (12), 2961-2969.

Sarin, P., Snoeyink, V.L., Lytle, D.A., Kriven, W.M. 2004b. Iron corrosion scales: Model for scale growth, iron release, and colored water formation. *J. Environ. Eng*. **130** (4), 364-373.

Scherer, M.M., Balko, B.A., Tratnyek, P.G. 1998. The role of oxides in reduction reactions at the metal-water interface. *Mineral-Water Interfacial Reaction*. Chapter 15, 301-322. American Chemical Society, USA.

Schlautman, M.A., Morgan, J.J. 1994. Adsorption of aquatic humic substances on colloidal-size aluminum oxide particles: Influence of solution chemistry. *Geochim. Cosmochim. Acta* **58** (20), 4293-4303.

Schock, M.R. 1999. Internal corrosion and deposition control. Chapter 17 In Ed. Letterman, *Water Quality and Treatment*. 5th Ed. McGraw-Hill Inc., NY, USA.

Schwertmann, U., Cornell, R.M. 2000. *Iron Oxides in the Laboratory* : *Preparation and Characterization*. 2nd Ed., John Wiley & Sons, Inc., NY, USA.

Sellers, K., Mackay, C., Bergeson, L.L., .Clough, S.R., Hoyt, M., Chen, J., Henry, K., Hamblen, J. 2009. *Nanotechnology and the Environment*. CRC Press, Florida, USA.

Serikov, L.V., Tropina, E.A., Shiyan, L.N., Frimmel, F.H., Metreveli, G., Delay, M. 2009. Iron oxidation in different types of groundwater of western Siberia. *J. Soils Sediments* **9** (2), 103-110.

Sharma, S.K., Kappelhof, J., Groenendijk, M. Schippers, J.C. 2001. Comparison of physicochemical iron removal mechanisms in filters. *J. Water Supply Res. Technol.-AQUA* **50** (4), 187-198.

Shen, Y.H. 1999. Sorption of natural dissolved organic matter on soil. *Chemosphere* **38** (7), 1505-1515.

Shi, H., Ding, J., Timmons, T., Adams, C. 2012. pH effects on the adsorption of saxitoxin by powdered activated carbon. *Harmful Algae*. **19**, 61-67.

Shimazu, H., Kouchi, M., Sugita, Y., Yonekura, Y., Kumano, H., Hashiwata, K., Hirota, T., Ozaki, N., Fukushima, T. 2005. Developing a model for disinfection by-products based on multiple regression analysis in a water distribution system. *J. Water Supply Research & Tech.-AQUA* **54** (4), 225-237.

Shipley, J.W., McHaffic, I.R., Clare, N.D. 1925. Corrosion of iron in absence of oxygen. *Ind. Eng. Chem*. **17** (4), 381-385.

Shorney, H.L. 1998. *Disinfection By-product Precursor Removal by Enhanced Softening and Coagulation*. PhD Dissertation, Unievrsity of Kansas, USA.

Shwertmann, U., Cornell, R.M. 2000. *Iron Oxides in the Laboratory*: *Preparation and Characterization.* 2nd Ed., John Wiley & Sons, Inc., NY, USA.

Siantar, D.P., Schreier, C.G., Chou, C.S., Reinhard, M. 1996. Treatment of 1,2-dibromo-3-chloropropane and nitrate contaminated water with zero-valent iron or hydrogen/palladium catalysts. *Water Res*. **30** (10), 2315-2322.

Singer, P.C., Obolensky, A., Greiner, A. 1995. DBPs in chlorinated North Carolina drinking waters. *J. Am. Water Works Assoc*. **87** (10), 83-92.

Speight, V.L., Singer, P.C. 2005. Association between residual chlorine and reduction in haloacetic acid concentrations in distribution systems. *J. Am. Water Works Assoc.* **97** (2), 82-91.

Sposito, G. 1984. *The Surface Chemistry of Soils*. Oxford University Press, NY, USA.

Stevenson, F.J. 1994. *Humus Chemistry*: *Genesis, Composition, Reactions*. 2nd Ed., John Wiley & Sons, Inc., NY, USA.

Stumm, W. 1990. *Aquatic Chemical Kinetics: Reaction Rates of Processes in Natural Waters*. 1st Ed., John Wiley & Sons, Inc., NY, USA.

Stumm, W. 1992. *Chemistry of the Solid-Water Interface*. John Wiley & Sons, Inc., NY, USA.

Stumm, W., Lee, G.F. 1961. Oxygenation of ferrous iron. *Ind. Eng. Chem.* **53** (2), 143-146.

Stumm, W., Sulzberger, B. 1992. The cycling of iron in natural environments: Considerations based on laboratory studies of heterogeneous redox processes. *Geochimica et Cosmochimica Acta* **56** (8), 3233-3257.

Summers R.S., Robert P.V. 1988. Activated carbon adsorption of humic substances. *J. Colloid Interface Sci.* **122** (2), 367-381.

Summers, R.S., Hooper, S.M., Shukairy, H.M., Solarik, G., Owen, D.C. 1996. Assessing DBP yield: Uniform formation conditions. *J. Am. Water Works Assoc.* **88** (6), 80-93.

Sun, Z., Su, F., Forsling, W., Samskog, P. 1998. Surface characteristics of magnetite in aqueous suspension. *J. Colloid Interface Sci*. **197** (1), 151-159.

Sung, W., Morgan, J. 1980. Kinetics and products of ferrous iron oxygenation in aqueous systems. *Environ. Sci. Technol.* **14** (5), 561-568.

Sung, W., Reiley-Matthews, B., O'Day, D.K., Horrigan, K. 2000. Modeling DBP formation. *J. Am. Water Works Assoc.* **92** (5), 53-63.

Świetlik, J., Raczyk-Stanisławiak, U., Biłozor, S., Ilecki, W., Nawrocki, J. 2002. Effect of oxidation with chlorine dioxide on the adsorption of natural organic matter on granular activated carbon. *Pol. J. Environ. Stud.* **11**(4), 435-439.

Tam, Y.S., Elefsiniotis, P. 2009. Corrosion control in water supply systems: Effects of pH, alkalinity, and orthophosphate on lead and copper leaching from brass plumbing. *J. Environ. Sci. Health A Tox. Hazard. Subs. Environ. Eng.* **44** (12), 1251-1260.

Tamura, H., Goto, K., Nagayama, M. 1976. Effect of anions on the oxygenation of ferrous iron in natural solutions. *J. Inorg. Nucl. Chem*. **38**(1), 113-117.

Teker, M., İmamoğlu, M. 1999. Adsorption of copper and cadmium ions by activated carbon from rice hulls. *Turk. J. Chem*. **23** (2), 185-191.

Theis, T.L., Singer, P.C. 1974. Complexation of iron(II) by organic matter and its effect on iron(II) oxygenation. *Environ. Sci. Technol.* **8** (6), 569-573.

Thurman, E.M., Malcolm, R.L. 1983. Structural study of humic substances: New approaches and methods. *Terrestrial Humic Materials*. R.F. Christman and E.T. Gjessing, (Ed.), Ann Arbor Sci., Michigan.

Tipping, E. 1981. Adsorption by goethite (α-FeOOH) of humic substances from three different lakes. *Chem. Geol.* **33** (1-4), 81-89.

Tombacz, E., Libor, Z., Illes, E., Majzik, A., Klumpp, E. 2004. The role of reactive surface sites and complexation by humic acids in the interaction of clay mineral and iron oxide particles. *Org. Geochem*. **35** (3), 257-267.

Truong, G.L., Laat, J.D., Legube, B. 2004. Effects of chloride and sulfate on the rate of oxidation of ferrous ion by H_2O_2. *Water Res.* **38** (9), 2383-2393.

Tuovinen, O.H., Mair, D.M., Banovic, J. 1984. Chlorine demand and trihalomethane formation by tubercles from cast iron water mains. *Environ. Technol. Lett.* **5** (1-11), 97-108.

USEPA. 1995a. Determination of haloacetic acids and dalapon in drinking water by liquid-liquid extraction, derivatization and gas chromatography with electron capture detection. Method 552.2. US Environmental Protection Agency, Cincinnati, OH, USA.

USEPA. 1995b. Determination of chlorination disinfection byproducts, chlorinated solvents, and halogenated pesticides/herbicides in drinking water by liquid-liquid extraction and gas chromatography with electron-capture detection. Method 551.1. US Environmental Protection Agency, Cincinnati, OH, USA.

USEPA. 2006. United States Environmental Protection Agency. 40 CFR Parts 9, 141, and 142. National primary drinking water regulations: Stage 2 Disinfectants and disinfection byproducts rule; Final rule. *Fed. Regist.* (Part II) **71**, 388-493.

Uyak, V., Ozdemir, K., Toroz, I. 2007. Multiple linear regression modeling of disinfection by-products formation in Istanbul drinking water reservoirs. *Sci. Total Envir*. **378** (3), 269-280.

Valencia, S., Marín, J., Velásquez, J., Restrepo, G., Frimmel, F.H. 2012. Study of pH effects on the evolution of properties of brown-water natural organic matter as

revealed by size-exclusion chromatography during photocatalytic degradation. *Water Res*. **46** (4), 1198-1206.

Valentine, R.L., Vikesland, P.J., Angerman, B.D., Hackett, S.A., Shoup, M., Slattenow, S. 2000. *The Role of the Pipe-Water Interface in DBP Formation and Disinfectant Loss*. AWWARF and AWWA, Denver, CO, USA.

Velten, S., Knappe, D.R.U., Traber, J., Kaiser, H.P., Gunten, U., Boller, M., Meylan, S. 2011. Characterization of natural organic matter adsorption in granular activated carbon adsorbers. *Water Res*. **45** (13), 3951-3959.

Vik, E.A., Ryder, R.A., Wanger, I., Ferguson, J.F. 1996. Mitigation of Corrosion effects. In *Internal Corrosion of Water Distribution Systems*. AWWARF and DVGW, Denver, USA.

Vikesland, P.J., Ozekin, K., Valentine, R.L. 1998 Effect of natural organic matter on monochloramine decomposition: Pathway elucidation through the use of mass and redox balances. *Environ. Sci. Technol*. **32** (10), 1409-1416.

Volk, C., Dundore, E., Schiermann, J., Lechevallier, M. 2000. Practical evaluation of iron corrosion control in drinking water distribution system. *Water Res.* **34** (6), 1967-1974.

Wallace, B., Purcell, M., Furlong, J. 2002. Total organic carbon analysis as a precursor to disinfection by-product in portable water: Oxidation technique considerations. *J. Environ. Monit*. **4** (1), 35-42.

Walpersdorf, E., Heiberg, L., Kjærgaard, C., Koch, C.B., O'Connell, D., Jensen, H.S., Hansen, H.C.B. 2012. Does vivianite ($FeII_3(PO_4)_2$. $8H_2O$) control phosphate solubility in anoxic soils? University of Copenhagen, Denmark. <www.cost869.alterra.nl/Spain/Hansen.pdf> (access on 12.06.12).

Wang, H., Hu, C., Hu, X., Yang, M., Qu, J. 2012. Effects of disinfectant and biofilm on the corrosion of cast iron pipes in a reclaimed water distribution system. *Water Res.* **6** (4), 1070-1078.

Wang, L., Chin, Y.-P., Traina, S.J. 1997. Adsorption of (poly)maleic acid and an aquatic fulvic acid by goethite. *Geochimica et Cosmochimica Acta* **61** (24), 5313-5324.

Wang, X.M., Waite T.D. 2010. Iron speciation and iron species transformation in activated sludge membrane bioreactors. *Water Res.* **44** (11), 3511-3521.

Weiss, J. 1935. Elektronenübergangsprozesse im mechanismus von oxydations-undReduktionsreaktionen in Lösungen. *Naturwissenschaften* **23** (4), 64-69.

White, G.C. 1992. *Handbook of Chlorination and Alternative Disinfectants*. Van Nostrand Reinhold. NY, USA.

WHO. 2008. *Guidelines for Drinking Water Quality*. 3rd Ed., Geneva, Switzerland.

Williams, D.T., LeBel, G.L., M.Benoit, F. 1997. Disinfection byproducts in Canadian drinking water. *Chemosphere* **34** (2), 299-316.

Wolthoorn, A., Temminghoff, E.J.M., Weng, L., van Riemsdijk, W.H. 2004. Colloid formation in groundwater: effect of phosphate, manganese, silicate and dissolved organic matter on the dynamic heterogeneous oxidation of ferrous iron. *Appl. Geochem.* **19** (4), 611-622.

Xie, Y.F. 2003. *Disinfection Byproducts in Drinking Water: Formation, Analysis, and Control*. CRC Press, USA.

Yang, X., Shang, C. 2004. Chlorination byproduct formation in the presence of humic acid, model nitrogenous organic compounds, ammonia, and bromide. *Environ. Sci. Technol*. **38** (19), 4995-5001.

Ye, B., Wang, W., Yang, L., Wei, J., E, X. 2009. Factors influencing disinfection by-products formation in drinking water of six cities in China. *J. Hazard. Mater*. **171** (1-3), 147-152.

Zhang, H., Andrews, S.A. 2012. Effects of phosphate-based corrosion inhibitors on the kinetics of chlorine degradation and haloacetic acid formation in contact with three metal materials. *Can. J. Civ. Eng*. **39** (1), 44-54.

Zhang, L., Arnold, W.A., Hozalski, R.M. 2004. Kinetics of haloacetic acid reactions with Fe(0). *Environ. Sci. Technol.* **38** (24), 6881-6889.

Zhang, X., Echigo, S., Minear, R.A., Plewa, M.J. 2000. Characterization and comparison of disinfection by-products of four major disinfectants. *Natural Organic Matter and Disinfection By-products*: *Characterization and Control in Drinking Water.* Ed Barrett S.E., Krasner S.W., Amy G.L. 299-314, American Chemical Society, Washington DC, USA.

Zhang, Y., Li P., Zhou, Y., Han, G., Li G., Xu, B., Jiang, T. 2012. Adsorption of lignite humic acid onto magnetite particle surface. *J. Cent. South Univ*. **19** (7), 1967-1972.

Zhang, Y., Martinez, D., Collins, C., Graham, N., Templeton, M.R., Huang, J., Nieuwenhuijsen, M. 2011. Modelling of haloacetic acid concentrations in a United Kingdom drinking water system. *J. Water Supply Research & Tech.-AQUA* **60** (5), 275-285.

Zhou, Q., Maurice, P.A., Cabaniss, S.E. 2001. Size fractionation upon adsorption of fulvic acid on goethite: Equilibrium and kinetic studies. *Geochim. Cosmochim. Acta* **65** (5), 803-812.

Zou, H., Yang, S., Xu, X., Xu, O. 1997. Formation of POX and NPOX with chlorination of fulvic acids in water: Empirical models. *Water Res*. **31** (6), 1536-1541.

APPENDIX A. Chapter 4 Raw data and supplementary information

Table A1. Coded and level of variables chosen for this factorial experiments.

Factors	Symbol	Coded variable levels	
		Low (-1)	High (+1)
pH value	A	6.50	8.50
DOM dosage (mg-C/L)	B	0 mg/L	2.85 mg/L
Phosphate dosage (mg PO_4/L)	C	0 mg/L	1.5 mg/L
Chlorine dosage (mg/L)	D	0 mg/L	2.2 mg/L

Table A2. Model matrixfor the 2^4 factorial design approach.

Exp. No.	Treatment combination	(A) pH	(B) HA	(C) PO_4	(D) Chlorine
1	-	-	-	-	-
2	A	+	-	-	-
3	B	-	+	-	-
4	AB	+	+	-	-
5	C	-	-	+	-
6	AC	+	-	+	-
7	BC	-	+	+	-
8	ABC	+	+	+	-
9	D	-	-	-	+
10	AD	+	-	-	+
11	BD	-	+	-	+
12	ABD	+	+	-	+
13	CD	-	-	+	+
14	ACD	+	-	+	+
15	BCD	-	+	+	+
16	ABCD	+	+	+	+

Table A3. Analysis of variance (ANOVA) test for the rate constants in ferrous iron oxidation process following 2^4 full factorial design approach.

Source	Sum Square	Degree of Freedom	Mean Square	*F*-value (calc)	Remark
Principal					
A. pH value	0.000659	1	0.000659	18.83	Significant
B. DOM dosage	0.000003	1	0.000003	0.08	Insignificant
C. PO_4 dosage	0.000353	1	0.000353	10.07	Significant
D. Chlorine dosage	0.000081	1	0.000081	2.33	Insignificant
Two way interactive					
A*B	0.000029	1	0.000029	0.83	Insignificant
A*C	0.000143	1	0.000143	4.10	Insignificant
A*D	0.000051	1	0.000051	1.45	Insignificant
B*C	0.000054	1	0.000054	1.55	Insignificant
B*D	0.000000	1	0.000000	0.00	Insignificant
C*D	0.000005	1	0.000005	0.14	Insignificant
Error (higher)	0.000175	5	0.0000080		
Total		15			

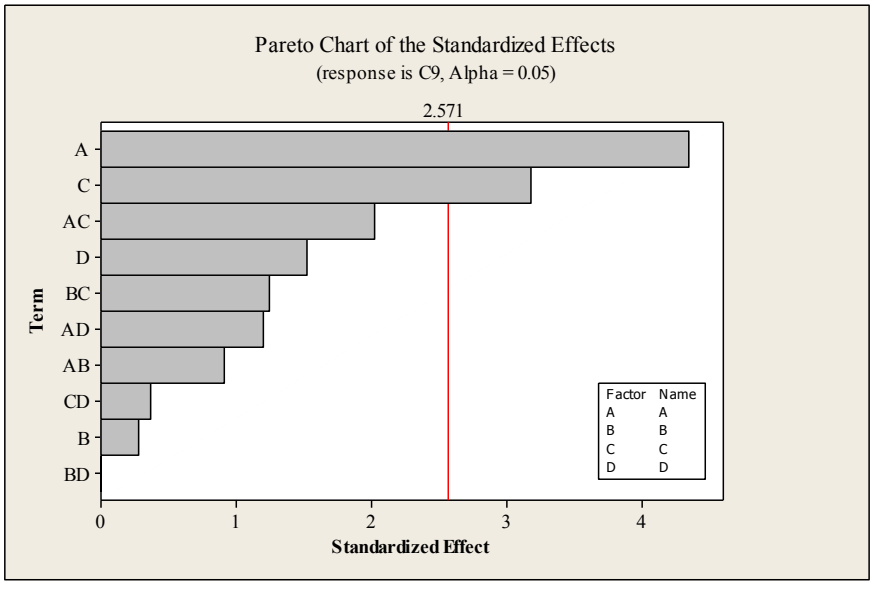

Figure. A1. Pareto chart of the standardized effects

Validation for factorial design approach:

One of the main objectives of the experimental design is to obtain mathematical modeling that directly relates the various factors with the statistically significant variables and their interactions. Based on *F*-test (ANOVA) and student's *t*-test, a simple linear mathematical model using the relevant variables describing the experimental response was constructed as follows:

$$\text{Rate constant } (k)_{\text{predicted}} = 0.01399 + (0.00642) * (\text{Fe}^{2+}\text{ions}) - (0.00469) * (\text{pH})$$

The validation of the mathematical model was performed using a normal probability plot of the residual values, defined as the difference between the predicted values according to the equation mentioned above and the observed (experimental) values for each response factor. The values of the calculated residuals for the response factor were plotted in a normal probability plot shown in following Figure. It was observed that the all data points for the response factors lied close to a straight line and within the 95% confidence intervals line with mean value near to zero. Since the residuals lied approximately along a straight line, we did not suspect any severe non-normality in the data. Therefore, it could be concluded agreeing to the above observations that there was a good agreement between the experimental values and the simple mathematical model developed and the observed differences.

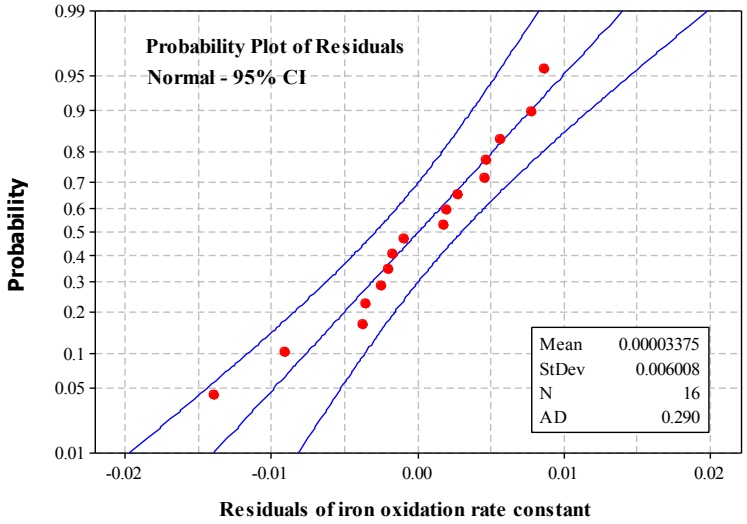

Figure A2. Normal probability plot of the residuals at 95% confidence interval for the response factor *k* (rate constants for Fe^{2+} ions oxidation).

Table A4. The effect of different variables (i.e. pH, DOM, phosphate and chlorine dosages) with two (02) levels (low and high) on the changes of rate constant (*k*) of Fe(II) ions oxidation process in $NaHCO_3$ buffered synthetic water ($[Fe(II)]_o \approx 3$ mg/L, 21 ± 1 °C).

Effect of pH values		Effect of DOM dosages		Effect of PO_4 dosages		Effect of chlorine dosages	
Low	High	Low	High	Low	High	Low	High
0.0085	0.0337	0.0085	0.0097	0.0085	0.0046	0.0085	0.0087
0.0097	0.0160	0.0337	0.0160	0.0337	0.0018	0.0337	0.0329
0.0046	0.0018	0.0046	0.0056	0.0097	0.0056	0.0097	0.0102
0.0056	0.0140	0.0018	0.0140	0.0160	0.0140	0.0160	0.0298
0.0087	0.0329	0.0087	0.0102	0.0087	0.0048	0.0046	0.0048
0.0102	0.0298	0.0329	0.0298	0.0329	0.0203	0.0018	0.0203
0.0048	0.0203	0.0048	0.0085	0.0102	0.0085	0.0056	0.0085
0.0085	0.0148	0.0203	0.0148	0.0298	0.0148	0.0140	0.0148
Average rate constants (k)							
0.0076	0.0204	0.0144	0.0136	0.0187	0.0093	0.0117	0.0163

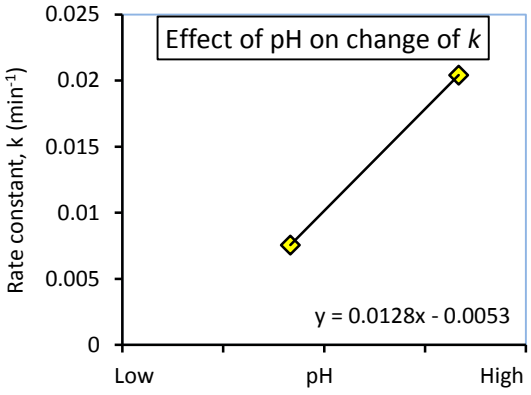

(a). For changing pH value from a lower to a higher level, Fe(II) ions oxidation rate (k) increased significantly (α = 0.05) having a positive slope of 0.0128.

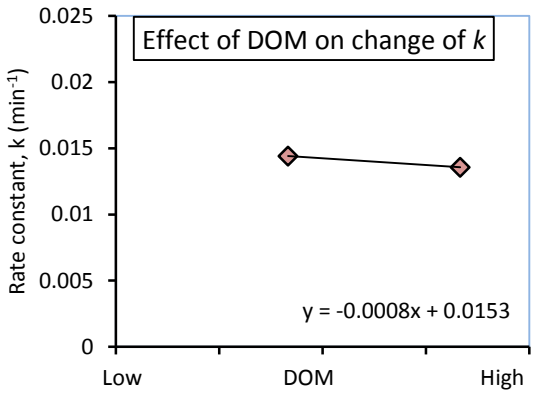

(b). For changing DOM dosage from a lower to a higher level, Fe(II) ions oxidation rate (k) does not change significantly having a slope < 0.001.

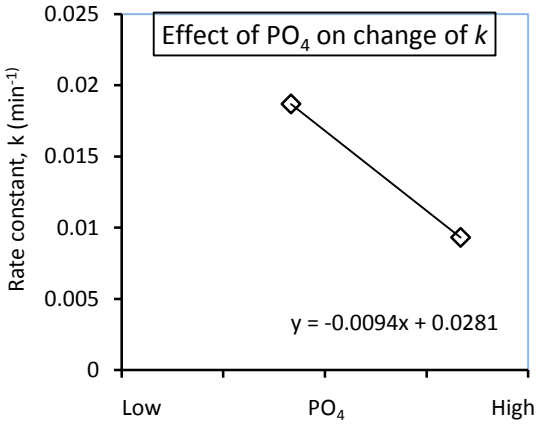

(c). For changing PO4 dosage from a lower to a higher level, Fe(II) ions oxidation rate (k) decreased significantly (α = 0.05) having a negative slope of 0.0094.

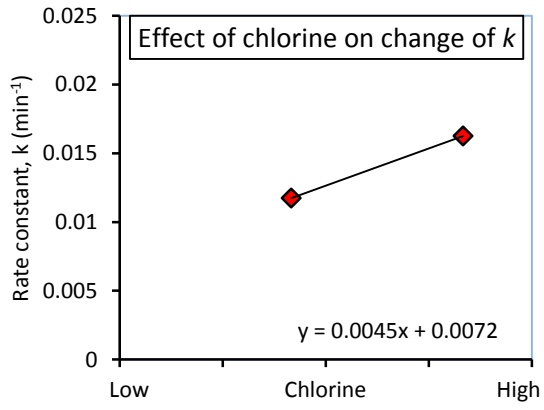

(d). For changing chlorine dosage from a lower to a higher level, Fe(II) ions oxidation rate (k) increased with a positive slope of 0.0045.

Figure A3. Plots of Fe(II) ions oxidation rate constants (k) for the main effects of solution (a) pH, (b) DOM, (c) phosphate dosages and (d) chlorine concentrations following the factorial design approach (α = 0.05).

Table A5. The effect of different pH values on the oxidation of Fe(II) ions process in $NaHCO_3$ buffered synthetic water ($[Fe(II)]_o \approx 3$ mg/L, 21 ± 1 °C).

pH values	Fe(II) ions conc. (mg/L)		Fe(II) ions oxidation %		k (min^{-1}) for 150 min of reaction time	Half life $t_{½}$
	After 60 min reaction	After 150 min reaction	After 60 min reaction	After 150 min reaction		
5.5	2.15	1.33	28.33	55.67	0.0054	128.33
6.5	1.76	0.82	41.33	72.66	0.0085	81.53
7.5	0.98	0.07	67.33	97.69	0.0238	29.12
8.5	0.832	0.030	72.27	99.00	0.0336	20.63

Table A6. Effect of phosphate dosages on the changes of k and half-life for Fe(II) ions oxidation process in $NaHCO_3$ buffered synthetic water ($[Fe(II)]_o \approx 3$ mg/L, 21 ± 1 °C).

Exp. No	PO_4 dosage (mg/L)	PO_4:Fe(II) mole ratio	k (min^{-1})	r^2	$t_{1/2}$
1	0.0	0	0.0086	0.992	80.58
2	0.5	0.098	0.0075	0.986	92.40
3	1.0	0.196	0.0064	0.974	108.28
4	1.5	0.294	0.0056	0.983	123.75
5	2.5	0.489	0.0062	0.976	111.77
6	5.0	0.979	0.0111	0.992	62.43
7	7.5	1.371	0.0118	0.947	58.73
8	10.0	1.959	0.0126	0.971	55.00
9	12.5	2.939	0.0139	0.975	49.86

APPENDIX B. Chapter 5 Raw data and supplementary information

Color (Co-Pt)

Table B1. Design matrix and experimental results for iron suspension color (Co-Pt) for average result.

Exp. No.	Composition of synthetic water	Factors				Average Color (Co-Pt)
		pH Unit.	DOM Conc.	PO_4^{3-} Conc.	Chlorine Conc.	
1	Fe(II) + O_2	6.5	0 mg/L	0 mg/L	0 mg/L	287
2	Fe(II) + O_2	8.5	0 mg/L	0 mg/L	0 mg/L	313
3	Fe(II) + O_2 + DOM	6.5	2.85 mg/L	0 mg/L	0 mg/L	311
4	Fe(II) + O_2 + DOM	8.5	2.85 mg/L	0 mg/L	0 mg/L	332
5	Fe(II) + O_2 + PO_4^{3-}	6.5	0 mg/L	1.5 mg/L	0 mg/L	115
6	Fe(II) + O_2 + PO_4^{3-}	8.5	0 mg/L	1.5 mg/L	0 mg/L	212
7	Fe(II) + O_2 + DOM + PO_4^{3-}	6.5	2.85 mg/L	1.5 mg/L	0 mg/L	251
8	Fe(II) + O_2 + DOM + PO_4^{3-}	8.5	2.85 mg/L	1.5 mg/L	0 mg/L	280
9	Fe(II) + O_2 + Cl_2	6.5	0 mg/L	0 mg/L	2.2 mg/L	163
10	Fe(II) + O_2 + Cl_2	8.5	0 mg/L	0 mg/L	2.2 mg/L	286
11	Fe(II) + O_2 + DOM + Cl_2	6.5	2.85 mg/L	0 mg/L	2.2 mg/L	275
12	Fe(II) + O_2 + DOM + Cl_2	8.5	2.85 mg/L	0 mg/L	2.2 mg/L	309
13	Fe(II) + O_2 + PO_4^{3-} + Cl_2	6.5	0 mg/L	1.5 mg/L	2.2 mg/L	81
14	Fe(II) + O_2 + PO_4^{3-} + Cl_2	8.5	0 mg/L	1.5 mg/L	2.2 mg/L	184
15	Fe(II) + O_2+DOM+ PO_4^{3-} + Cl_2	6.5	2.85 mg/L	1.5 mg/L	2.2 mg/L	219
16	Fe(II) + O_2+DOM+ PO_4^{3-} + Cl_2	8.5	2.85 mg/L	1.5 mg/L	2.2 mg/L	228

Table B2. Estimated effects and coefficients for color (coded units)

Term	Effect	Coef	SE Coef	T	P
Constant		240.38	6.153	39.07	0.000
pH	55.25	27.62	6.153	4.49	0.006
DOM	70.50	35.25	6.153	5.73	0.002
PO4	-88.25	-44.13	6.153	-7.17	0.001
Cl2	-44.51	-22.25	6.153	-3.62	0.015
pH*DOM	-32.00	-16.00	6.153	-2.60	0.048
pH*PO4	4.25	2.12	6.153	0.35	0.744
pH*Cl2	12.01	6.01	6.153	0.98	0.374
DOM*PO4	26.00	13.00	6.153	2.11	0.088
DOM*Cl2	8.75	4.38	6.153	0.71	0.509
PO4*Cl2	8.00	4.00	6.153	0.65	0.544

Table B3. Analysis of Variance for Color (coded units)

Source	DF	Seq SS	Adj SS	Adj MS	F	P
Main Effect						
pH	1	12210	12210	12210	20.16	0.006
DOM	1	19881	19881	19881	32.82	0.002
PO4	1	31152	31152	31152	51.43	0.001
Cl2	1	7921	7921	7921	13.08	0.015
2-Way Interactions						
pH*DOM	1	4096	4096	4096	6.76	0.048
pH*PO4	1	72.2	72	72	0.12	0.744
pH*Cl2	1	576	576	576	0.95	0.374
DOM*PO4	1	2704	2704	2704	4.46	0.088
DOM*Cl2	1	306	306	306	0.51	0.509
PO4*Cl2	1	256	256	256	0.42	0.544
Residual Error						
Total	15	82203				

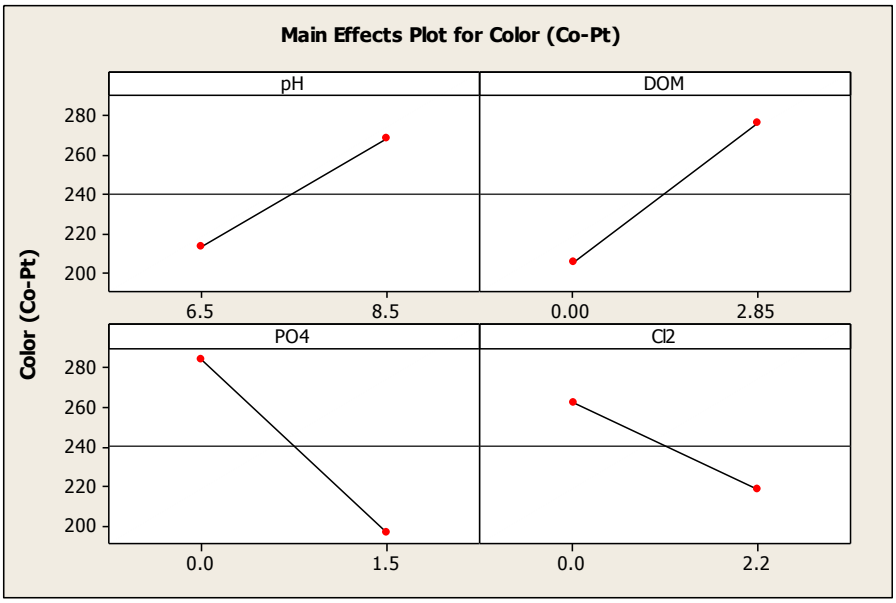

Figure B1. Main effects plot for color (Pt-Co)

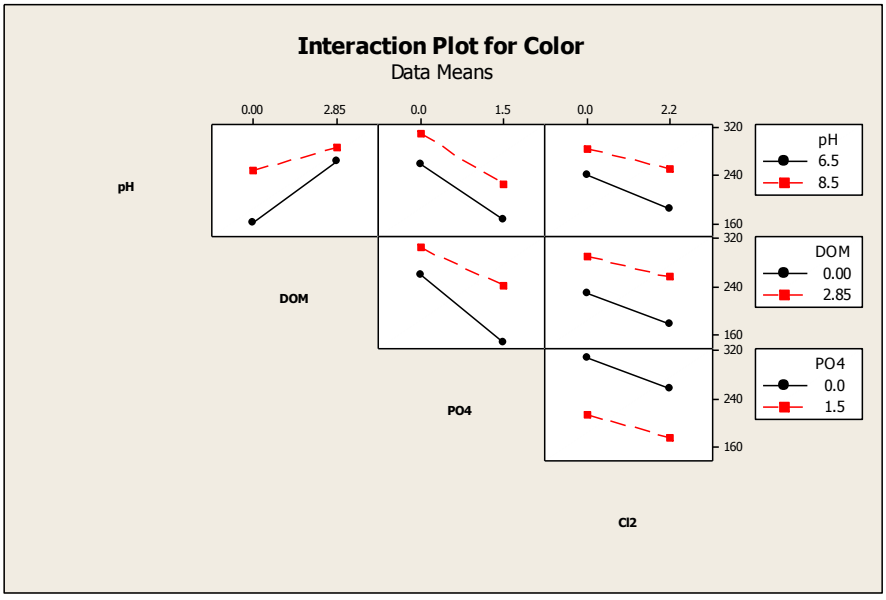

Figure B2. Interaction effects plot for color (Pt-Co)

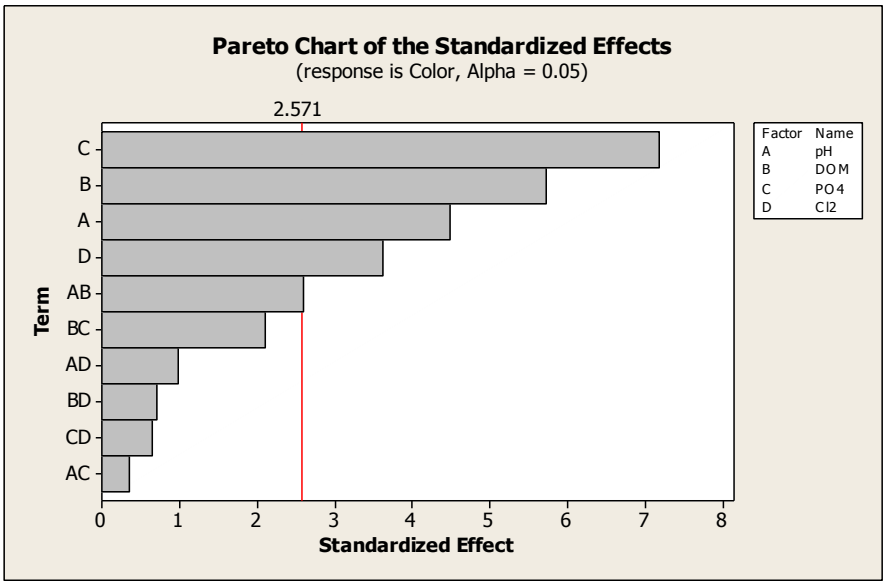

Figure B3. Pareto chart of the standardized effects for color (Pt-Co)

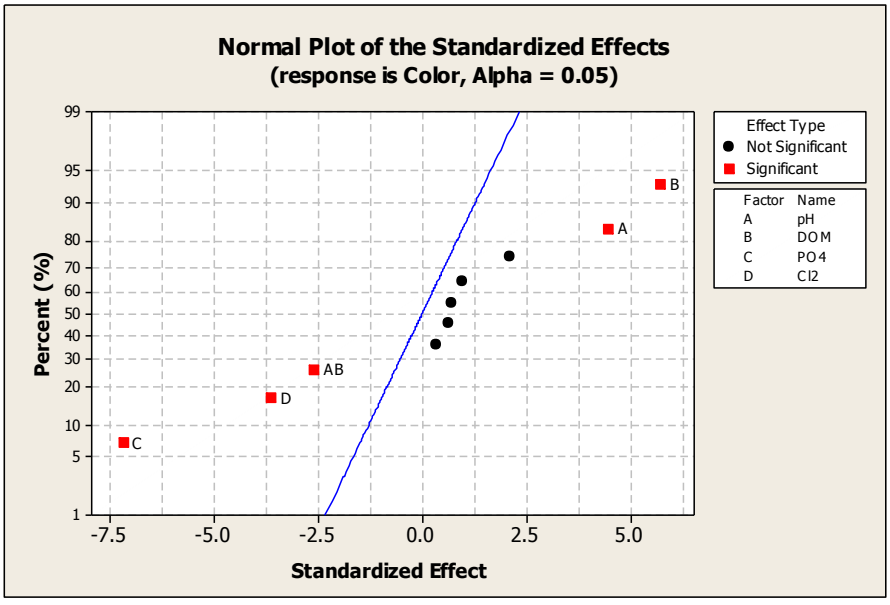

Figure B4. Normal plot of the standardized effects for color (Co-Pt).

Turbidity (NTU)

Table B4. Design matrix and experimental results (average) for iron suspension turbidity (NTU) for average result.

Exp. No.	Composition of synthetic water	Factors				Average Turbidity (NTU)
		pH unit.	DOM conc.	PO_4^{3-} conc.	Chlorine conc.	
1	Fe(II) + O_2	6.5	0 mg/L	0 mg/L	0 mg/L	5.17
2	Fe(II) + O_2	8.5	0 mg/L	0 mg/L	0 mg/L	7.17
3	Fe(II) + O_2 + DOM	6.5	2.85 mg/L	0 mg/L	0 mg/L	4.34
4	Fe(II) + O_2 + DOM	8.5	2.85 mg/L	0 mg/L	0 mg/L	4.17
5	Fe(II) + O_2 + PO_4^{3-}	6.5	0 mg/L	1.5 mg/L	0 mg/L	2.19
6	Fe(II) + O_2 + PO_4^{3-}	8.5	0 mg/L	1.5 mg/L	0 mg/L	3.26
7	Fe(II) + O_2 + DOM + PO_4^{3-}	6.5	2.85 mg/L	1.5 mg/L	0 mg/L	2.37
8	Fe(II) + O_2 + DOM + PO_4^{3-}	8.5	2.85 mg/L	1.5 mg/L	0 mg/L	3.71
9	Fe(II) + O_2 + Cl_2	6.5	0 mg/L	0 mg/L	2.2 mg/L	3.91
10	Fe(II) + O_2 + Cl_2	8.5	0 mg/L	0 mg/L	2.2 mg/L	5.62
11	Fe(II) + O_2 + DOM + Cl_2	6.5	2.85 mg/L	0 mg/L	2.2 mg/L	3.07
12	Fe(II) + O_2 + DOM + Cl_2	8.5	2.85 mg/L	0 mg/L	2.2 mg/L	3.93
13	Fe(II) + O_2 + PO_4^{3-} + Cl_2	6.5	0 mg/L	1.5 mg/L	2.2 mg/L	3.12
14	Fe(II) + O_2 + PO_4^{3-} + Cl_2	8.5	0 mg/L	1.5 mg/L	2.2 mg/L	3.42
15	Fe(II) + O_2+DOM+ PO_4^{3-} + Cl_2	6.5	2.85 mg/L	1.5 mg/L	2.2 mg/L	2.79
16	Fe(II) + O_2+DOM+ PO_4^{3-} + Cl_2	8.5	2.85 mg/L	1.5 mg/L	2.2 mg/L	3.16

Factorial Fit: Turbidity versus pH, DOM, PO4, Chlorine

Table B5. Estimated Effects and Coefficients for Turbidity (coded units)

Term	*Effect*	*Coef*	*SE Coef*	*T*	*P*
Constant		3.836	0.146	26.22	0.000
pH	0.938	0.469	0.146	3.20	0.024
DOM	-0.788	-0.394	0.146	-2.69	0.043
PO_4	-1.668	-0.834	0.146	-5.70	0.002
Chlorine	-0.418	-0.209	0.146	-1.43	0.213
pH*DOM	-0.338	-0.169	0.146	-1.15	0.301
pH*PO_4	-0.168	-0.084	0.146	-0.57	0.592
pH*Chlorine	-0.128	-0.064	0.146	-0.44	0.681
DOM*PO_4	0.798	0.399	0.146	2.73	0.042
DOM*Chlorine	0.008	0.004	0.146	0.03	0.981
PO4*Chlorine	0.658	0.329	0.146	2.25	0.075

Table B6. Analysis of Variance for Turbidity (coded units)

Source	*DF*	*Seq SS*	*Adj SS*	*Adj MS*	*F*	*P*
Main Effects						
pH	1	3.52	3.52	3.52	10.27	0.024
DOM	1	2.48	2.48	2.48	7.24	0.043
PO_4	1	11.12	11.12	11.12	32.48	0.002
Chlorine	1	0.70	0.70	0.70	2.04	0.213
2-Way Interactions						
pH*DOM	1	0.46	0.46	0.46	1.33	0.301
pH*PO_4	1	0.11	0.11	0.11	0.33	0.592
pH* Chlorine	1	0.07	0.07	0.07	0.19	0.681
DOM*PO_4	1	2.54	2.54	2.54	7.43	0.042
DOM* Chlorine	1	0.00	0.00	0.00	0.00	0.981
PO4* Chlorine	1	1.73	1.73	1.73	5.05	0.075
Residual Error						
Total	15	24.43				

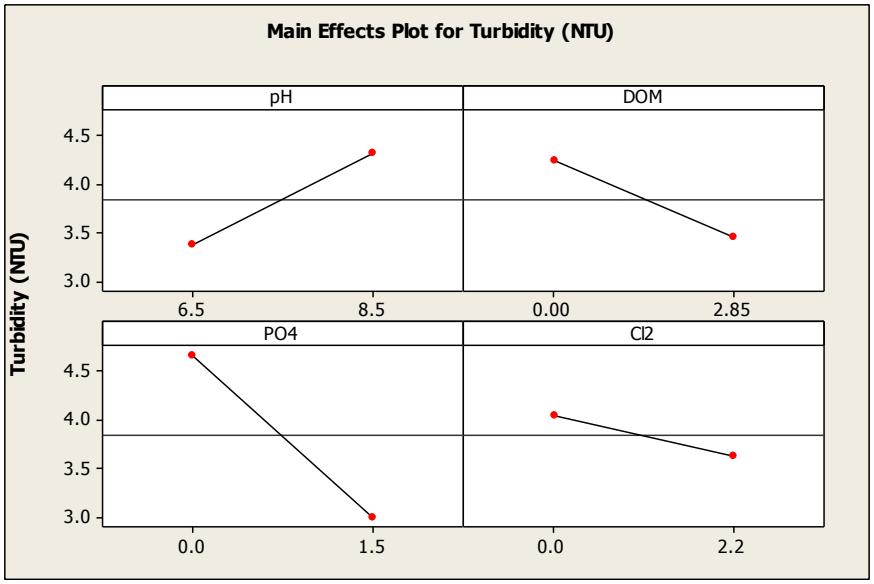

Figure B5. Main effects plot for turbidity (NTU)

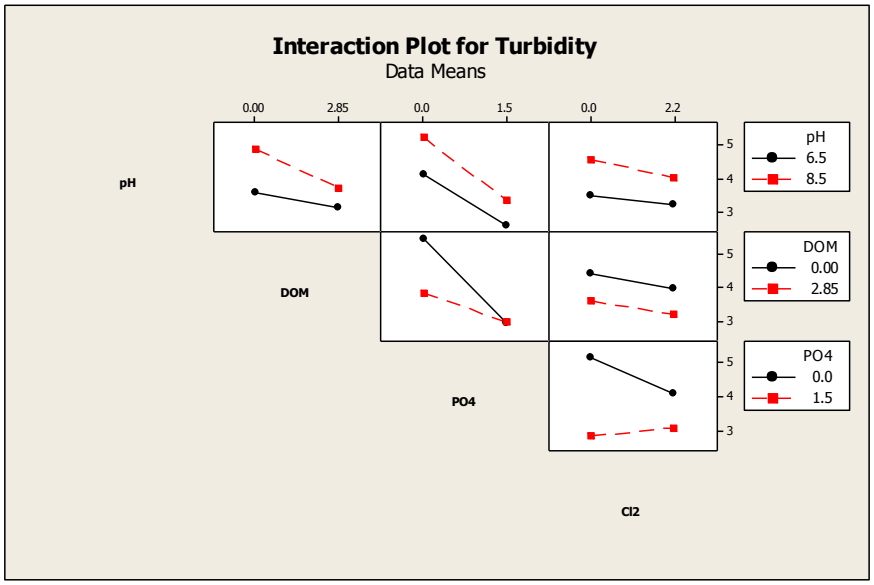

Figure B6 . Interaction effects plot for turbidity (NTU)

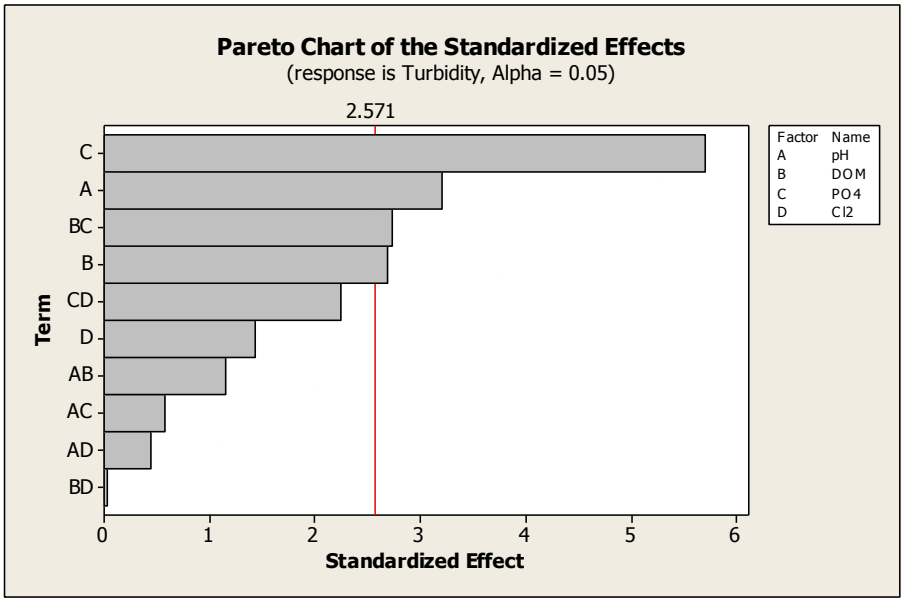

Figure B7. Pareto chart of the standardized effects for turbidity (NTU)

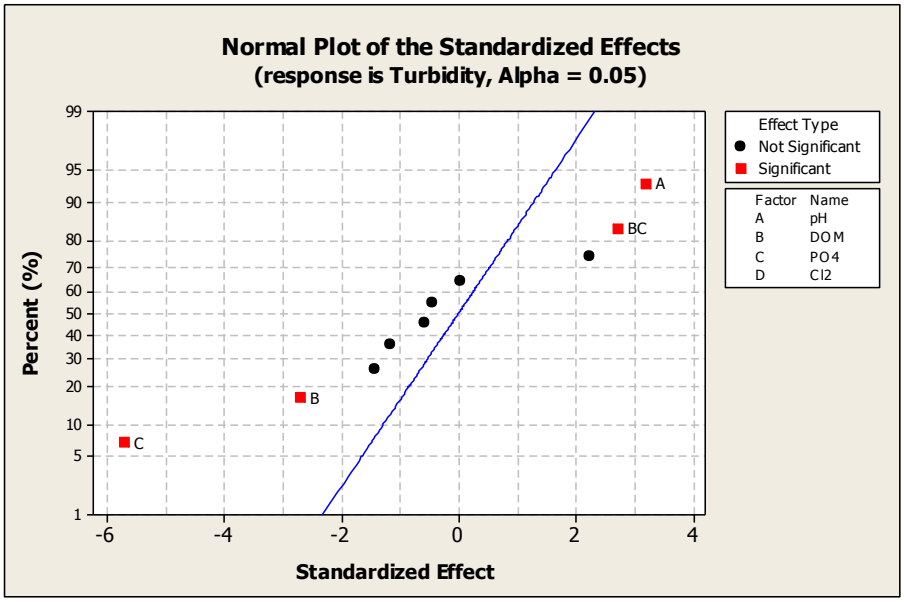

Figure B8. Normal plot of the standardized effects for turbidity.

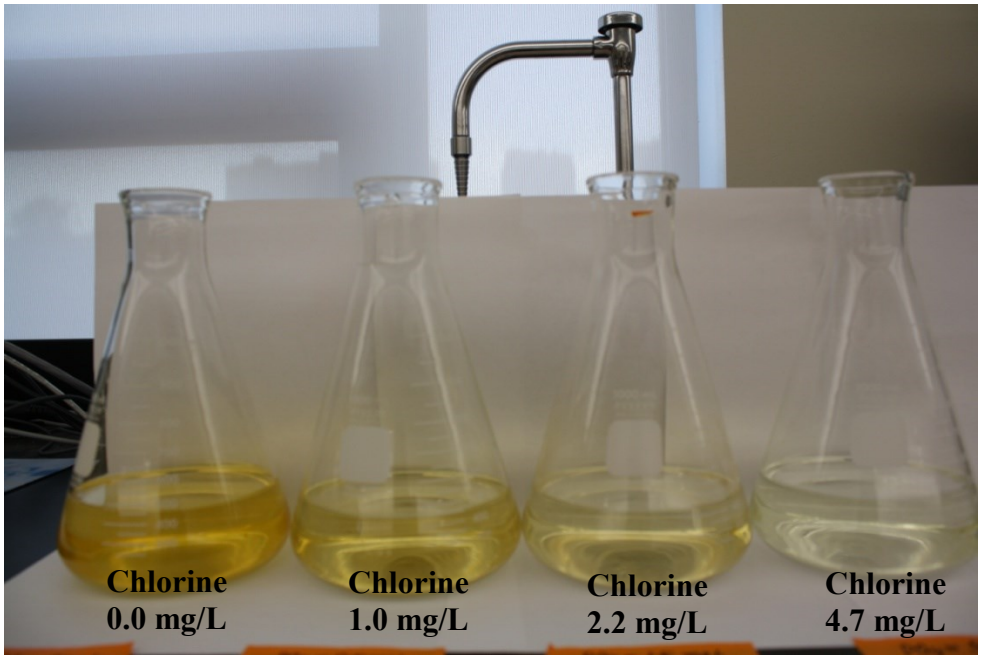

Figure B9. Effect of chlorine dosages on the changes of color in $NaHCO_3$ buffered synthetic water ([Fe(II)]o ≈ 3 mg/L, pH 6.5, at 25 ± 0.1 °C temp).

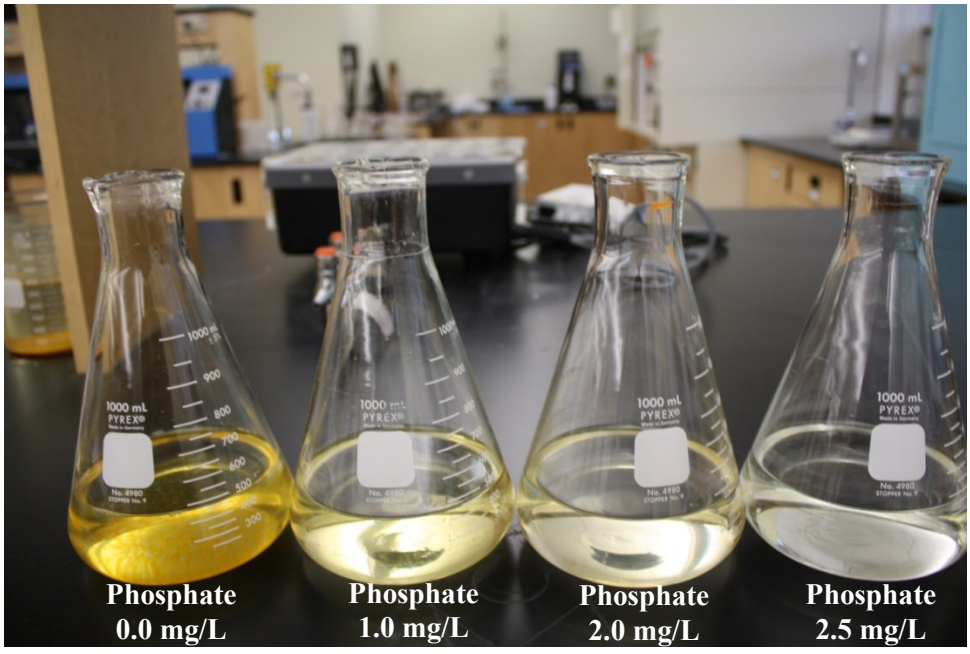

Figure B10. Effect of phosphate dosage on the changes of color in $NaHCO_3$ buffered synthetic water ([Fe(II)]o ≈ 3 mg/L, pH 6.5, at 25 ± 0.1 °C temp).

Zeta potential

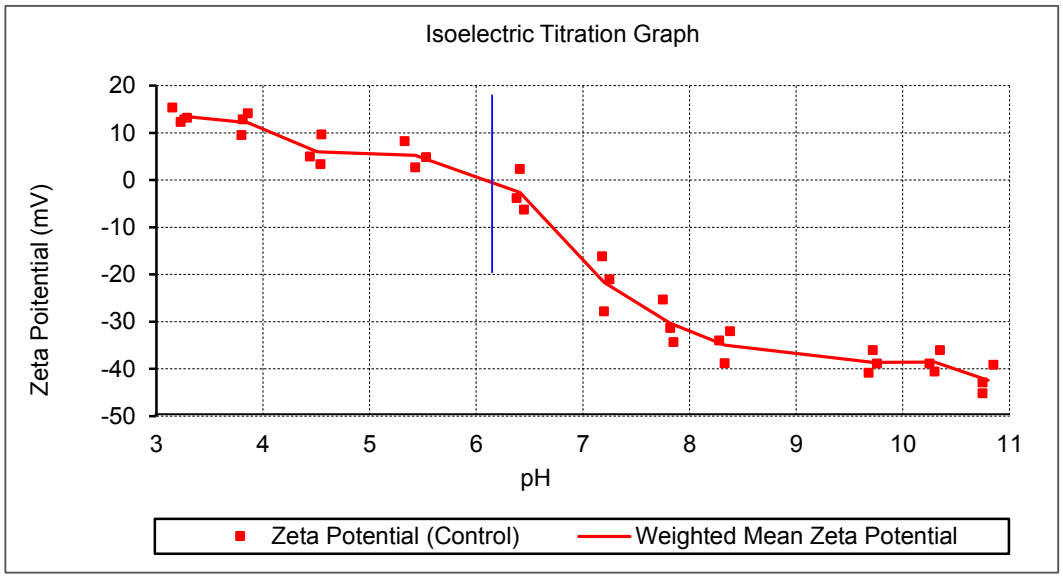

Figure B11. Isoelectric titration graph (pH_{PZC} = 6.11) for the iron particles in $NaHCO_3$ buffered synthetic water for control system ([Fe(II)]o ≈ 3 mg/L, at 25 ± 0.1 °C temperature).

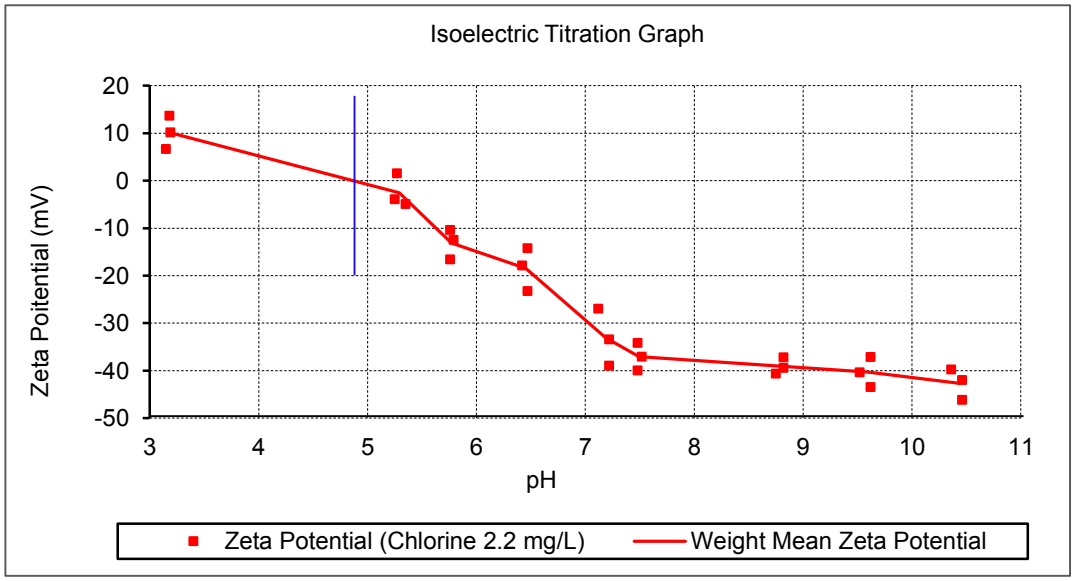

Figure B12. Isoelectric titration graph pH_{PZC} = 4.87 for the iron particles in $NaHCO_3$ buffered synthetic water for the chlorine dosage of 4.7 mg/L, ([Fe(II)]o ≈ 3 mg/L, at 25 ± 0.1 °C temp).

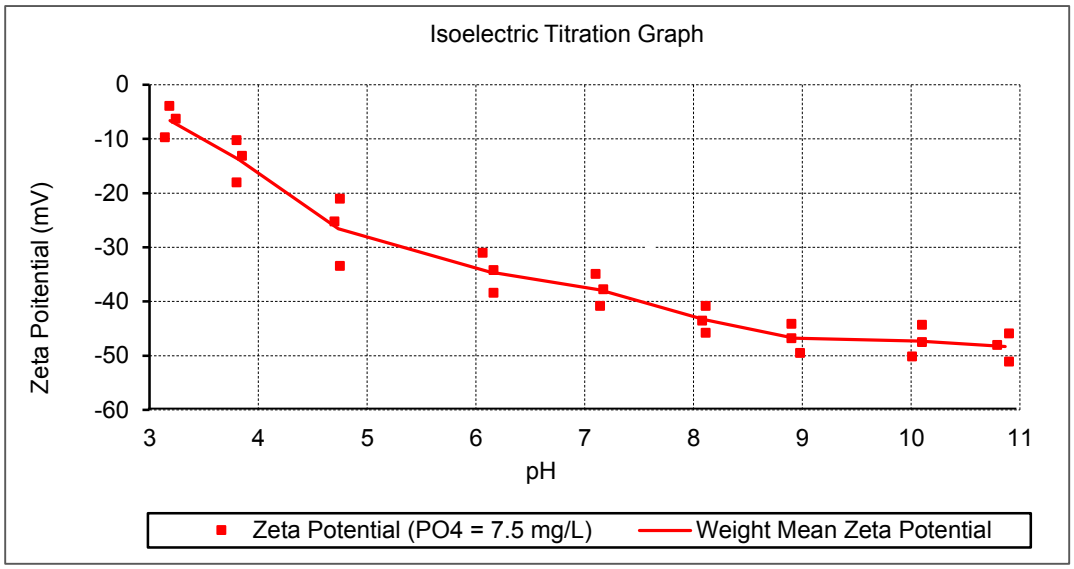

Figure B13. Isoelectric titration graph (pH_{PZC} = 0.0) for the iron particles in $NaHCO_3$ buffered synthetic water for the phosphate dosage of 5 mg/L (Fe(II)]o ≈ 3 mg/L, at 25 ± 0.1 °C temp).

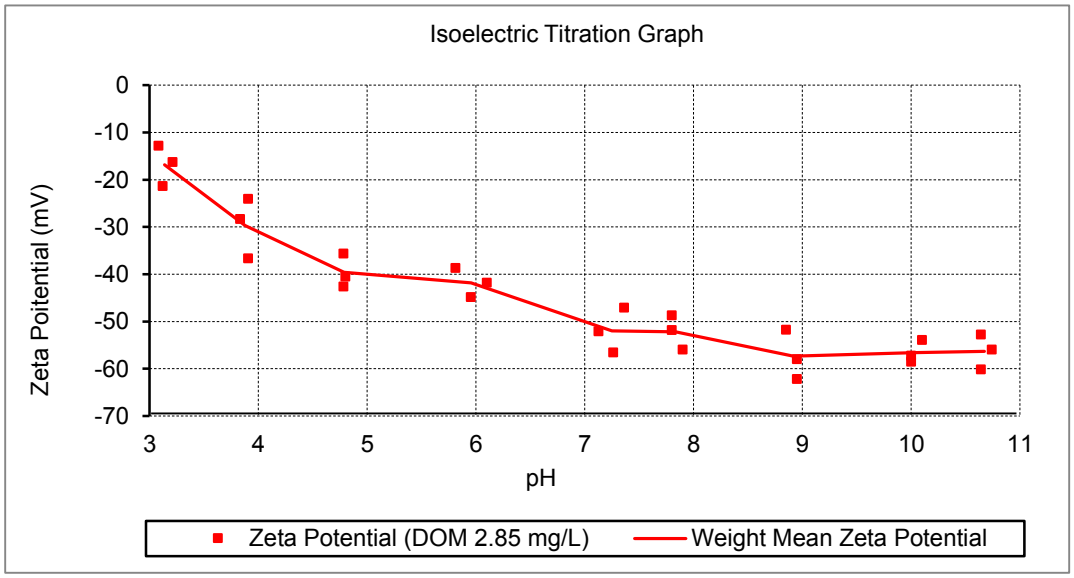

Figure B14. Isoelectric titration graph (pH_{PZC} = 0.0) for the iron particles in $NaHCO_3$ buffered synthetic water for the DOM dosage of 2.85 mg/L (([Fe(II)]o ≈ 3 mg/L, at 25 ± 0.1 °C temp).

Table B7. Effect of different variables (i.e. chlorine, phosphate and DOM dosage on the changes in iron particles size distribution in $NaBCO_3$ buffered synthetic water systems,

	Variables in experiment			
Experiment	Control study	Chlorine dosage 4.7 mg/L	PO_4 dosage 10 mg/L	DOM dosage 2.85 mg/L
Exp. 1	410.30	174.10	31.91	96.85
Exp. 2	395.20	180.00	31.91	98.34
Exp. 3	353.20	174.50	30.95	97.37
Average	386.23	176.20	31.59	97.52
Standard deviation	29.59	3.30	0.55	0.76

ANOVA (analysis of variance) test calculation: single factor

Total sum of square is obtained by the following equation

$$SS_T = \sum_{i=1}^{a}\sum_{i=1}^{n} y_{ij}^2 - \frac{y_{\cdot\cdot}^2}{N}$$

$$= (410.3)^2 + (174.1)^2 + \cdots + (97.37)^2 - \frac{(2074.63)^2}{12}$$

$$SS_T = 215292.29$$

The treatment sum of square is obtained by the following equation

$$SS_{treatment} = \sum_{i=1}^{a} \frac{y_i^2}{n} - \frac{y_{\cdot\cdot}^2}{N}$$

$$= \frac{(1158.7)^2 + (528.6)^2 + (94.77)^2 + (292.56)^2}{3} - \frac{(2074.63)^2}{12}$$

$$SS_{treatment} = 21351.98$$

The error sum of square is obtained by the following equation

$$SS_E = SS_T - SS_{treatment}$$

$$SS_E = 215292.29 - 21351.98 = 1774.30$$

The treatment mean of square is obtained by the following equation

$$MS_{treatment} = \frac{SS_{treatment}}{a-1} = \frac{21351.98}{3}$$

$MS_{treatment} = 71172.66$

The error mean of square is obtained by the following equation

$$MS_E = \frac{SS_E}{N - a} = \frac{1774.308}{8}$$

$$MS_E = 221.79$$

F_{obs} is computed by the following equation

$$F_{obs} = \frac{MS_{treatment}}{MS_E} = \frac{71172.66}{221.79}$$

$$F_{obs} = 320.9$$

Table B8. Analysis of variance (ANOVA) test (single factor) for the iron particle size distribution data.

Source of Variation	*SS*	*Df*	*MS*	F_{obs}	*P-value*	F_{crit}
Water variables	213517.98	3	71172.66	320.90	1.13152E-08	7.59
Error	1774.30	8	221.79			
Total	215292.29	11				

Comments:
The ANOVA for testing $H_o: \beta_1 = 0$ is summarized in Table B8. Noting that F_{obs} = 320.9 > $F_{0.01,\ 3,\ 8}$ = 7.59, we reject the H_o and concluded that experimental variables (chlorine, phosphate and DOM dosage) significantly affects the iron particle size distribution.

Iron particle size distribution

Table B9. Effect of phosphate dosage= 0.0 mg/L (control system) on iron particles size distribution in $NaHCO_3$ buffered synthetic water (pH 6.5, 21 ± 1° C)

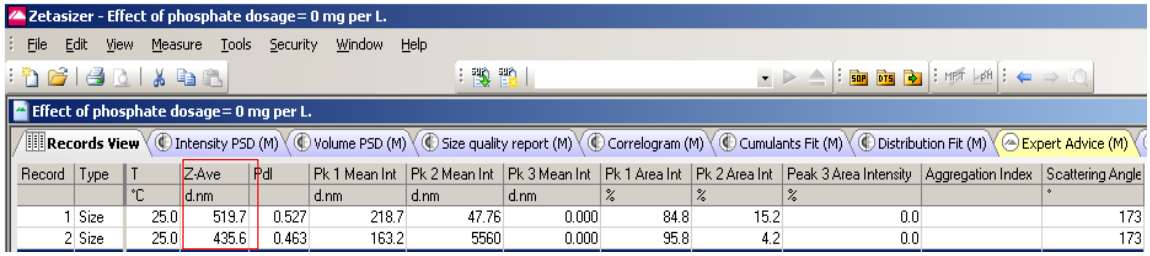

Record	Type	T	Z-Ave	PdI	Pk 1 Mean Int	Pk 2 Mean Int	Pk 3 Mean Int	Pk 1 Area Int	Pk 2 Area Int	Peak 3 Area Intensity	Aggregation Index	Scattering Angle
		°C	d.nm		d.nm	d.nm	d.nm	%	%	%		°
1	Size	25.0	519.7	0.527	218.7	47.76	0.000	84.8	15.2	0.0		173
2	Size	25.0	435.6	0.463	163.2	5560	0.000	95.8	4.2	0.0		173

Record: 1			Diam (nm)	% Intensity	Width (nm)
Z-average(nm):	519.7	Peak 1:	218.7	84.8	64.3
PdI:	0.527	Peak 2:	47.76	15.2	10.5
Intercept:	0.356	Peak 3:	0.00	0.00	0.00

			Diam (nm)	% Intensity	Width (nm)
Record: 2					
Z-average(nm):	435.6	Peak 1:	163.2	95.8	48.5
PdI:	0.463	Peak 2:	5560	4.2	0.0
Intercept:	0.354	Peak 3:	0.00	0.0	0.0

Z-Average: 477.6 ±59.5 (nm)

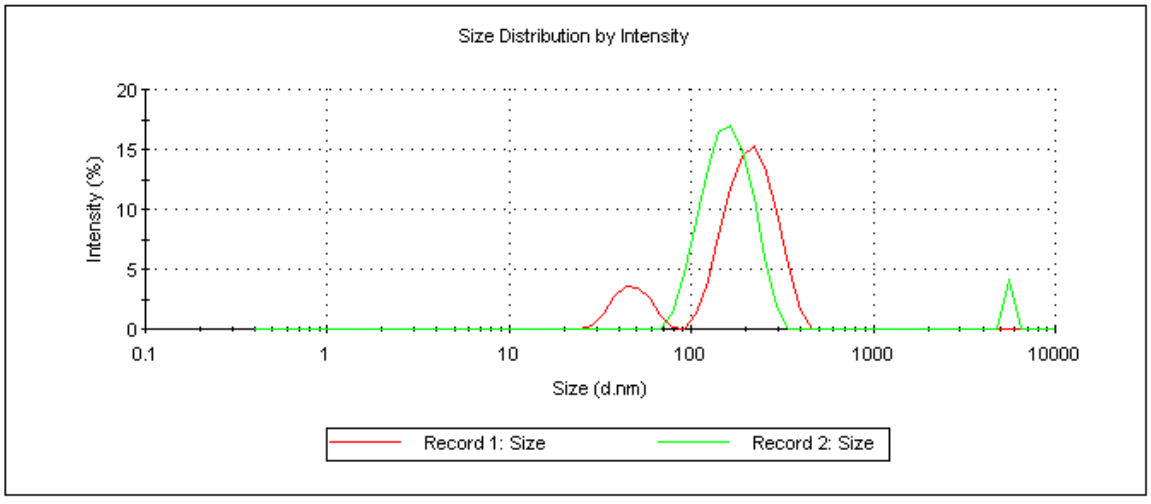

Figure B15. Iron particles size distribution for the phosphate dosage of 0.0 mg/L

Table B10. Effect of phosphate dosage= 0.0 mg/L (control system) on iron particles size distribution in $NaHCO_3$ buffered synthetic water (pH 6.5, 21 ± 1° C)

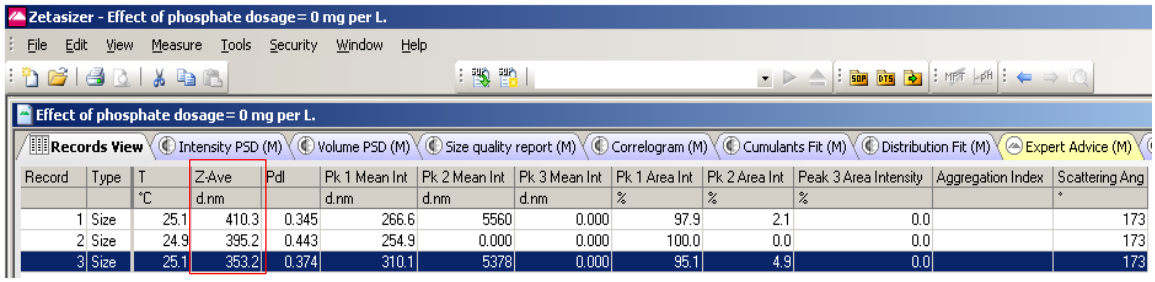

Record	Type	T	Z-Ave	PdI	Pk 1 Mean Int	Pk 2 Mean Int	Pk 3 Mean Int	Pk 1 Area Int	Pk 2 Area Int	Peak 3 Area Intensity	Aggregation Index	Scattering Ang
		°C	d.nm		d.nm	d.nm	d.nm	%	%	%		°
1	Size	25.1	410.3	0.345	266.6	5560	0.000	97.9	2.1	0.0		173
2	Size	24.9	395.2	0.443	254.9	0.000	0.000	100.0	0.0	0.0		173
3	Size	25.1	353.2	0.374	310.1	5378	0.000	95.1	4.9	0.0		173

Record: 1			Diam (nm)	% Intensity	Width (nm)
Z-average(nm):	410.3	Peak 1:	266.6	97.9	79.15
PdI:	0.345	Peak 2:	5560	2.1	0.000
Intercept:	0.530	Peak 3:	0.000	0.00	0.000

Record: 2			Diam (nm)	% Intensity	Width (nm)
Z-average(nm):	395.2	Peak 1:	254.9	100.0	68.35
PdI:	0.443	Peak 2:	0.000	0.00	0.00
Intercept:	0.527	Peak 3:	0.00	0.00	0.00

Record: 3			Diam (nm)	% Intensity	Width (nm)
Z-average(nm):	353.2	Peak 1:	310.1	95.1	117.2
PdI:	0.372	Peak 2:	5378	4.9	324.1
Intercept:	0.484	Peak 3:	0.00	0.00	0.00

Z-Average: 386.2 ± 29.66 (nm)

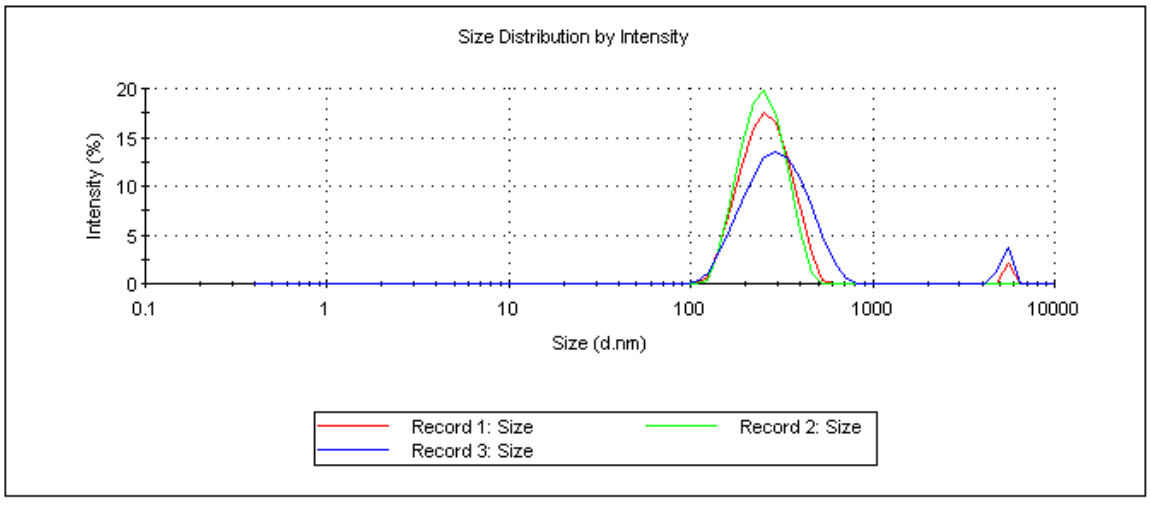

Figure B16. Iron particles size distribution for the phosphate dosage of 0.0 mg/L
The grand average particle size (No of observation= 5) in control system= 422.8 ± 61.88 nm

Table B11. Effect of phosphate dosage= 0.5 mg/L on iron particles size distribution in $NaHCO_3$ buffered synthetic water (pH 6.5, 21 ± 1° C)

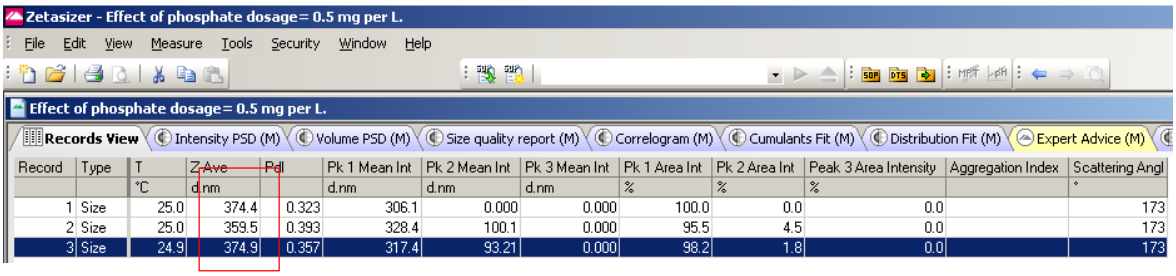

Record	Type	T	Z-Ave	PdI	Pk 1 Mean Int	Pk 2 Mean Int	Pk 3 Mean Int	Pk 1 Area Int	Pk 2 Area Int	Peak 3 Area Intensity	Aggregation Index	Scattering Angl
		°C	d.nm		d.nm	d.nm	d.nm	%	%	%		°
1	Size	25.0	374.4	0.323	306.1	0.000	0.000	100.0	0.0	0.0		173
2	Size	25.0	359.5	0.393	328.4	100.1	0.000	95.5	4.5	0.0		173
3	Size	24.9	374.9	0.357	317.4	93.21	0.000	98.2	1.8	0.0		173

Record: 1			Diam (nm)	% Intensity	Width (nm)
Z-average(nm):	374.9	Peak 1:	317.4	98.2	98.06
PdI:	0.357	Peak 2:	93.2	1.8	15.51
Intercept:	0.883	Peak 3:	0.000	0.00	0.000

Record: 2			Diam (nm)	% Intensity	Width (nm)
Z-average(nm):	359.5	Peak 1:	328.4	95.5	108.0
PdI:	0.393	Peak 2:	100.1	4.5	16.35
Intercept:	0.878	Peak 3:	0.00	0.00	0.00

Record: 3			Diam (nm)	% Intensity	Width (nm)
Z-average(nm):	374.4	Peak 1:	316.6	100.0	91.83
PdI:	0.323	Peak 2:	5378	0.00	0.00
Intercept:	0.875	Peak 3:	0.00	0.00	0.00

Z-Average: 369.2 ± 8.75 (nm)

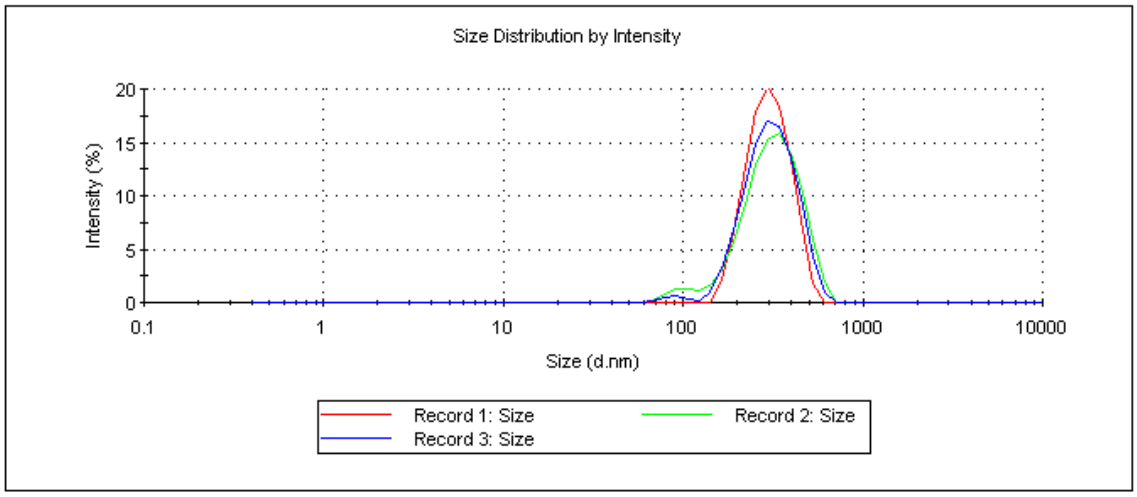

Figure B17. Iron particles size distribution for the phosphate dosage of 0.5 mg/L

Table B12. Effect of phosphate dosage (0.5 mg/L) on iron particles size distribution in $NaHCO_3$ buffered synthetic water (pH 6.5, 21 ± 1° C)

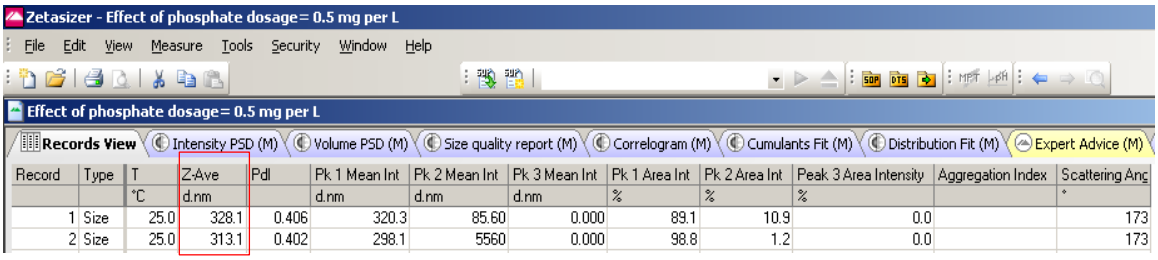

Record	Type	T	Z-Ave	PdI	Pk 1 Mean Int	Pk 2 Mean Int	Pk 3 Mean Int	Pk 1 Area Int	Pk 2 Area Int	Peak 3 Area Intensity	Aggregation Index	Scattering Ang
		°C	d.nm		d.nm	d.nm	d.nm	%	%	%		°
1	Size	25.0	328.1	0.406	320.3	85.60	0.000	89.1	10.9	0.0		173
2	Size	25.0	313.1	0.402	298.1	5560	0.000	98.8	1.2	0.0		173

Record: 1			Diam (nm)	% Intensity	Width (nm)
Z-average(nm):	328.1	Peak 1:	320.3	89.1	110.8
PdI:	0.406	Peak 2:	85.60	10.9	22.29
Intercept:	0.882	Peak 3:	0.000	0.00	0.000

			Diam (nm)	% Intensity	Width (nm)
Record: 2					
Z-average(nm):	313.1	Peak 1:	298.1	98.8	157.7
PdI:	0.402	Peak 2:	5560	1.20	0.00
Intercept:	0.892	Peak 3:	0.00	0.00	0.00

Z-Average: 320.6 ± 10.6 (nm)

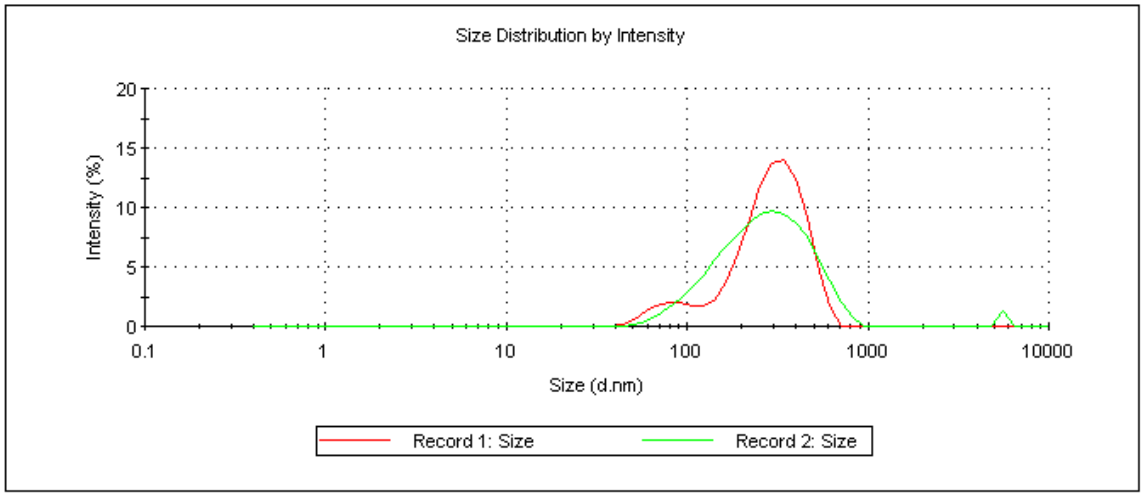

Figure B18. Iron particles size distribution for phosphate dosage= 0.5 mg/L

The grand average particle size (No of observation= 5) in control system= 350 ± 28.05 nm

Table B13. Effect of phosphate dosage (1.0 mg/L) on iron particles size distribution in $NaHCO_3$ buffered synthetic water (pH 6.5, 21 ± 1° C)

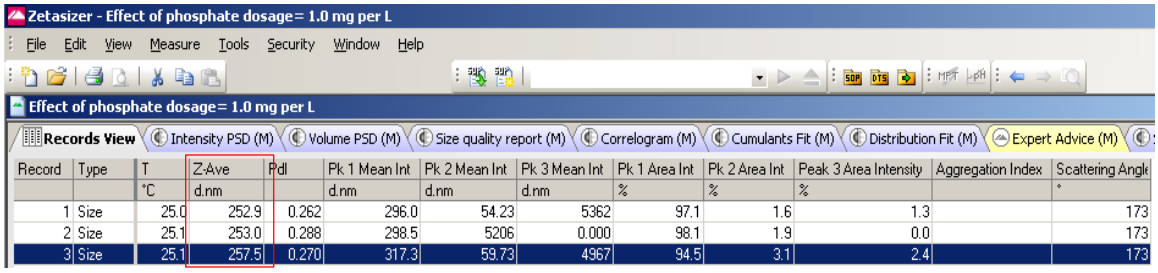

Record	Type	T	Z-Ave	PdI	Pk 1 Mean Int	Pk 2 Mean Int	Pk 3 Mean Int	Pk 1 Area Int	Pk 2 Area Int	Peak 3 Area Intensity	Aggregation Index	Scattering Angle
		°C	d.nm		d.nm	d.nm	d.nm	%	%	%		°
1	Size	25.0	252.9	0.262	296.0	54.23	5362	97.1	1.6	1.3		173
2	Size	25.1	253.0	0.288	298.5	5206	0.000	98.1	1.9	0.0		173
3	Size	25.1	257.5	0.270	317.3	59.73	4967	94.5	3.1	2.4		173

Record: 1			Diam (nm)	% Intensity	Width (nm)
Z-average(nm):	252.9	Peak 1:	296.0	97.1	137.2
PdI:	0.262	Peak 2:	54.23	1.6	10.13
Intercept:	0.922	Peak 3:	5362	1.3	335.0

Record: 2			Diam (nm)	% Intensity	Width (nm)
Z-average(nm):	253.0	Peak 1:	298.5	98.1	143.5
PdI:	0.288	Peak 2:	5206	1.9	471.6
Intercept:	0.922	Peak 3:	0.00	0.00	0.00

Record: 3			Diam (nm)	% Intensity	Width (nm)
Z-average(nm):	257.5	Peak 1:	317.3	94.5	149.0
PdI:	0.270	Peak 2:	59.73	3.1	12.04
Intercept:	0.892	Peak 3:	4967	2.4	624.0

Z-Average: 254.47 ± 2.67 (nm)

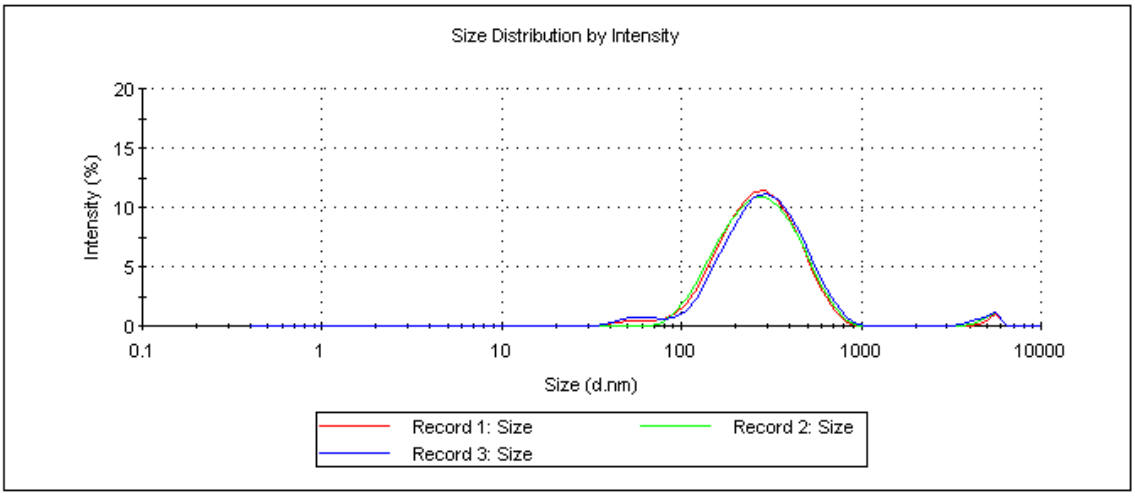

Figure B19. Iron particles size distribution for the phosphate dosage of 1.0 mg/L

Table B14. Effect of phosphate dosage= 1.0 mg/L on iron particles size distribution in $NaHCO_3$ buffered synthetic water (pH 6.5, 21 ± 1° C)

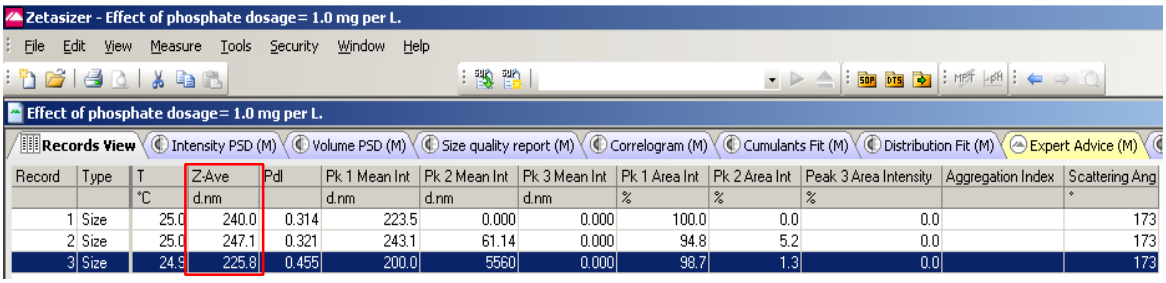

Record	Type	T	Z-Ave	PdI	Pk 1 Mean Int	Pk 2 Mean Int	Pk 3 Mean Int	Pk 1 Area Int	Pk 2 Area Int	Peak 3 Area Intensity	Aggregation Index	Scattering Ang
		°C	d.nm		d.nm	d.nm	d.nm	%	%	%		°
1	Size	25.0	240.0	0.314	223.5	0.000	0.000	100.0	0.0	0.0		173
2	Size	25.0	247.1	0.321	243.1	61.14	0.000	94.8	5.2	0.0		173
3	Size	24.9	225.8	0.455	200.0	5560	0.000	98.7	1.3	0.0		173

Record: 1			Diam (nm)	% Intensity	Width (nm)
Z-average(nm):	240.0	Peak 1:	223.5	100.0	65.74
PdI:	0.314	Peak 2:	0.00	0.00	0.000
Intercept:	0.764	Peak 3:	0.00	0.00	0.000

			Diam (nm)	% Intensity	Width (nm)
Record: 2					
Z-average(nm):	247.1	Peak 1:	243.1	94.8	89.57
PdI:	0.321	Peak 2:	61.14	5.2	11.85
Intercept:	0.743	Peak 3:	0.000	0.00	0.000

			Diam (nm)	% Intensity	Width (nm)
Record: 3					
Z-average(nm):	225.8	Peak 1:	200.0	98.7	62.54
PdI:	0.455	Peak 2:	5560	1.3	0.000
Intercept:	0.743	Peak 3:	0.000	0.00	0.000

Z-Average: 237.63 ± 10.85 (nm)

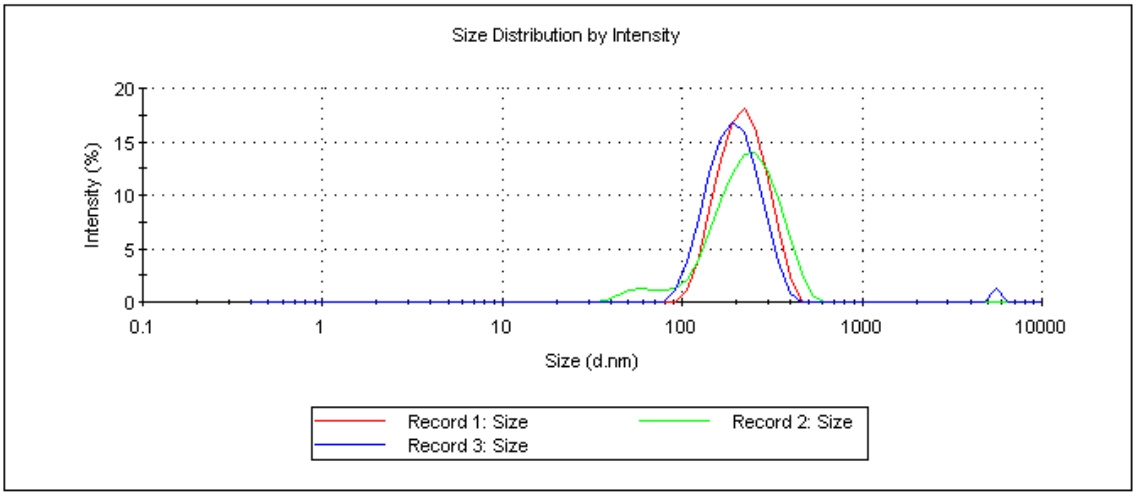

Figure B20. Iron particles size distribution for the phosphate dosage of 1.0 mg/L

The grand average particle size (No of observation= 6) in control system= 246.05 ± 11.61 nm

Table B15. Effect of phosphate dosage (1.5 mg/L) on iron particles size distribution in $NaHCO_3$ buffered synthetic water (pH 6.5, 21 ± 1° C)

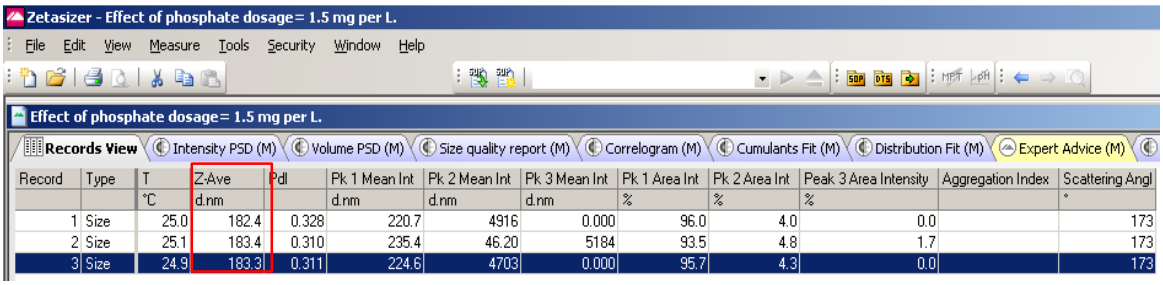

Record	Type	T	Z-Ave	PdI	Pk 1 Mean Int	Pk 2 Mean Int	Pk 3 Mean Int	Pk 1 Area Int	Pk 2 Area Int	Peak 3 Area Intensity	Aggregation Index	Scattering Angl
		°C	d.nm		d.nm	d.nm	d.nm	%	%	%		°
1	Size	25.0	182.4	0.328	220.7	4916	0.000	96.0	4.0	0.0		173
2	Size	25.1	183.4	0.310	235.4	46.20	5184	93.5	4.8	1.7		173
3	Size	24.9	183.3	0.311	224.6	4703	0.000	95.7	4.3	0.0		173

			Diam (nm)	% Intensity	Width (nm)
Record: 1					
Z-average(nm):	182.4	Peak 1:	220.7	96.0	124.9
PdI:	0.328	Peak 2:	4916	4.00	665.0
Intercept:	0.652	Peak 3:	0.00	0.00	0.000
			Diam (nm)	% Intensity	Width (nm)
Record: 2					
Z-average(nm):	183.4	Peak 1:	235.1	93.5	112.2
PdI:	0.310	Peak 2:	46.20	4.8	8.869
Intercept:	0.672	Peak 3:	5184	1.70	483.5
			Diam (nm)	% Intensity	Width (nm)
Record: 3					
Z-average(nm):	183.3	Peak 1:	224.6	95.7	124.2
PdI:	0.311	Peak 2:	4703	4.3	782.0
Intercept:	0.685	Peak 3:	0.000	0.00	0.000

Z-Average: 183.03 ± 0.55 (nm)

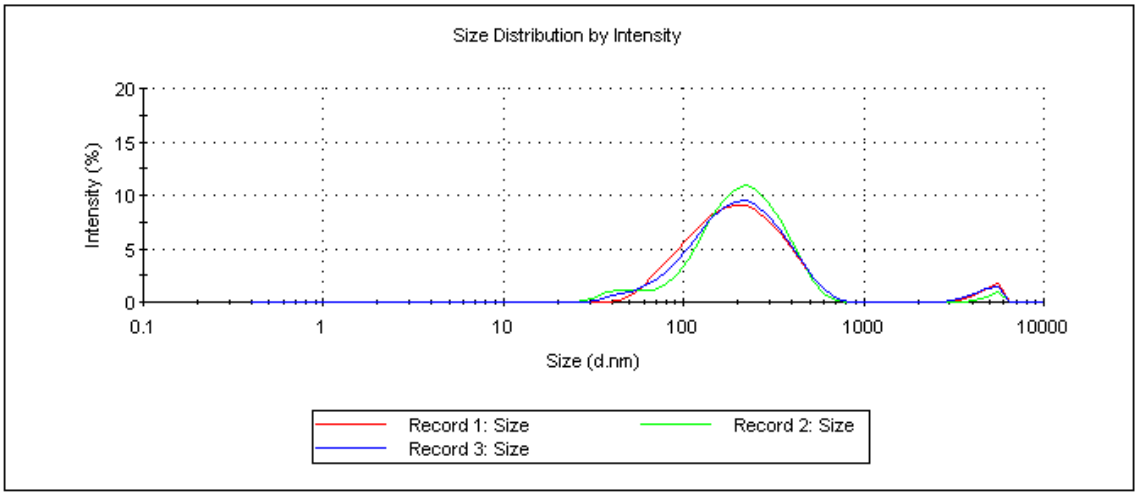

Figure B21. Iron particles size distribution for the phosphate dosage of 1.5 mg/L

Table B16. Effect of phosphate dosage (1.5 mg/L) on iron particles size distribution in $NaHCO_3$ buffered synthetic water (pH 6.5, 21 ± 1° C)

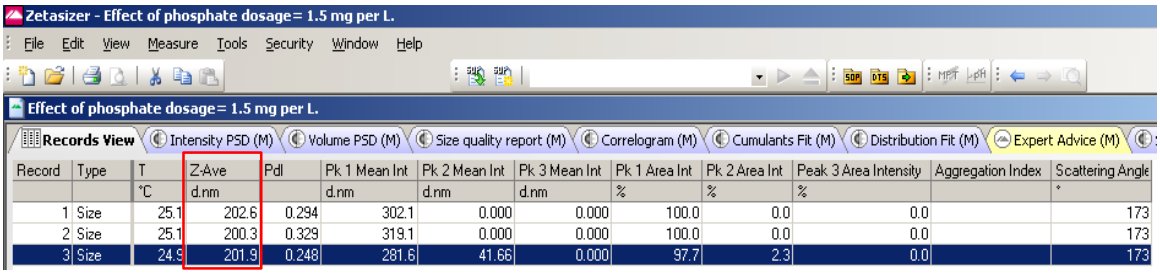

Record	Type	T	Z-Ave	PdI	Pk 1 Mean Int	Pk 2 Mean Int	Pk 3 Mean Int	Pk 1 Area Int	Pk 2 Area Int	Peak 3 Area Intensity	Aggregation Index	Scattering Angle
		°C	d.nm		d.nm	d.nm	d.nm	%	%	%		°
1	Size	25.1	202.6	0.294	302.1	0.000	0.000	100.0	0.0	0.0		173
2	Size	25.1	200.3	0.329	319.1	0.000	0.000	100.0	0.0	0.0		173
3	Size	24.9	201.9	0.248	281.6	41.66	0.000	97.7	2.3	0.0		173

Record: 1			Diam (nm)	% Intensity	Width (nm)
Z-average(nm):	202.6	Peak 1:	302.1	100.0	187.9
PdI:	0.294	Peak 2:	0.00	0.00	0.000
Intercept:	0.707	Peak 3:	0.00	0.00	0.000

Record: 2			Diam (nm)	% Intensity	Width (nm)
Z-average(nm):	200.3	Peak 1:	319.1	100.0	225.7
PdI:	0.329	Peak 2:	0.000	0.00	0.00
Intercept:	0.715	Peak 3:	0.000	0.00	0.00

Record: 3			Diam (nm)	% Intensity	Width (nm)
Z-average(nm):	201.9	Peak 1:	281.6	97.7	158.5
PdI:	0.248	Peak 2:	41.66	2.3	7.085
Intercept:	0.723	Peak 3:	0.000	0.00	0.000

Z-Average: 201.60 ± 1.18 (nm)

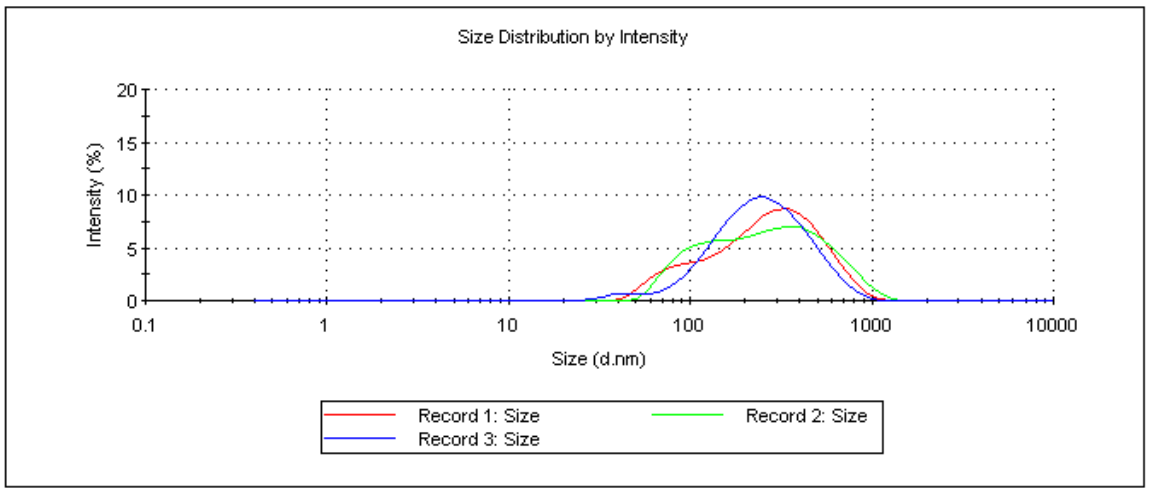

Figure B22. Iron particles size distribution for the phosphate dosage of 1.5 mg/L

The grand average particle size (No of observation= 6) in control system= 192.32 ± 10.2 nm

Table B17. Effect of phosphate dosage (2.5 mg/L) on iron particles size distribution in $NaHCO_3$ buffered synthetic water (pH 6.5, 21 ± 1° C)

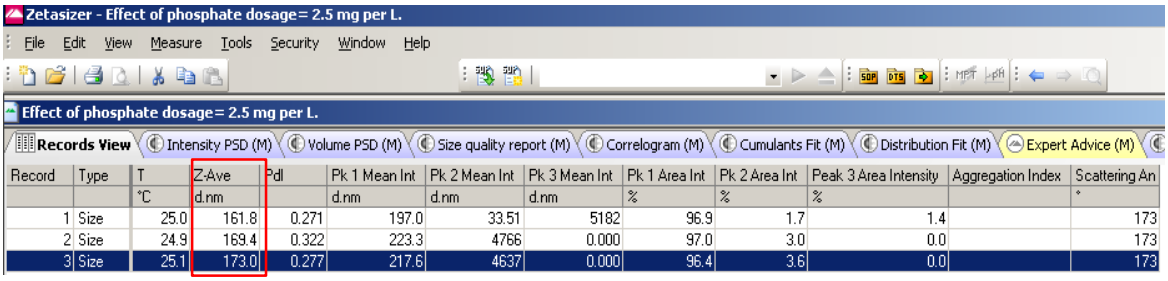

Record	Type	T	Z-Ave	PdI	Pk 1 Mean Int	Pk 2 Mean Int	Pk 3 Mean Int	Pk 1 Area Int	Pk 2 Area Int	Peak 3 Area Intensity	Aggregation Index	Scattering An
		°C	d.nm		d.nm	d.nm	d.nm	%	%	%		°
1	Size	25.0	161.8	0.271	197.0	33.51	5182	96.9	1.7	1.4		173
2	Size	24.9	169.4	0.322	223.3	4766	0.000	97.0	3.0	0.0		173
3	Size	25.1	173.0	0.277	217.6	4637	0.000	96.4	3.6	0.0		173

			Diam (nm)	% Intensity	Width (nm)
Record: 1					
Z-average(nm):	161.8	Peak 1:	197.0	96.9	93.45
PdI:	0.271	Peak 2:	33.51	1.7	6.023
Intercept:	0.781	Peak 3:	5182	1.4	484.4
			Diam (nm)	% Intensity	Width (nm)
Record: 2					
Z-average(nm):	169.4	Peak 1:	223.3	97.0	140.8
PdI:	0.322	Peak 2:	4766	3.00	747.0
Intercept:	0.794	Peak 3:	0.000	0.00	0.000
			Diam (nm)	% Intensity	Width (nm)
Record: 3					
Z-average(nm):	173.0	Peak 1:	217.6	96.4	135.2
PdI:	0.277	Peak 2:	4637	3.6	818.7
Intercept:	0.802	Peak 3:	0.000	0.00	0.000

Z-Average: 171.32 ± 6.02 (nm)

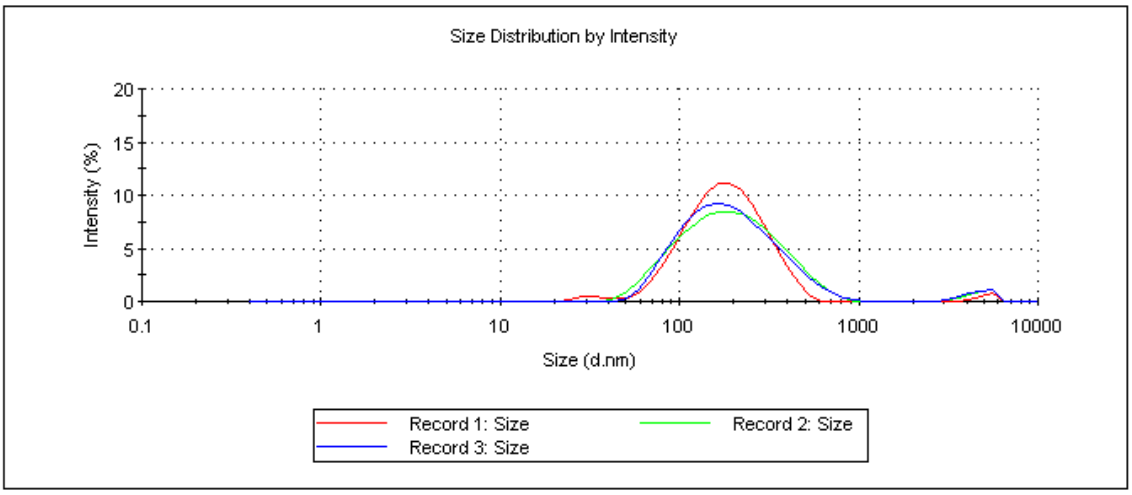

Figure B23. Iron particles size distribution for the phosphate dosage of 2.5 mg/L

Table B18. Effect of phosphate dosage (2.5 mg/L) on iron particles size distribution in $NaHCO_3$ buffered synthetic water (pH 6.5, 21 ± 1° C).

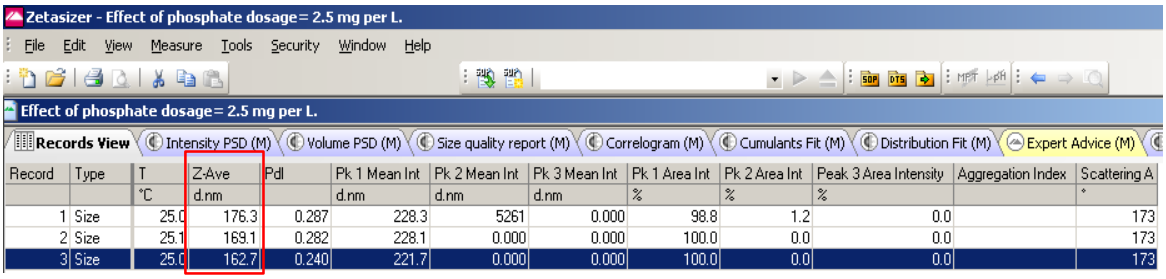

Record	Type	T	Z-Ave	PdI	Pk 1 Mean Int	Pk 2 Mean Int	Pk 3 Mean Int	Pk 1 Area Int	Pk 2 Area Int	Peak 3 Area Intensity	Aggregation Index	Scattering A
		°C	d.nm		d.nm	d.nm	d.nm	%	%	%		°
1	Size	25.0	176.3	0.287	228.3	5261	0.000	98.8	1.2	0.0		173
2	Size	25.1	169.1	0.282	228.1	0.000	0.000	100.0	0.0	0.0		173
3	Size	25.0	162.7	0.240	221.7	0.000	0.000	100.0	0.0	0.0		173

Record: 1			Diam (nm)	% Intensity	Width (nm)
Z-average(nm):	176.3	Peak 1:	228.3	98.8	132.3
PdI:	0.278	Peak 2:	5261	1.2	433.9
Intercept:	0.803	Peak 3:	0.000	0.00	0.000

Record: 2			Diam (nm)	% Intensity	Width (nm)
Z-average(nm):	169.1	Peak 1:	228.1	100.0	130.6
PdI:	0.282	Peak 2:	0.000	0.00	0.000
Intercept:	0.803	Peak 3:	0.000	0.00	0.000

Record: 3			Diam (nm)	% Intensity	Width (nm)
Z-average(nm):	162.7	Peak 1:	221.7	100.0	126.4
PdI:	0.240	Peak 2:	0.000	0.00	0.000
Intercept:	0.800	Peak 3:	0.000	0.00	0.000

Z-Average: 171.70 ± 7.79 (nm)

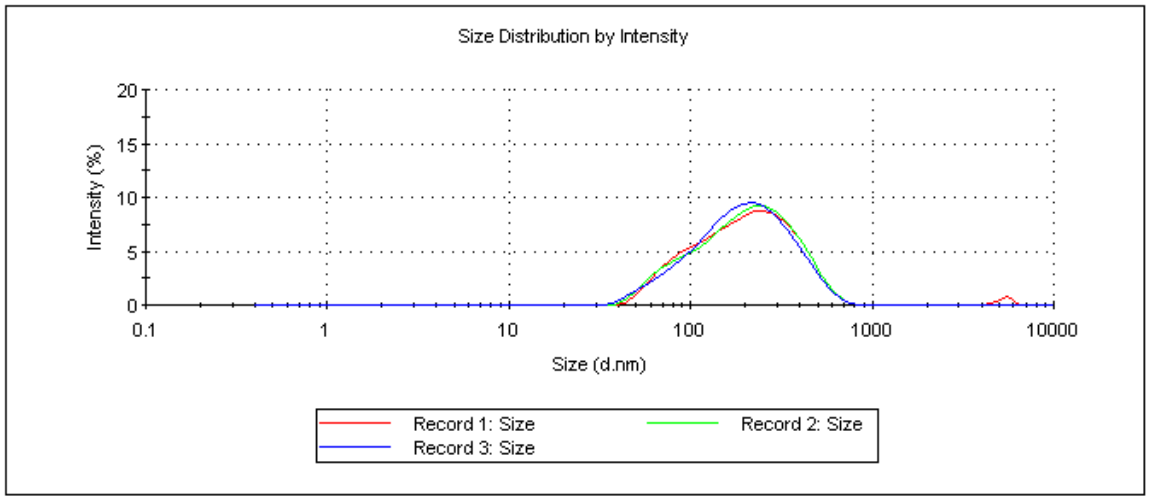

Figure B24. Iron particles size distribution for the phosphate dosage of 2.5 mg/L

The grand average particle size (No of observation= 6) in control system= 169.88 ± 6.43 nm

Table B19. Effect of phosphate dosage (5.0 mg/L) on iron particles size distribution in $NaHCO_3$ buffered synthetic water (pH 6.5, 21 ± 1° C).

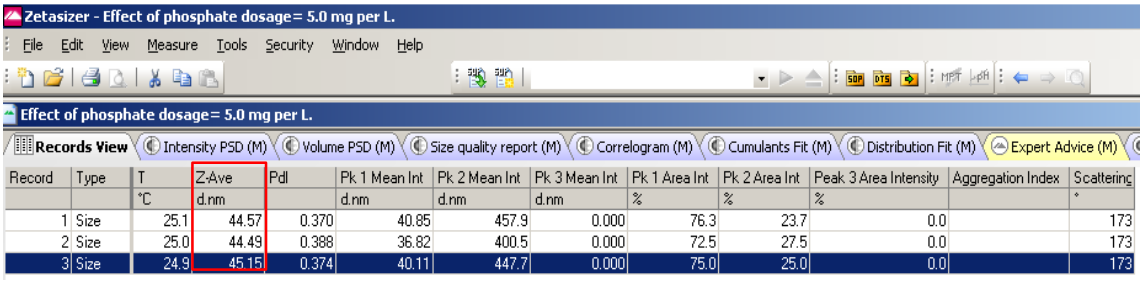

Record	Type	T	Z-Ave	PdI	Pk 1 Mean Int	Pk 2 Mean Int	Pk 3 Mean Int	Pk 1 Area Int	Pk 2 Area Int	Peak 3 Area Intensity	Aggregation Index	Scattering
		°C	d.nm		d.nm	d.nm	d.nm	%	%	%		°
1	Size	25.1	44.57	0.370	40.85	457.9	0.000	76.3	23.7	0.0		173
2	Size	25.0	44.49	0.388	36.82	400.5	0.000	72.5	27.5	0.0		173
3	Size	24.9	45.15	0.374	40.11	447.7	0.000	75.0	25.0	0.0		173

Record: 1			Diam (nm)	% Intensity	Width (nm)
Z-average(nm):	44.57	Peak 1:	40.85	76.3	18.17
PdI:	0.370	Peak 2:	457.9	23.7	212.1
Intercept:	0.851	Peak 3:	0.000	0.0	0.000

Record: 2			Diam (nm)	% Intensity	Width (nm)
Z-average(nm):	44.49	Peak 1:	36.82	72.5	12.32
PdI:	0.388	Peak 2:	400.5	27.5	168.1
Intercept:	0.851	Peak 3:	0.000	0.0	0.000

Record: 3			Diam (nm)	% Intensity	Width (nm)
Z-average(nm):	45.15	Peak 1:	40.11	75.0	16.86
PdI:	0.374	Peak 2:	447.7	25.0	206.2
Intercept:	0.846	Peak 3:	0.000	0.0	0.000

Z-Average: 43.97 ± 1.08 (nm)

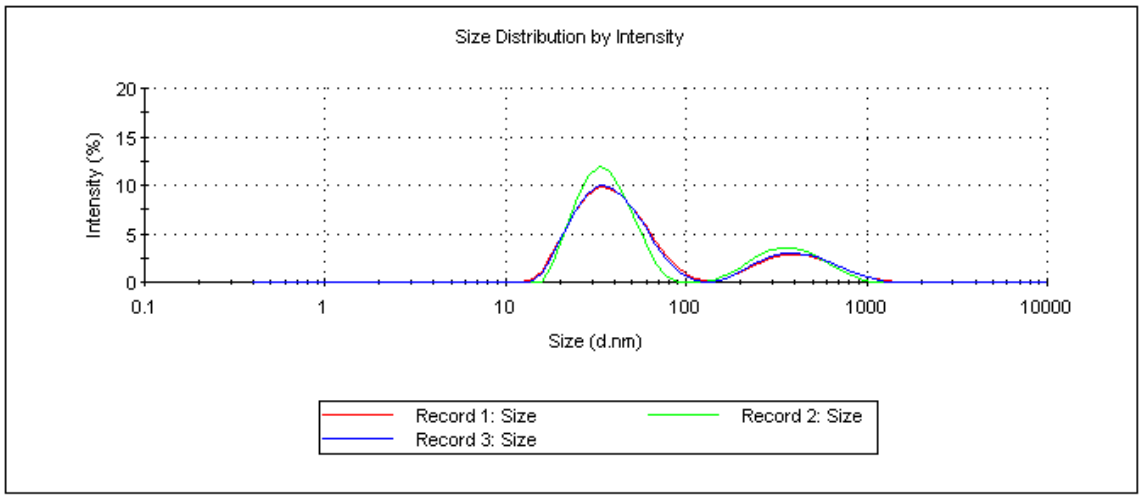

Figure B25. Iron particles size distribution for the phosphate dosage of 5.0 mg/L

Table B20. Effect of phosphate dosage (5.0 mg/L) on iron particles size distribution in $NaHCO_3$ buffered synthetic water (pH 6.5, 21 ± 1° C).

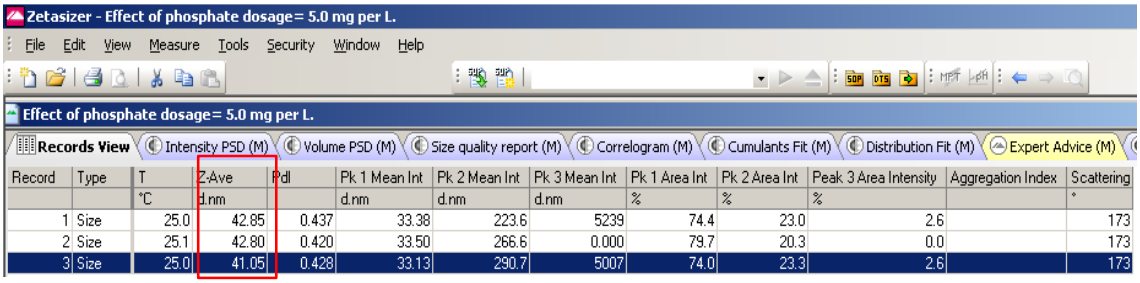

Record	Type	T	Z-Ave	PdI	Pk 1 Mean Int	Pk 2 Mean Int	Pk 3 Mean Int	Pk 1 Area Int	Pk 2 Area Int	Peak 3 Area Intensity	Aggregation Index	Scattering
		°C	d.nm		d.nm	d.nm	d.nm	%	%	%		°
1	Size	25.0	42.85	0.437	33.38	223.6	5239	74.4	23.0	2.6		173
2	Size	25.1	42.80	0.420	33.50	266.6	0.000	79.7	20.3	0.0		173
3	Size	25.0	41.05	0.428	33.13	290.7	5007	74.0	23.3	2.6		173

Record: 1			Diam (nm)	% Intensity	Width (nm)
Z-average(nm):	42.85	Peak 1:	33.38	74.4	10.66
PdI:	0.437	Peak 2:	223.6	23.0	73.23
Intercept:	0.909	Peak 3:	5239	2.6	450.6

Record: 2			Diam (nm)	% Intensity	Width (nm)
Z-average(nm):	42.80	Peak 1:	33.50	79.7	9.833
PdI:	0.420	Peak 2:	266.6	20.3	76.27
Intercept:	0.917	Peak 3:	0.000	0.0	0.000

Record: 3			Diam (nm)	% Intensity	Width (nm)
Z-average(nm):	41.05	Peak 1:	33.13	74.0	10.70
PdI:	0.428	Peak 2:	290.7	23.3	105.6
Intercept:	0.903	Peak 3:	5007	2.6	606.1

Z-Average: 42.23 ± 1.03 (nm)

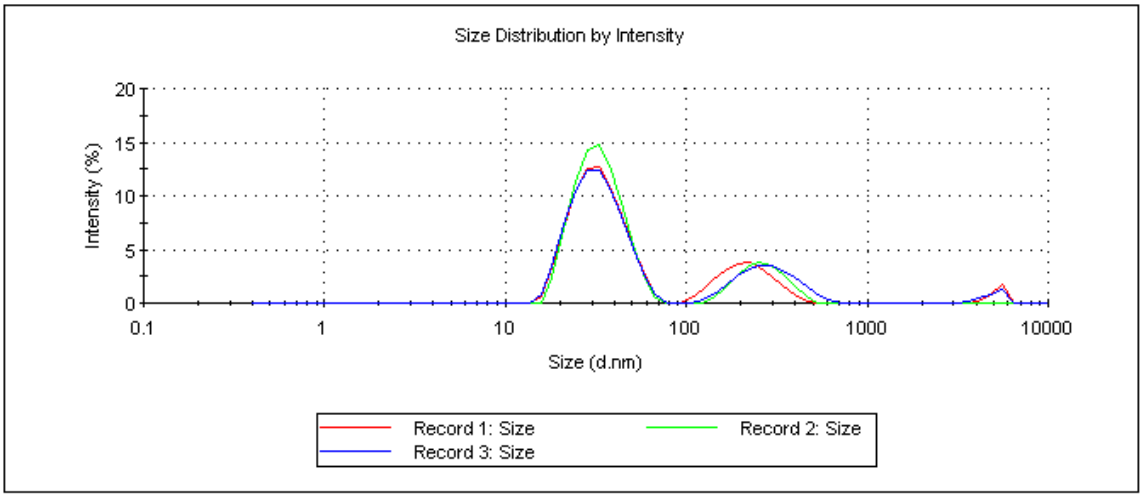

Figure B26. Iron particles size distribution for the phosphate dosage of 5.0 mg/L

The grand average particle size (No of observation= 6) in control system= 43.49 ± 1.53 nm

Table B21. Effect of phosphate dosage (7.5 mg/L) on iron particles size distribution in $NaHCO_3$ buffered synthetic water (pH 6.5, 21 ± 1° C).

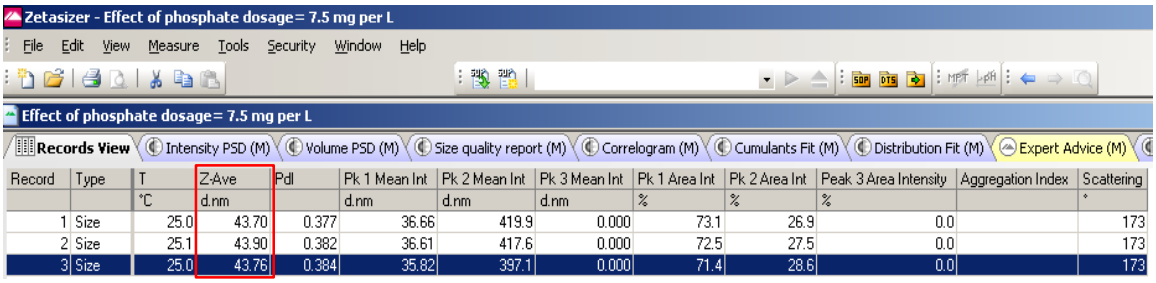

Record	Type	T	Z-Ave	PdI	Pk 1 Mean Int	Pk 2 Mean Int	Pk 3 Mean Int	Pk 1 Area Int	Pk 2 Area Int	Peak 3 Area Intensity	Aggregation Index	Scattering
		°C	d.nm		d.nm	d.nm	d.nm	%	%	%		°
1	Size	25.0	43.70	0.377	36.66	419.9	0.000	73.1	26.9	0.0		173
2	Size	25.1	43.90	0.382	36.61	417.6	0.000	72.5	27.5	0.0		173
3	Size	25.0	43.76	0.384	35.82	397.1	0.000	71.4	28.6	0.0		173

Record: 1			Diam (nm)	% Intensity	Width (nm)
Z-average(nm):	43.70	Peak 1:	36.66	73.1	13.21
PdI:	0.377	Peak 2:	419.9	26.9	178.8
Intercept:	0.890	Peak 3:	0.000	0.0	0.000

Record: 2			Diam (nm)	% Intensity	Width (nm)
Z-average(nm):	43.90	Peak 1:	36.61	72.5	13.50
PdI:	0.382	Peak 2:	417.6	27.5	188.3
Intercept:	0.890	Peak 3:	0.000	0.0	0.000

Record: 3			Diam (nm)	% Intensity	Width (nm)
Z-average(nm):	43.76	Peak 1:	35.82	71.4	12.98
PdI:	0.384	Peak 2:	397.1	28.6	181.3
Intercept:	0.889	Peak 3:	0.000	0.0	0.000

Z-Average: 43.34 ± 2.30 (nm)

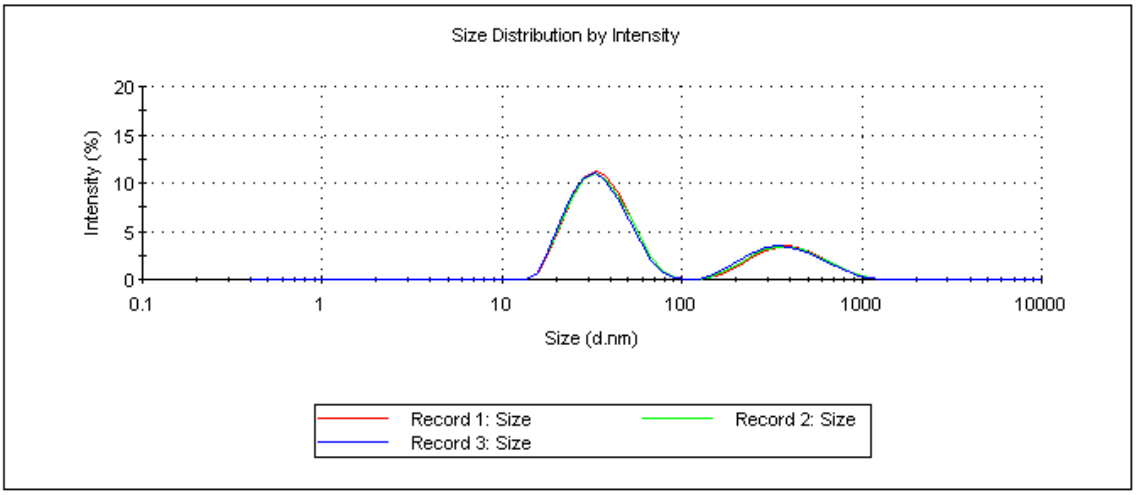

Figure B27. Iron particles size distribution for the phosphate dosage of 7.5 mg/L

Table B22. Effect of phosphate dosage (7.5 mg/L) on iron particles size distribution in $NaHCO_3$ buffered synthetic water (pH 6.5, 21 ± 1° C).

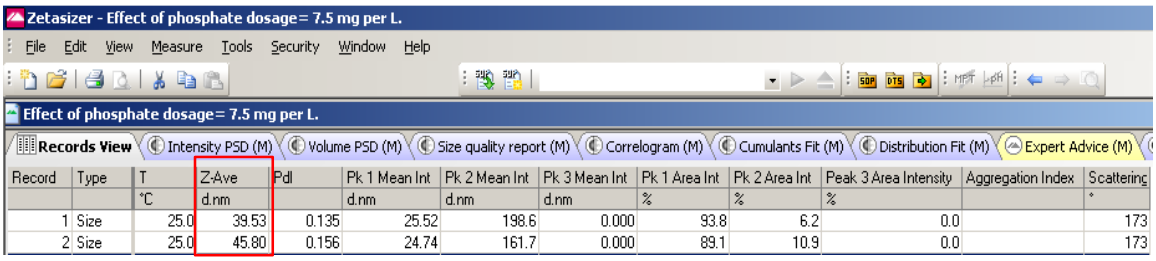

Record	Type	T	Z-Ave	PdI	Pk 1 Mean Int	Pk 2 Mean Int	Pk 3 Mean Int	Pk 1 Area Int	Pk 2 Area Int	Peak 3 Area Intensity	Aggregation Index	Scattering
		°C	d.nm		d.nm	d.nm	d.nm	%	%	%		°
1	Size	25.0	39.53	0.135	25.52	198.6	0.000	93.8	6.2	0.0		173
2	Size	25.0	45.80	0.156	24.74	161.7	0.000	89.1	10.9	0.0		173

Record: 1			Diam (nm)	% Intensity	Width (nm)
Z-average(nm):	39.53	Peak 1:	25.52	93.8	6.966
PdI:	0.136	Peak 2:	198.6	6.2	42.78
Intercept:	0.888	Peak 3:	0.000	0.0	0.000

			Diam (nm)	% Intensity	Width (nm)
Record: 2					
Z-average(nm):	45.80	Peak 1:	24.74	89.1	7.067
PdI:	0.156	Peak 2:	161.7	10.9	38.14
Intercept:	0.886	Peak 3:	0.000	0.0	0.000

Z-Average: 42.67 ± 4.43 (nm)

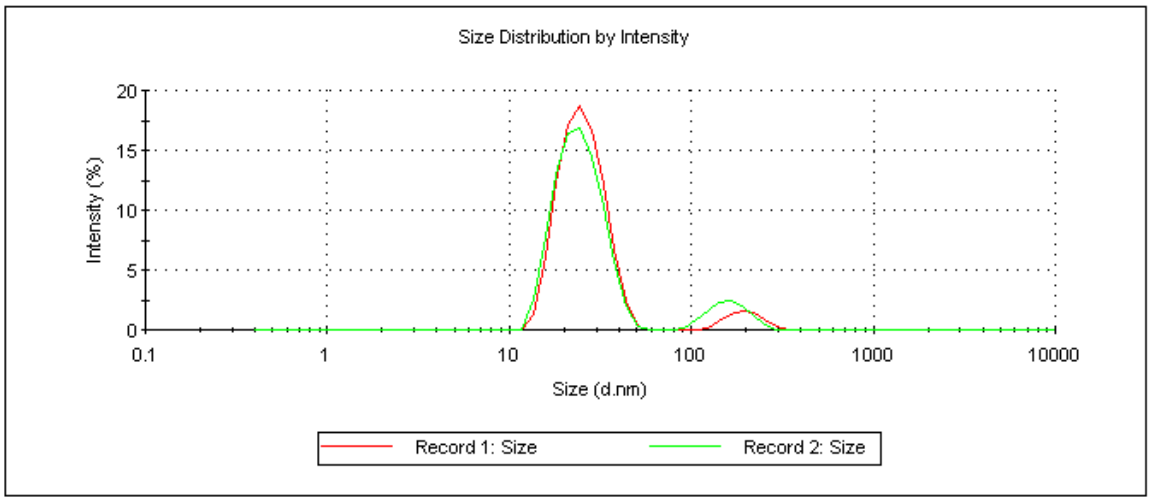

Fig. B28. Iron particles size distribution for phosphate dosage= 7.5 mg/L

The grand average particle size (No of observation= 5) in control system= 43.34 ± 2.30 nm

Table B23. Effect of phosphate dosage (10.0 mg/L) on iron particles size distribution in $NaHCO_3$ buffered synthetic water (pH 6.5, 21 ± 1° C).

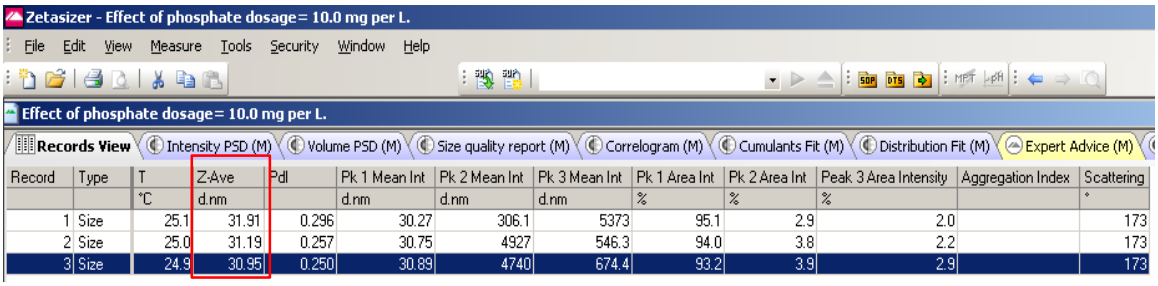

Record	Type	T	Z-Ave	PdI	Pk 1 Mean Int	Pk 2 Mean Int	Pk 3 Mean Int	Pk 1 Area Int	Pk 2 Area Int	Peak 3 Area Intensity	Aggregation Index	Scattering
		°C	d.nm		d.nm	d.nm	d.nm	%	%	%		°
1	Size	25.1	31.91	0.296	30.27	306.1	5373	95.1	2.9	2.0		173
2	Size	25.0	31.19	0.257	30.75	4927	546.3	94.0	3.8	2.2		173
3	Size	24.9	30.95	0.250	30.89	4740	674.4	93.2	3.9	2.9		173

Record: 1			Diam (nm)	% Intensity	Width (nm)
Z-average(nm):	31.91	Peak 1:	30.27	95.1	9.659
PdI:	0.296	Peak 2:	306.1	2.9	69.96
Intercept:	0.907	Peak 3:	5373	2.0	326.6

Record: 2			Diam (nm)	% Intensity	Width (nm)
Z-average(nm):	31.19	Peak 1:	30.75	94.0	9.803
PdI:	0.257	Peak 2:	4927	3.8	660.0
Intercept:	0.904	Peak 3:	546.3	2.2	147.7

Record: 3			Diam (nm)	% Intensity	Width (nm)
Z-average(nm):	30.95	Peak 1:	30.89	93.2	10.22
PdI:	0.250	Peak 2:	4740	3.9	769.0
Intercept:	0.903	Peak 3:	674.4	2.9	205.3

Z-Average: 31.27 ± 0.59 (nm)

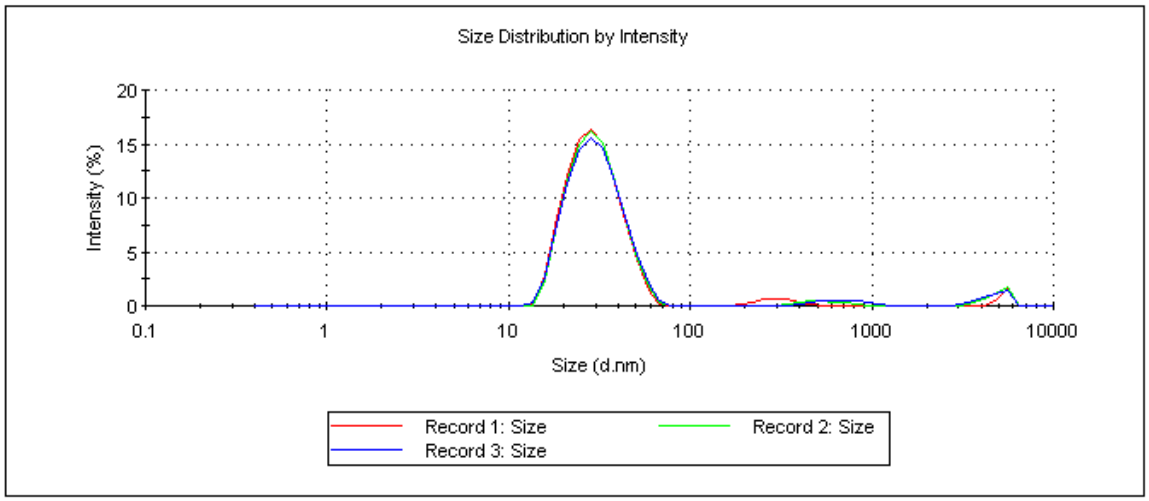

Figure B29. Iron particles size distribution for phosphate dosage= 10.0 mg/L

Table B24. Effect of phosphate dosage= 10.0 mg/L on iron particles size distribution in $NaHCO_3$ buffered synthetic water (pH 6.5, 21 ± 1° C).

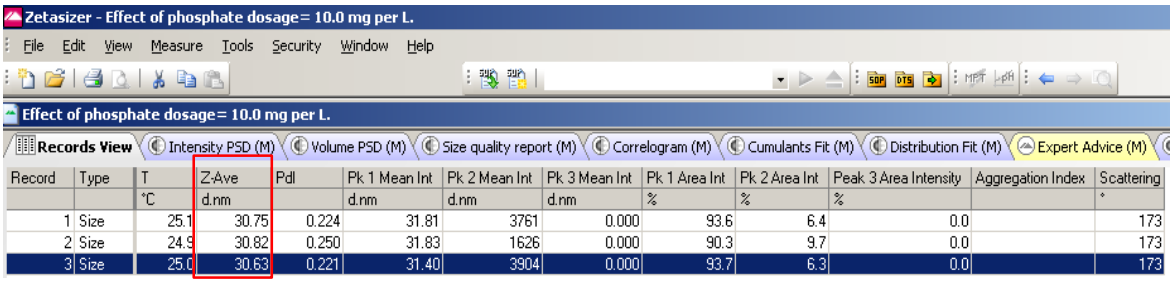

Record	Type	T	Z-Ave	PdI	Pk 1 Mean Int	Pk 2 Mean Int	Pk 3 Mean Int	Pk 1 Area Int	Pk 2 Area Int	Peak 3 Area Intensity	Aggregation Index	Scattering
		°C	d.nm		d.nm	d.nm	d.nm	%	%	%		°
1	Size	25.1	30.75	0.224	31.81	3761	0.000	93.6	6.4	0.0		173
2	Size	24.9	30.82	0.250	31.83	1626	0.000	90.3	9.7	0.0		173
3	Size	25.0	30.63	0.221	31.40	3904	0.000	93.7	6.3	0.0		173

Record: 1			Diam (nm)	% Intensity	Width (nm)
Z-average(nm):	30.75	Peak 1:	31.81	93.6	11.02
PdI:	0.224	Peak 2:	3761	6.4	1152
Intercept:	0.901	Peak 3:	0.000	0.0	0.000

Record: 2			Diam (nm)	% Intensity	Width (nm)
Z-average(nm):	30.82	Peak 1:	31.83	90.3	11.85
PdI:	0.250	Peak 2:	1626	9.7	901.1
Intercept:	0.904	Peak 3:	0.000	0.0	0.000

			Diam (nm)	% Intensity	Width (nm)
Record: 3					
Z-average(nm):	30.63	Peak 1:	31.40	93.7	10.55
PdI:	0.221	Peak 2:	3904	6.3	1112
Intercept:	0.901	Peak 3:	0.000	0.0	0.000

Z-Average: 30.73 ± 0.10 (nm)

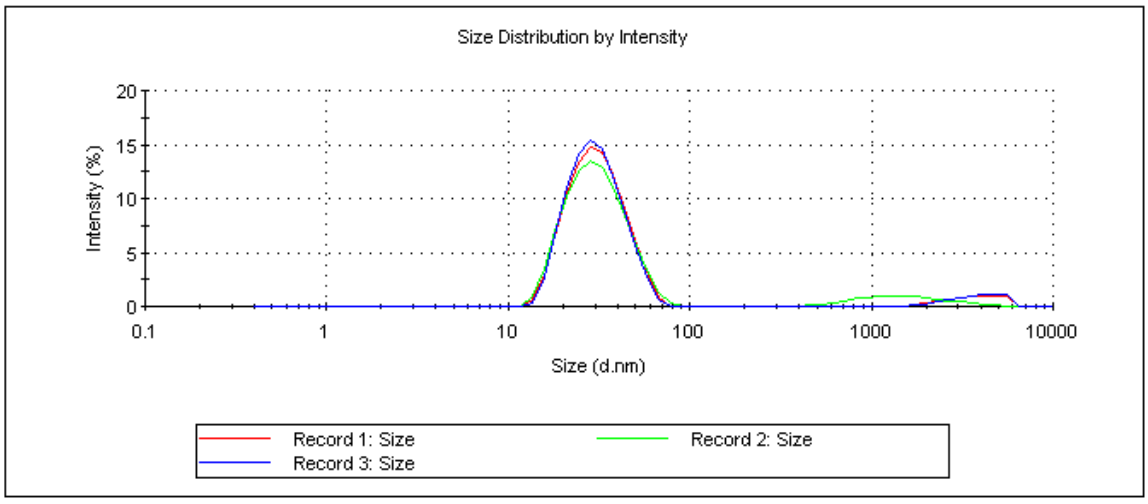

Figure B30. Iron particles size distribution for phosphate dosage= 10.0 mg/L

The grand average particle size (No of observation= 6) in control system= 31.16 ± 0.59 nm.

APPENDIX C. Chapter 6 Raw data and supplementary information

Table C1. Gas chromatograph (GC) operating conditions for HAAs analysis

Parameter	Description
System	: Varian CP-3800 GC
Auto sampler	: Varian CP-8400
Column	: VF-5 capillary column
Injector Temperature	: 200°C
Detector Temperature	: 300°C
Temperature Program	: 35°C for 10 min
	2.5°C/min temperature ramp to 65 °C
	10°C/min temperature ramp to 85 °C
	20°C/min temperature ramp to 205 °C, hold for 7 min
Carrier Gas	: Helium
Flow Rate	: 1.2 ml/min at 35°C

Table C2. Gas chromatograph (GC) operating conditions for THMs analysis

Parameter	Description
System	: Varian CP-3800 GC
Auto sampler	: Varian CP-8400
Column	: VF-5 capillary column
Injector temperature	: 220 °C
Detector temperature	: 320 °C
Injection volume	: 1 µL
Flow rate	: 1 mL/min
Temperature program	: 50 °C for 7 min
	5 °C/min temperature ramp to 115 °C
	50 °C/min temperature ramp to 295 °C, held for 0.5 min
Carrier gas	: Helium

Table C3. Method of detection limit (MDL) for nine haloacetic acids (HAAs)

No	HAA Species	Chemical formula	MDL
1	Monochloroacetic acid (MCAA)	$CH_2ClCOOH$	4.0 µg/L
2	Monobromoacetic acid (BCAA)	$CH_2BrCOOH$	2.5 µg/L
3	Dichloroacetic acid (DCAA)	$CHCl_2COOH$	2.0 µg/L
4	Trichloroacetic acid (TCAA)	Cl_3COOH	1.5 µg/L
5	Bromochloroacetic acid (BCAA)	$CHBrClCOOH$	1.5 µg/L
6	Dibromoacetic acid (DBAA)	$CHBr_2COOH$	1.0 µg/L
7	Bromodichloroacetic acid (BDCAA)	$CBrCl_2COOH$	2.0 µg/L
8	Chlorodibromoacetic acid (CDBAA)	$CBr_2ClCOOH$	3.2 µg/L
9	Tribromoacetic acid (TBAA)	CBr_3COOH	8.5 µg/L

Table C4. Method of detection limit (MDL) for nine trihalomethanes (THMs).

No	THM Species	Chemical formula	MDL
1	Chloroform (TCM)	$CHCl_3$	5.50 µg/L
2	Dichlorobromomethane (BDCM)	$CHBrCl_2$	2.50 µg/L
3	Dibromochloromethane (CDBM)	$CHBr_2Cl$	2.50 µg/L
9	Bromoform (TBM)	$CHBr_3$	3.00 µg/L

Effect of Fe(II) ions concentration in the formation HAAs and their speciation in synthetic water (chlorine to carbon ratio 0.79, pH 6.5, 21 ± 1 °C)

Table C5. The effect of initial Fe(II) ions concentrations (mg/L) for the reaction period of 3.5 h in the formation and speciation of HAAs in synthetic water.

Sl. No.	HAA species	Average HAAs conc. in presence of different dosages of Fe(II) ions					
		Fe(II) ions (0.0 g/L)	Fe(II) ions (0.35 mg/L)	Fe(II) ions (0.7 mg/L)	Fe(II) ions (1.5 mg/L)	Fe(II) ions (2.0 mg/L)	Fe(II) ions (3.0 mg/L)
1	MCAA	1.32	0.00	0.00	0.00	0.00	0.00
2	MBAA	0.38	0.00	0.00	0.40	0.00	0.00
3	DCAA	38.49	24.23	13.98	15.24	10.95	10.45
4	TCAA	38.18	23.61	17.40	16.40	12.77	12.91
5	BCAA	0.86	0.00	0.32	0.34	0.31	0.33
6	DBAA	0.20	0.00	0.00	0.00	0.00	0.00
7	BDCAA	2.35	0.00	0.00	0.00	0.00	0.00
8	CDBAA	0.00	0.00	0.00	0.00	0.00	0.00
9	TBAA	0.00	0.00	0.00	0.00	0.00	0.00
	Total HAAs =	81.79	47.84	31.69	32.38	24.02	23.70

Table C6. The effect of initial Fe(II) ions concentrations (mg/L) for the reaction period of 24 h in the formation and speciation of HAAs in synthetic water samples.

Sl. No.	HAA species	Average HAAs conc. in presence of different dosages of Fe(II) ions					
		Fe(II) ions (0.0 g/L)	Fe(II) ions (0.35 mg/L)	Fe(II) ions (0.7 mg/L)	Fe(II) ions (1.5 mg/L)	Fe(II) ions (2.0 mg/L)	Fe(II) ions (3.0 mg/L)
1	MCAA	1.22	0.00	0.00	0.00	0.00	0.00
2	MBAA	0.35	0.00	0.00	0.00	0.00	0.48
3	DCAA	42.16	23.34	14.95	14.97	12.38	13.26
4	TCAA	41.07	22.66	18.31	15.11	13.96	16.00
5	BCAA	0.98	0.33	0.33	0.33	0.31	0.36
6	DBAA	0.49	0.00	0.52	0.00	0.00	0.50
7	BDCAA	1.13	0.00	1.67	0.00	0.00	0.00
8	CDBAA	0.00	0.00	0.00	0.00	0.00	0.00
9	TBAA	0.92	0.00	0.00	0.00	0.00	0.00
	Total HAAs =	88.32	46.33	35.78	30.41	26.64	30.61

Table C7. The effect of initial Fe(II) ions concentrations (mg/L) for the reaction period of 48 h in the formation and speciation of HAAs in synthetic water samples.

Sl. No.	HAA species	Average HAAs conc. in presence of different dosages of Fe(II) ions					
		Fe(II) ions (0.0 g/L)	Fe(II) ions (0.35 mg/L)	Fe(II) ions (0.7 mg/L)	Fe(II) ions (1.5 mg/L)	Fe(II) ions (2.0 mg/L)	Fe(II) ions (3.0 mg/L)
1	MCAA	0.00	0.00	0.00	0.00	3.17	0.00
2	MBAA	0.00	0.00	0.00	0.00	0.69	0.37
3	DCAA	37.17	24.26	17.26	14.37	13.47	13.04
4	TCAA	55.70	23.46	22.45	14.80	14.12	16.01
5	BCAA	0.00	0.32	0.71	0.32	0.73	0.34
6	DBAA	0.00	0.00	0.00	0.00	0.00	0.39
7	BDCAA	0.00	0.00	0.00	0.00	0.00	0.00
8	CDBAA	0.00	0.00	0.00	0.00	0.00	0.00
9	TBAA	0.00	0.00	0.00	0.00	0.00	0.00
	Total HAAs =	92.87	48.05	40.42	29.49	32.18	30.16

Table C8. The effect of initial Fe(II) ions concentrations (mg/L) for the reaction period of 84 h in the formation and speciation of HAAs in synthetic water samples.

Sl. No.	HAA species	Average HAAs conc. in presence of different dosages of Fe(II) ions					
		Fe(II) ions (0.0 g/L)	Fe(II) ions (0.35 mg/L)	Fe(II) ions (0.7 mg/L)	Fe(II) ions (1.5 mg/L)	Fe(II) ions (2.0 mg/L)	Fe(II) ions (3.0 mg/L)
1	MCAA	0.00	0.00	0.00	0.00	1.78	0.00
2	MBAA	0.00	0.00	0.00	0.00	0.57	0.21
3	DCAA	39.59	26.89	17.32	15.01	13.46	12.71
4	TCAA	59.16	26.08	22.40	15.45	14.66	16.03
5	BCAA	0.00	0.36	0.51	0.32	0.41	0.32
6	DBAA	0.00	0.00	0.00	0.00	0.00	0.22
7	BDCAA	0.00	0.00	0.60	0.00	0.00	0.00
8	CDBAA	0.00	0.00	0.00	0.00	0.00	0.00
9	TBAA	0.00	0.00	0.00	0.00	0.00	0.00
	Total HAAs =	98.75	53.34	41.01	30.79	30.88	29.49

Table C9. The effect of initial Fe(II) ions concentrations (mg/L) for the reaction period of 84 h in the formation and speciation of HAAs in synthetic water samples.

Sl. No.	HAA species	Average HAAs conc. in presence of different dosages of Fe(II) ions					
		Fe(II) ions (0.0 g/L)	Fe(II) ions (0.35 mg/L)	Fe(II) ions (0.7 mg/L)	Fe(II) ions (1.5 mg/L)	Fe(II) ions (2.0 mg/L)	Fe(II) ions (3.0 mg/L)
1	MCAA	0.00	0.00	0.00	0.00	0.00	0.00
2	MBAA	0.00	0.00	0.00	0.00	0.42	0.00
3	DCAA	42.58	30.26	17.40	15.87	13.45	12.29
4	TCAA	63.68	29.43	22.39	16.27	15.35	16.04
5	BCAA	0.00	0.40	0.44	0.32	0.00	0.30
6	DBAA	0.00	0.00	0.00	0.00	0.00	0.00
7	BDCAA	0.00	0.00	1.55	0.00	0.00	0.00
8	CDBAA	0.00	0.00	0.00	0.00	0.00	0.00
9	TBAA	0.00	0.00	0.00	0.00	0.00	0.00
	Total HAAs =	106.26	60.09	41.78	32.46	29.22	28.63

Two way ANOVA (analysis of variance) test

Table C10. Total HAAs concentration data (μg/L) in presence of different Fe(II) ions concentration for the different reaction time (h)

Fe(II) ions Conc. (mg/L)	Average HAAs formation (μg/L) for different reaction time (h)					Total
	4 (h)	24 (h)	48(h)	84 (h)	130(h)	
0.35	47.84	46.33	48.05	53.34	65.09	260.65
0.7	31.69	35.78	40.42	41.01	41.78	190.68
1.5	32.38	30.41	29.49	30.80	32.46	155.53
2.0	24.02	26.64	32.18	30.88	29.22	142.95
3.0	23.70	30.61	29	28.84	28.63	140.78
Total	159.63	169.77	179.14	184.87	197.19	890.60

Table C11. Summary for sum, average and variance for HAAs formation data

SUMMARY	*Count*	*Sum*	*Average*	*Variance*
Row 1: HAAs concentration (µg/L)	5	260.65	52.13	59.51
Row 2: HAAs concentration (µg/L)	5	190.68	38.14	18.47
Row 3: HAAs concentration (µg/L)	5	155.53	31.11	1.66
Row 4: HAAs concentration (µg/L)	5	142.95	28.59	10.80
Row 5: HAAs concentration (µg/L)	5	140.78	28.16	6.82
Column 1: HAAs concentration (µg/L)	5	159.63	31.93	95.94
Column 2: HAAs concentration (µg/L)	5	169.77	33.95	58.47
Column 3: HAAs concentration (µg/L)	5	179.14	35.83	67.61
Column 4: HAAs concentration (µg/L)	5	184.87	36.97	106.36
Column 5: HAAs concentration (µg/L)	5	197.19	39.44	233.32

Sum square (SS):

$$\mathrm{SS}_{treatment} = \sum_{i=1}^{a} \frac{y_{i.}^2}{b} - \frac{y_{..}^2}{ab}$$

$$\mathrm{SS}_{treatment} = \frac{(260.65)^2 + (190.68)^2 + (155.53)^2 + (142.95)^2 + (140.78)^2}{5} - \frac{(890.6)^2}{25}$$

$$\mathrm{SS}_{treatment} = 2022.16$$

$$\mathrm{SS}_{blocks} = \sum_{j=1}^{b} \frac{y_{.j}^2}{b} - \frac{y_{..}^2}{ab}$$

$$\mathrm{SS}_{blocks} = \frac{(159.63)^2 + (169.77)^2 + (179.14)^2 + (184.87)^2 + (197.2)^2}{5} - \frac{(890.6)^2}{25}$$

$$\mathrm{SS}_{blocks} = 164.35$$

$$\mathrm{SS}_{Total} = \sum_{i=1}^{a} \sum_{j=1}^{b} y_{ij}^2 - \frac{y_{..}^2}{ab}$$

$$\mathrm{SS}_{Total} = (47.84)^2 + (31.69)^2 + \cdots\cdots\cdots + (28.63)^2 - \frac{(890.6)^2}{25} = 2411.19$$

$$\mathrm{SS}_{Error} = SS_{Total} - SS_{treatment} - SS_{blocks}$$

$$SS_{Error} = 2411.19 - 2022.16 - 164.35 = 224.68$$

Mean square (MS):

$$\mathrm{MS}_{treatment} = \frac{\mathrm{SS}_{treatment}}{a-1} = 505.54$$

$$\mathrm{MS}_{blocks} = \frac{\mathrm{SS}_{blocks}}{b-1} = 41.09$$

$$\mathrm{MS}_{Error} = \frac{\mathrm{SS}_{Error}}{(a-1)(b-1)} = 14.04$$

Table C12. ANOVA (analysis of variance) test for HAAs formation study.

Source of Variation	*SS*	*df*	*MS*	*F*	*P-value*	*F crit*
Fe(II) ions conc. (treatment)	2022.16	4	505.54	36.001	< 0.0001	3.007
Reaction time (blocks)	164.35	4	41.09	2.926	0.0542	3.007
Error	224.68	16	14.04			
Total	2411.19	24				

Comments:
For Fe(II) ions concentration, $F_{obs} > F_{crit}$ (36.001 > 3.007). Therefore, it could be said that changes of Fe(II) ions concentrations in solution, HAAs formation significantly changed at a 95 % confidence level. However, reaction time does not have significant impact as well $F_{obs} < F_{crit}$ (32.926 < 3.007).

THMs formation study

Table C13. Effect of Fe(II) ions and reaction them (h) on trihalomethane (THMs) formation in synthetic water ((chlorine to carbon ratio 0.79, pH 6.5, 21 ± 1 °C))

Sl No.	Presence of Fe(II) ions (mg/L)	Average THMs (ug/L) conc. for different reaction time (h)				
		3.5 h	24 h	48 h	84 h	130 h
1	0 mg/L	26.84	31.72	35.23	36.58	38.34
2	0.35 mg/L	20.53	23.77	23.14	23.95	25.01
3	0.7 mg/L	16.39	18.55	17.69	19.89	22.76
4	1.5 mg/L	17.06	18.14	16.71	19.39	22.89
5	2.0 mg/L	17.10	18.67	16.04	16.74	17.65
6	3.0 mg/L	14.74	16.14	14.16	14.63	15.23

Table C14. Summary for sum, average and variance for HAAs formation data

SUMMARY	*Count*	*Sum*	*Average*	*Variance*
Row 1: THMs concentration (µg/L)	5	116.40	23.28	2.83
Row 2: THMs concentration (µg/L)	5	95.28	19.06	5.91
Row 3: THMs concentration (µg/L)	5	94.18	18.84	6.22
Row 4: THMs concentration (µg/L)	5	86.21	17.24	0.98
Row 5: THMs concentration (µg/L)	5	74.91	14.98	0.56
Column 1: THMs concentration (µg/L)	5	85.82	17.16	4.44
Column 2: THMs concentration (µg/L)	5	95.28	19.06	8.00
Column 3: THMs concentration (µg/L)	5	87.74	17.55	11.42
Column 4: THMs concentration (µg/L)	5	94.60	18.92	12.41
Column 5: THMs concentration (µg/L)	5	103.54	20.71	16.71

Sum square (SS):

$$\mathrm{SS}_{treatment} = \sum_{i=1}^{a} \frac{y_{i.}^2}{b} - \frac{y_{..}^2}{ab}$$

$$\mathrm{SS}_{treatment} = \frac{(116.4)^2 + (95.28)^2 + (94.18)^2 + (86.21)^2 + (74.91)^2}{5} - \frac{(466.98)^2}{25}$$

$$\mathrm{SS}_{treatment} = 185.39$$

$$\mathrm{SS}_{blocks} = \sum_{j=1}^{b} \frac{y_{.j}^2}{b} - \frac{y_{..}^2}{ab}$$

$$\mathrm{SS}_{blocks} = \frac{(85.82)^2 + (95.28)^2 + (87.74)^2 + (94.60)^2 + (103.54)^2}{5} - \frac{(466.98)^2}{25} = 39.4$$

$$\mathrm{SS}_{Total} = \sum_{i=1}^{a} \sum_{j=1}^{b} y_{ij}^2 - \frac{y_{..}^2}{ab}$$

$$\mathrm{SS}_{Total} = (20.53)^2 + (16.39)^2 + \cdots\cdots\cdots + (15.23)^2 - \frac{(466.98)^2}{25} = 251.39$$

$$\mathrm{SS}_{Error} = SS_{Total} - SS_{treatment} - SS_{blocks} = 26.55$$

Mean square (MS):

$$\mathrm{MS}_{treatment} = \frac{\mathrm{SS}_{treatment}}{a-1} = 46.35$$

$$\mathrm{MS}_{blocks} = \frac{\mathrm{SS}_{blocks}}{b-1} = 9.86$$

$$\mathrm{MS}_{Error} = \frac{\mathrm{SS}_{Error}}{(a-1)(b-1)} = 1.66$$

Table C15. ANOVA (analysis of variance) test for THMs formation study.

Source of Variation	*SS*	*df*	*MS*	*F*	*P-value*	*F crit*
Fe(II) ions conc. (treatment)	185.39	4	46.35	27.93	0.0000	3.007
Reaction time (blocks)	39.45	4	9.86	5.94	0.00397	3.007
Error	26.55	16	1.66			
Total	251.39	24				

Comments: For Fe(II) ions concentration, $F_{obs} > F_{crit}$ (27.93 > 3.007) and for reaction time , $F_{obs} > F_{crit}$ (5.94 > 3.007) . It could be said that changes of Fe(II) ions concentrations in solution and reaction, HAAs formation significantly changed at a 95 % confidence level.

Effect of PO_4 dosage (1.5 mg/L) along with different dosages of Fe(II) ions in synthetic water (chlorine to carbon ratio 0.79, pH 6.5, 21 ± 1 °C).

Table C16. The effect of PO_4 dosage (1.5 mg/L) along with different dosages of Fe(II) ions for the reaction of the reaction period of 0.35 h in the formation and speciation of HAAs.

Sl. No.	HAA species	Average HAAs conc. in presence of different dosages of Fe(II) ions					
		Fe(II) ions (0.0 g/L)	Fe(II) ions (0.35 mg/L)	Fe(II) ions (0.7 mg/L)	Fe(II) ions (1.5 mg/L)	Fe(II) ions (2.0 mg/L)	Fe(II) ions (3.0 mg/L)
1	MCAA	1.32	1.72	0.00	0.00	0.00	0.00
2	MBAA	0.38	0.00	0.00	0.00	0.00	0.00
3	DCAA	38.49	22.18	16.32	10.66	9.34	8.27
4	TCAA	38.18	21.44	15.03	10.98	8.08	8.71
5	BCAA	0.86	0.37	0.34	0.32	0.33	0.00
6	DBAA	0.20	0.53	0.00	0.00	0.00	0.00
7	BDCAA	2.35	1.59	0.00	0.00	0.00	0.00
8	CDBAA	0.00	0.00	0.00	0.00	0.00	0.00
9	TBAA	0.00	0.00	0.00	0.00	0.00	0.00
	Total HAAs =	81.79	47.84	31.69	21.95	17.74	16.98

Table C17. The effect of PO_4 dosage (1.5 mg/L) along with different dosages of Fe(II) ions for the reaction of the reaction period of 24 h in the formation and speciation of HAAs.

Sl. No.	HAA species	Average HAAs conc. in presence of different dosages of Fe(II) ions					
		Fe(II) ions (0.0 g/L)	Fe(II) ions (0.35 mg/L)	Fe(II) ions (0.7 mg/L)	Fe(II) ions (1.5 mg/L)	Fe(II) ions (2.0 mg/L)	Fe(II) ions (3.0 mg/L)
1	MCAA	1.22	0.00	0.00	0.00	0.00	0.04
2	MBAA	0.35	0.00	0.00	0.00	0.00	0.00
3	DCAA	42.16	22.19	14.38	10.22	9.67	10.01
4	TCAA	41.07	20.96	12.75	10.06	8.25	9.89
5	BCAA	0.98	0.33	0.35	0.32	0.32	0.34
6	DBAA	0.49	0.00	0.00	0.00	0.00	0.53
7	BDCAA	1.13	0.00	0.00	0.00	0.00	0.00
8	CDBAA	0.00	0.00	0.00	0.00	0.00	0.00
9	TBAA	0.92	0.00	0.00	0.00	0.00	0.00
	Total HAAs =	88.32	43.49	27.47	20.60	18.24	20.80

Table C18. The effect of PO_4 dosage (1.5 mg/L) along with different dosages of Fe(II) ions for the reaction of the reaction period of 48 h in the formation and speciation of HAAs.

Sl. No.	HAA species	Average HAAs conc. in presence of different dosages of Fe(II) ions					
		Fe(II) ions (0.0 g/L)	Fe(II) ions (0.35 mg/L)	Fe(II) ions (0.7 mg/L)	Fe(II) ions (1.5 mg/L)	Fe(II) ions (2.0 mg/L)	Fe(II) ions (3.0 mg/L)
1	MCAA	0.00	0.00	0.00	0.00	0.00	0.00
2	MBAA	0.00	0.00	0.00	0.00	0.00	0.00
3	DCAA	37.17	21.15	18.69	11.74	10.97	10.68
4	TCAA	55.70	19.82	16.51	10.32	11.32	9.44
5	BCAA	0.00	0.34	0.62	0.80	0.35	0.37
6	DBAA	0.00	0.00	0.00	0.00	0.00	0.00
7	BDCAA	0.00	0.00	0.00	0.00	0.00	0.00
8	CDBAA	0.00	0.00	0.00	0.00	0.00	0.00
9	TBAA	0.00	0.00	0.00	0.00	0.00	0.00
	Total HAAs =	92.87	41.31	35.82	22.85	22.64	20.49

Table C19. The effect of PO_4 dosage (1.5 mg/L) along with different dosages of Fe(II) ions for the reaction of the reaction period of 84 h in the formation and speciation of HAAs.

Sl. No.	HAA species	Average HAAs conc. in presence of different dosages of Fe(II) ions					
		Fe(II) ions (0.0 g/L)	Fe(II) ions (0.35 mg/L)	Fe(II) ions (0.7 mg/L)	Fe(II) ions (1.5 mg/L)	Fe(II) ions (2.0 mg/L)	Fe(II) ions (3.0 mg/L)
1	MCAA	0.00	0.16	0.00	0.00	0.00	0.00
2	MBAA	0.00	0.00	0.00	0.00	0.00	0.00
3	DCAA	39.59	14.30	12.36	8.07	6.99	8.65
4	TCAA	59.16	27.01	18.40	10.44	11.54	7.87
5	BCAA	0.00	0.50	0.63	0.73	0.47	0.36
6	DBAA	0.00	0.00	0.00	0.00	0.00	0.00
7	BDCAA	0.00	0.00	0.00	0.00	0.00	0.00
8	CDBAA	0.00	0.00	0.00	0.00	0.00	0.00
9	TBAA	0.00	0.00	0.00	0.00	0.00	0.00
	Total HAAs =	98.750	41.97	31.39	19.24	19.01	16.88

Table C20. The effect of PO_4 dosage (1.5 mg/L) along with different dosages of Fe(II) ions for the reaction of the reaction period of 130 h in the formation and speciation of HAAs.

Sl. No.	HAA species	Average HAAs conc. in presence of different dosages of Fe(II) ions					
		Fe(II) ions (0.0 g/L)	Fe(II) ions (0.35 mg/L)	Fe(II) ions (0.7 mg/L)	Fe(II) ions (1.5 mg/L)	Fe(II) ions (2.0 mg/L)	Fe(II) ions (3.0 mg/L)
1	MCAA	0.00	0.35	0.00	0.00	0.00	0.00
2	MBAA	0.00	0.00	0.00	0.00	0.00	0.00
3	DCAA	42.58	5.54	4.27	3.39	1.91	6.05
4	TCAA	63.68	36.20	20.81	10.60	11.82	5.87
5	BCAA	0.00	0.71	0.64	0.64	0.63	0.34
6	DBAA	0.00	0.00	0.00	0.00	0.00	0.00
7	BDCAA	0.00	0.00	0.00	0.00	0.00	0.00
8	CDBAA	0.00	0.00	0.00	0.00	0.00	0.00
9	TBAA	0.00	0.00	0.00	0.00	0.00	0.00
	Total HAAs =	106.26	42.80	25.72	14.63	14.37	12.26

Effect of PO_4 dosage in formation of HAAs

The paired Student's *t*- test between the effects of different dosages (0 to 3.0 mg/L) of Fe(II) ions alone and phosphate (1.5 mg/L) along with the different dosages Fe(II) ions on HAAs formation.

Table C21. The paired Student's *t*-test for the reaction period of 3.5 h in HAAs formation study

	54.230	*47.840*
Mean	29.703	22.090
Variance	52.208	45.738
Observations	4.000	4.000
Pooled Variance	48.973	
Hypothesized Mean Difference	0.000	
df	6.000	
t Stat	1.538	
P(T<=t) one-tail	0.087	
t Critical one-tail	1.943	
P(T<=t) two-tail	0.175	
t Critical two-tail	2.447	

Comments:
Here, $t_{stat} < t_{critic}$. Therefore, it could be concluded that the difference between the HAAs data in presence of Fe(II) ions and PO4 long along with Fe(II) ions for the reaction period of 3.5 h is not statistically significant at a 95% confidence level.

Table C22. The paired Student's *t*-test for the reaction period of 24 h in HAAs formation study.

	46.330	*43.490*
Mean	30.860	21.783
Variance	14.093	15.741
Observations	4.000	4.000
Pooled Variance	14.917	
Hypothesized Mean Difference	0.000	
df	6.000	
t Stat	3.324	
P(T<=t) one-tail	0.008	
t Critical one-tail	1.943	
P(T<=t) two-tail	0.016	
t Critical two-tail	2.447	

Comments: Here, $t_{stat} > t_{critic}$. The difference between two sets of data is significant (α = 0.05).

Table C23. The paired Student's *t*-test for the reaction period of 48 h in HAAs formation study

	48.050	*41.310*
Mean	34.623	25.440
Variance	29.952	49.064
Observations	4.000	4.000
Pooled Variance	39.508	
Hypothesized Mean Difference	0.000	
df	6.000	
t Stat	2.066	
P(T<=t) one-tail	0.042	
t Critical one-tail	1.943	
P(T<=t) two-tail	0.084	
t Critical two-tail	2.447	

Comments: Here, $t_{stat} > t_{critic}$. The difference between two sets of data is significant (α = 0.05).

Table C24. The paired Student's *t*-test for the reaction period of 84 h in HAAs formation study

	53.335	*41.966*
Mean	33.046	21.630
Variance	28.626	43.450
Observations	4.000	4.000
Pooled Variance	36.038	
Hypothesized Mean Difference	0.000	
df	6.000	
t Stat	2.689	
P(T<=t) one-tail	0.018	
t Critical one-tail	1.943	
P(T<=t) two-tail	0.036	
t Critical two-tail	2.447	

Comments; Here, $t_{stat} > t_{critic}$. The difference between two sets of data is significant (α = 0.05).

Table C25. The paired Student's *t*-test for the reaction period of 130 h in HAAs formation study

	60.090	*42.800*
Mean	33.023	16.745
Variance	36.921	36.927
Observations	4.000	4.000
Pooled Variance	36.924	
Hypothesized Mean Difference	0.000	
df	6.000	
t Stat	3.788	
P(T<=t) one-tail	0.005	
t Critical one-tail	1.943	
P(T<=t) two-tail	0.009	
t Critical two-tail	2.447	

Comments: Here, $t_{stat} > t_{critic}$. The difference between two sets of data is significant (α = 0.05).

Table C26. Summary of the paired Student's *t*-test for the effect of phosphate dosage on HAAs formation in synthetic water different reaction.

Statistical factors	Reaction time (h)				
	4 h	24 h	48 h	84 h	130 h
Pooled variance	48.973	14.92	39.51	36.038	36.92
t_{stat}	1.538	3.324	2.066	2.689	3.79
t_{crit}	1.943	1.943	1.943	1.943	1.943
P(T<=t)	0.874	0.008	0.042	0.036	0.005
Remark	*Insignificant*	*Significant*	*Significant*	*Significant*	*Significant*

Effect of PO_4 on THMs formation study

Table C27. Effect of PO_4 dosage (1.5 mg/L) in presence of different dosages of Fe(II) ions on THMs formation (chlorine to carbon ratio 0.79, pH 6.5, 21 ± 1 °C).

Sl No.	Presence of Fe(II) ions (mg/L)	Average THMs (ug/L) conc. for different reaction time (h)				
		3.5 h	24 h	48 h	84 h	130 h
1	0 mg/L	26.84	31.73	35.02	36.58	38.34
2	0.35 mg/L	21.09	22.19	22.88	24.33	23.51
3	0.7 mg/L	17.09	19.53	17.57	13.71	15.89
4	1.5 mg/L	14.05	14.765	14.09	12.59	13.44
5	2.0 mg/L	14.69	15.78	14.76	20.61	17.30
6	3.0 mg/L	13.68	14.36	13.11	10.77	12.09

Table C28. Summary for sum, average and variance for HAAs formation data

SUMMARY	*Count*	*Sum*	*Average*	*Variance*
Row 1	5	114.00	22.80	1.53
Row 2	5	83.81	16.76	4.62
Row 3	5	68.93	13.79	0.67
Row 4	5	83.15	16.63	6.07
Row 5	5	64.02	12.80	1.98
Column 1	5	80.61	16.12	9.50
Column 2	5	86.62	17.32	11.56
Column 3	5	82.42	16.48	15.54
Column 4	5	82.01	16.40	33.50
Column 5	5	82.24	16.45	19.72

Sum square (SS):

$$\mathrm{SS}_{treatment} = \sum_{i=1}^{a} \frac{y_{i.}^2}{b} - \frac{y_{..}^2}{ab}$$

$$\mathrm{SS}_{treatment} = \frac{(114)^2 + (83.81)^2 + (68.93)^2 + (83.15)^2 + (64.02)^2}{5} - \frac{(413.9)^2}{25}$$

$$\mathrm{SS}_{treatment} = 303.93$$

$$\mathrm{SS}_{blocks} = \sum_{j=1}^{b} \frac{y_{.j}^2}{b} - \frac{y_{..}^2}{ab}$$

$$\mathrm{SS}_{blocks} = \frac{(80.61)^2 + (86.62)^2 + (82.42)^2 + (82.01)^2 + (82.24)^2}{5} - \frac{(419.9)^2}{25}$$

$$= 4.10$$

$$\mathrm{SS}_{Total} = \sum_{i=1}^{a} \sum_{j=1}^{b} y_{ij}^2 - \frac{y_{..}^2}{ab}$$

$$\mathrm{SS}_{Total} = (26.84)^2 + (21.1)^2 + \cdots\cdots\cdots + (12.09)^2 - \frac{(419.9)^2}{25}$$

$$\mathrm{SS}_{Total} = 363.42$$

$$\mathrm{SS}_{Error} = SS_{Total} - SS_{treatment} - SS_{blocks} = 55.38$$

Mean square (MS):

$$\mathrm{MS}_{treatment} = \frac{\mathrm{SS}_{treatment}}{a-1} = 75.98$$

$$\mathrm{MS}_{blocks} = \frac{\mathrm{SS}_{blocks}}{b-1} = 1.02$$

$$\mathrm{MS}_{Error} = \frac{\mathrm{SS}_{Error}}{(a-1)(b-1)} = 3.46$$

Table C29. ANOVA (analysis of variance) test for THMs formation study in presence of PO4 (1.5 mg/L) and different dosages of Fe(II) ions in solution.

Source of Variation	*SS*	*df*	*MS*	*F*	*P-value*	*F crit*
Fe(II) ions conc. (*treatment*)	303.93	4	75.98	21.95	< 0.0001	3.007
Reaction time (*blocks*)	4.10	4	1.02	0.30	0.8762	3.007
Error	55.38	16	3.46			
Total	363.42	24				

Comments:

For Fe(II) ions concentration, $F_{obs} > F_{crit}$ (27.93 > 3.007) and for reaction time , $F_{obs} > F_{crit}$ (5.94 > 3.007) . It could be said that changes of Fe(II) ions concentrations in solution and reaction, HAAs formation significantly changed at a 95 % confidence level.

Molecular weight (MW) distribution of DOM in solution

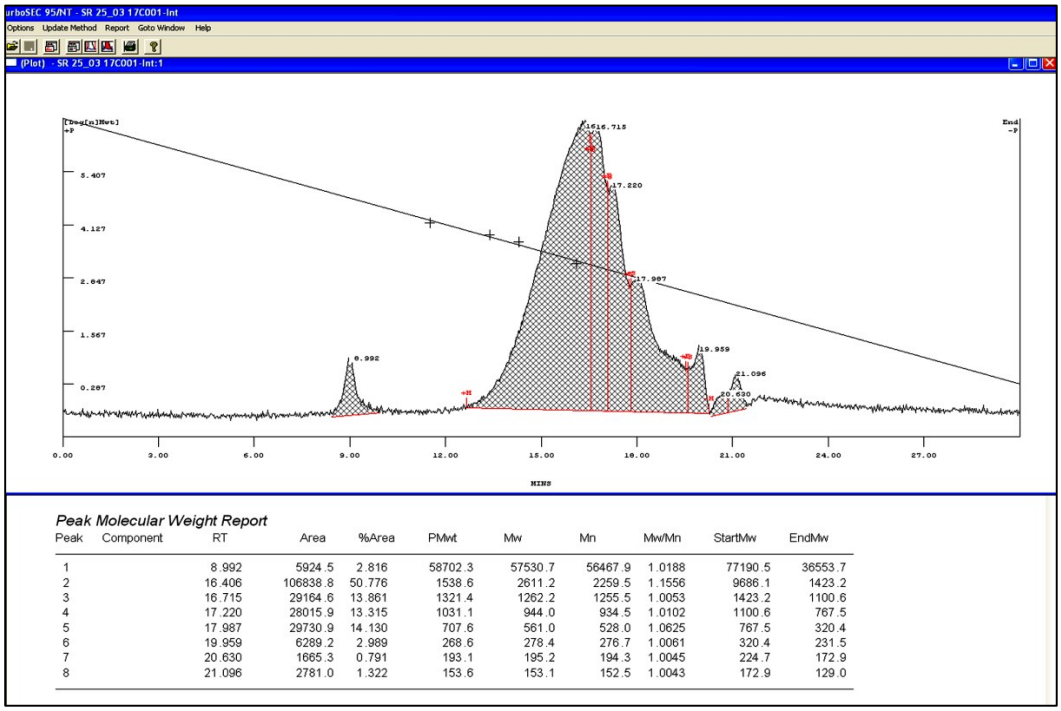

Peak Molecular Weight Report

Peak	Component	RT	Area	%Area	PMwt	Mw	Mn	Mw/Mn	StartMw	EndMw
1		8.992	5924.5	2.816	58702.3	57530.7	56467.9	1.0188	77190.5	36553.7
2		16.406	106838.8	50.776	1538.6	2611.2	2259.5	1.1556	9686.1	1423.2
3		16.715	29164.6	13.861	1321.4	1262.2	1255.5	1.0053	1423.2	1100.6
4		17.220	28015.9	13.315	1031.1	944.0	934.5	1.0102	1100.6	767.5
5		17.987	29730.9	14.130	707.6	561.0	528.0	1.0625	767.5	320.4
6		19.959	6289.2	2.989	268.6	278.4	276.7	1.0061	320.4	231.5
7		20.630	1665.3	0.791	193.1	195.2	194.3	1.0045	224.7	172.9
8		21.096	2781.0	1.322	153.6	153.1	152.5	1.0043	172.9	129.0

Figure C1. Molecular weight (MW) distribution of DOM in control water system (exp. 1).

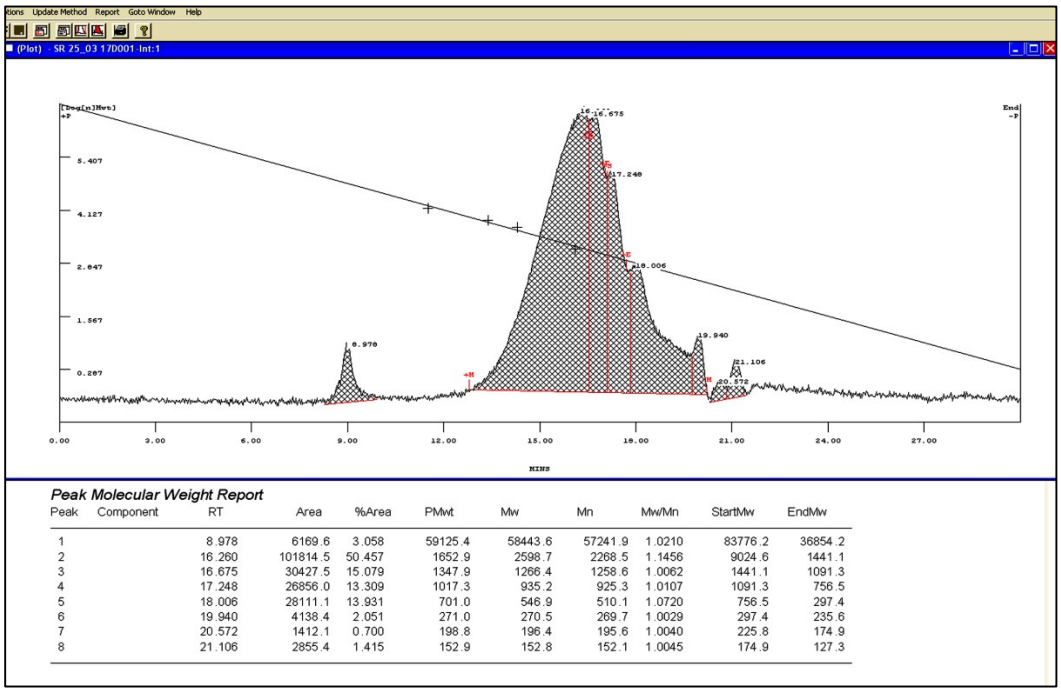

Peak Molecular Weight Report

Peak	Component	RT	Area	%Area	PMwt	Mw	Mn	Mw/Mn	StartMw	EndMw
1		8.978	6169.6	3.058	59125.4	58443.6	57241.9	1.0210	83776.2	36854.2
2		16.260	101814.5	50.457	1652.9	2598.7	2268.5	1.1456	9024.6	1441.1
3		16.675	30427.5	15.079	1347.9	1266.4	1258.6	1.0062	1441.1	1091.3
4		17.248	26856.0	13.309	1017.3	935.2	925.3	1.0107	1091.3	756.5
5		18.006	28111.1	13.931	701.0	546.9	510.1	1.0720	756.5	297.4
6		19.940	4138.4	2.051	271.0	270.5	269.7	1.0029	297.4	235.6
7		20.572	1412.1	0.700	198.8	196.4	195.6	1.0040	225.8	174.9
8		21.106	2855.4	1.415	152.9	152.8	152.1	1.0045	174.9	127.3

Figure C2. Molecular weight (MW) distribution of DOM in control water system (exp. 2).

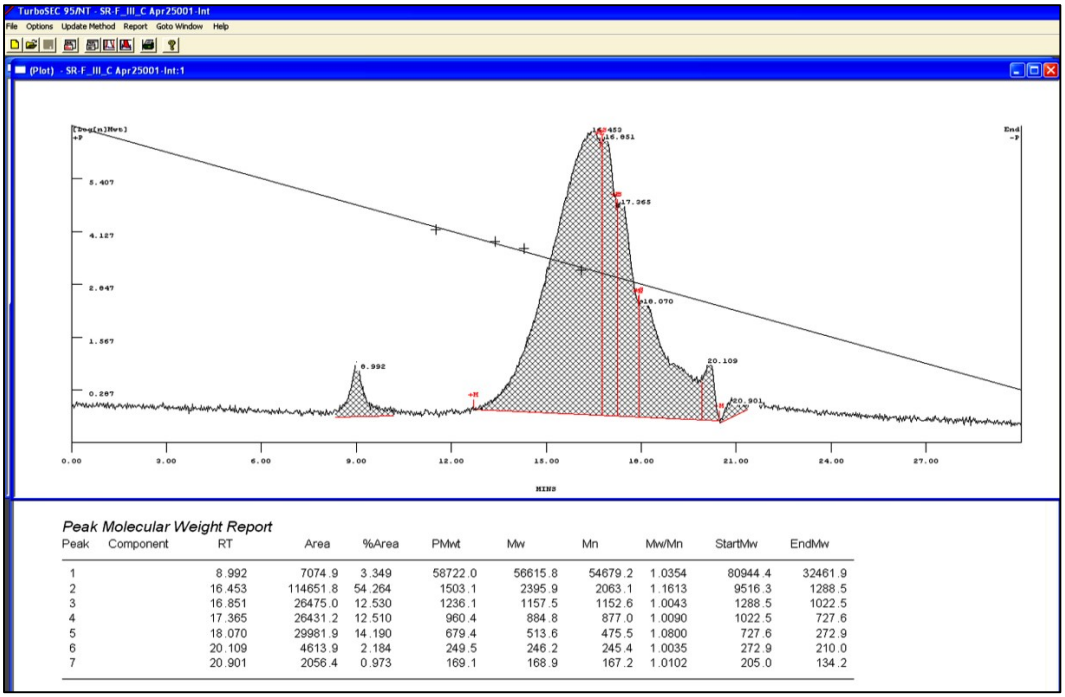

Peak Molecular Weight Report

Peak	Component	RT	Area	%Area	PMwt	Mw	Mn	Mw/Mn	StartMw	EndMw
1		8.992	7074.9	3.349	58722.0	56615.8	54679.2	1.0354	80944.4	32461.9
2		16.453	114651.8	54.264	1503.1	2395.9	2063.1	1.1613	9516.3	1288.5
3		16.851	26475.0	12.530	1236.1	1157.5	1152.6	1.0043	1288.5	1022.5
4		17.365	26431.2	12.510	960.4	884.8	877.0	1.0090	1022.5	727.6
5		18.070	29981.9	14.190	679.4	513.6	475.5	1.0800	727.6	272.9
6		20.109	4613.9	2.184	249.5	246.2	245.4	1.0035	272.9	210.0
7		20.901	2056.4	0.973	169.1	168.9	167.2	1.0102	205.0	134.2

Figure C3. Molecular weight (MW) distribution of DOM in synthetic water for the presence of chlorine (exp. 1).

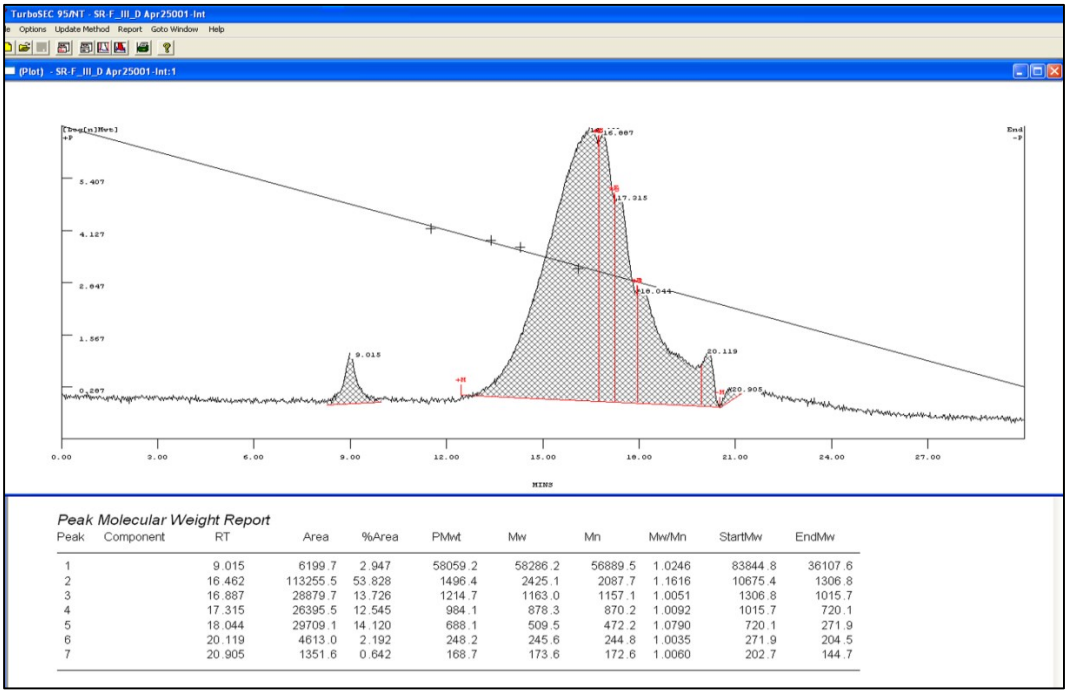

Peak Molecular Weight Report

Peak	Component	RT	Area	%Area	PMwt	Mw	Mn	Mw/Mn	StartMw	EndMw
1		9.015	6199.7	2.947	58059.2	58286.2	56889.5	1.0246	83844.8	36107.6
2		16.462	113255.5	53.828	1496.4	2425.1	2087.7	1.1616	10675.4	1306.8
3		16.887	28879.7	13.726	1214.7	1163.0	1157.1	1.0051	1306.8	1015.7
4		17.315	26395.5	12.545	984.1	878.3	870.2	1.0092	1015.7	720.1
5		18.044	29709.1	14.120	688.1	509.5	472.2	1.0790	720.1	271.9
6		20.119	4613.0	2.192	248.2	245.6	244.8	1.0035	271.9	204.5
7		20.905	1351.6	0.642	168.7	173.6	172.6	1.0060	202.7	144.7

Figure C4. Molecular weight (MW) distribution of DOM in synthetic water for the presence of chlorine (exp. 2)

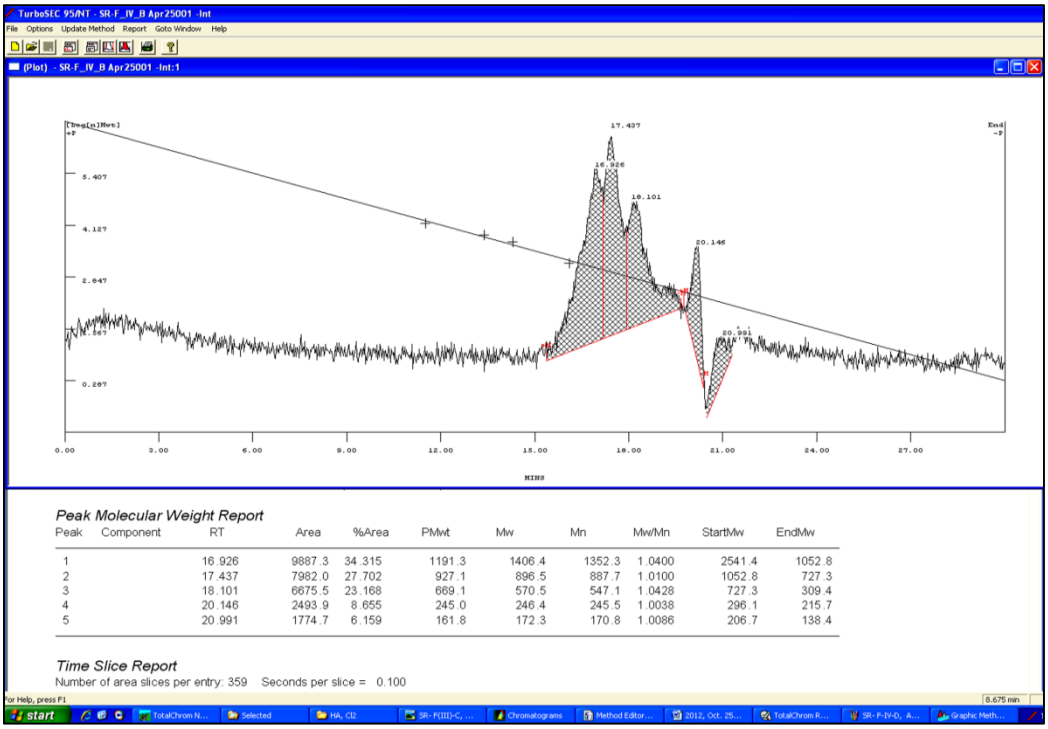

Figure C5. Molecular weight (MW) distribution of DOM in synthetic water for the presence of iron (exp. 1).

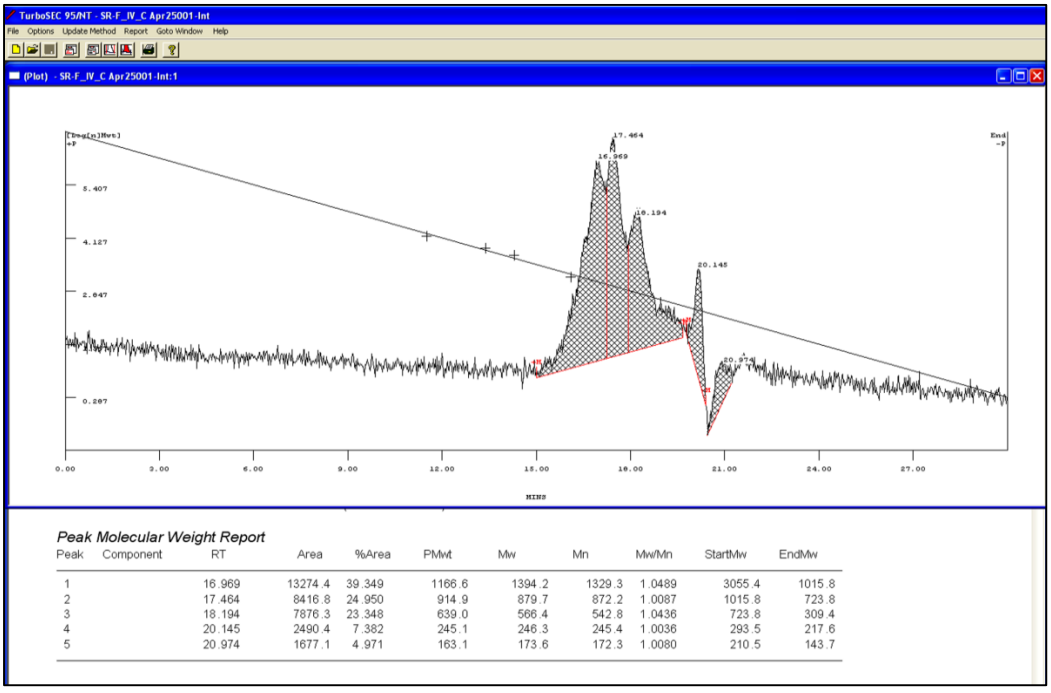

Figure C6. Molecular weight (MW) distribution of DOM in synthetic water for the presence of iron (exp. 2).

Table C30. Summary of molecular weight (MW) distribution of DOM in control system.

Peak No.	MW distribution				Area of each peak			
	Control A	Control B	Average (Dalton)	Stdev	Control A	Control B	Average (Dalton)	Stdev
1	57530.7	58443.6	57987.1	645.5	5924.5	6169.6	6047.5	173.31
2	2611.2	2598.7	2604.9	8.84	106838.8	101814.5	104326.7	3552.72
3	1262.2	1266.4	1264.3	2.97	29164.6	30427.5	29796.05	893.01
4	944.0	935.2	939.6	6.22	28015.9	26856	27435.95	820.17
5	561.0	546.9	553.95	9.97	29730.9	28111.1	28921	1145.37
6	278.4	270.5	274.45	5.59	6289.2	4138.4	5213.8	1520.85
7	195.2	195.6	195.4	0.28	1665.3	1412.1	1538.7	179.04
8	153.1	152.8	152.95	0.21	2781	2855.4	2818.2	52.61

Table C31. Summary of molecular weight (MW) distribution of DOM in presence of chlorine.

Peak No.	MW distribution				Area of each peak			
	Chlorine A	Chlorine B	Average (Dalton)	Stdev	Chlorine A	Chlorine B	Average (Dalton)	Stdev
1	58722	58286.2	58504.1	308.16	7074.9	6199.7	6637.3	618.86
2	1503.1	2425.1	1964.1	651.95	107651.8	108255.5	107953.7	426.88
3	1236.1	1163	1199.55	51.69	26475	28879.7	27677.35	1700.38
4	960.4	878.3	919.35	58.05	26431.2	26395.5	26413.35	25.24
5	679.4	509.5	594.45	120.14	29981.9	29709.1	29845.5	192.90
6	249.5	245.6	247.55	2.76	4613.9	4613	4613.45	0.64
7	169.1	173.6	171.35	3.18	2056.4	1351.6	1704	498.37

Table C32. Summary of molecular weight (MW) distribution of DOM in presence of iron.

Peak No.	MW distribution				Area of each peak			
	Iron A	Iron B	Average (Dalton)	Stdev	Iron A	Iron B	Average (Dalton)	Stdev
1	1406.4	1394.2	1400.3	8.63	9887.3	13274.4	11580.85	2395.04
2	896.5	879.7	888.1	11.88	7982	8416.8	8199.4	307.45
3	570.5	566.4	568.45	2.90	6675.5	7876.3	7275.9	849.09
4	246.4	246.3	246.35	0.07	2493.9	2490.4	2492.15	2.47
5	172.3	173.6	172.95	0.92	1774.7	1677.1	1725.9	69.01

Factorial design approach for HAAs formation study

Table C33 [F.D.A. # 1]. The formation and speciation of HAAs in synthetic water (chlorine to carbon ratio 0.79, pH 6.5, 21 ± 1 °C, reaction time 3.5 h)

Sl. No	HAA species	HAAs concentration (µg/L)			
		Data 1	Data 2	Average	Stdev.
1	Monochloroacetic acid ($CH_2ClCOOH$)	2.64	0.00	1.32	1.87
2	Monobromoacetic acid ($CH_2BrCOOH$)	0.76	0.00	0.38	0.54
3	Dichloroacetic acid ($CHCl_2COOH$)	36.04	39.99	38.01	2.79
4	Trichloroacetic acid (Cl_3COOH)	36.21	40.15	38.18	2.79
5	Bromochloroacetic acid ($CHBrClCOOH$)	0.87	0.86	0.86	0.01
6	Dibromoacetic acid ($CHBr_2COOH$)	0.00	0.39	0.20	0.28
7	Bromodichloroacetic acid ($CBrCl_2COOH$)	2.35	2.36	2.35	0.01
8	Chlorodibromoacetic acid ($CBr_2ClCOOH$)	0.00	0.00	0.00	0.00
9	Tribromoacetic acid (CBr_3COOH)	0.00	0.00	0.00	0.00
	Total HAAs =	78.87	83.75	81.31	3.46

Table C34 [F.D.A. # 2]. The formation and speciation of HAAs in synthetic water (chlorine to carbon ratio 0.79, pH 6.5, Fe(II) ions = 3 mg/L, 21 ± 1 °C, reaction time 3.5 h)

Sl. No	HAA species	HAAs concentration (µg/L)			
		Data 1	Data 2	Average	Stdev.
1	Monochloroacetic acid ($CH_2ClCOOH$)	0.00	0.00	0.00	0.00
2	Monobromoacetic acid ($CH_2BrCOOH$)	0.00	0.00	0.00	0.00
3	Dichloroacetic acid ($CHCl_2COOH$)	14.83	13.71	14.27	0.79
4	Trichloroacetic acid (Cl_3COOH)	11.85	11.34	11.59	0.36
5	Bromochloroacetic acid ($CHBrClCOOH$)	1.07	1.02	1.05	0.03
6	Dibromoacetic acid ($CHBr_2COOH$)	0.00	0.00	0.00	0.00
7	Bromodichloroacetic acid ($CBrCl_2COOH$)	0.00	2.36	1.18	1.67
8	Chlorodibromoacetic acid ($CBr_2ClCOOH$)	0.00	0.00	0.00	0.00
9	Tribromoacetic acid (CBr_3COOH)	0.00	0.00	0.00	0.00
	Total HAAs =	27.76	28.43	28.09	0.48

Table C35 [F.D.A. # 3]. The formation and speciation of HAAs in synthetic water (chlorine to carbon ratio 0.79, pH 8.5, 21 ± 1 °C, reaction time 3.5 h).

Sl. No	HAA species	HAAs concentration (μg/L)			
		Data 1	Data 2	Average	Stdev.
1	Monochloroacetic acid ($CH_2ClCOOH$)	0.00	0.00	0.00	0.00
2	Monobromoacetic acid ($CH_2BrCOOH$)	0.00	0.00	0.00	0.00
3	Dichloroacetic acid ($CHCl_2COOH$)	33.58	34.51	34.05	0.65
4	Trichloroacetic acid (Cl_3COOH)	41.98	40.44	41.21	1.08
5	Bromochloroacetic acid (CHBrClCOOH)	0.00	0.00	0.00	0.00
6	Dibromoacetic acid ($CHBr_2COOH$)	0.00	0.00	0.00	0.00
7	Bromodichloroacetic acid ($CBrCl_2COOH$)	0.00	0.00	0.00	0.00
8	Chlorodibromoacetic acid ($CBr_2ClCOOH$)	0.00	0.00	0.00	0.00
9	Tribromoacetic acid (CBr_3COOH)	0.00	0.00	0.00	0.00
	Total HAAs =	75.56	74.95	75.26	0.43

Table C36 [F.D.A. # 4]. The formation and speciation of HAAs in synthetic water (chlorine to carbon ratio 0.79, pH 8.5, Fe(II) ions = 3 mg/L, 21 ± 1 °C, reaction time 3.5 h).

Sl. No	HAA species	HAAs concentration (μg/L)			
		Data 1	Data 2	Average	Stdev.
1	Monochloroacetic acid ($CH_2ClCOOH$)	1.04	0.00	0.52	0.74
2	Monobromoacetic acid ($CH_2BrCOOH$)	0.00	0.00	0.00	0.00
3	Dichloroacetic acid ($CHCl_2COOH$)	38.74	31.63	35.18	5.03
4	Trichloroacetic acid (Cl_3COOH)	45.23	39.59	42.41	3.99
5	Bromochloroacetic acid (CHBrClCOOH)	1.66	1.55	1.61	0.07
6	Dibromoacetic acid ($CHBr_2COOH$)	0.00	0.74	0.37	0.53
7	Bromodichloroacetic acid ($CBrCl_2COOH$)	0.00	0.00	0.00	0.00
8	Chlorodibromoacetic acid ($CBr_2ClCOOH$)	0.00	0.00	0.00	0.00
9	Tribromoacetic acid (CBr_3COOH)	0.00	0.00	0.00	0.00
	Total HAAs =	86.67	73.51	80.09	9.30

Table C37 [F.D.A. # 5]. The formation and speciation of HAAs in synthetic water (chlorine to carbon ratio 0.79, pH 6.5, PO4 = 1.5 mg/L, 21 ± 1 °C, reaction time 3.5 h)

Sl. No	HAA species	HAAs concentration (µg/L)			
		Data 1	Data 2	Average	Stdev.
1	Monochloroacetic acid ($CH_2ClCOOH$)	0.00	0.00	0.00	0.00
2	Monobromoacetic acid ($CH_2BrCOOH$)	0.00	0.00	0.00	0.00
3	Dichloroacetic acid ($CHCl_2COOH$)	29.63	34.12	31.87	3.18
4	Trichloroacetic acid (Cl_3COOH)	34.50	40.61	37.56	4.33
5	Bromochloroacetic acid ($CHBrClCOOH$)	0.00	0.00	0.00	0.00
6	Dibromoacetic acid ($CHBr_2COOH$)	0.00	0.00	0.00	0.00
7	Bromodichloroacetic acid ($CBrCl_2COOH$)	0.00	0.00	0.00	0.00
8	Chlorodibromoacetic acid ($CBr_2ClCOOH$)	0.00	0.00	0.00	0.00
9	Tribromoacetic acid (CBr_3COOH)	0.00	0.00	0.00	0.00
	Total HAAs =	64.12	74.74	69.43	7.50

Table C38 [F.D.A. # 6]. The formation and speciation of HAAs in synthetic water (chlorine to carbon ratio 0.79, pH 6.5, Fe(II) ions = 3 mg/L, PO_4 = 1.5 mg/L, 21 ± 1 °C, reaction time 3.5 h).

Sl. No	HAA species	HAAs concentration (µg/L)			
		Data 1	Data 2	Average	Stdev.
1	Monochloroacetic acid ($CH_2ClCOOH$)	0.00	0.00	0.00	0.00
2	Monobromoacetic acid ($CH_2BrCOOH$)	0.00	0.00	0.00	0.00
3	Dichloroacetic acid ($CHCl_2COOH$)	6.78	7.78	7.28	0.71
4	Trichloroacetic acid (Cl_3COOH)	8.35	9.15	8.75	0.57
5	Bromochloroacetic acid ($CHBrClCOOH$)	0.00	0.00	0.00	0.00
6	Dibromoacetic acid ($CHBr_2COOH$)	0.00	0.00	0.00	0.00
7	Bromodichloroacetic acid ($CBrCl_2COOH$)	0.00	0.00	0.00	0.00
8	Chlorodibromoacetic acid ($CBr_2ClCOOH$)	0.00	0.00	0.00	0.00
9	Tribromoacetic acid (CBr_3COOH)	0.00	0.00	0.00	0.00
	Total HAAs =	15.13	16.93	16.03	1.27

Table C39 [F.D.A. # 7]. The formation and speciation of HAAs in synthetic water (chlorine to carbon ratio 0.79, pH 8.5, PO_4 = 1.5 mg/L, 21 ± 1 °C, reaction time 3.5 h).

Sl. No	HAA species	HAAs concentration (μg/L)			
		Data 1	Data 2	Average	Stdev.
1	Monochloroacetic acid ($CH_2ClCOOH$)	0.00	0.00	0.00	0.00
2	Monobromoacetic acid ($CH_2BrCOOH$)	0.40	0.41	0.40	0.01
3	Dichloroacetic acid ($CHCl_2COOH$)	27.35	22.30	24.83	3.57
4	Trichloroacetic acid (Cl_3COOH)	31.86	26.24	29.05	3.97
5	Bromochloroacetic acid (CHBrClCOOH)	1.51	1.52	1.52	0.01
6	Dibromoacetic acid ($CHBr_2COOH$)	0.00	0.00	0.00	0.00
7	Bromodichloroacetic acid ($CBrCl_2COOH$)	0.00	0.00	0.00	0.00
8	Chlorodibromoacetic acid ($CBr_2ClCOOH$)	0.00	0.00	0.00	0.00
9	Tribromoacetic acid (CBr_3COOH)	0.00	0.00	0.00	0.00
	Total HAAs =	61.12	50.48	55.80	7.52

Table C40 [F.D.A. # 8]. The formation and speciation of HAAs in synthetic water (chlorine to carbon ratio 0.79, pH 8.5, Fe(II) ions = 3 mg/L, PO_4 = 1.5 mg/L, 21 ± 1 °C, reaction time 3.5 h).

Sl. No	HAA species	HAAs concentration (μg/L)			
		Data 1	Data 2	Average	Stdev.
1	Monochloroacetic acid ($CH_2ClCOOH$)	0.00	1.39	0.69	0.98
2	Monobromoacetic acid ($CH_2BrCOOH$)	0.62	0.57	0.59	0.04
3	Dichloroacetic acid ($CHCl_2COOH$)	11.08	12.98	12.03	1.34
4	Trichloroacetic acid (Cl_3COOH)	11.50	13.64	12.57	1.51
5	Bromochloroacetic acid (CHBrClCOOH)	0.96	0.99	0.98	0.02
6	Dibromoacetic acid ($CHBr_2COOH$)	0.00	0.00	0.00	0.00
7	Bromodichloroacetic acid ($CBrCl_2COOH$)	2.35	2.35	2.35	0.00
8	Chlorodibromoacetic acid ($CBr_2ClCOOH$)	0.00	0.00	0.00	0.00
9	Tribromoacetic acid (CBr_3COOH)	0.00	0.00	0.00	0.00
	Total HAAs =	26.51	31.91	29.21	3.82

Table C41 [F.D.A. # 9]. The formation and speciation of HAAs in synthetic water (chlorine to carbon ratio 0.79, pH 6.5, 21 ± 1 °C, reaction time 24 h).

Sl. No	HAA species	HAAs concentration (μg/L)			
		Data 1	Data 2	Average	Stdev.
1	Monochloroacetic acid ($CH_2ClCOOH$)	2.45	0.00	1.22	1.73
2	Monobromoacetic acid ($CH_2BrCOOH$)	0.69	0.00	0.35	0.49
3	Dichloroacetic acid ($CHCl_2COOH$)	35.02	39.31	37.16	3.03
4	Trichloroacetic acid (Cl_3COOH)	33.93	38.45	36.19	3.20
5	Bromochloroacetic acid (CHBrClCOOH)	0.91	1.04	0.97	0.09
6	Dibromoacetic acid ($CHBr_2COOH$)	0.66	0.31	0.49	0.25
7	Bromodichloroacetic acid ($CBrCl_2COOH$)	0.00	2.38	1.19	1.69
8	Chlorodibromoacetic acid ($CBr_2ClCOOH$)	0.00	0.00	0.00	0.00
9	Tribromoacetic acid (CBr_3COOH)	1.84	0.00	0.92	1.30
	Total HAAs =	75.51	81.49	78.50	4.23

Table C42 [F.D.A. # 10]. The formation and speciation of HAAs in synthetic water (chlorine to carbon ratio 0.79, pH 6.5, Fe(II) ions = 3 mg/L, 21 ± 1 °C, reaction time 24 h).

Sl. No	HAA species	HAAs concentration (μg/L)			
		Data 1	Data 2	Average	Stdev.
1	Monochloroacetic acid ($CH_2ClCOOH$)	0.00	0.00	0.00	0.00
2	Monobromoacetic acid ($CH_2BrCOOH$)	0.00	0.00	0.00	0.00
3	Dichloroacetic acid ($CHCl_2COOH$)	14.35	14.21	14.28	0.10
4	Trichloroacetic acid (Cl_3COOH)	11.47	11.43	11.45	0.03
5	Bromochloroacetic acid (CHBrClCOOH)	0.95	1.05	1.00	0.07
6	Dibromoacetic acid ($CHBr_2COOH$)	0.00	0.35	0.18	0.25
7	Bromodichloroacetic acid ($CBrCl_2COOH$)	2.36	2.35	2.36	0.00
8	Chlorodibromoacetic acid ($CBr_2ClCOOH$)	0.00	0.00	0.00	0.00
9	Tribromoacetic acid (CBr_3COOH)	0.00	0.00	0.00	0.00
Total HAAs =		29.13	29.39	29.26	0.19

Table C43 [F.D.A. # 11]. The formation and speciation of HAAs in synthetic water (chlorine to carbon ratio 0.79, pH 8.5, 21 ± 1 °C, reaction time 24 h).

Sl. No	HAA species	HAAs concentration (μg/L)			
		Data 1	Data 2	Average	Stdev.
1	Monochloroacetic acid ($CH_2ClCOOH$)	0.00	0.00	0.00	0.00
2	Monobromoacetic acid ($CH_2BrCOOH$)	0.00	0.00	0.00	0.00
3	Dichloroacetic acid ($CHCl_2COOH$)	36.11	37.14	36.62	0.73
4	Trichloroacetic acid (Cl_3COOH)	44.05	46.04	45.05	1.41
5	Bromochloroacetic acid ($CHBrClCOOH$)	0.00	0.00	0.00	0.00
6	Dibromoacetic acid ($CHBr_2COOH$)	0.00	0.00	0.00	0.00
7	Bromodichloroacetic acid ($CBrCl_2COOH$)	0.00	0.00	0.00	0.00
8	Chlorodibromoacetic acid ($CBr_2ClCOOH$)	0.00	0.00	0.00	0.00
9	Tribromoacetic acid (CBr_3COOH)	0.00	0.00	0.00	0.00
	Total HAAs =	80.16	83.18	81.67	2.14

Table C44 [F.D.A. # 12]. The formation and speciation of HAAs in synthetic water (chlorine to carbon ratio 0.79, pH 8.5, Fe(II) ions = 3 mg/L, 21 ± 1 °C, reaction time 24 h).

Sl. No	HAA species	HAAs concentration (μg/L)			
		Data 1	Data 2	Average	Stdev.
1	Monochloroacetic acid ($CH_2ClCOOH$)	0.00	0.00	0.00	0.00
2	Monobromoacetic acid ($CH_2BrCOOH$)	0.00	0.44	0.22	0.31
3	Dichloroacetic acid ($CHCl_2COOH$)	30.59	35.63	33.11	3.56
4	Trichloroacetic acid (Cl_3COOH)	38.99	42.29	40.64	2.33
5	Bromochloroacetic acid ($CHBrClCOOH$)	1.59	1.71	1.65	0.09
6	Dibromoacetic acid ($CHBr_2COOH$)	0.00	0.00	0.00	0.00
7	Bromodichloroacetic acid ($CBrCl_2COOH$)	0.00	0.00	0.00	0.00
8	Chlorodibromoacetic acid ($CBr_2ClCOOH$)	0.00	0.00	0.00	0.00
9	Tribromoacetic acid (CBr_3COOH)	0.00	0.00	0.00	0.00
	Total HAAs =	71.16	80.07	75.62	6.30

Table C45 [F.D.A. # 13]. The formation and speciation of HAAs in synthetic water (chlorine to carbon ratio 0.79, pH 6.5, PO_4 = 1.5 mg/L, 21 ± 1 °C, reaction time 24 h).

Sl. No	HAA species	HAAs concentration (μg/L)			
		Data 1	Data 2	Average	Stdev.
1	Monochloroacetic acid ($CH_2ClCOOH$)	1.20	0.00	0.60	0.85
2	Monobromoacetic acid ($CH_2BrCOOH$)	0.00	0.00	0.00	0.00
3	Dichloroacetic acid ($CHCl_2COOH$)	34.14	35.39	34.76	0.88
4	Trichloroacetic acid (Cl_3COOH)	40.74	43.17	41.95	1.72
5	Bromochloroacetic acid (CHBrClCOOH)	-0.24	0.00	-0.12	0.17
6	Dibromoacetic acid ($CHBr_2COOH$)	0.00	0.00	0.00	0.00
7	Bromodichloroacetic acid ($CBrCl_2COOH$)	0.00	0.00	0.00	0.00
8	Chlorodibromoacetic acid ($CBr_2ClCOOH$)	0.00	0.00	0.00	0.00
9	Tribromoacetic acid (CBr_3COOH)	0.00	0.00	0.00	0.00
	Total HAAs =	75.83	78.55	77.19	1.92

Table C46 [F.D.A. # 14]. The formation and speciation of HAAs in synthetic water (chlorine to carbon ratio 0.79, pH 6.5, Fe(II) ions = 3 mg/L, PO_4 = 1.5 mg/L, 21 ± 1 °C, reaction time 24 h).

Sl. No	HAA species	HAAs concentration (μg/L)			
		Data 1	Data 2	Average	Stdev.
1	Monochloroacetic acid (CH2ClCOOH)	0.00	0.00	0.00	0.00
2	Monobromoacetic acid (CH2BrCOOH)	0.00	0.00	0.00	0.00
3	Dichloroacetic acid (CHCl2COOH)	8.04	8.09	8.07	0.04
4	Trichloroacetic acid (Cl3COOH)	9.26	9.20	9.23	0.04
5	Bromochloroacetic acid (CHBrClCOOH)	0.00	0.00	0.00	0.00
6	Dibromoacetic acid (CHBr2COOH)	0.00	0.00	0.00	0.00
7	Bromodichloroacetic acid (CBrCl2COOH)	0.00	0.00	0.00	0.00
8	Chlorodibromoacetic acid (CBr2ClCOOH)	0.00	0.00	0.00	0.00
9	Tribromoacetic acid (CBr3COOH)	0.00	0.00	0.00	0.00
	Total HAAs =	17.30	17.30	17.30	0.00

Table C47 [F.D.A. # 15]. The formation and speciation of HAAs in synthetic water (chlorine to carbon ratio 0.79, pH 8.5, PO_4 = 1.5 mg/L, 21 ± 1 °C, reaction time 24 h).

Sl. No	HAA species	HAAs concentration (µg/L)			
		Data 1	Data 2	Average	Stdev.
1	Monochloroacetic acid ($CH_2ClCOOH$)	0.00	0.00	0.00	0.00
2	Monobromoacetic acid ($CH_2BrCOOH$)	0.51	0.00	0.25	0.36
3	Dichloroacetic acid ($CHCl_2COOH$)	36.74	28.33	32.54	5.95
4	Trichloroacetic acid (Cl_3COOH)	43.42	33.99	38.71	6.67
5	Bromochloroacetic acid ($CHBrClCOOH$)	1.69	1.49	1.59	0.15
6	Dibromoacetic acid ($CHBr_2COOH$)	0.00	0.00	0.00	0.00
7	Bromodichloroacetic acid ($CBrCl_2COOH$)	2.37	2.34	2.35	0.02
8	Chlorodibromoacetic acid ($CBr_2ClCOOH$)	0.00	0.00	0.00	0.00
9	Tribromoacetic acid (CBr_3COOH)	0.00	0.00	0.00	0.00
	Total HAAs =	84.74	66.15	75.44	13.14

Table C48 [F.D.A. # 16]. The formation and speciation of HAAs in synthetic water (chlorine to carbon ratio 0.79, pH 8.5, Fe(II) ions = 3 mg/L, PO4 = 1.5 mg/L, 21 ± 1 °C, reaction time 24 h).

Sl. No	HAA species	HAAs concentration (µg/L)			
		Data 1	Data 2	Average	Stdev.
1	Monochloroacetic acid ($CH_2ClCOOH$)	0.00	0.00	0.00	0.00
2	Monobromoacetic acid ($CH_2BrCOOH$)	0.67	0.58	0.62	0.07
3	Dichloroacetic acid ($CHCl_2COOH$)	14.62	15.69	15.16	0.76
4	Trichloroacetic acid (Cl_3COOH)	15.20	16.58	15.89	0.98
5	Bromochloroacetic acid ($CHBrClCOOH$)	1.01	1.01	1.01	0.01
6	Dibromoacetic acid ($CHBr_2COOH$)	0.00	0.00	0.00	0.00
7	Bromodichloroacetic acid ($CBrCl_2COOH$)	2.35	2.35	2.35	0.00
8	Chlorodibromoacetic acid ($CBr_2ClCOOH$)	0.00	1.51	0.76	1.07
9	Tribromoacetic acid (CBr_3COOH)	0.00	0.00	0.00	0.00
	Total HAAs =	33.85	37.72	35.79	2.74

Table C49 [F.D.A. # I]. The formation and speciation of HAAs in synthetic water (chlorine to carbon ratio 0.79, pH 7.5, Fe(II) ions = 1.5 mg/L, PO_4 = 0.75 mg/L, 21 ± 1 °C, time 13.5 h).

Sl. No	HAA species	HAAs concentration (μg/L)			
		Data 1	Data 2	Average	Stdev.
1	Monochloroacetic acid ($CH_2ClCOOH$)	0.81	0.00	0.41	0.57
2	Monobromoacetic acid ($CH_2BrCOOH$)	0.00	0.00	0.00	0.00
3	Dichloroacetic acid ($CHCl_2COOH$)	29.81	28.75	29.28	0.75
4	Trichloroacetic acid (Cl_3COOH)	35.49	33.59	34.54	1.34
5	Bromochloroacetic acid (CHBrClCOOH)	1.46	1.14	1.30	0.22
6	Dibromoacetic acid ($CHBr_2COOH$)	0.00	0.74	0.37	0.53
7	Bromodichloroacetic acid ($CBrCl_2COOH$)	0.00	0.00	0.00	0.00
8	Chlorodibromoacetic acid ($CBr_2ClCOOH$)	0.00	0.00	0.00	0.00
9	Tribromoacetic acid (CBr_3COOH)	0.00	0.00	0.00	0.00
	Total HAAs =	67.57	64.23	65.90	2.36

Table C50 [F.D.A.-II]. The formation and speciation of HAAs in synthetic water (chlorine to carbon ratio 0.79, pH 7.5, Fe(II) ions = 1.5 mg/L, PO_4 = 0.75 mg/L, 21 ± 1 °C, time 13.5 h).

Sl. No	HAA species	HAAs concentration (μg/L)			
		Data 1	Data 2	Average	Stdev.
1	Monochloroacetic acid ($CH_2ClCOOH$)	0.74	0.00	0.37	0.52
2	Monobromoacetic acid ($CH_2BrCOOH$)	0.00	0.00	0.00	0.00
3	Dichloroacetic acid ($CHCl_2COOH$)	23.49	20.63	22.06	2.02
4	Trichloroacetic acid (Cl_3COOH)	36.57	31.49	34.03	3.60
5	Bromochloroacetic acid (CHBrClCOOH)	0.31	0.00	0.16	0.22
6	Dibromoacetic acid ($CHBr_2COOH$)	0.00	0.00	0.00	0.00
7	Bromodichloroacetic acid ($CBrCl_2COOH$)	0.00	0.00	0.00	0.00
8	Chlorodibromoacetic acid ($CBr_2ClCOOH$)	0.00	0.00	0.00	0.00
9	Tribromoacetic acid (CBr_3COOH)	0.00	0.00	0.00	0.00
	Total HAAs =	61.12	52.12	56.62	6.37

Table C51 [F.D.A. # III]. The formation and speciation of HAAs in synthetic water (chlorine to carbon ratio 0.79, pH 7.5, Fe(II) ions = 1.5 mg/L, PO_4 = 0.75 mg/L, 21 ± 1 °C, time 13.5 h).

Sl. No	HAA species	HAAs concentration (μg/L)			
		Data 1	Data 2	Average	Stdev.
1	Monochloroacetic acid ($CH_2ClCOOH$)	0.00	0.47	0.24	0.33
2	Monobromoacetic acid ($CH_2BrCOOH$)	0.00	0.00	0.00	0.00
3	Dichloroacetic acid ($CHCl_2COOH$)	16.58	16.48	16.53	0.07
4	Trichloroacetic acid (Cl_3COOH)	21.14	23.08	22.11	1.37
5	Bromochloroacetic acid ($CHBrClCOOH$)	0.00	0.26	0.13	0.18
6	Dibromoacetic acid ($CHBr_2COOH$)	0.00	0.00	0.00	0.00
7	Bromodichloroacetic acid ($CBrCl_2COOH$)	0.00	0.00	0.00	0.00
8	Chlorodibromoacetic acid ($CBr_2ClCOOH$)	0.00	0.00	0.00	0.00
9	Tribromoacetic acid (CBr_3COOH)	0.00	0.00	0.00	0.00
	Total HAAs =	37.72	40.30	39.01	1.82

Table C52 [F.D.A. # IV]. The formation and speciation of HAAs in synthetic water (chlorine to carbon ratio 0.79, pH 7.5, Fe(II) ions = 1.5 mg/L, PO_4 = 0.75 mg/L, 21 ± 1 °C, time 13.5 h).

Sl. No	HAA species	HAAs concentration (μg/L)			
		Data 1	Data 2	Average	Stdev.
1	Monochloroacetic acid ($CH_2ClCOOH$)	0.48	0.74	0.61	0.18
2	Monobromoacetic acid ($CH_2BrCOOH$)	0.00	0.00	0.00	0.00
3	Dichloroacetic acid ($CHCl_2COOH$)	18.23	15.21	16.72	2.14
4	Trichloroacetic acid (Cl_3COOH)	31.09	28.43	29.76	1.88
5	Bromochloroacetic acid ($CHBrClCOOH$)	0.31	1.05	0.68	0.52
6	Dibromoacetic acid ($CHBr_2COOH$)	0.00	0.35	0.18	0.25
7	Bromodichloroacetic acid ($CBrCl_2COOH$)	0.36	0.00	0.18	0.25
8	Chlorodibromoacetic acid ($CBr_2ClCOOH$)	0.00	0.00	0.00	0.00
9	Tribromoacetic acid (CBr_3COOH)	0.00	0.00	0.00	0.00
	Total HAAs =	50.48	45.78	48.13	3.32

Table C53 . The paired Student *t*-test for HAAs formation data obtained by the 2^4 full factorial design approach with center point level.

Exp. No.	Reaction conditions	HAAs-1	HAAs-2	Difference, d_i (HAA1-HAA2)	d_i^2
1	Factorial design approach [F1]	78.87	83.75	-4.88	23.81
2	Factorial design approach [F2]	27.76	28.43	-0.67	0.45
3	Factorial design approach [F3]	75.56	74.95	0.61	0.37
4	Factorial design approach [F4]	86.67	73.51	13.16	173.19
5	Factorial design approach [F5]	64.12	74.74	-10.62	112.78
6	Factorial design approach [F6]	15.13	16.93	-1.80	3.24
7	Factorial design approach [F7]	61.12	50.48	10.64	113.21
8	Factorial design approach [F8]	26.51	31.91	-5.40	29.16
9	Factorial design approach [F9]	75.51	81.49	-5.98	35.76
10	Factorial design approach [F10]	29.13	29.39	-0.26	0.07
11	Factorial design approach [F11]	80.16	83.18	-3.02	9.12
12	Factorial design approach [F12]	80.07	71.16	8.91	79.39
13	Factorial design approach [F13]	75.83	78.55	-2.72	7.40
14	Factorial design approach [F14]	17.31	17.30	0.01	0.00
15	Factorial design approach [F15]	84.74	66.15	18.59	345.59
16	Factorial design approach [F16]	33.85	37.72	-3.87	14.98
17	Center point level I	67.57	64.23	3.34	11.16
18	Center point level II	61.12	52.12	9.00	81.00
19	Center point level III	37.72	40.30	-2.58	6.66
20	Center point level IV	50.48	45.78	4.70	22.09
Sum				$\sum d_i = 27.16$	$\sum d_i^2$ =1069.42

Average of the paired difference ($\bar{d}$):

$$\bar{d} = \frac{\sum d_i}{n} = \frac{27.16}{20} = 1.358$$

Root of the variance of the paired difference

$$s_d = \sqrt{\frac{\sum d_i^2}{(n-1)} - \frac{n}{n-1}(\bar{d})^2}$$

$$s_d = \sqrt{\frac{1069.42}{(19)} - \frac{20}{19}(1.358)^2} = 7.372$$

Standard error of the average of the paired difference ($S_{\bar{d}}$):

$$S_{\bar{d}} = \frac{S_d}{\sqrt{n}} = \frac{7.372}{\sqrt{20}} = 1.648$$

The paired Student t-test (t_{stat}):

$$t_{stat} = \frac{\bar{d}\sqrt{n}}{S_d} = \frac{1.358 * \sqrt{20}}{7.372} = 0.8238$$

At a 95% confidence interval with ν = n-1 degree of freedom, the critic value for t is $t_{0.025,\ (n-1)} = t_{0.025,19} = 2.093$.

Comment:

Here, $t_{stat} < t_{critic}$ (0.824 < 2.093); it reveals that there is no significance difference between the two sets of data for HAAs formation.

Table C54. ANOVA test for 2^4 full factorial design for HAAs formation model.

Source	*DF*	*Seq SS*	*Adj SS*	*Adj MS*	*F*	*P*	*%*
Main Effect	4	7347.37	7347.37	1836.84	38.56	0.001	74.53
Fe(II)	1	5013.17	5013.17	5013.17	105.25	0.000[s]	50.85
pH	1	780.57	780.57	780.57	16.39	0.010[s]	7.92
PO4	1	1474.66	1474.66	1474.66	30.96	0.003[s]	14.96
Time	1	78.97	78.97	78.97	1.66	0.254	0.80
2-Way Interaction	6	2272.75	2272.75	378.79	7.95	0.019[s]	23.05
Fe(II).*pH	1	1374.09	1374.09	1374.09	28.85	0.003[s]	13.94
Fe(II)*PO4	1	359.72	359.72	359.72	7.55	0.040[s]	3.65
Fe(II)*Time	1	43.81	43.81	43.81	0.92	0.382	0.44
pH*PO4	1	391.79	391.79	391.79	8.23	0.035	3.97
pH*Time	1	26.98	26.98	26.98	0.57	0.486	0.27
PO4*Time	1	76.37	76.37	76.37	1.60	0.261	0.77
Residual Error	5	238.16	238.16	47.63			
Total	15	9858.28					

[s] significant factor on HAAs formation study at a 95% confidence level.

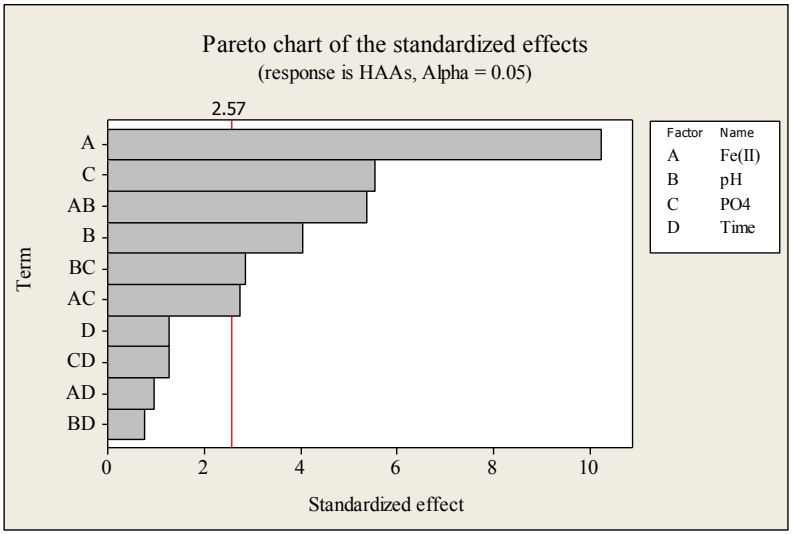

Figure C7. Pareto chart of the standardized effects for THMs formation

Table C55. ANOVA for the 2^4 factorial design with center point approach for lack of fit test of HAAs formation model.

Source	*DF*	*Seq SS*	*Adj SS*	*Adj MS*	*F*	*t*
Main Effect	4	7331.40	7331.40	1832.85	18.20	0.008
Fe(II)	1	4990.01	4990.01	4990.01	49.55	0.002
pH	1	770.90	770.90	770.90	7.65	0.051
PO_4	1	1488.42	1488.42	1488.42	14.78	0.018
Time	1	82.08	82.08	82.08	0.82	0.418
2-Way Interaction	6	2252.39	2252.39	375.40	3.73	0.112
Fe(II)*pH	1	1360.50	1360.50	1360.50	13.51	0.021
Fe(II)*PO_4	1	366.72	366.72	366.72	3.64	0.129
Fe(II)*Time	1	41.60	41.60	41.60	0.41	0.555
pH*PO_4	1	385.14	385.14	385.14	3.82	0.122
pH*Time	1	25.15	25.15	25.15	0.25	0.644
PO_4*Time	1	73.27	73.27	73.27	0.73	0.442
3-Way Interaction	4	233.91	233.91	58.48	0.58	0.694
Fe(II)*pH*PO_4	1	179.16	179.16	179.16	1.78	0.253
Fe(II)*pH*Time	1	30.75	30.75	30.75	0.31	0.610
Fe(II)*PO_4*Time	1	11.22	11.22	11.22	0.11	0.755
pH*PO_4*Time	1	12.78	12.78	12.78	0.13	0.740
Curvature	1	57.90	57.94	57.94	0.58	0.49
Residual Error	4	402.85	402.85	100.71		
Lack of Fit	1	5.00	5.00	5.00	0.04	0.859
Pure Error	3	397.85	397.85	132.62		
Total	19	10278.5				

Table C56. ANOVA test for 2^4 full factorial design with center point for HAAs formation study mentioning the significant factors.

Source	*DF*	*Seq SS*	*SS (Adj)*	*MS*	*F*	*P*
Main Effect	3	7249.30	7249.32	2416.44	33.76	0.000
Fe(II)	1	4990.00	4990.01	4990.01	69.72	0.000
pH	1	770.90	770.90	770.90	10.77	0.007
PO_4	1	1488.40	1488.42	1488.42	20.80	0.001
2-Way Interaction	3	2112.40	2112.37	704.12	9.84	0.001
Fe(II)*pH	1	1360.50	1360.50	1360.50	19.01	0.001
Fe(II)*PO_4	1	366.70	366.72	366.72	5.12	0.043
pH*PO_4	1	385.10	385.14	385.14	5.38	0.039
Curvature	1	57.90	57.94	57.94	0.81	0.386
Residual Error	12	858.90	858.86	71.57		
Lack of Fit	1	179.20	179.16	179.16	2.90	0.117
Pure Error	11	679.70	679.71	61.79		
Total	19	10278.50				

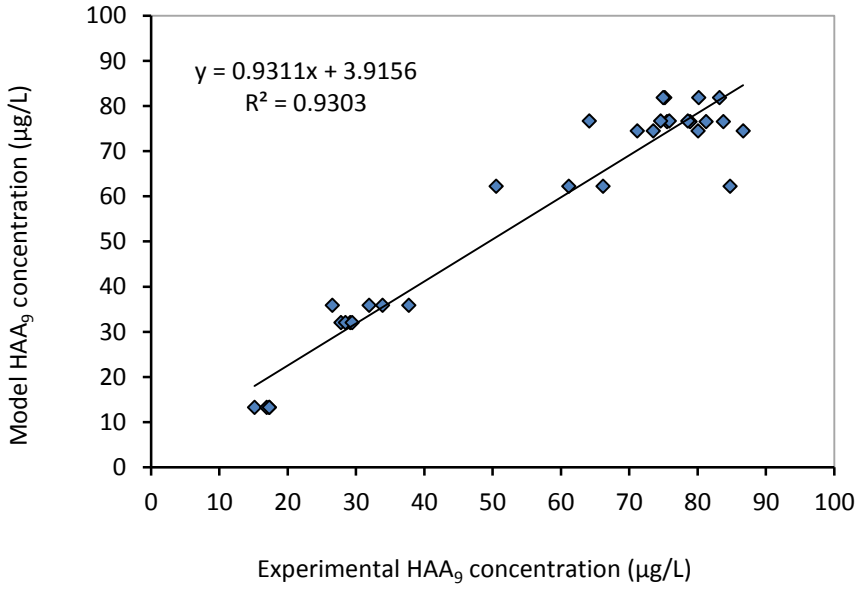

Figure C8. A liner graph between the experimental and model data for THMs formation study.

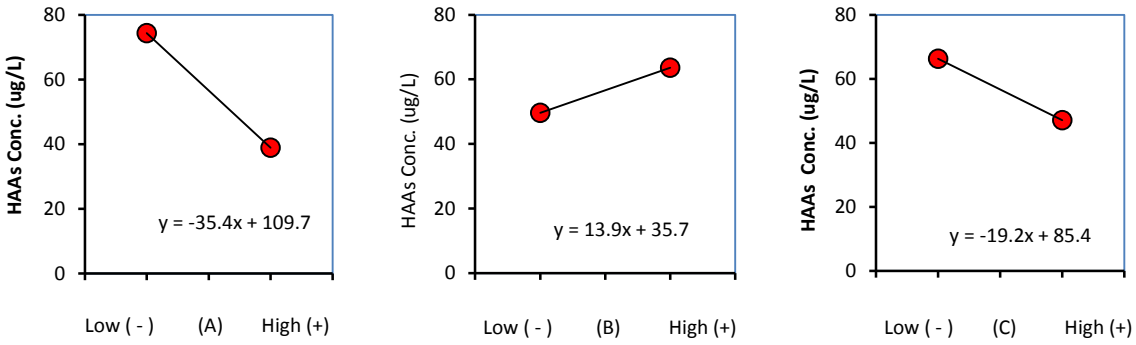

Figure C9. Main effect plots of A (Fe(II) ions concentration), B (pH) and C (PO_4) for HAAs formation study.

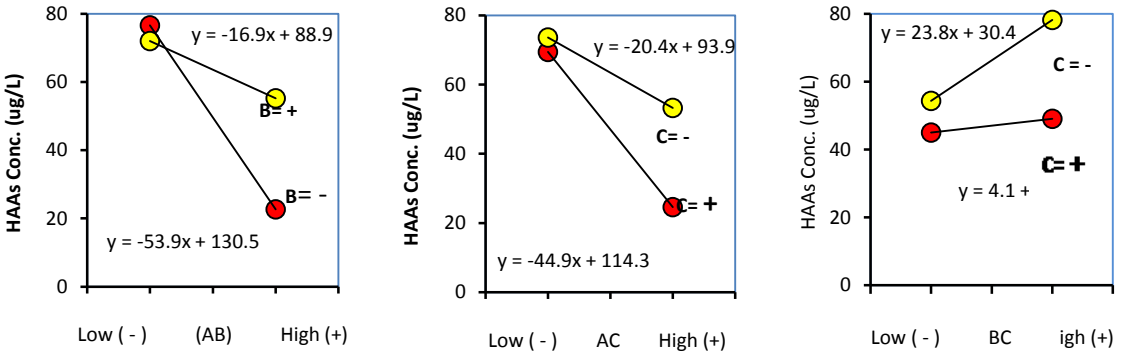

Figure C10. Interaction effect plots for AB (Fe(II) ions & pH), AC (Fe(II) ions & PO_4) and BC (pH & PO_4) for HAAs formation study.

Table C57. The paired Student t-test for THMs formation data obtained by the 2_4 full factorial design approach with center point level

Exp. No.	Reaction conditions	THMs-1	THMs-2	Difference, d_i (THM1-THM2)	d_i^2
1	Factorial design approach [F1]	14.74	15.44	-0.69	0.48
2	Factorial design approach [F2]	0.44	1.65	-1.21	1.47
3	Factorial design approach [F3]	22.38	26.34	-3.95	15.64
4	Factorial design approach [F4]	9.20	9.55	-0.35	0.12
5	Factorial design approach [F5]	30.91	24.92	5.99	35.83
6	Factorial design approach [F6]	17.02	19.03	-2.00	4.02
7	Factorial design approach [F7]	16.24	16.54	-0.31	0.09
8	Factorial design approach [F8]	4.03	5.68	-1.65	2.73
9	Factorial design approach [F9]	23.47	26.47	-3.00	9.02
10	Factorial design approach [F10]	0.72	1.53	-0.81	0.66
11	Factorial design approach [F11]	32.23	30.79	1.43	2.06
12	Factorial design approach [F12]	11.51	11.38	0.13	0.02
13	Factorial design approach [F13]	42.00	42.40	-0.41	0.16
14	Factorial design approach [F14]	11.17	17.46	-6.29	39.56
15	Factorial design approach [F15]	27.63	23.98	3.65	13.32
16	Factorial design approach [F16]	10.60	10.82	-0.22	0.05
17	Center point level I	16.54	18.38	-1.84	3.39
18	Center point level II	15.54	13.94	1.60	2.56
19	Center point level III	21.01	17.05	3.96	15.68
20	Center point level IV	15.44	17.04	-1.60	2.56
Sum				$\sum d_i$ = -7.58	$\sum d_i^2$ = 149.4

Average of the paired difference ($\bar{d}$):

$$\bar{d} = \frac{\sum d_i}{n} = \frac{7.58}{20} = 0.379$$

Root of the variance of the paired difference (s_d) = 2.78

Standard error of the average of the paired difference ($S_{\bar{d}}$) =0.621

The paired Student t-test (t_{stat}) = 0.61

Comments: At a 95% confidence interval with ν = n-1 degree of freedom, the critic value for t is $t_{0.025,\ (n-1)} = t_{0.025,19} = 2.093$. Here, $t_{stat} < t_{critic}$ (0.61 < 2.093); it reveals that there is no significance difference between the two sets of data for THMs formation.

Table C58. ANOVA test for 2^4 full factorial design for THMs formation model.

Source	*DF*	*Seq SS*	*Adj SS*	*Adj MS*	*F*	*P*	*%*
Main Effect	4	1418.53	1418.53	354.63	46.97	0.000	
Fe(II)	1	1178.81	1178.81	1178.81	156.12	0.000	60.41
pH	1	6.55	6.55	6.55	0.87	0.394	0.34
PO4	1	106.53	106.53	106.53	14.11	0.013	5.46
Time	1	126.65	126.65	126.65	16.77	0.009	6.49
2-Way Interaction	6	495.15	495.15	82.53	10.93	0.009	
Fe(II).*pH	1	12.21	12.21	12.21	1.62	0.259	0.63
Fe(II)*PO4	1	4.55	4.55	4.55	0.6	0.473	0.23
Fe(II)*Time	1	82.97	82.97	82.97	10.99	0.021	4.25
pH*PO4	1	391.69	391.69	391.69	51.88	0.001	20.07
pH*Time	1	0.97	0.97	0.97	0.13	0.734	0.05
PO4*Time	1	2.76	2.76	2.76	0.37	0.572	0.14
Residual Error	5	37.75	37.75	7.55			
Total	15	1951.44					

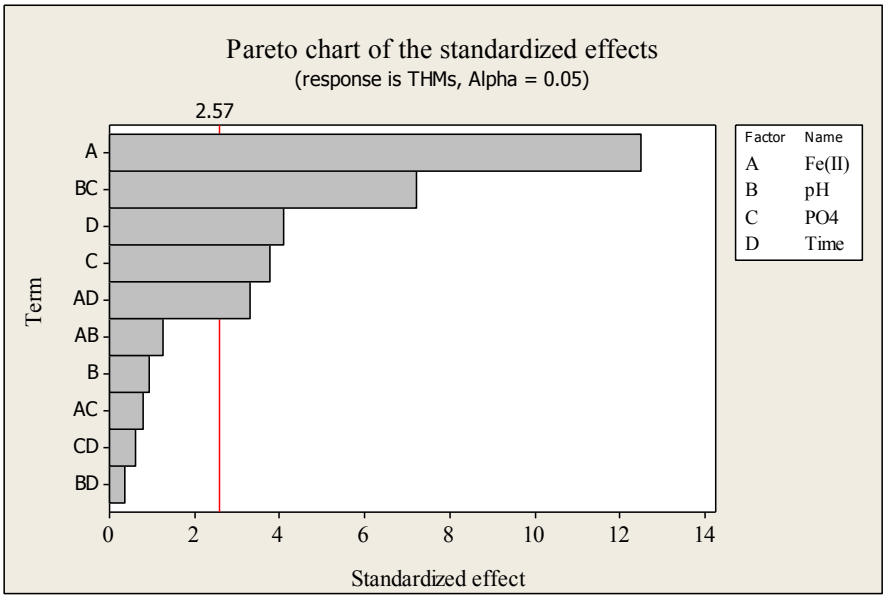

Figure C11. Pareto chart of the standardized effects for THMs formation.

Table C59. ANOVA test for 2^4 full factorial design with center point for THMs formation study.

Source	DF	Seq SS	Adj SS	Adj MS	*F*	*P*
Main Effects	4	1418.53	1418.53	354.63	89.59	0.000
Fe(II)	1	1178.81	1178.81	1178.81	297.79	0.000
pH	1	6.55	6.55	6.55	1.65	0.268
PO4	1	106.53	106.53	106.53	26.91	0.007
Time	1	126.65	126.65	126.65	31.99	0.005
2-Way Interactions	6	495.15	495.15	82.53	20.85	0.006
Fe(II)*pH	1	12.21	12.21	12.21	3.08	0.154
Fe(II)*PO4	1	4.55	4.55	4.55	1.15	0.344
Fe(II)*Time	1	82.97	82.97	82.97	20.96	0.010
pH*PO4	1	391.69	391.69	391.69	98.95	0.001
pH*Time	1	0.97	0.97	0.97	0.25	0.646
PO4*Time	1	2.76	2.76	2.76	0.70	0.451
3-Way Interactions	4	31.87	31.87	7.97	2.01	0.257
Fe(II)*pH*PO4	1	4.31	4.31	4.31	1.09	0.356
Fe(II)*pH*Time	1	22.93	22.93	22.93	5.79	0.074
Fe(II)*PO4*Time	1	2.78	2.78	2.78	0.70	0.449
pH*PO4*Time	1	1.85	1.85	1.85	0.47	0.532
Curvature	1	1.07	1.07	1.07	0.27	0.631
Residual Error	4	15.83	15.83	3.96		
Lack of Fit	1	5.89	5.89	5.89	1.78	0.275
Pure Error	3	9.95	9.95	3.32		
Total	19	1962.45				

Table C60. ANOVA (analysis of variance) test for 2^4 full factorial design with center point for THMs formation study.

Source	*DF*	*Seq SS*	*Adj SS*	*Adj MS*	*F*	*P*
Main Effect	4	1418.53	1418.53	354.63	62.41	0.000
Fe(II)	1	1178.81	1178.81	1178.81	207.44	0.000*
pH	1	6.55	6.55	6.55	1.15	0.304
PO_4	1	106.53	106.53	106.53	18.75	0.001*
Time	1	126.65	126.65	126.65	22.29	0.000*
2-Way Interaction	2	474.66	474.66	237.33	41.76	0.000
Fe(II)*Time	1	82.97	82.97	82.97	14.60	0.002*
pH*PO_4	1	391.69	391.69	391.69	68.93	0.000*
Curvature	1	1.07	1.07	1.07	0.19	0.673
Residual Error	12	68.19	68.19	5.68		
Lack of Fit	9	58.24	58.24	6.47	1.95	0.316
Pure Error	3	9.95	9.95	3.32		
Total	19	1962.45				

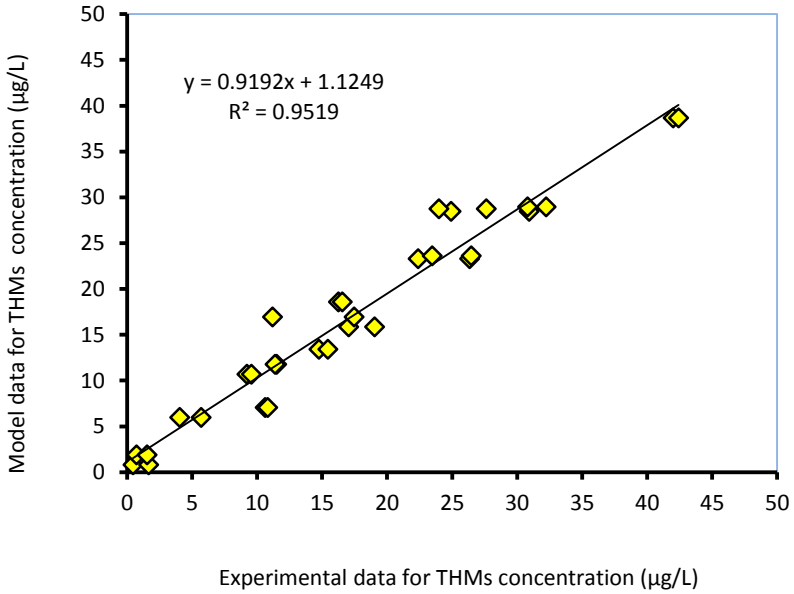

Figure C12. A liner graph between the experimental and model data for THMs formation study.

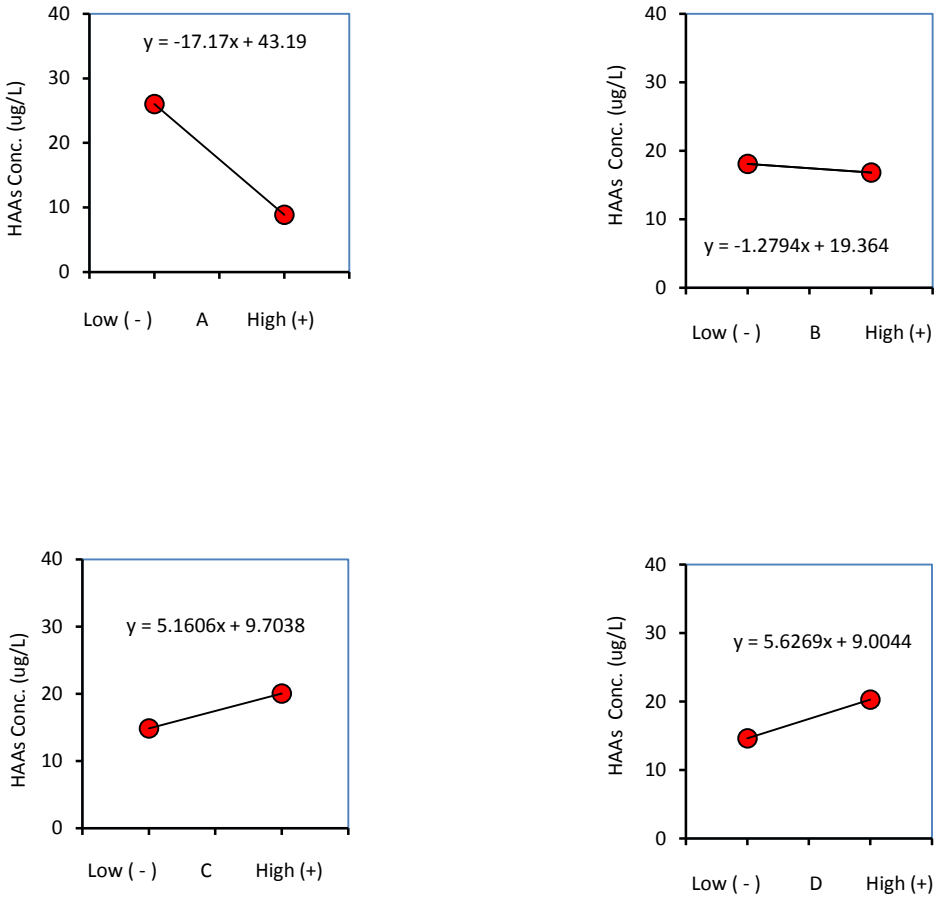

Figure C13. Main effect plots of A (Fe(II) ions concentration), C (PO_4) and D (reaction time) for THMs formation study.

APPENDIX D. Chapter 7: Raw and Supplemental Data

Table D1. The average HAAs concentration for different reaction time (h) in control systems using JDK post filtered water samples [Chlorine dosage = 2.24 mg/L, pH =7.4, lab temperature (21 ± 1 °C)]

Sl No	HAA species	Average HAAs concentration for different reaction time (h)					
		2 h	24 h	48 h	72 h	96 h	120 h
1	MCAA	0.00	0.00	0.00	0.00	3.38	0.00
2	MBAA	0.00	0.66	0.75	0.00	0.00	0.00
3	DCAA	44.49	46.08	53.76	57.94	58.89	59.39
4	TCAA	29.72	37.63	36.10	45.05	41.64	36.93
5	BCAA	1.34	1.89	2.56	2.64	2.41	2.27
6	DBAA	0.40	0.40	0.33	0.00	0.28	0.00
7	BDCAA	2.31	3.24	3.66	2.03	1.26	3.49
8	CDBAA	0.41	0.00	0.00	0.00	0.00	0.00
9	TBAA	0.00	0.00	0.00	0.00	0.00	0.00
	Total HAAs	78.67	89.90	97.16	107.65	107.86	102.07

Table D2. The Average HAAs concentration for different reaction time (h) in presence of 4 g/L goethite in JDK post filtered water samples [Chlorine dosage = 2.24 mg/L, pH =7.4, lab temperature (21 ± 1 °C)].

Sl No	HAA species	Average HAAs concentration for different reaction time (h)					
		2 h	24 h	48 h	72 h	96 h	120 h
1	MCAA	1.52	0.00	0.00	2.69	2.83	2.38
2	MBAA	0.00	0.00	0.00	0.00	0.64	1.42
3	DCAA	46.00	56.39	64.79	73.06	76.70	79.70
4	TCAA	21.84	51.93	66.08	61.04	53.76	57.76
5	BCAA	0.15	1.27	1.34	1.98	2.05	2.05
6	DBAA	0.00	0.00	0.00	0.00	0.00	0.00
7	BDCAA	2.82	3.49	3.66	2.38	4.90	3.89
8	CDBAA	0.00	0.00	0.00	0.00	0.00	0.00
9	TBAA	0.00	0.00	0.00	0.00	0.00	0.00
	Total HAAs	72.00	113.07	135.00	141.00	140.00	147.00

Table D3. The average haloacetic acids (HAAs) concentration for different reaction time (h) in presence of 4 g/L magnetite in JDK post filtered water samples [Chlorine dosage = 2.24 mg/L, pH =7.4, lab temperature (21 ± 1 °C)].

Sl No	HAA species	Average HAAs concentration for different reaction time (h)					
		2 h	24 h	48 h	72 h	96 h	120 h
1	MCAA	2.64	1.54	2.67	1.95	1.27	0.00
2	MBAA	0.00	0.00	0.00	0.00	0.00	0.00
3	DCAA	43.39	46.77	49.89	47.33	42.24	41.79
4	TCAA	26.84	29.68	34.63	38.03	34.37	39.08
5	BCAA	0.98	0.80	0.84	1.17	1.46	1.34
6	DBAA	0.00	0.00	0.00	0.00	0.00	0.00
7	BDCAA	1.74	3.28	3.41	3.95	4.53	3.66
8	CDBAA	0.00	0.00	0.00	0.00	0.00	0.00
9	TBAA	0.00	0.00	0.00	0.00	0.00	0.00
Total HAAs		75.00	82.07	91.00	92.00	83.00	85.00

Table D4. The Average trihalomethanes (THMs) concentration for different reaction time (h) in control water systems [Chlorine dosage = 2.24 mg/L, pH =7.4, lab temperature (21 ± 1 °C)]

Sl No	HAA species	Average THMs concentration for different reaction time (h)					
		2 h	24 h	48 h	72 h	96 h	120 h
1	TCM	78.37	116.40	126.58	139.38	149.52	141.06
2	DCBM	8.83	10.10	9.90	10.93	11.00	9.58
3	CDBM	0.00	0.00	0.00	0.00	0.00	0.56
4	TBM	0.00	0.00	0.00	1.44	1.43	0.00
Total THMs		87.00	126.51	136.51	151.75	161.95	151.00

Table D5. The average trihalomethanes (THMs) concentration for different reaction time (h) in presence of 4 g/L gpethite in JDK post filtered water samples [Chlorine dosage = 2.24 mg/L, pH =7.4, lab temperature (21 ± 1 °C)]

Sl No	HAA species	Average THMs concentration for different reaction time (h)					
		2 h	24 h	48 h	72 h	96 h	120 h
1	TCM	56.06	109.31	151.29	149.32	157.50	158.52
2	DCBM	5.58	8.32	8.23	11.38	10.80	11.07
3	CDBM	1.56	1.73	0.00	1.52	1.05	1.43
4	TBM	0.00	0.00	0.00	0.00	0.00	0.00
Total THMs		63.21	119.36	159.36	162.22	169.00	171.00

Table D6. The average trihalomethanes (THMs) concentration for different reaction time (h) in presence of 4 g/L magnetite in JDK post filtered water samples [Chlorine dosage = 2.24 mg/L, pH =7.4, lab temperature (21 ± 1 °C)]

Sl No	HAA species	Average THMs concentration for different reaction time (h)					
		2 h	24 h	48 h	72 h	96 h	120 h
1	TCM	71.95	106.05	119.72	111.59	119.28	109.97
2	DCBM	8.58	8.13	7.75	8.12	7.69	10.44
3	CDBM	1.42	1.54	0.73	1.62	1.64	1.58
4	TBM	0.00	0.00	0.00	0.00	0.00	0.00
Total THMs		82.00	115.00	128.73	121.00	128.92	122.00

Table D7a. Two-way ANOVA for the effect of iron oxide dosages and type of iron oxides on residual chlorine concentration in JDK post filtered water samples.

Table D7a. ANOVA: Two-Factor Without Replication

SUMMARY	*Count*	*Sum*	*Average*	*Variance*
Row 1	2	1.63	0.815	0.09245
Row 2	2	1.465	0.7325	0.137813
Row 3	2	1.24	0.62	0.19845
Row 4	2	1.15	0.575	0.18605
Row 5	2	1.136	0.568	0.188498
Column 1	5	1.906	0.3812	0.022095
Column 2	5	4.715	0.943	0.004733

Table D7b. ANOVA: Two-way for iron oxide dosage and types of iron oxides on residual chlorine concentration in JDK post filtered water samples

Source of Variation	*SS*	*df*	*MS*	*F*	*P-value*	*F crit*
Iron oxide dosage	0.093096	4	0.023274	6.550364	0.047978	6.388233
Types of iron oxide	0.789048	1	0.789048	222.0731	0.000118	7.708647
Error	0.014212	4	0.003553			
Total	0.896357	9				

Molecular weight distribution of DOM in JDK post filtered water samples

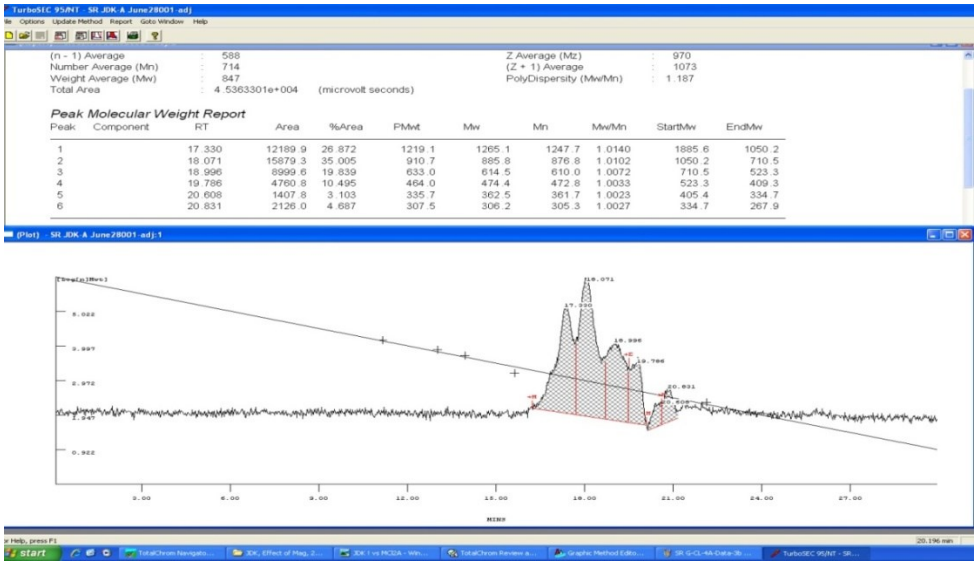

Figure D1. HPSEC Chromatograms for JDK water in control system

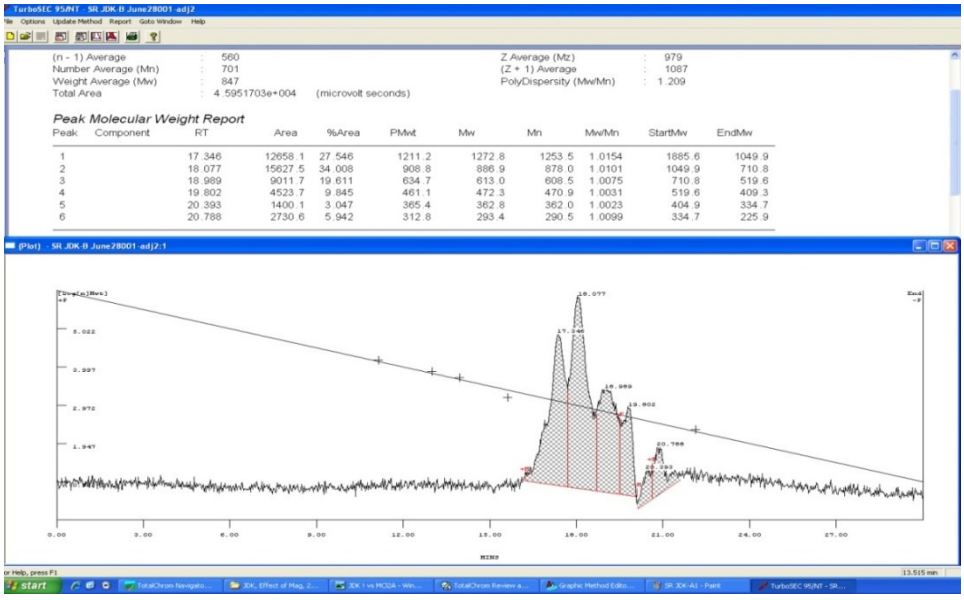

Figure D2. HPSEC Chromatograms for JDK water in control system

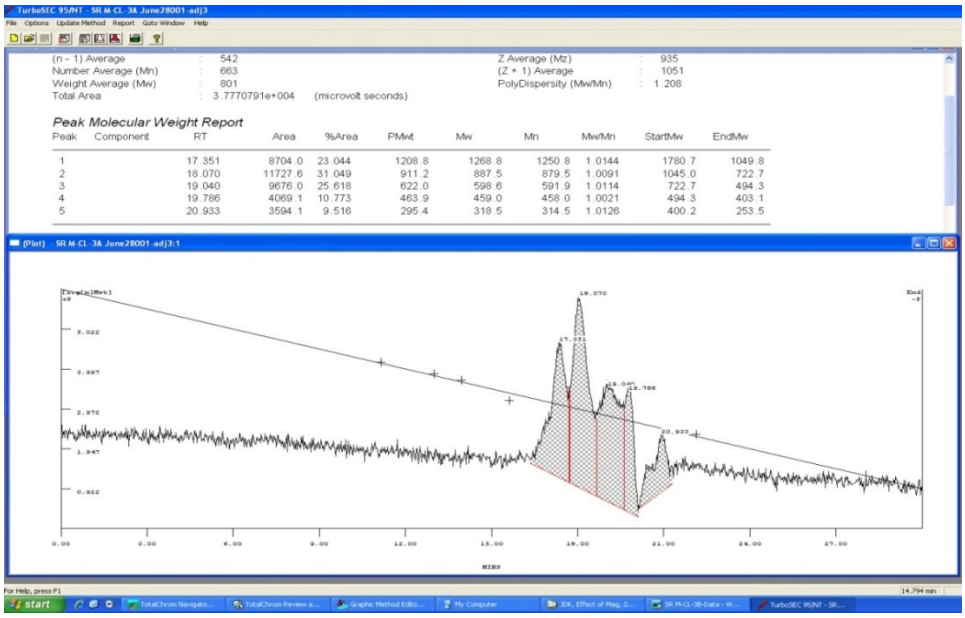

Figure D3. HPSEC Chromatograms for JDK water in aqueous-magnetite system

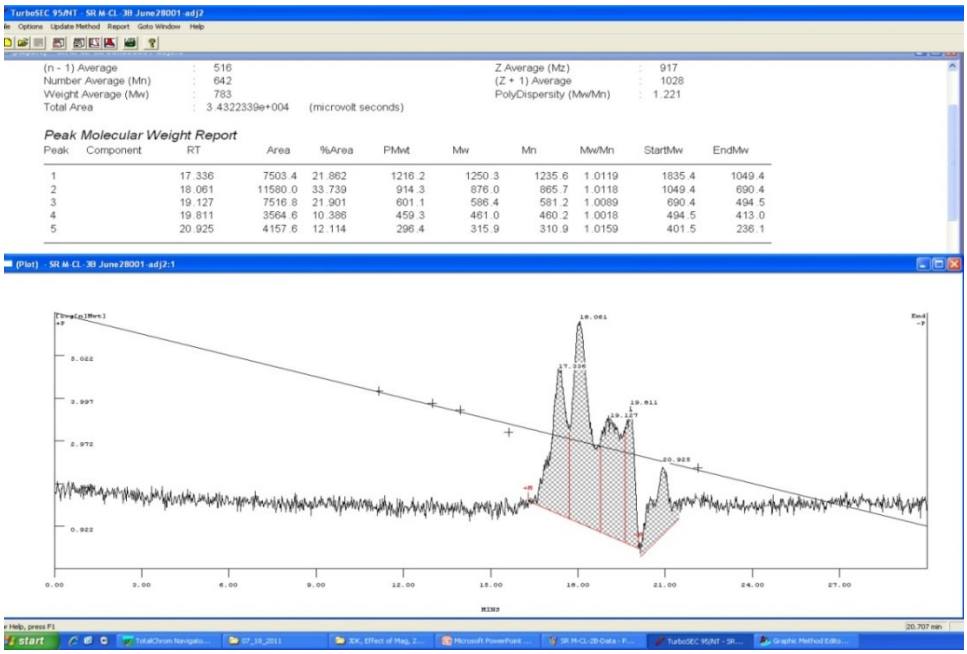

Figure D4. HPSEC Chromatograms for JDK water in aqueous magnetite system

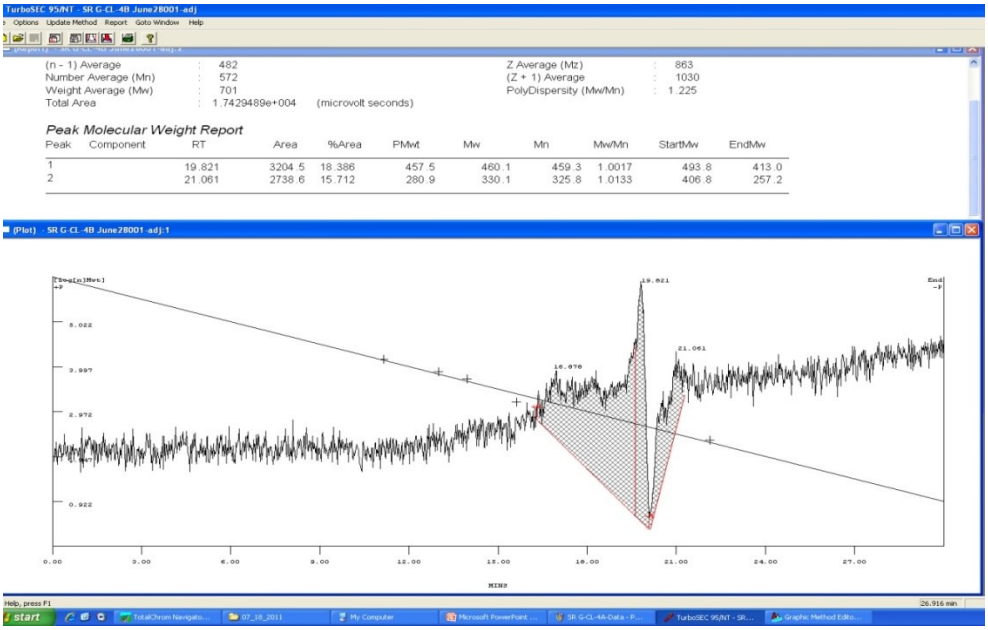

Figure D5. HPSEC Chromatograms for JDK water in aqueous goethite system

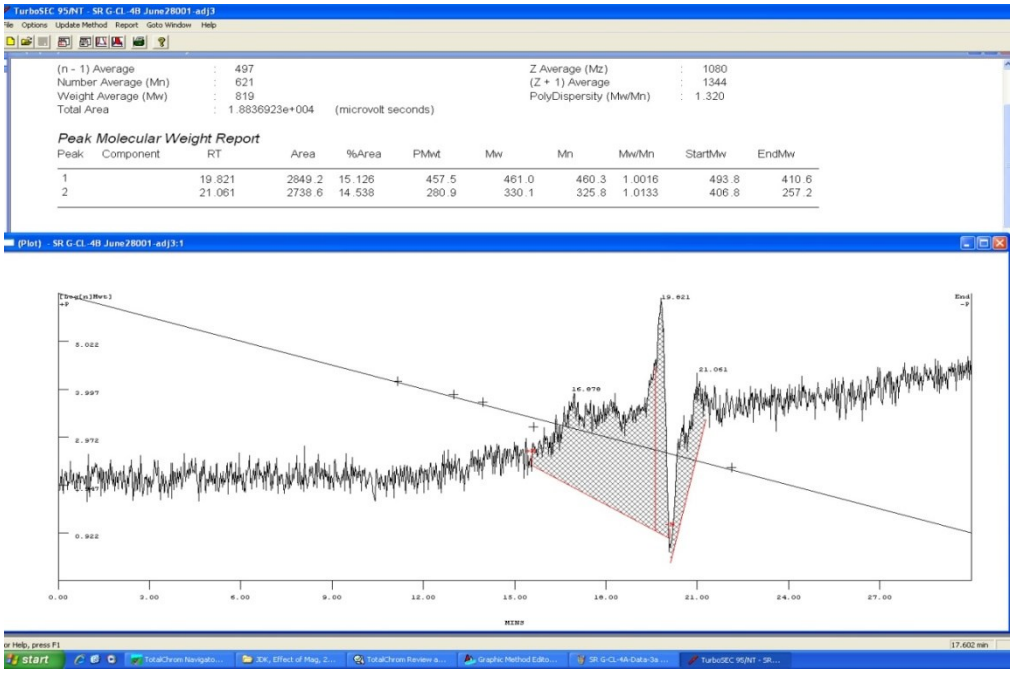

Figure D6. HPSEC Chromatograms for JDK water in aqueous goethite system

APPENDIX E. Chapter 8: Raw and Supplemental Data

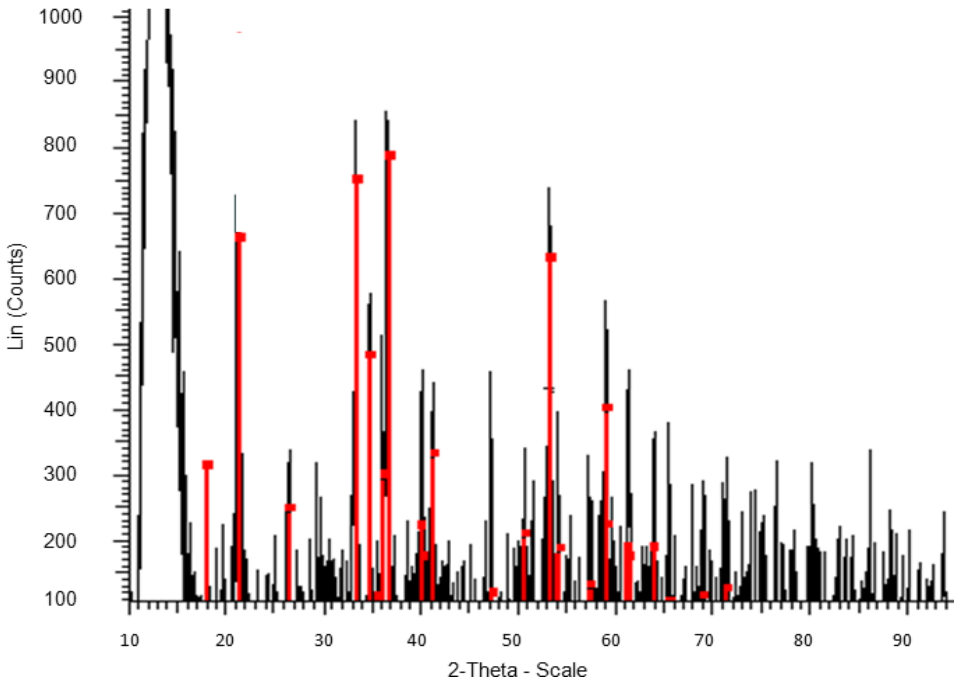

Figure E1. XRD patterns of the synthesized goethite, measured in Process Engineering Department at Dalhousie University using a high-speed XRD system (XRD D8 Advance, Bruker, Germany). Black colored spectrums represent the peaks for model raw goethite and red colored spectrums represent synthesized goethite (Type: 2Th/Th locked – Start: 20.000° -End: 95.197° -Step: 0.050° - Temp.: 25 °C (Room) –T Operation: Strip kAlpha2 0.500.

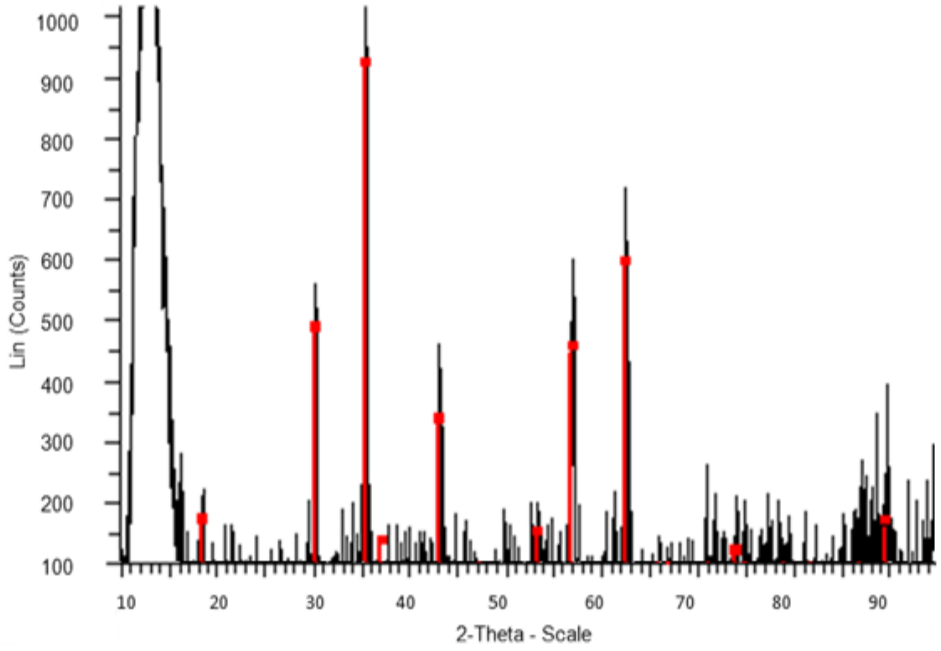

Figure E2. XRD patterns of the synthesized magnetite, measured in Process Engineering Department at Dalhousie University using a high-speed XRD system (XRD D8 Advance, Bruker, Germany). Black colored spectrums represent the peaks for model raw magnetite and red colored spectrums represent synthesized magnetite (Type: 2Th/Th locked – Start: 20.000° -End: 95.197° -Step: 0.050° - Temp.: 25 °C (Room) –T Operation: Strip kAlpha2 0.500.

Table E1. Adsorption of DOM onto goethite at pH 2.5

Goethite Dose, M (g/L)	Initial Conc., C_i (mg-C/L)	Equilibrium Conc., C_e (mg-C/L)	Mass Adsorbed q_e (Exp.) (mg-C/L)	$\frac{C_e}{q_e}$	Mass Adsorbed q_e (Model) (mg-C/L)
0.25	6.39	5.400	4.000	1.350	4.029
0.5	6.39	4.450	3.900	1.141	3.929
1	6.39	2.500	3.900	0.641	3.540
1.5	6.39	1.551	3.233	0.480	3.110
2	6.39	1.042	2.679	0.389	2.691
2.5	6.39	0.533	2.347	0.227	1.930
3.5	6.39	0.497	1.687	0.295	1.854
4.5	6.39	0.389	1.336	0.291	1.591
5.5	6.39	0.310	1.107	0.280	1.364
6.5	6.39	0.240	0.948	0.253	1.133
1.5	2.85	0.421	1.619	0.260	1.674
2.5	2.85	0.380	0.988	0.385	1.567
3.5	2.85	0.234	0.747	0.313	1.112
4.5	2.85	0.022	0.629	0.034	0.131
6.5	2.85	0.013	0.436	0.030	0.080

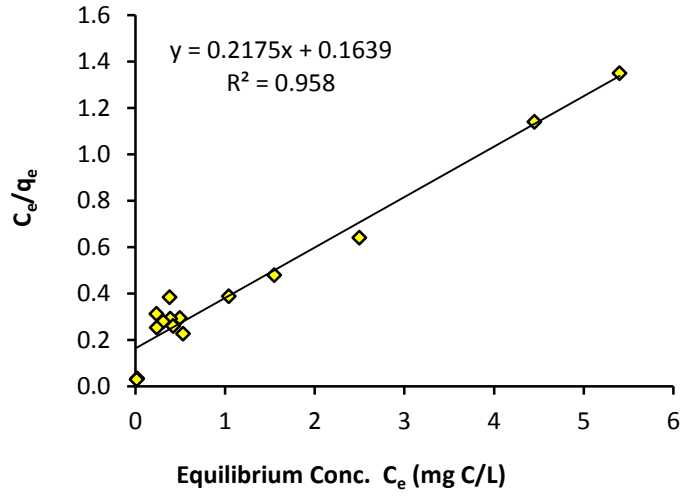

Figure E3. The Langmuir adsorption isotherm in linearized form: C_e/q_e vs C_e for goethite at pH 2.5.

$$Slope = m = \frac{1}{q_m} = 0.2715$$

$$q_m = 4.572$$

$$Maximum\ adsorption\ capacity\ (q_m) = 4.572\ mg - C/g\ \ goethite$$

$$Intercept = C = \frac{1}{q_m K_L} = 0.1639$$

$$K_L = 1.3\ L/mg$$

$$The\ Langmuir\ adsorption\ constant\ (K_L) = 1.3\ L/mg$$

Table E2. Student paired *t*-test for DOM adsorption capacity of experimental and model data at pH 2.5

	Variable 1	*Variable 2*
Mean	1.97	1.98
Variance	1.63	1.54
Observations	15.00	15.00
Pooled Variance	1.58	
Hypothesized Mean Difference	0.00	
df	28.00	
t Stat	-0.03	
P(T<=t) one-tail	0.49	
t Critical one-tail	1.70	
P(T<=t) two-tail	0.98	
t Critical two-tail	2.05	

Remark: The student paired *t*-test revealed that the *t* observation value is smaller than *t* table value ($t_{stat} \leq t_{crit}$). Therefore, it can be concluded that the model data is found to be indistinguishable from the experimental data at the significance level of 0.05 (95% confidence level).

Table E3. Student paired *t*-test for DOM adsorption capacity of experimental and model data at pH 4.5

Goethite Dose, M (g/L)	Initial Conc., C_i (mg-C/L)	Equilibrium Conc., C_e (mg-C/L)	Mass Adsorbed q_e (Exp.) (mg-C/L)	$\frac{C_e}{q_e}$	Mass Adsorbed q_e (Model) (mg-C/L)
0.25	6.39	5.650	3.400	1.662	3.509
0.5	6.39	4.765	3.470	1.373	3.391
1	6.39	3.172	3.329	0.953	3.062
1.5	6.39	2.352	2.765	0.851	2.780
2	6.39	1.390	2.555	0.544	2.231
2.5	6.39	1.198	2.121	0.565	2.071
3.5	6.39	0.850	1.614	0.527	1.707
4.5	6.39	0.780	1.271	0.614	1.619
5.5	6.39	0.650	1.064	0.611	1.439
6.5	6.39	0.472	0.927	0.509	1.150
1.5	2.85	0.450	1.600	0.281	1.110
2.5	2.85	0.410	0.976	0.420	1.035
3.5	2.85	0.251	0.743	0.338	0.699
4.5	2.85	0.027	0.627	0.043	0.088
6.5	2.85	0.190	0.409	0.464	0.551

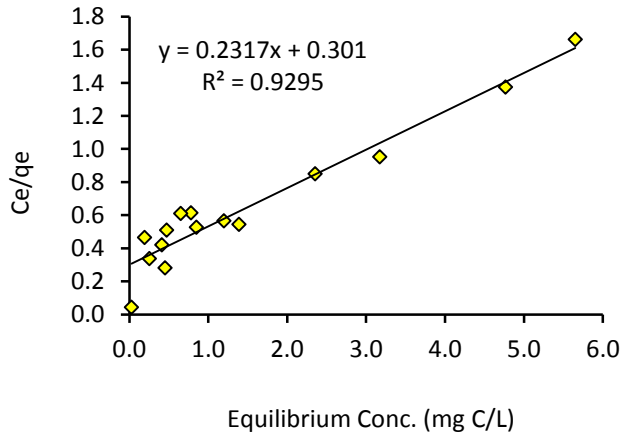

Figure E4. The Langmuir adsorption isotherm in linearized form: C_e/q_e *vs* C_e for goethite at pH 4.5.

$$Slope = m = \frac{1}{q_m} = 0.232$$

$$q_m = 4.316$$

$$Maximum\ adsorption\ capacity\ (q_m) = 4.316\ mg - C/g\ \ goethite$$

$$Intercept = C = \frac{1}{q_m K_L} = 0.301$$

$$K_L = 0.77\ L/mg$$

$$The\ Langmuir\ adsorption\ constant\ (K_L) = 0.77\ L/mg$$

Table E4. Student paired *t*-test for DOM adsorption capacity of experimental and model data at pH 4.5

	Variable 1	*Variable 2*
Mean	1.79	1.76
Variance	1.15	1.11
Observations	15.00	15.00
Pooled Variance	1.13	
Hypothesized Mean Difference	0.00	
df	28.00	
t Stat	0.07	
P(T<=t) one-tail	0.47	
t Critical one-tail	1.70	
P(T<=t) two-tail	0.94	
t Critical two-tail	2.05	

Remark: The student paired *t*-test revealed that the *t* observation value is smaller than *t* table value ($t_{stat} \leq t_{crit}$). Therefore, it can be concluded that the model data is found to be indistinguishable from the experimental data at the significance level of 0.05 (95% confidence level).

Table E5. Adsorption of DOM onto goethite at pH 6.5

Goethite Dose, M (g/L)	Initial Conc., C_i (mg-C/L)	Equilibrium Conc., C_e (mg-C/L)	Mass Adsorbed q_e (Exp.) (mg-C/L)	$\frac{C_e}{q_e}$	Mass Adsorbed q_e (Model) (mg-C/L)
0.25	6.39	5.758	2.968	1.940	3.065
0.5	6.39	5.041	2.918	1.728	2.962
1	6.39	3.655	2.845	1.285	2.688
1.5	6.39	2.575	2.617	0.984	2.356
2	6.39	1.989	2.256	0.882	2.098
2.5	6.39	1.450	2.020	0.718	1.779
3.5	6.39	1.250	1.500	0.833	1.632
4.5	6.39	0.971	1.229	0.790	1.393
5.5	6.39	0.880	1.022	0.861	1.305
6.5	6.39	0.764	0.882	0.866	1.183
1.5	2.85	0.696	1.436	0.484	1.106
2.5	2.85	0.463	0.955	0.485	0.810
3.5	2.85	0.340	0.717	0.474	0.628
4.5	2.85	0.290	0.569	0.510	0.549
6.5	2.85	0.210	0.406	0.517	0.413

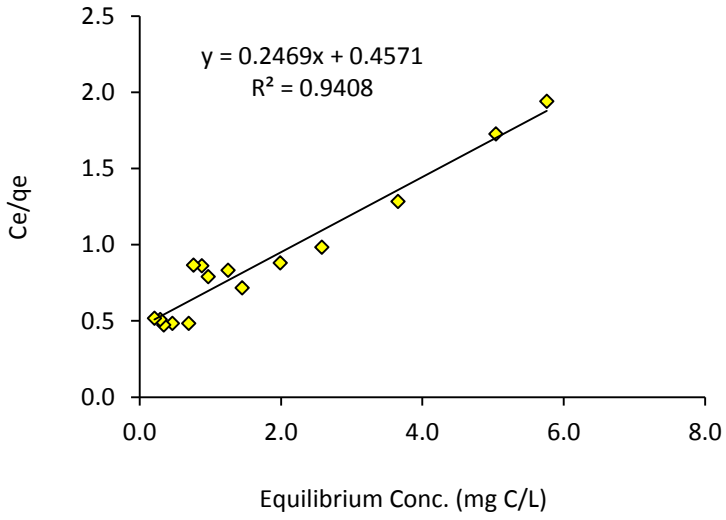

Figure E5. The Langmuir adsorption isotherm in linearized form: C_e/q_e vs C_e for goethite at pH 6.5.

$$Slope = m = \frac{1}{q_m} = 0.247$$

$$q_m = 4.05$$

$$Maximum\ adsorption\ capacity\ (q_m) = 4.05\ mg - C/g\ \ goethite$$

$$Intercept = C = \frac{1}{q_m K_L} = 0.457$$

$$K_L = 0.54\ L/mg$$

$$The\ Langmuir\ adsorption\ constant\ (K_L) = 0.54\ L/mg$$

Table E6. Student paired *t*-test DOM adsorption capacity of experimental and model data at pH 6.5

	Variable 1	*Variable 2*
Mean	1.62	1.60
Variance	0.82	0.76
Observations	15.00	15.00
Pooled Variance	0.79	
Hypothesized Mean Difference	0.00	
df	28.00	
t Stat	0.08	
P(T<=t) one-tail	0.47	
t Critical one-tail	1.70	
P(T<=t) two-tail	0.94	
t Critical two-tail	2.05	

Remark: The student paired *t*-test revealed that the *t* observation value is smaller than *t* table value ($t_{stat} \leq t_{crit}$). Therefore, it can be concluded that the model data is found to be indistinguishable from the experimental data at the significance level of 0.05 (95% confidence level).

Table E7. Adsorption of DOM onto goethite at pH 8.5

Goethite Dose, M (g/L)	Initial Conc., C_i (mg-C/L)	Equilibrium Conc., C_e (mg-C/L)	Mass Adsorbed q_e (Exp.) (mg-C/L)	$\frac{C_e}{q_e}$	Mass Adsorbed q_e (Model) (mg-C/L)
0.25	6.39	5.969	2.125	2.809	2.189
0.5	6.39	5.453	2.093	2.605	2.145
1	6.39	4.400	2.100	2.095	2.029
1.5	6.39	3.375	2.083	1.620	1.871
2	6.39	2.748	1.876	1.465	1.738
2.5	6.39	2.195	1.722	1.274	1.585
3.5	6.39	1.725	1.364	1.264	1.416
4.5	6.39	1.697	1.067	1.590	1.405
5.5	6.39	1.088	0.984	1.106	1.097
6.5	6.39	0.816	0.859	0.950	0.912
1.5	2.85	0.865	1.323	0.654	0.949
2.5	2.85	0.450	0.960	0.469	0.588
3.5	2.85	0.370	0.709	0.522	0.503
4.5	2.85	0.320	0.562	0.569	0.445
6.5	2.85	0.290	0.394	0.736	0.410

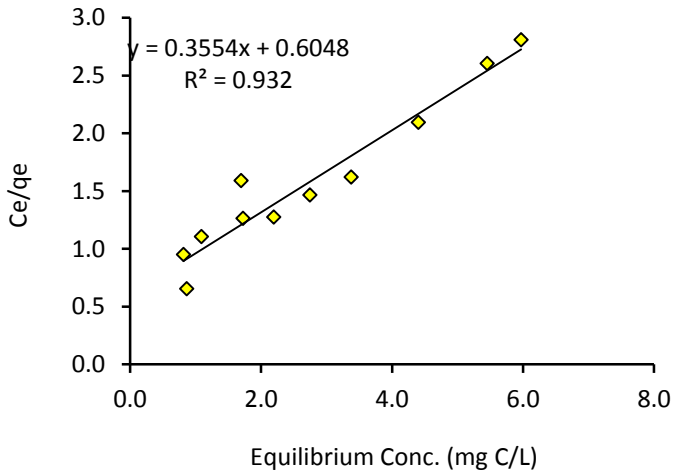

Figure E6. The Langmuir adsorption isotherm in linearized form: C_e/q_e vs C_e for goethite at pH 8.5.

$$Slope = m = \frac{1}{q_m} = 0.355$$

$$q_m = 2.814$$

$$Maximum\ adsorption\ capacity\ (q_m) = 2.814\ mg - C/g\ \ goethite$$

$$Intercept = C = \frac{1}{q_m K_L} = 0.605$$

$$K_L = 0.588\ L/mg$$

$$The\ Langmuir\ adsorption\ constant\ (K_L) = 0.588\ L/mg$$

Table E8. Student paired *t*-test DOM adsorption capacity of experimental and model data at pH 8.5

	Variable 1	*Variable 2*
Mean	1.35	1.29
Variance	0.37	0.40
Observations	15.00	15.00
Pooled Variance	0.39	
Hypothesized Mean Difference	0.00	
df	28.00	
t Stat	0.28	
P(T<=t) one-tail	0.39	
t Critical one-tail	1.70	
P(T<=t) two-tail	0.78	
t Critical two-tail	2.05	

Remark: The student paired *t*-test revealed that the *t* observation value is smaller than *t* table value ($t_{stat} \leq t_{crit}$). Therefore, it can be concluded that the model data is found to be indistinguishable from the experimental data at the significance level of 0.05 (95% confidence level).

Table E9. Adsorption of DOM onto goethite at pH 10.5

Goethite Dose, M (g/L)	Initial Conc., C_i (mg-C/L)	Equilibrium Conc., C_e (mg-C/L)	Mass Adsorbed q_e (Exp.) (mg-C/L)	$\frac{C_e}{q_e}$	Mass Adsorbed q_e (Model) (mg-C/L)
0.25	6.39	6.111	1.556	0.643	1.588
0.5	6.39	5.713	1.574	0.635	1.570
1	6.39	4.950	1.550	0.645	1.527
1.5	6.39	4.268	1.488	0.672	1.478
2	6.39	3.615	1.443	0.693	1.419
2.5	6.39	2.945	1.422	0.703	1.339
3.5	6.39	2.120	1.251	0.799	1.198
4.5	6.39	1.780	1.049	0.953	1.118
5.5	6.39	1.539	0.902	1.109	1.049
6.5	6.39	1.316	0.797	1.254	0.975
1.5	2.85	1.212	1.092	0.916	0.935
2.5	2.85	0.850	0.800	1.250	0.767
3.5	2.85	0.610	0.640	1.563	0.621
4.5	2.85	0.410	0.542	1.844	0.467
6.5	2.85	0.320	0.389	2.569	0.385

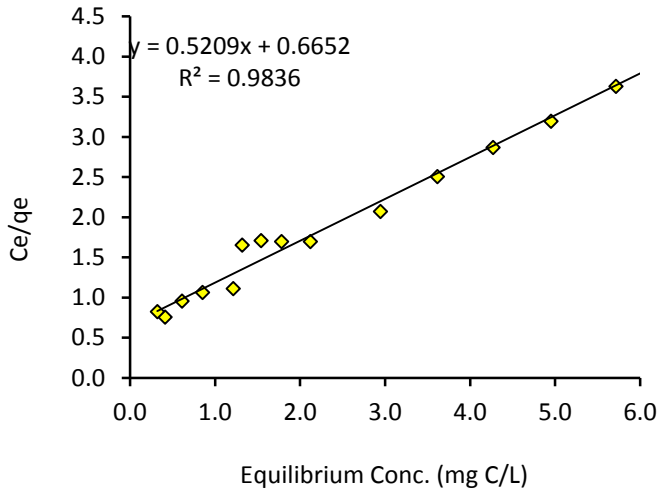

Figure E7. The Langmuir adsorption isotherm in linearized form: $C_e/q_e \ vs \ C_e$ for goethite at pH 10.5.

$$Slope = m = \frac{1}{q_m} = 0.521$$

$$q_m = 1.92$$

$$Maximum\ adsorption\ capacity\ (q_m) = 2.814\ mg - C/g\ \ goethite$$

$$Intercept = C = \frac{1}{q_m K_L} = 0.665$$

$$K_L = 0.783\ L/mg$$

$$The\ Langmuir\ adsorption\ constant\ (K_L) = 0.783\ L/mg$$

Table E10. Student paired *t*-test DOM adsorption capacity of experimental and model data at pH 10.5.

	Variable 1	*Variable 2*
Mean	1.10	1.10
Variance	0.16	0.16
Observations	15.00	15.00
Pooled Variance	0.16	
Hypothesized Mean Difference	0.00	
df	28.00	
t Stat	0.03	
P(T<=t) one-tail	0.49	
t Critical one-tail	1.70	
P(T<=t) two-tail	0.98	
t Critical two-tail	2.05	

Remark: The student paired *t*-test revealed that the *t* observation value is smaller than *t* table value ($t_{stat} \leq t_{crit}$). Therefore, it can be concluded that the model data is found to be indistinguishable from the experimental data at the significance level of 0.05 (95% confidence level).

Table E11. Adsorption of DOM onto magnetite at pH 2.5

Goethite Dose, M (g/L)	Initial Conc., C_i (mg-C/L)	Equilibrium Conc., C_e (mg-C/L)	Mass Adsorbed q_e (Exp.) (mg-C/L)	$\frac{C_e}{q_e}$	Mass Adsorbed q_e (Model) (mg-C/L)
0.25	6.39	5.658	2.967	1.907	3.044
0.5	6.39	4.895	3.010	1.626	2.953
1	6.39	3.581	2.819	1.271	2.730
1.5	6.39	2.480	2.613	0.949	2.426
2	6.39	1.789	2.305	0.776	2.129
2.5	6.39	1.520	1.952	0.779	1.975
3.5	6.39	1.125	1.507	0.746	1.690
4.5	6.39	0.901	1.222	0.738	1.486
5.5	6.39	0.679	1.040	0.653	1.239
6.5	6.39	0.627	0.888	0.706	1.173
1.5	2.85	0.652	1.465	0.445	1.205
2.5	2.85	0.518	0.933	0.555	1.024
3.5	2.85	0.304	0.727	0.418	0.677
4.5	2.85	0.202	0.589	0.342	0.477
6.5	2.85	0.091	0.424	0.215	0.232

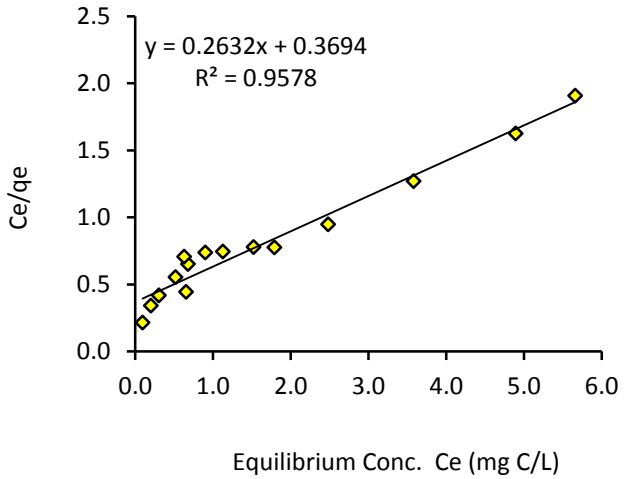

Figure E8. The Langmuir adsorption isotherm in linearized form: C_e/q_e vs C_e for magnetite at pH 2.5.

$$Slope = m = \frac{1}{q_m} = 0.2632$$

$$q_m = 3.799$$

$$Maximum\ adsorption\ capacity\ (q_m) = 2.814\ mg - \frac{C}{g}\ goethite$$

$$Intercept = C = \frac{1}{q_m K_L} = 0.3694$$

$$K_L = 0.713\ L/mg$$

$$The\ Langmuir\ adsorption\ constant\ (K_L) = 0.713\ L/mg$$

Table E12. Student paired *t*-test DOM adsorption capacity onto magnetite for experimental and model data at pH 2.5 (α = 0.05, p < 0.05).

	Variable 1	*Variable 2*
Mean	1.63	1.61
Variance	0.83	0.81
Observations	15.00	15.00
Pooled Variance	0.82	
Hypothesized Mean Difference	0.00	
df	28.00	
t Stat	0.07	
P(T<=t) one-tail	0.47	
t Critical one-tail	1.70	
P(T<=t) two-tail	0.95	
t Critical two-tail	2.05	

Remark: The student paired *t*-test revealed that the *t* observation value is smaller than *t* table value ($t_{stat} \leq t_{crit}$). Therefore, it can be concluded that the model data is found to be indistinguishable from the experimental data at the significance level of 0.05 (95% confidence level).

Table E13. Adsorption of DOM onto magnetite at pH 4.5

Goethite Dose, M (g/L)	Initial Conc., C_i (mg-C/L)	Equilibrium Conc., C_e (mg-C/L)	Mass Adsorbed q_e (Exp.) (mg-C/L)	$\frac{C_e}{q_e}$	Mass Adsorbed q_e (Model) (mg-C/L)
0.25	6.39	5.748	2.609	2.210	2.544
0.5	6.39	5.120	2.560	2.000	2.498
1	6.39	3.890	2.510	1.550	2.373
1.5	6.39	3.041	2.239	1.358	2.242
2	6.39	2.479	1.961	1.264	2.120
2.5	6.39	1.794	1.842	0.974	1.907
3.5	6.39	1.450	1.414	1.025	1.755
4.5	6.39	0.942	1.213	0.777	1.434
5.5	6.39	0.870	1.005	0.865	1.375
6.5	6.39	0.747	0.870	0.859	1.263
1.5	2.85	0.766	1.390	0.551	1.281
2.5	2.85	0.530	0.928	0.571	1.021
3.5	2.85	0.378	0.706	0.149	0.807
4.5	2.85	0.105	0.610	0.344	0.278
6.5	2.85	0.210	0.406	0.000	0.509

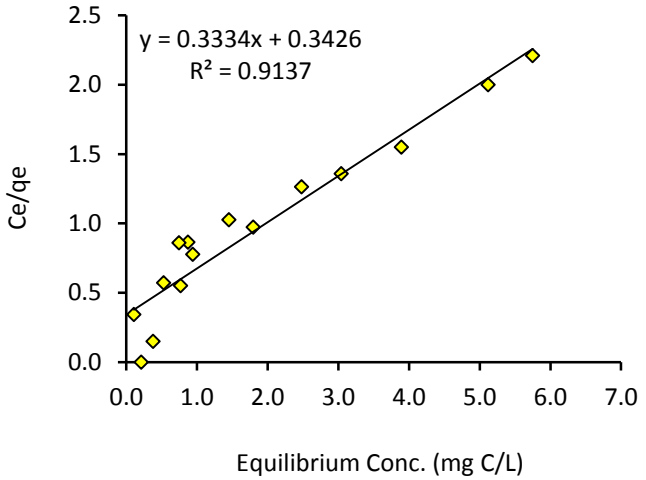

Figure E9. The Langmuir adsorption isotherm in linearized form: C_e/q_e vs C_e for magnetite at pH 4.5.

$$Slope = m = \frac{1}{q_m} = 0.3334$$

$q_m = 2.999$

$Maximum\ adsorption\ capacity\ (q_m) = 2.999\ mg - C/g\ \ goethite$

$Intercept = C = \frac{1}{q_m K_L} = 0.34256$

$K_L = 0.973\ L/mg$

$The\ Langmuir\ adsorption\ constant\ (K_L) = 0.973\ L/mg$

Table E14. Student paired *t*-test DOM adsorption capacity onto magnetite for experimental and model data at pH 4.5 (α = 0.05, p < 0.05).

	Variable 1	*Variable 2*
Mean	1.48	1.56
Variance	0.57	0.52
Observations	15.00	15.00
Pooled Variance	0.54	
Hypothesized Mean Difference	0.00	
df	28.00	
t Stat	-0.28	
P(T<=t) one-tail	0.39	
t Critical one-tail	1.70	
P(T<=t) two-tail	0.78	
t Critical two-tail	2.05	

Remark: The student paired *t*-test revealed that the *t* observation value is smaller than *t* table value ($t_{stat} \leq t_{crit}$). Therefore, it can be concluded that the model data is found to be indistinguishable from the experimental data at the significance level of 0.05 (95% confidence level).

Table E15. Adsorption of DOM on magnetite at pH 6.5

Goethite Dose, M (g/L)	Initial Conc., C_i (mg-C/L)	Equilibrium Conc., C_e (mg-C/L)	Mass Adsorbed q_e (Exp.) (mg-C/L)	$\frac{C_e}{q_e}$	Mass Adsorbed q_e (Model) (mg-C/L)
0.25	6.39	5.963	2.148	2.776	2.152
0.5	6.39	5.453	2.093	2.605	2.116
1	6.39	4.400	2.100	2.095	2.021
1.5	6.39	3.415	2.057	1.660	1.895
2	6.39	2.748	1.876	1.465	1.774
2.5	6.39	2.195	1.722	1.274	1.639
3.5	6.39	1.674	1.379	1.214	1.467
4.5	6.39	1.697	1.067	1.590	1.476
5.5	6.39	1.088	0.984	1.106	1.184
6.5	6.39	0.896	0.862	1.040	1.060
1.5	2.85	0.990	1.240	0.798	1.123
2.5	2.85	0.565	0.914	0.618	0.785
3.5	2.85	0.414	0.696	0.595	0.625
4.5	2.85	0.320	0.562	0.569	0.511
6.5	2.85	0.129	0.419	0.308	0.233

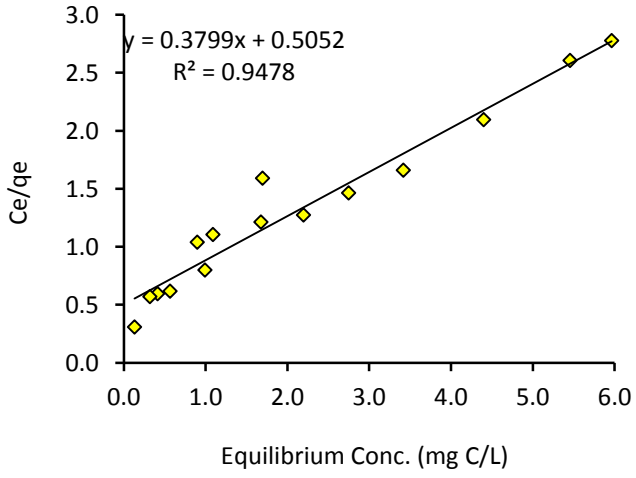

Figure E10. The Langmuir adsorption isotherm in linearized form: C_e/q_e vs C_e for magnetite at pH 6.5.

$$Slope = m = \frac{1}{q_m} = 0.3799$$

$$q_m = 2.632$$

$$Maximum\ adsorption\ capacity\ (q_m) = 2.632\ mg - C/g\ \ goethite$$

$$Intercept = C = \frac{1}{q_m K_L} = 0.5052$$

$$K_L = 0.752\ L/mg$$

$$The\ Langmuir\ adsorption\ constant\ (K_L) = 0.752\ L/mg$$

Table E16. Student paired *t*-test DOM adsorption capacity onto magnetite for experimental and model data at pH 6.5 (α = 0.05, $p < 0.05$).

	Variable 1	*Variable 2*
Mean	1.34	1.34
Variance	0.37	0.37
Observations	15.00	15.00
Pooled Variance	0.37	
Hypothesized Mean Difference	0.00	
df	28.00	
t Stat	0.02	
P(T<=t) one-tail	0.49	
t Critical one-tail	1.70	
P(T<=t) two-tail	0.99	
t Critical two-tail	2.05	

Remark: The student paired *t*-test revealed that the *t* observation value is smaller than *t* table value ($t_{stat} \leq t_{crit}$). Therefore, it can be concluded that the model data is found to be indistinguishable from the experimental data at the significance level of 0.05 (95% confidence level).

Table E17. Adsorption of DOM onto magnetite at pH 8.5

Goethite Dose, M (g/L)	Initial Conc., C_i (mg-C/L)	Equilibrium Conc., C_e (mg-C/L)	Mass Adsorbed q_e (Exp.) (mg-C/L)	$\frac{C_e}{q_e}$	Mass Adsorbed q_e (Model) (mg-C/L)
0.25	6.39	6.195	1.220	5.078	1.255
0.5	6.39	5.896	1.207	4.884	1.246
1	6.39	5.291	1.209	4.376	1.226
1.5	6.39	4.650	1.233	3.770	1.199
2	6.39	4.016	1.242	3.232	1.166
2.5	6.39	3.548	1.181	3.005	1.136
3.5	6.39	2.450	1.157	2.117	1.033
4.5	6.39	1.850	1.033	1.790	0.943
5.5	6.39	1.650	0.882	1.871	0.904
6.5	6.39	1.420	0.782	1.817	0.852
1.5	2.85	1.480	0.913	1.620	0.866
2.5	2.85	1.110	0.696	1.595	0.763
3.5	2.85	0.940	0.546	1.723	0.702
4.5	2.85	0.490	0.524	0.934	0.475
6.5	2.85	0.350	0.385	0.910	0.374

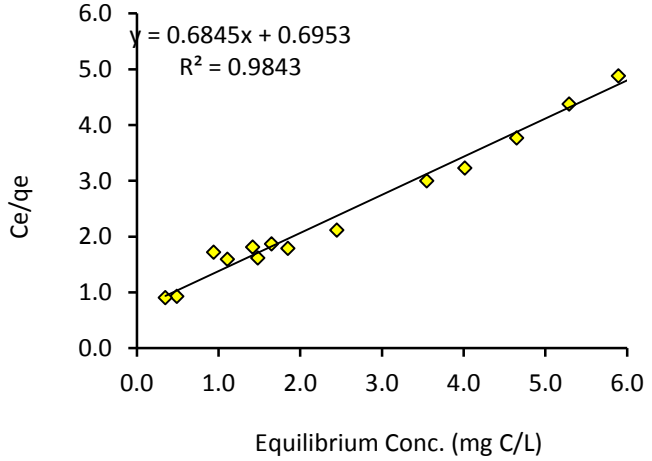

Figure E11. The Langmuir adsorption isotherm in linearized form: C_e/q_e vs C_e for magnetite at pH 8.5.

$$Slope = m = \frac{1}{q_m} = 0.6845$$

$$q_m = 1.461$$

$$Maximum\ adsorption\ capacity\ (q_m) = 1.461\ mg - C/g\ \ goethite$$

$$Intercept = C = \frac{1}{q_m K_L} = 0.6953$$

$$K_L = 0.984\ L/mg$$

$$Langmuir\ adsorption\ constant\ (K_L) = 0.984\ L/mg$$

Table E18. Student paired *t*-test DOM adsorption capacity onto magnetite for experimental and model data at pH 8.5 (α = 0.05, p < 0.05).

	Variable 1	*Variable 2*
Mean	0.95	0.94
Variance	0.09	0.08
Observations	15.00	15.00
Pooled Variance	0.08	
Hypothesized Mean Difference	0.00	
df	28.00	
t Stat	0.04	
P(T<=t) one-tail	0.48	
t Critical one-tail	1.70	
P(T<=t) two-tail	0.96	
t Critical two-tail	2.05	

Remark: The student paired *t*-test revealed that the *t* observation value is smaller than *t* table value ($t_{stat} \leq t_{crit}$). Therefore, it can be concluded that the model data is found to be indistinguishable from the experimental data at the significance level of 0.05 (95% confidence level).

Table E19. Adsorption of DOM onto magnetite at pH 10.5

Goethite Dose, M (g/L)	Initial Conc., C_i (mg-C/L)	Equilibrium Conc., C_e (mg-C/L)	Mass Adsorbed q_e (Exp.) (mg-C/L)	$\frac{C_e}{q_e}$	Mass Adsorbed q_e (Model) (mg-C/L)
0.25	6.39	6.231	1.076	5.791	1.059
0.5	6.39	5.980	1.039	5.754	1.053
1	6.39	5.456	1.045	5.223	1.041
1.5	6.39	5.043	0.972	5.190	1.029
2	6.39	4.461	1.019	4.377	1.009
2.5	6.39	4.022	0.991	4.058	0.991
3.5	6.39	3.124	0.965	3.239	0.943
4.5	6.39	2.270	0.940	2.415	0.871
5.5	6.39	1.750	0.864	2.026	0.804
6.5	6.39	1.420	0.782	1.817	0.746
1.5	2.85	1.565	0.857	1.826	0.773
2.5	2.85	1.110	0.696	1.595	0.674
3.5	2.85	0.940	0.546	1.723	0.624
4.5	2.85	0.650	0.489	1.330	0.513
6.5	2.85	0.510	0.360	1.417	0.443

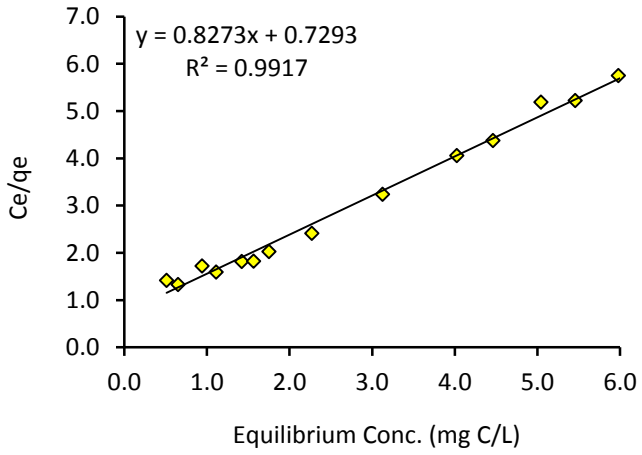

Figure E12. The Langmuir adsorption isotherm in linearized form: C_e/q_e vs C_e for magnetite at pH 10.5.

$$Slope = m = \frac{1}{q_m} = 0.8273$$

$$q_m = 1.209$$

$$Maximum\ adsorption\ capacity\ (q_m) = 1.461\ mg - C/g\ \ goethite$$

$$Intercept = C = \frac{1}{q_m K_L} = 0.7293$$

$$K_L = 1.134\ L/mg$$

$$The\ Langmuir\ adsorption\ constant\ (K_L) = 1.134\ L/mg$$

Table E20. Student paired *t*-test DOM adsorption capacity onto magnetite for experimental and model data at pH 10.5 (α = 0.05, p < 0.05).

	Variable 1	*Variable 2*
Mean	0.84	0.84
Variance	0.05	0.04
Observations	15.00	15.00
Pooled Variance	0.05	
Hypothesized Mean Difference	0.00	
df	28.00	
t Stat	0.06	
P(T<=t) one-tail	0.48	
t Critical one-tail	1.70	
P(T<=t) two-tail	0.95	
t Critical two-tail	2.05	

Remark: The student paired *t*-test revealed that the *t* observation value is smaller than *t* table value ($t_{stat} \leq t_{crit}$). Therefore, it can be concluded that the model data is found to be indistinguishable from the experimental data at the significance level of 0.05 (95% confidence level).

Zeta potential data

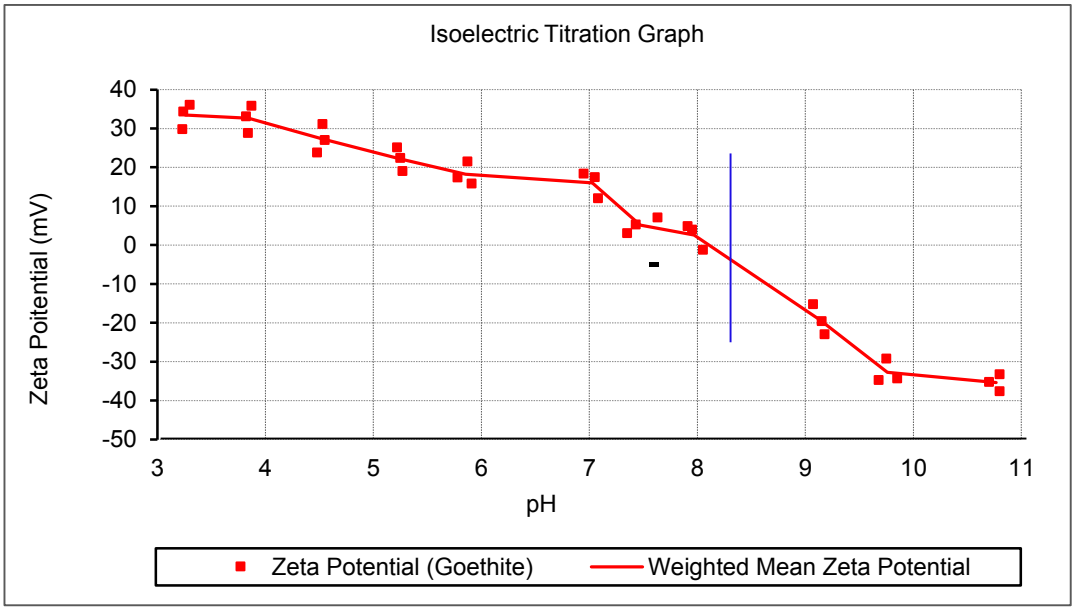

Figure E13. Zeta potential for goethite as a function of pH in the absence of DOM in solution at 25 ± 0.1°C temp.

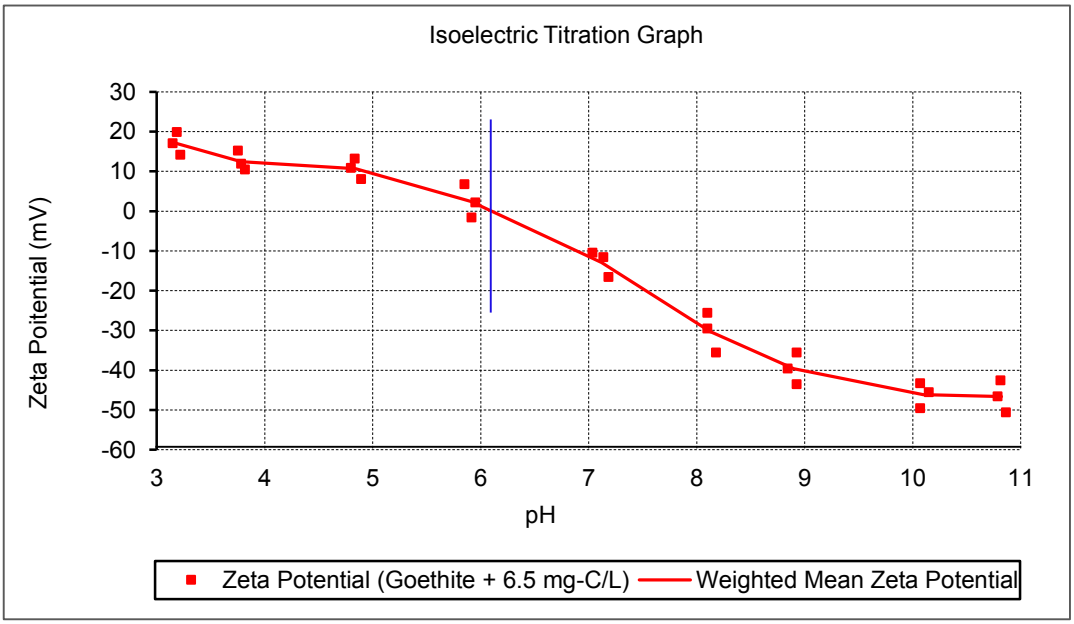

Figure E14. Zeta potential for goethite as a function of pH in the presence of DOM (6.67 mg/L) in solution at 25 ± 0.1°C temp.

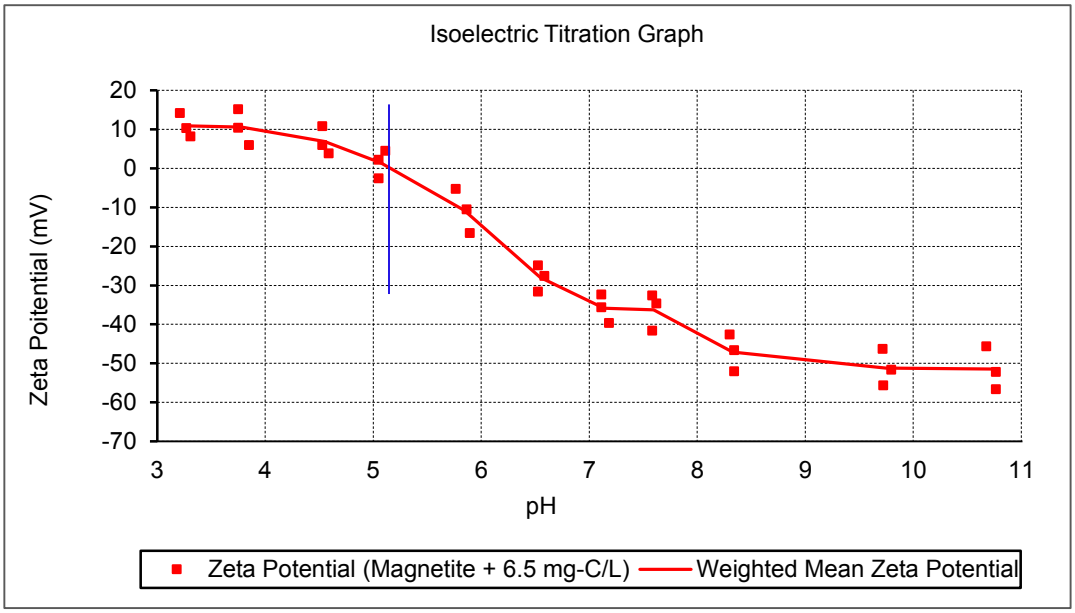

Figure E15. Zeta potential of magnetite as a function of pH in the absence of DOM in solution at 25 ± 0.1°C temp.

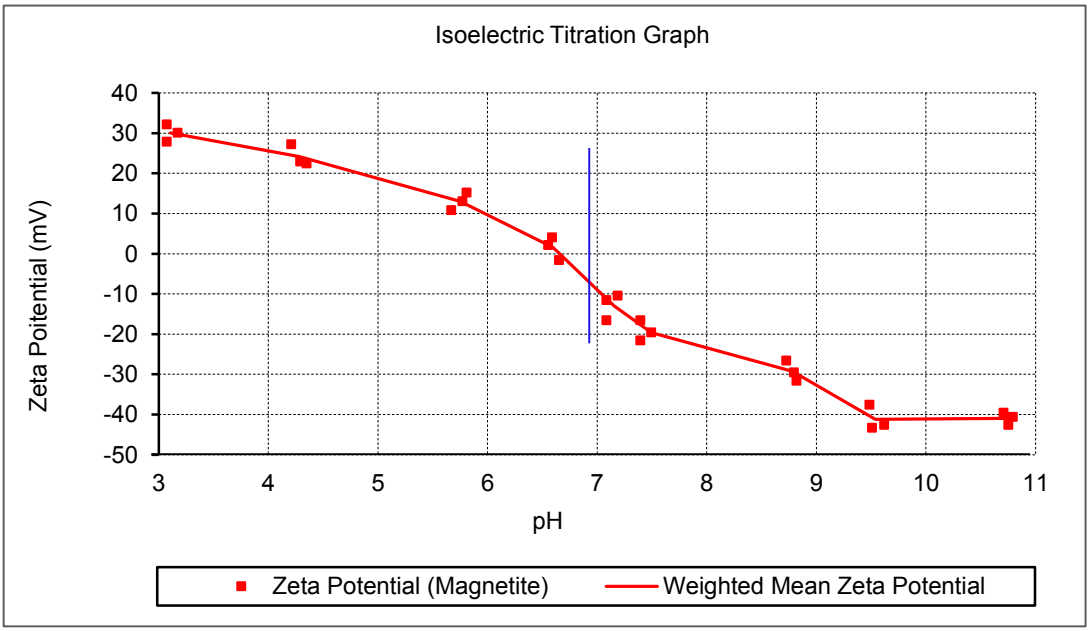

Figure E16. Zeta potential of magnetite as a function of pH in the presence of DOM (6.65 mg/L) in solution at 25 ± 0.1°C temp.

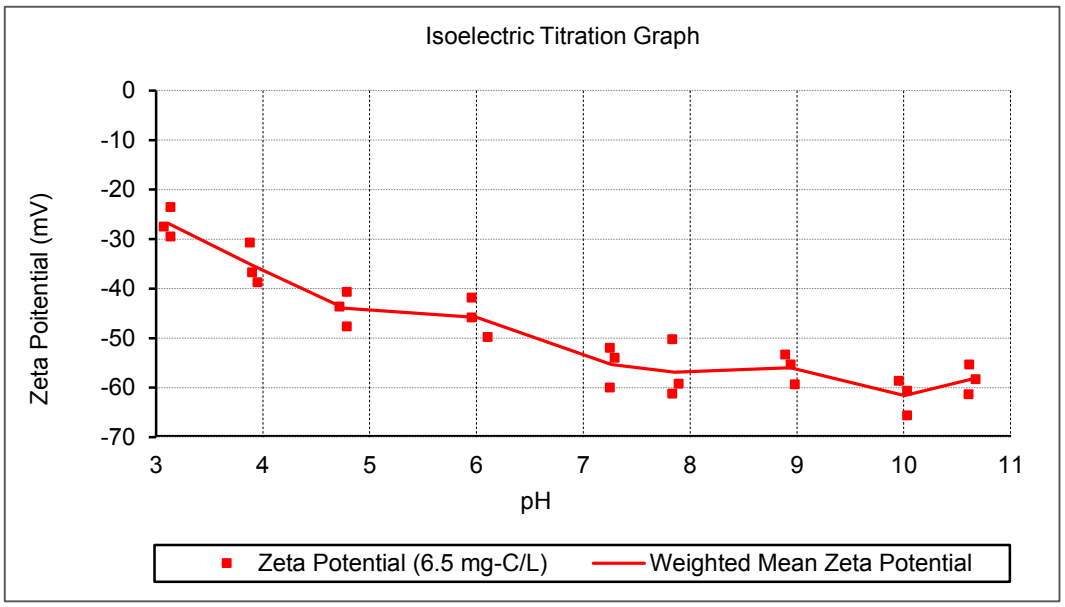

Figure E17. Zeta potential of dissolved organic carbon (6.67 mg/L) as a function of pH in solution at 25 ± 0.1°C temp.

Table E21. Summary for zeta potential reading for different reaction medias

SL No.	Reaction media	Zeta potential reading (mV)		
		Starting reading	End reading	pH_{PZC}
1	Goethite	33.45 at pH 3.18	- 35.34 at pH 10.77	8.09
2	Goethite + 6.5 mg/L DOM	17.01 at pH 3.18	- 46.61 at pH 10.82	6.11
3	Magnetite	30.01 at pH 3.11	- 44.94 at pH 10.75	6.65
4	Magnetite + 6.5 mg/L DOM	10.86 at pH 3.26	- 51.47 at pH 10.74	5.14
5	6.5 mg/L DOM	26.83 at pH 3.12	- 58.3 at pH 10.63	--

High Performance Size Exclusion Chromatography (HPSEC) data for DOM

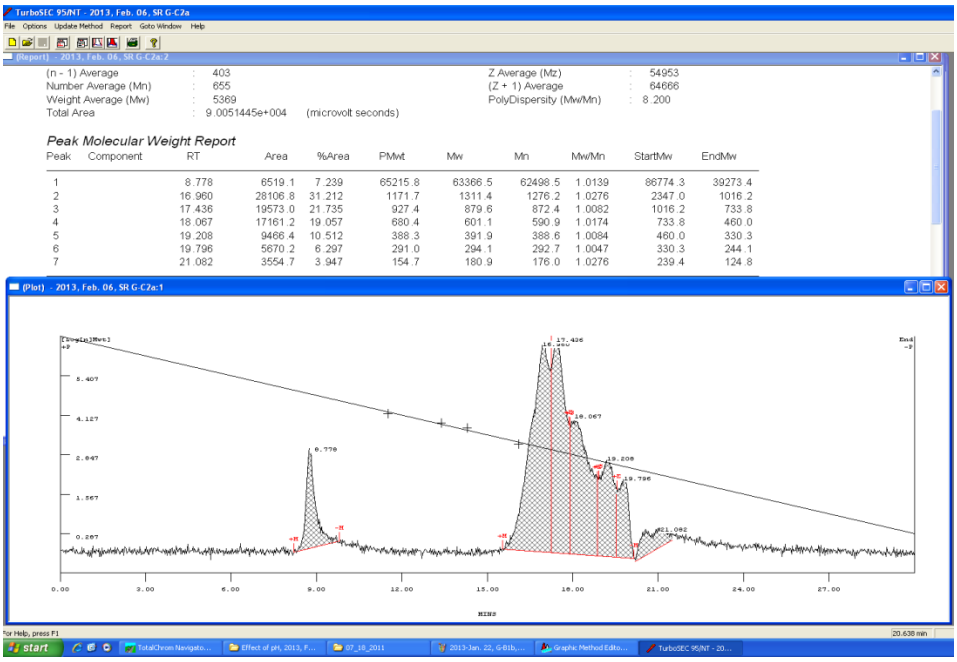

Figure E18. Molecular weight distribution of DOM at pH 10.5 using goethite.

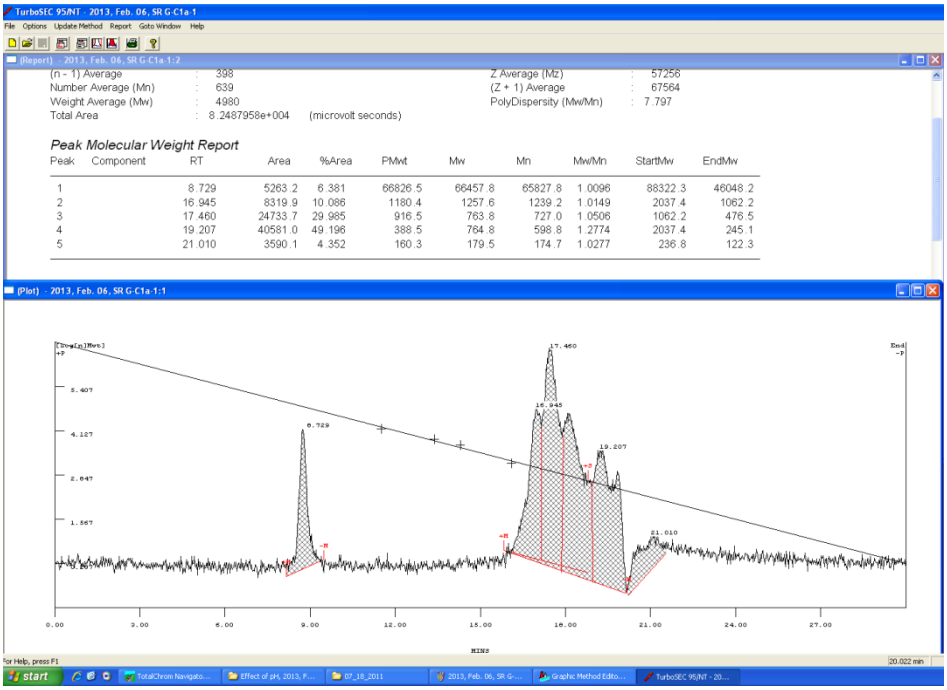

Figure E19. Molecular weight distribution of DOM at pH 8.5 using goethite.

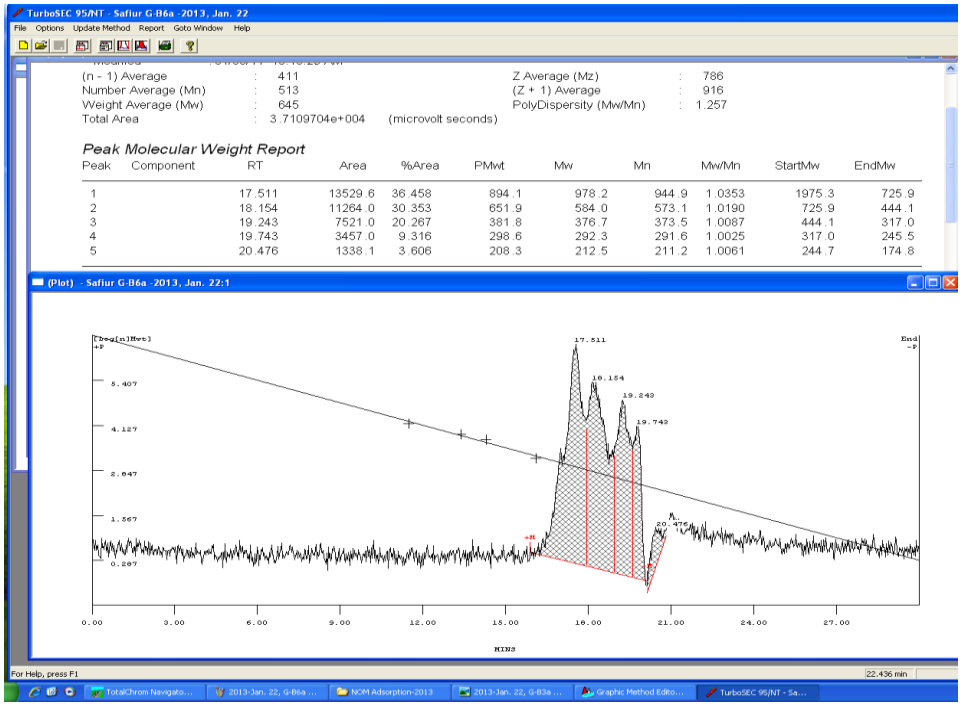

Figure E20. Molecular weight distribution of DOM at pH 6.5 using goethite.

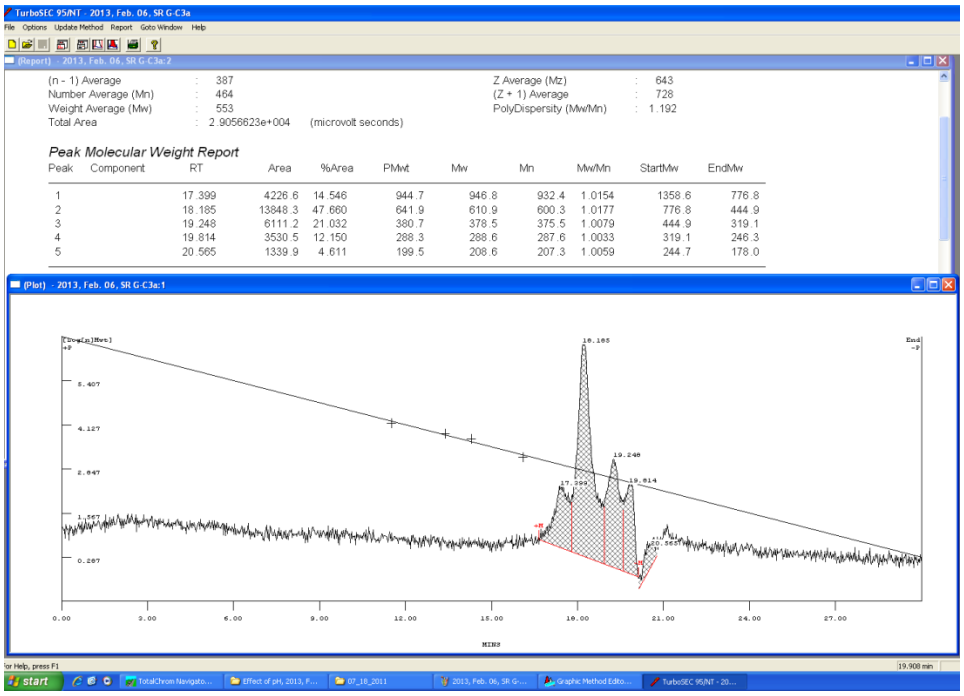

Figure E21. Molecular weight distribution of DOM at pH 4.5 using goethite.

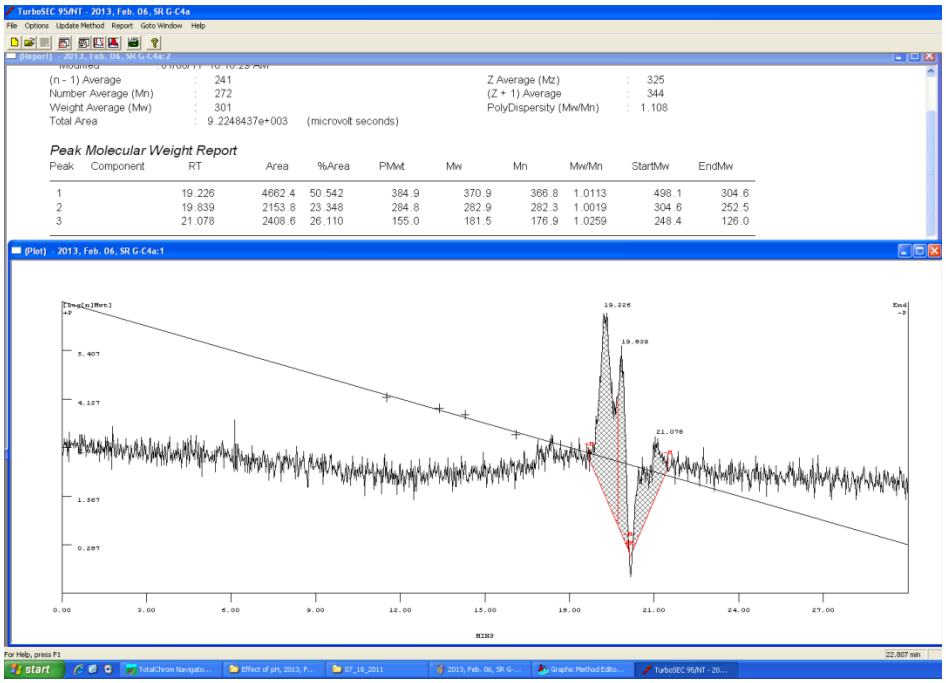

Figure E22. Molecular weight distribution of DOM at pH 2.5 using goethite.

Table E22. The changes of molecular weight (MW) distribution of dissolved organic matter due to adsorption study at different pH values in presence of 4.5 g/L goethite and 4.5 g/L magnetite.

Studied pH values	Weight average MW distribution (in presence of 4.5 mg/L goethite)				Weight average MW distribution (in presence of 4.5 mg/L magnetite)			
	Read-1	Read-2	Average	Stdev.	Read-1	Read-2	Average	Stdev.
10.5	5369	6215	5792	598.21	10899	10507	10703	277.19
8.5	4980	6065	5522.5	767.21	7291	6777	7034	363.45
6.5	636	645	640.5	6.36	2761	3179	2970	295.57
4.5	553	640	596.5	61.52	635	587	611	33.94
2.5	301	479	390	125.87	515	555	535	28.28

Table E23. Two-way analysis of variance (ANOVA) for DOM adsorption study using iron pipe corrosion scales (goethite and magnetite).

Source of Variation	*SS*	*df*	*MS*	*F*	*P-value*	F_{crit}
Iron scale	3.38	1	3.38	70.57	0.00	7.71
pH	10.05	4	2.51	52.54	0.00	6.39
Error	0.19	4	0.05			
Total	13.62	9				

Remark: ANOVA tests revealed that the pH values were statistically significant (α = 0.05, p < 0.005 and $F_{stat} = 52.54 > F_{crit} = 6.39$) on the change in adsorption capacity. On the other hand, in ANOVA analysis, there was significant difference (α = 0.05, p < 0.005 and $F_{stat} = 70.57 > F_{crit} = 7.71$) on adsorption capacity for goethite and magnetite in various solutions pH indicating that goethite and magnetite adsorbents performed differently at adsorbing DOM from the aqueous solutions.

APPENDIX F. Letter of Copyright Permission/Acceptance from Journals

(1). *Journal of Environmental Science and Health, Part A*, Taylor & Francis

Taylor & Francis Group
an informa business

For the Attention of:
Md. Safiur Rahman
PhD Candidate
Department of Civil and Resource Engineering
Dalhousie University
Canada
safiur.rahman@dal.ca

January 17, 2014

Dear Md. Safiur Rahman,

We are in receipt of your request to include the contents of the following article;

"Bench-scale evaluation of ferrous iron oxidation kinetics in drinking water: effect of corrosion control and dissolved organic matter," Graham A. Gagnon and M. Safiur Rahman, *Journal of Environmental Science and Health, Part A, Toxic/Hazardous Substances and Environmental Engineering,* Volume 49, Issue 1.

to be incorporated in a PhD Thesis by Md. Safiur Rahman for submission to the Faculty of Graduate Studies at Dalhousie University, Canada.

As the author, you retain the right to include this article in a thesis or dissertation that is not to be published commercially, provided that acknowledgement to prior publication in the relevant Taylor & Francis journal is made explicit.

Sincerely,

Mary Ann Muller
Permissions Coordinator
maryann.muller@taylorandfrancis.com

(2). *Water Research Journal* (IWA), Elsevier Inc.

Copyright Clearance Center RightsLink®

Home | Account Info | Help

Title: Bench-scale evaluation of drinking water treatment parameters on iron particles and water quality
Author: M. Safiur Rahman,Graham A. Gagnon
Publication: Water Research
Publisher: Elsevier
Date: 1 January 2014

Logged in as:
M. Safiur Rahman
Account #:
3000633722
LOGOUT

Order Completed

Thank you very much for your order.

This is a License Agreement between M. Safiur Rahman ("You") and Elsevier ("Elsevier"). The license consists of your order details, the terms and conditions provided by Elsevier, and the payment terms and conditions.

Get the printable license.

License Number	3280450377751
License date	Dec 01, 2013
Licensed content publisher	Elsevier
Licensed content publication	Water Research
Licensed content title	Bench-scale evaluation of drinking water treatment parameters on iron particles and water quality
Licensed content author	M. Safiur Rahman,Graham A. Gagnon
Licensed content date	1 January 2014
Licensed content volume number	48
Number of pages	11
Type of Use	reuse in a thesis/dissertation
Portion	full article
Format	electronic
Are you the author of this Elsevier article?	Yes
Will you be translating?	No
Title of your thesis/dissertation	Impact and management of iron corrosion by-products on drinking water quality in distribution systems
Expected completion date	Mar 2014
Estimated size (number of pages)	300
Elsevier VAT number	GB 494 6272 12
Permissions price	0.00 USD
VAT/Local Sales Tax	0.00 USD / 0.00 GBP
Total	0.00 USD

ORDER MORE... CLOSE WINDOW

(3). *Journal of Water Supply: Research and Technology–AQUA,* IWA Publishing

Alliance House
12 Caxton Street
London SW1H 0QS
United Kingdom
Tel: +44 (0)20 7654 5500
Fax: +44 (0)20 7654 5555
Email: publications@iwap.co.uk
www.iwapublishing.com

Md. Safiur Rahman
PhD Candidate
Department of Civil & Resource Engineering
Dalhousie University,
Canada

25 November 2013

Dear Md. Safiur Rahman,

Permissions request relating to material published in *Journal of Water Supply: Research and Technology - Aqua:*

In response to your request for copyright clearance to incorporate material from the following publication:

> Rahman, M.S. and Gagnon, G.A. (2013). "Bench scale evaluation of Fe(II) ions on haloacetic acids (HAAs) formation in synthetic water". *J. Water Supply Res. Technol. –AQUA* 63 (3), 155-168.© IWA Publishing 2013.

Into a PhD thesis by Md. Safiur Rahman for submission to the Faculty of Graduate Studies at Dalhousie University, Canada; we are very happy to grant you permission to reproduce the material specified above without charge, provided that:

- the material to be used has appeared in our publication without credit or acknowledgement to another source;
- The version of the paper which is reproduced is the author's proof and not the final published version;
- suitable acknowledgement to the source is given in accordance with standard editorial practice, e.g.,

  "Reproduced from Rahman, M.S. and Gagnon, G.A. 2013. "Bench scale evaluation of Fe(II) ions on haloacetic acids (HAAs) formation in synthetic water". *J. Water Supply Res. Technol. –AQUA* 63 (3), 155-168 with permission from the copyright holders, IWA Publishing".

- Reproduction of this material is confined to the purpose for which this permission is given.

I trust this permission will be satisfactory; if any point needs clarification or you have any further queries, please do not hesitate to contact us again.

Yours sincerely

Chloe Parker
Digital Publishing Assistant

(4). *Journal of Water Supply: Research and Technology–AQUA,* IWA Publishing

Alliance House
12 Caxton Street
London SW1H 0QS
United Kingdom
Tel: +44 (0)20 7654 5500
Fax: +44 (0)20 7654 5555
Email: publications@iwap.co.uk
www.iwapublishing.com

From: Saroj Kumar Sharma
Subject: Your Submission
Date: 17 December, 2013
To: Graham A Gagnon

Dear Dr. Gagnon,

I am pleased to tell you that your submission "Iron corrosion as a factor contributing to haloacatic acids (HAAs) formation in the distribution system: Experimental assessment and model development" (JWSRTAQUA-D-13-00071R1) has now been ACCEPTED for publication in Journal of Water Supply: Research and Technology -AQUA.

It was accepted on 17 Dec 2013.

You will hear from IWA Publishing soon regarding the publication of your paper.

Thank you for submitting your work to Journal of Water Supply: Research and Technology - AQUA.

Sincerely yours,

Saroj Kumar Sharma, Ph.D.
Editor
Journal of Water Supply: Research and Technology - AQUA
IWA Publishing

s.sharma@unesco-ihe.org

(5). *Chemical Engineering Journal*, Elsevier Inc.

Copyright Clearance Center RightsLink®

Home | Account Info | Help

Title: Adsorption of dissolved organic matter (DOM) onto the synthetic iron pipe corrosion scales (goethite and magnetite): Effect of pH

Author: M. Safiur Rahman,Marc Whalen,Graham A. Gagnon

Publication: Chemical Engineering Journal

Publisher: Elsevier

Date: December 2013

Logged in as:
M. Safiur Rahman
Account #:
3000633722

LOGOUT

Order Completed

Thank you very much for your order.

This is a License Agreement between M. Safiur Rahman ("You") and Elsevier ("Elsevier"). The license consists of your order details, the terms and conditions provided by Elsevier, and the payment terms and conditions.

Get the printable license.

License Number	3280441320621
License date	Dec 01, 2013
Licensed content publisher	Elsevier
Licensed content publication	Chemical Engineering Journal
Licensed content title	Adsorption of dissolved organic matter (DOM) onto the synthetic iron pipe corrosion scales (goethite and magnetite): Effect of pH
Licensed content author	M. Safiur Rahman,Marc Whalen,Graham A. Gagnon
Licensed content date	December 2013
Licensed content volume number	234
Number of pages	9
Type of Use	reuse in a thesis/dissertation
Portion	full article
Format	electronic
Are you the author of this Elsevier article?	Yes
Will you be translating?	No
Title of your thesis/dissertation	Impact and management of iron corrosion by-products on drinking water quality in distribution systems
Expected completion date	Mar 2014
Estimated size (number of pages)	300
Elsevier VAT number	GB 494 6272 12
Permissions price	0.00 USD
VAT/Local Sales Tax	0.00 USD / 0.00 GBP
Total	0.00 USD

ORDER MORE... CLOSE WINDOW